

# Molecular and cellular mechanisms of heart failure: Pathophysiology, pathogenesis and therapeutics

**Edited by**

Kenneth Scott Campbell, Amy Li  
and Sean Lal

**Published in**

Frontiers in Cardiovascular Medicine



## FRONTIERS EBOOK COPYRIGHT STATEMENT

The copyright in the text of individual articles in this ebook is the property of their respective authors or their respective institutions or funders. The copyright in graphics and images within each article may be subject to copyright of other parties. In both cases this is subject to a license granted to Frontiers.

The compilation of articles constituting this ebook is the property of Frontiers.

Each article within this ebook, and the ebook itself, are published under the most recent version of the Creative Commons CC-BY licence. The version current at the date of publication of this ebook is CC-BY 4.0. If the CC-BY licence is updated, the licence granted by Frontiers is automatically updated to the new version.

When exercising any right under the CC-BY licence, Frontiers must be attributed as the original publisher of the article or ebook, as applicable.

Authors have the responsibility of ensuring that any graphics or other materials which are the property of others may be included in the CC-BY licence, but this should be checked before relying on the CC-BY licence to reproduce those materials. Any copyright notices relating to those materials must be complied with.

Copyright and source acknowledgement notices may not be removed and must be displayed in any copy, derivative work or partial copy which includes the elements in question.

All copyright, and all rights therein, are protected by national and international copyright laws. The above represents a summary only. For further information please read Frontiers' Conditions for Website Use and Copyright Statement, and the applicable CC-BY licence.

ISSN 1664-8714  
ISBN 978-2-8325-3318-5  
DOI 10.3389/978-2-8325-3318-5

## About Frontiers

Frontiers is more than just an open access publisher of scholarly articles: it is a pioneering approach to the world of academia, radically improving the way scholarly research is managed. The grand vision of Frontiers is a world where all people have an equal opportunity to seek, share and generate knowledge. Frontiers provides immediate and permanent online open access to all its publications, but this alone is not enough to realize our grand goals.

## Frontiers journal series

The Frontiers journal series is a multi-tier and interdisciplinary set of open-access, online journals, promising a paradigm shift from the current review, selection and dissemination processes in academic publishing. All Frontiers journals are driven by researchers for researchers; therefore, they constitute a service to the scholarly community. At the same time, the *Frontiers journal series* operates on a revolutionary invention, the tiered publishing system, initially addressing specific communities of scholars, and gradually climbing up to broader public understanding, thus serving the interests of the lay society, too.

## Dedication to quality

Each Frontiers article is a landmark of the highest quality, thanks to genuinely collaborative interactions between authors and review editors, who include some of the world's best academicians. Research must be certified by peers before entering a stream of knowledge that may eventually reach the public - and shape society; therefore, Frontiers only applies the most rigorous and unbiased reviews. Frontiers revolutionizes research publishing by freely delivering the most outstanding research, evaluated with no bias from both the academic and social point of view. By applying the most advanced information technologies, Frontiers is catapulting scholarly publishing into a new generation.

## What are Frontiers Research Topics?

Frontiers Research Topics are very popular trademarks of the *Frontiers journals series*: they are collections of at least ten articles, all centered on a particular subject. With their unique mix of varied contributions from Original Research to Review Articles, Frontiers Research Topics unify the most influential researchers, the latest key findings and historical advances in a hot research area.

Find out more on how to host your own Frontiers Research Topic or contribute to one as an author by contacting the Frontiers editorial office: [frontiersin.org/about/contact](https://frontiersin.org/about/contact)



# Molecular and cellular mechanisms of heart failure: Pathophysiology, pathogenesis and therapeutics

## Topic editors

Kenneth Scott Campbell — University of Kentucky, United States

Amy Li — La Trobe University, Australia

Sean Lal — The University of Sydney, Australia

## Citation

Campbell, K. S., Li, A., Lal, S., eds. (2023). *Molecular and cellular mechanisms of heart failure: Pathophysiology, pathogenesis and therapeutics*.

Lausanne: Frontiers Media SA. doi: 10.3389/978-2-8325-3318-5

# Table of contents

- 05 **Editorial: Molecular and cellular mechanisms of heart failure: pathophysiology, pathogenesis and therapeutics**  
Sean Lal, Kenneth Campbell and Amy Li
- 08 **Long non-coding RNAs in the pathogenesis of heart failure: A literature review**  
Xiaoyan Fan, Zhenwei Zhang, Liang Zheng, Wei Wei and Zetao Chen
- 18 **Transcriptional bursts and heterogeneity among cardiomyocytes in hypertrophic cardiomyopathy**  
Valentin Burkart, Kathrin Kowalski, David Aldag-Niebling, Julia Beck, Dirk Alexander Frick, Tim Holler, Ante Radocaj, Birgit Piep, Andre Zeug, Denise Hilfiker-Kleiner, Cristobal G. dos Remedios, Jolanda van der Velden, Judith Montag and Theresia Kraft
- 34 **Chronic intermittent hypoxia accelerates cardiac dysfunction and cardiac remodeling during cardiac pressure overload in mice and can be alleviated by PHD3 overexpression**  
Xuan Xu, Peng-Hao Zhen, Fu-Chao Yu, Tao Wang, Sheng-Nan Li, Qin Wei and Jia-Yi Tong
- 51 **Functional comparison of phosphomimetic S15D and T160D mutants of myosin regulatory light chain exchanged in cardiac muscle preparations of HCM and WT mice**  
Katarzyna Kazmierczak, Jingsheng Liang, Michelle Gomez-Guevara and Danuta Szczesna-Cordary
- 65 **New factors in heart failure pathophysiology: Immunity cells release of extracellular vesicles**  
Alba Vilella-Figuerola, Teresa Padró, Eulàlia Roig, Sònia Mirabet and Lina Badimon
- 77 **Suppression of lusitropy as a disease mechanism in cardiomyopathies**  
Steven Marston and Jose Renato Pinto
- 89 **Role of Connexin 43 phosphorylation on Serine-368 by PKC in cardiac function and disease**  
Renju Pun, Michael H. Kim and Brian J. North
- 108 **Implications of S-glutathionylation of sarcomere proteins in cardiac disorders, therapies, and diagnosis**  
Paola C. Rosas and R. John Solaro
- 120 **Affimers targeting proteins in the cardiomyocyte Z-disc: Novel tools that improve imaging of heart tissue**  
Francine Parker, Anna A. S. Tang, Brendan Rogers, Glenn Carrington, Cris dos Remedios, Amy Li, Darren Tomlinson and Michelle Peckham
- 130 **Indoxyl sulfate induces left ventricular hypertrophy via the AhR-FGF23-FGFR4 signaling pathway**  
Hiroshi Kishimoto, Toshiaki Nakano, Kumiko Torisu, Masanori Tokumoto, Yushi Uchida, Shunsuke Yamada, Masatomo Taniguchi and Takanari Kitazono

- 143 **Myofibroblast Ccn3 is regulated by Yap and Wwtr1 and contributes to adverse cardiac outcomes**  
Michael A. Flinn, Santiago Alvarez-Argote, Makenna C. Knas, Victor Alencar Almeida, Samantha J. Paddock, Xiaoxu Zhou, Tyler Buddell, Ayana Jamal, Reiauna Taylor, Pengyuan Liu, Jenny Drnevich, Michaela Patterson, Brian A. Link and Caitlin C. O'Meara
- 161 **Association polymorphism of guanine nucleotide-binding protein  $\beta 3$  subunit (*GNB3*) C825T and insertion/deletion of the angiotensin-converting enzyme (*ACE*) gene with peripartum cardiomyopathy**  
Ivana Purnama Dewi, Louisa Fadjri Kusuma Wardhani, Irma Maghfirah, Kristin Purnama Dewi, Agus Subagjo, Mochamad Yusuf Alsagaff and Johannes Nugroho
- 169 **Alterations in cytoskeletal and  $\text{Ca}^{2+}$  cycling regulators in atria lacking the obscurin Ig58/59 module**  
Alyssa Grogan, Weiliang Huang, Annie Brong, Maureen A. Kane and Aikaterini Kontrogianni-Konstantopoulos



## OPEN ACCESS

EDITED BY  
Matteo Cameli,  
University of Siena, Italy

\*CORRESPONDENCE  
Amy Li  
✉ amy.li@torrens.edu.au

RECEIVED 17 July 2023  
ACCEPTED 19 July 2023  
PUBLISHED 04 August 2023

CITATION  
Lal S, Campbell K and Li A (2023) Editorial:  
Molecular and cellular mechanisms of heart  
failure: pathophysiology, pathogenesis and  
therapeutics.  
Front. Cardiovasc. Med. 10:1260483.  
doi: 10.3389/fcvm.2023.1260483

COPYRIGHT  
© 2023 Lal, Campbell and Li. This is an open-  
access article distributed under the terms of the  
[Creative Commons Attribution License \(CC BY\)](#).  
The use, distribution or reproduction in other  
forums is permitted, provided the original  
author(s) and the copyright owner(s) are  
credited and that the original publication in this  
journal is cited, in accordance with accepted  
academic practice. No use, distribution or  
reproduction is permitted which does not  
comply with these terms.

# Editorial: Molecular and cellular mechanisms of heart failure: pathophysiology, pathogenesis and therapeutics

Sean Lal<sup>1</sup>, Kenneth Campbell<sup>2</sup> and Amy Li<sup>1,3,4\*</sup>

<sup>1</sup>School of Medical Sciences, The University of Sydney, Camperdown, NSW, Australia, <sup>2</sup>Department of Physiology, University of Kentucky, Lexington, KY, United States, <sup>3</sup>Department of Rural Clinical Sciences, La Trobe Rural Health School, La Trobe University, Flora Hill, VIC, Australia, <sup>4</sup>Centre for Healthy Futures, Torrens University Australia, Surrey Hill, NSW, Australia

## KEYWORDS

heart failure, cardiomyopathy, molecular, cellular, pathophysiology

## Editorial on the Research Topic

**Molecular and cellular mechanisms of heart failure: pathophysiology, pathogenesis and therapeutics**

Heart failure is the common endpoint of a diverse group of cardiac disorders including inherited or acquired (or a combination of the two) cardiomyopathies, myocardial ischemia and pressure/volume overload from valvular disease. Despite continuous advances in therapeutics, heart failure remains a major burden on the health care system with a high incidence of morbidity and mortality (up to 75% at 5 years) (1). Several physiological processes contribute to the development of heart failure including impaired contractility, alterations in energy metabolism, neurohormonal dysregulation, and maladaptive remodeling of the myocardium (2). Within cardiomyocytes, aberrant calcium handling and modulation of contractile proteins and ion channels caused by genetic mutations or post-translational modification are key contributors to impaired contractility. The collection of research papers in this issue highlights recent advances at the molecular and cellular level that contribute to the pathophysiology of heart failure with a major focus on cardiomyopathies, followed by insights gained from chronic multi-systemic diseases. Collectively, the mechanistic insight revealed by the authors offer novel therapeutic approaches and/or targets that are gaining traction towards translation in patients.

Molecular studies in this issue provide valuable insights into the pathogenesis of heart failure. Suppression of lusitropy is recognized as a contributor to impaired relaxation and diastolic dysfunction, a key mechanism in cardiomyopathies (Marston and Pinto). Marston and Pinto discuss how altered calcium handling by protein kinase A (PKA) phosphorylation of troponin I and how phospholamban impacts lusitropy. They identify therapeutic targets in conditions where diastolic dysfunction is prevalent. Similarly, S-glutathionylation of sarcomere proteins has emerged as a molecular modifier in contractile dysfunction and disease progression associated with oxidative stress (Rosas and Solaro). In this study, Rosas and Solaro outline the possibility of screening serum S-glutathionylated sarcomeric proteins as a clinical tool for early diagnosis in patients at risk of heart failure, stratification and determination

of progression, and even to identify the effectiveness of new therapeutic approaches. Another way to investigate the functional impact of specific phosphorylation sites is to engineer amino acid substitutions that mimic phosphorylation, known as phosphomimetics. This was accomplished by [Kazmierczak et al.](#) who demonstrated the therapeutic potential of myosin regulatory light chain phosphomimetics by showing that they could rescue the contractile defects caused by hypertrophic cardiomyopathy.

Besides post-translational modification, dysfunctional cytoskeletal and calcium cycling regulators have been implicated in atrial and ventricular dysfunction and susceptibility to arrhythmias ([Grogan et al.](#)) (3). [Grogan et al.](#) examined the functional deletions of the Obscurin immunoglobulin 58/59 domains (Ig58/59) and demonstrated their essential role in regulating cytoskeleton structure and  $\text{Ca}^{2+}$  cycling in the atria. This new knowledge provides a mechanistic explanation of the previously characterized phenotype with an onset of atrial enlargement and fibrillation in the ageing heart (4). Additionally, [Dewi et al.](#) discovered a genetic susceptibility of peripartum cardiomyopathy by linking the association of guanine nucleotide-binding protein  $\beta 3$  subunit (GNB3) C825T polymorphism and insertion/deletion of the angiotensin-converting enzyme (ACE) gene to the disease. Unravelling these molecular mechanisms and their functional consequences opens new avenues for therapeutic interventions aimed at restoring normal cardiac function.

The next set of studies illustrate the cellular processes that contributes to heart failure pathogenesis. [Pun et al.](#) provide a comprehensive review of Connexin 43, an essential gap junction protein localized to the intercalated discs which connect adjacent cardiomyocytes. Phosphorylation of connexin 43 S368 by protein kinase C (PKC) has been identified as a key regulator of cardiac function where both hypo- and hyper-phosphorylation are associated with disease, impacting cell-cell coupling and arrhythmogenesis ([Pun et al.](#)). Transcriptional burst was an interesting concept first described by the Kraft group in hypertrophic cardiomyopathy patients with heterogenous mutations (5). This causes independent transcription of mutated and wild-type alleles giving rise to a mosaic expression in the ratio of mRNA between individual cardiomyocytes. [Burkart et al.](#) demonstrated that sarcomeric proteins also exhibited mosaic patterns and contributed to highly variable  $\text{Ca}^{2+}$ -dependent force generation between individual cardiomyocytes. The contractile imbalance between individual cardiomyocytes promotes HCM-development contributing to disease progression ([Burkart et al.](#)).

Three further articles in this issue consider the role of adverse cardiac remodeling and fibrosis induced by myofibroblasts in [Flinn et al.](#), chronic kidney disease in [Kishimoto et al.](#), and chronic intermittent hypoxia in [Xuan et al.](#) These diverse pathological pathways underpin the cardiac consequences of many multi-systemic diseases.

Advancements in understanding of heart failure pathophysiology have paved the way for innovative therapeutic approaches targeting specific molecular and cellular

mechanisms. Novel tools such as affimers, extracellular vesicles and long non-coding RNAs (lncRNAs) offer new possibilities for diagnostic and therapeutic development. [Parker et al.](#) provide evidence that affimers, small engineered non-antibody binding proteins, can target proteins in cardiomyocytes. This proof-of-concept offers a novel tool that improves imaging of heart tissue, aiding in diagnosis and monitoring of heart failure ([Parker et al.](#)). New factors, such as the shedding of extracellular vesicles by adaptive and innate immune cells confirmed by [Vilella-Figuerola et al.](#), unveil previously unrecognized contributors to heart failure pathophysiology. Moreover, long non-coding RNAs (lncRNAs) have emerged as an important epigenetic regulator of DNA, RNA and proteins with diverse implications in heart failure pathogenesis (6). [Fan et al.](#) conducted a comprehensive literature review of lncRNAs' involvement in heart failure that highlights their potential as diagnostic markers and epigenetic-based therapeutic targets. These advances provide opportunities to developing personalized therapeutic strategies beyond the now standard therapeutic inhibitors and highlight the increasing interaction between genetic pre-disposition and environment.

This topical issue represents some of the most recent progress in our understanding of the complex cellular mechanisms underlying heart failure. The suppression of lusitropy, S-glutathionylation of sarcomere proteins, connexin 43 phosphorylation, alterations in cytoskeletal and calcium cycling regulators, and transcriptional heterogeneity in cardiomyocyte are some of the key molecular mechanisms implicated in cardiomyopathies. Insights into cellular processes, such as myofibroblast regulation, signaling pathways, and the impact of chronic intermittent hypoxia provide valuable information underpinning the more generalized progression towards heart failure. Together, the research presented in this issue opens new avenues for the development of targeted diagnostics and design of novel treatment strategies that improve cardiac function, prevent aberrant myocardial remodeling, and reduce fibrosis. These measures could be aimed at restoring normal cardiac function and ultimately improve patient outcomes.

## Author contributions

SL: Writing – review & editing. KC: Writing – review & editing. AL: Writing – original draft, Writing – review & editing.

## Funding

This work was supported by NIH R01 HL149164 (KC).

## Acknowledgments

We thank all the authors and reviewers who contributed to this Research Topic.



## Conflict of interest

The authors declare that the research was conducted in the absence of any commercial or financial relationships that could be construed as a potential conflict of interest.

The author(s) declared that they were an editorial board member of Frontiers, at the time of submission. This had no impact on the peer review process and the final decision.

## Publisher's note

All claims expressed in this article are solely those of the authors and do not necessarily represent those of their affiliated organizations, or those of the publisher, the editors and the reviewers. Any product that may be evaluated in this article, or claim that may be made by its manufacturer, is not guaranteed or endorsed by the publisher.

## References

1. Savarese G, Lund LH. Global public health burden of heart failure. *Card Fail Rev.* (2017) 3(1):7–11. doi: 10.15420/cfr.2016:25:2
2. Mann DL, Bristow MR. Mechanisms and models in heart failure. *Circulation.* (2005) 111(21):2837–49. doi: 10.1161/CIRCULATIONAHA.104.500546
3. Sequeira V, Nijenkamp LLAM, Regan JA, van der Velden J. The physiological role of cardiac cytoskeleton and its alterations in heart failure. *Biochim Biophys Acta Biomembr* (2014) 1838(2):700–22. doi: 10.1016/j.bbmem.2013.07.011
4. Grogan A, Coleman A, Joca H, Granzier H, Russel MW, Ward CW, et al. Deletion of obscurin immunoglobulin domains Ig58/59 leads to age-dependent cardiac remodeling and arrhythmia. *Basic Res Cardiol.* (2020) 115(6):60. doi: 10.1007/s00395-020-00818-8
5. Montag J, Kowalski K, Makul M, Ernstberger P, Radocaj A, Beck J, et al. Burst-like transcription of mutant and wildtype Myh7-alleles as possible origin of cell-to-cell contractile imbalance in hypertrophic cardiomyopathy. *Front Physiol.* (2018) 9:359. doi: 10.3389/fphys.2018.00359
6. Papait R, Serio S, Condorelli G. Role of the epigenome in heart failure. *Physiol Rev.* (2020) 100(4):1753–77. doi: 10.1152/physrev.00037.2019



## OPEN ACCESS

## EDITED BY

Matteo Pagnesi,  
ASST Spedali Civili di Brescia, Italy

## REVIEWED BY

Vincenzo Castiglione,  
Sant'Anna School of Advanced  
Studies, Italy  
Emma Louise Robinson,  
University of Colorado, United States

## \*CORRESPONDENCE

Wei Wei  
869641942@qq.com  
Zetao Chen  
zetaochen2007@126.com

## SPECIALTY SECTION

This article was submitted to  
Heart Failure and Transplantation,  
a section of the journal  
Frontiers in Cardiovascular Medicine

RECEIVED 22 May 2022

ACCEPTED 11 July 2022

PUBLISHED 03 August 2022

## CITATION

Fan X, Zhang Z, Zheng L, Wei W and  
Chen Z (2022) Long non-coding RNAs  
in the pathogenesis of heart failure: A  
literature review.  
*Front. Cardiovasc. Med.* 9:950284.  
doi: 10.3389/fcvm.2022.950284

## COPYRIGHT

© 2022 Fan, Zhang, Zheng, Wei and  
Chen. This is an open-access article  
distributed under the terms of the  
[Creative Commons Attribution License  
\(CC BY\)](#). The use, distribution or  
reproduction in other forums is  
permitted, provided the original  
author(s) and the copyright owner(s)  
are credited and that the original  
publication in this journal is cited, in  
accordance with accepted academic  
practice. No use, distribution or  
reproduction is permitted which does  
not comply with these terms.

# Long non-coding RNAs in the pathogenesis of heart failure: A literature review

Xiaoyan Fan<sup>1,2</sup>, Zhenwei Zhang<sup>3</sup>, Liang Zheng<sup>2</sup>, Wei Wei<sup>4\*</sup> and Zetao Chen<sup>5,6\*</sup>

<sup>1</sup>Postdoctoral Mobile Station of Shandong University of Traditional Chinese Medicine, Shandong University of Traditional Chinese Medicine, Jinan, China, <sup>2</sup>Department of Cardiovascular Disease, Affiliated Hospital of Shandong University of Traditional Chinese Medicine, Jinan, China, <sup>3</sup>Department of Urinary Surgery, No.3 People's Hospital, Jinan, China, <sup>4</sup>Postdoctoral Mobile Station of Wangjing Hospital, Wangjing Hospital, China Academy of Chinese Medicine Sciences, Beijing, China, <sup>5</sup>Section of Integrated Chinese and Western Medicine, Shandong university of Traditional Chinese Medicine, Jinan, China, <sup>6</sup>Department of Geriatrics, Affiliated Hospital of Shandong University of Traditional Chinese Medicine, Jinan, China

Heart failure (HF) is a common cardiovascular disorder and a major cause of mortality and morbidity in older people. The mechanisms underlying HF are still not fully understood, restricting novel therapeutic target discovery and drug development. Besides, few drugs have been shown to improve the survival of HF patients. Increasing evidence suggests that long non-coding RNAs (lncRNAs) serve as a critical regulator of cardiac physiological and pathological processes, regarded as a new target of treatment for HF. lncRNAs are versatile players in the pathogenesis of HF. They can interact with chromatin, protein, RNA, or DNA, thereby modulating chromatin accessibility, gene expressions, and signaling transduction. In this review, we summarized the current knowledge on how lncRNAs involve in HF and categorized them into four aspects based on their biological functions, namely, cardiomyocyte contractility, cardiac hypertrophy, cardiac apoptosis, and myocardial fibrosis. Along with the extensive laboratory data, RNA-based therapeutics achieved great advances in recent years. These indicate that targeting lncRNAs in the treatment of HF may provide new strategies and address the unmet clinical needs.

## KEYWORDS

heart failure, long non-coding RNA, pathogenesis, cardiac remodeling, cardiac hypertrophy

## Introduction

Heart failure (HF) is one of the most common cardiovascular disorders in the elderly, caused by left (or global) ventricular dysfunction, which is manifested by fatigue and dyspnea, often with signs of volume overload. Its prevalence and cost are still rising. In the guidelines for the diagnosis and treatment of HF issued by the European Society of Cardiology (ESC), HF is divided into three types according to the left ventricular ejection fraction (EF), namely, HF with reduced ejection fraction (HFrEF, EF < 40%), HF with preserved ejection fraction (HFpEF, EF > 50%), and the newly defined HF with mildly

reduced ejection fraction (HFmrEF, 40–49%) (1). The American College of Cardiology Foundation/American Heart Association and Japanese Circulation Society/Japanese Heart Failure Society guidelines introduced a category called “HF with improved EF (HFiEF),” which is defined as patients with previous LVEF <35% and a follow-up measurement of LVEF >40% (2). Past decades have seen great achievements made in the treatment of HFmrEF. However, seldom has been clinically demonstrated to improve the survival. New insights in the pathogenesis and treatment of HF are warranted (3).

Our understanding regarding the pathogenesis of HF has changed over decades. In the past, HF has been viewed as a hemodynamic disorder. Gradually, evidence unravels that activation of the renin–angiotensin–aldosterone system (RAAS) is independent of the hemodynamics and further gives birth to the neurohormonal hypothesis (4). Now, the prevailing view is that HF is a multisystemic disorder, which involves various organ pathologies, such as renal, pulmonary, and skeletal muscle diseases, as well as obesity (5). Besides, different types of HF share similarities in proposed cellular and molecular mechanisms, such as mitochondrial dysfunction, oxidative stress, cardiomyocyte and extracellular matrix-based stiffening, reduced NO bioavailability, impaired cation channel homeostasis, inflammation, and endoplasmic reticulum stress (6, 7). In the last decades, increasing evidence suggests that long non-coding RNAs (lncRNAs) serve as a critical regulator of cardiac physiological and pathological processes, regarded as a new target of treatment for heart failure. Long non-coding RNAs are transcripts exceeding 200 nucleotides in length without functional protein-coding potential.

In this study, we summarized the current advances made using the involvement of lncRNA in the pathogenesis of HF, as well as its possible clinical applications in diagnosis and treatments.

## Molecular and biological functions of lncRNAs

The Human Genome Project prevailed that the human genome comprises about 3.1 billion base pairs with only about 22,300 protein-coding genes, whereas the remaining was considered “junk DNA” (8). Consistent with this, RNA sequencing technology in recent years revealed only 2% of transcribed genomes eventually translated into proteins (9, 10). Apart from protein-coding messenger RNAs (mRNAs), transfer RNA (tRNAs), and ribosomal RNAs (rRNAs), non-coding RNAs (ncRNAs) are classified into long non-coding RNAs (lncRNAs), circular RNAs (circRNAs), small non-coding RNAs (sncRNAs), and PIWI-interacting RNAs (piRNAs) based on their structural features (11, 12).

Among these, lncRNAs are longer than ~200 nucleotides (nt), and their biogenesis is similar to mRNAs. lncRNAs are transcribed by RNA polymerase II (RNAPII) from intergenic, exonic, or distal protein-coding regions of the genome, and they often undergo 3′-polyadenylation, 5′-methyl-guanosine capping, and splicing (13). lncRNAs are versatile gene expression regulators at different levels, and their functions largely depend on interacting partners.

## lncRNAs regulate chromatin structure and accessibility

In the nucleus, lncRNAs with negative charge bind to positively charged histone tails resulting in chromatin de-compaction, which may function as a rapid switch of gene expression (14). In addition, lncRNAs directly bind to DNA forming a hybrid structure, termed triple triplexes or R-loops, which influence chromatin accessibility and DNA repair (15, 16). Recently, it was reported that NEAT1 is responsible for the assembly of paraspeckles, a form of nuclear condensates, through liquid–liquid phase separation (17).

## lncRNAs modulate transcriptional activity

lncRNA can recruit or guide chromatin modifiers, thus affecting the transcriptional activity, such as epigenetic regulatory enzymes (18). A widely known example is that HOX antisense intergenic RNA (HOTAIR) regulates chromatin dynamics and induces gene silencing *via* acting as a guide of histone methylase (PRC2) and histone demethylase (LSD1) to the correct genomic loci (19).

Besides, lncRNA can serve as a scaffold or platform at a specific genomic locus for other regulators. For instance, SPRY4-intronic transcript 1 (SPRY4-IT1) scaffolds enhancer of zeste homolog 2 (EZH2) along with LSD1 or DNA methyltransferase 1 (DNMT1) induces downstream gene silencing (20). In addition, lncRNAs compete for binding sites and prevent gene-modifying proteins from acting on the loci of interest, known as decoys.

## lncRNAs involve in translational process

In the cytoplasm, lncRNAs can alter mRNA splicing by interacting with ribosomes, competing with endogenous RNAs (CeRNA), and directly bind or sponge microRNAs (21). lncRNA, the antisense transcript of the gene ZNF1 (ZFAS1), can interact with 40S subunit of ribosome. It is involved in ribosome production and assembly (22).

Regarding CeRNA, the antisense transcript for beta-secretase-1 (BACE1-AS) competes with miR-485-5p for binding within the same region in the open reading frame of the BACE1 mRNA (23).

In addition to these functions, lncRNAs can interact with mitochondria and exosomes. lncRNAs can be encoded by mitochondrial DNA and are specifically located in mitochondria affecting mitochondrial functions and the crosstalk of mitochondria with nuclei (24, 25). A previous study found that in gene imprinting, lncRNA directly acts as a signal molecule without translation to protein, which enables a prompt response to stimulation (26). lncRNAs can also be packed into exosomes and delivered to recipient cells (27).

## Roles of LncRNAs in the pathogenesis of HF

### LncRNAs modulating cardiomyocyte contractility

A critical way for cardiomyocytes to overcome insufficient blood output is to increase their contractility. From another perspective, pathological insults impairing the cardiac contractility are considered a reason for HF.

Rhythmically, heart pumping largely relies on cellular  $\text{Ca}^{2+}$  homeostasis and excitation-contraction coupling (28). Under pathological conditions, cardiomyocytes expand contractility by elevating  $\text{Ca}^{2+}$  release from the sarcoplasmic reticulum (SR), a convoluted membrane structure serving as an iron critical storage site, into the cytoplasm (29). Cellular  $\text{Ca}^{2+}$  dynamics is controlled by two major regulators. One is the ryanodine receptors (RyRs), mediating the calcium release from the SR. The other is sarcoplasmic/endoplasmic reticulum  $\text{Ca}^{2+}$  ATPase 2a (SERCA2a), responsible for  $\text{Ca}^{2+}$  retrieval back into SR (30).

Several lines of data have revealed that lncRNAs interact with these key  $\text{Ca}^{2+}$  regulators, such as zinc finger antisense 1 (ZFAS1), myocardial infarction (MI) associated transcript (Miat), and zinc finger protein 593 antisense RNA (ZNF593-AS). Mechanistically, myocardial infarction induces the expression of ZFAS1, which is controlled by the nuclear factor of activated T-cells C2 (NFATc2). ZFAS1 binds SERCA2a and restricts its activity, thus leading to intracellular  $\text{Ca}^{2+}$  overload, abnormal  $\text{Ca}^{2+}$  transient in cardiomyocytes, and finally impaired contractile function (31). Besides, it has been identified that Miat jeopardizes cardiomyocyte calcium handling by interfering pan-RNA splicing, reducing the levels of two important calcium releasing and intaking proteins, **namely**, SERCA2a and RyR2, thereby contributing to contractility damage (32). Contrary to the mentioned lncRNAs, ZNF593-AS enhances the stability of RYR2 mRNA by recruiting HNRNPC (heterogeneous nuclear ribonucleoprotein C [C1/C2]) to the poly-U tracts of RYR2

mRNA, thereby contributing to the improvement of cardiac  $\text{Ca}^{2+}$  handling and contractile function (33). In addition, SR is physically and functionally linked with mitochondria. It controls ATP production by  $\text{Ca}^{2+}$  transferring and drives mitochondrial dynamics (34). lncRNA cardiomyocyte-enriched non-coding transcript (Caren) preserves cardiac function during pressure overload by suppressing the ataxia telangiectasia mutated (ATM)/DNA damage response (DDR) pathway, thus maintaining mitochondrial biogenesis and function (35). lncHrt modulates the deacetylase activity of sirtuin 2, which enhances the oxidative phosphorylation (OXPHOS) capacity of mitochondria, thereby preserving cardiac metabolic homeostasis and function (36).

In addition, potassium channels are key regulators in maintaining action potential prolongation and cardiac rhythm (37). Abnormal potassium channel expression results in aberrant cardiac currents and even sudden cardiac death (38). One of the major outward currents responsible for potential repolarization is the delayed rectifier potassium current ( $I_K$ ) and is dominated by Kv1.2, a subunit of the voltage-gated shaker channel family (39). An antisense RNA of Kv1.2, known as Kcna2 AS, has been shown to be elevated in cardiomyocyte hypertrophy. This lncRNA is complementary to Kcna2 mRNA, thus repressing its expression and thereby leading to malignant ventricular arrhythmias and HF (40) (Table 1).

### LncRNAs regulating cardiac hypertrophy

Cardiomyocytes are terminally differentiated cells, and therefore they cannot expand stroke work by cell division. When the contractility cannot counteract loading conditions, the cardiomyocytes synthesize excessive contractile proteins and increase in size to serve as a compensatory alternation to maintain wall stress and oxygen consumption, termed as cardiac hypertrophy (41). However, this structural change can lead to impaired subcellular organelles for efficient  $\text{Ca}^{2+}$  signaling, contraction/relaxation, and energy metabolism, and it collectively results in cardiomyocyte apoptosis, which further triggers inflammation, fibrosis, and extracellular matrix protein aggregation.

Cardiac hypertrophy has been observed in various heart diseases, such as hypertension, myocardial infarction, and valvular disease. Besides, enlarged cardiomyocytes result in ventricular hypertrophy, which increases the risk of heart failure and malignant arrhythmia. Two different types of cardiac hypertrophy have been reported. One is concentric hypertrophy, characterized by lateral growth of individual cardiomyocytes and parallel addition of sarcomeres, and the other is eccentric hypertrophy, characterized by longitudinal cellular growth and addition of sarcomeres in series (42). Mechanisms involved in pathological hypertrophy have been recognized as metabolic

TABLE 1 lncRNAs modulating cardiomyocyte contractility.

lncRNA	Published year	Role in the pathogenesis of HF	Mechanism	References
ZFAS1	2018	Promote	ZFAS1 is an endogenous SERCA2a inhibitor, impairs the contractility of cardiac muscles.	Zhang et al. (31)
Miat	2021	Promote	It interferes with Ca <sup>2+</sup> transport proteins, SERCA2a, and RyR2, thereby impairing Ca <sup>2+</sup> homeostasis.	Yang et al. (32)
ZNF593-AS	2021	Inhibit	It recruits HNRNPC to RYR2 which stabilizes RYR2 mRNA, improving cardiac Ca <sup>2+</sup> handling and contractile function.	Fan et al. (33)
Caren	2021	Inhibit	It suppresses Hint1, which activates ATM-DDR pathway and reduces oxidative phosphorylation in cardiomyocytes.	Sato et al. (35)
lncHrt	2021	Inhibit	It interacts with sirtuin2 to preserve sirtuin2 deacetylase activity thereby ameliorating mitochondrial dysfunction.	Liu et al. (36)
Kcna2 AS	2017	Promote	It downregulates Kcna2 and attributes to arrhythmia.	Long et al. (40)

Caren, lncRNA cardiomyocyte-enriched non-coding transcript; Hint1, histidine triad nucleotide-binding protein 1; HNRNPC, heterogeneous nuclear ribonucleoprotein C [C1/C2]; Kcna2, potassium voltage-gated channel subfamily A member 2; Miat, lncRNA myocardial infarction associated transcript; RYR2, ryanodine receptor type 2; SERCA2a, sarcoplasmic/endoplasmic reticulum Ca<sup>2+</sup> ATPase 2a; ZFAS1, zinc finger antisense 1; ZNF593-AS, zinc finger protein 593 antisense RNA.

reprogramming, mitochondrial dysfunction, fetal gene program, and impaired Ca<sup>2+</sup> homeostasis (43).

lncRNA H19 is becoming a hotspot in recent decades, due to its important role in both early postnatal development and various diseases (44, 45). H19 is a highly conserved lncRNA, transcribed from H19-insulin growth factor 2 (IGF2) locus, and rich in muscle (46). In the heart, it is mainly expressed in endothelial cells and is located in both the nucleus and the cytoplasm. Previous studies revealed its important role in various cardiovascular diseases such as ischemic myocardial injuries (47), diabetic cardiomyopathy (48), and calcific aortic valve disease (49). In heart failure, H19 is reported to be upregulated in a transverse aortic constriction model, and it inhibits cardiomyocyte hypertrophy by encoding miR-675, which targets CaMKII $\delta$  (50). Contrary to that, another line of data finds a low expression of H19 in heart failure mice (51). Mechanistically, suppression of H19 disembarasses the polycomb repressive complex 2 (PRC2). Then, PRC2 increases H3K27 tri-methylation of Tescalcin, followed by GSK activation and calcineurin inhibition, which finally leads to the expression and activation of NFAT, a well-known hypertrophic-promoting factor (51). Similarly, another epigenetic regulatory lncRNA, cardiac-hypertrophy-associated epigenetic regulator (Chaer), directly binds with PRC2, thereby repressing its genomic targeting ability and reducing H3K27me3 levels at the promoter regions of genes involved in cardiac hypertrophy (52). lncRNA antihypertrophic interrelated transcript (Ahit) also represses the H3K27me3 level of a critical hypertrophy-inducer, myocyte enhancer factor 2a (MEF2A). It acts as a scaffold to guide the suppressor of zeste 12 protein homolog (SUZ12) to the promotor of MEF2A, thereby mitigating hypertrophic modifications (53).

In addition to functions within nucleus, several lncRNAs have been shown to serve as the sponge of miRNA in the cytoplasm in HF. It is reported that lncRNA cardiac hypertrophy-related factor (CHRF) acts as an endogenous sponge, thus downregulating miR-489 and thereby elevating the level of myeloid differentiation primary response gene 88 (Myd88) in cardiomyocytes, and finally it contributes to cardiac hypertrophy (54). Plscr4 negatively regulates cardiac hypertrophy by sponging miR-214, which suppresses the expression of Mitofusin 2 (Mfn2) (55) (Table 2).

## lncRNAs involving in cardiac apoptosis

Apoptosis is an evolutionarily conserved programmed cell death that participates in embryonic development, tissue homeostasis, and pathological remodeling (56). Cardiac myocytes sustain apoptosis in response to various insults, such as hypoxia, acidosis, oxidative stress, metabolic crisis,  $\beta$ 1-adrenergic agonists, and angiotensin II (57, 58). Cardiac myocyte apoptotic is one of the major pathological processes during heart failure. Analyses from postmortem samples reveal a small portion (<1%) of apoptotic cells in failed hearts, which is 10- to 100-fold higher than that of functional healthy control (59, 60). Apoptotic myocyte has also been shown to present in different heart failure animal models, such as ascending aortic constriction and left coronary ligation (61–63). Besides, conditionally activated procaspase-8 resulting in 0.023% of apoptotic myocardial cells generated a lethal dilated cardiomyopathy (64). Therefore, it is believed that low level, but persistent loss, of the cardiac myocyte apoptosis leads to functional limitation and finally decompensated heart failure.



TABLE 2 lncRNAs regulating cardiac hypertrophy.

lncRNA	Published year	Role in the pathogenesis of HF pathogenesis of HF	Mechanism	References
H19	2016	Inhibit	H19 sponges miR-675 to target CaMKII $\delta$ as a negative regulator of cardiac hypertrophy.	Liu et al. (50)
H19	2020	Promote	H19 suppresses H3K27m3 of the anti-hypertrophic Tescalcin locus which further halts NFAT expression.	Viereck et al. (51)
Chaer	2016	Promote	Chaer directly interacts with PRC2 targeting to genomic loci, thereby inhibiting H3L27m1 at the promoter regions of genes involved in cardiac hypertrophy.	Wang et al., (52)
Ahit	2020	Inhibit	Ahit serves as a scaffold to guide the SUZ12 to the promoter of MEF2A (a critical inducer of cardiac hypertrophy), leading to repressive H3K27me3 and decline in MEF2A expression.	Yu et al. (53)
CHRF	2014	Promote	CHRF sponges miR-489 and regulates Myd88 expression and hypertrophy.	Wang et al. (54)
Plscr4	2018	Inhibit	Plscr4 sponges miR-214 that targets Mfn2 thereby interfering with mitochondrial dynamics.	Lv et al. (55)

Ahit, lncRNA antihypertrophic interrelated transcript; Chaer, cardiac-hypertrophy-associated epigenetic regulator; CHRF, lncRNA cardiac hypertrophy-related factor; MEF2A, myocyte enhancer factor 2a; Mfn2, Mitofusin 2; PRC2, polycomb repressive complex 2; SUZ12, suppressor of zeste 12 protein homolog.

TABLE 3 lncRNAs involving in cardiac apoptosis.

lncRNA	Published year	Role in the pathogenesis of HF	Mechanism	References
CAIF	2018	Inhibit	It inhibits p53-dependent expression of myocardin and autophagy induced cell death and cardiac dysfunction.	Liu et al. (65)
MHRT	2019	Inhibit	Unknown	Zhang et al. (66)
MIAT	2017	Promote	MIAT sponges miR-22-3p thus counteracting the inhibitory effect of miR-22-3p on DAPK2 and promoting cardiac apoptosis.	Zhou et al., (67)
SOX2-OT	2020	Promote	SOX2-OT sponges miR-455-3p which targets TRAF6 therefore enhances inflammation and apoptosis.	Gu et al. (68)
H19	2019	Inhibit	H19 sponges miR-877-3p thereby represses the Bcl-2 induced apoptosis.	Li et al. (69)
Snhg1	2021	Inhibit	Snhg1 elicits cardiomyocyte proliferation by sustaining PI3K/Akt signaling activation.	Li. (70)
CMDL-1	2021	Inhibit	CMDL-1 suppresses DOX-induced cardiotoxicity by regulating Drp1 phosphorylation and mitochondrial dynamics.	Aung et al. (71)

CAIF, lncRNA cardiac autophagy inhibitory factor; CMDL-1, cardiomyocyte mitochondrial dynamic-related lncRNA 1; Drp1, dynamin-related protein 1; DAPK2, death-associated protein kinase 2; Miat, lncRNA myocardial infarction-associated transcript; MHRT, lncRNA myosin heavy-chain-associated RNA transcripts; Snhg1, lncRNA small nucleolar RNA host gene 1; SOX2-OT, sex-determining region Y-box 2 overlapping transcript; TRAF6, TNF receptor-associated factor 6.

lncRNA cardiac autophagy inhibitory factor (CAIF) directly binds to p53 protein and hence inhibits the activation and expression of myocardin, which suppresses autophagic apoptosis and cardiac dysfunction (65). Another protective lncRNA, myosin heavy-chain-associated RNA transcripts

(MHRT), has been shown to inhibit ROS-induced apoptosis and can be used as a prognostic factor of survival in patients with heart failure (66). In diabetic cardiomyopathy, high glucose induces the expression of myocardial infarction-associated transcript (MIAT) and upregulates the death-associated protein

TABLE 4 lncRNAs participating in cardiac fibrosis.

lncRNA	Published year	Role in the pathogenesis of HF	Mechanism	References
lncRNA-Safe	2019	Promote	It enhances the expression of Sfrp2 and stabilizes Sfrp2 mRNA by forming a Safe-Sfrp2-HuR complex.	Hao et al. (74)
Wisp2	2017	Promote	It binds TIA1-related protein facilitating the expression of a profibrotic form of lysyl hydroxylase 2, which leads to enhanced matrix deposition and fibrosis.	Micheletti et al. (75)
Cfast	2021	Promote	It competitively inhibits the COTL1 interaction with TRAP1, which boosts TGF- $\beta$ signaling by enhancing SMAD2/SMAD4 complex formation.	Zhang et al. (76)
MEG3	2017	Promote	It regulates the binding of p53 to the promotor region of Mmp-2.	Piccoli et al. (77)

Cfast, lncRNA cardiac fibroblast-associated transcript; COTL1, coactosin-like 1; HuR, human antigen R; MEG3, lncRNA maternally expressed gene 3; Sfrp2, secreted frizzled-related protein 2; TIA1, T-cell intracellular antigen 1; TRAP1, transforming growth factor- $\beta$  receptor-associated protein 1; Wisp2, Wisp2 super-enhancer-associated RNA.

kinase 2 (DAPK2) expression by sponging miR-22-3p, which consequently leads to cardiomyocyte apoptosis (67). It is reported that ischemia induces the elevation of sex-determining region Y-box 2 (SOX2) overlapping transcript (SOX2-OT), and hence a lncRNA sponging miR-455-3p exacerbates apoptosis rate, cell oxidative damage, and inflammatory response (68). Another ischemic-related lncRNA is H19, which has been shown to bind miR-877-3p thereby inhibiting mitochondrial apoptosis (69). Besides, lncRNA small nucleolar RNA host gene 1 (Snhg1) exerts anti-apoptotic effects on cardiomyocyte and myocardial infarction (MI) heart, by activating the PI3K/AKT/c-Myc pathway, which in turn enhances the expression of Snhg1, thus forming a positive feedback loop (70). Apart from these, cardiomyocyte mitochondrial dynamic-related lncRNA 1 (CMDL-1) has been shown to interact with dynamin-related protein 1, thereby regulating mitochondrial fission and apoptosis in cardiomyocytes (71) (Table 3).

## lncRNAs participating in cardiac fibrosis

Consistent detrimental stimuli contribute to cardiomyocyte cell death and hypertrophic changes, which in turn prompts an inflammatory circumstance, and excessive accumulation of collagen stiffens the ventricles, which further damages the contraction and relaxation activity of the myocardium. This adverse structural remodeling is termed as cardiac fibrosis and is characterized by collagen type I deposition, as well as cardiac fibroblast activation and differentiation into myofibroblasts.

Several types of myocardial fibrosis have been reported based on etiology and pathological features: (1) reactive interstitial fibrosis, (2) replacement fibrosis, (3) infiltrative interstitial fibrosis, and (4) endomyocardial fibrosis (72, 73).

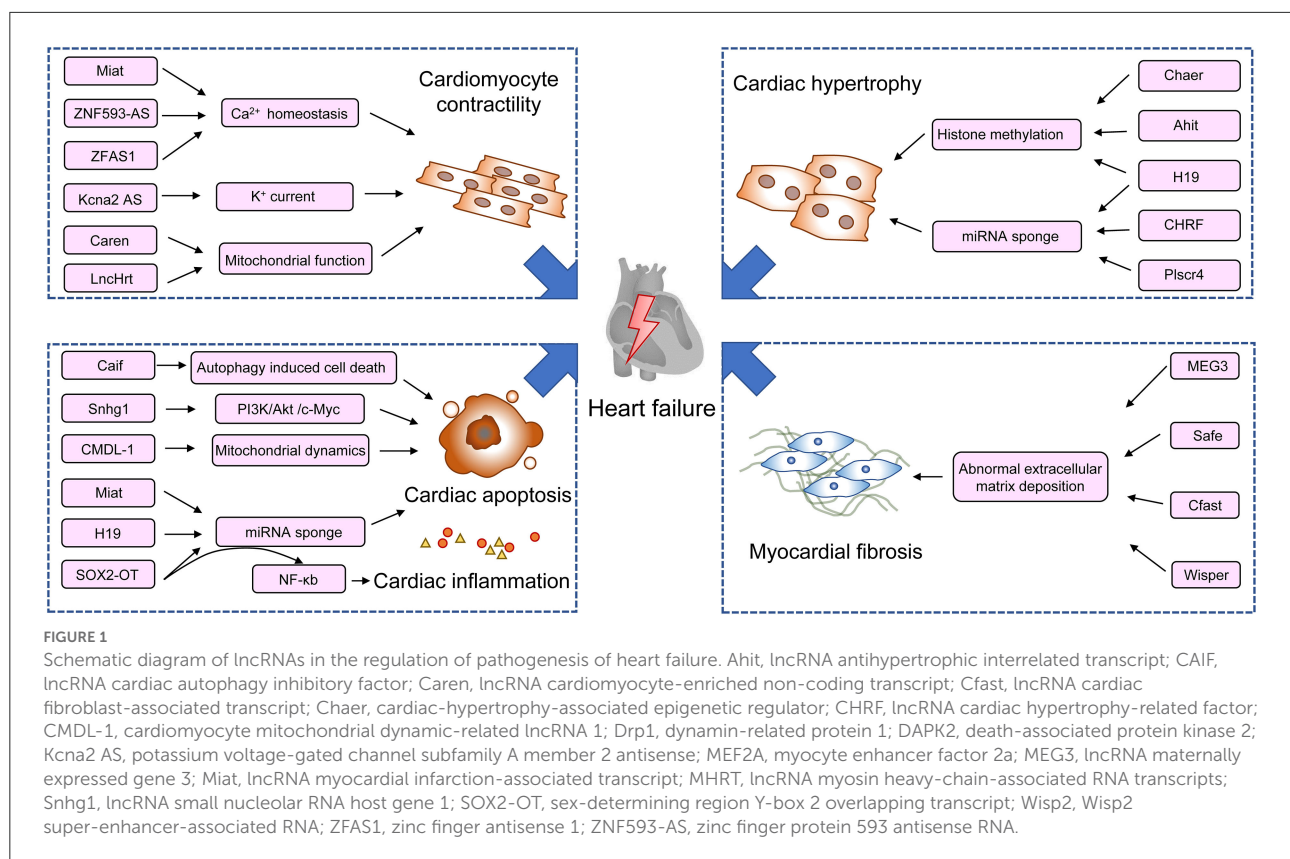
It has been well established that lncRNAs play an important role in myocardial infarction (MI)-induced cardiac fibrosis and HF, such as lncRNA-Safe (74), lncHrt (36), Wisp2 super-enhancer-associated RNA (Wisper) (75), and cardiac fibroblast-associated transcript (Cfast) (76). All of them are enriched in fibroblasts.

lncRNA-Safe elevates in both MI and TGF- $\beta$ -induced cardiac fibrosis. It acts in cis by controlling the expression of neighboring gene, secreted frizzled related protein 2 (Sfrp2) (74). Wisper enhances the proliferation and survival of fibroblast and extracellular matrix synthesis, by interacting with T-cell intracellular antigen 1 (TIA1)-related protein to regulate the expression of lysyl hydroxylase 2 (75). Cfast competitively suppresses the coactosin-like 1 (COTL1) interaction with TRAP1 (transforming growth factor- $\beta$  receptor-associated protein 1) and further transdifferentiation of myofibroblasts into cardiac fibroblasts (76).

However, less is known about how pressure overload-associated lncRNAs involve in the pathogenesis of cardiac fibrosis. A recent study revealed that a chromatin-associated lncRNA, lncRNA maternally expressed gene 3 (MEG3), regulates the transcriptional activity of p53 by direct interaction, which further enhances the expression of Mmp-2 and cardiac remodeling (77) (Table 4).

## lncRNAs mediating inflammation in HF

In addition, the inflammatory response has been shown to play a vital role in the pathogenesis of ventricular remodeling after MI. Piles of data from both laboratory and clinical aspects identify an inflammatory state, in the circulation and the heart tissue during MI with or without established HF, and have been well reviewed elsewhere (78–80). The CANTOS trial proved anti-cytokine therapy to be a promising approach toward



an improved clinical outcome regarding cardiac function in patients with MI (81). However, the details of how lncRNAs mediate cardiac dysfunction remain largely unknown. One recent study revealed that SOX2-OT drives the onset of HF by sponging miR-455-3p, thereby augmenting the level of TNF receptor-associated factor 6 (TRAF6) and the activation of NF- $\kappa$ B signaling (68).

## Therapeutic potential of lncRNAs in heart failure

With the expansion of our understanding in lncRNAs and other non-coding RNAs, and their roles in the pathogenesis of cardiac remodeling and heart failure (Figure 1), efforts are taken to focus on their therapeutic potential. Along with the extensive preclinical data, RNA-based therapeutic development has achieved enormous advances in recent years rapidly in the field of biotherapeutics. RNA therapy is termed as an approach using RNA-based molecules to modulate specific proteins and biological pathways to treat diseases (82). It bears several advantages over traditional drugs. It can target every disease-relevant protein or gene theoretically and can be produced much faster than protein and small molecule drugs at lower costs (83). The first RNA aptamer, Pegaptanib, which is an anti-VEGF agent for the treatment of retinal diseases is licensed

by the FDA in 2004 (84). After two decades of development, more antisense oligonucleotide drugs have been approved by the FDA for clinical use, such as fomivirsin, eteplirsin, nusinersen, defibrotide, inotersen, mipomersen, golodirsen, and casimersen. Another example of RNA-based therapeutic is the successful use of two mRNA vaccines, namely, tozinameran and elasomeran, which translate to a modified spike protein from COVID-19, thus facilitating a specific immune response in recipients (85). Although great achievements in RNA therapeutics have been made, the drugs to directly modulate lncRNAs' expression are still in infancy. The challenges are that several drawbacks halt the clinical translation of RNA-based therapeutics, including adverse effects, off-target activity, and aspecific delivery (12).

The future endeavor would pay on a deeper understanding of lncRNA pathology in heart failure, optimizing specificity and efficiency of the delivery system, and reducing adverse events, so as to fuel the clinical transformation of lncRNAs.

## Concluding remarks

Given the versatility of RNA properties, lncRNAs extensively participate in the cardiac physiology and pathological remodeling (Figure 1). Unraveling the details of their regulatory activities will incontestably help seek more potential therapeutic targets to supplement traditional Treatments. In addition,

recent years have seen the sprouting up of innovative RNA-based technologies. The successful application of RNA-based therapeutics in the treatment of HF requires interdisciplinary collaboration, which includes chemistry, molecular biology, immunology, and pharmacology. Although challenging, with the development of the state-of-the-art technology, these laboratory efforts will pave the way for the translation of transformative therapies and to achieve accessible and personalized healthcare.

## Author contributions

WW, ZC, and LZ participated in the conception of the review. XF and ZZ drafted the initial full manuscript. WW and ZC edited the manuscript. All authors contributed to the article and approved the submitted version.

## Funding

This study was supported by the National Key Research and Development Program for Key Research

Project of Modernization of Traditional Chinese Medicine (2018YFC1707402) and the Natural Science Foundation of Shandong Province (Grant Number: ZR2021MH410).

## Conflict of interest

The authors declare that the research was conducted in the absence of any commercial or financial relationships that could be construed as a potential conflict of interest.

## Publisher's note

All claims expressed in this article are solely those of the authors and do not necessarily represent those of their affiliated organizations, or those of the publisher, the editors and the reviewers. Any product that may be evaluated in this article, or claim that may be made by its manufacturer, is not guaranteed or endorsed by the publisher.

## References

- McDonagh TA, Metra M, Adamo M, Gardner RS, Baumbach A, Böhm M, et al. ESC Guidelines for the diagnosis and treatment of acute and chronic heart failure. *Eur Heart J*. (2021) 42:3599–726. doi: 10.1093/eurheartj/ehab368
- Gulati G, Udelson JE. Heart failure with improved ejection fraction: is it possible to escape one's past? *JACC Heart Fail*. (2018) 6:725–33. doi: 10.1016/j.jchf.2018.05.004
- Van Linthout S, Tschöpe C. Inflammation - cause or consequence of heart failure or both? *Curr Heart Fail Rep*. (2017) 14:251–65. doi: 10.1007/s11897-017-0337-9
- Packer M. The neurohormonal hypothesis: a theory to explain the mechanism of disease progression in heart failure. *J Am Coll Cardiol*. (1992) 20:248–54. doi: 10.1016/0735-1097(92)90167-L
- Mishra S, Kass DA. Cellular and molecular pathobiology of heart failure with preserved ejection fraction. *Nat Rev Cardiol*. (2021) 18:400–23. doi: 10.1038/s41569-020-00480-6
- Jia G, Hill MA, Sowers JR. Diabetic cardiomyopathy: an update of mechanisms contributing to this clinical entity. *Circ Res*. (2018) 122:624–38. doi: 10.1161/CIRCRESAHA.117.311586
- Paulus WJ. Unfolding discoveries in heart failure. *N Engl J Med*. (2020) 382:679–82. doi: 10.1056/NEJMcibr1913825
- Collins FS, Morgan M, Patrinos A. The human genome project: lessons from large-scale biology. *Science*. (2003) 300:286–29. doi: 10.1126/science.1084564
- Hon C, Ramilowski JA, Harshbarger J, Bertin N, Rackham OJ, et al. An atlas of human long non-coding RNAs with accurate 5' ends. *Nature*. (2017) 543:199–204. doi: 10.1038/nature21374
- Zhao L, Wang J, Li Y, Song T, Wu Y, Fang S, et al. NONCODEV6: an updated database dedicated to long non-coding RNA annotation in both animals and plants. *Nucleic Acids Res*. (2021) 49:D165–71. doi: 10.1093/nar/gkaa1046
- Anastasiadou E, Jacob LS, Slack FJ. Non-coding RNA networks in cancer. *Nat Rev Cancer*. (2018) 18:5–18. doi: 10.1038/nrc.2017.99
- Winkle M, El-Daly SM, Fabbri M, Calin GA. Noncoding RNA therapeutics—challenges and potential solutions. *Nature Rev Drug Discovery*. (2021) 20:629–51. doi: 10.1038/s41573-021-00219-z
- Dhanoo JK, Sethi RS, Verma R, Arora JS, Mukhopadhyay CS. Long non-coding RNA: its evolutionary relics and biological implications in mammals: a review. *J Anim Sci Technol*. (2018) 60:25. doi: 10.1186/s40781-018-0183-7
- Dueva R, Akopyan K, Pederiva C, Trevisan D, Dhanjal S, Lindqvist A, et al. Neutralization of the positive charges on histone tails by RNA promotes an open chromatin structure. *Cell Chem Biol*. (2019) 26:1436–49.e1435. doi: 10.1016/j.chembiol.2019.08.002
- Micheli F, Pitchiaya S, Vitelli V, Sharma S, Gioia U, Pessina F, et al. Damage-induced lncRNAs control the DNA damage response through interaction with DDRNAs at individual double-strand breaks. *Nat Cell Biol*. (2017) 19:1400–11. doi: 10.1038/ncb3643
- Niehurs C, Luke B. Regulatory R-loops as facilitators of gene expression and genome stability. *Nat Rev Mol Cell Biol*. (2020) 21:167–78. doi: 10.1038/s41580-019-0206-3
- Yamazaki T, Souquere S, Chujo T, Kobelke S, Chong YS, Fox AH, et al. Functional Domains of NEAT1 Architectural lncRNA Induce Paraspeckle Assembly through Phase Separation. *Mol Cell*. (2018) 70:1038–53.e1037 doi: 10.1016/j.molcel.2018.05.019
- Morlando M, Fatica A. Alteration of epigenetic regulation by long noncoding RNAs in cancer. *Int J Mol Sci*. (2018) 19: 570. doi: 10.3390/ijms19020570
- Bhan A, Mandal SS. lncRNA HOTAIR: a master regulator of chromatin dynamics and cancer. *Biochim Biophys Acta*. (2015) 1856:151–64. doi: 10.1016/j.bbcan.2015.07.001
- Xu Y, Yao Y, Jiang X, Zhong X, Wang Z, Li C, et al. SP1-induced upregulation of lncRNA SPRY4-IT1 exerts oncogenic properties by scaffolding EZH2/LSD1/DNMT1 and sponging miR-101-3p in cholangiocarcinoma. *J Exp Clin Cancer Res*. (2018) 37:81. doi: 10.1186/s13046-018-0747-x
- Rashid F, Shah A, Shan G. Long Non-coding RNAs in the Cytoplasm. *Genomics Proteomics Bioinformatics*. (2016) 14:73–80. doi: 10.1016/j.gpb.2016.03.005

22. Hansji H, Leung EY, Baguley BC, Finlay GJ, Cameron-Smith D, Figueiredo VC, et al. ZFAS1: a long noncoding RNA associated with ribosomes in breast cancer cells. *Biol Direct*. (2016) 11:62. doi: 10.1186/s13062-016-0165-y
23. Faghihi MA, Zhang M, Huang J, Modarresi F, Van der Brug MP, Nalls MA, et al. Evidence for natural antisense transcript-mediated inhibition of microRNA function. *Genome Biol*. (2010) 11:R56. doi: 10.1186/gb-2010-11-5-r56
24. Leucci E, Vendramin R, Spinazzi M, Laurette P, Fiers M, Wouters J, et al. Melanoma addiction to the long non-coding RNA SAMMSON. *Nature*. (2016) 531:518–22. doi: 10.1038/nature17161
25. Vendramin R, Verheyden Y, Ishikawa H, Goedert L, Nicolas E, Saraf K, et al. SAMMSON fosters cancer cell fitness by concertedly enhancing mitochondrial and cytosolic translation. *Nat Struct Mol Biol*. (2018) 25:1035–46. doi: 10.1038/s41594-018-0143-4
26. Mohammad F, Mondal T, Kanduri C. Epigenetics of imprinted long noncoding RNAs. *Epigenetics*. (2009) 4:277–86. doi: 10.4161/epi.4.5.9242
27. Dragomir M, Chen B, Calin GA. Exosomal lncRNAs as new players in cell-to-cell communication. *Transl Cancer Res*. (2018) 7:S243–s252. doi: 10.21037/tcr.2017.10.46
28. Cortassa S, Juhaszova M, Aon MA, Zorov DB, Sollott SJ. Mitochondrial Ca<sup>2+</sup>, redox environment and ROS emission in heart failure: two sides of the same coin? *J Mol Cell Cardiol*. (2021) 151:113–25. doi: 10.1016/j.yjmcc.2020.11.013
29. Denniss AL, Dashwood AM, Molenaar P, Beard NA. Sarcoplasmic reticulum calcium mishandling: central tenet in heart failure? *Biophys Rev*. (2020) 12:865–78. doi: 10.1007/s12551-020-00736-y
30. Rossini M, Filadi R. Sarcoplasmic reticulum-mitochondria kissing in cardiomyocytes: Ca<sup>2+</sup>, ATP, and undisclosed secrets. *Front Cell Dev Biol*. (2020) 8:532. doi: 10.3389/fcell.2020.00532
31. Zhang Y, Jiao L, Sun L, Li Y, Gao Y, Xu C, et al. LncRNA ZFAS1 as a SERCA2a inhibitor to cause intracellular Ca<sup>2+</sup> overload and contractile dysfunction in a mouse model of myocardial infarction. *Circ Res*. (2018) 122:1354–68. doi: 10.1161/CIRCRESAHA.117.312117
32. Yang L, Deng J, Ma W, Qiao A, Xu S, Yu Y, et al. Ablation of lncRNA Miat attenuates pathological hypertrophy and heart failure. *Theranostics*. (2021) 11:7995–8007. doi: 10.7150/thno.50990
33. Fan J, Li H, Xie R, Zhang X, Nie X, Shi X, et al. LncRNA ZNF593-AS alleviates contractile dysfunction in dilated cardiomyopathy. *Circ Res*. (2021) 128:1708–23. doi: 10.1161/CIRCRESAHA.120.318437
34. Lopez-Crisosto C, Pennanen C, Vasquez-Trincado C, Morales PE, Bravo-Sagua R, Quest AFG, et al. Sarcoplasmic reticulum-mitochondria communication in cardiovascular pathophysiology. *Nat Rev Cardiol*. (2017) 14:342–60. doi: 10.1038/nrcardio.2017.23
35. Sato M, Kadomatsu T, Miyata K, Warren JS, Tian Z, Zhu S, et al. The lncRNA Caren antagonizes heart failure by inactivating DNA damage response and activating mitochondrial biogenesis. *Nat Commun*. (2021) 12:2529. doi: 10.1038/s41467-021-22735-7
36. Liu N, Kataoka M, Wang Y, Pu L, Dong X, Fu X, et al. LncRNA LncHrt preserves cardiac metabolic homeostasis and heart function by modulating the LKB1-AMPK signaling pathway. *Basic Res Cardiol*. (2021) 116:48. doi: 10.1007/s00395-021-00887-3
37. Burg S, Attali B. Targeting of potassium channels in cardiac arrhythmias. *Trends Pharmacol Sci*. (2021) 42:491–506. doi: 10.1016/j.tips.2021.03.005
38. Walsh KB. Targeting cardiac potassium channels for state-of-the-art drug discovery. *Expert Opin Drug Discov*. (2015) 10:157–69. doi: 10.1517/17460441.2015.983471
39. Jost N, Papp JG, Varró A. Slow delayed rectifier potassium current (IKs) and the repolarization reserve. *Ann Noninvasive Electrocardiol*. (2007) 12:64–78. doi: 10.1111/j.1542-474X.2007.00140.x
40. Long QQ, Wang H, Gao W, Fan Y, Li YF, Ma Y, et al. Long noncoding RNA Kcna2 antisense RNA contributes to ventricular arrhythmias via silencing Kcna2 in rats with congestive heart failure. *J Am Heart Assoc*. (2017) 6:e005965. doi: 10.1161/JAHA.117.005965
41. Shimizu I, Minamino T. Physiological and pathological cardiac hypertrophy. *J Mol Cell Cardiol*. (2016) 97:245–62. doi: 10.1016/j.yjmcc.2016.06.001
42. Dorn GW, Robbins J, Sugden PH. "Phenotyping hypertrophy: eschew obfuscation" *Am Heart Assoc*. (2003). doi: 10.1161/01.RES.0000077012.11088.BC
43. Nakamura M, Sadoshima J. Mechanisms of physiological and pathological cardiac hypertrophy. *Nature Reviews Cardiol*. (2018) 15:387–407. doi: 10.1038/s41569-018-0007-y
44. Lecerc F, Le Bourhis X, Adriaenssens E. The long non-coding RNA H19: an active player with multiple facets to sustain the hallmarks of cancer. *Cell Mol Life Sci*. (2019) 76:4673–87. doi: 10.1007/s00118-019-03240-z
45. Ghafouri-Fard S, Esmaili M, Taheri M. H19. lncRNA: Roles in tumorigenesis. *Biomed Pharmacother*. (2020) 123:109774. doi: 10.1016/j.biopha.2019.109774
46. Ratajczak MZ. Igf2-H19, an imprinted tandem gene, is an important regulator of embryonic development, a guardian of proliferation of adult pluripotent stem cells, a regulator of longevity, and a 'passkey' to cancerogenesis. *Folia Histochem Cytobiol*. (2012) 50:171–9. doi: 10.5603/FHC.2012.0026
47. Luo H, Wang J, Liu D, Zang S, Ma N, Zhao L, et al. The lncRNA H19/miR-675 axis regulates myocardial ischemic and reperfusion injury by targeting PPARα. *Mol Immunol*. (2019) 105:46–54. doi: 10.1016/j.molimm.2018.11.011
48. Li X, Wang H, Yao B, Xu W, Chen J, Zhou X, et al. lncRNA H19/miR-675 axis regulates cardiomyocyte apoptosis by targeting VDAC1 in diabetic cardiomyopathy. *Sci Rep*. (2016) 6:36340. doi: 10.1038/srep36340
49. Hadji F, Boulanger MC, Guay SP, Gaudreault N, Amellah S, Mkannez G, et al. Altered DNA methylation of long noncoding RNA H19 in calcific aortic valve disease promotes mineralization by silencing NOTCH1. *Circulation*. (2016) 134:1848–62. doi: 10.1161/CIRCULATIONAHA.116.023116
50. Liu L, An X, Li Z, Song Y, Li L, Zuo S, et al. The H19 long noncoding RNA is a novel negative regulator of cardiomyocyte hypertrophy. *Cardiovasc Res*. (2016) 111:56–65. doi: 10.1093/cvr/cvw078
51. Viereck J, Bührke A, Foinquinos A, Chatterjee S, Kleeberger JA, Xiao K, et al. Targeting muscle-enriched long non-coding RNA H19 reverses pathological cardiac hypertrophy. *Eur Heart J*. (2020) 41:3462–74. doi: 10.1093/eurheartj/ehaa519
52. Wang Z, Zhang XJ, Ji YX, Zhang P, Deng KQ, Gong J, et al. The long noncoding RNA Chaf1 defines an epigenetic checkpoint in cardiac hypertrophy. *Nat Med*. (2016) 22:1131–9. doi: 10.1038/nm.4179
53. Yu J, Yang Y, Xu Z, Lan C, Chen C, Li C, et al. Long Noncoding RNA Ahit protects against cardiac hypertrophy through SUZ12 (suppressor of Zeste 12 protein homolog)-mediated downregulation of MEF2A (myocyte enhancer factor 2A). *Circ Heart Fail*. (2020) 13:e006525. doi: 10.1161/CIRCHEARTFAILURE.119.006525
54. Wang K, Liu F, Zhou LY, Long B, Yuan SM, Wang Y, et al. The long noncoding RNA CHRF regulates cardiac hypertrophy by targeting miR-489. *Circ Res*. (2014) 114:1377–88. doi: 10.1161/CIRCRESAHA.114.302476
55. Lv L, Li T, Li X, Xu C, Liu Q, Jiang H, et al. The lncRNA Plscr4 controls cardiac hypertrophy by regulating miR-214. *Mol Ther Nucleic Acids*. (2018) 10:387–97. doi: 10.1016/j.omtn.2017.12.018
56. D'Arcy MS. Cell death: a review of the major forms of apoptosis, necrosis and autophagy. *Cell Biol Int*. (2019) 43:582–92. doi: 10.1002/cbin.11137
57. Del Re DP, Amgalan D, Linkermann A, Liu Q, Kitsis RN. Fundamental mechanisms of regulated cell death and implications for heart disease. *Physiol Rev*. (2019) 99:1765–817. doi: 10.1152/physrev.00022.2018
58. Nair N. Epidemiology and pathogenesis of heart failure with preserved ejection fraction. *Rev Cardiovasc Med*. (2020) 21:531–40. doi: 10.31083/j.rcm.2020.04.154
59. Olivetti G, Abbi R, Quaini F, Kajstura J, Cheng W, Nitahara JA, et al. Apoptosis in the failing human heart. *New Engl J Med*. (1997) 336:1131–41. doi: 10.1056/NEJM199704173361603
60. Saraste A, Pulkki K, Kallajoki M, Heikkilä P, Laine P, Mattila S, et al. Cardiomyocyte apoptosis and progression of heart failure to transplantation. *Eur J Clin Invest*. (1999) 29:380–6. doi: 10.1046/j.1365-2362.1999.00481.x
61. Bae S, Siu PM, Choudhury S, Ke Q, Choi JH, Koh YY, et al. Delayed activation of caspase-independent apoptosis during heart failure in transgenic mice overexpressing caspase inhibitor CrmA. *Am J Physiol Heart Circ Physiol*. (2010) 299:H1374–81. doi: 10.1152/ajpheart.00168.2010
62. Wang K, Long B, Liu F, Wang JX, Liu CY, Zhao B, et al. A circular RNA protects the heart from pathological hypertrophy and heart failure by targeting miR-223. *Eur Heart J*. (2016) 37:2602–11. doi: 10.1093/eurheartj/ehv713
63. Yao Y, Lu Q, Hu Z, Yu Y, Chen Q, Wang QK, et al. A non-canonical pathway regulates ER stress signaling and blocks ER stress-induced apoptosis and heart failure. *Nat Commun*. (2017) 8:133. doi: 10.1038/s41467-017-00171-w
64. Wencker D, Chandra M, Nguyen K, Miao W, Garantziotis S, Factor SM, et al. A mechanistic role for cardiac myocyte apoptosis in heart failure. *J Clin Invest*. (2003) 111:1497–504. doi: 10.1172/JCI17664
65. Liu CY, Zhang YH, Li RB, Zhou LY, et al. LncRNA CAIF inhibits autophagy and attenuates myocardial infarction by blocking p53-mediated myocardial transcription. *Nature commun*. (2018) 9:1–12. doi: 10.1038/s41467-017-02280-y
66. Zhang L, Wu YJ, Zhang SL. Circulating lncRNA MHRT predicts survival of patients with chronic heart failure. *J Geriatr Cardiol*. (2019) 16:818–21. doi: 10.11909/j.issn.1671-5411.2019.11.006



67. Zhou X, Zhang W, Jin M, Chen J, Xu W, Kong X, et al. lncRNA MIAT functions as a competing endogenous RNA to upregulate DAPK2 by sponging miR-22-3p in diabetic cardiomyopathy. *Cell Death Dis.* (2017) 8:1–8. doi: 10.1038/cddis.2017.321
68. Gu Q, Wang B, Zhao H, Wang W, Wang P, Deng Y, et al. lncRNA promoted inflammatory response in ischemic heart failure through regulation of miR-455-3p/TRAFA6 axis. *Inflammation Res.* (2020) 69:667–81. doi: 10.1007/s00011-020-01348-8
69. Li X, Luo S, Zhang J, Yuan Y, Jiang W, Zhu H, et al. lncRNA H19 alleviated myocardial I/RI via suppressing miR-877-3p/Bcl-2-mediated mitochondrial apoptosis. *Molecular Therapy-Nucleic Acids.* (2019) 17:297–309. doi: 10.1016/j.omtn.2019.05.031
70. Li M. lncRNA Snhg1-driven self-reinforcing regulatory network promoted cardiac regeneration and repair after myocardial infarction. *Theranostics.* (2021) 11:9397. doi: 10.7150/thno.57037
71. Chen X, Yu H, Li Z, Ye W, Liu Z, Gao J, et al. (2021). Cardiomyocyte mitochondrial dynamic-related lncRNA 1 (CMDL-1) may serve as a potential therapeutic target in doxorubicin cardiotoxicity. *Mol Ther Nucleic Acid.* (2021) 25:638–51. doi: 10.1016/j.omtn.2021.08.006
72. Tian J, An X, Niu L. Myocardial fibrosis in congenital and pediatric heart disease. *Exp Ther Med.* (2017) 13:1660–4. doi: 10.3892/etm.2017.4224
73. Hinderer S, Schenke-Layland K. Cardiac fibrosis - a short review of causes and therapeutic strategies. *Adv Drug Deliv Rev.* (2019) 146:77–82. doi: 10.1016/j.addr.2019.05.011
74. Hao K, Lei W, Wu H, Wu J, Yang Z, Yan S, et al. lncRNA-Safe contributes to cardiac fibrosis through Safe-Sfrp2-HuR complex in mouse myocardial infarction. *Theranostics.* (2019) 9:7282–97. doi: 10.7150/thno.33920
75. Micheletti R, Plaisance I, Abraham BJ, Sarre A, Ting CC, Alexanian M, et al. The long noncoding RNA Wisper controls cardiac fibrosis and remodeling. *Sci Transl Med.* (2017) 9:eaa9118. doi: 10.1126/scitranslmed.aai9118
76. Zhang F, Fu X, Kataoka M, Liu N, Wang Y, Gao F, et al. Long noncoding RNA Cfast regulates cardiac fibrosis. *Mol Ther Nucleic Acids.* (2021) 23:377–92. doi: 10.1016/j.omtn.2020.11.013
77. Piccoli MT, Gupta SK, Viereck J, Foinquinos A, Samolovac S, Kramer FL, et al. Inhibition of the cardiac fibroblast-enriched lncRNA Meg3 prevents cardiac fibrosis and diastolic dysfunction. *Circ Res.* (2017) 121:575–83. doi: 10.1161/CIRCRESAHA.117.310624
78. Briasoulis A, Androulakis E, Christophides T, Tousoulis D. The role of inflammation and cell death in the pathogenesis, progression and treatment of heart failure. *Heart Fail Rev.* (2016) 21:169–76. doi: 10.1007/s10741-016-9533-z
79. Zhang Y, Bauersachs J, Langer HF. Immune mechanisms in heart failure. *Eur J Heart Fail.* (2017) 19:1379–89. doi: 10.1002/ejhf.942
80. Adamo L, Rocha-Resende C, Prabhu SD, Mann DL. Reappraising the role of inflammation in heart failure. *Nat Rev Cardiol.* (2020) 17:269–85. doi: 10.1038/s41569-019-0315-x
81. Ridker PM, Everett BM, Thuren T, MacFadyen JG, Chang WH, Ballantyne C, et al. Antiinflammatory therapy with canakinumab for atherosclerotic disease. *N Engl J Med.* (2017) 377:1119–31. doi: 10.1056/NEJMoa1707914
82. Damase TR, Sukhovshin R, Boada C, Taraballi F, Pettigrew RI, Cooke JP, et al. The limitless future of RNA therapeutics. *Front Bioengineering Biotechnol.* (2021) 161:628137. doi: 10.3389/fbioe.2021.628137
83. Kaczmarek JC, Kowalski PS, Anderson DG. Advances in the delivery of RNA therapeutics: from concept to clinical reality. *Genome Med.* (2017) 9:60. doi: 10.1186/s13073-017-0450-0
84. Yu AM, Tu MJ. Deliver the promise: RNAs as a new class of molecular entities for therapy and vaccination. *Pharmacol Ther.* (2021) 230:107967. doi: 10.1016/j.pharmthera.2021.107967
85. Kim YK. RNA therapy: rich history, various applications and unlimited future prospects. *Experiment Mol Med.* (2022) 54:455–65. doi: 10.1038/s12276-022-00724-0



## OPEN ACCESS

## EDITED BY

Amy Li,  
La Trobe University, Australia

## REVIEWED BY

J. Carter Ralphie,  
University of Wisconsin-Madison,  
United States  
Nazha Hamdani,  
Ruhr University Bochum, Germany

## \*CORRESPONDENCE

Judith Montag  
montag.judith@mh-hannover.de  
Valentin Burkart  
burkart.valentin@mh-hannover.de

## †PRESENT ADDRESS

Denise Hilfiker-Kleiner,  
Medical Department,  
Philipps-University Marburg, Marburg,  
Germany

†These authors have contributed  
equally to this work

## SPECIALTY SECTION

This article was submitted to  
Cardiovascular Biologics and  
Regenerative Medicine,  
a section of the journal  
Frontiers in Cardiovascular Medicine

RECEIVED 06 July 2022

ACCEPTED 02 August 2022

PUBLISHED 23 August 2022

## CITATION

Burkart V, Kowalski K,  
Aldag-Niebling D, Beck J, Frick DA,  
Holler T, Radocaj A, Piep B, Zeug A,  
Hilfiker-Kleiner D, dos Remedios CG,  
van der Velden J, Montag J and Kraft T  
(2022) Transcriptional bursts and  
heterogeneity among cardiomyocytes  
in hypertrophic cardiomyopathy.  
*Front. Cardiovasc. Med.* 9:987889.  
doi: 10.3389/fcvm.2022.987889

## COPYRIGHT

© 2022 Burkart, Kowalski,  
Aldag-Niebling, Beck, Frick, Holler,  
Radocaj, Piep, Zeug, Hilfiker-Kleiner,  
dos Remedios, van der Velden, Montag  
and Kraft. This is an open-access  
article distributed under the terms of  
the [Creative Commons Attribution  
License \(CC BY\)](#). The use, distribution  
or reproduction in other forums is  
permitted, provided the original  
author(s) and the copyright owner(s)  
are credited and that the original  
publication in this journal is cited, in  
accordance with accepted academic  
practice. No use, distribution or  
reproduction is permitted which does  
not comply with these terms.

# Transcriptional bursts and heterogeneity among cardiomyocytes in hypertrophic cardiomyopathy

Valentin Burkart<sup>1\*</sup>, Kathrin Kowalski<sup>1</sup>, David Aldag-Niebling<sup>1</sup>,  
Julia Beck<sup>1</sup>, Dirk Alexander Frick<sup>1</sup>, Tim Holler<sup>1</sup>, Ante Radocaj<sup>1</sup>,  
Birgit Piep<sup>1</sup>, Andre Zeug<sup>2</sup>, Denise Hilfiker-Kleiner<sup>3†</sup>,  
Cristobal G. dos Remedios<sup>4</sup>, Jolanda van der Velden<sup>5</sup>,  
Judith Montag<sup>1\*†</sup> and Theresia Kraft<sup>1†</sup>

<sup>1</sup>Institute for Molecular and Cell Physiology, Hannover Medical School, Hannover, Germany,

<sup>2</sup>Institute for Cellular Neurophysiology, Hannover Medical School, Hannover, Germany, <sup>3</sup>Clinic of  
Cardiology and Angiology, Hannover Medical School, Hannover, Germany, <sup>4</sup>Mechanosensory

Biophysics Laboratory, Victor Chang Cardiac Research Institute, Darlinghurst, NSW, Australia,

<sup>5</sup>Department of Physiology, VU University Medical Center, Amsterdam, Netherlands

Transcriptional bursting is a common expression mode for most genes where independent transcription of alleles leads to different ratios of allelic mRNA from cell to cell. Here we investigated burst-like transcription and its consequences in cardiac tissue from Hypertrophic Cardiomyopathy (HCM) patients with heterozygous mutations in the sarcomeric proteins cardiac myosin binding protein C (cMyBP-C, *MYBPC3*) and cardiac troponin I (cTnI, *TNNI3*). Using fluorescence *in situ* hybridization (RNA-FISH) we found that both, *MYBPC3* and *TNNI3* are transcribed burst-like. Along with that, we show unequal allelic ratios of *TNNI3*-mRNA among single cardiomyocytes and unequally distributed wildtype cMyBP-C protein across tissue sections from heterozygous HCM-patients. The mutations led to opposing functional alterations, namely increasing (cMyBP-C<sub>c.927-2A>G</sub>) or decreasing (cTnI<sub>R145W</sub>) calcium sensitivity. Regardless, all patients revealed highly variable calcium-dependent force generation between individual cardiomyocytes, indicating contractile imbalance, which appears widespread in HCM-patients. Altogether, we provide strong evidence that burst-like transcription of sarcomeric genes can lead to an allelic mosaic among neighboring cardiomyocytes at mRNA and protein level. In HCM-patients, this presumably induces the observed contractile imbalance among individual cardiomyocytes and promotes HCM-development.

## KEYWORDS

hypertrophic cardiomyopathy, burst-like transcription, cell-to-cell allelic imbalance, contractile imbalance, cardiomyocyte heterogeneity

## Introduction

Burst-like transcription and cell-to-cell allelic imbalance has been described for a variety of genes in global mRNA-transcriptome analyses (1, 2). Bursts originate from stochastic binding and unbinding of the transcription initiation complex to the promotor of a respective gene and depend on biochemical attachment and detachment rates (3). This stochastic process leads to pulses of transcription (4). Most likely, for each allele of a gene binding and unbinding occurs independently. This can be concluded from different fractions of mRNA from each allele that were detected among different cells and in basal variability in mRNA and protein expression among cells from the same population (5, 6). If both alleles encode for the identical protein, heterogeneity of allelic transcription from cell to cell is most likely negligible. However, in heterozygous patients, where one allele encodes for a disease causing mutation, allelic imbalance may exacerbate disease phenotype (7).

A severe disease that is caused by heterozygous mutations in genes encoding for sarcomeric proteins in almost all mutation-positive patients is Hypertrophic Cardiomyopathy (HCM) (8, 9). HCM is characterized by asymmetric hypertrophy of the left ventricle, the interventricular septum, or both. The myocardium of HCM-patients often shows a marked cardiomyocyte and myofibrillar disarray and increased fibrosis (10). Approximately 80% of mutation-positive HCM-cases carry a mutation in one of two sarcomeric proteins,  $\beta$ -myosin heavy chain ( $\beta$ -MyHC, *MYH7*) and cardiac myosin-binding protein C (cMyBP-C, *MYBPC3*). Mutations in cardiac troponin T (cTnT, *TNNT2*) and cardiac troponin I (cTnI, *TNNI3*) account for another 10% of mutation-positive HCM-cases (11). Notably, HCM-mutations alter sarcomeric function and thereby affect force generation of cardiomyocytes. Most mutations in  $\beta$ -MyHC, cTnI and cTnT are missense mutations. Amino acid substitutions affect e.g., ATPase function of  $\beta$ -MyHC, acto-myosin binding kinetics, stiffness of myosin heads, or activation of the thin filament (12). Most mutations in cMyBP-C are truncation mutations, where premature termination codons lead to nonsense-mediated decay of mutated mRNA (13). This leads to haploinsufficiency, a reduction in functional cMyBP-C protein, which also affects force generation (14). Yet, it remains unclear how mutations in different genes with different primary effects on force generation, e.g., calcium-sensitization (hypercontractility) or calcium-desensitization (hypocontractility), can lead to the same HCM-phenotype.

We hypothesized that burst-like transcription of sarcomeric genes in HCM-patients with heterozygous mutations could induce imbalanced expression of mutated and wildtype (WT) alleles at mRNA and protein level among neighboring cardiomyocytes. In patients with missense mutations, this would lead to cardiomyocytes with variable fractions of mutant protein. Since mutations directly affect mechanical function of cardiomyocytes, such heterogeneity is expected to

have functional consequences for the myocardial syncytium. Cardiomyocytes with a larger proportion of mutated protein may show more severely altered contraction as compared to cells with lower fractions. In patients with truncation mutations, cells would contain divergent amounts of WT-protein and may thereby show differently altered force generation. Thus, burst-like transcription of HCM-genes may well cause contractile imbalance from cell to cell independent of the primary mutation effect and could thereby provide an important mechanism that promotes disease development in HCM. The resulting mosaic-like, variable force generation within the myocardium over time could disrupt the cardiac syncytium and lead to cardiomyocyte disarray and other HCM characteristics (15–17).

To test our hypothesis we analyzed single cardiomyocytes from patients with cMyBP-C truncation mutations which show calcium sensitization (18) and from patients with a missense mutation in cTnI which leads to calcium desensitization (19). We show that both genes are transcribed in bursts alongside a large variability in mutant vs. WT cTnI-mRNA and in WT-cMyBP-C-protein from cell to cell. The mosaic-like distribution of WT or WT/mutant protein from cell to cell most likely underlies the variable force generation among individual cardiomyocytes that we observed for patients with both kinds of mutations. Together with previous observations on HCM-related missense mutations in  $\beta$ -MyHC (15–17), our finding of transcriptional and functional heterogeneity among cardiomyocytes from patients with mutations that cause different primary effects suggests a common pathomechanism in heterozygous HCM-patients.

## Methods

An expanded methods section is available in the [Supplementary material](#).

## Patients and donors

The ethics committee of Hannover Medical School approved the study on anonymized human tissue and experiments were carried out in accordance with the given recommendations (No. 2276–2014). Written informed consent according to the Declaration of Helsinki (20) was given by all subjects. Left ventricular septum tissue from HCM-patients was obtained either during myectomy surgery, or after heart transplantation. All patients were diagnosed with hypertrophic obstructive cardiomyopathy (HOCM) as evident from increased septal thickness (>13 mm). Myocardial samples of non-transplanted donor hearts without any known cardiovascular condition were obtained from the Sydney Heart Bank (21). Detailed information on mutations and clinical characteristics are given in [Supplementary Table 1](#).

## Visualization of aTS by smRNA-FISH

Cryosections (10–14  $\mu\text{m}$ ) from frozen left ventricular heart tissue were hybridized with fluorescently labeled sets of 20-mer oligonucleotides for intronic or exonic sequences of RNA. Custom designed (Stellaris® Probe Designer) intronic pre-mRNA probe sets labeled with fluorophore Quasar 670 (LGC Biosearch Technologies) and exonic mRNA probe sets with fluorophore Quasar 570 (LGC Biosearch Technologies) were used (Supplementary Table 2). After hybridization, aTS were counted as spots with co-localization of both Quasar 570 and Quasar 670 fluorescence in cardiomyocyte nuclei.

## Absolute quantification of *TNNI3*- and *MYBPC3*-mRNA in single cardiomyocytes

Cardiomyocytes were isolated from left ventricular cryosections (5  $\mu\text{m}$ ) by laser-microdissection (LMD) with a LMD6 setup (Leica). Cardiomyocytes were identified by striation pattern and staining of intercalated discs with an anti-cadherin antibody. Cells were cut by laser and captured in PCR-tubes. Successful capture of cardiomyocytes was verified microscopically within the Leica LMD6. After reverse transcription of *TNNI3* or *MYBPC3*-mRNA, cDNA from single cells and from *in vitro* transcribed *TNNI3* or *MYBPC3*-mRNA in serial dilutions was pre-amplified and quantified by real-time PCR, using a QuantStudio™ 6 Flex System (Thermo Fisher). RNA copies per cell were calculated from serially diluted standard-RNA.

## Relative quantification of mutant to WT *TNNI3*-mRNA in single cardiomyocytes

*TNNI3*-mRNA from LMD-isolated cardiomyocytes was reverse transcribed on a custom-made micro-mixer. Nested PCR was performed after splitting the whole sample as technical replicate. Reconditioned PCR-products were subjected to allele-specific restriction analyses with *MwoI* for *TNNI3*<sub>c.433C>T</sub> and *BbsI* for donor *TNNI3*<sub>SNP</sub> (single nucleotide polymorphism rs3729841). Allele-specific band patterns on agarose gels were quantified densitometrically and relative allelic fractions were calculated from band intensities.

## Identification of cMyBP-C truncation fragments and cMyBP-C protein quantification

Tissue samples from donors and HCM-patients were ground in a cryo-mortar and re-suspended in sample buffer. Proteins

were separated by polyacrylamide gel electrophoresis and transferred to a nitrocellulose membrane by western blotting. cMyBP-C and  $\alpha$ -actinin were detected by incubation with antibodies against the N-terminus of cMyBP-C or against  $\alpha$ -actinin, respectively.

## Immunofluorescence protein staining in cryosections

Cryosections (5  $\mu\text{m}$ ) from cMyBP-C<sub>trunc</sub> patient and donor tissue were fixed in 4% paraformaldehyde and immunofluorescently co-stained against cMyBP-C,  $\alpha$ -actinin and N-cadherin. As secondary antibodies, Alexa Fluor 488, Alexa Fluor 555 and Alexa Fluor 680 were used simultaneously. DAPI was used to stain nuclei. Cryosections were analyzed by epifluorescent microscopy (H84) or confocal microscopy (H36, H45 and H89).

## Force measurements

Cardiomyocyte force generation and cross-bridge kinetics were characterized after mechanical isolation of single cardiomyocytes from flash frozen myocardial tissue as previously described (15, 17). Briefly, isolated and permeabilized cardiomyocytes were attached to a cantilever and a force transducer and treated with protein phosphatase 1- $\alpha$  (PP1- $\alpha$ ) and protein kinase A (PKA) to adjust phosphorylation levels. Force was measured at different calcium concentrations (pCa-values) from relaxing (pCa 9.0) to maximal activating (pCa 4.18) calcium concentrations.

## Immunofluorescence protein staining in individual cardiomyocytes

Individual cardiomyocytes from cMyBP-C<sub>trunc</sub> patient and donor were co-stained after functional measurements for cMyBP-C and  $\alpha$ -actinin by specific antibodies and respective secondary antibodies in relaxing solution. Fluorescence was determined by confocal microscopy in the center of the cell.

## Quantification of hypertrophy and fibrosis marker expression by real-time PCR

RNA was extracted from donor and patient cardiac tissue and reverse transcribed using random decamers in three independent experiments. Fibrosis and hypertrophy marker gene expression was analyzed in duplicates by real-time

PCR relative to four reference genes. Primers are given in [Supplementary Table 3](#).

## Mathematical model of *TNNI3*-expression

The previously published (17) mathematical simulation of gene expression in individual cardiomyocytes was adapted for *TNNI3* and compared to results from smRNA-FISH, qPCR and functional measurements in donor and *TNNI3*<sub>c.433C>T</sub>-patients.

## Statistical analysis

Values are presented as mean  $\pm$  SD unless otherwise indicated. Groups were compared using Mann-Whitney *U* test and group variances were compared using Levene's test. In multi-group comparisons one-way analysis of variance (ANOVA) and appropriate *post-hoc* tests were applied. Significance for all tests was accepted when  $p < 0.05$ . Statistical analysis and linear correlation test (Pearson correlation coefficient) was performed using GraphPad Prism and R.

## Results

### Burst-like transcription of *TNNI3* and *MYBPC3*

Single cardiomyocytes from donors (H89, H108 and H113, cf. [Supplementary Table 1](#)) and HCM-patients with a missense mutation in cTnI (H146 and H147 *TNNI3*<sub>c.433C>T</sub>, cTnI<sub>R145W</sub>) (19) or truncation mutations in cMyBP-C (H84, *MYBPC3*<sub>c.927-2A>G</sub>; H45, *MYBPC3*<sub>c.1458-6G>A</sub>; H36, *MYBPC3*<sub>c.2864\_2865delCT</sub>; all denominated as cMyBP-C<sub>trunc</sub>) were analyzed. To test whether *TNNI3* and *MYBPC3* are transcribed continuous or burst-like, we used single molecule RNA fluorescence *in situ* hybridization (smRNA-FISH) analysis as previously described (17). Burst-like vs. continuous transcription can be tested by visualization of actively transcribed alleles. A continuously expressed gene would show two active alleles (or the maximal number of alleles in polyploid cells), determined as active transcription sites (aTS) in all cells. Stochastic, burst-like and independent expression of the alleles would appear as cells without aTS and cells with different numbers of aTS in the same tissue. Active transcription sites (aTS) in nuclei contain pre-mRNA – consisting of intronic and exonic sequences – and spliced mRNA – consisting only of exonic sequences. Fluorescently labeled probe sets for intronic (Quasar 670) and exonic (Quasar 570) RNA were hybridized to cryosections from heart tissue. Co-localization

of both probes sets indicated aTS. To restrict the analysis to cardiomyocytes exclusively, cells with striation patterns and/or specific cytoplasmic mRNA spots were examined.

High sensitivity and specificity of our RNA-FISH assays was assessed in short-term cultivated human pluripotent stem cell derived cardiomyocytes (hPSC-CMs) where all nuclei reveal aTS for *MYBPC3*, indicating essentially continuous transcription ([Supplementary Figure 1A](#)). This demonstrates that the sensitivity of our assay will allow us to distinguish continuous and burst-like transcription. For *TNNI3*, modulation of transcriptional activity indicated high sensitivity of this FISH-assay. Treatment with triiodothyronine ( $T_3$ ) led to a substantial reduction of nuclei with aTS ([Supplementary Figure 1A](#)), indicating that a sensitive analysis of transcriptional activity is possible with our assay. To test whether we can depict differences in transcriptional activity in cardiac tissue, we analyzed left ventricular tissue from a one year old child. We show that transcription of both genes was substantially increased as detected by more nuclei with aTS. Furthermore, reproducibility among individual experiments, absence of specific signals in RNase-treated cardiac tissue and in human skeletal muscle tissue for both, *MYBPC3* and *TNNI3* ([Supplementary Figures 1B–D](#)), supports the high specificity of our assays.

To study the mode of transcription in adult human myocardium, smRNA-FISH was performed for *TNNI3* transcription in three donors and two cTnI<sub>R145W</sub> patients and for *MYBPC3* transcription in three donors and three cMyBP-C<sub>trunc</sub> patients. For donors and patients, myocardium from left ventricular wall and interventricular septum was analyzed ([Supplementary Table 1](#)). [Figure 1A](#) shows representative intronic and exonic signals in a nucleus from cMyBP-C<sub>trunc</sub> heart tissue with one *MYBPC3*-aTS (further exemplary nuclei in [Supplementary Figure 2](#)). All patient and donor tissues contained cardiomyocyte nuclei without aTS and nuclei with one, two or more aTS of *TNNI3* or *MYBPC3*, respectively. Quantitative analysis revealed that most cardiomyocyte nuclei show no active *TNNI3*-transcription ([Figure 1B](#)). Donors showed 61, 64 and 55% of nuclei without aTS, cTnI<sub>R145W</sub> patients had 70% and 71% nuclei without aTS. All individuals showed very few nuclei with more than two aTS. More active transcription was seen for *MYBPC3*, however, also here nuclei without aTS were detected; 23, 23, and 10% of nuclei in donors and 13, 21, and 1% in cMyBP-C<sub>trunc</sub> patients were without aTS, respectively ([Figure 1B](#)).

In continuous transcription with constant rates for mRNA production, mRNA counts should follow a Poisson distribution, where mean and variance are equal. In contrast, burst-like transcription is associated with a non-Poisson distribution of mRNA per cell for a respective gene (22). To test this for *TNNI3* and *MYBPC3*, we quantified the total number of mRNA copies per cardiomyocyte from donor and the cMyBP-C<sub>trunc</sub> patient tissue by real-time PCR. We determined a large heterogeneity of



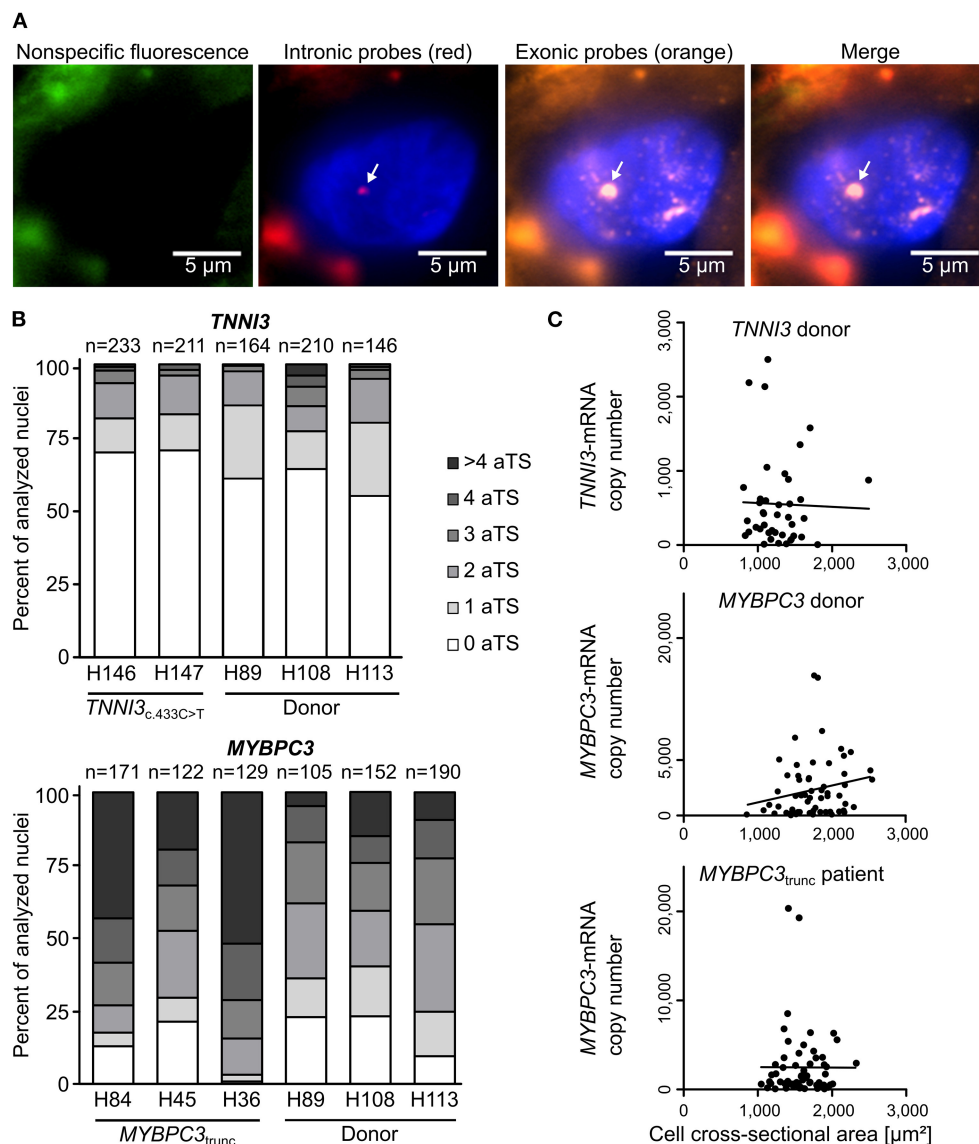


FIGURE 1

Independent, stochastic transcription of *TNNI3*- and *MYBPC3*-alleles. (A) Exonic and intronic mRNA of either *TNNI3* or *MYBPC3* were hybridized with fluorescently labeled DNA probes to visualize active transcription in cardiomyocyte nuclei in cryosections from left ventricular heart tissue. Representative cardiomyocyte nucleus with one active transcription site (aTS) for *MYBPC3* from the cMyBP-C<sub>trunc</sub> patient. Left panel (green) non-specific fluorescence, middle panels intronic RNA (red) and exonic RNA (orange) and right panel merge. Intronic and exonic signals are shown merged with DAPI (blue) to stain the nucleus. One layer of the z-stack is shown. White arrow indicates aTS with co-localization of Quasar 570 and Quasar 670 fluorescence. The other fluorescent spots in the nucleus are only stained by exonic probes and presumably represent spliced mRNA. (B) Distribution of the numbers of aTS per nucleus in cardiomyocytes for *TNNI3* and *MYBPC3*. Percentage of nuclei with 0, 1, 2, 3, 4, and >4 aTS was plotted for different individuals. (C) *TNNI3*- or *MYBPC3*-mRNA copy number per cell plotted against the cell cross-sectional area. Linear correlation was tested using the Pearson correlation coefficient (*TNNI3*:  $r = -0.0263$ ,  $n = 41$ ,  $p = 0.870$ ; *MYBPC3* donor:  $r = 0.1970$ ,  $n = 63$ ,  $p = 0.122$  and *MYBPC3*<sub>trunc</sub> patient:  $r = -0.0030$ ,  $n = 61$ ,  $p = 0.982$ ).

*TNNI3*-mRNA ranging from <20 to 2,499 copies per isolated cell with a mean of 552 molecules and a variance of  $3.8 \cdot 10^5$  ( $n = 41$ , SD = 613). A similar heterogeneity was found for *MYBPC3*-mRNA with copy numbers ranging from <200 to 15,776 per isolated cell with a mean of 2,937 molecules and a variance of  $1.1 \cdot 10^7$  ( $n = 63$ , SD = 3,329) in the donor. For

the cMyBP-C<sub>trunc</sub> patient a range from <200 to 20,338 with a mean of 2,486 molecules and a variance of  $1.4 \cdot 10^7$  ( $n = 61$ , SD = 3,769) was observed. In addition, mRNA copy numbers did not correlate with the cross-sectional area of isolated cardiomyocytes (Figure 1C), which would have been expected for cell-size specific transcription (23). Also, the frequency

distribution of mRNA counts per cell showed no bimodality, which would be expected from continuous transcription from mono- and binucleated cells. This is in line with findings from human pluripotent stem cell derived cardiomyocytes (hPSC-CMs) where we show that the number of *MYH7*-mRNA molecules per cell varies significantly but does not correlate with the number of nuclei (Supplementary Figure 3). Similar results from single cell RNA-sequencing show that mono- and binucleated cells show comparable total mRNA levels for specific genes (24). Together, our findings strongly indicate burst-like transcription of *TNNI3*- and *MYBPC3*-alleles in donors and HCM-patients. Moreover, we found burst-like transcription in both, interventricular septum and left ventricular wall samples, in HCM-patients and donors.

## Unequal expression of mutated per WT *TNNI3*-mRNA in donor and patient cardiomyocytes

To examine whether burst-like transcription can induce allelic imbalance from cell to cell, the ratio of mutant per WT-mRNA in single cardiomyocytes from *TNNI3*<sub>c.433C>T</sub> (cTnI<sub>R145W</sub>) patients and donors was analyzed. Single cardiomyocytes were isolated from cryosections *via* laser-microdissection and examined by RT-PCR in two technical replicates to detect dropout events. To quantify allelic expression, PCR-products were subjected to allele-specific restriction and resulting fragments were separated on agarose gels. PCR-linearity was validated with a set of plasmid mixtures of mutant and WT-allele (Supplementary Figure 4). Relative quantification in three independent experiments in duplicates showed, that both allelic templates were amplified and detected in the correct proportion with high accuracy (root mean square error = 5.3%). In Figure 2A representative restriction analyses of *TNNI3*-mRNA from individual *TNNI3*<sub>c.433C>T</sub> cardiomyocytes are shown. The restriction enzyme *Mwo*I generates a 202 base pair (bp) mutation-specific fragment, a 160 bp WT-specific fragment and a 115 bp fragment from both alleles (Figure 2A). In this example, cell 1 showed comparable signal intensities for both mutant and WT-mRNA, whereas cells 2 and 3 had more intense signals for mutant specific fragments.

To analyze allelic expression in donor cardiomyocytes, we made use of a heterozygous non-pathogenic single nucleotide polymorphism (SNP rs3729841). Quantitative RT-PCR was performed with the same protocol as for patient cardiomyocytes and *Bbs*I was used for allele-specific restriction of PCR-products, generating a mutation-specific fragment of 273 bp and a WT-specific fragment of 317 bp. Figure 2B shows an exemplary gel analysis. Cell 1 shows a higher intensity for the WT-fragment, cell 2 for the SNP-fragment and cell 3 shows comparable intensities for both fragments.

To quantify allelic ratios in HCM-patients and donor, integrated optical densities (IOD) of allele-specific fragments were determined for each replicate and fractions of mutated or SNP- per WT-mRNA were calculated from respective IODs. Some cells showed a large difference between replicates, presumably due to technical limitations. Therefore, we performed a multialiquot control to determine the experimental scatter. Total RNA was extracted from five donor cryosections and diluted to single cell equivalent amount as determined by PCR-product intensity. We analyzed 18 aliquots using the same protocol as for single cardiomyocytes (Figure 2C). The mean of aliquots was 49.0% of SNP-mRNA with a standard deviation of 6.5%. Two-fold of this standard deviation (13.0%) was used as cut-off for the deviation between the two replicates that we generated upon quantification of transcripts from each single cardiomyocyte. In the final analyses, only cells where technical replicates from one cell differed <13.0% were included (Figure 2C).

We detected highly variable fractions of transcript from the mutated allele among single *TNNI3*<sub>c.433C>T</sub> cardiomyocytes (Figure 2C, red symbols) and from the SNP-allele in donor cardiomyocytes (Figure 2C, blue symbols). Cells displayed the full range containing essentially only WT through variable mixtures of WT and mutant or SNP to essentially only mutant or SNP-mRNA. This variability was significantly larger than the experimental scatter and was similar for donor and *TNNI3*<sub>c.433C>T</sub> cardiomyocytes (Figure 2C). It suggests similar heterogeneity of *TNNI3* allelic expression in donor cardiomyocytes and in HCM-patient cardiomyocytes. Importantly, the average fraction of mRNA from the two alleles (donor: 46.9% SNP-mRNA, patients: 50.4 and 43.0% mutant mRNA) was comparable to the mean fraction of mutant or SNP-mRNA from tissue sections (donor: 43.2% SNP-mRNA, patients: 46.0 and 54.4% mutant mRNA; Supplementary Table 5). This suggests that the analyzed single cardiomyocytes display a representative sample of cells from donor and patient tissue, respectively.

## Intra- and intercellular heterogeneous distribution of cMyBP-C protein in patient cardiomyocytes

Mutations *MYBPC3*<sub>c.927-2A>G</sub> (H84) and *MYBPC3*<sub>c.1458-6G>A</sub> (H45) induce aberrant splicing and mutation *MYBPC3*<sub>c.2864\_2865delCT</sub> (H36) causes a frameshift; all mutations lead to a premature stop codon (25). Western blot analysis of cMyBP-C<sub>trunc</sub> patient cardiac tissues showed no evidence for truncated cMyBP-C<sub>trunc</sub> proteins (Figure 3A). Even with long exposure times of 120 seconds, only unspecific bands present in all analyzed samples could be detected (Supplementary Figure 5). Therefore, it seems unlikely that

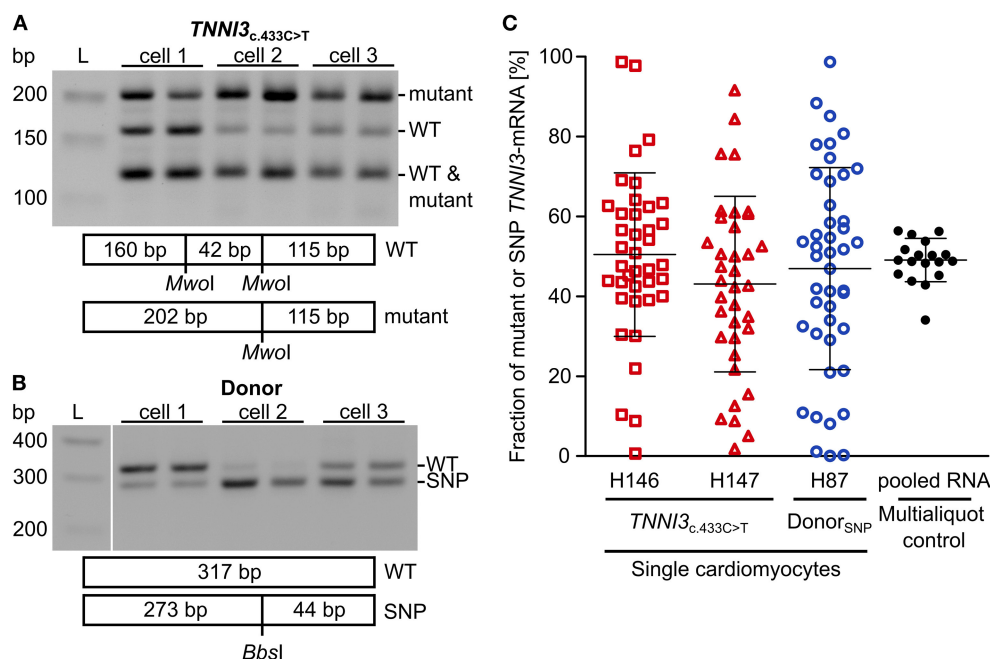


FIGURE 2

Allelic imbalance of *TNNI3* in cTnR145W patient and donor cardiomyocytes. Individual cTnR145W cardiomyocytes and donor cardiomyocytes were isolated by laser-microdissection from cryosections and reverse transcribed. cDNA was split in two technical replicates and subjected to nested PCR. **(A)** RT-PCR-products from single laser-microdissected cTnR145W cardiomyocytes were treated with *MwoI* to generate allele-specific restriction fragments. Shown are three different cells in technical replicates. Expected fragment sizes are 202 bp for *TNNI3*<sub>c.433C>T</sub>-allele, 160 bp for WT-allele and 115 bp for both WT- and *TNNI3*<sub>c.433C>T</sub>-allele corresponding to 100% of the PCR-product. L indicates the DNA standard. **(B)** RT-PCR-products from donor cardiomyocytes with heterozygous SNP rs3729841 were treated with *BbsI* to generate allele-specific restriction fragments. Shown are three different cells in technical replicates. Expected fragment sizes are 317 bp for WT-allele and 273 bp for SNP-allele. L indicates the DNA standard. **(C)** Fractions of mutant *TNNI3*-allele from single cTnR145W cardiomyocytes (two patients) and of SNP-allele from donor cardiomyocytes. Each dot represents the mean of two replicates from one cell. Multiquot control, 18 individual PCR-analyses from pooled donor RNA with a concentration mimicking single cell level indicating the experimental error. Homogeneity of variance was tested by Levene's test, showing a significant difference between group variance [ $F(3, 133) = 6.72, p = 0.00029$ ]. Lines indicate mean  $\pm$  SD.

truncated protein was incorporated into the sarcomeres of cMyBP-C<sub>trunc</sub> patients. Total full-length cMyBP-C per  $\alpha$ -actinin was reduced to 80, 80, and 59%, respectively indicating haploinsufficiency (Figure 3B).

Burst-like transcription of mutant and WT-alleles may lead to different levels of WT-protein among cells. To test this, cryosections from patient's tissue were co-stained with antibodies against cMyBP-C and  $\alpha$ -actinin. We observed a patchy distribution of cMyBP-C between individual neighboring cardiomyocytes in all three patients (Figure 3C, left column). Some cardiomyocytes showed no staining for cMyBP-C, whereas neighboring cardiomyocytes showed strong signals. In addition, we observed different intensities of cMyBP-C staining among cardiomyocytes. In contrast,  $\alpha$ -actinin (Figure 3C, middle column) or  $\beta$ -MyHC (Supplementary Figure 6) as markers for sarcomere alignment showed a substantially more homogeneous pattern. In donor heart tissue, cMyBP-C distribution was homogenous (Figure 3C, lower row left panel) and similar to  $\alpha$ -actinin (Figure 3C, lower row middle panel) and the

$\beta$ -MyHC pattern (Supplementary Figure 6). Z-stack and 3D views of cMyBP-C and  $\alpha$ -actinin staining in patient tissue presented uneven cMyBP-C distribution also in z-dimension compared to donor tissue (Supplementary Videos 1–3). In summary, immunostaining of tissue from patients with three different haploinsufficiency-causing mutations reveals a substantial variability of WT-protein from cardiomyocyte to cardiomyocyte. Interestingly, as already evident from tissue staining, uneven distribution of cMyBP-C was also often found within patient cardiomyocytes (*MYBPC3*<sub>c.927–2A>G</sub>) when single, demembranated cardiomyocytes were co-stained for cMyBP-C and  $\alpha$ -actinin (Figure 3D; Supplementary Figure 7). Whereas essentially all sarcomeres in individual cardiomyocytes could be stained for  $\alpha$ -actinin, some sarcomeres or areas of these cardiomyocytes showed no signal for cMyBP-C (Figure 3D). In contrast, cardiomyocytes from donor heart tissue showed a considerably more even staining pattern for cMyBP-C and  $\alpha$ -actinin over all sarcomeres (Figure 3D). Also, the confocal images of individual cardiomyocytes analyzed in functional measurements show lower levels and patchy distribution of

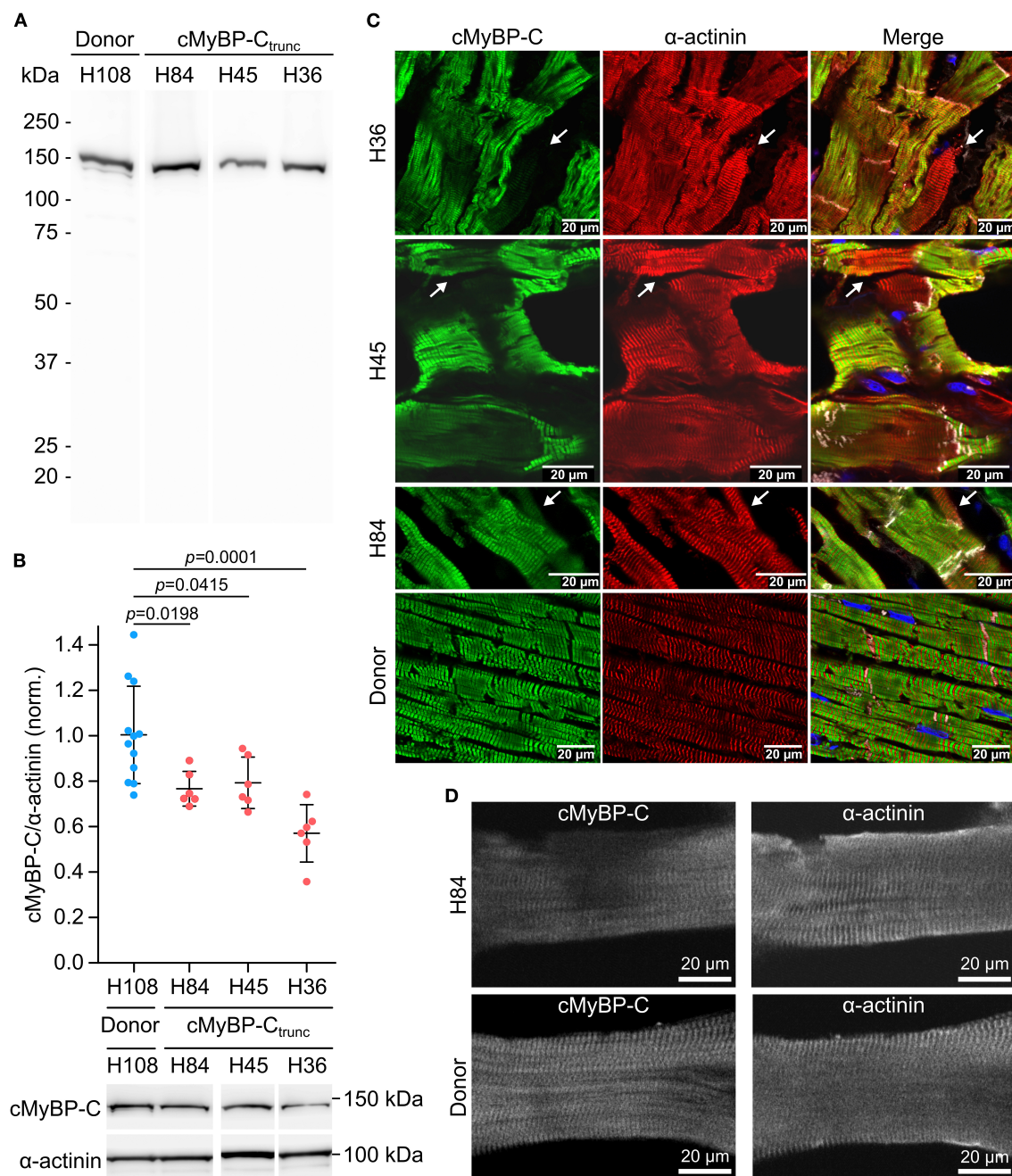


FIGURE 3

Unequal expression of cMyBP-C in cardiomyocytes of the cMyBP-C<sub>trunc</sub> patient. **(A)** Western blot of one donor sample and three cMyBP-C<sub>trunc</sub> patients H84 (*MYBPC3*<sub>c.927-2A>G</sub>), H45 (*MYBPC3*<sub>c.1458-6G>A</sub>) and H36 (*MYBPC3*<sub>c.2864\_2865delCT</sub>) was incubated with an N-terminal cMyBP-C antibody. Detection of full-length WT-cMyBP-C (~140 kDa) and possible truncated cMyBP-C was performed with 5 s exposure time. **(B)** Relative protein amount of cMyBP-C was calculated from IOD of the cMyBP-C band divided by IOD of α-actinin for normalization. IOD of α-actinin band at 103 kDa was quantified as loading control. IOD ratio (cMyBP-C/α-actinin) from one donor sample (blue dots, n = 12 lanes) and compared to data from cMyBP-C<sub>trunc</sub> patients (red dots, n = 6 lanes each). For comparison of patient results (H84, H45, H36) with donor (H108) reference one-way analysis of variance (ANOVA) and Dunnett's *post-hoc* test were performed. ANOVA yielded significant variation among groups [ $F(3, 26) = 10.17$ ,  $p = 0.00013$ ]. Mean ± SD and p-values from Dunnett's test are indicated in the figure. **(C)** Cryosections (5 or 10 μm) from cMyBP-C<sub>trunc</sub> patients and donor myocardium were stained with an N-terminus-specific antibody for cMyBP-C (left panels, green) to visualize cell-to-cell cMyBP-C distribution. Co-staining with an α-actinin antibody (middle panels, red) reveals sarcomeric Z-lines. Right panels, merge with N-cadherin (white) and DAPI (blue) staining. Images were either taken by confocal laser scanning microscopy (H36, *MYBPC3*<sub>c.2864\_2865delCT</sub> and H45, *MYBPC3*<sub>c.1458-6G>A</sub>) or by epifluorescent microscopy (H84, *MYBPC3*<sub>c.927-2A>G</sub>). White arrows indicate cells with substantially reduced cMyBP-C signals. **(D)** Confocal microscopy of single cardiomyocytes from cMyBP-C<sub>trunc</sub> (c.927-2A>G, H84) patient or donor co-stained for cMyBP-C and α-actinin.



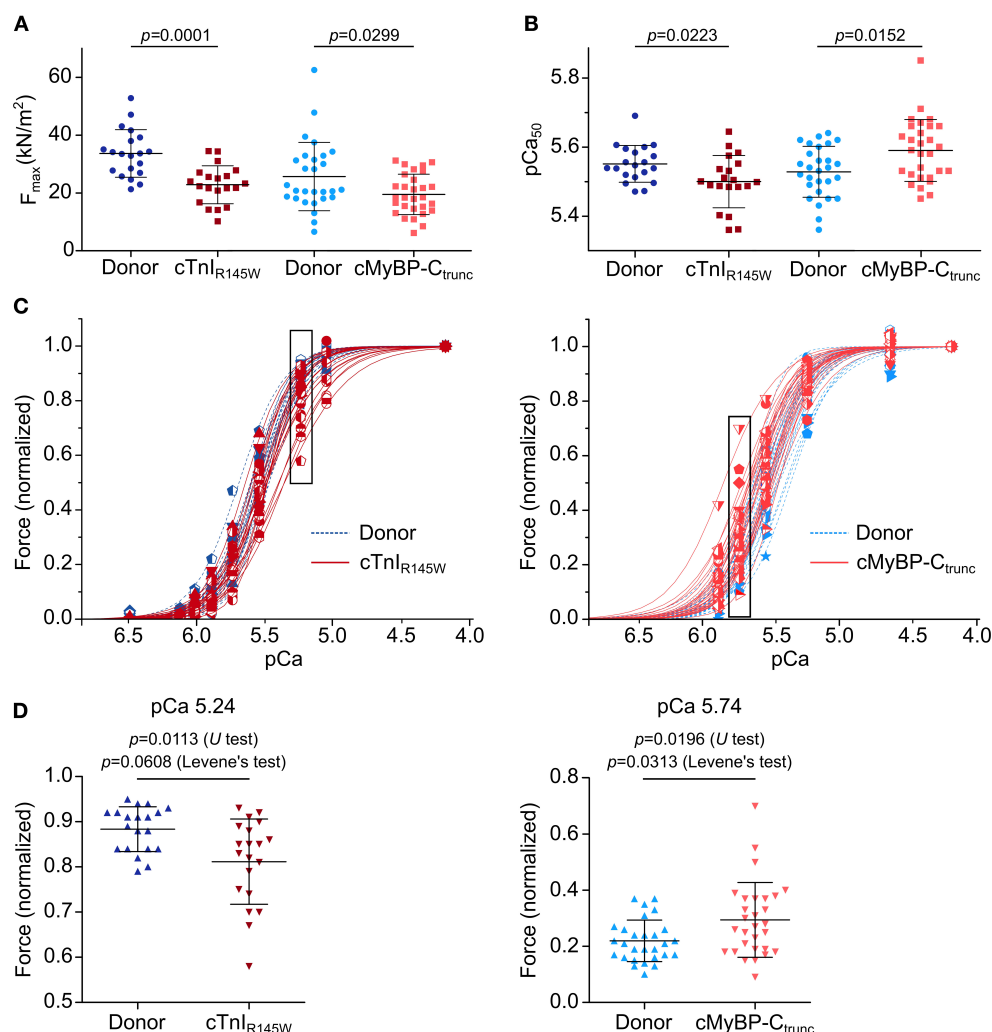


FIGURE 4

Contractile imbalance among cardiomyocytes from cMyBP-C<sub>trunc</sub> and cTnIR145W. Individual cardiomyocytes from cTnIR145W patient, cMyBP-C<sub>trunc</sub> (c.927-2G>A) patient and respective donors were permeabilized and subjected to different calcium concentrations to measure calcium-dependent force generation. **(A)** Maximum force generation (pCa 4.18) and **(B)** pCa<sub>50</sub> values of individual cTnIR145W cardiomyocytes ( $n = 20$ ), of cMyBP-C<sub>trunc</sub> ( $n = 28$ ) and of the corresponding donor cardiomyocytes ( $n = 20$  and  $n = 29$ ). pCa<sub>50</sub> was derived from Hill-fits of normalized force-pCa relations. p-values of U test are indicated in the figure. **(C)** Force-pCa relations were plotted for individual cTnIR145W cardiomyocytes, for cMyBP-C<sub>trunc</sub> cardiomyocytes and the respective donor cardiomyocytes. Patient cardiomyocytes, red symbols and solid lines; donor cardiomyocytes, blue symbols and dashed lines. Force values in black boxes are plotted in **(D)**. **(D)** Normalized forces of individual cardiomyocytes are shown for cTnIR145W vs. the respective donor at pCa 5.24, and for cMyBP-C<sub>trunc</sub> versus the respective donor at pCa 5.74. Each symbol represents an individual cardiomyocyte. Mean  $\pm$  SD and p-values for U-test and Levene's test are indicated in the figure.

cMyBP-C in patient cardiomyocytes compared to donor cells (Supplementary Figures 7A,B).

## Contractile imbalance among single cardiomyocytes

To test whether unequal expression of mutant and WT-alleles at mRNA and protein level also has consequences for cardiomyocyte contractile function or represents negligible fluctuations, calcium-dependent isometric force generation and

cross-bridge kinetics of single, demembranated cardiomyocytes were examined. Cardiomyocytes isolated from flash frozen tissue of HCM-patients with cTnIR145W and cMyBP-C mutation c.927-2A>G, respectively, were analyzed in comparison to donors as previously described (15). To adjust phosphorylation levels for patients and donor, cardiomyocytes were incubated with PP1- $\alpha$  and PKA prior to mechanical experiments (Supplementary Figure 8).

On average, cardiomyocytes from the cTnIR145W patient showed significant reduction of maximum isometric force by 32% and cardiomyocytes from the cMyBP-C<sub>trunc</sub> patient by 24%

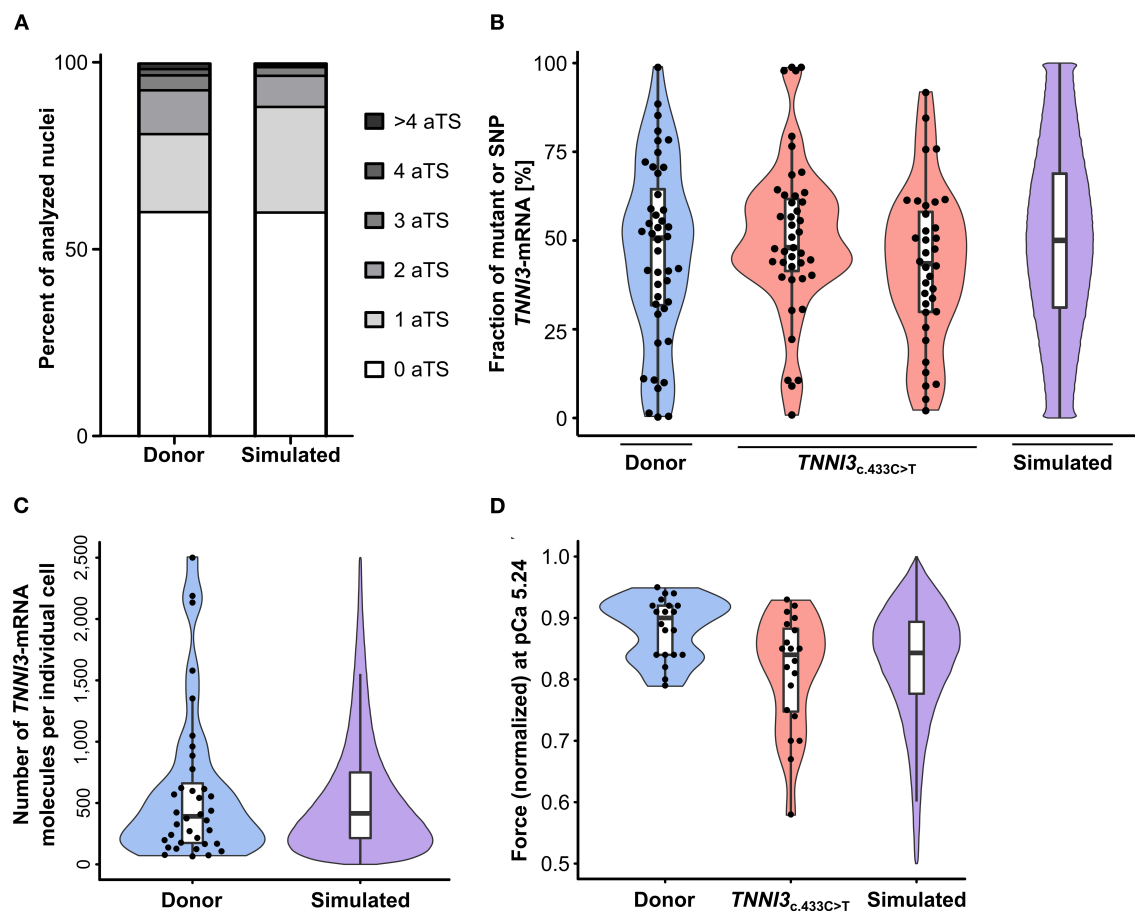


FIGURE 5

Experimental results from donor and from patients with *TNNI3*-mutations in comparison to simulation results from the model. **(A)** *TNNI3*-aTS distribution from three donors (H89, H108, and H113) compared to aTS distribution simulated by model. Percentage of nuclei with 0, 1, 2, 3, 4, and >4 aTS was plotted. **(B)** Percentage of *TNNI3*-SNP-allele transcripts from a donor and of *TNNI3*-mutant-allele transcripts from two cTnI<sub>R145W</sub> patients (densitometric analysis of allele-specific restriction fragments), compared to the simulated distribution. Each data point represents the mean of replicates from one cell. Violin plots represent probability density of experimental data (blue and red) and probability density simulated by model (violet). Horizontal bar, median; white rectangle, interquartile range. **(C)** Total *TNNI3*-mRNA counts in donor cardiomyocytes. Violin plot probability density of the data (blue) compared to outcome of model simulation (violet). **(D)** Force values of individual cardiomyocytes for donor and for *TNNI3*<sub>c.433C>T</sub> patient at pCa 5.24, normalized to respective maximum force, compared to simulation outcome. Dots represent individual cardiomyocytes. Violin plots, probability density of data (blue and red) and of model simulation (violet).

compared to the respective donor (Figure 4A). This is in line with reports from the same patient with mutation cTnI<sub>R145W</sub> and from patients with the same mutation in cMyBP-C (18, 19, 26). The rate constant of force redevelopment as measure for cross-bridge cycling kinetics was only slightly reduced (Supplementary Figure 9A). Interestingly, cardiomyocytes from the two patients showed opposite alterations in the calcium concentration needed for half maximal force generation (pCa<sub>50</sub>). pCa<sub>50</sub> of the cTnI<sub>R145W</sub> patient was significantly reduced to  $5.50 \pm 0.08$  (mean  $\pm$  SD) compared to the respective donor [pCa<sub>50</sub>  $5.55 \pm 0.05$  (mean  $\pm$  SD)] indicating calcium desensitization (Figure 4B; Supplementary Figure 9B). In contrast, cMyBP-C<sub>trunc</sub> cardiomyocytes had a significantly increased pCa<sub>50</sub> of  $5.59 \pm 0.09$  (mean  $\pm$  SD) compared

to the respective donor with a pCa<sub>50</sub> of  $5.53 \pm 0.07$  (mean  $\pm$  SD), indicating calcium sensitization (Figure 4B; Supplementary Figure 9C). In addition, we observed that the Hill-fit did not characterize the force-pCa relationship of the cTnI<sub>R145W</sub> cardiomyocytes well at higher calcium concentrations. Therefore, logit transformed force values were fitted with two linear functions (Supplementary Figure 9D). At low calcium concentrations, force generation of donor and cTnI<sub>R145W</sub> cardiomyocytes was very similar, while at higher calcium concentrations (pCa < 5.54) the slope for cTnI<sub>R145W</sub> cardiomyocytes was significantly more shallow than for donor cardiomyocytes.

Analysis of calcium dependent force generation in individual cardiomyocytes from both patients revealed a marked variability



that was considerably larger than that of donor cardiomyocytes. Some cTnI<sub>R145W</sub> cardiomyocytes showed comparable force-pCa relations as donor cardiomyocytes, while others were significantly shifted to the right (Figure 4C). Variability in force generation between individual cTnI<sub>R145W</sub> cardiomyocytes was strikingly visible at pCa values  $\leq 5.54$  (Figure 4D). The variance in force generation among the cTnI<sub>R145W</sub> cardiomyocytes at pCa 5.54 was significantly increased by 3.6 fold as compared to donor cardiomyocytes (Levene's test  $p = 0.0608$ ). cMyBP-C<sub>trunc</sub> cardiomyocytes presented a similar large cell-to-cell variability, however, with a shift to the left (Figure 4C, right panel). The variance between the cMyBP-C<sub>trunc</sub> cardiomyocytes was significantly increased by 3.2 fold compared to donor cardiomyocytes (Figure 4D, Levene's test  $p = 0.0313$ ).

## Model calculations to connect transcriptional bursting to contractile imbalance of *TNNI3*

Since the different analyses could not be performed on one identical cardiomyocyte, we used a mathematical simulation to survey a potential direct link of the experimental findings in one cell. We modeled aTS distribution of *TNNI3*, allele-specific *TNNI3* transcription, allelic *TNNI3*-mRNA-fractions, number of total *TNNI3*-mRNA per cell and force generated at pCa 5.24 for 100,000,000 cells and compared them to experimental data from donors and from cTnI<sub>R145W</sub> patients. For each individual simulated cell, relative force generation was consequence of the particular bursting and subsequent allelic mRNA and protein synthesis and degradation.

*TNNI3*-aTS distribution from all three donors was averaged and compared to the simulation, which reproduced the trend to low numbers of nuclei with aTS (Figure 5A). Simulation of *TNNI3*-mRNA allelic expression revealed a comparable imbalance from cell to cell as determined experimentally, ranging from almost only mutant allele *via* different fraction of both alleles to essentially only wildtype allele (Figure 5B). The simulated *TNNI3*-allele ratio showed a broader and smoother distribution compared to the experimental data. This is presumably due to smaller numbers of data points in the experimental data. We next modeled the total number of *TNNI3*-mRNA copy number per cell. The mean of 580 *TNNI3* copies/cell was comparable to experimental data (552 copies per cell). Furthermore, the simulation could reproduce the distribution of *TNNI3*-mRNA counts (Figure 5C). To test whether mRNA allelic imbalance may lead to unequal fractions of mutant and wildtype protein and subsequently to contractile imbalance we simulated force generation of single cardiomyocytes based on the respective calculated fraction of mutant per wildtype cTnI-protein. This was done based on the assumption that higher fractions of mutant protein produce a

higher effect on force development in the cardiomyocyte. The resulting simulated distribution of force generation was similar to the distribution of force generation at pCa 5.24 in patient cardiomyocytes (Figure 5D).

Additionally, the model also predicts the effect of burst-like transcription in individual cardiomyocytes over time, since our analysis on human tissue provided a snapshot of expression during tissue extraction. The model shows that fractions of mRNA from each allele change over time, resulting in changing fractions of mutant per wildtype protein and consequently force generation (Supplementary Figure 10).

## Discussion

Evidence accumulates that burst-like transcription is a general expression mode for most genes (2, 22). Both alleles of a respective gene are switched on and off stochastically and independently from each other. This leads to unequal fractions of mRNA from the alleles among individual cells within a tissue (17, 27). In heterozygous patients with mutations that alter protein function and biomechanical properties of a cell, such imbalanced allelic expression may cause functional heterogeneity from cell to cell, which could exacerbate disease phenotype (7, 16, 28). A vast majority of HCM-patients are heterozygous. Mutations occur in several different proteins and alter force generation in cardiomyocytes. However, primary effects of HCM-mutations are highly divergent, e.g. often causing calcium-sensitization but also calcium-desensitization (12). In addition, missense mutations impose their effect by incorporation of mutant protein into the sarcomere, whereas truncation mutations mostly lead to a reduction of functional protein, so-called haploinsufficiency (13). To date, HCM pathomechanisms are not fully understood. If burst-like transcription is a principle feature of sarcomeric gene transcription, it could represent an important general mechanism that exacerbates disease development in HCM.

To test this, we chose patients with mutations in different sarcomeric genes that cause opposing primary effects on force generation and analyzed sarcomeric gene transcription, allelic mRNA or protein expression, and force generation in donors and HCM-patients. We provide evidence that burst-like transcription is a physiological expression mode of sarcomeric genes, which leads to unequal fractions of mRNA from both alleles among individual cardiomyocytes. It does not affect protein expression in donor controls, since both alleles encode for the identical protein. In HCM-patients, however, we show that it leads to highly heterogeneous protein expression among cardiomyocytes. Along with that, we measured a substantial contractile heterogeneity among cardiomyocytes from each HCM-patient compared to donor cardiomyocytes. We suppose that this functional variability triggers the increased expression

of marker genes for hypertrophy and fibrosis, which we detected in the patients.

## Burst-like transcription is a physiological transcription pattern that causes heterogeneity in heterozygous HCM-patients

Our finding that the sarcomeric genes *MYBPC3* and *TNNI3* are transcribed in bursts in donors indicates that this is a physiological transcription mode of these genes. Since it is also found for *MYH7* in donors (Supplementary Figure 11), we provide evidence that three of the most commonly affected genes in HCM are principally transcribed in bursts. This leads to transcriptional noise (29), as we show by variable mRNA-counts among cardiomyocytes for each gene. This variability is in a comparable range in single cell transcriptomic studies for cardiomyocytes in humans and mice (30, 31). Thus, it likely represents natural fluctuation, which can be tolerated within the myocardium. The variability also exists for other sarcomeric genes such as *TNNT2*, *TMP1*, *MYL2*, *MYL3*, and *ACTC1* (30) indicating a general expression mode for sarcomeric, HCM-associated genes. Therefore, we assume that the mechanisms we detected for *MYBPC3*, *TNNI3*, and *MYH7* can be transferred to further HCM-genes.

Variability in absolute mRNA molecule numbers per cell for each gene is accompanied by an unequal expression of the two alleles among individual cells (5), as we can show here for *TNNI3*. However, in donors this does not cause differential functionality of cells, since both alleles code for an identical protein. Nonetheless, burst-like transcription is maintained upon HCM-development, as seen by only small differences in transcriptional activity between HCM-patients and donors. *cTnI*<sub>R145W</sub> patients showed comparable *TNNI3* transcriptional activity compared to donors. HCM-patients with cMyBP-C<sub>trunc</sub> mutations showed a modest increase in *MYBPC3* transcriptional activity, which is still compatible with burst-like transcription. In HCM-patients, transcriptional bursts lead to unequal ratios of mutant per wildtype mRNA among individual cardiomyocytes. Here we showed for *cTnI*<sub>R145W</sub> that the average mutant vs. wildtype mRNA ratio is 50:50 but ranges from 0:100 to 100:0 in individual cells. We suppose that mRNA allelic imbalance translates to imbalance at protein level. To date it is not possible to perform allele-specific quantification of single amino acid exchanges at protein level. However, in cMyBP-C<sub>trunc</sub> patients, where mutated mRNA is degraded, unequal expression would lead to an inhomogeneous distribution of WT-cMyBP-C among cardiomyocytes, which we demonstrated in tissue sections from myocardium of three cMyBP-C<sub>trunc</sub> patients with different truncation mutations. Previous reports showing unequal cMyBP-C distribution in HCM-patient cardiomyocytes

with the same (32) and other truncation mutations in cMyBP-C (33) strengthen our observation.

Some cMyBP-C<sub>trunc</sub> patients may exhibit altered cMyBP-C protein degradation or compensatory upregulation of cMyBP-C, which might correct for degradation of the mutated allele. These patients show no reduction in total cMyBP-C (33, 34). Here, the burden of truncated proteins could trigger disease, either by excess protein production and degradation or by inefficient incorporation of truncated protein in the sarcomeres and disruption of its structure (34). We assume that such mechanisms will affect cells with different fractions of mutant protein to different degrees, which would also cause heterogeneity among cells. The finding that patients without haploinsufficiency show an uneven distribution of cMyBP-C among cardiomyocytes supports this (33). Therefore, restoration of total cMyBP-C at tissue level still retains variable levels from cell to cell. In the patient analyzed in this study, upregulation of *MYBPC3*-transcriptional activity did not lead to increased amounts of *MYBPC3*-mRNA. The reduction of cMyBP-C in the same patient indicates that the increased transcriptional activity could not restore cMyBP-C protein level.

Most interestingly, we also observed a marked uneven intracellular distribution of cMyBP-C in patient cardiomyocytes but not in donors which is in line with cMyBP-C stainings in tissue from HCM-patients shown by Theis and colleagues (33). In rat cardiomyocytes it has been reported that mRNA from several sarcomeric genes is transported from the nucleus to the sarcomeres and translated directly at the Z-disc (35). The mRNA transcribed from one allele during a particular burst may thus be translocated to sarcomeres within a distinct cellular area. Upon translation at the Z-disc, the protein might be incorporated in adjacent sarcomeres. In cMyBP-C<sub>trunc</sub> patients, where mutant protein is not found, this possibly causes areas without functional cMyBP-C leading to patchy intracellular distribution (36). If mRNAs transcribed from each nucleus in binucleated cardiomyocytes are transported to different areas of the cell similarly to skeletal muscle cells (37), this could additionally contribute to intracellular heterogeneity.

## Contractile imbalance between individual cardiomyocytes from HCM-patients with mutations in cTnI and cMyBP-C

We tested our hypothesis that highly variable force generation among individual cardiomyocytes can occur irrespective of the primary effect of the mutation on force generation. For missense mutations, different fractions of mutant protein will shift the force-pCa relationship to a different extent in each cardiomyocyte. For truncation mutations, different levels of wildtype cMyBP-C per cardiomyocyte can have the same effect. The direction of changes differs with

the initial effect of the mutation on acto-myosin interaction. Thus, we analyzed calcium-dependent force generation of individual cardiomyocytes with mutation cTnI<sub>R145W</sub> that causes a calcium-desensitization (19), and of cardiomyocytes with truncation mutation *MYBPC3*<sub>c.927-2A>G</sub> that causes calcium-sensitization (18, 38). For both mutations, we detected a substantial heterogeneity in force generation among the individual cardiomyocytes from the patients. Even though also donor cardiomyocytes showed some variability in force generation, which reflects the experimental scatter and intrinsic physiological differences among cells, variability among patient's cardiomyocytes was significantly larger than that of the donors.

Importantly, we often encountered cells – mostly from patient tissue – with a low structural integrity presumably due to disease-associated cardiomyocyte damage in which force generation over the full range of calcium concentrations could not be examined. Since such cells were mainly found in patient tissue, variability between individual cardiomyocytes in HCM-patients most likely is even larger than shown by our analysis. A low number of cardiomyocytes, which show a large shift in force generation, presumably reflects this.

## Possible consequences of burst-like transcription for the pathomechanism of HCM

We show here for the first time that three of the most commonly affected genes in HCM are transcribed burst-like in donors, thus under physiological conditions. This general transcription mode is maintained in HCM-patients. It will have no functional effect in healthy individuals since they express only WT-allele transcripts and proteins (28). However, if one allele encodes for a mutated protein, which alters biomechanical function of cardiomyocytes, burst-like transcription creates not just fluctuation of transcripts but likely attains clinical impact, as shown here for mutations in *TNNI3* and *MYBPC3*. The observed heterogeneous force generation among cardiomyocytes from HCM-myocardium with either of the mutations most likely results from allele transcription in bursts. It is found in patients with truncation mutations as well as in patients with mutations that cause a poison peptide effect.

This contractile imbalance could disrupt the cardiac syncytium and induce disarray of cardiomyocytes (16, 17, 28). Aberrant stretch can induce expression of atrial natriuretic peptide, angiotensin II, endothelin I and transforming growth factor  $\beta$  (TGF- $\beta$ ) in isolated cardiomyocytes (39, 40) and TGF- $\beta$  in an HCM mouse model (41) and thereby lead to hypertrophy and fibrosis (39–41). In line with this, we show upregulated expression of several marker genes for fibrosis and hypertrophy in HCM-patients as compared to donors (Supplementary Figure 12). Interestingly, the extent

of upregulation differed largely among individual patients, putatively reflecting the large variability in disease development which is characteristic for HCM (12). Future studies will reveal whether upregulation of these genes is also heterogeneous from cell to cell. Overall, contractile imbalance may activate pro-hypertrophic and pro-fibrotic pathways and for many different mutations exacerbate the HCM phenotype by inducing cardiomyocyte disarray and interstitial fibrosis (16, 17, 28).

It should be noted that the mutation effects, reduction in functional cMyBP-C or incorporation of functionally altered proteins into the sarcomeres, provide the primary disease mechanism. Homozygous patients, which presumably do not exhibit functional heterogeneity but develop heart failure, indicate this. Interestingly, the identical mutation affects homozygous and heterozygous patients differently. Whereas homozygous patients developed dilated cardiomyopathy, heterozygous patients developed HCM (42). This indicates that next to the direct effect of the mutation, functional heterogeneity among cardiomyocytes most likely exacerbates HCM phenotype development. Furthermore, HCM-development can be influenced by environmental stress, lifestyle and comorbidities like coronary artery disease, obstructive sleep apnea and renal diseases (43) as well as polymorphisms in other genes (44). This gets apparent in a family where several members carry the cTnI mutation R145W. However not all of them developed HCM and some even developed RCM (45). Burst-like transcription could also contribute to differences in disease severity within a family if the kinetics of bursting and/or mRNA and protein turnover would differ among family members, thus increasing or reducing cell-to-cell heterogeneity.

## Limitations of the study

One limitation of our study is that we cannot perform all analyses in the identical cell. Even though fluorescent staining of sarcomeres indicated different levels of cMyBP-C, robust absolute quantification was not feasible using this approach. To meet this limitation, we set up a mathematical simulation and tested whether variable force generation from cell to cell could result from burst-like transcription. We used our previously described computational model (17) and adjusted its rate constants for *TNNI3*. The model calculations show that burst-like transcription of *TNNI3* results in variable counts of aTS in the cells, marked cell-to-cell allelic imbalance and heterogeneous numbers of *TNNI3*-mRNA copies per cell, similar to our experimental data. Using our mathematical model we have previously shown that increased ploidy in HCM-patients does not influence the outcome of allelic imbalance among cardiomyocytes (17). The model also showed that the cell-to-cell allelic imbalance in HCM-patients results in large differences in force generation of patient cardiomyocytes, comparable to our experimental data.

We performed our study on isolated cardiomyocytes. In tissue, sarcomere length-dependent force generation was suggested to provide a smoothing effect on physiologically different layers of cardiomyocytes (46). Increased stretching of weaker cardiomyocytes by neighboring cells would accordingly increase their force and could thereby counteract contractile heterogeneity in a physiological range. However, loss of cMyBP-C was shown to lead to aberrant stretch activation (47) and perturbation of length-dependent force generation has been reported to be common in HCM (19). This feedback-mechanism could therefore fail to equalize forces of cardiomyocytes in HCM-tissue. Nevertheless, in future studies it may be feasible to investigate force generation of individual cardiomyocytes in larger preparations of HCM-patient's cardiac tissue.

Cellular adaptations to different forces may also occur *via* phosphorylation of regulatory proteins, such as cTnI, cMyBP-C or the regulatory myosin light chain. However, these mechanisms mostly act globally on all cells, whereas bursts will lead to diverse force levels among cardiomyocytes, which also change over time, as shown by our mathematical model. This would require constant and specific adaptations of phosphorylation for each cell to counteract the altered function, which seems unlikely. In addition, for HCM-mutation cTnI<sub>R145W</sub> it was shown that it may induce a structural state of cTnI similar to PKC induced phosphorylation of cTnI at threonine 143 (48), which may contribute to inadequate adaptations to altered force generation. On the other hand, differential phosphorylation among cardiomyocytes could also cause heterogeneity in force generation. Analysis of both, adaption to differential forces by phosphorylation and differential phosphorylation as cause of heterogeneity would require single cell analysis of protein phosphorylation, which is not possible to date. To minimize potential influences of differential phosphorylation in individual cells on our measurements, we adjusted phosphorylation in all cardiomyocytes by treatment with PP1- $\alpha$  and PKA. Thus, the detected heterogeneity is most likely not due to differential phosphorylation, however we cannot exclude possible effects of other kinases such as PKC on sarcomeric proteins.

## Conclusion

We addressed the question whether sarcomeric proteins cMyBP-C and cTnI are transcribed burst-like, and how this may affect expression of mutated and WT-proteins as well as function of HCM-patient's cardiomyocytes. Alterations of the force generating mechanism in cardiomyocytes due to the respective HCM-mutation are the primary cause of the disease. Yet, transcription is stochastic, independent bursts of each allele at least for the sarcomeric proteins we studied so far (*TNNI3*, *MYBPC3* and *MYH7*) most likely is the cause of the observed contractile imbalance

among cardiomyocytes. This over time may well contribute substantially to development of cardiomyocyte disarray, fibrosis and hypertrophy and thus exacerbate disease phenotype. Our current study provides evidence that functional heterogeneity among patient cardiomyocytes occurs irrespective whether the direct effect of the mutation is calcium-sensitization or calcium-desensitization. Thus, it seems likely that also alteration of other parameters of cardiac contraction such as shortening velocity or relaxation lead to contractile imbalance. Since three of the most commonly affected genes in HCM are transcribed in bursts, it is quite likely that transcriptional bursting will occur for other HCM-genes as well and promote development of hallmarks of HCM.

## Data availability statement

The original contributions presented in the study are included in the article/[Supplementary material](#), further inquiries can be directed to the corresponding authors.

## Ethics statement

The studies involving human participants were reviewed and approved by Ethikkommission der Medizinischen Hochschule Hannover. Written informed consent to participate in this study was provided by the participants' legal guardian/next of kin.

## Author contributions

TK and JM designed the research. VB, KK, DA-N, JB, DE, TH, AR, BP, and AZ performed the research. DH-K, CR, and JV contributed patient or donor tissue. VB, JM, and TK wrote the paper. All authors contributed to the article and approved the submitted version.

## Funding

This work was supported by the Deutsche Forschungsgemeinschaft [grant number KR1187/22-1 to TK] and the European Research Area Network on Cardiovascular Disease [grant "SCALE", BMBF Number 01KL2007 to JM].

## Acknowledgments

The authors thank Torsten Beier, and Alexander Lingk, Molecular and Cell Physiology, Hannover Medical School, for excellent technical assistance and Britta Keyser, formerly Department of Human Genetics, Hannover Medical School for sequence analysis of HCM-genes in patients and donors.



## Conflict of interest

The authors declare that the research was conducted in the absence of any commercial or financial relationships that could be construed as a potential conflict of interest.

## Publisher's note

All claims expressed in this article are solely those of the authors and do not necessarily represent those of their affiliated

organizations, or those of the publisher, the editors and the reviewers. Any product that may be evaluated in this article, or claim that may be made by its manufacturer, is not guaranteed or endorsed by the publisher.

## Supplementary material

The Supplementary Material for this article can be found online at: <https://www.frontiersin.org/articles/10.3389/fcvm.2022.987889/full#supplementary-material>

## References

- Borel C, Ferreira PG, Santoni F, Delaneau O, Fort A, Popadin KY, et al. Biased allelic expression in human primary fibroblast single cells. *Am J Hum Genet.* (2015) 96:70–80. doi: 10.1016/j.ajhg.2014.12.001
- Jiang Y, Zhang NR, Li M. SCALE: Modeling allele-specific gene expression by single-cell RNA sequencing. *Genome Biol.* (2017) 18:1–15. doi: 10.1186/s13059-017-1200-8
- Rodriguez J, Larson DR. Transcription in living cells: molecular mechanisms of bursting. *Annu Rev Biochem.* (2020) 89:189–212. doi: 10.1146/annurev-biochem-011520-105250
- Suter DM, Molina N, Gatfield D, Schneider K, Schibler U, Naef F. Mammalian genes are transcribed with widely different bursting kinetics. *Science.* (2011) 332:472–4. doi: 10.1126/science.1198817
- Levesque MJ, Ginart P, Wei Y, Raj A. Visualizing SNVs to quantify allele-specific expression in single cells. *Nat Methods.* (2013) 10:865–7. doi: 10.1038/nmeth.2589
- Sun M, Zhang J. Allele-specific single-cell RNA sequencing reveals different architectures of intrinsic and extrinsic gene expression noises. *Nucleic Acids Res.* (2020) 48:533–47. doi: 10.1093/nar/gkz1134
- Deng Q, Ramsköld D, Reinius B, Sandberg R. Single-Cell RNA-Seq reveals dynamic, random monoallelic gene expression in mammalian cells. *Science.* (2014) 334:193–6. doi: 10.1126/science.1245316
- Maron BJ, Gardin JM, Flack JM, Gidding SS, Kurosaki TT, Bild DE. Prevalence of hypertrophic cardiomyopathy in a general population of young adults. *Circulation.* (1995) 92:785–9. doi: 10.1161/01.CIR.92.4.785
- Semsarian C, Ingles J, Maron MS, Maron BJ. New perspectives on the prevalence of hypertrophic cardiomyopathy. *J Am Coll Cardiol.* (2015) 65:1249–54. doi: 10.1016/j.jacc.2015.01.019
- Elliot P, McKenna WJ. Hypertrophic cardiomyopathy. *Lancet.* (2004) 363:1881–91. doi: 10.1016/S0140-6736(04)16358-7
- Walsh R, Buchan R, Wilk A, John S, Felkin LE, Thomson KL, et al. Defining the genetic architecture of hypertrophic cardiomyopathy: re-evaluating the role of non-sarcomeric genes. *Eur Heart J.* (2017) 38:3461–8. doi: 10.1093/eurheartj/ehw603
- Marian AJ, Braunwald E. Hypertrophic cardiomyopathy genetics, pathogenesis, clinical manifestations, diagnosis, and therapy. *Circ Res.* (2017) 121:749–70. doi: 10.1161/CIRCRESAHA.117.311059
- Glazier AA, Thompson A, Day SM. Allelic imbalance and haploinsufficiency in MYBPC3-linked hypertrophic cardiomyopathy. *Pflugers Arch.* (2019) 471:781–93. doi: 10.1007/s00424-018-2226-9
- Saber W, Begin KJ, Warshaw DM, VanBuren P. Cardiac myosin binding protein-C modulates actomyosin binding and kinetics in the in vitro motility assay. *J Mol Cell Cardiol.* (2008) 44:1053–61. doi: 10.1016/j.yjmcc.2008.03.012
- Kraft T, Witjas-Paalberends ER, Boontje NM, Tripathi S, Brandis A, Montag J, et al. Familial hypertrophic cardiomyopathy: functional effects of myosin mutation R723G in cardiomyocytes. *J Mol Cell Cardiol.* (2013) 57:13–22. doi: 10.1016/j.yjmcc.2013.01.001
- Brenner B, Seeböhm B, Tripathi S, Montag J, Kraft T. Familial hypertrophic cardiomyopathy: functional variance among individual cardiomyocytes as a trigger of FHC-phenotype development. *Front Physiol.* (2014) 5:392. doi: 10.3389/fphys.2014.00392
- Montag J, Kowalski K, Makul M, Ernstberger P, Radocaj A, Beck J, et al. Burst-like transcription of mutant and wildtype MYH7-alleles as possible origin of cell-to-cell contractile imbalance in hypertrophic cardiomyopathy. *Front Physiol.* (2018) 9:359. doi: 10.3389/fphys.2018.00359
- van Dijk SJ, Paalberends ER, Najafi A, Michels M, Sadayappan S, Carrier L, et al. Contractile dysfunction irrespective of the mutant protein in human hypertrophic cardiomyopathy with normal systolic function. *Circ Heart Fail.* (2012) 5:36–46. doi: 10.1161/CIRCHEARTFAILURE.111.963702
- Sequeira V, Wijnker PJM, Nijenkamp LLAM, Kuster DWD, Najafi A, Witjas-Paalberends ER, et al. Perturbed length-dependent activation in human hypertrophic cardiomyopathy with missense sarcomeric gene mutations. *Circ Res.* (2013) 112:1491–505. doi: 10.1161/CIRCRESAHA.111.300436
- WMA. World medical association declaration of Helsinki. *JAMA* (1997) 277:925–926. doi: 10.1001/jama.1997.03540350075038.
- dos Remedios CG, Li A, Lal S. Non-sarcomeric causes of heart failure: a Sydney Heart Bank perspective. *Biophys Rev.* (2018) 10:949–54. doi: 10.1007/s12551-018-0441-4
- Raj A, Peskin CS, Tranchina D, Vargas DY, Tyagi S. Stochastic mRNA synthesis in mammalian cells. *PLoS Biol.* (2006) 4:1707–19. doi: 10.1371/journal.pbio.0040309
- Zhurinsky J, Leonhard K, Watt S, Marguerat S, Bähler J, Nurse P, et al. A coordinated global control over cellular transcription. *Curr Biol.* (2010) 20:2010–5. doi: 10.1016/j.cub.2010.10.002
- Yekelchik M, Guenther S, Preussner J, Braun T. Mono- and multi-nucleated ventricular cardiomyocytes constitute a transcriptionally homogenous cell population. *Basic Res Cardiol.* (2019) 114:1–13. doi: 10.1007/s00395-019-0744-z
- Flashman E, Redwood C, Moolman-Smook J, Watkins H. Cardiac myosin binding protein C: its role in physiology and disease. *Circ Res.* (2004) 94:1279–89. doi: 10.1161/01.RES.0000127175.21818.C2
- Witjas-Paalberends ER, Piroddi N, Stam K, van Dijk SJ, Sequeira Oliviera V, Ferrara C, et al. Mutations in MYH7 reduce the force generating capacity of sarcomeres in human familial hypertrophic cardiomyopathy. *Cardiovasc Res.* (2013) 99:432–41. doi: 10.1093/cvr/cvt119
- Symmons O, Chang M, Mellis IA, Kalish JM, Park J, Suszták K, et al. Allele-specific RNA imaging shows that allelic imbalances can arise in tissues through transcriptional bursting. *PLoS Genet.* (2019) 15:e1007874. doi: 10.1371/journal.pgen.1007874
- Kraft T, Montag J, Radocaj A, Brenner B. Hypertrophic cardiomyopathy: cell-to-cell imbalance in gene expression and contraction force as trigger for disease phenotype development. *Circ Res.* (2016) 119:992–5. doi: 10.1161/CIRCRESAHA.116.309804
- Urban EA, Johnston RJ. Buffering and amplifying transcriptional noise during cell fate specification. *Front Genet.* (2018) 9:1–14. doi: 10.3389/fgene.2018.00591
- Litvinuková M, Talavera-López C, Maatz H, Reichart D, Worth CL, Lindberg EL, et al. Cells of the adult human heart. *Nature.* (2020) 588:466–72. doi: 10.1038/s41586-020-2797-4

31. The Tabula Muris Consortium, Overall coordination Schaum Nicholas, Karkanas Jim, Neff Norma F, May Andrew P. Single-cell transcriptomics of 20 mouse organs creates a Tabula Muris. *Nature*. (2018) 562:367–372. doi: 10.1038/s41586-018-0590-4
32. Parbhudayal RY, Garra AR, Götte MJW, Michels M, Pei J, Harakalova M, et al. Variable cardiac myosin binding protein-C expression in the myofilaments due to MYBPC3 mutations in hypertrophic cardiomyopathy. *J Mol Cell Cardiol*. (2018) 123:59–63. doi: 10.1016/j.jmcc.2018.08.023
33. Theis JL, Bos JM, Theis JD, Miller D V, Dearani JA, Schaff H V, et al. Expression patterns of cardiac myofilament proteins. *Circ Hear Fail*. (2009) 2:325–33. doi: 10.1161/CIRCHEARTFAILURE.108.789735
34. Helms AS, Davis F, Coleman D, Bartolone S, Glazier AA, Pagani F, et al. Sarcomere mutation-specific expression patterns in human hypertrophic cardiomyopathy. *Circ Cardiovasc Genet*. (2014) 7:434–43. doi: 10.1161/CIRCGENETICS.113.000448
35. Lewis YE, Moskovitz A, Mutlak M, Heineke J, Caspi LH, Kehat I. Localization of transcripts, translation, and degradation for spatiotemporal sarcomere maintenance. *J Mol Cell Cardiol*. (2018) 116:16–28. doi: 10.1016/j.jmcc.2018.01.012
36. Montag J, Kraft T. Stochastic allelic expression as trigger for contractile imbalance in hypertrophic cardiomyopathy. *Biophys Rev*. (2020) 12:1055–64. doi: 10.1007/s12551-020-00719-z
37. Pavlath GK, Rich K, Webster SG, Blau HM. Localization of muscle gene products in nuclear domains. *Nature*. (1989) 337:570–3. doi: 10.1038/337570a0
38. van Dijk SJ, Dooijes D, Remedios C, Michels M, Lamers MJM, Winegrad S, et al. Cardiac myosin-binding protein C mutations and hypertrophic cardiomyopathy. *Circulation*. (2009) 119:1473–84. doi: 10.1161/CIRCULATIONAHA.108.838672
39. van Wamel AJET, Ruwhof C, Van Der Valk-Kokshoorn LEJM, Schriern PI, Van Der Laarse A. The role of angiotensin II, endothelin-1 and transforming growth factor- $\beta$  as autocrine/paracrine mediators of stretch-induced cardiomyocyte hypertrophy. *Mol Cell Biochem*. (2001) 218:113–24. doi: 10.1023/A:1007279700705
40. Ruwhof C, van Wamel AET, Egas JM, Van Der Laarse A. Cyclic stretch induces the release of growth promoting factors from cultured neonatal cardiomyocytes and cardiac fibroblasts. *Mol Cell Biochem*. (2000) 208:89–98. doi: 10.1023/A:1007046105745
41. Teekakirikul P, Eminaga S, Toka O, Alcalai R, Wang L, Wakimoto H, et al. Cardiac fibrosis in mice with hypertrophic cardiomyopathy is mediated by non-myocyte proliferation and requires Tgf- $\beta$ . *J Clin Invest*. (2010) 120:3520–9. doi: 10.1172/JCI42028
42. Tanjore R, RangaRaju A, Vadapalli S, Remersu S, Narsimhan C, Nallari P. Genetic variations of  $\beta$ -MYH7 in hypertrophic cardiomyopathy and dilated cardiomyopathy. *Indian J Hum Genet*. (2010) 16:67–71. doi: 10.4103/0971-6866.69348
43. Finocchiaro G, Magavern E, Sinagra G, Ashley E, Papadakis M, Tome-Esteban M, et al. Impact of demographic features, lifestyle, and comorbidities on the clinical expression of hypertrophic cardiomyopathy. *J Am Heart Assoc*. (2017) 6:1–11. doi: 10.1161/JAHA.117.007161
44. Perkins MJ, Van Driest SL, Ellsworth EG, Will ML, Gersh BJ, Ommen SR, et al. Gene-specific modifying effects of pro-LVH polymorphisms involving the renin-angiotensin-aldosterone system among 389 unrelated patients with hypertrophic cardiomyopathy. *Eur Heart J*. (2005) 26:2457–62. doi: 10.1093/eurheartj/ehi438
45. Hwang JW, Jang MA, Jang SY, Seo SH, Seong MW, Park SS, et al. Diverse phenotypic expression of cardiomyopathies in a family with TNNI3 pArg145Trp mutation. *Korean Circ J*. (2017) 47:270–7. doi: 10.4070/kcj.2016.0213
46. Pitoulis FG, Hasan W, Papadaki M, Clavere NG, Perbellini F, Harding SE, et al. Intact myocardial preparations reveal intrinsic transmural heterogeneity in cardiac mechanics. *J Mol Cell Cardiol*. (2020) 141:11–6. doi: 10.1016/j.jmcc.2020.03.007
47. Mamidi R, Gresham KS, Stelzer JE. Length-dependent changes in contractile dynamics are blunted due to cardiac myosin binding protein-C ablation. *Front Physiol*. (2014) 5:1–11. doi: 10.3389/fphys.2014.00461
48. Dvornikov A V, Smolin N, Zhang M, Martin JL, Robia SL, de Tombe PP. Restrictive cardiomyopathy Troponin-I R145W mutation does not perturb myofilament length dependent activation in human cardiac sarcomeres. *J Biol Chem*. (2016) 291:21817–28. doi: 10.1074/jbc.M116.746172





## OPEN ACCESS

## EDITED BY

Amy Li,  
La Trobe University, Australia

## REVIEWED BY

James Todd Pearson,  
National Cerebral and Cardiovascular  
Center, Japan  
Yunhui Du,  
Capital Medical University, China

## \*CORRESPONDENCE

Jia-Yi Tong  
101007925@seu.edu.cn

<sup>†</sup>These authors have contributed  
equally to this work

## SPECIALTY SECTION

This article was submitted to  
Heart Failure and Transplantation,  
a section of the journal  
Frontiers in Cardiovascular Medicine

RECEIVED 21 June 2022

ACCEPTED 19 August 2022

PUBLISHED 12 September 2022

## CITATION

Xu X, Zhen P-H, Yu F-C, Wang T,  
Li S-N, Wei Q and Tong J-Y (2022)  
Chronic intermittent hypoxia  
accelerates cardiac dysfunction and  
cardiac remodeling during cardiac  
pressure overload in mice and can be  
alleviated by PHD3 overexpression.  
*Front. Cardiovasc. Med.* 9:974345.  
doi: 10.3389/fcvm.2022.974345

## COPYRIGHT

© 2022 Xu, Zhen, Yu, Wang, Li, Wei  
and Tong. This is an open-access  
article distributed under the terms of  
the [Creative Commons Attribution  
License \(CC BY\)](#). The use, distribution  
or reproduction in other forums is  
permitted, provided the original  
author(s) and the copyright owner(s)  
are credited and that the original  
publication in this journal is cited, in  
accordance with accepted academic  
practice. No use, distribution or  
reproduction is permitted which does  
not comply with these terms.

# Chronic intermittent hypoxia accelerates cardiac dysfunction and cardiac remodeling during cardiac pressure overload in mice and can be alleviated by PHD3 overexpression

Xuan Xu<sup>1,2†</sup>, Peng-Hao Zhen<sup>2†</sup>, Fu-Chao Yu<sup>1</sup>, Tao Wang<sup>2</sup>,  
Sheng-Nan Li<sup>2</sup>, Qin Wei<sup>1</sup> and Jia-Yi Tong<sup>1\*</sup>

<sup>1</sup>Department of Cardiology, Zhongda Hospital, Southeast University, Nanjing, China, <sup>2</sup>Medical School of Southeast University, Nanjing, China

Obstructive sleep apnea (OSA) accelerates the progression of chronic heart failure (CHF). OSA is characterized by chronic intermittent hypoxia (CIH), and CIH exposure accelerates cardiac systolic dysfunction and cardiac remodeling in a cardiac afterload stress mouse model. Mechanistic experiments showed that long-term CIH exposure activated hypoxia-inducible factor 1 $\alpha$  (HIF-1 $\alpha$ ) expression in the mouse heart and upregulated miR-29c expression and that both HIF-1 $\alpha$  and miR-29c simultaneously inhibited sarco-/endoplasmic reticulum calcium ATPase 2a (SERCA2a) expression in the mouse heart. Cardiac HIF-1 $\alpha$  activation promoted cardiomyocyte hypertrophy. SERCA2a expression was suppressed in mouse heart in middle- and late-stage cardiac afterload stress, and CIH exposure further downregulated SERCA2a expression and accelerated cardiac systolic dysfunction. Prolyl hydroxylases (PHDs) are physiological inhibitors of HIF-1 $\alpha$ , and PHD3 is most highly expressed in the heart. Overexpression of PHD3 inhibited CIH-induced HIF-1 $\alpha$  activation in the mouse heart while decreasing miR-29c expression, stabilizing the level of SERCA2a. Although PHD3 overexpression did not reduce mortality in mice, it alleviated cardiac systolic dysfunction and cardiac remodeling induced by CIH exposure.

## KEYWORDS

chronic intermittent hypoxia, cardiac dysfunction, cardiac remodeling, SERCA2a, HIF-1 $\alpha$

## Introduction

Obstructive sleep apnea (OSA) is a sleep disorder resulting from disordered breathing, and its hallmark feature is chronic intermittent hypoxia (CIH) during sleep (1). OSA is an independent risk factor for serious cardiovascular events and is involved in the occurrence and development of events such as hypertension, myocardial

infarction, congestive heart failure and stroke (2). In addition, OSA is associated with adverse cardiac outcomes of chronic heart failure (CHF). According to reports, 20% of symptomatic CHF patients have OSA (3, 4). Notably, large prospective cohort studies have demonstrated an increased incidence of HF in patients with severe OSA (5). Much evidence suggests that the pathophysiological effects of OSA in heart failure (HF) are mediated by multiple mechanisms, including neurohormonal activation, oxidative stress, and inflammation. These effects can accelerate the progression of HF and of symptoms associated with it (6). In animal models, CIH exposure for 5 weeks was shown to increase the heart/body weight ratio, increase the left ventricle (LV)/total heart weight ratio and decrease left ventricular function in SD rats (7). C57BL/6 mice had increased left ventricular perivascular fibrosis after 6 weeks of CIH exposure (8).

Continuous positive airway pressure (CPAP) therapy is currently the main treatment used for sleep apnea. In 2017, the American Heart Association/American College of Cardiology gave CPAP strategies a class IIb recommendation for people with HF and OSA (9). However, meta-analyses have shown that CPAP therapy does not significantly improve the left ventricular ejection fraction (LVEF), number of hospitalizations for HF events, or all-cause mortality in patients with or without HF (10). Furthermore, CPAP therapy appears to be only partially effective in patients with HF and does not reduce the incidence of cardiovascular events in patients with OSA and HF (11). In addition to the limited treatment effect, the poor long-term compliance of patients with CPAP therapy, which is only 40%–80%, is a limitation of this treatment modality (12). CPAP therapy is indeed an effective treatment for OSA, but effective combination therapy therapies are still needed to improve the adverse cardiac consequences of OSA.

Hypoxia-inducible factor 1 (HIF-1) is a transcription factor that consists of two subunits: HIF-1 $\alpha$ , whose expression is regulated by O<sub>2</sub>, and HIF-1 $\beta$ , which is constitutively expressed (13). Clinical studies have shown that the expression of HIF-1 is upregulated in the organs, tissues, and circulating blood of OSA patients (14, 15). In an animal model of cardiac pressure overload, the long-term elevation of cardiac-specific HIF-1 $\alpha$  expression was found to accelerate the impairment of cardiac function (16). In a cardiomyocyte hypertrophy model, HIF-1 $\alpha$  transcriptional activation was shown to promote the cardiomyocyte hypertrophy induced by Ang II (17, 18). Ang II or transverse aortic constriction (TAC) surgery-induced cardiac pressure overload in animals can lead to HF. Oxygen-derived radicals, especially superoxide anion, produced during CIH lead to HIF-1 $\alpha$  upregulation and its long-term high expression in cardiac tissue (19, 20). We therefore speculate that CIH exposure could accelerate cardiac pressure overload-induced HF and that HIF-1 $\alpha$  may be a new therapeutic target.

Our previous study showed that HIF-1 $\alpha$  upregulation during intermittent hypoxia induces endothelial cell

mesenchymalization and thus increases cardiac fibrosis and cardiac dysfunction (21). To alleviate the effects of HIF-1 $\alpha$ , we overexpressed PHD3, which is a physiological inhibitor of HIF-1 $\alpha$  that is abundantly expressed in the heart (22). We found that inhibition of HIF-1 $\alpha$  by overexpression of PHD3 reduced endothelial mesenchymalization and improved fibrosis and systolic function. However, the study was limited to endothelial cells and did not involve cardiomyocytes. Notably, PHD3 was also overexpressed in cardiomyocytes in the study, and cardiomyocytes had a greater effect on myocardial contractile function. Therefore, we wanted to further explore whether the overexpression of PHD3 in cardiomyocytes can mitigate the adverse cardiac effects of CIH.

In the present study, we investigated the mechanisms underlying the CIH acceleration of cardiac injury in TAC mice and the involvement of HIF-1 $\alpha$  in this pathology. We explored the molecular basis associated with HIF-1 $\alpha$  function and the possible therapeutic role of PHD3.

## Methods

### Animals

A total of 351 10-week-old male C57BL/6 mice were purchased from the Animal Experimental Middle School of Southeast University. For details on the experimental procedures and groups, please refer to [Supplementary Figures 1, 2](#). All animal experiments were carried out in accordance with the guidelines for the care and use of laboratory animals formulated by the Animal Care and Use Committee of Southeast University School of Medicine. The TAC and CIH exposure protocols were approved by the Animal Experiment Ethics Committee of Southeast University School of Medicine. The afterload stress mouse model was established as reported (23). In short, mice were anesthetized with isoflurane (3% isoflurane for induction, 2% isoflurane for maintenance). The aorta was ligated with a bent 26-G needle and a 6–0 silk suture between the origin of the right innominate and left common carotid arteries, and then the needle was removed to induce narrowing of the blood vessel. Buprenorphine (0.01 mg/kg) was given subcutaneously for postoperative analgesia. The mouse was kept warm until it recovered from the anesthesia. CIH exposure was performed as described (21). Mice were placed in a plexiglass container (48\*33\*23 cm, 5 mice in each container) with a constant temperature of 22–24°C. Nitrogen was introduced to reduce the oxygen concentration in the container to 4–5% within 8 s, and it was kept there for 12 s. Then air was introduced to restore the oxygen concentration to 21% within 40 s. This made for a 60-s cycle. The mice were exposed to this intermittent hypoxia treatment for 8 h/day during the 12-h dark period. CIH animals were kept in a normoxic environment during the 12-h light

period. When investigating the mechanism, we divided the mice into five groups (Figure 1A): (1) Sham group: Only thoracotomy. The mice were placed in containers with free air circulation for 8 h/day for 6 weeks according to the protocol. (2) CIH group: Only thoracotomy. The protocol for CIH exposure was followed for 6 weeks. (3) TAC group: After TAC surgery, the mice were placed in containers with free air circulation for 8 h/day for 6 weeks according to the protocol. (4) TAC+CIH group: Three days after TAC surgery, CIH exposure was performed according to the protocol (a total of 6 weeks from the time of TAC surgery). (5) CIH+TAC group: The mice were first exposed to CIH for 3 days and then underwent TAC surgery. They were submitted to CIH again after surgery (a total of 6 weeks from the time of first CIH exposure). When exploring the effect of PHD3 treatment, we also divided the mice into five groups (Figure 5A): (1) TAC group: The protocol was the same as above. (2) CIH control group: CIH exposure was performed 3 days after TAC surgery, and CIH exposure was stopped after 2 weeks (a total of 6 weeks from the time of TAC surgery). The goal was to simulate cases in which OSA is cured during CHF. (3) TAC+CIH group: The protocol was the same as above. (4) Adeno-associated virus 9 (AAV9)-NC group: CIH exposure was performed 3 days after TAC surgery, followed by tail vein injection of AAV9-vehicle ( $5 \times 10^{11}$  vg) 1 week later (a total of 6 weeks from the time of TAC surgery). (5) AAV9-PHD3 group: CIH exposure was performed 3 days after TAC surgery, followed by tail vein injection of AAV9-PHD3 ( $5 \times 10^{11}$  vg; GeneChem, China) 1 week later (a total of 6 weeks from the time of TAC surgery). All mice were housed in a room with an alternating light and dark cycle at 26°C and were provided free access to food and water. Animals were euthanized using cervical dislocation according to AVMA guidelines.

## Echocardiography

The mice were anesthetized with isoflurane (0.5–4%) and fixed horizontally on the operating table at 37°C. The hair on the chest of each mouse was removed with depilatory cream, and the coupling agent was applied evenly after cleaning. The MS400 probe was placed vertically on the left side of the chest of the mouse with the notch facing the head, and then the probe was rotated 45 degrees counterclockwise. Parasternal long-axis section images of the mouse heart were obtained by the small animal ultrasound imaging system (Vevo 2100, Canada). The left ventricular end-diastolic diameter (LVDd) and the left ventricular end-systolic diameter (LVDs) were measured, and the left ventricular ejection fraction (LVEF) and left ventricular fraction shortening (LVFS) were automatically calculated. Each value was measured over six consecutive cardiac cycles and averaged.

## Luciferase reporter assay

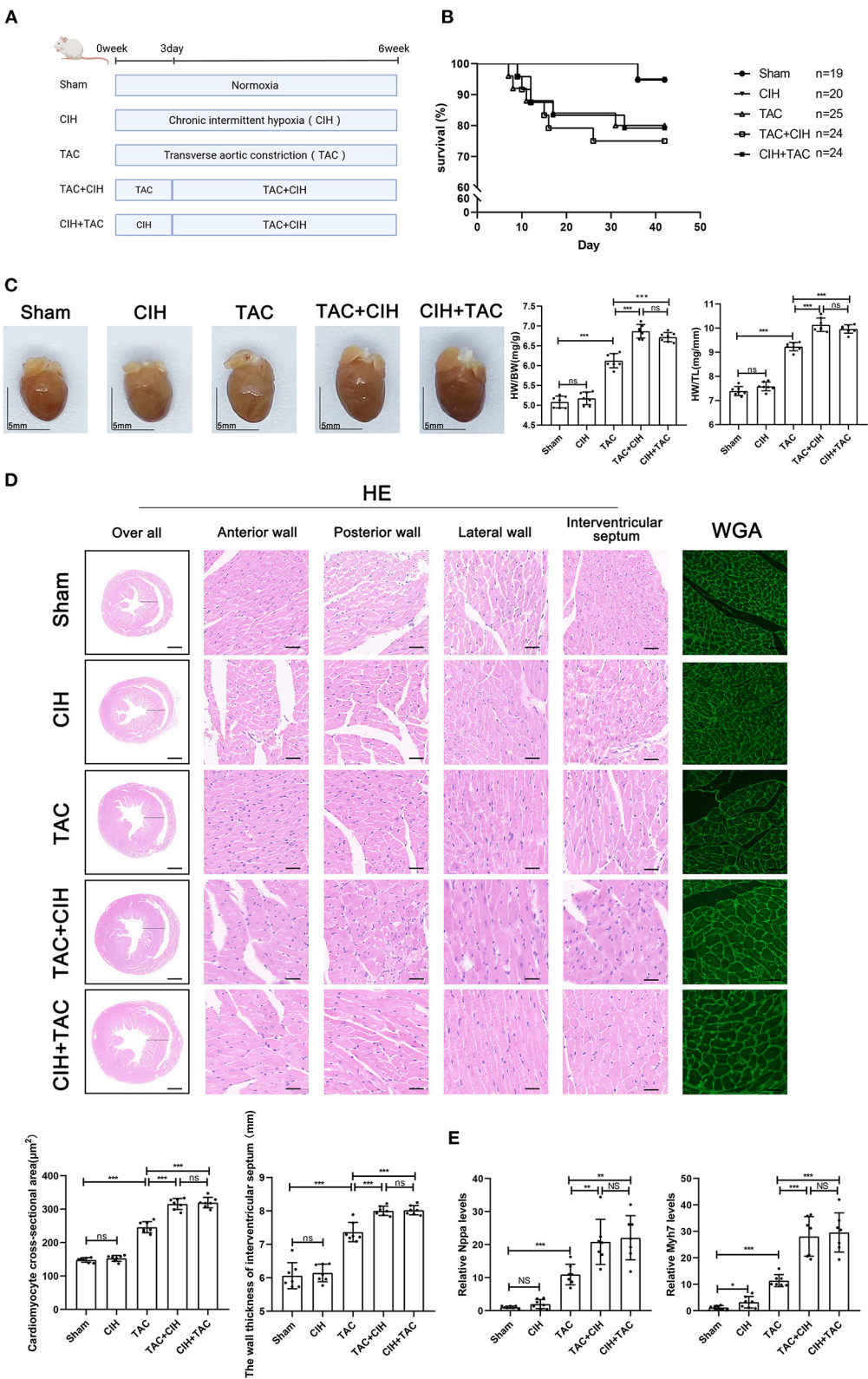
We performed a luciferase reporter gene experiment in HEK293T cells to verify miRNA targets and conserved sites bound by miR-29c. We cloned the total length of the 3'UTR of mouse SERCA2a into the pmir-RB-Report™ vector to generate a SERCA2a wild-type plasmid (SERCA2a-WT) (GenePharma, China) and constructed a mutant plasmid (SERCA2a-MUT) (GenePharma, China). Vectors containing SERCA2a-WT or SERCA2a-MUT were cotransfected into HEK293T cells with miR-29c mimic or NC mimic. Vectors were transfected using Lipofectamine 3000 reagent (Invitrogen, USA). The cells were harvested 48 h after transfection, and luciferase activity was measured using a dual-luciferase assay system (Promega, USA). Regarding the relationship between SERCA2a and HIF-1 $\alpha$ , we constructed the pGL3-SERCA2a (GenePharma, China) promoter plasmid as previously described (24). The empty cloning vector pGL3-Basic was used as a control. The vector was transfected into HL-1 cells using Lipofectamine 3000 reagent (Invitrogen, USA). Luciferase assays were performed 48 h after transfection.

## Cell culture and treatments

HL-1 cells and HEK293 T cells were kindly donated from Dr. Ma Bo. Cells were cultured in high-glucose Dulbecco's modified Eagle medium (Gibco, USA) and HL-1 cells were cultured in Claycomb medium (Sigma, USA). HL-1 cells were exposed to 0.6  $\mu$ M Ang II for up to 72 h to establish a hypertrophy model concurrent with CIH exposure. Cellular CIH exposure was performed using a special intermittent cell hypoxia box (PUHE Biotechnology Company LTD, China). The cells were cultured in a humidified 5% CO<sub>2</sub> incubator at 37°C. Cells were treated with CIH for 72 h (air phase set point consisting of 35 min of hypoxia followed by 25 min of reoxygenation [21% O<sub>2</sub> and 5% CO<sub>2</sub>]). HL-1 cells were transfected with LV-PHD3 and LV-NC lentivirus vectors (GenePharma, China) following the manufacturer's instructions. The HIF-1 $\alpha$ -PPN plasmid (GenePharma, China) was constructed according to a previously described method for cell transfection to achieve overexpression of HIF-1 $\alpha$  under normoxia (25). For miRNA transfection, according to the manufacturer's instructions, the miR-29c inhibitor, miR-29c mimic and respective negative controls were transfected into cells with Lipofectamine 3000 reagent (Invitrogen, USA).

## Real-time PCR

mRNA expression analysis: Total RNA was isolated from mouse left ventricular tissue using the RNeasy Mini Kit (Qiagen) according to the manufacturer's instructions. cDNA was then



**FIGURE 1**  
CIH exposure does not affect basal mortality rates after TAC but promotes cardiomyocyte hypertrophy. **(A)** Grouping and experimental protocols for each group. Sham: thoracotomy only without transverse aortic constriction surgery, followed by 6 weeks in normoxia; CIH: thoracotomy only without transverse aortic constriction surgery, followed by 6 weeks in CIH exposure; TAC: transverse aortic constriction surgery, followed by 6 weeks in normoxia; TAC+CIH: transverse aortic constriction surgery, followed by 3 days in CIH exposure and then 6 weeks in normoxia; CIH+TAC: CIH exposure for 3 days, followed by transverse aortic constriction surgery and then 6 weeks in normoxia. *(Continued)*



**FIGURE 1 (Continued)**

surgery, followed by normoxia for 6 weeks; TAC+CIH: CIH exposure was performed 3 days after transverse aortic constriction surgery for a total of 6 weeks. CIH+TAC: transverse aortic constriction surgery was performed 3 days after CIH exposure and CIH exposure was continued for 6 weeks thereafter. **(B)** Survival rates of all groups; the sample size of each group is noted in the figure. **(C)** Left: representative images of hearts; right: quantification of the heart weight-to-body weight ratio and heart weight-to-tibia length ratio.  $n = 7$ ; scale bar = 5 mm;  $***p < 0.001$ . **(D)** HE staining and WGA staining of mouse hearts. The wall thickness of interventricular septum was measured according to HE staining pictures. The cardiomyocyte cross-sectional area was quantified according to WGA staining.  $n = 7$ ; scale bar = 1 mm and 25  $\mu\text{m}$ ;  $***p < 0.001$ . **(E)** Real-time PCR analysis of relative Nppa and Myh7 levels in heart tissue at week 6.  $n = 7$ ;  $*p < 0.05$ ,  $**p < 0.01$ ,  $***p < 0.001$ .

prepared by using the Omniscript RT Kit (Qiagen, USA). qRT-PCR was performed using SYBR Green (miScript SYBR Green PCR Kit, Qiagen, USA) and the Mx3000p Real-time PCR system (Agilent). The expression of the target genes was normalized to GAPDH gene expression levels. miRNA expression analysis: miRNA was extracted from left ventricular tissue and HL-1 cells using the miRNeasy Mini Kit (Qiagen, USA) and then reverse-transcribed with the miScript II RT Kit (Qiagen, USA) using miScript HiSpec buffer. qRT-PCR was performed using SYBR Green (miScript SYBR Green PCR Kit, Qiagen, USA) and the Mx3000p Real-time PCR system (Agilent). U6 was used as the reference gene. Each sample was processed in triplicate. All data were analyzed for relative expression using the  $2^{-\Delta\Delta C_t}$  method. The primers used in our experiments are provided in [Supplementary Table 1](#).

## Western blot

Protein was extracted from frozen left ventricular tissue and HL-1 cells using standard RIPA buffer. HL-1 nuclear protein extraction, using a nuclear isolation kit (P0027, Beyotime, China) according to the manufacturer's instructions, was used to determine HIF-1 $\alpha$  protein expression. The protein concentration was determined with a BCA protein assay kit (P0012, Beyotime, China). The samples were electrophoresed on 10% SDS-PAGE gels (Gsebio) and then transferred to PVDF membranes (Immobilon). After the membranes were blocked with 5% skim milk at room temperature for 2 h, they were incubated with HIF-1 $\alpha$  (1:1000, ab179483, Abcam, USA), sarco-/endoplasmic reticulum calcium ATPase 2a (SERCA2a) expression (SERCA2a) (1:1000, ab150435, Abcam, USA), prolyl 4-hydroxylase domain protein 3 (PHD3) (1:1000, A8001, ABclonal, China), and GAPDH (1:10000, db106, DiDiBio, China) primary antibodies overnight at 4°C. The membranes were washed three times with TBST and incubated with secondary antibody for 2 h. Finally, the blots were scanned using the LI-COR Odyssey imaging system, and ImageJ software was used for quantification.

## Histological staining

Mouse hearts were removed at the appropriate time point and then fixed with 4% polyformaldehyde. Finally, the hearts

were embedded in paraffin and cut into 5  $\mu\text{m}$  sections for hematoxylin and eosin (HE), wheat germ agglutinin (WGA), and Masson staining. HE staining: Sections were stained with Harris hematoxylin for 5 min and washed with 0.6% ammonia in water to return the color of the staining to blue; they were then washed again, stained with eosin for 3 min, and finally mounted and observed with a fluorescence microscope. WGA staining: The sections were stained with WGA, incubated at 37°C for 30 min in a dark incubator and observed under a fluorescence microscope. Images of the stained left ventricle and interventricular septum were obtained under a 40x microscope. The cross-sectional area of all cardiomyocytes was then quantitatively analyzed by the Image-Pro Plus 4.0 image analysis system, and the average value was obtained. Masson staining: Sections were stained with Masson's staining solution for 5 min, washed and counterstained with aniline blue solution for 5 min, mounted and observed under a fluorescence microscope. The fibrotic area was calculated by Image-Pro Plus 4.0. Phalloidin staining: Treated HL-1 cells were treated with Actin-Tracker Red-Rhodamine (C2207, Beyotime, China) following the manufacturer's instructions. The cell area measurement method was the same as above.

## Statistical analysis

Each experiment was performed at least three times with consistent results, and the data are presented as the mean  $\pm$  standard deviation (SD). Differences between two groups were analyzed using a two-tailed Student's *t*-test. One-way analysis of variance (ANOVA) followed by Tukey's pairwise multiple comparisons test was used to compare multiple groups. Results with *P*-values of  $< 0.05$  were considered statistically significant.

## Results

### CIH exposure promotes TAC-induced cardiomyocyte hypertrophy

To prolong the total duration of heart failure induced by TAC in mice, 26-G needles were used as surgical pad needles. We calculated the mortality rate of mice in the five groups. The mortality rate of mice that underwent TAC was significantly higher than that of mice that had not undergone TAC, and the

difference in mortality between the three groups that underwent TAC was minimal (Figure 1B). By measuring the heart weight, body weight and tibia length of mice in each group, we obtained the mouse heart/body weight and heart weight/tibia length ratios. CIH exposure for 6 weeks alone had no effect on the mouse heart/body weight or heart weight/tibia length ratio. The heart/body weight and heart weight/tibia length ratios of the mice were increased in the TAC group. The heart/body weight and heart weight/tibia length ratios of mice were further increased in the TAC+CIH and CIH+TAC groups, but there was no difference between these two groups (Figure 1C). HE and WGA staining results showed that TAC induced hypertrophy of mouse cardiomyocytes. The cardiomyocyte hypertrophy was further aggravated in the TAC+CIH and CIH+TAC groups, with no significant difference in the level of cardiomyocyte hypertrophy between these two groups (Figure 1D). In addition, the thickness of the interventricular septal wall measured in the cross-section of the heart (Figure 1D) and the expression of cardiac pro-hypertrophy genes (*Nppa* and *Myh7*) (Figure 1E) confirmed the above results. In summary, CIH exposure before or after TAC accelerates TAC-induced cardiomyocyte hypertrophy in mice.

### CIH exposure accelerates TAC-induced left cardiac fibrosis and ventricular systolic dysfunction

Cardiac fibrosis can lead to cardiac dysfunction in mice. By Masson staining, we found that the CIH group exhibited higher levels of cardiac fibrosis than the sham group (Figure 2A). Cardiac fibrosis was significantly worse in mice that underwent both CIH and TAC than in mice that underwent only TAC (Figure 2A). We determined the expression levels of cardiac fibrosis-related genes (*Col1a1* and *Col3a1*) by qPCR, and the results were similar to those observed in the cardiac fibrosis phenotype (Figure 2B). We also performed echocardiography on mice from all groups in the third and sixth weeks. In the third week, the echocardiography data showed that the LVEF and FS in the TAC+CIH and CIH+TAC groups were lower than those in the TAC group (Figure 2C). There was no difference in echocardiography data between the CIH group and the sham group (Figure 2C). In the sixth week, a greater decrease in LVEF and FS was observed in the TAC+CIH and CIH+TAC groups than in the TAC group. There was no significant difference in mouse echocardiography data between the group exposed to CIH first and the group subjected to TAC first (Figure 2C). The LVEF and FS were slightly decreased in the CIH group, but the difference was not significant (Figure 2C). In general, CIH exposure accelerated TAC-induced left ventricular systolic dysfunction, and whether the mice were exposed to CIH first or underwent TAC first had no significant effect on the results.

### CIH exposure induces long-term elevation of HIF-1 $\alpha$ expression levels

It was reported that in mice subjected to TAC, the expression levels of HIF-1 $\alpha$  in the heart gradually increased within seven days after surgery, decreased after seven days, and returned to normal by 4 weeks (26). We chose to measure HIF-1 $\alpha$  levels in the hearts of mice from all groups at 3 days, 3 weeks, and 6 weeks. The Western blot results showed that both CIH exposure and TAC increased the expression levels of HIF-1 $\alpha$  in mouse hearts at 3 days (Figure 3A). Three weeks later, the expression of HIF-1 $\alpha$  in the heart was higher to varying degrees in the four groups of mice subjected to different treatments than in the sham group. The TAC+CIH and CIH+TAC groups exhibited the highest expression levels of HIF-1 $\alpha$  in the heart, but there was no significant difference in HIF-1 $\alpha$  expression between the two groups. The TAC groups had higher levels of HIF-1 $\alpha$  in the heart than the CIH group (Figure 3A). At 6 weeks, the expression level of HIF-1 $\alpha$  in the heart was still higher in the CIH group than in the sham group. The level of HIF-1 $\alpha$  in the heart was still the highest in the TAC+CIH and CIH+TAC groups, and there was no significant difference in HIF-1 $\alpha$  expression between these two groups (Figure 3A). The HIF-1 $\alpha$  level in the heart had returned to normal at 6 weeks in the TAC group, but it remained high in the TAC+CIH and CIH+TAC groups.

### Long-term elevations in HIF-1 $\alpha$ expression in the heart upregulates miR-29c expression and inhibits SERCA2a expression

The expression level of SERCA2a determines the Ca<sup>2+</sup> balance of cardiomyocytes and cardiac contractile function (27). During hypoxia, HIF-1 can bind to hypoxia response elements (HREs) in the SERCA2a promoter region in a competitive manner, thus inhibiting the transcription and expression of SERCA2a (Figure 3B) (24). In addition, high expression of HIF-1 $\alpha$  has been reported to lead to the upregulation of miR-29c expression, and miR-29c was shown to negatively regulate the expression of SERCA2a (Figure 3C) (28). We verified the existence of binding sites between SERCA2a mRNA and miR-29c by bioinformatic analysis (Figure 3C). Therefore, we measured the expression levels of SERCA2a and miR-29c in the hearts of mice from all groups after 3 days, 3 weeks, and 6 weeks. After 3 days, the SERCA2a protein and mRNA levels in the hearts of mice that underwent CIH exposure or TAC were slightly increased, but not significantly (Figures 3D,E). The four groups of mice subjected to CIH exposure or TAC exhibited a small but non-significant increase in cardiac miR-29c expression (Figure 3F). After 3 weeks, there was no significant difference in SERCA2a protein or mRNA levels in the heart between the



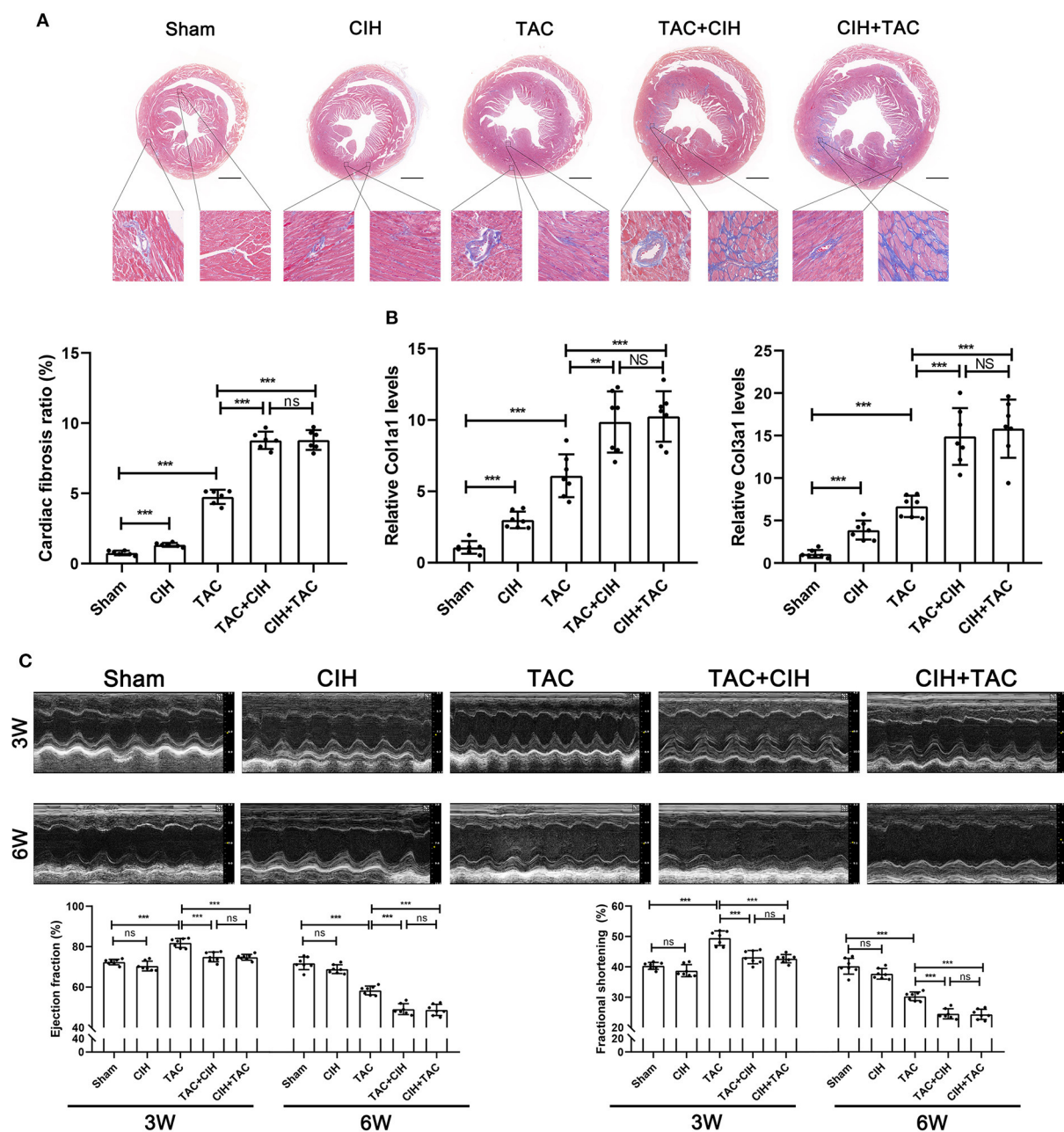


FIGURE 2

CIH exposure accelerates cardiac fibrosis and cardiac dysfunction in mice subjected to TAC. (A) Masson staining of heart cross-section images and representative perivascular and interstitial fibrosis images magnified in boxes; the fibrosis area ratio was quantified.  $n = 7$ ;  $**p < 0.01$ ,  $***p < 0.001$ . (B) Real-time PCR analysis of relative Col1a1 and Col3a1 levels in heart tissue at week 6.  $n = 7$ ;  $***p < 0.001$ . (C) M-mode echocardiographic images of the left ventricle along the left parasternal long axis. Quantification of the LVEF and LVFS from the echocardiography data.  $n = 7$ ;  $***p < 0.001$ .

CIH group and the sham group. Interestingly, SERCA2a protein and mRNA levels were significantly increased in the TAC group, and they were significantly higher than those in the TAC+CIH and CIH+TAC groups (Figures 3E,D). This finding may have been related to adaptation to the early increase in SERCA2a expression levels in the mouse heart in response to disease

(29). However, CIH exposure suppressed this adaptive change. Moreover, miR-29c levels in the hearts of mice in all groups were slightly different. The TAC+CIH and CIH+TAC groups exhibited the highest expression of miR-29c, with no difference between the groups. The expression of miR-29 in the TAC group was lower than that in the TAC+CIH and CIH+TAC groups.

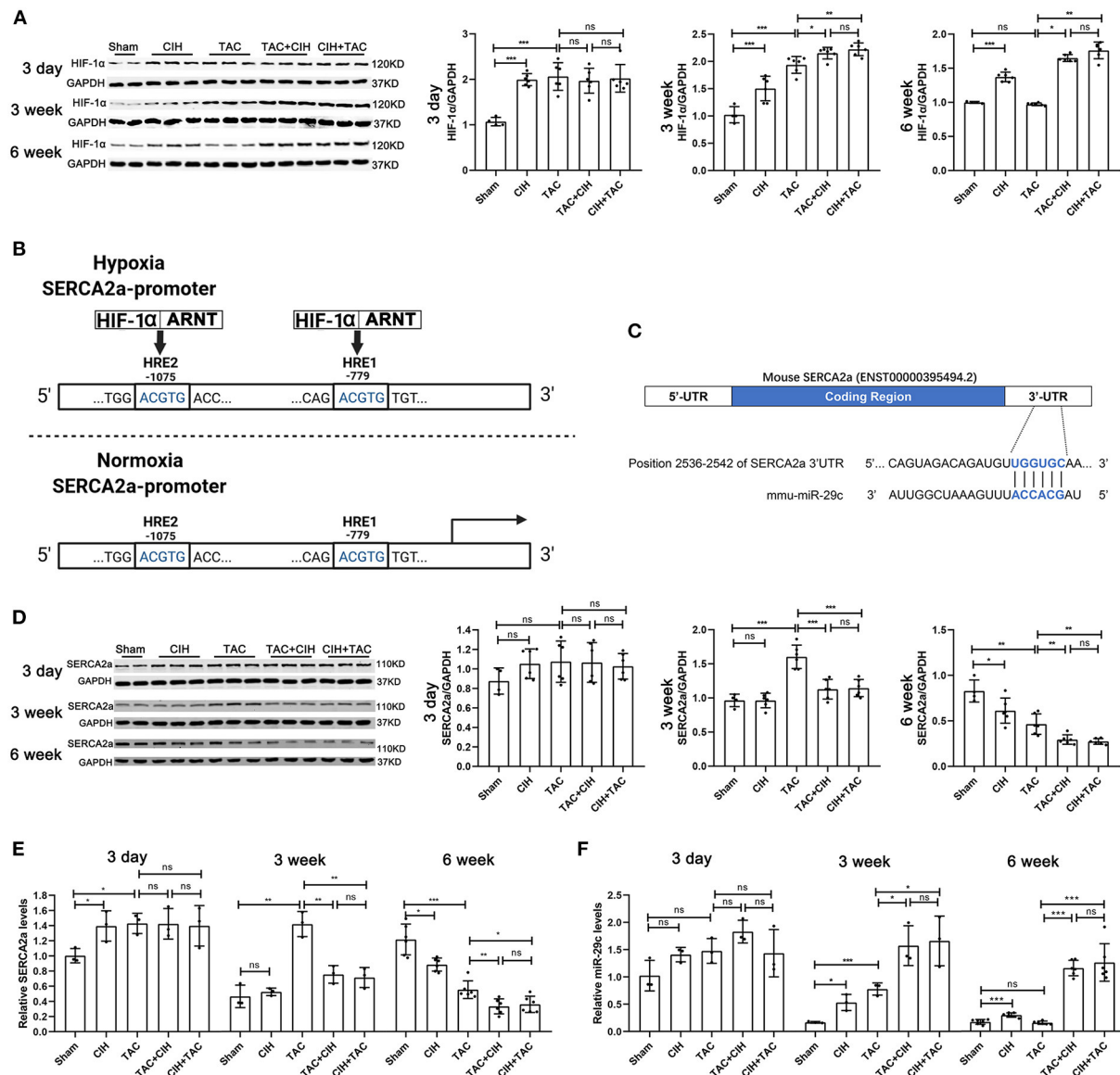
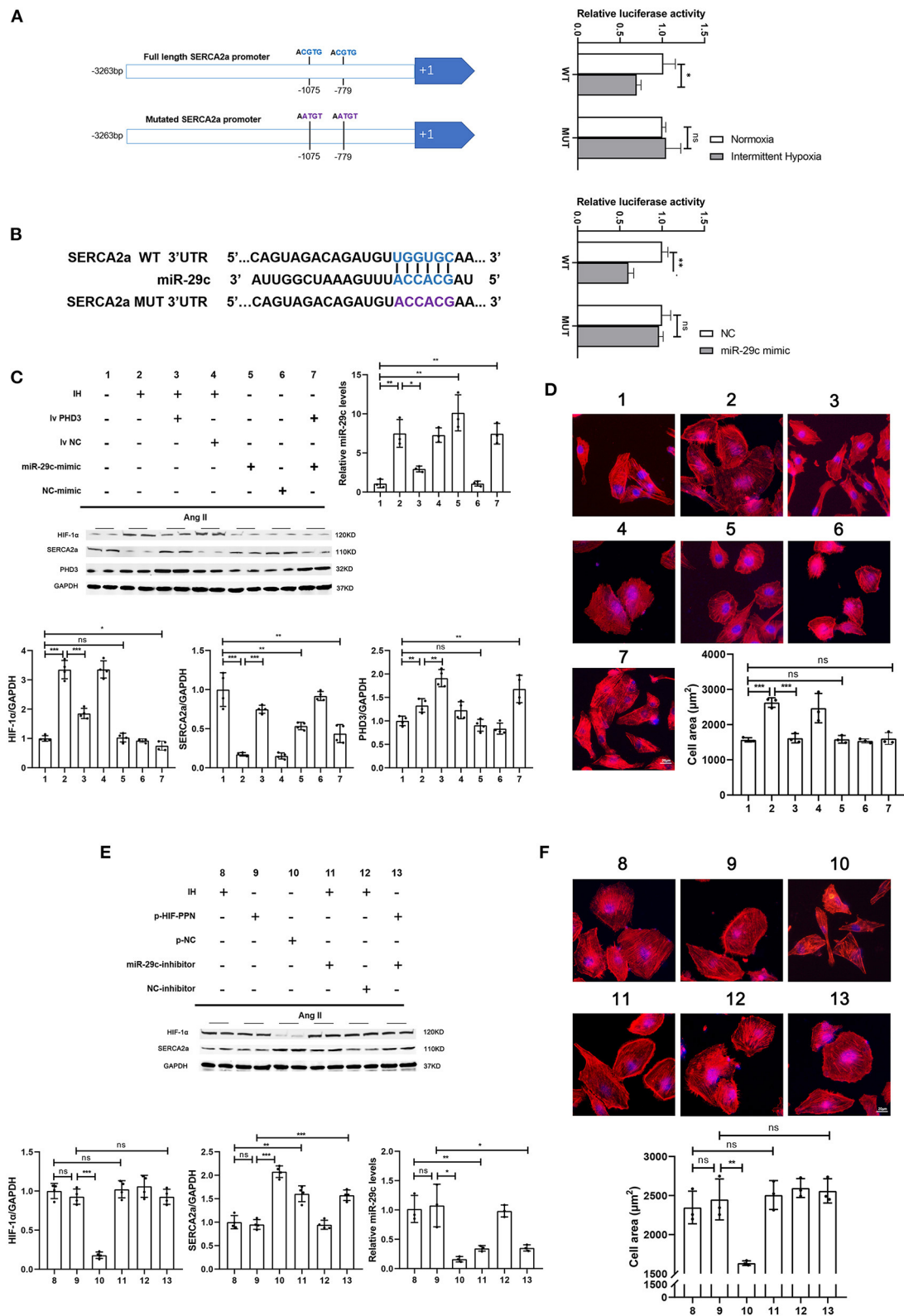


FIGURE 3

CIH exposure maintains long-term elevations in the expression of HIF-1 $\alpha$  and induces a sustained decrease in SERCA2a levels and a sustained increase in miR-29c levels in the hearts of mice subjected to TAC. (A) Western blot analysis of HIF-1 $\alpha$  expression in the heart in all groups at day 3, week 3 and week 6.  $n = 6$  (sham group  $n = 4$ );  $*p < 0.05$ ,  $**p < 0.01$ ,  $***p < 0.001$ . (B) Schematic diagram of the competitive binding of HIF-1 to the SERCA2a promoter region under hypoxic conditions. (C) Schematic representation of the miR-29c and SERCA2a mRNA binding sites. (D) Western blot analysis of SERCA2a expression in the heart in all groups at day 3, week 3 and week 6.  $n = 6$  (sham group  $n = 4$ );  $*p < 0.05$ ,  $**p < 0.01$ ,  $***p < 0.001$ . (E) Real-time PCR analysis of relative SERCA2a levels in heart tissue at day 3, week 3 and week 6.  $n = 3$  (week 6  $n = 6$ );  $*p < 0.05$ ,  $**p < 0.01$ ,  $***p < 0.001$ . (F) Real-time PCR analysis of relative miR-29c levels in heart tissue at day 3, week 3 and week 6.  $n = 3$  (week 6  $n = 6$ );  $*p < 0.05$ ,  $**p < 0.01$ ,  $***p < 0.001$ .

The expression of miR-29c was higher in the hearts of mice exposed to CIH or TAC than in the sham group (Figure 3F). After 6 weeks, the protein and mRNA levels of SERCA2a in the heart were the lowest in the TAC+CIH and CIH+TAC groups, which had similar levels. The levels of SERCA2a protein and mRNA in the heart were lower in the TAC group than in the

sham group (Figures 3D,E). In contrast, the expression level of miR-29c was the highest in the TAC+CIH and CIH+TAC groups, which had similar levels. The expression level of miR-29c in the heart returned to normal in the TAC group (Figure 3F). These data combined with the results presented in section 3 of the Results indicate that, as expected, the expression of miR-29c



**FIGURE 4**  
HIF-1α inhibits SERCA2a expression, promotes miR-29c expression and induces cardiomyocyte hypertrophy, while miR-29c only inhibits SERCA2a expression. (A) Two HIF-1 binding core sequences (HRE1 and HRE2) on the SERCA2 promoter were mutated to construct a SERCA2 promoter-luciferase reporter construct. HL-1 cells were transfected and then assayed for luciferase activity in normoxia and hypoxia.  $n = 3$ ; (Continued)

## FIGURE 4 (Continued)

\* $p < 0.05$ . (B) Relative luciferase activity of the SERCA2a mRNA wild-type or mutant 3'-UTR in HEK293T cells after transfection with the miR-29c mimic or NC mimic.  $n = 3$ ; \*\* $p < 0.05$ . (C) Western blot analysis of HIF-1 $\alpha$ , SERCA2a, PHD3 expression and real-time PCR analysis of relative miR-29c in the HL-1 cells in all groups.  $n = 4$  (Western blot); \* $p < 0.05$ , \*\* $p < 0.01$ , \*\*\* $p < 0.001$ ;  $n = 3$  (RT-PCR); \* $p < 0.05$ , \*\* $p < 0.01$ . (D) HL-1 cells treated with corresponding groups in "(C)" and stained with phalloidin. Then the cell area was quantified. scale bar = 20 $\mu$ m; \*\*\* $p < 0.001$ . (E) Western blot analysis of HIF-1 $\alpha$ , SERCA2a expression and real-time PCR analysis of relative miR-29c in the HL-1 cells in all groups.  $n = 4$  (Western blot); \*\* $p < 0.01$ , \*\*\* $p < 0.001$ ;  $n = 3$  (RT-PCR); \* $p < 0.05$ , \*\* $p < 0.01$ . (F) HL-1 cells treated with corresponding groups in "(E)" and stained with phalloidin. Then the cell area was quantified. scale bar = 20 $\mu$ m; \*\* $p < 0.01$ .

in the heart was consistent with the expression of HIF-1 $\alpha$  in each group. In this study, we observed that the CIH+TAC-induced long-term elevations of HIF-1 $\alpha$  and miR-29c in the mouse heart promoted further downregulation of SERCA2a expression. In addition, the compensatory increase in SERCA2a expression in the early stage counteracted the inhibitory effect of HIF-1 $\alpha$  and miR-29c, but under the long-term effect of chronic diseases, the body eventually decompensates, and the expression of SERCA2a is downregulated.

### HIF-1 $\alpha$ regulates both cardiomyocyte hypertrophy and SERCA2a expression, while miR-29c only regulates SERCA2a expression

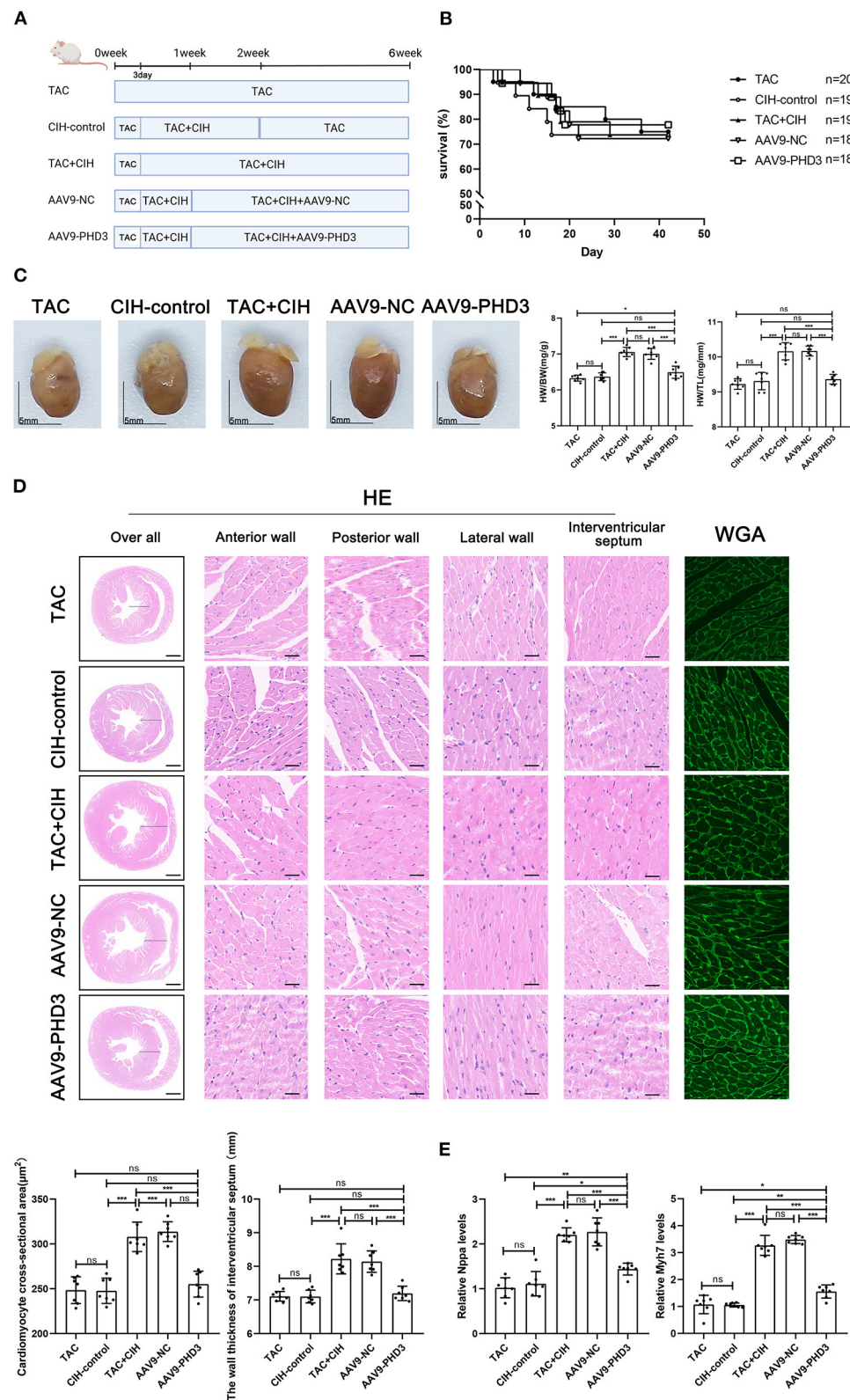
We further verified the regulatory relationship between HIF-1 $\alpha$ , miR-29c and SERCA2a. First, we tested the regulatory effect of HIF-1 $\alpha$  on SERCA2a. After a previous study (24), we mutated two sites in the SERCA2a promoter that may bind to HIF-1 to construct a SERCA2 promoter-mutant luciferase reporter plasmid (Figure 4A). The SERCA2a promoter-mutant plasmid was transfected into HL-1 cells under normoxia or intermittent hypoxia, followed by a luciferase assay. The results showed that luciferase activity was not affected by intermittent hypoxia after mutation of the HIF-1-binding core sequence in the SERCA2a promoter (Figure 4A). To test the regulatory effect of miR-29c on SERCA2a, we constructed a SERCA2a 3'UTR-mutant luciferase reporter plasmid. Tool cells were cotransfected with miR-29c mimics and plasmids (Figure 4B). The results showed that after the wild-type SERCA2a 3'UTR was mutated and cotransfected with the miR-29c mimic into cells, the luciferase activity was not affected by the miR-29c mimic (Figure 4B). Then, we performed CIH exposure on the basis of an Ang II-induced cardiomyocyte hypertrophy model to establish a corresponding cellular model. Overexpression of PHD3 attenuated CIH-induced cardiomyocyte hypertrophy, with upregulation of miR-29c and downregulation of SERCA2a (Figures 4C,D). We also attempted to overexpress miR-29c under normoxia. The results showed that miR-29c only affected SERCA2a expression without causing cardiomyocyte hypertrophy regardless of whether it increased PHD3 expression

(Figures 4C,D). In addition, we used the plasmid HIF-PPN (25), which encodes a HIF-1 $\alpha$  mutant resistant to PHD degradation under normoxia. The results showed that overexpression of HIF-1 $\alpha$  under normoxia still accelerated Ang II-induced cardiomyocyte hypertrophy, with upregulation of miR-29c and downregulation of SERCA2a (Figures 4E,F). Similar to the previous results, the miR-29c inhibitor only alleviated the downregulation of SERCA2a promoted by CIH or overexpression of HIF-1 $\alpha$  but did not significantly alleviate cardiomyocyte hypertrophy (Figures 4E,F). These results validate the hypothesis of previous *in vivo* experiments and clarify the regulatory effects of HIF-1 $\alpha$  and miR-29c on cardiomyocytes.

### AAV9-PHD3 can alleviate left ventricular systolic dysfunction in mice after both CIH exposure and TAC and inhibit further cardiac remodeling

*In vitro* experiments verified the therapeutic effect of PHD3 overexpression. Next, we used AAV9-PHD3 to increase the expression of PHD3 in the mouse heart to clarify the therapeutic effect *in vivo*. In the *in vivo* experiment presented above, our data showed that the mice that underwent both CIH exposure and TAC showed no difference in heart function after 6 weeks, regardless of whether the mice were exposed to CIH before or after TAC. Therefore, when exploring the effect of PHD3, we subjected mice to CIH exposure after TAC surgery. There was no significant difference in mortality between the five groups of mice after 6 weeks, indicating that AAV9-PHD3 had no effect on the mortality of the mice (Figure 5B). After both CIH exposure and TAC, the heart/body weight and heart weight/tibia length ratios of heart-PHD3-overexpressing mice were significantly lower, though they had no significant differences from those in the CIH control group, but the heart/body weight ratio was slightly higher than that in the TAC group (Figure 5C). HE and WGA staining results showed that further cardiomyocyte hypertrophy was inhibited in mice that were treated with AAV9-PHD3, unlike in the mice in the TAC+CIH group (Figure 5D). The thickness of the interventricular septal wall measured in the cross-section of the heart also confirmed the above





**FIGURE 5**  
PHD3 overexpression alleviates the cardiomyocyte hypertrophy induced by CIH exposure. **(A)** Grouping and experimental protocol for each group. TAC: Transverse aortic constriction surgery was performed, followed by normoxia for 6 weeks; CIH-control: CIH exposure was performed 3 days after transverse aortic constriction surgery and CIH exposure was discontinued at the second week for a total of 6 weeks. *(Continued)*

## FIGURE 5 (Continued)

TAC+CIH: CIH exposure was performed 3 days after transverse aortic constriction surgery for a total of 6 weeks. AAV9-NC: CIH exposure was performed 3 days after transverse aortic constriction surgery and tail vein injection of AAV9-NC on day 7 for a total of 6 weeks. AAV9-PHD3: CIH exposure was performed 3 days after transverse aortic constriction surgery and tail vein injection of AAV9-PHD3 on day 7 for a total of 6 weeks. (B) Survival rates of all groups; the sample size of each group is noted in the figure. (C) Left: representative images of hearts; right: quantification of the heart weight-to-body weight ratio and heart weight-to-tibia length ratio.  $n = 7$ ; scale bar = 5 mm;  $*p < 0.05$ ,  $***p < 0.001$ . (D) HE staining and WGA staining of mouse hearts. The wall thickness of the interventricular septum was measured according to HE staining pictures. The cardiomyocyte cross-sectional area was quantified according to WGA staining.  $n = 7$ ; scale bar = 1mm and 25 $\mu$ m;  $***p < 0.001$ . (E) Real-time PCR analysis of relative Nppa and Myh7 levels in heart tissue at week 6.  $n = 7$ ;  $*p < 0.05$ ,  $**p < 0.01$ ,  $***p < 0.001$ .

result (Figure 5D). Notably, the qPCR analysis of hypertrophic genes (Nppa and Myh7) showed that the AAV9-PHD3 group still expressed slightly higher levels than the TAC and CIH control groups, but significantly lower than the TAC+CIH group (Figure 5E). Masson staining and the analysis of fibrosis-related gene expression also showed that overexpression of PHD3 in mouse heart alleviated CIH+TAC-induced cardiac fibrosis, but these mice still had more cardiac fibrosis than the TAC and CIH control groups (Figures 6A,B). Echocardiography showed that mice that underwent interrupted CIH exposure or received AAV9-PHD3 treatment exhibited higher LVEF and FS than mice in the TAC+CIH group (Figure 6C). In summary, interruption of CIH exposure and AAV9-PHD3 treatment can delay the cardiac remodeling and left ventricular systolic dysfunction induced by CIH exposure but cannot alter the cardiac remodeling and left ventricular systolic dysfunction induced by TAC.

### AAV9-PHD3 maintains the expression level of SERCA2a by inhibiting HIF-1 $\alpha$ expression in the mouse heart

By comparing the expression levels of PHD3 in the hearts of mice injected with AAV9-vehicle and AAV9-PHD3, we verified the efficacy of AAV9-PHD3 in upregulating the expression of PHD3 in the heart (Supplementary Figure 3). We used Western blotting and qPCR to determine the levels of HIF-1 $\alpha$  mRNA, SERCA2a mRNA, miR-29c, PHD3 protein and SERCA2a protein in the hearts of all groups of mice 6 weeks later. The results were as expected. Cardiac PHD3 was significantly elevated in the AAV9-PHD3 group (Figure 6D). Heart HIF-1 $\alpha$  and miR-29c were the lowest in the AAV9-PHD3 group, and the levels of HIF-1 $\alpha$  and miR-29c were similar between the CIH control and TAC groups (Figures 6E,H). In contrast, cardiac SERCA2a mRNA and protein levels were significantly higher in the AAV9-PHD3 group than in the TAC+CIH group (Figures 6F,G). These results indicate that AAV9-PHD3 increases the expression of PHD3 in the mouse heart while downregulating HIF-1 $\alpha$  and miR-29c and preserving the expression level of SERCA2a in the heart.

## Discussion

In this study, we show that CIH exposure in combination with TAC can cause further cardiac remodeling and promote a decline in left ventricular contractile function in mice. In-depth research showed that CIH exposure in combination with TAC leads to long-term elevations in the expression of HIF-1 $\alpha$ . HIF-1 $\alpha$ , as a transcription factor, promotes miR-29c expression, and both HIF-1 $\alpha$  and miR-29c can negatively regulate SERCA2a expression. Our results also showed that cardiomyocytes overexpressing PHD3 could reverse left ventricular contractile dysfunction and cardiac remodeling by inhibiting the upregulation of HIF-1 $\alpha$ .

TAC can induce left ventricle systolic dysfunction and cardiac remodeling in mice (23). The results of previous experiments on the conditional increase/decrease in HIF-1 $\alpha$  expression observed in mice following TAC surgery appear to be contradictory. Marion et al. subjected HIF-1 $\alpha$ -overexpressing HIF-1 $\alpha^{\text{tg}}$  mice to TAC for 8 weeks. Continued upregulation of HIF-1 $\alpha$  expression accelerated cardiac dysfunction in TAC mice. In addition, they found more stable HIF-1 $\alpha$  expression in heart samples from patients with end-stage heart failure (16). In contrast, Masanori Sano et al. conditionally knocked out Hif-1 $\alpha$  in mouse cardiomyocytes and performed TAC surgery, and the cardiac dysfunction in Hif-1 $\alpha$  knockout mice was more obvious 2 weeks later (30). Notably, high expression of Hif-1 $\alpha$  promoted cardiac hypertrophy, and low expression of Hif-1 $\alpha$  reduced the cross-sectional area of cardiomyocytes, suggesting that the pro-hypertrophic effect of HIF-1 $\alpha$  is non-controversial. Both high HIF-1 $\alpha$  expression at 8 weeks and low HIF-1 $\alpha$  expression at 2 weeks after TAC surgery aggravated cardiac dysfunction, which both seem to be related to the time at which HIF-1 $\alpha$  expression is assessed. This is similar to the role of HIF-1 $\alpha$  in ischemic cardiomyopathy (19). Short-term HIF-1 $\alpha$  upregulation confers some benefit, whereas long-term HIF-1 $\alpha$  upregulation overrides the beneficial effects. Our findings emphasize the adverse effects of long-term high HIF-1 $\alpha$  expression and do not cover any beneficial effects of short-term high HIF-1 $\alpha$  expression.

The important role of SERCA2a in cardiac systolic function has been extensively studied. Increasing the level of cardiac SERCA2a can alleviate cardiac dysfunction (31). *In vitro*, we verified by luciferase assays that HIF-1 $\alpha$  inhibits SERCA2a



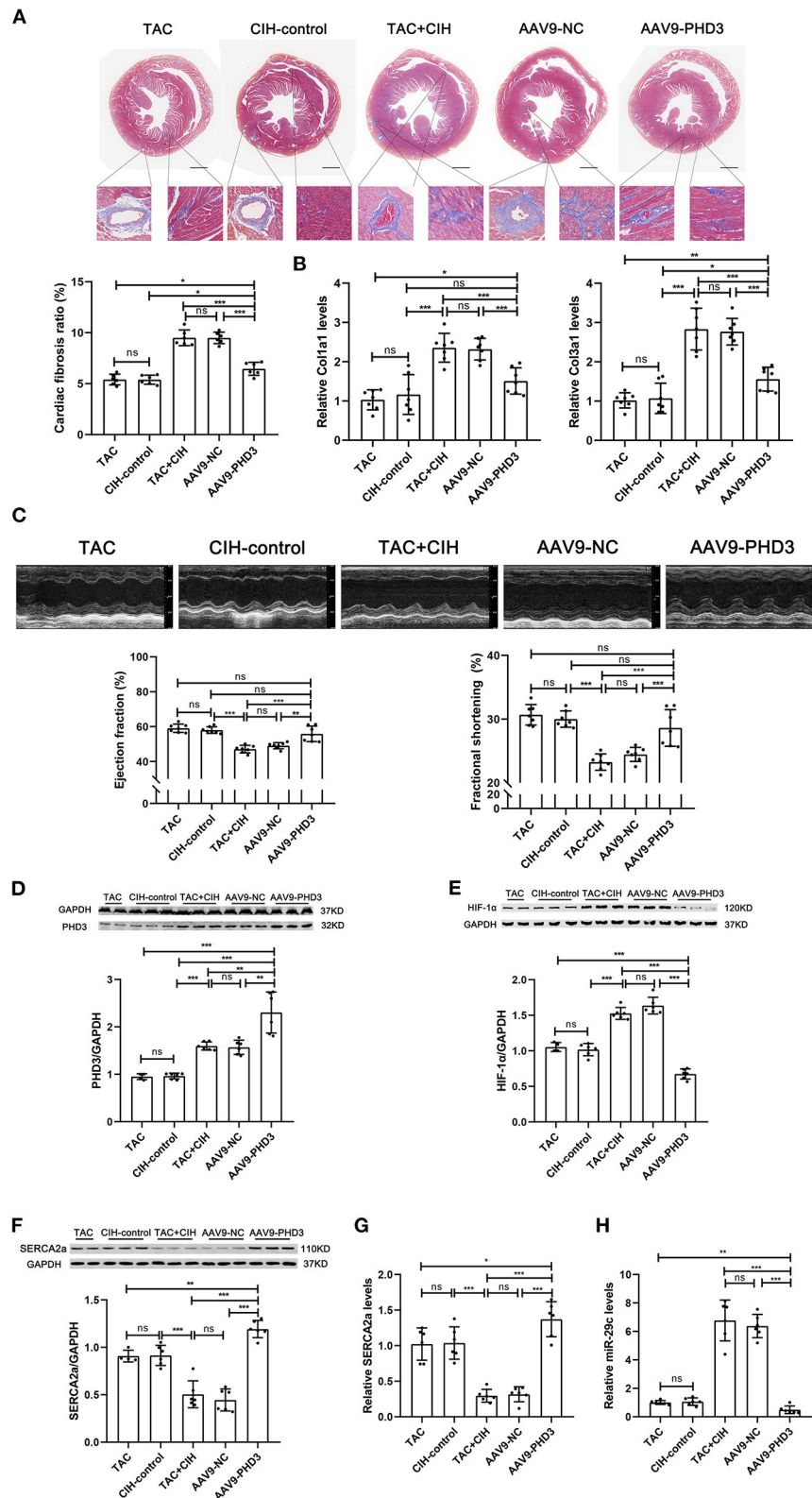


FIGURE 6

PHD3 overexpression downregulates HIF-1 $\alpha$  and miR-29 expression to stabilize SERCA2a expression and alleviate cardiac fibrosis and cardiac dysfunction. (A) Masson staining of heart cross-section images and representative perivascular and interstitial fibrosis images magnified in boxes; the fibrosis area ratio was quantified. *n* = 7; \*\*\**p* < 0.001. (B) Real-time PCR analysis of relative Col1a1 and Col3a1 levels in heart tissue at (Continued)

## FIGURE 6 (Continued)

week 6.  $n = 7$ ;  $***p < 0.001$ . (C) M-mode echocardiographic images of the left ventricle along the left parasternal long axis. Quantification of the LVEF and LVFS from the echocardiography data.  $n = 7$ ;  $***p < 0.001$ . (D) Western blot analysis of PHD3 expression in the heart in all groups.  $n = 6$  (TAC group  $n = 4$ );  $**p < 0.01$ ,  $***p < 0.001$ . (E) Western blot analysis of HIF-1 $\alpha$  expression in the heart in all groups.  $n = 6$  (TAC group  $n = 4$ );  $***p < 0.001$ . (F) Western blot analysis of SERCA2a expression in the heart in all groups.  $n = 6$  (TAC group  $n = 4$ );  $***p < 0.001$ . (G) Real-time PCR analysis of relative SERCA2a levels in heart tissue.  $n = 6$ ;  $*p < 0.05$ ,  $***p < 0.001$ . (H) Real-time PCR analysis of relative miR-29c levels in heart tissue.  $n = 6$ ;  $**p < 0.01$ ,  $***p < 0.001$ .

expression through both direct and indirect pathways. Cardiac injury from CIH-induced HIF-1 $\alpha$  overexpression is only a factor that accelerates cardiac dysfunction in TAC mice. Cardiac dysfunction caused by TAC still plays an important role. TAC results in downregulation of SERCA2a expression in the heart *via* multiple pathways (32, 33). This is faster than the HIF-1 $\alpha$  inhibition of SERCA2a. Therefore, we observed lower SERCA2a expression and worse cardiac function in the TAC group than in the CIH group at 6 weeks. Earlier in our study, we observed that HIF-1 $\alpha$  expression was upregulated 3 days and 3 weeks after CIH exposure or TAC, at which time SERCA2a was also upregulated in the CIH and TAC groups. However, there was no simultaneous upregulation of HIF-1 $\alpha$  and SERCA2a in our cell experiments. This reflects a strong compensatory ability in animals that can compensate for an early external pressure to increase the level of SERCA2a (34, 35). At this time, the inhibition of SERCA2a expression by HIF-1 $\alpha$  is not enough to offset the upregulation by the body's compensation. When the external stress exceeds the body's compensatory ability, the level of SERCA2a gradually decreases, as shown by the expression of SERCA2a in the TAC+CIH and CIH+TAC groups at 3 weeks. CIH exposure in combination with TAC further upregulated HIF-1 $\alpha$  expression, leading to cardiac decompensation. Long-term elevations in the expression of HIF-1 $\alpha$  led to a more obvious impairment in cardiac function at 6 weeks. In addition, we observed that mice subjected to CIH alone for 6 weeks showed an increase in the levels of the hypertrophic factor Myh7 and cardiac fibrosis, although there was no significant decrease in left ventricular function. This finding suggests that 6 weeks of elevated HIF-1 $\alpha$  expression in normal mice also induced some cardiac damage, but within the compensable range of the heart. In summary, our study once again demonstrates that long-term activation of HIF-1 $\alpha$  accelerates the development of cardiac injury in mice.

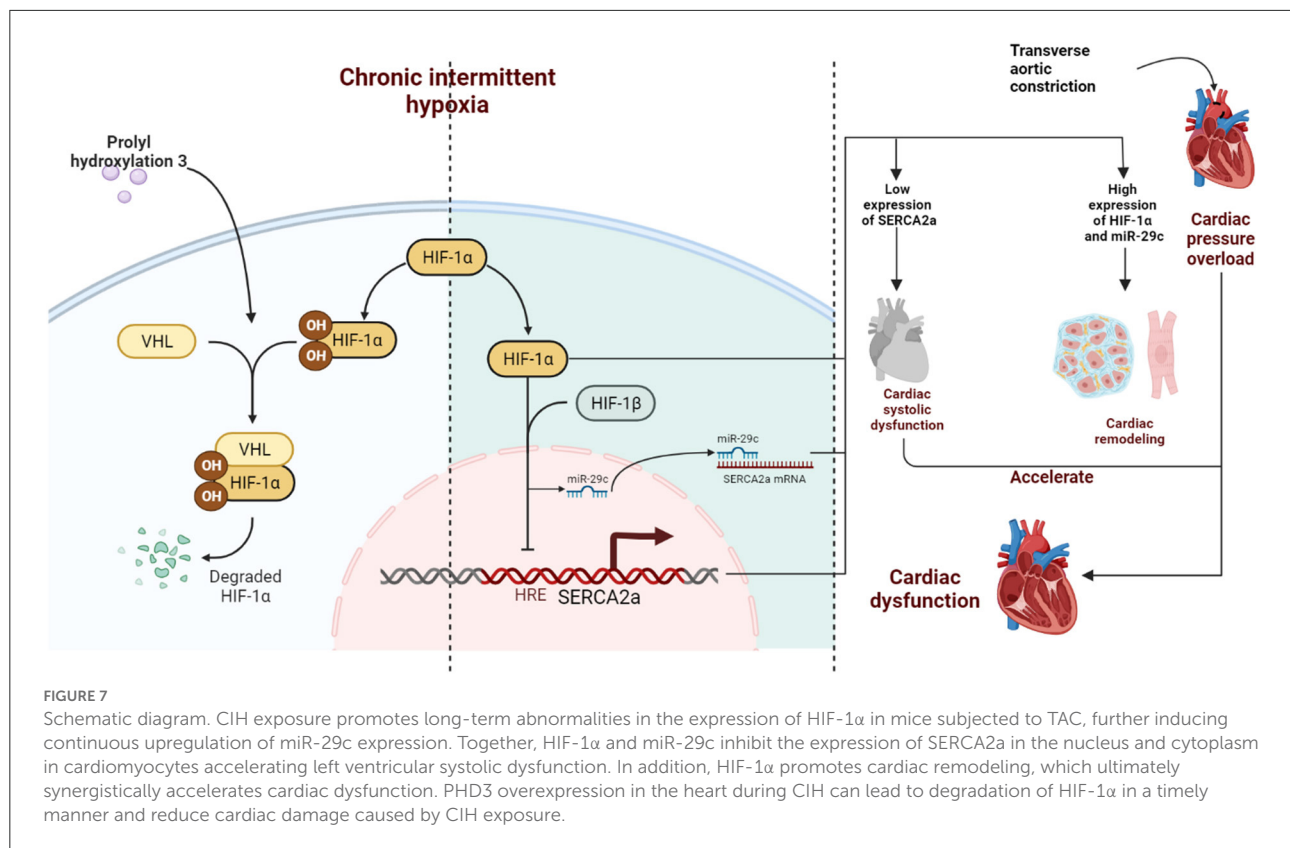
Under normoxic conditions, PHD3 hydroxylates 2 specific proline residues in the oxygen-dependent degradation (ODD) domain of HIF-1 $\alpha$ , and then von Hippel–Lindau protein mediates HIF-1 $\alpha$  degradation. Under hypoxic conditions, PHD activity is inhibited, and HIF-1 $\alpha$  escapes hydroxylation and is transported into the nucleus to play a regulatory role in transcription (36). Cardiac PHD3 activation mimics the inhibition of HIF-1 $\alpha$  activation under normoxic conditions, which is more similar to what is observed under physiological conditions. In this experiment, we first overexpressed PHD3 in a model of cardiomyocyte injury induced by the combination

of Ang II and CIH to verify the therapeutic effect. Then we verified the therapeutic effect of AAV9-PHD3 on cardiac systolic dysfunction and cardiac remodeling induced by CIH exposure in mice with overload stress. We also observed that CIH accelerated cardiac fibrosis in TAC mice. We alleviated the cardiac fibrosis in TAC mice by overexpressing PHD3 in the heart, including but not limited to cardiomyocytes. Similarly, in our previous study (21), CIH activated HIF-1 $\alpha$ , which increased endothelial mesenchymalization, leading to cardiac fibrosis. Notably, miR-29c is also one of the influencing factors of cardiac fibrosis (37). However, this study mainly focused on cardiomyocytes and did not further elaborate on the specific reasons. We hope to explore these issues in more depth in follow-up studies.

Although this seems to be a satisfactory result, we noticed that AAV9-PHD3 treatment reduced the adverse cardiac effects of CIH exposure but did not have a therapeutic effect on the TAC-induced basic heart damage. We also observed that PHD3 overexpression did not reduce mortality in mice. This may be due to the limited effect on mortality in mice with an EF of approximately 50%, and more deaths were due to infection or complications from TAC surgery. Between the TAC+CIH, CIH+TAC, and TAC groups, there were differences in cardiac function but no significant difference in mortality. However, we think that the effect of PHD3 on mortality may become visible in the animal model after longer experimental times. In addition, there are some limitations to our study. First, because of the cardiovascular protective effect of estrogen in adult female mice, we only selected male C57BL/6 mice, which are more sensitive to CIH exposure. Second, the role of SERCA2a and PHD3 is affected not only by their expression levels but also by SERCA2a and PHD3 activity. Finally, due to the limitations of experimental conditions, we could not directly verify the contractile function of cells *in vitro* but chose to use SERCA2a expression for verification.

## Conclusion

Our findings, which are shown in the schematic illustration (Figure 7), identify therapeutic targets for CIH exposure-induced upregulation of HIF-1 $\alpha$  expression, which accelerates TAC-induced left ventricular systolic dysfunction and cardiac remodeling. We also demonstrate that high expression of myocardial PHD3 promotes the downregulation of HIF-1 $\alpha$



induced by intermittent hypoxia and that downregulation of HIF-1 $\alpha$  expression leads to transcriptional repression of miR-29c, upregulating SERCA2a expression and ultimately alleviating cardiac remodeling and dysfunction.

## Data availability statement

The original contributions presented in the study are included in the article/[Supplementary material](#), further inquiries can be directed to the corresponding author/s.

## Ethics statement

The animal study was reviewed and approved by Animal Care and Use Committee of Southeast University School of Medicine.

## Author contributions

J-YT and XX: conception and design of the research and drafting manuscript. XX, P-HZ, F-CY, TW, S-NL, and QW: acquisition of data and analysis and interpretation of data. XX and P-HZ: statistical analysis. J-YT: obtaining funding. All authors read and approved the final manuscript.

## Funding

This study was supported by Natural Science Foundation of Jiangsu Province (BK20210231).

## Acknowledgments

The authors thanked the AJE Company for their language editing and proofreading. [Figure 7](#) created with [BioRender.com](#).

## Conflict of interest

The authors declare that the research was conducted in the absence of any commercial or financial relationships that could be construed as a potential conflict of interest.

## Publisher's note

All claims expressed in this article are solely those of the authors and do not necessarily represent those of their affiliated organizations, or those of the publisher, the editors and the reviewers. Any product that may be evaluated in this article, or

claim that may be made by its manufacturer, is not guaranteed or endorsed by the publisher.

## Supplementary material

The Supplementary Material for this article can be found online at: <https://www.frontiersin.org/articles/10.3389/fcvm.2022.974345/full#supplementary-material>

### SUPPLEMENTARY FIGURE 1

Flow chart of the experimental process. Surgical death: Mice that died during TAC surgery due to vascular rupture or pneumothorax and other

causes. Surgical failed: TAC surgical ligation was wrongly positioned or the operation time was too long, the mice suffered from respiratory disturbance and were forced to stop the operation.

### SUPPLEMENTARY FIGURE 2

Flow chart of the experimental process.

### SUPPLEMENTARY FIGURE 3

Left: CIH exposure after TAC surgery, tail vein injection of AAV9-PHD3 on week 1, and PHD3 protein expression was measured in cardiac tissue on week 6. Right: PHD3 protein expression in heart tissue after 4 weeks of AAV9-PHD3 tail vein injection under normoxia.

### SUPPLEMENTARY TABLE 1

Primer sequences used for qRT-PCR.

## References

- Lévy P, Kohler M, McNicholas WT, Barbé F, McEvoy RD, Somers VK, et al. Obstructive sleep apnoea syndrome. *Nat Rev Dis Prim.* (2015) 1:15015. doi: 10.1038/nrdp.2015.15
- Jordan AS, McSharry DG, Malhotra A. Adult obstructive sleep apnoea. *Lancet (London, England).* (2014) 383:736–47. doi: 10.1016/S0140-6736(13)60734-5
- Oldenburg O, Lamp B, Faber L, Teschler H, Horstkotte D, Töpfer V. Sleep-disordered breathing in patients with symptomatic heart failure: a contemporary study of prevalence in and characteristics of 700 patients. *Eur J Heart Fail.* (2007) 9:251–7. doi: 10.1016/j.ejheart.2006.08.003
- Cai A, Wang L, Zhou Y. Hypertension and obstructive sleep apnea. *Hyperten Res Offic J Japanese Soc Hypertens.* (2016) 39:391–5. doi: 10.1038/hr.2016.11
- Gottlieb DJ, Yenokyan G, Newman AB, O'Connor GT, Punjabi NM, Quan SF, et al. Prospective study of obstructive sleep apnea and incident coronary heart disease and heart failure: the sleep heart health study. *Circulation.* (2010) 122:352–60. doi: 10.1161/CIRCULATIONAHA.109.901801
- Yeghiazarians Y, Jneid H, Tietjens JR, Redline S, Brown DL, El-Sherif N, et al. Obstructive sleep apnea and cardiovascular disease: a scientific statement from the american heart association. *Circulation.* (2021) 144:e56–67. doi: 10.1161/CIR.0000000000000988
- Chen L, Einbinder E, Zhang Q, Hasday J, Balke CW, Scharf SM. Oxidative stress and left ventricular function with chronic intermittent hypoxia in rats. *Am J Respir Crit Care Med.* (2005) 172:915–20. doi: 10.1164/rccm.200504-560OC
- Castro-Grattoni AL, Alvarez-Buvé R, Torres M, Farré R, Montserrat JM, Dalmau M, et al. Intermittent hypoxia-induced cardiovascular remodeling is reversed by normoxia in a mouse model of sleep apnea. *Chest.* (2016) 149:1400–8. doi: 10.1016/j.chest.2015.11.010
- Yancy CW, Jessup M, Bozkurt B, Butler J, Casey DE, Colvin MM, et al. ACC/AHA/HFSA Focused Update of the 2013 ACCF/AHA guideline for the management of heart failure: a report of the american college of cardiology/american heart association task force on clinical practice guidelines and the heart failure society of America. *Circulation.* (2017) 136:e137–e161. doi: 10.1161/CIR.0000000000000509
- Patil SP, Ayappa IA, Caples SM, Kimoff RJ, Patel SR, Harrod CG. Treatment of adult obstructive sleep apnea with positive airway pressure: an american academy of sleep medicine systematic review, meta-analysis, and GRADE assessment. *J Clin Sleep Med JCSM: Offic Publicat Am Acad Sleep Med.* (2019) 15:301–34. doi: 10.5664/jcsm.7638
- McEvoy RD, Antic NA, Heeley E, Luo Y, Ou Q, Zhang X, et al. CPAP for prevention of cardiovascular events in obstructive sleep apnea. *n Engl J Med.* (2016) 375:919–31. doi: 10.1056/NEJMoa1606599
- Kakkar RK, Berry RB. Positive airway pressure treatment for obstructive sleep apnea. *Chest.* (2007) 132:1057–72. doi: 10.1378/chest.06-2432
- Wang GL, Semenza GL. Purification and characterization of hypoxia-inducible factor 1. *J Biol Chem.* (1995) 270:1230–7. doi: 10.1074/jbc.270.3.1230
- Gabryelska A, Turkiewicz S, Karuga FF, Sochal M, Strzelecki D, Białasiewicz P. Disruption of circadian rhythm genes in obstructive sleep apnea patients: possible mechanisms involved and clinical implication. *Int J Mol Sci.* (2022). 23:709. doi: 10.3390/ijms23020709
- Gabryelska A, Szmyd B, Szemraj J, Stawski R, Sochal M, Białasiewicz P. Patients with obstructive sleep apnea present with chronic upregulation of serum HIF-1α protein. *J Clin Sleep Med JCSM: Offic Publicat Am Acad Sleep Med.* (2020) 16:1761–8. doi: 10.5664/jcsm.8682
- Hölscher M, Schäfer K, Krull S, Farhat K, Hesse A, Silter M, et al. Unfavorable consequences of chronic cardiac HIF-1α stabilization. *Cardiovasc Res.* (2012) 94:77–86. doi: 10.1093/cvr/cvs014
- Yan X, Zhao R, Feng X, Mu J, Li Y, Chen Y, et al. Sialyltransferase7A promotes angiotensin II-induced cardiomyocyte hypertrophy via HIF-1α-TAK1 signaling pathway. *Cardiovasc Res.* (2020) 116:114–26. doi: 10.1093/cvr/cvz064
- Yang Y, Zou P, He L, Shao J, Tang Y, Li J, et al. aggravates Ang II-induced cardiac hypertrophy via the VHL/HIF-1α pathway. *Exp Cell Res.* (2021) 405:112730. doi: 10.1016/j.yexcr.2021.112730
- Belaidi E, Joyeux-Faure M, Ribuot C, Launois SH, Levy P, Godin-Ribuot D. Major role for hypoxia inducible factor-1 and the endothelin system in promoting myocardial infarction and hypertension in an animal model of obstructive sleep apnea. *J Am Coll Cardiol.* (2009) 53:1309–17. doi: 10.1016/j.jacc.2008.12.050
- Wang W, Gu H, Li W, Lin Y, Yao X, Luo W, et al. SRC-3 Knockout attenuates myocardial injury induced by chronic intermittent hypoxia in mice. *Oxid Med Cell Longev.* (2021) 2021:6372430. doi: 10.1155/2021/6372430
- Zhang GH, Yu FC, Li Y, Wei Q, Song SS, Zhou FP, et al. Prolyl 4-Hydroxylase domain protein 3 overexpression improved obstructive sleep apnea-induced cardiac perivascular fibrosis partially by suppressing endothelial-to-mesenchymal transition. *J Am Heart Assoc.* (2017). 6:10. doi: 10.1161/JAHA.117.006680
- Lieb ME, Menzies K, Moschella MC Ni R, Taubman MB. Mammalian EGLN genes have distinct patterns of mRNA expression and regulation. *Biochem Cell Biol.* (2002) 80:421–6. doi: 10.1139/o02-115
- Deng H, Ma LL, Kong FJ, Qiao Z. Distinct phenotypes induced by different degrees of transverse aortic constriction in C57BL/6N Mice. *Front Cardiovascul Med.* (2021) 8:641272. doi: 10.3389/fcvm.2021.641272
- Ronkainen VP, Skoumal R, Tavi P. Hypoxia and HIF-1 suppress SERCA2a expression in embryonic cardiac myocytes through two interdependent hypoxia response elements. *J Mol Cell Cardiol.* (2011) 50:1008–16. doi: 10.1016/j.yjmcc.2011.02.017
- Bekeredjian R, Walton CB, MacCannell KA, Ecker J, Kruse F, Outten JT, et al. Conditional HIF-1α expression produces a reversible cardiomyopathy. *PLoS One.* (2010) 5:e11693. doi: 10.1371/journal.pone.0011693
- Guo J, Mihic A, Wu J, Zhang Y, Singh K, Dhingra S, et al. Canopy 2 attenuates the transition from compensatory hypertrophy to dilated heart failure in hypertrophic cardiomyopathy. *Eur Heart J.* (2015) 36:2530–40. doi: 10.1093/eurheartj/ehv294
- Zhihao L, Jingyu N, Lan L, Michael S, Rui G, Xiyun B, et al. SERCA2a: a key protein in the Ca(2+) cycle of the heart failure. *Heart Fail Rev.* (2020) 25:523–35. doi: 10.1007/s10741-019-09873-3
- Williams AL, Walton CB, MacCannell KA, Avelar A, Shohet RV. HIF-1 regulation of miR-29c impairs SERCA2 expression and cardiac contractility. *Am J Physiol Heart Circulat Physiol.* (2019) 316:H554–h565. doi: 10.1152/ajpheart.00617.2018

29. Lee A, Jeong D, Mitsuyama S, Oh JG, Liang L, Ikeda Y, et al. The role of SUMO-1 in cardiac oxidative stress and hypertrophy. *Antioxid Redox Signal*. (2014) 21:1986–2001. doi: 10.1089/ars.2014.5983
30. Sano M, Minamino T, Toko H, Miyauchi H, Orimo M, Qin Y, et al. p53-induced inhibition of Hif-1 causes cardiac dysfunction during pressure overload. *Nature*. (2007) 446:444–8. doi: 10.1038/nature05602
31. Korf-Klingebiel M, Rebol M, Polten F, Weber N, Jäckle F, Wu X, et al. Myeloid-derived growth factor protects against pressure overload-induced heart failure by preserving sarco/endoplasmic reticulum Ca(2+)-ATPase expression in cardiomyocytes. *Circulation*. (2021) 144:1227–40. doi: 10.1161/CIRCULATIONAHA.120.053365
32. Wu X, Liu X, Wang H, Zhou Z, Yang C, Li Z, et al. Seipin deficiency accelerates heart failure due to calcium handling abnormalities and endoplasmic reticulum stress in mice. *Front Cardiovascul Med*. (2021) 8:644128. doi: 10.3389/fcvm.2021.644128
33. Bartoli F, Bailey MA, Rode B, Mateo P, Antigny F, Bedouet K, et al. Orai1 Channel inhibition preserves left ventricular systolic function and normal Ca(2+) handling after pressure overload. *Circulation*. (2020) 141:199–216. doi: 10.1161/CIRCULATIONAHA.118.038891
34. Fredersdorf S, Thumann C, Zimmermann WH, Vetter R, Graf T, Luchner A, et al. Increased myocardial SERCA expression in early type 2 diabetes mellitus is insulin dependent: *In vivo* and *In vitro* data. *Cardiovasc Diabetol*. (2012) 11:57. doi: 10.1186/1475-2840-11-57
35. Toischer K, Teucher N, Unsöld B, Kuhn M, Kögler H, Hasenfuss G, et al. controls early load-dependent regulation of SERCA through calcineurin. *Basic Res Cardiol*. (2010) 105:795–804. doi: 10.1007/s00395-010-0115-2
36. Jaakkola P, Mole DR, Tian YM, Wilson MI, Gielbert J, Gaskell SJ, et al. Targeting of HIF- $\alpha$  to the von Hippel-Lindau ubiquitylation complex by O<sub>2</sub>-regulated prolyl hydroxylation. *Science*. (2001) 292:468–72. doi: 10.1126/science.1059796
37. Liang JN, Zou X, Fang XH, Xu JD, Xiao Z, Zhu JN, et al. The Smad3-miR-29b/miR-29c axis mediates the protective effect of macrophage migration inhibitory factor against cardiac fibrosis. *Biochimica et biophysica acta Molecular basis of disease*. (2019) 1865:2441–50. doi: 10.1016/j.bbdis.2019.06.004





## OPEN ACCESS

## EDITED BY

Amy Li,  
La Trobe University, Australia

## REVIEWED BY

Tom Burghardt,  
Mayo Clinic, United States  
Michael A. Flinn,  
Medical College of Wisconsin,  
United States

## \*CORRESPONDENCE

Danuta Szczesna-Cordary  
dszczesna@miami.edu

## SPECIALTY SECTION

This article was submitted to  
Cardiovascular Biologics and  
Regenerative Medicine,  
a section of the journal  
Frontiers in Cardiovascular Medicine

RECEIVED 06 July 2022

ACCEPTED 31 August 2022

PUBLISHED 20 September 2022

## CITATION

Kazmierczak K, Liang J,  
Gomez-Guevara M and  
Szczesna-Cordary D (2022) Functional  
comparison of phosphomimetic S15D  
and T160D mutants of myosin  
regulatory light chain exchanged in  
cardiac muscle preparations of HCM  
and WT mice.  
*Front. Cardiovasc. Med.* 9:988066.  
doi: 10.3389/fcvm.2022.988066

## COPYRIGHT

© 2022 Kazmierczak, Liang,  
Gomez-Guevara and  
Szczesna-Cordary. This is an  
open-access article distributed under  
the terms of the [Creative Commons  
Attribution License \(CC BY\)](#). The use,  
distribution or reproduction in other  
forums is permitted, provided the  
original author(s) and the copyright  
owner(s) are credited and that the  
original publication in this journal is  
cited, in accordance with accepted  
academic practice. No use, distribution  
or reproduction is permitted which  
does not comply with these terms.

# Functional comparison of phosphomimetic S15D and T160D mutants of myosin regulatory light chain exchanged in cardiac muscle preparations of HCM and WT mice

Katarzyna Kazmierczak, Jingsheng Liang,  
Michelle Gomez-Guevara and Danuta Szczesna-Cordary\*

Department of Molecular and Cellular Pharmacology, University of Miami Miller School of Medicine, Miami, FL, United States

In this study, we investigated the rescue potential of two phosphomimetic mutants of the myosin regulatory light chain (RLC, *MYL2* gene), S15D, and T160D RLCs. S15D-RLC mimics phosphorylation of the established serine-15 site of the human cardiac RLC. T160D-RLC mimics the phosphorylation of threonine-160, identified by computational analysis as a high-score phosphorylation site of myosin RLC. Cardiac myosin and left ventricular papillary muscle (LVPM) fibers were isolated from a previously generated model of hypertrophic cardiomyopathy (HCM), Tg-R58Q, and Tg-wild-type (WT) mice. Muscle specimens were first depleted of endogenous RLC and then reconstituted with recombinant human cardiac S15D and T160D phosphomimetic RLCs. Preparations reconstituted with recombinant human cardiac WT-RLC and R58Q-RLC served as controls. Mouse myosins were then tested for the actin-activated myosin ATPase activity and LVPM fibers for the steady-state force development and  $\text{Ca}^{2+}$ -sensitivity of force. The data showed that S15D-RLC significantly increased myosin ATPase activity compared with T160D-RLC or WT-RLC reconstituted preparations. The two S15D and T160D phosphomimetic RLCs were able to rescue  $V_{\text{max}}$  of Tg-R58Q myosin reconstituted with recombinant R58Q-RLC, but the effect of S15D-RLC was more pronounced than T160D-RLC. Low tension observed for R58Q-RLC reconstituted LVPM from Tg-R58Q mice was equally rescued by both phosphomimetic RLCs. In the HCM Tg-R58Q myocardium, the S15D-RLC caused a shift from the super-relaxed (SRX) state to the disordered relaxed (DRX) state, and the number of heads readily available to interact with actin and produce force was increased. At the same time, T160D-RLC stabilized the SRX state at a level similar to R58Q-RLC reconstituted fibers. We report here on the functional superiority of the established S15 phospho-site of

the human cardiac RLC vs. C-terminus T160-RLC, with S15D-RLC showing therapeutic potential in mitigating a non-canonical HCM behavior underlined by hypocontractile behavior of Tg-R58Q myocardium.

#### KEYWORDS

**myosin RLC, phosphorylation, phosphomimetic S15D and T160D RLCs, reconstituted cardiac muscle preparations, super-relaxed state of myosin, transgenic mice**

## Introduction

Phosphorylation of cardiac sarcomeric proteins is a critical regulator of cardiac muscle contraction and a modulator of the physiological performance of the heart. Among essential phosphorylatable proteins is the regulatory light chain (RLC) of cardiac myosin (*MYL2* gene), which is attached to the myosin heavy chain (MHC) at the distal part of the neck region (lever arm) of the myosin head (1). The RLC, together with the adjacent myosin essential light chain (ELC), provides structural stability to the lever arm and supports an ATP-dependent rotational movement of this region of the myosin head to execute the power stroke and sarcomere shortening (2–4). The N-terminus of myosin RLC comprises a  $\text{Ca}^{2+}/\text{Mg}^{2+}$  binding site and myosin light chain kinase (MLCK)-dependent phosphorylation site, both regions capable of altering the alpha-helical structure of the RLC and its  $\text{Ca}^{2+}$  binding properties (5, 6). Under physiological conditions, the cardiac regulatory light chain is phosphorylated at  $\sim 0.4$  moles of phosphate per mole of RLC in various species, including humans (7, 8). RLC phosphorylation has been proposed to result in the movement of myosin heads toward thin filaments facilitating cross-bridge formation, accelerating rates of actin-myosin interaction, and increasing the  $\text{Ca}^{2+}$  sensitivity of force development (9–12). Studies from the Irving group suggest that RLC phosphorylation induces changes in the  $\text{Ca}^{2+}$  sensitivity of force through structural changes in thin filaments rather than by phosphorylation-induced availability of myosin heads for thin-filament binding (13).

In rodent hearts, RLC can be unphosphorylated or occur in a single or double phosphorylated form at two serine residues,

S14 and S15. At the same time, the human ventricular RLC can only be singly-phosphorylated at S15 (14). Using an *in vitro* phosphorylation assay with cardiac MLCK, it was shown that S15 of the human cardiac RLC is the only N-terminal RLC site that is phosphorylated by cardiac MLCK (10). This result confirmed the physiological relevance of the S15-RLC site in the heart.

The question that we asked in this investigation was whether there are other phosphorylatable residues in the human cardiac RLC that could play functional roles in actomyosin interaction and cardiac muscle contraction. Besides the established S15 site, *in-silico* analysis identified two new sites at T125 and T160 as highly scored phosphorylatable residues in the human cardiac RLC (15, 16) (Figure 1). Relevant to this investigation is the fact that T160 is localized in the C-terminus of the RLC molecule. This region encompasses many *MYL2* variants associated with hypertrophic cardiomyopathy (HCM). One of the first *MYL2* mutations identified to cause HCM and located in the C-terminus RLC was D166V, where the last amino acid, aspartate-166, was replaced by valine (17). Notably, the D166V mutation was also associated with malignant HCM outcomes. The same aspartate-166 residue was found to be mutated to alanine (D166A) in a cohort of 124 consecutive HCM patients in the study by Alvarez-Acosta et al. (18). The authors also reported on I158L-RLC mutation causing obstructive hypertrophy and atrial fibrillation but with a good prognosis (18). In 2020, D166 residue was again found to be mutated to histidine (D166H) (19). D166H was found among multigenerational family members and appeared to be highly penetrant. A high restrictive filling pattern and atrial fibrillation incidence were observed (19). In the same year, the Garg group reported on another missense *MYL2* variant (G162R) located in the vicinity of T160 in the C-terminus of RLC (20).

Therefore, this investigation focused on the C-terminal T160-RLC residue that comprises several *MYL2* missense mutations of benign to malignant HCM phenotypes (17–20). The goal was to study whether the phosphorylation of T160 *via* the RLC phosphomimetic approach, replacing aspartate for threonine (T160D), would be able to mitigate any of the HCM adverse phenotypes in a mouse model of HCM reconstituted with recombinant human cardiac T160D-RLC. The function of T160D-RLC phosphomimetic was compared to that of S15D-RLC, which was assessed along with T160D

Abbreviations: DRX, Disordered relaxed state; ELC, Essential light chain of myosin; HCM, Hypertrophic cardiomyopathy; Mant-ATP, (N-Methylanthraniloyl)-ATP (fluorescent); MHC, Myosin heavy chain; MLCK, Myosin light chain kinase;  $n_H$ , Hill coefficient; P1, Amplitude of fast DRX phase; P2, Amplitude of slow SRX phase; R58Q, Arg → Gln mutation in myosin RLC; RLC, Regulatory light chain of myosin; S15D, Phosphomimetic RLC where serine-15 is replaced by aspartic acid; SRX, Super-relaxed state; T1, Nucleotide turnover lifetime in DRX; T2, Nucleotide turnover lifetime in SRX; T160D, Phosphomimetic RLC where threonine 160 is replaced by aspartic acid; Tg, Transgenic; WT, Wild-type.

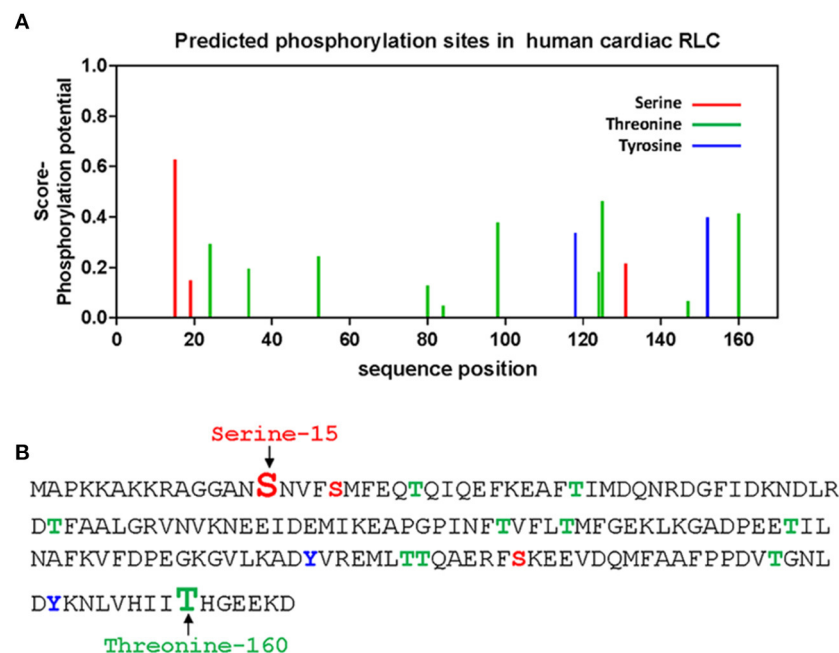


FIGURE 1

*In-silico* prediction of phosphorylation sites of the human cardiac RLC. (A) Phosphorylation of Ser/Tyr/Thr sites in the RLC was predicted by PhosphoSVM search <http://sysbio.unl.edu/PhosphoSVM/prediction.php/>. (B) Amino acid sequence of the human cardiac RLC (NCBI\_P10916) with the location of predicted pSer, pTyr, and pThr residues. Bolded and enlarged, the S15 (in red font) and T160 (in green font) sites are studied in this report.

and served as a control. We also compared the data on S15D-RLC phosphomimetic to previous studies of S15D-RLC phosphomimetic-induced effects on heart function *in vitro* (21, 22) and *in vivo* (23, 24). Specifically, we previously showed that S15D phosphomimetic in the background of HCM-D166V RLC mutation was able to rescue the binding of D166V-myosin to actin and increased force generation capacity in the *in vitro* motility assays compared with D166V reconstituted porcine myosin (21). Likewise, S15D phosphomimetic in the background of human cardiac HCM-R58Q RLC mutation rescued R58Q-exerted low isometric force and Vmax of actin-activated myosin ATPase activity in S15D-R58Q- vs. R58Q-reconstituted porcine cardiac muscle preparations (22). We also showed improved heart function *in vivo* in HCM-D166V mice injected with AAV9-S15D-RLC (24) and in double transgenic mice expressing the S15D phosphomimetic in the background of HCM-D166V mutation (23).

We cloned and expressed human cardiac T160D and S15D phosphomimetic RLC mutants and tested them in chemically skinned, and RLC-depleted left ventricular papillary muscles (LVPM) and cardiac myosin from transgenic wild-type (Tg-WT) and HCM Tg-R58Q mice. Both mouse models expressed the human cardiac RLC-WT or RLC-R58Q mutant.

The R58Q model displays a non-canonical HCM phenotype that is hypo- rather than hypercontractile and stabilizes the

OFF state of myosin in LVPM fibers from Tg-R58Q mice, and in R58Q recombinant protein-reconstituted porcine fibers (22). A similar observation of the R58Q-mediated hypocontractile activity was reported by Kampourakis et al. who demonstrated that R58Q promotes an OFF state that reduces the number of myosin cross-bridges readily available for actin interaction and ATP utilization (25). Using a loaded *in vitro* motility assay, we previously showed an R58Q-mediated decrease in actin sliding velocity resulting in a significant reduction in force production (26, 27). Interestingly, actin sliding velocity and force were restored upon MLCK-induced phosphorylation of the R58Q mutant (26).

In this report, we showed that in Tg-R58Q preparations, both T160D and S15D phosphomimetics -could restore myosin ATPase activity and maximal isometric tension to the level observed for WT-RLC-reconstituted HCM Tg-R58Q preparations. However, S15D-RLC was more efficient than T160D-RLC in activating myosin ATPase activity ( $V_{max}$ ) in Tg-R58Q and Tg-WT hearts. In addition, in LVPM fibers of HCM-R58Q myocardium, S15D-RLC was observed to cause a shift in the myosin energetic states from the super-relaxed (SRX) to disordered relaxed (DRX) state, while T160D-RLC maintained the SRX-to-DRX ratio at the level observed for R58Q-reconstituted fibers. Alterations of cardiac SRX may result in changes in sarcomere force production and energy utilization

in the heart (28). Therefore, the S15D-RLC-mediated increase in the DRX heads readily available to interact with actin and produce force suggests that S15D-RLC phosphomimetic may serve as a therapeutic modality to counteract the hypocontractile activity of HCM-R58Q myocardium.

## Materials and methods

### Transgenic mice

This work was performed in accordance with the Guide for the Care and Use of Laboratory Animals published by the U.S. National Institutes of Health (NIH Publication no. 85–23, revised 2011). Animal protocols were endorsed by the Institutional Animal Care and Use Committee at the University of Miami Miller School of Medicine (protocol #21-106 LF). The assurance number is #A-3224-01, approved through November 30, 2023. Mice were euthanized by CO<sub>2</sub> inhalation that was followed by cervical dislocation.

The characterization of transgenic (Tg) mice, including the determination of Tg protein expression, has been previously described (29). For this study, we used Tg-WT line 2 (L2), expressing ~90% of human cardiac WT-RLC (NCBI\_P10916), and two Tg-R58Q lines, L8 and L9, showing ~95% expression of human cardiac R58Q-RLC (29, 30).

### Cloning, expression, and purification of recombinant RLC proteins

Reverse transcription-polymerase chain reaction and primers based on the published cDNA RLC sequence (GenBank™ Accession No. AF020768) were used to generate the cDNAs of human cardiac WT-RLC and RLC mutants. Standard methods described previously (5) were utilized to produce cDNAs of WT-RLC and two phosphomimetic RLC mutants, S15D (GenBank accession number ON950401) and T160D (GenBank accession number ON950400). Briefly, the cDNAs were obtained by overlapping sequential polymerase chain reaction and subsequently transformed into BL21 expression host cells to express proteins in 16L cultures. Proteins were then purified by ion-exchange chromatography and eluted with a salt gradient of 0–450 mM NaCl. In the first step an S-Sepharose column was used equilibrated with 2 M urea, 20 mM sodium citrate, 0.1 mM PMSE, 1 mM 1,4-dithiothreitol (DTT), and 0.02% NaN<sub>3</sub>, pH 6.0. Eluted proteins were purified further using a Q-Sepharose column equilibrated with 2 M urea, 25 mM Tris-HCl, 0.1 mM PMSE, 1 mM DTT, and 0.02% NaN<sub>3</sub>, pH 7.5. The purity of all recombinant RLC proteins was determined by 15% SDS-PAGE (5, 21).

### Isolation and purification of mouse cardiac myosin

Cardiac myosin was isolated from mouse hearts of 9–12 month-old male and female Tg-WT and Tg-R58Q mice as described earlier (31). In short, myosin was extracted from the homogenized ventricular tissue in an ice-cold Guba Straub-type buffer (300 mM NaCl, 100 mM NaH<sub>2</sub>PO<sub>4</sub>, 50 mM Na<sub>2</sub>HPO<sub>4</sub>, 1 mM MgCl<sub>2</sub>, 10 mM EDTA, 0.1% NaN<sub>3</sub>, 10 mM Na<sub>4</sub>P<sub>2</sub>O<sub>7</sub>, 1 mM DTT, and a protease inhibitor cocktail, pH 6.5). The extract was incubated on ice for 40 min and then ultracentrifuged at 200,000 g for 1 h (4°C). The supernatant was diluted 60-fold (by volume) with 2 mM DTT and left on ice for 60 min to precipitate filamentous myosin. Precipitated myosin was then centrifuged at 8,000 g for 10 min (4°C). The pellet was dissolved in a small volume of myosin buffer containing 0.4 M KCl, 10 mM 3-(n-morpholino) propane sulfonic acid (MOPS) (pH 7.0), 5 mM DTT, and a protease inhibitor cocktail. Myosin samples were diluted with glycerol in a 1:1 ratio and stored at –20°C until used. The purity of myosin preparations was tested by SDS-PAGE. Gel samples were prepared by mixing myosin solution 1:1 by volume with Laemmli buffer (62.5 mM Tris-HCl, pH 6.8, 25% glycerol, 2% SDS, 0.01% Bromophenol blue, and 5% β-mercaptoethanol, BME). Mixtures were heated at 95°C for 5 min and stored at –20°C until used for SDS-PAGE.

### Replacement of endogenous RLC from mouse cardiac myosin with the human cardiac WT and mutant RLCs

Depletion of endogenous RLC from mouse cardiac myosin (Tg-WT and Tg-R58Q) was achieved by using the buffer containing 1% Triton X-100 and 5 mM CDTA (cyclohexane-1,2-diamine tetra acetic acid), pH 8.5, as described earlier for porcine cardiac myosin (21). Reconstitution of depleted myosins was achieved by mixing them with a 3-fold molar excess of recombinant human cardiac RLC proteins, WT, S15D, T160D for Tg-WT myosin, and WT, S15D, T160D, and R58Q for Tg-R58Q myosin in a buffer containing 0.4 M KCl, 50 mM MOPS, pH 7.0, 2 mM MgCl<sub>2</sub>, and 1 mM DTT. After the brief incubation, the complexes were placed in dialyzing tubes and dialyzed against the same buffer for 2 h at 4°C. Subsequently, the complexes were transferred to 5 mM DTT and dialyzed overnight at 4°C. This process resulted in the precipitation of myosin reconstituted with different recombinant RLC proteins. Reconstituted myosin complexes were then centrifuged at 8,000 g for 10 min (4°C). Pelleted myosin-RLC complexes were resuspended in the buffer consisting of 0.4 M KCl, 10 mM MOPS, pH 7.0, and 1 mM DTT, mixed 1:1 with glycerol and stored at –20°C until needed. The quality of myosin-RLC complexes was tested by SDS-PAGE.

## ATPase measurements

Rabbit skeletal F-actin was used in the ATPase experiments. The protocol for actin purification was detailed in our earlier publication (21). Reconstituted mouse cardiac myosins (stored previously in 50% glycerol) were precipitated with 13 volumes of ice-cold 2 mM DTT and centrifuged at 8,000 g for 10 min (4°C). Pelleted myosins were resuspended in myosin buffer (0.4 M KCl, 10 mM MOPS, and 1 mM DTT, pH 7.0) and dialyzed against it overnight at 4°C. Following determination of the concentration of reconstituted myosin preparations with Coomassie Plus protein assay (Pierce, Rockford, IL, USA), myosin at 0.5  $\mu$ M concentration was titrated with 0.1, 0.5, 1.5, 3, 5, 7.5, 10, and 15  $\mu$ M F-actin. The assay was performed in duplicate on a 96-well plate in a buffer consisting of 25 mM imidazole (pH 7.0), 4 mM  $\text{MgCl}_2$ , 1 mM EGTA, 1 mM DTT, and 77.7 mM final KCl salt concentration. The reaction, performed in a Jitterbug incubator shaker, was initiated by adding 2.5 mM ATP and continued for 15 min at 30°C. The reaction was terminated with 4% ice-cold trichloroacetic acid (TCA). Precipitated proteins were then centrifuged, and the supernatants were used for the assessment of inorganic phosphate by Fiske and Subbarow method (21, 32). Data points were fitted to Michaelis–Menten equation, yielding  $V_{\text{max}}$  (maximal activity) and  $K_m$  (Michaelis–Menten dissociation constant) (21, 33).

## Preparation of skinned LVPM fibers

Left ventricular papillary muscle (LVPM) fibers were isolated from 5 to 7 month-old Tg-WT and Tg-R58Q mice. They were dissected into small muscle bundles ( $\sim 2\text{--}3 \times 0.5\text{--}1$  mm in size) in an ice-cold relaxing (pCa 8) solution ( $10^{-8}$  M  $\text{Ca}^{2+}$ , 1 mM free  $\text{Mg}^{2+}$ , total MgPr, propionate = 3.88 mM, 7 mM EGTA, 2.5 mM Mg-ATP $^{2-}$ , 20 mM MOPS pH 7.0, 15 mM creatine phosphate, and 15 U/ml of phosphocreatine kinase, ionic strength = 150 mM adjusted with KPr) and in the presence of 30 mM 2,3-Butanedione 2-monoxime (BDM) and 15% glycerol. Muscle bundles were then transferred to a fresh pCa 8 solution mixed with 50% glycerol (storage solution) and incubated for 1 h on ice. Muscle strips were chemically skinned in 1% Triton X-100 added to the mixture of pCa 8 solution and glycerol (50:50 by volume) overnight at 4°C. The bundles were transferred to a new storage solution and kept for 5–10 days at  $-20^\circ\text{C}$  (30).

## CDTA-Extraction of endogenous RLC from LVPM fibers and reconstitution with recombinant RLC proteins

Endogenous RLC depletion from mouse LVPM preparations was achieved by treatment of fibers  $\sim 100 \mu\text{m} \times \sim 1.5$  mm

in size isolated from glycerinated LVPM bundles with an extraction buffer composed of 5 mM CDTA, 1% Triton X-100, 50 mM KCl, 40 mM Tris, 0.6 mM  $\text{NaN}_3$ , 0.2 mM PMSF at pH 8.4, and protease inhibitor cocktail for 40 min at room temperature. The CDTA/Triton-treated fibers were incubated with 15  $\mu$ M of cardiac troponin C (TnC) in pCa 8 solution due to the potential extraction of endogenous TnC under these conditions. RLC-depleted and TnC reconstituted LVPM strips were subsequently incubated in pCa 8 solution containing 40  $\mu$ M recombinant WT, T160D, or S15D RLC proteins for Tg-WT strips and 40  $\mu$ M recombinant WT, R58Q, T160D, and S15D RLCs for Tg-R58Q strips for 45 min at room temperature. RLC and TnC reconstituted LVPM fibers were washed in a pCa 8 buffer and kept at  $-20^\circ\text{C}$  for 1–5 days until needed for experiments. SDS-PAGE tested the degree of RLC depletion and RLC reconstitution in LVPM fibers.

## SDS-PAGE experiments

The myosin and LVPM samples were run on 15% SDS-PAGE gels. For myosin,  $\sim 20 \mu\text{g}$  of protein was used per well, and for LVPM, one fiber per well. The bands were stained with Coomassie Brilliant Blue. The gels were scanned using the Odyssey infrared imaging system (LICOR Biosciences, Lincoln, NE, USA). The level of RLC depletion and reconstitution was determined by densitometry analysis using ImageJ software (<https://imagej.nih.gov/ij/>) measuring RLC/ELC band intensities in native myosin/LVPM, RLC-depleted, and RLC-reconstituted myosin/LVPM. Myosin ELC that was not extracted during the RLC-depletion/reconstitution experiment was used as a loading control (34).

## Force-pCa study

LVPM fibers  $\sim 1.5$  mm in length and  $\sim 100 \mu\text{m}$  in diameter were isolated from glycerinated muscle bundles, rinsed several times in pCa 8 solution, and mounted on the force transducer of the Guth Muscle Research System (Heidelberg, Germany). The fibers were treated with 1% Triton X-100 in pCa 8 buffer for 30 min at room temperature. After skinning with Triton X-100, muscle fibers were washed in pCa 8 buffer (3 times  $\times$  5 min), and their sarcomere length was adjusted to 2.1–2.2  $\mu\text{m}$ . Then LVPM fibers were tested for maximal steady-state force development in pCa 4 solution, which has the same composition as pCa 8 buffer except the  $[\text{Ca}^{2+}] = 10^{-4}$  M, and relaxed in pCa 8 solution. For the force-pCa relationship, the fibers were placed in solutions of increasing  $\text{Ca}^{2+}$  concentration from pCa 8 to pCa 4 and the level of force was measured in each “pCa” solution. The force-pCa dependence for RLC-depleted fibers was performed after the fibers were reconstituted with TnC. Maximal tension (in  $\text{kN/m}^2$ ) was determined from



averaged values of tension measured before and after the force-pCa dependence and divided by the cross-sectional area of fibers. The diameter of fibers was estimated using an SZ6045 Olympus microscope with the measurement taken at 3 points along the fiber length and averaged. Force-pCa data were fitted to the Hill equation and the pCa<sub>50</sub> (midpoint of force-pCa dependence and measure of calcium sensitivity) and n<sub>H</sub> (Hill coefficient and measure of myofilament cooperativity) values were established for LVPM from Tg-WT, and Tg-R58Q mice reconstituted with recombinant RLCs proteins.

## Measurement of SRX ↔ DRX equilibrium by mant-ATP chase assay

Tg-WT and Tg-R58Q reconstituted LVPM fibers (~100 μm in diameter) were subjected to measurements of the super-relaxed (SRX) state of myosin. ATP turnover rates were measured by rapid exchange of fluorescent N-methylanthraniloyl (mant)-ATP with non-fluorescent (dark) ATP in skinned LVPM from all groups of mice using the previously described IonOptix Instrument (22, 35). The experiment was initiated with the fiber placed in a chamber under the microscope and incubated in a solution containing 250 μM mant-ATP in a rigor solution [120 mM KPr, 5 mM MgPr, 2.5 mM K<sub>2</sub>HPO<sub>4</sub>, 2.5 mM KH<sub>2</sub>PO<sub>4</sub>, 50 mM MOPS (pH 6.8), and fresh 2 mM DTT]. After fluorescence intensity reached a stable level, the fiber was chased with 4 mM non-labeled (dark) ATP. Fluorescence intensity decay isotherms were plotted as a function of time and fitted to a double-exponential equation  $Y = 1 - P1[1 - \exp(-t/T1)] - P2[1 - \exp(-t/T2)]$ , where P1 and P2 are the amplitudes of the fast phase, and slow phase of decay, respectively, and T1 and T2 are their respective lifetimes (36). To relate the P1 and P2 values to the number of myosin heads directly occupying the DRX and SRX states, the rapid phase of the fluorescence decay, P1, was corrected for the fast release of non-specifically bound mant-ATP. The correction was established experimentally using a competition assay and was equal to  $0.44 \pm 0.02$ , and the fraction of myosin heads directly occupying the SRX state was calculated as  $P2/(1-0.44)$  (35).

## Secondary structure prediction of WT and R58Q RLCs as well as their phosphomimetic mutants

The secondary structure prediction was executed using the I-TASSER approach developed by the Zhang laboratory, University of Michigan, and available online at <http://zhanglab.ccmb.med.umich.edu/ITASSER/>. The amino acid sequences of S15D/T160D phosphomimetic RLCs in the background of WT-RLC or R58Q-RLC were compared against template proteins

of similar structures chosen from the protein data bank (PDB) library. High similarity structures were used: 5tbyE (Chain E, Myosin regulatory light chain 2, ventricular/cardiac muscle isoform), 3dtpE, 3jvtB (Chain B, calcium-bound Scallop Myosin Regulatory Domain (Lever Arm) with reconstituted complete Light Chains), 3pn7E, 3j04B (Chain B, EM structure of the heavy meromyosin subfragment of Chick smooth muscle myosin with regulatory light chain in phosphorylated state), 3i5iB, 2w4aB (Chain B, isometrically contracting Insect Asynchronous Flight Muscle), 2bl0C, 6iihA, 6k7yI. Fragments of the above templates were used for the assembly of the full-length protein, which was further simulated into the lowest-energy model using specific algorithms. Each predicted model structure was given a confidence C-score, ranging from -5 to 2, estimating the quality of the predicted models (37). The predicted protein structures were then visualized using PyMol ([www.pymol.org](http://www.pymol.org)).

## Statistical analysis

All values are shown as means ± SD with statistical significance determined as  $p < 0.05$  using one-way ANOVA and Tukey's multiple comparison test (GraphPad Prism software version 7.0 for Windows).

## Results

To elucidate the effects of T160D and S15D phosphomimetic RLCs on cardiac muscle contraction and myosin energetics in HCM vs. WT hearts, we isolated cardiac myosin and LVPM preparations from Tg-R58Q and Tg-WT mouse models and subjected them to the depletion/reconstitution procedures. Reconstituted myosin and LVPM preparations were then used to measure actin-activated myosin ATPase activity, force-pCa relationship, and the super-relaxed state of myosin (36, 38). The latter is essential to understanding cardiac muscle's structure-function relationship and myosin energetic states (28).

## Effects of S15D and T160D phosphomimetic RLCs on myosin ATPase activity

Myosin was extracted from heart ventricles of Tg-WT and Tg-R58Q mice and subjected to the depletion/reconstitution protocol, as described in Yadav et al. (22). The depletion of endogenous RLC resulted in ~40% of residual RLC still present in myosin from Tg-WT and Tg-R58Q hearts (Figure 2). The reconstitution of RLC-depleted Tg-WT or Tg-R58Q (Figure 2A) myosin with recombinant T160D, S15D, R58Q, and WT RLC proteins was achieved by incubation of RLC-depleted myosin with a 3-fold molar excess of recombinant RLC proteins.

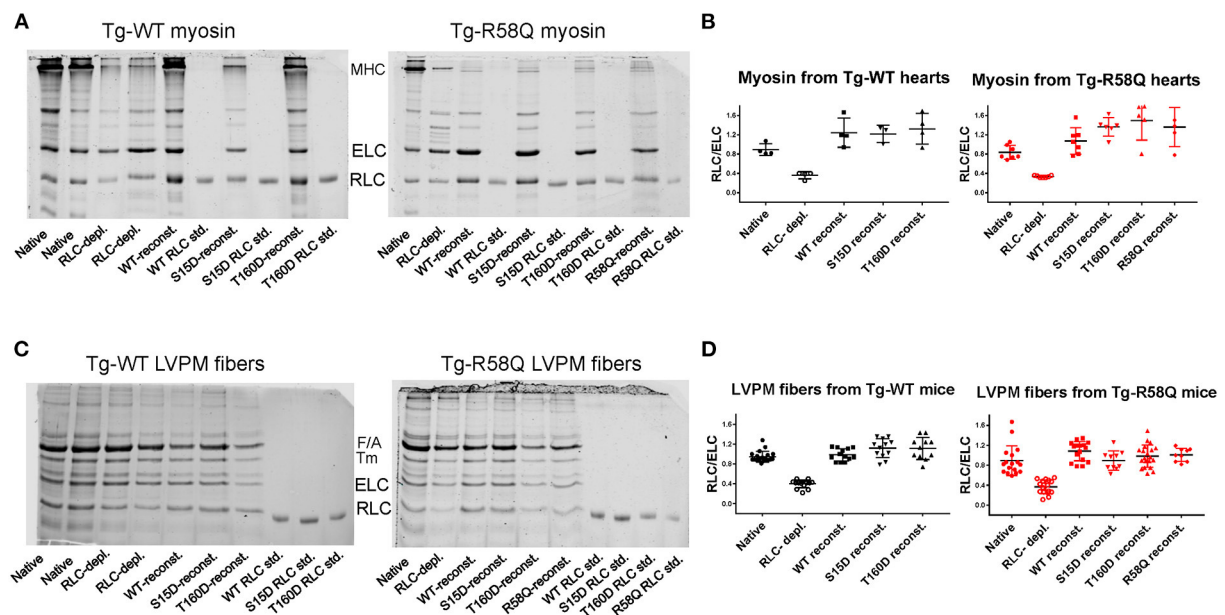


FIGURE 2

Representative SDS-PAGE images of RLC-depleted and mutant-reconstituted cardiac muscle preparations from Tg-WT and Tg-R58Q mice. (A) Depletion and reconstitution experiments in mouse-purified cardiac myosin. (B) Myosin gels' quantification. (C) Depletion and reconstitution experiments in LVPM fibers. (D) LVPM gels' quantification. Cardiac preparations were CDTA/Triton-depleted of endogenous RLC and reconstituted with recombinant WT-RLC, R58Q, T160D, and S15D RLC proteins. Three to Four different myosin preparations from Tg-WT and 5–7 from Tg-R58Q mice were used to deplete  $60 \pm 6\%$  endogenous RLC, followed by myosin reconstitution with recombinant RLC proteins at  $140 \pm 30\%$  in Tg-WT and  $155 \pm 40\%$  Tg-R58Q myosin (A,B). Eleven to Twenty LVPM fibers from Tg-WT and 9–20 from Tg-R58Q mice were employed to deplete  $60 \pm 12\%$  RLC from LVPM, followed by  $112 \pm 20\%$  reconstitution with recombinant RLC proteins in Tg-WT and  $106 \pm 21\%$  in Tg-R58Q LVPM fibers (C,D). Data in (B,D) are presented as means  $\pm$  SD.

As shown in Figure 2B, RLC-depleted myosin was  $>100\%$  reconstituted with recombinant RLC proteins, as judged by the RLC/ELC bands' ratios of SDS-PAGE. Reconstituted myosin preparations at a concentration of  $0.5 \mu\text{M}$  were complexed with  $0\text{--}15 \mu\text{M}$  actin, and the ATPase activity assays were performed.

As shown in Figure 3A, the titration isotherms for T160D-RLC reconstituted Tg-WT myosin were similar to WT-RLC-reconstituted but significantly different than those of Tg-WT myosin reconstituted with S15D RLC. The  $V_{\text{max}}$  of S15D-RLC reconstituted Tg-WT myosin was 1.2 and 1.3-fold higher than that of WT or T160D-RLC reconstituted, respectively (Figure 3A; Table 1). The summary of statistical analysis of actin-activated myosin ATPase activity isotherms of Tg-WT and Tg-R58Q reconstituted myosin is presented in Table 2. Titration isotherms for HCM Tg-R58Q myosin reconstituted with WT-RLC, T160D, S15D, and R58Q are shown in Figure 3B and analyzed for significance in Table 2. For Tg-R58Q myosin, the  $V_{\text{max}}$  was the lowest in R58Q-RLC reconstituted compared with WT-RLC, T160D-RLC, or S15D-RLC-reconstituted (Figure 3B; Table 1). Both T160D and S15D phosphomimetic RLCs could restore the maximal ATPase activity in Tg-R58Q myosin to the level observed for WT-RLC reconstituted, but S15D-RLC appeared to be more effective, with significantly

higher  $V_{\text{max}}$  compared to T160D-RLC-reconstituted Tg-R58Q myosin (Figure 3B; Table 1). Interestingly, in our previous study of actin-activated myosin ATPase activity measured in reconstituted porcine cardiac myosin, a significantly lower  $V_{\text{max}}$  of R58Q-RLC vs. WT-RLC reconstituted myosin could be rescued by the S15D phosphomimetic R58Q protein (22). In summary, significant differences were noted between S15D-RLC vs. T160D-RLC RLCs, with the S15D-RLC surpassing the T160D-RLC in rescuing the low ATPase activity of R58Q-RLC-reconstituted myosin purified from HCM Tg-R58Q myocardium (Figure 3B; Tables 1, 2). The  $K_m$  values were not significantly different among all tested proteins (Table 1).

### Isometric force generation in mutant-reconstituted LVPM fibers from HCM-R58Q mice is rescued by S15D and T160D phosphomimetic RLC proteins

The effects of RLC phosphomimetics on the force-pCa dependence were assessed in skinned LVPM fibers from Tg-WT and HCM Tg-R58Q mice that were depleted of endogenous

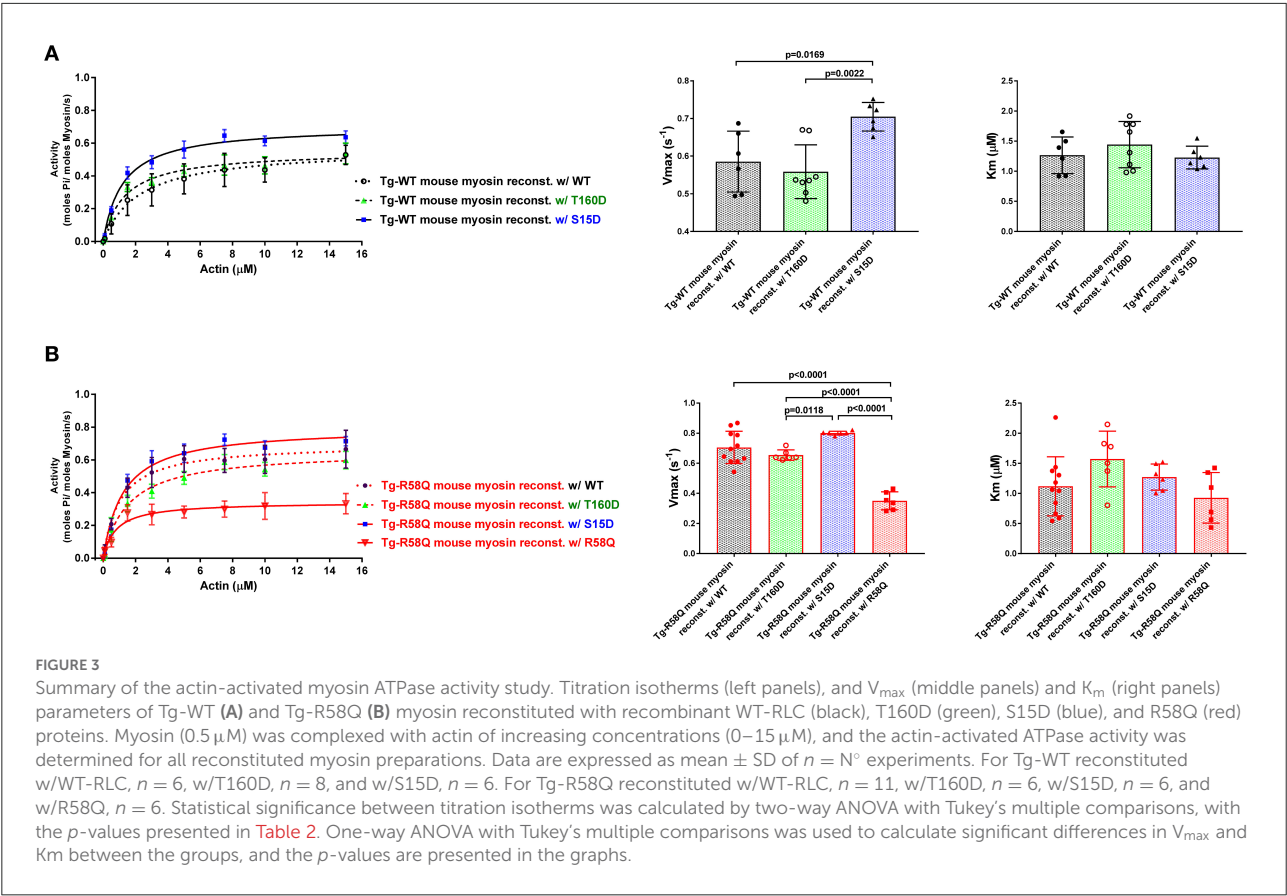


TABLE 1 Summary of actin-activated myosin ATPase activity study.

Parameter/recombinant RLC protein	Myosin from Tg-WT mice			Myosin from Tg-R58Q mice			
	WT	T160D	S15D	WT	T160D	S15D	R58Q
$V_{max}$ ( $s^{-1}$ ) $\pm$ SD	$0.59 \pm 0.08$	$0.56 \pm 0.07^{*#}$	$0.71 \pm 0.04^*$	$0.71 \pm 0.11$	$0.66 \pm 0.04^{*,\wedge,\wedge,\wedge}$	$0.80 \pm 0.01^{\wedge,\wedge,\wedge}$	$0.35 \pm 0.06^{****}$
$K_m \pm$ SD	$1.27 \pm 0.31$	$1.44 \pm 0.38$	$1.23 \pm 0.19$	$1.12 \pm 0.49$	$1.57 \pm 0.46$	$1.27 \pm 0.22$	$0.93 \pm 0.42$
$n = N^\circ$ experiments	6	8	6	11	6	6	6

Values are means  $\pm$  SD for  $n = N^\circ$  of independent experiments. Significance was calculated by one-way ANOVA with Tukey's multiple comparison test with  $^*p < 0.05$  and  $****p < 0.0001$  for S15D, T160D or R58Q for mutant vs. WT protein,  $^{\#}p < 0.05$  and  $^{##}p < 0.01$  for T160D vs. S15D,  $^{\wedge,\wedge,\wedge}p < 0.0001$  for T160D and S15D vs. R58Q.

RLC protein and reconstituted with either S15D or T160D RLCs along with WT and R58Q RLC controls (Figures 4A,B). Representative images of CDTA/Triton-depleted and RLC/TnC-reconstituted mouse LVPM from Tg-WT and Tg-R58Q hearts are presented in Figure 2C. As illustrated in Figure 2D,  $\sim 60\%$  of RLC depletion could be achieved in Tg-WT and Tg-R58Q LVPM fibers that were subsequently  $\sim 110\%$  reconstituted with recombinant RLC proteins (Figure 2D).

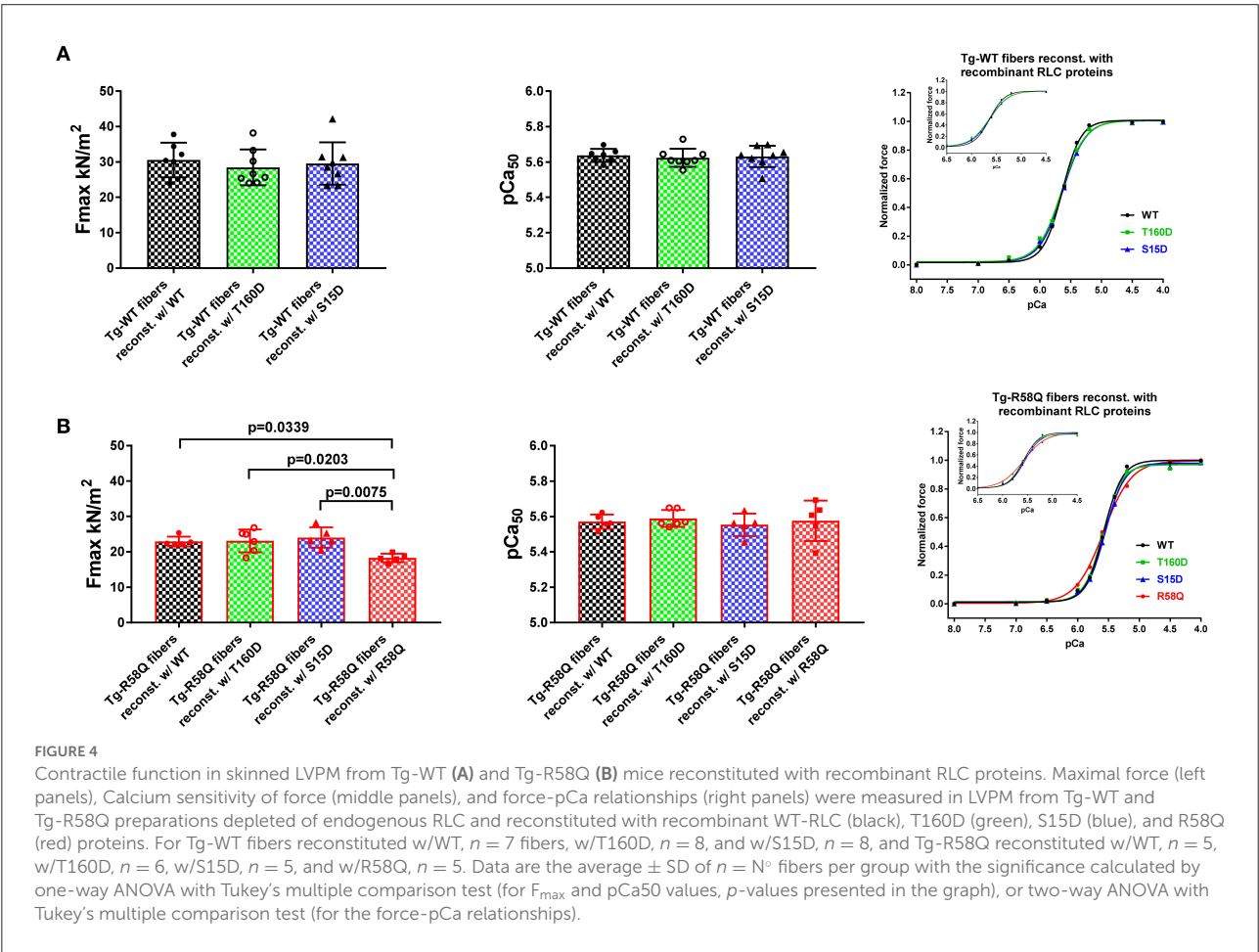
In Tg-WT, maximum isometric tension per cross-section of muscle (in  $\text{kN/m}^2$ ) and force-pCa relationship were similar among all reconstituted fibers (Figure 4A; Table 3). However, LVPM fibers from Tg-R58Q show the lowest

level of force for R58Q-reconstituted compared with S15D, T160D, and WT-RLC-reconstituted LVPM (Figure 4B). Both S15D and T160D phosphomimetic RLC mutants were equally efficient in bringing up the level of force to that observed for WT-RLC-reconstituted fibers from Tg-R58Q mice (Figure 4B; Table 3). Like for LVPM from Tg-WT mice, the calcium sensitivity of force, represented by  $pCa_{50}$ , was not different among all tested RLC proteins reconstituted in Tg-R58Q fibers (Figure 4; Table 3). Differences were noted in the Hill coefficient ( $n_H$ ) between WT and mutant-reconstituted fibers from both groups of transgenic fibers (Table 3).

**TABLE 2** Summary of statistical analysis of actin-activated myosin ATPase activity of Tg-WT and Tg-R58Q myosin reconstituted with recombinant human cardiac WT-RLC, S15D and T160D phosphomimetics, and R58Q mutant.

System/actin concentration ( $\mu$ M)	<i>p</i> -values							
	0.1	0.5	1.5	3	5	7.5	10	15
Tg-WT reconst. w/WT vs. w/S15D	NS	NS	0.0037	0.0032	0.0002	<0.0001	<0.0001	0.0005
Tg-WT reconst. w/WT vs. w/T160D	NS	NS	NS	NS	NS	0.0459	NS	NS
Tg-WT reconst. w/T160D vs. w/S15D	NS	NS	0.0011	<0.0001	<0.0001	<0.0001	<0.0001	<0.0001
Tg-R58Q reconst. w/WT vs. w/R58Q	NS	0.001	<0.0001	<0.0001	<0.0001	<0.0001	<0.0001	<0.0001
Tg-R58Q reconst. w/WT vs. w/T160D	NS	NS	0.0056	0.0007	0.0006	NS	NS	NS
Tg-R58Q reconst. w/WT vs. w/S15D	NS	NS	NS	NS	NS	0.0001	NS	NS
Tg-R58Q reconst. w/T160D vs. w/S15D	NS	NS	0.0002	<0.0001	<0.0001	0.0003	0.0005	0.0033
Tg-R58Q reconst. w/T160D vs. w/R58Q	NS	NS	NS	0.0002	<0.0001	<0.0001	<0.0001	<0.0001
Tg-R58Q reconst. w/S15D vs. w/R58Q	NS	NS	<0.0001	<0.0001	<0.0001	<0.0001	<0.0001	<0.0001

Two-way ANOVA with Tukey's multiple comparison test was applied.



# Mutant RLC-mediated regulation of SRX↔DRX equilibrium in LVPM from HCM Tg-R58Q vs. Tg-WT mice

In contracting muscle, myosin cross-bridges oscillate between the active and relaxed states, with the latter

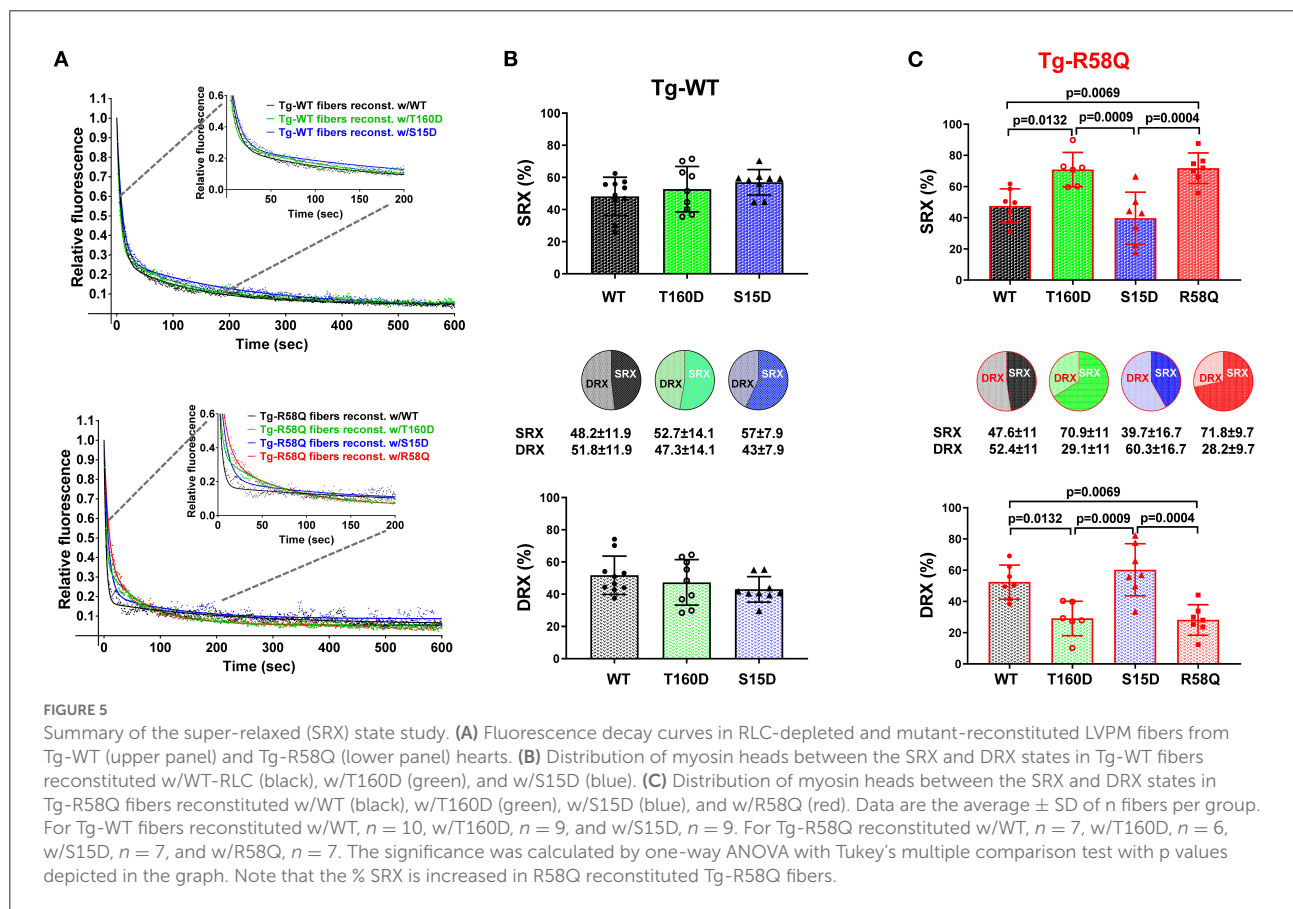
comprising the SRX energy-saving conformation and the DRX state facilitating cross-bridge formation with greater ATP consumption (39). Under relaxation conditions, myosin cross-bridges may exist in various structural and biochemical states, and each state is associated with different energy consumption rates (40). Modulation of myosin function



TABLE 3 Contractile function in skinned LVPM from Tg-WT and Tg-R58Q mice reconstituted with recombinant RLCs proteins.

Parameter/recombinant RLC protein	LVPM from Tg-WT mice			LVPM from Tg-R58Q mice			
	WT	T160D	S15D	WT	T160D	S15D	R58Q
Fmax (kN/m <sup>2</sup> ) ± SD	30.54 ± 4.9	28.44 ± 5.07	29.57 ± 6.01	22.92 ± 1.39 <sup>^</sup>	23.09 ± 3.22 <sup>^</sup>	24.04 ± 1.3 <sup>^^</sup>	18.28 ± 1.22
pCa <sub>50</sub> ± SD	5.64 ± 0.04	5.62 ± 0.05	5.63 ± 0.06	5.57 ± 0.04	5.59 ± 0.05	5.55 ± 0.06	5.58 ± 0.11
n <sub>H</sub> Hill coeff. ± SD	3.01 ± 0.58	2.45 ± 0.42	2.41 ± 0.33 <sup>*</sup>	2.98 ± 0.3	2.9 ± 0.23 <sup>^^^</sup>	2.9 ± 0.19 <sup>^^^</sup>	2 ± 0.28 <sup>***</sup>
n = N° fibers	7	8	8	5	6	5	5

Values are means ± SD for n = N° of independent experiments. Significance was calculated by one-way ANOVA with Tukey's multiple comparison test with \*p < 0.05 and \*\*\*p < 0.0001 for S15D, T160D or R58Q mutant vs. WT protein, <sup>^</sup>p < 0.05, <sup>^^</sup>p < 0.01, <sup>^^^</sup>p = 0.001, and <sup>^^^</sup>p < 0.0001 for S15D, T160D, or WT vs. R58Q.



through the SRX mechanism is essential for sarcomere contraction, and many factors, e.g., mutations in sarcomeric proteins, may affect SRX ↔ DRX equilibrium. To further explore the differences and similarities between the two RLC phosphorylation sites at S15 and T160, we assessed the effect of phosphomimetic RLC mutants on the SRX state and SRX ↔ DRX equilibrium following their exchange for the endogenous cardiac RLC in LVPM from Tg-WT and HCM Tg-R58Q mice (Figure 5; Table 4). LVPM fibers underwent the RLC-depletion/reconstitution procedure and then were subjected to mant-ATP chase assay (22, 35). The fluorescence

decay curves vs. time were collected on the rapid exchange of fluorescent mant-ATP for non-labeled (dark) ATP (Figure 5A). The data were fitted to a two-state exponential equation, and the amplitudes of the fast (P1) and slow (P2) phases of fluorescence decay and their respective T1 and T2 lifetimes (in seconds) were obtained (22, 35, 41). To estimate the number of myosin heads directly occupying the SRX state in reconstituted LVPM fibers from Tg-WT (Figure 5B) and Tg-R58Q hearts (Figure 5C), the rapid phase of the fluorescence decay (P1) was corrected for the fast release of nonspecifically bound mant-ATP and the number of SRX heads calculated as P2/(1–0.44) (35). No



TABLE 4 The SRX state of myosin measured by mant-ATP/ATP chase assays in skinned LVPM from Tg-WT and Tg-R58Q mice reconstituted with recombinant RLCs proteins.

Parameter/recombinant RLC protein	LVPM from Tg-WT mice			LVPM from Tg-R58Q mice			
	WT	T160D	S15D	WT	T160D	S15D	R58Q
DRX $\pm$ SD (%)	51.8 $\pm$ 11.9	47.3 $\pm$ 14.1	43 $\pm$ 7.9	52.4 $\pm$ 11	29.1 $\pm$ 11 <sup>*,###</sup>	60.3 $\pm$ 16.7 <sup>^^^</sup>	28.2 $\pm$ 9.7 <sup>**</sup>
SRX $\pm$ SD (%)	48.2 $\pm$ 11.9	52.7 $\pm$ 14.1	57 $\pm$ 7.9	47.6 $\pm$ 11	70.9 $\pm$ 11 <sup>*,###</sup>	39.7 $\pm$ 16.7 <sup>^^^</sup>	71.8 $\pm$ 9.7 <sup>**</sup>
T1 $\pm$ SD (s)	9.5 $\pm$ 6	5.9 $\pm$ 3	8.8 $\pm$ 3.9	3.9 $\pm$ 2.8	3.3 $\pm$ 2.5	7.8 $\pm$ 4.1	9 $\pm$ 8
T2 $\pm$ SD (s)	133.7 $\pm$ 93	111.5 $\pm$ 66.8	327.5 $\pm$ 313.7	107.4 $\pm$ 143.5	80 $\pm$ 85.9	225 $\pm$ 158.3	108.5 $\pm$ 158.2
n = N° fibers	10	9	9	7	6	7	7

Values are means  $\pm$  SD for n = N° of independent experiments. Significance was calculated by one-way ANOVA with Tukey's multiple comparison test with \*p < 0.05 and \*\*p < 0.01 for R58Q, T160D mutant vs. WT protein, ###p < 0.001 for T160D vs. S15D, ^^p < 0.001 for S15D vs. R58Q.

differences in the SRX-to-DRX ratio were observed for the mutant RLC-reconstituted LVPM from Tg-WT (Figure 5B; Table 4). However, assessment of mutant RLC-reconstituted LVPM fibers from Tg-R58Q showed a significantly higher proportion of myosin cross-bridges in the SRX state for fibers reconstituted with recombinant R58Q-RLC (~72%) compared with WT-RLC-reconstituted fibers (48%). This result supports our previous data on R58Q-RLC reconstituted porcine and mouse cardiac preparations showing that R58Q promotes the OFF state of myosin by stabilizing the SRX conformation characterized by a very low ATP turnover rate (22). Interestingly, S15D-RLC destabilized the SRX state and shifted the R58Q heads toward the DRX state (Figure 5C; Table 4). The T160D phosphomimetic RLC did not alter the SRX-to-DRX ratio in Tg-R58Q LVPM fibers and behaved similarly to fibers reconstituted with R58Q-RLC (Figure 5C; Table 4). No significant differences in the lifetimes of fast and slow phases of fluorescence decays curves were observed among all tested systems (Table 4). As for the ATPase assay shown in Figure 3, a significant difference was noted between S15D-RLC vs. T160D-RLC RLCs, with the S15D-RLC being superior to T160D-RLC in recusing the hypocontractile behavior of R58Q-RLC-reconstituted fibers from HCM Tg-R58Q myocardium (Figure 5C).

## Discussion

Human cardiac RLC contains a cardiac MLCK (MYLK3 gene)-specific phosphorylation site at serine-15 (S15) recognized by many research studies as being essential for heart performance in normal and disease conditions (42). Significantly decreased phosphorylation of the RLC occurs in heart failure patients (43–45) and is also observed in animal models of heart disease (23, 46, 47). The myocardium containing dephosphorylated myosin has a reduced ability to generate force and sustain cardiac function at steady-state levels (23, 48), suggesting that RLC phosphorylation may inspire the development of target-specific new therapies. Studies from

our laboratory identified a link between compromised RLC phosphorylation in animal models of HCM and decreased force generation (48–51). Our *in vitro* data suggested that S15D phosphomimetic RLC where S15 is replaced by aspartic acid (D15), could serve as a strategy to mitigate the adverse cardiac phenotypes *in vivo*. Beneficial effects of S15D were observed in S15D-D166V transgenic mice, where the expression of S15D in the background of HCM-D166V mutation prevented the development of hypertrophy and cardiac dysfunction associated with D166V (23). The effects of S15D phosphomimetic RLC protein were recently tested *in vivo* when the S15D-RLC molecule was delivered into the hearts of Tg-D166V mice via the adeno-associated virus AAV9 (24). We observed a significant improvement in heart function in AAV9-S15D-RLC injected hearts of HCM mice compared with empty vector/PBS injected hearts (24).

Our *in-silico* search for other potential phosphorylation sites in the human RLC brought about several Ser/Thr/Tyr sites (Figure 1), of which we chose to focus on threonine-160 (T160). This is because T160 is located in the very C-terminal region of the RLC that encompasses a hot spot for HCM-associated mutations in the MYL2 gene (17–20). As phosphorylation sites of myosin RLC may represent a potential target for therapeutic interventions, we tested whether S15D and T160D phosphomimetic RLCs can rescue cardiomyopathy phenotypes in a mouse model of HCM, Tg-R58Q mice (29). This approach has been previously tested in S15D phosphomimetic RLC-reconstituted cardiac preparations from HCM-D166V and HCM-R58Q mice, where S15D alleviated some of the detrimental HCM phenotypes *in vitro* (21, 22).

In this study, we compared the T160 RLC site with the established S15-RLC site and performed a series of reconstitution experiments using RLC-depleted myosin and LVPM fibers that were reconstituted with phosphomimetic T160D and S15D RLC proteins. The data demonstrated that when reconstituted in cardiac myosin and tested for actin-activated myosin ATPase activity, both phosphomimetic RLC proteins (T160D and S15D) were able to restore the

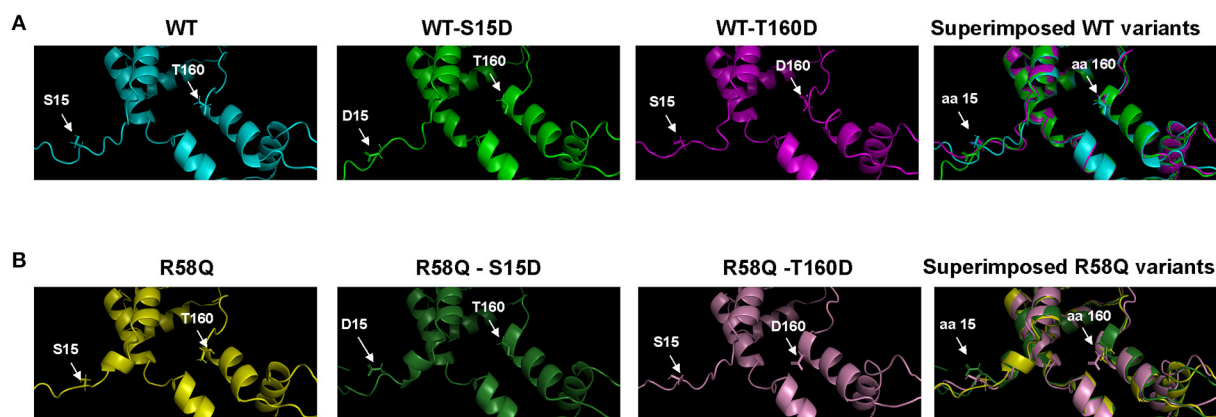


FIGURE 6

The S15 and T160 phosphorylation sites are visualized as phosphomimetics S15D and T160D in the human cardiac RLC-WT (A) and RLC-R58Q (B) proteins. I-TASSER derived secondary structures of the human cardiac RLC were built using protein templates selected from the Protein Data Bank (PDB): 5tbyE, 3dtpE, 3jvtB, 3pn7E, 3j04B, 3i5iB, 2w4aB, 2bl0C, 6iihA, and 6k7yl. Note that mild intramolecular rearrangements in the vicinity of phosphorylation sites at amino acids (aa) 15 and 160 are visible in the superimposed structures of WT and R58Q proteins.

maximal ATPase activity ( $V_{\max}$ ) in Tg-R58Q myosin to the level of WT-RLC-reconstituted HCM-R58Q myosin (Figure 3B; Table 1). A significant difference in  $V_{\max}$  was noted between S15D-RLC and T160D-RLC, with S15D-RLC showing higher ATPase than T160D reconstituted in Tg-WT and Tg-R58Q myosin, indicating functional superiority of the S15D vs. T160D phosphomimetic RLC protein. Significant differences were observed between both phosphomimetic RLCs in regulating SRX $\leftrightarrow$ DRX equilibrium in Tg-R58Q mice (Figure 5). Unlike S15D-RLC, T160D-RLC did not change the ratio of the SRX to DRX state in skinned LVPM fibers of HCM Tg-R58Q mice. At the same time, S15D-RLC fostered the transition from the energy-conserving SRX state to the DRX state and increased the number of DRX heads readily available to interact with actin and produce force (Figure 5). No changes were noted in SRX  $\leftrightarrow$  DRX equilibrium by S15D or T160D RLCs in Tg-WT mice, indicating that the phosphorylation of S15-RLC is essential for rescuing the energetic state of myosin altered by HCM-R58Q mutation of the RLC.

Several studies suggest that the primary effect of HCM-causing mutations is hypercontractility of the heart that results from an increase in the number of functionally accessible myosin heads for the interaction with thin filaments and force production (52). The R58Q model displays a non-canonical HCM phenotype that is hypo- rather than hypercontractile (Figure 5). It stabilizes the OFF state of myosin in LVPM fibers from Tg-R58Q mice (Table 4; Figure 5) and in R58Q recombinant protein-reconstituted porcine fibers (22). As demonstrated by Kampourakis et al. (25), R58Q promotes the OFF state by reducing the number of myosin cross-bridges readily available for actin interaction and ATP utilization. Altogether, our previous and current results suggest that the abnormal heart performance in Tg-R58Q mice (29,

49) originates from an R58Q-mediated decrease in RLC phosphorylation, diminished maximal tension, and stabilization of the hypocontractile SRX state of myosin cross-bridges. These adverse HCM phenotypes can be rescued in full by the S15D and to some degree by the T160D phosphomimetic mutant.

The I-TASSER/PyMol modeled secondary structures of the phosphomimetic S15D and T160D mutants in the background of either WT-RLC or HCM R58Q-RLC are presented in Figure 6. The S15D mutation causes slight conformational changes in the N-terminus of WT-RLC (Figure 6A) and HCM R58Q-RLC (Figure 6B), indicating phosphorylation-mediated intramolecular changes in the RLC molecule. The T160D mutation appears to render more structural changes in the WT-RLC background (Figure 6A) than in the R58Q-RLC (Figure 6B), supporting its lesser rescue ability of function in HCM myocardium compared with S15D-RLC.

## Conclusions

Our experimental approach allowed us to test the functional significance of two phosphomimetic RLCs when reconstituted in cardiac muscle preparations from HCM-R58Q myocardium compared with WT mice. We showed that several R58Q-exerted adverse phenotypes could be rescued by S15D or T160D phosphomimetic RLCs in cardiac preparations from Tg-R58Q mice. A low level of maximal isometric force or depressed ATPase activity observed for R58Q-reconstituted samples could be restored by both S15D and T160D RLCs with the significantly better rescue of the  $V_{\max}$  of myosin ATPase activity by S15D-RLC. Significantly, S15D but not T160D phosphomimetic RLC could modulate myosin energetic states in the resting

muscle and promote the DRX state reducing the fraction of SRX heads and counteracting the hypocontractile activity of R58Q-reconstituted HCM myocardium. This result supports the functional superiority of the established serine-15 phosphorylation site of the RLC that may serve as a therapeutic target for HCM.

## Data availability statement

The original contributions presented in the study are publicly available. This data can be found at: <https://www.ncbi.nlm.nih.gov/genbank/>, BankIt2600965 T160D ON950400 and BankIt2600993 S15D ON950401.

## Ethics statement

The animal study was reviewed and approved by this study conforms to the Guide for the Care and Use of Laboratory Animals published by the US National Institutes of Health (NIH Publication No. 85–23, revised 2011). All protocols were approved by the Institutional Animal Care and Use Committee at the University of Miami Miller School of Medicine (protocol #21-106 LF). The assurance number is #A-3224-01, approved through November 30, 2023. Euthanasia of mice was achieved through inhalation of isoflurane followed by thoracotomy.

## Author contributions

KK and DS-C conceived the research and wrote the paper. KK, JL, and MG-G performed experiments.

## References

1. Rayment I, Rypniewski WR, Schmidt-Base K, Smith R, Tomchick DR, Benning MM, et al. Three-dimensional structure of myosin subfragment-1: a molecular motor. *Science*. (1993) 261:50–8. doi: 10.1126/science.8316857
2. Geeves MA. Molecular motors: stretching the lever-arm theory. *Nature*. (2002) 415:129–31. doi: 10.1038/415129a
3. Burghardt TP, Josephson MP, Ajtai K. Single myosin cross-bridge orientation in cardiac papillary muscle detects lever-arm shear strain in transduction. *Biochemistry*. (2011) 50:7809–21. doi: 10.1021/bi2008992
4. Burghardt TP, Sikkink LA. Regulatory light chain mutants linked to heart disease modify the cardiac myosin lever arm. *Biochemistry*. (2013) 52:1249–59. doi: 10.1021/bi301500d
5. Szczesna D, Ghosh D, Li Q, Gomes AV, Guzman G, Arana C, et al. Familial hypertrophic cardiomyopathy mutations in the regulatory light chains of myosin affect their structure, Ca<sup>2+</sup> binding, and phosphorylation. *J Biol Chem*. (2001) 276:7086–92. doi: 10.1074/jbc.M009823200
6. Szczesna-Cordary D. Regulatory light chains of striated muscle myosin. Structure, function and malfunction. *Curr Drug Targets Cardiovasc Haematol Disord*. (2003) 3:187–97. doi: 10.2174/1568006033481474
7. Chang AN, Battiprolu PK, Cowley PM, Chen G, Gerard RD, Pinto JR, et al. Constitutive phosphorylation of cardiac myosin regulatory light chain in vivo. *J Biol Chem*. (2015) 290:10703–16. doi: 10.1074/jbc.M115.642165
8. Chang AN, Mahajan P, Knapp S, Barton H, Sweeney HL, Kamm KE, et al. Cardiac myosin light chain is phosphorylated by Ca<sup>2+</sup>/calmodulin-dependent and -independent kinase activities. *Proc Natl Acad Sci USA*. (2016) 113:E3824–33. doi: 10.1073/pnas.1600633113
9. Colson BA, Locher MR, Bekyarova T, Patel JR, Fitzsimons DP, Irving TC, et al. Differential roles of regulatory light chain and myosin binding protein-C phosphorylations in the modulation of cardiac force development. *J Physiol*. (2010) 588 (Pt. 6):981–93. doi: 10.1113/jphysiol.2009.183897
10. Kampourakis T, Irving M. Phosphorylation of myosin regulatory light chain controls myosin head conformation in cardiac muscle. *J Mol Cell Cardiol*. (2015) 85:199–206. doi: 10.1016/j.yjmcc.2015.06.002
11. Wang Y, Ajtai K, Burghardt TP. Ventricular myosin modifies in vitro step-size when phosphorylated. *J Mol Cell Cardiol*. (2014) 72:231–7. doi: 10.1016/j.yjmcc.2014.03.022
12. Yu H, Chakravorty S, Song W, Ferenczi MA. Phosphorylation of the regulatory light chain of myosin in striated muscle: methodological perspectives. *Eur Biophys J*. (2016) 45:779–805. doi: 10.1007/s00249-016-1128-z
13. Kampourakis T, Sun YB, Irving M. Myosin light chain phosphorylation enhances contraction of heart muscle via structural changes in both thick and thin filaments. *Proc Natl Acad Sci USA*. (2016) 113:E3039–47. doi: 10.1073/pnas.1602776113

All authors contributed to the article and approved the submitted version.

## Funding

This study was supported by the National Institutes of Health (Grant Nos. R01-HL143830 and R56-HL146133 to DS-C).

## Acknowledgments

The authors express their gratitude to Pardis Kaviani for help in reconstitution experiments and Judith Vinod for help in I-TASSER/PyMol modeling of RLC mutants.

## Conflict of interest

The authors declare that the research was conducted in the absence of any commercial or financial relationships that could be construed as a potential conflict of interest.

## Publisher's note

All claims expressed in this article are solely those of the authors and do not necessarily represent those of their affiliated organizations, or those of the publisher, the editors and the reviewers. Any product that may be evaluated in this article, or claim that may be made by its manufacturer, is not guaranteed or endorsed by the publisher.

14. Scruggs SB, Reisdorph R, Armstrong ML, Warren CM, Reisdorph N, Solaro RJ, et al. A novel, in-solution separation of endogenous cardiac sarcomeric proteins and identification of distinct charged variants of regulatory light chain. *Mol Cell Proteomics*. (2010) 9:1804–18. doi: 10.1074/mcp.M110.000075
15. Blom N, Sicheritz-Pontén T, Gupta R, Gammeltoft S, Brunak S. Prediction of post-translational glycosylation and phosphorylation of proteins from the amino acid sequence. *Proteomics*. (2004) 4:1633–49. doi: 10.1002/pmic.200300771
16. Dou Y, Yao B, Zhang C. PhosphoSVM: prediction of phosphorylation sites by integrating various protein sequence attributes with a support vector machine. *Amino Acids*. (2014) 46:1459–69. doi: 10.1007/s00726-014-1711-5
17. Richard P, Charron P, Carrier L, Ledebur C, Cheav T, Pichereau C, et al. Hypertrophic cardiomyopathy: distribution of disease genes, spectrum of mutations, and implications for a molecular diagnosis strategy. *Circulation*. (2003) 107:2227–32. doi: 10.1161/01.CIR.0000006323.15244.54
18. Alvarez-Acosta L, Mazzanti A, Fernández X, Ortí M, Barriales-Villa R, García D, et al. Regulatory light chain (MYL2) mutations in familial hypertrophic cardiomyopathy. *JCVD*. (2014) 2:82–90.
19. De Bortoli M, Vio R, Basso C, Calore M, Minervini G, Angelini A, et al. Novel missense variant in MYL2 gene associated with hypertrophic cardiomyopathy showing high incidence of restrictive physiology. *Circ Genom Precis Med*. (2020) 13:e002824. doi: 10.1161/CIRCGEN.119.002824
20. Manivannan SN, Darouich S, Masmoudi A, Gordon D, Zender G, Han Z, et al. Novel frameshift variant in MYL2 reveals molecular differences between dominant and recessive forms of hypertrophic cardiomyopathy. *PLOS Genet*. (2020) 16:e1008639. doi: 10.1371/journal.pgen.1008639
21. Muthu P, Liang J, Schmidt W, Moore JR, Szczesna-Cordary D. *In vitro* rescue study of a malignant familial hypertrophic cardiomyopathy phenotype by pseudo-phosphorylation of myosin regulatory light chain. *Arch Biochem Biophys*. (2014) 552:3:29–39. doi: 10.1016/j.abb.2013.12.011
22. Yadav S, Kazmierczak K, Liang J, Sitbon YH, Szczesna-Cordary D. Phosphomimetic-mediated in vitro rescue of hypertrophic cardiomyopathy linked to R58Q mutation in myosin regulatory light chain. *FEBS J*. (2019) 286:151–68. doi: 10.1111/febs.14702
23. Yuan CC, Muthu P, Kazmierczak K, Liang J, Huang W, Irving TC, et al. Constitutive phosphorylation of cardiac myosin regulatory light chain prevents development of hypertrophic cardiomyopathy in mice. *Proc Natl Acad Sci USA*. (2015) 112:E4138–46. doi: 10.1073/pnas.1505819112
24. Yadav S, Yuan CC, Kazmierczak K, Liang J, Huang W, Takeuchi LM, et al. Therapeutic potential of AAV9-S15D-RLC gene delivery in humanized MYL2 mouse model of HCM. *J Mol Med*. (2019) 97:1033–47. doi: 10.1007/s00109-019-01791-z
25. Kampourakis T, Ponnamp S, Irving M. Hypertrophic cardiomyopathy mutation R58Q in the myosin regulatory light chain perturbs thick filament-based regulation in cardiac muscle. *J Mol Cell Cardiol*. (2018) 117:72–81. doi: 10.1016/j.jmcc.2018.02.009
26. Karabina A, Kazmierczak K, Szczesna-Cordary D, Moore JR. Myosin regulatory light chain phosphorylation enhances cardiac beta-myosin *in vitro* motility under load. *Arch Biochem Biophys*. (2015) 580:14–21. doi: 10.1016/j.abb.2015.06.014
27. Greenberg MJ, Kazmierczak K, Szczesna-Cordary D, Moore JR. Cardiomyopathy-linked myosin regulatory light chain mutations disrupt myosin strain-dependent biochemistry. *Proc Natl Acad Sci USA*. (2010) 107:17403–8. doi: 10.1073/pnas.1009619107
28. Schmid M, Toepfer CN. Cardiac myosin super relaxation (SRX): a perspective on fundamental biology, human disease and therapeutics. *Biol Open*. (2021) 10:bio057646. doi: 10.1242/bio.057646
29. Wang Y, Xu Y, Kerrick WGL, Wang Y, Guzman G, Diaz-Perez Z, et al. Prolonged Ca<sup>2+</sup> and force transients in myosin RLC transgenic mouse fibers expressing malignant and benign FHC mutations. *J Mol Biol*. (2006) 361:286–99. doi: 10.1016/j.jmb.2006.06.018
30. Yuan CC, Kazmierczak K, Liang J, Zhou Z, Yadav S, Gomes AV, et al. Sarcomeric perturbations of myosin motors lead to dilated cardiomyopathy in genetically modified MYL2 mice. *Proc Natl Acad Sci USA*. (2018) 115:E2338–47. doi: 10.1073/pnas.1716925115
31. Szczesna-Cordary D, Jones M, Moore JR, Watt J, Kerrick WGL, Xu Y, et al. Myosin regulatory light chain E22K mutation results in decreased cardiac intracellular calcium and force transients. *FASEB J*. (2007) 21:3974–85. doi: 10.1096/fj.07-8630com
32. Fiske CH, Subbarow Y. The colorimetric determination of phosphorus. *J Biol Chem*. (1925) 66:375–400. doi: 10.1016/S0021-9258(18)84756-1
33. Kazmierczak K, Xu Y, Jones M, Guzman G, Hernandez OM, Kerrick WGL, et al. The role of the N-terminus of the myosin essential light chain in cardiac muscle contraction. *J Mol Biol*. (2009) 387:706–25. doi: 10.1016/j.jmb.2009.02.006
34. Pant K, Watt J, Greenberg M, Jones M, Szczesna-Cordary D, Moore JR. Removal of the cardiac myosin regulatory light chain increases isometric force production. *FASEB J*. (2009) 23:3571–80. doi: 10.1096/fj.08-126672
35. Yuan CC, Kazmierczak K, Liang J, Ma W, Irving TC, Szczesna-Cordary D. Molecular basis of force-pCa relation in MYL2 cardiomyopathy mice: role of the super-relaxed state of myosin. *Proc Natl Acad Sci USA*. (2022) 119:e2110328119. doi: 10.1073/pnas.2110328119
36. Hooijman P, Stewart MA, Cooke R. A new state of cardiac myosin with very slow ATP turnover: a potential cardioprotective mechanism in the heart. *Biophys J*. (2011) 100:1969–76. doi: 10.1016/j.bpj.2011.02.061
37. Yang J, Yan R, Roy A, Xu D, Poisson J, Zhang Y. The I-TASSER suite: protein structure and function prediction. *Nat Methods*. (2015) 12:7–8. doi: 10.1038/nmeth.3213
38. Stewart MA, Franks-Skiba K, Chen S, Cooke R. Myosin ATP turnover rate is a mechanism involved in thermogenesis in resting skeletal muscle fibers. *Proc Natl Acad Sci USA*. (2010) 107:430–5. doi: 10.1073/pnas.0909468107
39. Alamo L, Qi D, Wriggers W, Pinto A, Zhu J, Bilbao A, et al. Conserved intramolecular interactions maintain myosin interacting-heads motifs explaining tarantula muscle super-relaxed state structural basis. *J Mol Biol*. (2016) 428:1142–64. doi: 10.1016/j.jmb.2016.01.027
40. Garfinkel AC, Seidman JG, Seidman CE. Genetic pathogenesis of hypertrophic and dilated cardiomyopathy. *Heart Fail Clin*. (2018) 14:139–46. doi: 10.1016/j.hfc.2017.12.004
41. Sitbon YH, Kazmierczak K, Liang J, Yadav S, Veerasammy M, Kanashiro-Takeuchi RM, et al. Ablation of the N terminus of cardiac essential light chain promotes the super-relaxed state of myosin and counteracts hypercontractility in hypertrophic cardiomyopathy mutant mice. *FEBS J*. (2020) 287:3989–4004. doi: 10.1111/febs.15243
42. Yadav S, Szczesna-Cordary D. Pseudophosphorylation of cardiac myosin regulatory light chain: a promising new tool for treatment of cardiomyopathy. *Biophys Rev*. (2017) 9:57–64. doi: 10.1007/s12551-017-0248-8
43. van der Velden J, Papp Z, Boontje NM, Zaremba R, de Jong JW, Janssen PML, et al. The effect of myosin light chain 2 dephosphorylation on Ca<sup>2+</sup>-sensitivity of force is enhanced in failing human hearts. *Cardiovasc Res*. (2003) 57:505–14. doi: 10.1016/S0008-6363(02)00662-4
44. van der Velden J, Papp Z, Zaremba R, Boontje NM, de Jong JW, Owen VJ, et al. Increased Ca<sup>2+</sup>-sensitivity of the contractile apparatus in end-stage human heart failure results from altered phosphorylation of contractile proteins. *Cardiovasc Res*. (2003) 57:37–47. doi: 10.1016/S0008-6363(02)00606-5
45. van der Velden J, Papp Z, Boontje NM, Zaremba R, de Jong JW, Janssen PM, et al. Myosin light chain composition in non-failing donor and end-stage failing human ventricular myocardium. *Adv Exp Med Biol*. (2003) 538:3–15. doi: 10.1007/978-1-4419-9029-7\_1
46. Scruggs SB, Hinken AC, Thawornkaiwong A, Robbins J, Walker LA, de Tombe PP, et al. Ablation of ventricular myosin regulatory light chain phosphorylation in mice causes cardiac dysfunction in situ and affects neighboring myofibrillar protein phosphorylation. *J Biol Chem*. (2009) 284:5097–106. doi: 10.1074/jbc.M807414200
47. Sheikh F, Ouyang K, Campbell SG, Lyon RC, Chuang J, Fitzsimons D, et al. Mouse and computational models link Mlc2v dephosphorylation to altered myosin kinetics in early cardiac disease. *J Clin Invest*. (2012) 122:1209–21. doi: 10.1172/JCI61134
48. Muthu P, Kazmierczak K, Jones M, Szczesna-Cordary D. The effect of myosin RLC phosphorylation in normal and cardiomyopathic mouse hearts. *J Cell Mol Med*. (2012) 16:911–9. doi: 10.1111/j.1582-4934.2011.01371.x
49. Abraham TP, Jones M, Kazmierczak K, Liang H-Y, Pinheiro AC, Wagg CS, et al. Diastolic dysfunction in familial hypertrophic cardiomyopathy transgenic model mice. *Cardiovasc Res*. (2009) 82:84–92. doi: 10.1093/cvr/cvp016
50. Kerrick WGL, Kazmierczak K, Xu Y, Wang Y, Szczesna-Cordary D. Malignant familial hypertrophic cardiomyopathy D166V mutation in the ventricular myosin regulatory light chain causes profound effects in skinned and intact papillary muscle fibers from transgenic mice. *FASEB J*. (2009) 23:855–65. doi: 10.1096/fj.08-118182
51. Sitbon YH, Diaz F, Kazmierczak K, Liang J, Wangpaichitr M, Szczesna-Cordary D. Cardiomyopathic mutations in essential light chain reveal mechanisms regulating the super relaxed state of myosin. *J Gen Physiol*. (2021) 153:e202012801. doi: 10.1085/jgp.202012801
52. Spudich JA. Three perspectives on the molecular basis of hypercontractility caused by hypertrophic cardiomyopathy mutations. *Pflugers Arch*. (2019) 471:701–17. doi: 10.1007/s00424-019-02259-2





## OPEN ACCESS

## EDITED BY

Kenneth Scott Campbell,  
University of Kentucky, United States

## REVIEWED BY

Raquel Guillaumat-Prats,  
LMU Munich University Hospital,  
Germany  
Diego Vinicius Santinelli Pestana,  
Brigham and Women's Hospital  
and Harvard Medical School,  
United States  
Takehiro Funamizu,  
Juntendo University, Japan

## \*CORRESPONDENCE

Lina Badimon  
lbadimon@santpau.cat

†These authors have contributed  
equally to this work

## SPECIALTY SECTION

This article was submitted to  
Heart Failure and Transplantation,  
a section of the journal  
Frontiers in Cardiovascular Medicine

RECEIVED 09 May 2022

ACCEPTED 12 September 2022

PUBLISHED 03 November 2022

## CITATION

Vilella-Figuerola A, Padró T, Roig E,  
Mirabet S and Badimon L (2022) New  
factors in heart failure  
pathophysiology: Immunity cells  
release of extracellular vesicles.  
*Front. Cardiovasc. Med.* 9:939625.  
doi: 10.3389/fcvm.2022.939625

## COPYRIGHT

© 2022 Vilella-Figuerola, Padró, Roig,  
Mirabet and Badimon. This is an  
open-access article distributed under  
the terms of the [Creative Commons  
Attribution License \(CC BY\)](#). The use,  
distribution or reproduction in other  
forums is permitted, provided the  
original author(s) and the copyright  
owner(s) are credited and that the  
original publication in this journal is  
cited, in accordance with accepted  
academic practice. No use, distribution  
or reproduction is permitted which  
does not comply with these terms.

# New factors in heart failure pathophysiology: Immunity cells release of extracellular vesicles

Alba Vilella-Figuerola<sup>1,2</sup>, Teresa Padró<sup>1,3</sup>, Eulàlia Roig<sup>4</sup>,  
Sònia Mirabet<sup>3,4†</sup> and Lina Badimon<sup>1,3,5\*†</sup>

<sup>1</sup>Cardiovascular-Program ICCV, IR-Hospital Santa Creu i Sant Pau, IIB-Sant Pau, Barcelona, Spain,

<sup>2</sup>Department of Biochemical and Molecular Biology, Universitat Autònoma de Barcelona,

Barcelona, Spain, <sup>3</sup>Centro de Investigación Biomédica en Red Cardiovascular, Instituto de Salud

Carlos III, Madrid, Spain, <sup>4</sup>Heart Failure Group, Department of Cardiology, Hospital Santa Creu i Sant

Pau, Barcelona, Spain, <sup>5</sup>UAB-Chair Cardiovascular Research, Barcelona, Spain

Leukocyte-shed extracellular vesicles (EVs) can play effector roles in the pathophysiological mechanisms of different diseases. These EVs released by membrane budding of leukocytes have been found in high amounts locally in inflamed tissues and in the circulation, indicating immunity cell activation. These EVs secreted by immune cell subsets have been minimally explored and deserve further investigation in many areas of disease. In this study we have investigated whether in heart failure there is innate and adaptive immune cell release of EVs. Patients with chronic heart failure (CHF) ( $n = 119$ ) and in sex- and age-matched controls without this chronic condition ( $n = 60$ ). Specifically, EVs were quantified and phenotypically characterized by flow cytometry and cell-specific monoclonal antibodies. We observed that even in well medically controlled CHF patients (with guideline-directed medical therapy) there are higher number of blood annexin-V<sup>+</sup> (phosphatidylserine<sup>+</sup>)-EVs carrying activated immunity cell-epitopes in the circulation than in controls ( $p < 0.04$  for all cell types). Particularly, EVs shed by monocytes and neutrophils (innate immunity) and by T-lymphocytes and natural-killer cells (adaptive immunity) are significantly higher in CHF patients. Additionally, EVs-shed by activated leukocytes/neutrophils (CD11b<sup>+</sup>,  $p = 0.006$ ; CD29<sup>+</sup>/CD15<sup>+</sup>,  $p = 0.048$ ), and T-lymphocytes (CD3<sup>+</sup>/CD45<sup>+</sup>,  $p < 0.02$ ) were positively correlated with CHF disease severity (NYHA classification). Interestingly, CHF patients with ischemic etiology had the highest levels of EVs shed by lymphocytes and neutrophils ( $p < 0.045$ , all). In summary, in CHF patients there is a significant immune cell activation shown by high-release of EVs that is accentuated by clinical severity of CHF. These activated innate and adaptive immunity cell messengers may contribute by intercellular communication to the progression of the disease and to the common affection of distant organs in heart failure (paracrine regulation) that contribute to the clinical deterioration of CHF patients.

## KEYWORDS

extracellular microvesicles (EVs), chronic heart failure, immune cells, inflammation, liquid biopsies, extracellular vesicle (EV)



## Introduction

Leukocyte-shed extracellular vesicles (EVs) can play effector roles in the pathophysiological mechanisms of different diseases. These EVs released by membrane budding of leukocytes have been found in high amounts locally in inflamed tissues and in the circulation, indicating immunity cell activation. These EVs secreted by immune cell subsets have been minimally explored and deserve further investigation in many areas of disease (1). Heart failure (HF) is a complex syndrome that accounts for a high proportion of cardiovascular death worldwide (2, 3). It is characterized by an impairment of the cardiac function due to genetic and environmental insults and comorbidities such as ischemic disease, that induce significant alterations of heart structure (left ventricle hypertrophy or dilation, fibrosis, maladaptive remodeling) and function (decreased cardiac output, increased end-diastolic pressure and diastolic or systolic dysfunction) (4). HF can be classified in HF with preserved ejection fraction (HFpEF), HF with reduced ejection fraction (HFrEF) and in HF with mildly reduced ejection fraction (HFmrEF), according to their echographic values of left ventricular ejection fraction (LVEF) (2, 5). Although these groups present common symptomatology, their pathophysiological mechanisms and therapeutic approaches are slightly different. In that sense, although this is not universal, the vast majority of HFrEF have underlying ischemic etiology, while HFpEF patients tend to develop HF due to hypertensive or heart valve disease (6, 7).

The systemic inflammation of these patients represents a chronic and non-resolving health impairment with the presence of elevated levels of circulating cytokines or pro-inflammatory mediators, such as TNF $\alpha$ , IL- $\beta$ 1, IL-6, or CRP (4, 8). Further to the raised levels of inflammatory biomarkers, another source of organ damage is the defective equilibrium between pro-inflammatory and anti-inflammatory immune-cell subsets, such as monocytes/macrophages, neutrophils, lymphocytes (B, Treg, Th), that often results in impaired repair processes (9–11). Several clinical trials have tried to target the on-going inflammation with neutral results (12, 13). The failure of these approaches suggests that the potentially involved pathways are not well understood, and that further research in the pathophysiology of the disease is needed. Indeed, HF is a spectrum of overlapping phenotypes that need to be more accurately classified.

Circulating extracellular microvesicles (EVs) are a heterogeneous population of extracellular vesicles with a size range between 20 and 1,000 nm. Composed of a

phosphatidylserine-rich phospholipid bilayer that exposes transmembrane proteins and receptors from their parental cells, EVs are released after physiological stimuli such as cell activation, damage, stress, apoptotic or necrotic damage (14, 15). EVs play a role in physiology and pathophysiology since they are involved in various processes such as cell adhesion, communication (they carry miRNA, proteins and lipids), apoptosis, immune response, vascular function, remodeling, hemostasis or thrombosis (16). Their cargo reflects their parental cell condition and metabolic state and its numbers have been correlated with disease progression and severity (14, 16, 17). In cardiovascular disease, they have been related to several pathologies (18) including atherosclerosis (19–21), coronary artery disease (14), ischemia and myocardial infarction (22–24) and stroke (25).

To gain more insight in the pathophysiology of chronic HF (CHF), we aimed to investigate whether immune cells were activated in patients, even though treated according to guideline-directed medical therapy. Several studies have investigated endothelial-derived EVs in relation with cardiovascular risk factors and cardiovascular disease pathophysiology (26–29). However, to our knowledge, there are no studies investigating the type of immune cells that are activated and shed EVs in CHF.

In this study we have investigated whether in chronic heart failure there is innate and adaptive immune cell release of EVs and whether specific circulating EV patterns associate with the underlying CHF etiology (ischemic and non-ischemic) or the disease severity in CHF patients.

## Materials and methods

### Clinical study population

A total of 119 ambulatory patients with clinical diagnosis of CHF and under guideline-directed medical therapy were prospectively recruited in the outpatient HF unit of the Hospital de la Santa Creu i Sant Pau (Barcelona, Spain) between September 2016 and July 2018 and were followed-up until October 2019. During follow-up patients were treated according to international guidelines and at clinician discretion in the outpatient unit of our hospital. A control group was also included, comprising 60 sex- and age-matched controls without CHF. Baseline demographic data, classical cardiovascular risk factors and background medication of the study population (CHF and control groups) are shown in **Table 1**. Exclusion criteria were: HF with mildly reduced ejection fraction (40–50% of left ventricular ejection fraction [LVEF]), past history of cancer, inflammatory disorders, sepsis or infection. Pregnant women were also excluded. Characteristics of the CHF patients including biochemical and hematological data, CHF-etiology and CHF-severity (according to the New York

Abbreviations: AV, annexin V; CHF, chronic heart failure; EVs, extracellular microvesicles; HF-Isch, heart failure with an ischemic underlying etiology; HF-Nisch, heart failure with a non-ischemic underlying etiology; HFpEF, heart failure with preserved ejection fraction; HFrEF, heart failure with reduced ejection fraction; LVEF, left ventricle ejection fraction; NYHA, New York Heart Association.

TABLE 1 Patients and controls baseline characteristics.

	Controls <i>n</i> = 60	cHF <i>n</i> = 119	<i>P</i> -value controls-cHF
<b>Demographic characteristics; mean ± SD</b>			
Male/Female, <i>n</i>	34/26	81/38	0.133
Age, years	67.1 ± 7.1	67 ± 11.8	0.553
Systolic blood pressure, mmHg	144.8 ± 20.2	120.4 ± 19.1	<b>0.000</b>
Diastolic blood pressure, mmHg	83.7 ± 11.3	73.9 ± 11.1	<b>0.000</b>
Left ventricular ejection fraction, %	52–74 <sup>†</sup>	45.59 ± 18.98	–
<b>Risk factors; <i>n</i> (%)</b>			
Smokers	10 (16)	13 (10.9)	0.278
Hypertension	33 (55)	82 (68.9)	0.067
Pulmonary hypertension	–	49 (41.1)	–
Diabetes mellitus	10 (16)	53 (44.5)	<b>0.000</b>
Dyslipidaemia	45 (75)	64 (53.7)	<b>0.004</b>
Chronic kidney disease	2 (3.3)	46 (38.6)	<b>0.000</b>
Atrial fibrillation	–	50 (42)	–
<b>Background medication; <i>n</i> (%)</b>			
Angiotensin-converting-enzyme inhibitors	19 (31.6)	48 (40.3)	0.333
Angiotensin II receptor blockers	9 (15)	35 (29.4)	0.054
Beta-blockers	2 (3.3)	100 (84)	<b>0.000</b>
Aldosterone antagonists	–	66 (55.4)	–
Diuretics <sup>‡</sup>	6 (10)	104 (87.3)	<b>0.000</b>
Angiotensin receptor neprilysin inhibitors	–	17 (14.2)	–
Ivabradine	–	14 (11.7)	–
Statins	37 (61.6)	77 (64.7)	0.690
Insulin	3 (5)	16 (13.4)	0.083
Anti-diabetic drugs	8 (13.3)	40 (33.6)	<b>0.004</b>
Antiplatelet agents	12 (20)	46 (38.6)	<b>0.012</b>
Anticoagulants	2 (3.3)	61 (51.2)	<b>0.000</b>
Anti-arrhythmic drugs	–	26 (21.8)	–

<sup>†</sup>LVEF normal range (excerpted from <https://www.ncbi.nlm.nih.gov/books/NBK459131/> on 18/01/2021).

<sup>‡</sup>Includes: furosemide, hydrochlorothiazide, torasemide and indapamide.

SD, standard deviation; cHF, chronic heart failure. The statistically significant *p*-values are in bold.

Heart Association Classification [NYHA]) are given in **Table 2** and **Supplementary Tables 1, 2**. NYHA classification system considers cardiac functionality and disease severity, dividing cHF in four categories (5). Briefly, NYHA I patients do not present limitations in their physical activity and daily activity does not cause breathlessness, fatigue or palpitations. NYHA II patients have a slight limitation of physical activity, and whereas they are comfortable at rest, ordinary activity produces breathlessness, fatigue or palpitations. Patients in NYHA III present a marked limitation of physical activity. Although they are comfortable at rest, less than ordinary physical activity results in breathlessness, fatigue or palpitations. Finally, NYHA IV patients are unable to carry on any physical activity without discomfort and can have symptoms at rest. In patients with ischemic etiology, ischemia was defined as history of a previous myocardial infarction, or in the absence of an acute ischemic event, if there was stenosis equal or greater than 75% in the

common trunk or left anterior descending artery, as well as when stenosis was equal or greater than 75% in two or more of the principal coronary arteries.

The ethics committee at the Hospital de la Santa Creu i Sant Pau in Barcelona (Spain) approved the study (Ref 16/44) and it was conducted under the principles of the Declaration of Helsinki. A written informed consent was obtained from all participants prior recruitment.

## Blood sampling, circulating extracellular vesicles isolation and characterization

Venous blood was withdrawn from the cubital vein without tourniquet using a 20-gauge needle after 10–14 h of fasting into 3.8% sodium citrate tubes (BD Vacutainer, Becton Dickinson).

TABLE 2 Clinical characteristics of cHF patients at baseline (n = 119).

**Patients characteristics**

<b>Clinical history; n(%) cHF etiology</b>	
Ischemic	43 (36.1)
Non-ischemic	76 (63.9)
Hypertensive cardiomyopathy	19 (15.9)
Dilated cardiomyopathy	24 (20.1)
Hypertrophic cardiomyopathy	12 (10)
Heart valve disease	17 (14.2)
Other	4 (3.3)
<b>New York Heart Association cHF stage</b>	
NYHA I	0 (0)
NYHA II	52 (43.7)
NYHA III	66 (55.5)
NYHA IV	1 (0.8)
Hospitalizations in the 6 months prior study initiation	49 (41.1)
<b>Re-events in the year prior study initiation</b>	
Percutaneous coronary intervention	4 (44.5)
Coronary artery bypass grafting	2 (22.2)
Medical treatment	3 (33.3)
<b>Biochemistry; mean <math>\pm</math> SD</b>	
Hemoglobin, mg/dl	129.8 $\pm$ 18.5
Creatinine, mg/dl	1.3 $\pm$ 0.54
C-Reactive Protein, mg/ml	7.63 $\pm$ 11
NT-proBNP, pg/ml	2954.8 $\pm$ 4211.3
High-sensitive troponin T, ng/l	27.7 $\pm$ 20.9
Erythrocytes, 10 <sup>6</sup> /mm <sup>3</sup>	3.98 $\pm$ 0.74
Platelets, 10 <sup>3</sup> /mm <sup>3</sup>	173.2 $\pm$ 56.89
Leukocytes, mm <sup>3</sup>	7426.1 $\pm$ 1950
Neutrophils, 10 <sup>9</sup> /L	4.74 $\pm$ 1.54
Monocytes, 10 <sup>9</sup> /L	0.75 $\pm$ 0.54
<b>Major outcomes during follow-up; n (%)</b>	
<b>Cardiovascular event<sup>†</sup></b>	
Stroke	26 (21.8)
Aortic dissection	8 (6.7)
AMI + Cardiogenic shock	1 (0.8)
HTx/HTx waiting list	3 (2.5)
CV death	10 (8.4)/1 (0.8)
Emergency hospital admission for cHF	7 (5.8)
Rehospitalisation for cHF	16 (13.4)
Aortic aneurism	57 (47.8)
Other death causes <sup>‡</sup>	1 (0.8)
	10 (8.4)

<sup>†</sup>Includes patients that suffered a stroke, an aortic dissection, an AMI, a cardiogenic shock, a CV death (mainly due to cHF) or were admitted to the emergency department. It does not include patients that underwent a HTx.

<sup>‡</sup>Includes patients that died due to a septic shock, a hemorrhage or a non-successful HTx. AMI, acute myocardial infarction; CV, cardiovascular; cHF, chronic heart failure; HTx, heart transplantation; NT-proBNP, N-terminal pro-hormone of brain natriuretic peptide; NYHA, New York Heart Association; SD, standard deviation.

All samples were processed identically and within the first 2 h. Blood was centrifuged at 1,560 g for 20 min at 20°C (Eppendorf 5810R GLOOB04932 centrifuge, A-4-81 rotor,

Eppendorf) to avoid *in vitro* platelet activation. Platelet-poor plasma (PPP) was carefully aspirated, leaving about a 1 mm undisturbed layer on top of cells. A second centrifugation step was then performed at 1,500 g for 10 min at 20°C (Eppendorf 5415R centrifuge, FA45-24-11 rotor, Eppendorf) to ensure the complete removal of cells and obtain the platelet-free plasma (PFP). PFP aliquots were stored at  $-80^{\circ}\text{C}$  until flow cytometry studies.

The EVs fraction was isolated from PFP by a two-step high-speed centrifugation, according to the procedure previously described (20, 24, 30). Specifically, PFP was thawed and centrifuged at 1,500 g for 10 min at 20°C (Eppendorf 5417R centrifuge, FA45-24-11 rotor, Eppendorf). Next, 250  $\mu\text{l}$  of PFP were collected from the upper part of the vial and transferred to a new tube to pellet the EVs, and then centrifuged at 20,000 g for 30 min at 20°C (Eppendorf 5417R centrifuge, FA45-24-11 rotor, Eppendorf). The supernatant (225  $\mu\text{l}$ ) was discarded, and the EVs-enriched pellet was washed with 225  $\mu\text{l}$  of citrate-phosphate buffered saline (PBS) solution (citrate-PBS; 1.4 mmol/L phosphate, 154 mmol/L NaCl, 10.9 mmol/L trisodium citrate, pH 7.4) before a second equal centrifugation (20,000 g, 30 min, 20°C) was pursued. Finally, the remaining pellets were resuspended in a final volume of 100  $\mu\text{l}$  citrate-PBS.

## Flow cytometric analysis of extracellular vesicles

Extracellular vesicles were phenotypically characterized by three-label flow cytometric analysis, performed as described previously (20, 24, 30). Washed EVs suspensions were diluted in PBS containing 2.5 mmol of CaCl<sub>2</sub> (Annexin binding buffer [ABB], BD Biosciences, San Jose). Afterward, combinations of CFBlue-conjugated annexin V (AV) (Immunostep, Salamanca, Spain) to detect phosphatidylserine, and two specific monoclonal antibodies (mAb) (**Supplementary Table 3**) labeled with fluorescein isothiocyanate (FITC) and phycoerythrin (PE), or the isotype-matched control mAb, were added. Samples were incubated for 20 min at 20°C in the dark and diluted with ABB before being immediately analyzed on a FACSCantoII™ (Becton Dickinson, Franklin Lakes, NJ, USA) flow cytometer.

Sample acquisition was performed during 1 min per sample at “low flow” rate. Forward scatter (FSC), side scatter (SSC), and fluorescence data were obtained with the settings in the logarithmic scale. Gate limits were established as follows with the same criteria previously described (20, 24, 30). The upper threshold for FSC was set with the Megamix-Plus FSC beads (BioCytex, Marseille, France). Megamix-Plus FSC beads for cytometer setting are a mix of beads of the following bead-equivalent diameters: 0.1, 0.3, 0.5, and 0.9  $\mu\text{m}$ . According to the beads signal, the lower detection limit was placed as a

threshold above the electronic background noise of the flow cytometer for FSC and the second logarithm for SSC. EVs within the established gate limits ( $>0.1$  to  $1\ \mu\text{m}$ ) were identified and quantified based on their binding to AV and reactivity to cell-specific mAb. To identify positive marked events, thresholds of fluorescence were also set based on samples incubated with the same final concentration of isotype-matched control mAb after titration experiments. AV binding level was corrected for auto-fluorescence using fluorescence signals obtained with EVs in a calcium-free buffer (PBS). Additional controls to correct for FITC-, PE- and CFBlue-fluorescence were also pursued (unstained and single-stained controls), as well as serial dilutions to ensure proper event detection and to prevent swarming. Finally, to corroborate the presence of EVs in the EVs suspension, 5% saponin-treated controls were performed (see **Supplementary Figure 1**). To reduce background noise, buffers were prepared on the same day and filtered through  $0.22\ \mu\text{m}$  pore-size filters under vacuum. EVs markers observed in CHF patients by flow cytometry were validated by western blot as described in **Supplementary material** and shown in **Supplementary Figure 2**.

Data was analyzed with BD FACSDiva<sup>TM</sup> Software (version 6.1.3, Becton Dickinson, Franklin Lakes, NJ, USA). The concentration (number of EVs per  $\mu\text{l}$  of plasma) was determined according to Nieuwland's procedure (31), based on sample's volume, flow cytometer's flow rate and the number of fluorescence-positive events (N), as follows:  $\text{EVs}/\mu\text{l} = N \times (V_f/V_a) \times (V_t/FR) \times (1/V_i)$ , where  $V_f(\mu\text{l})$  = final volume of washed EVs suspension,  $V_a(\mu\text{l})$  = volume of washed EVs suspension used for each labeling analysis,  $V_t(\mu\text{l})$  = volume of EVs suspension before fluorescence-activated cell sorting analysis,  $FR(\mu\text{l}/\text{min})$  = flow rate of the cytometer at low mode (the average volume of EVs suspension analyzed in 1 min), 1 is the  $\mu\text{l}$  unit of volume, and  $V_i(\mu\text{l})$  = original volume of plasma used for EVs isolation.

## Statistical analysis

Statistical analysis was performed using SPSS Statistical Analysis System (version 26.0, IBM Corp. Armonk, NY). Normality of variables was assessed with Saphiro–Wilks test. Descriptive analysis for qualitative variables was performed using number of cases and percentages, while for quantitative variables, mean  $\pm$  SD were used except when specified. Frequencies of qualitative variables (clinical outcomes, risk factors, and medications) were compared between groups using Chi-squared analysis. Median values of quantitative variables were contrasted with non-parametric tests. Statistical significances between groups were determined with U Mann–Whitney tests. Correlation analyses were pursued using the Spearman correlation test. Receiver operating characteristic (ROC) curve analyses for predicted probabilities

were performed to identify threshold concentrations of EVs able to discriminate between CHF NYHA stages, or between severity in ischemic patients, and the corresponding area under the curve (AUC) with its 95% confidence interval (CI) was calculated. Binary logistic regression models were pursued to estimate predicted probabilities for NYHA severity using combinations of EVs and/or the currently used biomarker NT-proBNP. A  $p < 0.05$  was considered statistically significant. Sample size was determined using the GRANMO sample size calculator (version 7.12, April 2012). To detect mean differences in the number of EVs, a total of 126 subjects (controls and CHF) would be needed to complete the study ( $\alpha$  risk = 0.05, beta risk = 0.2, two-sided test).

## Results

### Clinical characteristics of the study population

Mean age of CHF was  $67 \pm 12$  years (68% of men). Sixty CHF patients presented reduced ejection fraction (HFrEF; LVEF  $< 40\%$ ;  $n = 60$ ) while 59 (49.6%) had CHF with preserved ejection fraction (HFpEF; LVEF  $> 50\%$ ). Additionally, 52 (43.7%) CHF presented a less severe CHF symptomatology according to the NYHA classification (class II), while 66 (55.5%) and 1 (0.8%) were in the higher severity spectrum, being in the NYHA stages III and IV, respectively. Demographics, classical risk factors and background medication are shown in **Table 1**, while etiology, biochemistry data and follow-up events and outcomes are listed in **Table 2**. Demographical, pharmacological and classical risk factor data of CHF according to their ejection fraction or severity (NYHA classification) is disclosed in **Supplementary Tables 1, 7**. Underlying etiology classification and clinical data of CHF according to these groups are listed in **Supplementary Tables 2, 8**.

### Immunity cell-derived circulating extracellular vesicles: Cell-origin and activation

Total levels of EVs-AV<sup>+</sup> shed by leukocytes were significantly higher in CHF patients than in controls. As shown in **Figure 1A**, EVs carrying the pan-leukocyte marker CD45<sup>+</sup>, the T-lymphocyte co-receptor (CD3<sup>+</sup>) or both (CD3<sup>+</sup>/CD45<sup>+</sup>), were significantly increased in CHF ( $p < 0.0001$ ). In addition, patients had significantly higher amounts of monocyte- and neutrophil-derived AV<sup>+</sup>-EVs carrying CD16<sup>+</sup> (receptor Fcγ III) and CD15<sup>+</sup> (sialyl Lewis X), respectively. EVs shed by natural-killer cells carrying the neural cell adhesion molecule-1 (CD56<sup>+</sup>) were significantly elevated in CHF compared to controls.

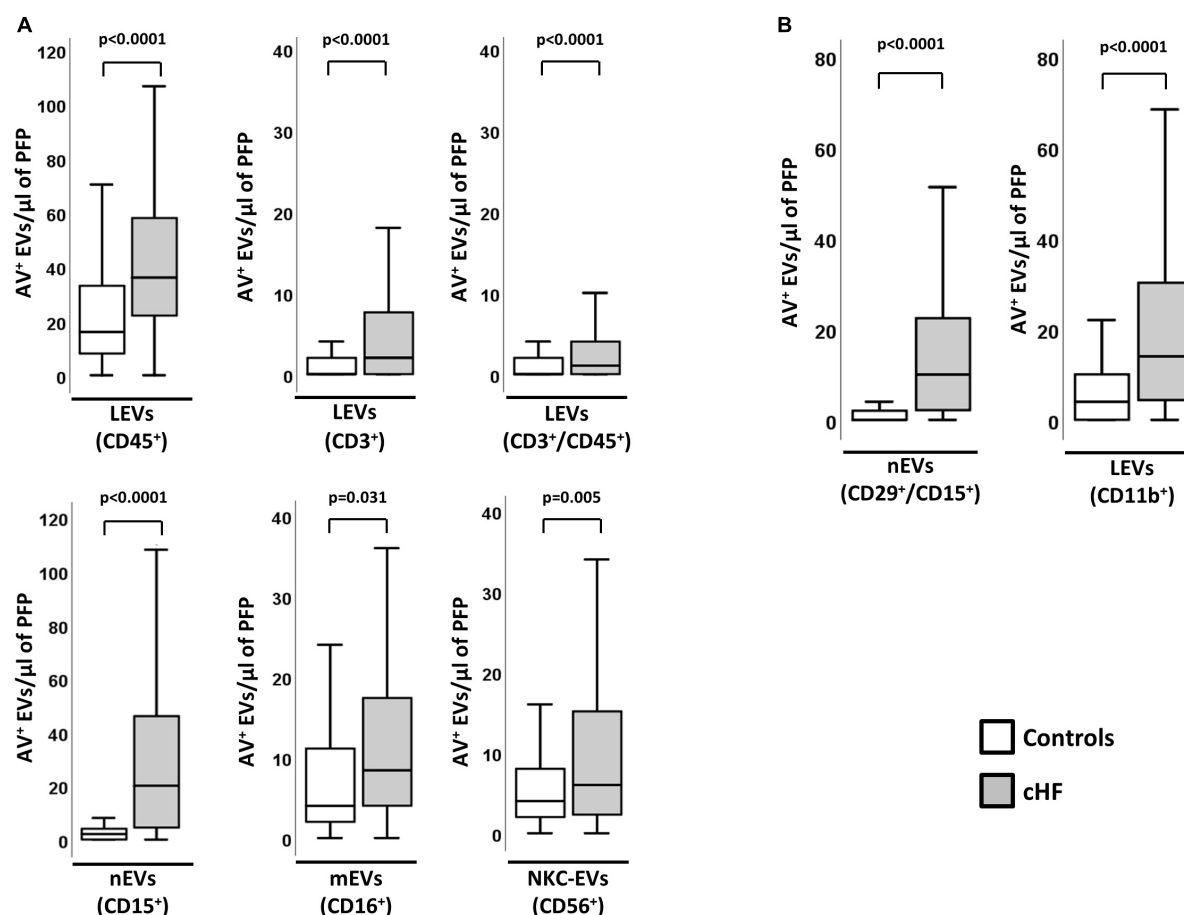


FIGURE 1

Cellular origin and distribution of AV<sup>+</sup> EVs in cHF and controls. **(A)** Distribution of EVs from total leukocytes (CD45<sup>+</sup>), T-lymphocytes (CD3<sup>+</sup> and CD3<sup>+</sup>/CD45<sup>+</sup>), neutrophils (CD15<sup>+</sup>), monocyte/macrophage (CD16<sup>+</sup>) and natural-killer cells (CD56<sup>+</sup>). **(B)** Distribution of EVs from activated neutrophils (CD29<sup>+</sup>/CD15<sup>+</sup>) and from activated leukocytes (CD11b<sup>+</sup>). A  $p < 0.05$  was considered significant (U Mann–Whitney test). AV<sup>+</sup>, annexin V<sup>+</sup>; cHF, chronic heart failure; EVs, extracellular microvesicles; LEVs, leukocyte-derived EVs; nEVs, neutrophil-derived EVs; mEVs, monocyte-derived EVs; NK-EVs, natural-killer cells-derived EVs; PFP, platelet-free plasma.

In addition, cHF patients had significantly higher levels of EVs derived from activated immune cells (identified for the shedding of activation markers in EVs). Specifically, AV<sup>+</sup>-EVs from activated leukocytes (integrin  $\alpha$ -M; CD11b<sup>+</sup>) and activated neutrophils (integrin  $\beta$ -1/sialyl Lewis X; CD29<sup>+</sup>/CD15<sup>+</sup>) were significantly increased in patients compared to controls (**Figure 1B**).

The activation of the immunity cells measured by EVs did not correlate with the number of blood leukocytes or CRP levels, indicating different pathophysiological pathways. Interestingly, circulating EVs from T-lymphocytes (CD3<sup>+</sup>/CD45<sup>+</sup>/AV<sup>+</sup>) significantly correlated with the cardiac damage markers hsTnT and NT-proBNP, while levels of EVs from activated neutrophils (CD29<sup>+</sup>/CD15<sup>+</sup>/AV<sup>+</sup>) and hsTnT and NT-proBNP showed a trend toward significance (**Supplementary Table 4**). cHF and control groups did not differ in the percentages of EVs shed by platelets (CD41a<sup>+</sup>;  $\alpha$ IIb  $\beta$  3-integrin).

## Immune cell-derived circulating extracellular vesicles signature and chronic heart failure severity

Chronic heart failure patients with more severe form of disease (a higher score in the NYHA classification [NYHA III–IV]) had higher values of EVs derived from leukocytes (CD45<sup>+</sup>/AV<sup>+</sup>) and specifically those shed by T-lymphocytes (CD3<sup>+</sup>/AV<sup>+</sup>, CD3<sup>+</sup>/CD45<sup>+</sup>/AV<sup>+</sup>). In addition, a significant increase in EVs from activated leukocytes (CD11b<sup>+</sup>/AV<sup>+</sup>) and activated neutrophils (CD29<sup>+</sup>/CD15<sup>+</sup>/AV<sup>+</sup>) was observed in these patients, compared to those with NYHA II (**Figure 2A**). Interestingly, these differences were maintained when both groups were compared with controls (**Supplementary Table 5**).

Distribution of the cHF population according to disease severity (according to the NYHA classification) is given in **Table 2**. Patients' characteristics according to degree of



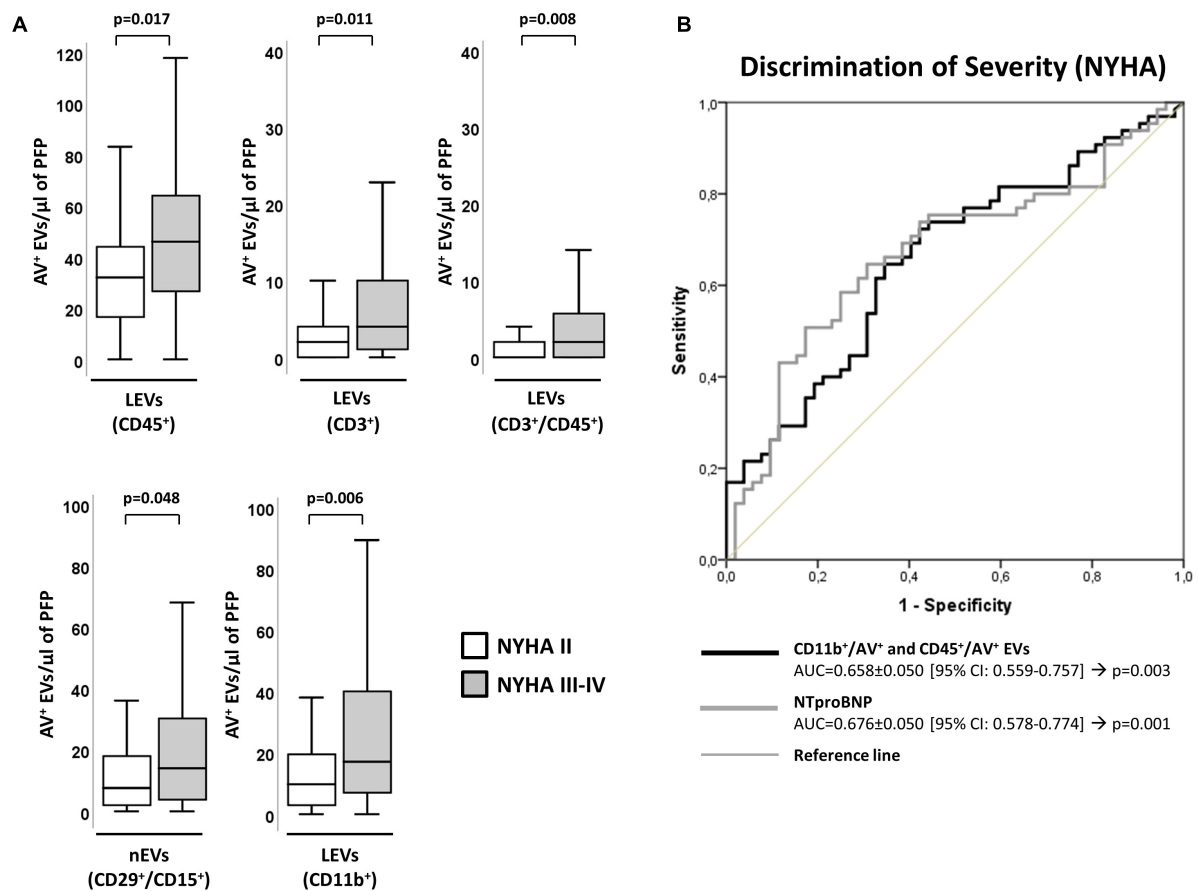


FIGURE 2

Distribution of AV<sup>+</sup>-EVs of immune-cell origin considering disease severity according to NYHA. (A) Distribution of EVs from total leukocytes (CD45<sup>+</sup>), T-lymphocytes (CD3<sup>+</sup> and CD3<sup>+</sup>/CD45<sup>+</sup>), activated leukocytes (CD11b<sup>+</sup>) and from activated neutrophils (CD29<sup>+</sup>/CD15<sup>+</sup>). A  $p < 0.05$  was considered significant (U Mann–Whitney test). (B) ROC curve analyses to evaluate EVs and NT-proBNP association to NYHA severity, with AUC indicated along its 95% CI. A  $p < 0.05$  was considered significant. AUC, area under the curve; AV<sup>+</sup>, annexin V<sup>+</sup>; CHF, chronic heart failure; CI, confidence interval; EVs, extracellular microvesicles; LEVs, leukocyte-derived EVs; IEVs, lymphocyte-derived EVs; nEVs, neutrophil-derived EVs; NYHA, New York Heart Association; PFP, platelet-free plasma; ROC, receiver operating characteristic curve.

severity (NYHA II and NYHA III-IV stages) are shown in **Supplementary Tables 1, 2**. Disease severity score according to NYHA correlated positively with hsTnT ( $\rho = 0.200$ ;  $p = 0.031$ ) and NT-proBNP ( $\rho = 0.313$ ;  $p = 0.001$ ).

Leukocyte-derived EVs subtypes showed a significant association to NYHA severity, evidencing their involvement in disease pathophysiology. By C-statistics analysis, the clustering of CD11b<sup>+</sup>/AV<sup>+</sup> and CD45<sup>+</sup>/AV<sup>+</sup> showed an AUC (AUC =  $0.658 \pm 0.050$  [95% CI: 0.559–0.757];  $p = 0.003$ ) (**Supplementary Table 6**) similar to NT-proBNP (AUC =  $0.676 \pm 0.050$  [95% CI: 0.578–0.774];  $p = 0.001$ ), hormone secreted by cardiomyocytes in the heart ventricles in response to stretching caused by increased ventricular blood volume that signals for a different pathophysiological pathway to that mapped by EVs (**Figure 2B** and **Supplementary Table 6**).

Interestingly, no differences in immune cell-derived EVs levels/phenotypes were detected in HFpEF and HFrEF patients.

Instead, as expected, a negative correlation of NT-proBNP and LVEF was observed ( $\rho = -0.222$ ,  $p = 0.015$ ). These results indicate that immune cell activation is a common feature in patients with both HFpEF and HFrEF. Demographic, biochemical and clinical classification of the patients according to their LVEF is shown in **Supplementary Tables 7–9**.

## Circulating extracellular vesicles and chronic heart failure etiology: Ischemic and non-ischemic disease

Chronic heart failure patients with ischemic etiology (HF-Isch) presented increased levels of EVs. Specifically, EVs derived from T-lymphocytes (CD3<sup>+</sup>/AV<sup>+</sup>,  $p = 0.045$ ) or carrying the leukocyte activation marker integrin  $\beta$ -1 (CD29<sup>+</sup>/AV<sup>+</sup>,  $p = 0.025$ ) were significantly increased in HF-Isch compared

to non-ischemic patients (HF-NIsch). Moreover, EVs from activated neutrophils (CD29<sup>+</sup>/CD15<sup>+</sup>/AV<sup>+</sup>) displayed higher levels in HF-Isch compared to HF-NIsch, although this trend was non-significant ( $p = 0.079$ ) (Figure 3A).

Within HF-Isch, different EVs profiles associated to disease severity (NYHA class). There were significantly higher levels of EVs derived from leukocytes (CD45<sup>+</sup>/AV<sup>+</sup>;  $p = 0.013$ ), T-lymphocytes (CD3<sup>+</sup>/AV<sup>+</sup> and CD45<sup>+</sup>/CD3<sup>+</sup>/AV<sup>+</sup>;  $p < 0.024$ ), and activated leukocytes, monocytes and neutrophils (CD11b<sup>+</sup>/AV<sup>+</sup>, CD11b<sup>+</sup>/CD14<sup>+</sup>/AV<sup>+</sup> and CD29<sup>+</sup>/CD15<sup>+</sup>/AV<sup>+</sup>, respectively;  $p < 0.05$ ) in severe disease patients. No differences associated to severity were detected in HF-NIsch (Figure 4). C-statistics analyses to assess the involvement of EVs in the pathophysiology and severity of disease in HF-Isch, showed that activated leukocytes (CD11b<sup>+</sup>/AV<sup>+</sup>) had the best discrimination power, with an AUC of  $0.848 \pm 0.058$  (95% CI: 0.734–0.961;  $p < 0.001$ ), followed by activated neutrophils (CD29<sup>+</sup>/CD15<sup>+</sup>/AV<sup>+</sup>), with an AUC of  $0.811 \pm 0.065$  (95% CI: 0.683–0.939;  $p = 0.001$ ). Again, in an order of magnitude comparable to the contribution of disease showed by NT-proBNP, with an AUC of  $0.816 \pm 0.071$  (95% CI: 0.676–0.955;  $p < 0.001$ ). When analyses were performed with the combined probabilities of EVs from activated leukocytes and neutrophils (CD11b<sup>+</sup>/AV<sup>+</sup> and CD29<sup>+</sup>/CD15<sup>+</sup>/AV<sup>+</sup>) the AUC increased to  $0.858 \pm 0.056$  (95% CI: 0.747–0.968;  $p < 0.001$ ), with a sensitivity and specificity of 80.0 and 83.3%, respectively. The addition of NT-proBNP to the analysis did not improve discrimination (AUC =  $0.858 \pm 0.056$  [0.747–0.968];  $p < 0.001$ ) (Figure 3B and Supplementary Table 10) indicating two types of contribution to disease progression of EVs and NT-proBNP, respectively.

Extracellular vesicles shedding levels, considering elapsed time between any ischemic event and sample collection, was similar in those patients with longer elapsed time between ischemic event and blood withdrawal (more than 1 year:  $7 \pm 7$  years) and those with lower time-periods (less than a year:  $5 \pm 2$  months) (Supplementary Table 11).

## Discussion

Heart failure is a complex syndrome where the heart is unable to maintain a correct blood supply to ensure that the metabolic needs of the body are met (2). This can occur due to structural and functional defects, which at the same time are the result of major pathogenic mechanisms like hemodynamic overload, ischemia-related dysfunction, or ventricular remodeling among others (32). CHF patients have shown in diverse studies to have a chronic and non-resolving inflammatory state (11, 33).

The immune system has an important role in the setting of structural and functional changes in many organs, especially

when the immune reparative processes become impaired. The present study has aimed at obtaining information on the activation state of different immunity cells in CHF patients. We have demonstrated that CHF patients present differential EVs profiles in comparison to control subjects, observing increased levels of EVs derived from leukocytes in CHF, reflecting the chronic activation state of these cells.

We have specifically detected EVs derived from lymphocytes, neutrophils, monocytes/macrophages and natural-killer cells in CHF compared to controls. In addition, we have shown that numbers of these EVs, except those shed by natural-killer cells and monocytes, correlated with the severity of the symptomatology. The combination of EVs CD11b<sup>+</sup>/AV<sup>+</sup> and CD45<sup>+</sup>/AV<sup>+</sup> was able to discriminate between NYHA stages II and III-IV, with an AUC of 0.658, indicating the implication of the activation of these immunity cells in disease severity pathophysiology. We also found that EVs could discriminate the etiology of CHF, with those patients with underlying ischemic etiology presenting significantly increased immune cell shed EVs. Further, we observed that in these patients EVs from activated leukocytes in combination with those from activated neutrophils, had a high discriminative potential in assessing CHF severity similar to NT-proBNP that measures another component of disease pathophysiology. We did not observe, however, differences in immune-cell-derived EVs profiles depending on the LVEF of CHF patients, indicating that both HFpEF and HFrEF patients have activation of immunity cells.

Several studies have shown how EVs can signal pathophysiological pathways of cardiovascular disease progression. For instance, our group has recently demonstrated that EVs can predict the presence of atherosclerotic plaques and discriminate plaque composition in familial hypercholesterolemia (21, 34). Further, it is widely accepted that EVs can identify severity of various pathologies (30, 35) and predict cardiovascular events (24, 36, 37), including cardiovascular death (22, 30). In fact, some studies have already observed increased levels of EVs in CHF, such as EVs from endothelial cells carrying the marker CD144<sup>+</sup> (29).

Here, we have shown in patients under guideline-directed medical therapy that immunity cells are activated. The amount of EVs shed by neutrophils (CD29<sup>+</sup>/CD15<sup>+</sup>/AV<sup>+</sup>), T-lymphocytes (CD3<sup>+</sup>/AV<sup>+</sup> and CD3<sup>+</sup>/CD45<sup>+</sup>/AV<sup>+</sup>) or carrying the activation marker CD11b<sup>+</sup>/AV<sup>+</sup>, positively correlates with disease severity. Further, we have shown for the first time that immune-cell-derived EVs associate to NYHA disease stage, and that immune cells are similarly activated in HFpEF and HFrEF patients. A non-resolving inflammation is a reported characteristic of HF (11, 38); in addition, our results indicate that there is an activated state of the innate and adaptive immune cells that may need be the target of future therapeutic interventions.

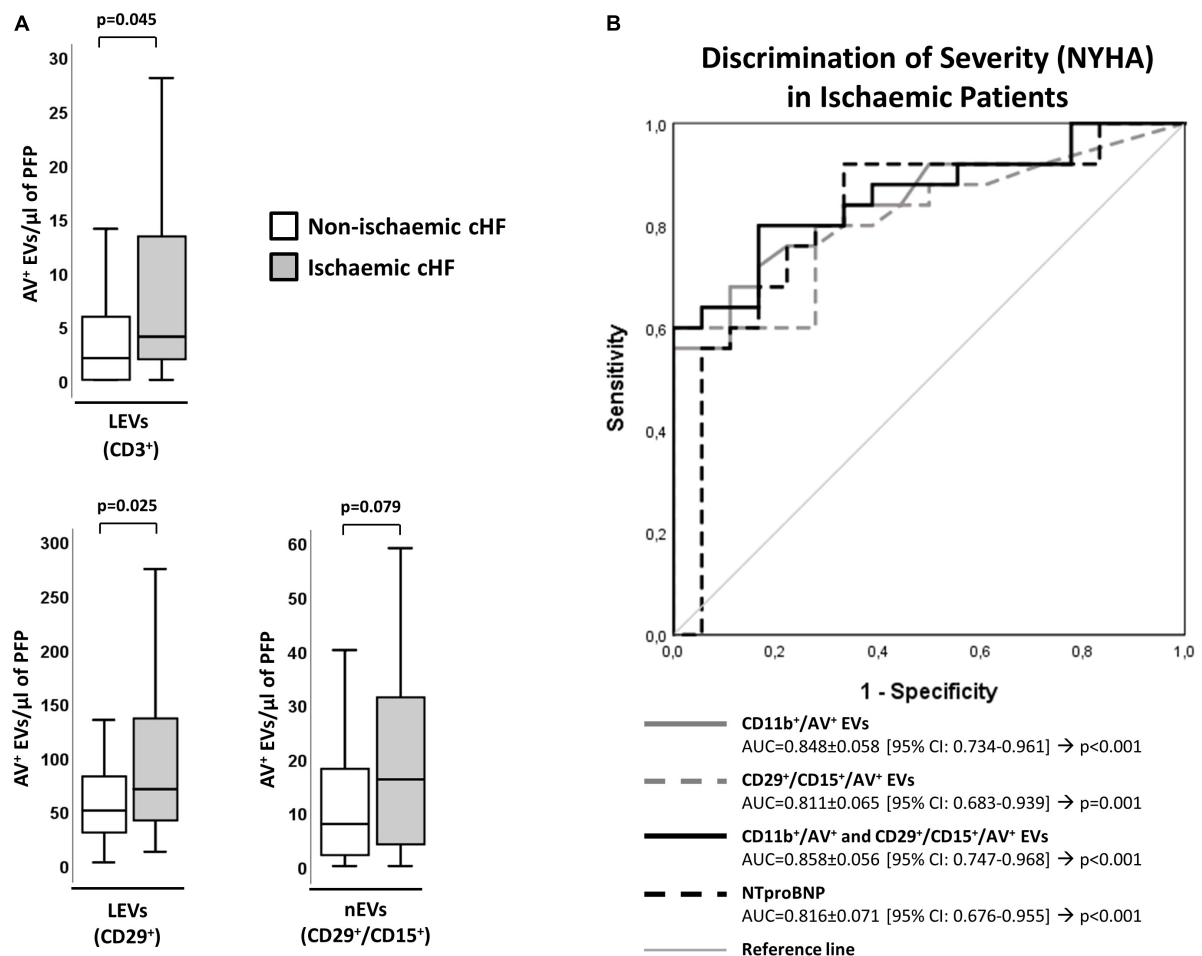


FIGURE 3

Distribution of AV<sup>+</sup>-EVs from immune-cell origin considering disease etiology. **(A)** Distribution of EVs from T-lymphocytes (CD3<sup>+</sup>), activated leukocytes (CD29<sup>+</sup>) and from activated neutrophils (CD29<sup>+</sup>/CD15<sup>+</sup>). A  $p < 0.05$  was considered significant (U Mann-Whitney test). **(B)** ROC curve analyses were used to evaluate the impact of EVs and combinations of EVs with NT-proBNP on HF severity (NYHA) in ischemic patients (AUC indicated along its 95% CI). A  $p < 0.05$  was considered significant. AUC, area under the curve; AV<sup>+</sup>, annexin V<sup>+</sup>; CHF, chronic heart failure; CI, confidence interval; EVs, extracellular microvesicles; LEVs, leukocyte-derived EVs; nEVs, neutrophil-derived EVs; NYHA, New York Heart Association; PFP, platelet-free plasma; ROC, receiver operating characteristic curve.

Patients with CHF of ischemic origin have significantly higher numbers of EVs from T-lymphocytes and neutrophils. This is a pathophysiological indication of the increase in neutrophils in the myocardium after an initial insult (10). Neutrophils are of the first cells mobilized to the damaged myocardium, where they clear diseased cells, start the reparative macrophages (M1) induction and promote inflammation, tissue reparation and fibrosis (10, 11, 39). Following the neutrophil and macrophage wave, T-lymphocytes infiltrate the heart and promote wound healing. However, if this pro-inflammatory state is prolonged in time and is not switched to a more anti-inflammatory phenotype, maladaptive remodeling and fibrosis occur, promoting HF (11, 39). This crosstalk among cells in the damaged myocardium is mapped by the phenotypically characterized EVs.

As study limitations we should first mention that the relatively small cohort size included in the study has impeded the adjustment for comorbidities and medications; however, this is a hypothesis generating study. Second, by experimental design, we did not include patients with HF with mildly reduced ejection fraction, which could have provided additional insights in the pathophysiology of the disease. Third, it is also worth mentioning that the CD11b marker (integrin  $\alpha$ -M) is expressed by activated cells and indicates the type of activated cell when is associated with another CD marker. Additionally, due to methodological issues we could not analyze EVs released by B lymphocytes, nor determine cell counts of all white blood cells analyzed. However, in view of our results, further studies addressing EVs from B cells are warranted.

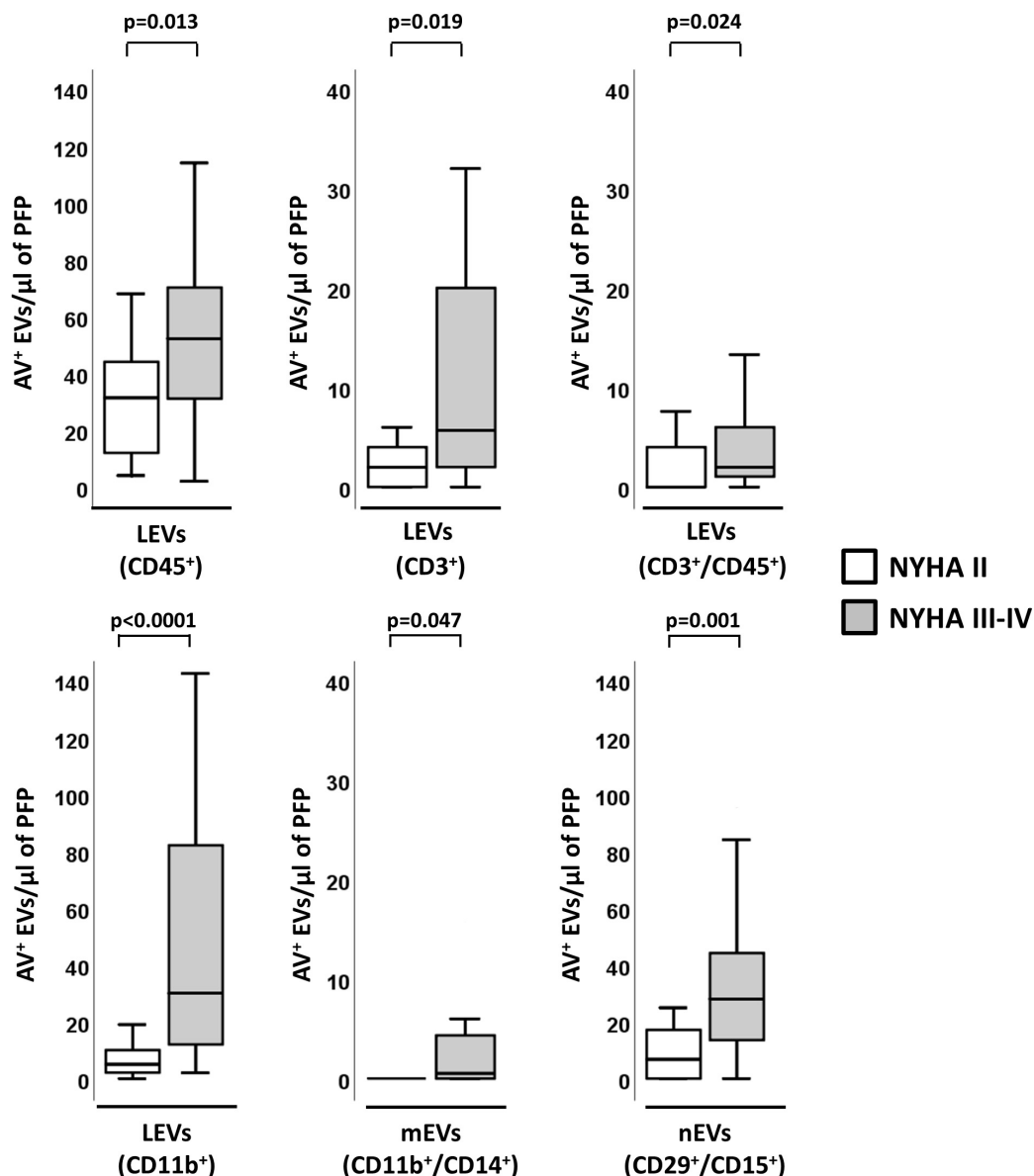


FIGURE 4

Distribution of AV<sup>+</sup>-EVs of immune-cell origin considering disease severity in ischemic patients. Distribution of EVs of total leukocytes (CD45<sup>+</sup>), T-lymphocytes (CD3<sup>+</sup> and CD3<sup>+</sup>/CD45<sup>+</sup>), activated leukocytes (CD11b<sup>+</sup>) and from activated monocytes (CD11b<sup>+</sup>/CD14<sup>+</sup>) and activated neutrophils (CD29<sup>+</sup>/CD15<sup>+</sup>). A  $p < 0.05$  was considered significant (U Mann–Whitney test). AV<sup>+</sup>, annexin V<sup>+</sup>; EVs, extracellular microvesicles; LEVs, leukocyte-derived EVs; IEVs, lymphocyte-derived EVs; mEVs, monocyte-derived EVs; nEVs, neutrophil-derived EVs; NYHA, New York Heart Association; PFP, platelet-free plasma.

## Conclusion

In conclusion, HF is a complex syndrome where multiple pathophysiological pathways converge. In well treated chronic heart failure patients, immunity cells, both innate and adaptive immunity cells, are activated and release high number of circulating EVs. The released EVs may amplify the underlying inflammatory processes in these patients, affecting different tissues. Indeed, EVs are involved in crosstalk with other cells,

acting as distant cell function regulators of targeted-receptor cells, even in distant organs.

## Data availability statement

The data that support the findings of this study are available from the corresponding author upon reasonable request.

## Ethics statement

The studies involving human participants were reviewed and approved by Ref 16/44; Ethics Committee of the Hospital de la Santa Creu i Sant Pau in Barcelona. The patients/participants provided their written informed consent to participate in this study.

## Author contributions

LB, TP, ER, and SM designed the research. AV-F performed the experiments. AV-F, TP, and LB analyzed the results. AV-F, TP, SM, and LB wrote and revised the manuscript. All authors contributed to the article and approved the submitted version.

## Funding

This work was supported by a Research Grant of the Spanish Society of Cardiology (SEC-2016) to LB; Spanish Ministry of Economy and Competitiveness of Science “Agencia Estatal de Investigación (AEI)” Proj Ref AEI/10.13039/501100011033-(PID2019-107160RB-I00) to LB; Institute of Health Carlos III (ISCIII) (Red RICORS TERA-V- RD21/0017/0013 to LB; FIS PI19/01687 to TP); and cofounded by FEDER “Una Manera de Hacer Europa”. AV-F was recipient of a research contract from the Cardiovascular Program-ICCC (IR-HSCSP). We thank Fundación Jesus Serra and Fundación de Investigación Cardiovascular (Barcelona, Spain) for their continuous support.

## Acknowledgments

We are indebted to heart failure patients for their participation in the study and the physicians that contributed

to recruitment. This work has been performed under the framework of the Doctoral Program in Biomedicine, Biochemistry and Molecular Biology of the Universitat Autònoma de Barcelona.

## Conflict of interest

LB declares to have acted as SAB member of Sanofi, to have a Research Grant of AstraZeneca, to have received speaker fees of Sanofi and Bayer and to have founded the Spin-offs Glycardial Diagnostics SL and Ivastatin Therapeutics S (all unrelated to this work). TP declares to be co-founder of the Spin-offs Glycardial Diagnostics SL and Ivastatin Therapeutics S (all unrelated to this work).

The remaining authors declare that the research was conducted in the absence of any commercial or financial relationships that could be construed as a potential conflict of interest.

## Publisher's note

All claims expressed in this article are solely those of the authors and do not necessarily represent those of their affiliated organizations, or those of the publisher, the editors and the reviewers. Any product that may be evaluated in this article, or claim that may be made by its manufacturer, is not guaranteed or endorsed by the publisher.

## Supplementary material

The Supplementary Material for this article can be found online at: <https://www.frontiersin.org/articles/10.3389/fcvm.2022.939625/full#supplementary-material>

## References

- Ridger VC, Boulanger CM, Angelillo-Scherrer A, Badimon L, Blanc-Brude OP, Bochaton-Piallat M-L, et al. Microvesicles in vascular homeostasis and diseases position paper of the European society of cardiology (ESC) working group on atherosclerosis and vascular biology. *Thromb Haemost.* (2017) 117:1296–316. doi: 10.1160/TH16-12-0943
- Kemp CD, Conte JV. The pathophysiology of heart failure. *Cardiovasc Pathol.* (2012) 21:365–71. doi: 10.1016/j.carpath.2011.11.007
- Virani SS, Alonso A, Benjamin EJ, Bittencourt MS, Callaway CW, Carson AP, et al. Heart disease and stroke statistics—2020 update: a report from the American Heart Association. *Circulation.* (2020) 141:e139–596. doi: 10.1161/CIR.0000000000000746
- Tanai E, Frantz S. Pathophysiology of heart failure. *Compr Physiol.* (2016) 6:187–214. doi: 10.1002/cphy.c140055
- McDonagh TA, Metra M, Adamo M, Gardner RS, Baumbach A, Böhm M, et al. 2021 ESC Guidelines for the diagnosis and treatment of acute and chronic heart failure. *Eur Heart J.* (2021) 42:3599–726.
- Campbell RT, McMurray JJV. Comorbidities and differential diagnosis in heart failure with preserved ejection fraction. *Heart Fail Clin.* (2014) 10:481–501. doi: 10.1016/j.hfc.2014.04.009
- Lee DS, Gona P, Vasan RS, Larson MG, Benjamin EJ, Wang TJ, et al. Relation of disease pathogenesis and risk factors to heart failure with preserved or reduced ejection fraction: insights from the framingham heart study of the national heart, lung, and blood institute. *Circulation.* (2009) 119:3070–7. doi: 10.1161/CIRCULATIONAHA.108.815944
- Testa M, Yeh M, Lee P, Fanelli R, Loperfido F, Berman JW, et al. Circulating levels of cytokines and their endogenous modulators in patients with mild to severe



congestive heart failure due to coronary artery disease or hypertension. *J Am Coll Cardiol.* (1996) 28:964–71. doi: 10.1016/S0735-1097(96)00268-9

9. Alvarez PA, Briassoulis A. Immune modulation in heart failure: the promise of novel biologics. *Curr Treat Options Cardiovasc Med.* (2018) 20:26. doi: 10.1007/s11936-018-0617-z

10. Kain V, Halade GV. Role of neutrophils in ischemic heart failure. *Physiol Genomics.* (2020) 205:107424. doi: 10.1016/j.pharmthera.2019.107424

11. Shirazi LF, Bissett J, Romeo F, Mehta JL. Role of inflammation in heart failure. *Curr Atheroscler Rep.* (2017) 19:27. doi: 10.1007/s11883-017-0660-3

12. Chung ES, Packer M, Lo KH, Fasanmade AA, Willerson JT. Randomized, double-blind, placebo-controlled, pilot trial of infliximab, a chimeric monoclonal antibody to tumor necrosis factor- $\alpha$ , in patients with moderate-to-severe heart failure: results of the anti-TNF therapy against congestive heart failure (ATTACH) trial. *Circulation.* (2003) 107:3133–40. doi: 10.1161/01.CIR.0000077913.60364.D2

13. Mann DL, McMurray JJV, Packer M, Swedberg K, Borer JS, Colucci WS, et al. Targeted anticytokine therapy in patients with chronic heart failure: results of the randomized etanercept worldwide evaluation (RENEWAL). *Circulation.* (2004) 109:1594–602. doi: 10.1161/01.CIR.0000124490.27666.B2

14. Boulanger CM, Loyer X, Rautou P-E, Amabile N. Extracellular vesicles in coronary artery disease. *Nat Rev Cardiol.* (2017) 14:259–72. doi: 10.1038/nrcardio.2017.7

15. Morel O, Jesel L, Freyssinet J-M, Toti F. Cellular mechanisms underlying the formation of circulating microparticles. *Arterioscler Thromb Vasc Biol.* (2011) 31:15–26. doi: 10.1161/ATVBAHA.109.200956

16. Suades R, Padró T, Badimon L. The role of blood-borne microparticles in inflammation and hemostasis. *Semin Thromb Hemost.* (2015) 41:590–606. doi: 10.1055/s-0035-1556591

17. Badimon L, Suades R, Fuentes E, Palomo I, Padró T. Role of platelet-derived microvesicles as crosstalk mediators in atherothrombosis and future pharmacology targets: a link between inflammation, atherosclerosis, and thrombosis. *Front Pharmacol.* (2016) 7:293. doi: 10.3389/fphar.2016.00293

18. Badimon L, Suades R, Vilella-Figuerola A, Crespo J, Vilahur G, Escate R, et al. Liquid biopsies: microvesicles in cardiovascular disease. *Antioxid Redox Signal.* (2020) 33:645–62. doi: 10.1089/ars.2019.7922

19. Leroyer AS, Isobe H, Lesèche G, Castier Y, Wassef M, Mallat Z, et al. Cellular origins and thrombogenic activity of microparticles isolated from human atherosclerotic plaques. *J Am Coll Cardiol.* (2007) 49:772–7. doi: 10.1016/j.jacc.2006.10.053

20. Suades R, Padró T, Vilahur G, Badimon L. Circulating and platelet-derived microparticles in human blood enhance thrombosis on atherosclerotic plaques. *Thromb Haemost.* (2012) 108:1208–19. doi: 10.1160/TH12-07-0486

21. Suades R, Padró T, Alonso R, Mata P, Badimon L. High levels of TSP1+/CD142+ platelet-derived microparticles characterise young patients with high cardiovascular risk and subclinical atherosclerosis. *Thromb Haemost.* (2015) 114:1310–21. doi: 10.1160/TH15-04-0325

22. Chiva-Blanch G, Bratseth V, Ritschel V, Andersen G, Halvorsen S, Eritsland J, et al. Monocyte-derived circulating microparticles (CD14+, CD14+/CD11b+ and CD14+/CD142+) are related to long-term prognosis for cardiovascular mortality in STEMI patients. *Int J Cardiol.* (2017) 227:876–81. doi: 10.1016/j.ijcard.2016.11.302

23. Sluijter JPG, Davidson SM, Boulanger CM, Buzás EI, De Kleijn DPV, Engel FB, et al. Extracellular vesicles in diagnostics and therapy of the ischaemic heart: position Paper from the working group on cellular biology of the heart of the european society of cardiology. *Cardiovasc Res.* (2018) 114:19–34. doi: 10.1093/cvr/cvx211

24. Suades R, Padró T, Crespo J, Ramaiola I, Martín-Yuste V, Sabaté M, et al. Circulating microparticle signature in coronary and peripheral blood of ST

elevation myocardial infarction patients in relation to pain-to-PCI elapsed time. *Int J Cardiol.* (2016) 202:378–87. doi: 10.1016/j.ijcard.2015.09.011

25. Chiva-Blanch G, Suades R, Crespo J, Peña E, Padró T, Jiménez-Xarrié E, et al. Microparticle shedding from neural progenitor cells and vascular compartment cells is increased in ischemic stroke. *PLoS One.* (2016) 11:e0148176. doi: 10.1371/journal.pone.0148176

26. Berezin AE, Kremzer AA, Martovitskaya YV, Samura TA, Berezina TA. The predictive role of circulating microparticles in patients with chronic heart failure. *BBA Clin.* (2015) 3:18–24. doi: 10.1016/j.bbacli.2014.11.006

27. Berezin AE, Kremzer AA, Samura TA, Berezina TA. Altered signature of apoptotic endothelial cell-derived microvesicles predicts chronic heart failure phenotypes. *Biomark Med.* (2019) 13:737–50. doi: 10.2217/bmm-2018-0449

28. Berezin AE, Kremzer AA, Martovitskaya YV, Berezina TA, Gromenko EA. Pattern of endothelial progenitor cells and apoptotic endothelial cell-derived microparticles in chronic heart failure patients with preserved and reduced left ventricular ejection fraction. *EBioMedicine.* (2016) 4:86–94. doi: 10.1016/j.ebiom.2016.01.018

29. Nozaki T, Sugiyama S, Sugamura K, Ohba K, Matsuzawa Y, Konishi M, et al. Prognostic value of endothelial microparticles in patients with heart failure. *Eur J Heart Fail.* (2010) 12:1223–8. doi: 10.1093/eurjhf/hfq145

30. Sionis A, Suades R, Sans-Roselló J, Sánchez-Martínez M, Crespo J, Padró T, et al. Circulating microparticles are associated with clinical severity of persistent ST-segment elevation myocardial infarction complicated with cardiogenic shock. *Int J Cardiol.* (2018) 258:249–58. doi: 10.1016/j.ijcard.2017.10.044

31. Nieuwland R, Berckmans RJ, McGregor S, Böing AN, Romijn FPHM, Westendorp RGJ, et al. Cellular origin and procoagulant properties of microparticles in meningococcal sepsis. *Blood.* (2000) 95:930–5. doi: 10.1182/blood.V95.3.930.003k46\_930\_935

32. Inamdar AA, Inamdar AC. Heart Failure: diagnosis, management and utilization. *J Clin Med.* (2016) 5:62. doi: 10.3390/jcm5070062

33. Biasucci LM, La Rosa G, Pedicino D, D'Aiello A, Galli M, Liuzzo G. Where does inflammation fit? *Curr Cardiol Rep.* (2017) 19:84. doi: 10.1007/s11886-017-0896-0

34. Chiva-Blanch G, Padró T, Alonso R, Crespo J, Perez De Isla L, Mata P, et al. Liquid biopsy of extracellular microvesicles maps coronary calcification and atherosclerotic plaque in asymptomatic patients with familial hypercholesterolemia: a computed tomographic angiography imaging study. *Arterioscler Thromb Vasc Biol.* (2019) 39:945–55. doi: 10.1161/ATVBAHA.118.312414

35. Gkaliagkousi E, Gavrilaki E, Yiannaki E, Vasileiadis I, Nikolaidou B, Lazaridis A, et al. Platelet microvesicles are associated with the severity of coronary artery disease: comparison between peripheral and coronary circulation. *J Thromb Thrombolysis.* (2021) 51:1138–43. doi: 10.1007/s12399-020-02302-5

36. Chiva-Blanch G, Crespo J, Suades R, Arderiu G, Padró T, Vilahur G, et al. CD142+/CD61+, CD146+ and CD45+ microparticles predict cardiovascular events in high risk patients following a Mediterranean diet supplemented with nuts. *Thromb Haemost.* (2016) 116:103–14. doi: 10.1160/TH16-02-0130

37. Chiva-Blanch G, Suades R, Crespo J, Vilahur G, Arderiu G, Padró T, et al. CD3+/CD45+ and SMA- $\alpha$ + circulating microparticles are increased in individuals at high cardiovascular risk who will develop a major cardiovascular event. *Int J Cardiol.* (2016) 208:147–9. doi: 10.1016/j.ijcard.2016.01.211

38. Dick SA, Epelman S. Chronic heart failure and inflammation. What do we really know? *Circ Res.* (2016) 119:159–76. doi: 10.1161/CIRCRESAHA.116.308030

39. Dutka M, Bobiński R, Ulman-Włodarz I, Hajduga M, Bujok J, Pająk C, et al. Various aspects of inflammation in heart failure. *Heart Fail Rev.* (2020) 25:537–48. doi: 10.1007/s10741-019-09875-1



## OPEN ACCESS

## EDITED BY

Kenneth Scott Campbell,  
University of Kentucky, United States

## REVIEWED BY

Farid Moussavi-Harami,  
University of Washington, United States  
Chiara Tesi,  
University of Florence, Italy

## \*CORRESPONDENCE

Steven Marston  
✉ S.marston@imperial.ac.uk

## SPECIALTY SECTION

This article was submitted to  
Cardiovascular Genetics and Systems  
Medicine,  
a section of the journal  
Frontiers in Cardiovascular Medicine

RECEIVED 26 October 2022

ACCEPTED 19 December 2022

PUBLISHED 09 January 2023

## CITATION

Marston S and Pinto JR (2023)  
Suppression of lusitropy as a disease  
mechanism in cardiomyopathies.  
*Front. Cardiovasc. Med.* 9:1080965.  
doi: 10.3389/fcvm.2022.1080965

## COPYRIGHT

© 2023 Marston and Pinto. This is an  
open-access article distributed under  
the terms of the [Creative Commons  
Attribution License \(CC BY\)](#). The use,  
distribution or reproduction in other  
forums is permitted, provided the  
original author(s) and the copyright  
owner(s) are credited and that the  
original publication in this journal is  
cited, in accordance with accepted  
academic practice. No use, distribution  
or reproduction is permitted which  
does not comply with these terms.

# Suppression of lusitropy as a disease mechanism in cardiomyopathies

Steven Marston <sup>1\*</sup> and Jose Renato Pinto <sup>2</sup>

<sup>1</sup>National Heart and Lung Institute, Imperial College London, London, United Kingdom,

<sup>2</sup>Department of Biomedical Sciences, Florida State University College of Medicine, Tallahassee, FL, United States

In cardiac muscle the action of adrenaline on  $\beta_1$  receptors of heart muscle cells is essential to adjust cardiac output to the body's needs. Adrenergic activation leads to enhanced contractility (inotropy), faster heart rate (chronotropy) and faster relaxation (lusitropy), mainly through activation of protein kinase A (PKA). Efficient enhancement of heart output under stress requires all of these responses to work together. Lusitropy is essential for shortening the heartbeat when heart rate increases. It therefore follows that, if the lusitropic response is not present, heart function under stress will be compromised. Current literature suggests that lusitropy is primarily achieved due to PKA phosphorylation of troponin I (TnI) and phospholamban (PLB). It has been well documented that PKA-induced phosphorylation of TnI releases  $\text{Ca}^{2+}$  from troponin C faster and increases the rate of cardiac muscle relaxation, while phosphorylation of PLB increases SERCA activity, speeding up  $\text{Ca}^{2+}$  removal from the cytoplasm. In this review we consider the current scientific evidences for the connection between suppression of lusitropy and cardiac dysfunction in the context of mutations in phospholamban and thin filament proteins that are associated with cardiomyopathies. We will discuss what advances have been made into understanding the physiological mechanism of lusitropy due to TnI and PLB phosphorylation and its suppression by mutations and we will evaluate the evidence whether lack of lusitropy is sufficient to cause cardiomyopathy, and under what circumstances, and consider the range of pathologies associated with loss of lusitropy. Finally, we will discuss whether suppressed lusitropy due to mutations in thin filament proteins can be therapeutically restored.

## KEYWORDS

adrenergic stimulation, lusitropy, contractility, protein kinase A, hypertrophic cardiomyopathy, dilated cardiomyopathy

## Introduction

It is 10 years since we wrote a review, based mainly on *in vitro* work, proposing that a major defect commonly connected with inherited cardiomyopathies (and perhaps some others) was their lack of response to TnI phosphorylation (1). The modulation of cardiac muscle relaxation rate due to TnI and phospholamban phosphorylation is a key determinant of the lusitropic response. This led us to propose that suppression of lusitropy could be a disease mechanism in cardiomyopathies. This review revisits the question in the light of recent research.

Calcium ions ( $\text{Ca}^{2+}$ ), released from the sarcoplasmic reticulum, bind to troponin C to switch the thin filament on, however, in cardiac muscle a more graded form of regulation is essential to tailor cardiac output to the body's needs. The level of contractility of heart muscle is determined by three factors: the initial sarcomere length (preload), the force against which the muscle must shorten (afterload), and the speed and force of contraction. Speed and force of contraction can be modulated independently of preload and afterload by changing the inotropic state. This is controlled largely, but not exclusively, by stimuli from the sympathoadrenal system and the parasympathetic nervous system.

Adrenergic activation acts mainly on  $\beta 1$  receptors to trigger a coordinated response of the heart during exercise or “flight-or-flight” that increases cardiac output up to fivefold. This is achieved by an increase in heart rate of up to threefold (chronotropy) and an increase in the force of contraction (inotropy). Ventricular pressure rises quicker and higher arterial pressure is produced. At the same time the duration of systole grows briefer and relaxation is faster (lusitropy).

The increased speed of relaxation is essential for the adrenergic response since the heart beat must become shorter if the heart rate is increased to avoid successive beats overlapping which would reduce stroke volume. Nevertheless, lusitropy is not often given the attention it deserves since heart rate and magnitude of contraction are obvious and easily measured parameters whilst relaxation rates are not commonly recorded. It is the objective of this review to consider the evidence that defects in lusitropy can be a significant contributor to heart disease.

The biochemical and physiological process of lusitropy is well understood.  $\beta$ -1 receptor activation leads to adenylate cyclase activation and cAMP production. cAMP acts directly on membrane channels and also activates the cyclic AMP-dependent protein kinase (PKA). PKA itself phosphorylates a variety of ion channels, ion pumps in the sarcolemma and sarcoplasmic reticulum (SR) and contractile proteins.

The SR in cardiac myocytes stores large quantities of  $\text{Ca}^{2+}$ . The SR is a complex cellular compartment that allows intracellular  $\text{Ca}^{2+}$  cycling that is coordinated with other cellular systems such as myofilament and sarcolemma proteins.  $\text{Ca}^{2+}$  release from the SR is driven by the opening of

Ryanodine Receptor whilst  $\text{Ca}^{2+}$  reuptake by the SR is mostly dictated by the  $\text{Ca}^{2+}$  pump called sarco/endoplasmic reticulum  $\text{Ca}^{2+}$  -ATPase (SERCA2a). In the sarcoplasmic reticulum PKA phosphorylates Phospholamban (PLB), an accessory protein crucial in the regulation of SERCA2a activity.

There are two phosphorylation sites in PLB, one at serine 16 and another at threonine 17 and the kinases involved are PKA for serine 16 and  $\text{Ca}^{2+}$ /CaM kinase for threonine 17. Unphosphorylated PLB is an inhibitor of SERCA2a; PKA-mediated phosphorylation of phospholamban relieves the inhibition, thus activating SERCA2a, resulting in faster sequestration of  $\text{Ca}^{2+}$  (lusitropy) and increased filling of the sarcoplasmic reticulum that contributes to positive inotropy. In addition, positive lusitropism is achieved by a PKA-mediated phosphorylation of troponin I, exclusively at serines 22 and 23 (2, 3); phosphorylation of TnI at these two serine sites increases the rate of  $\text{Ca}^{2+}$ -release from troponin C (4). To terminate these events when plasma concentrations of  $\beta$ -agonists fall, cyclic adenosine monophosphate (cAMP) is hydrolyzed by the cyclic nucleotide phosphodiesterases, and protein phosphatases hydrolyze the protein-bound phosphate. As will be discussed later, it is probable that both PLB and TnI phosphorylation are necessary for effective positive lusitropy. It is possible other targets of PKA, such as the L-type  $\text{Ca}^{2+}$  channel (5), may influence lusitropy, but comprehensive data is lacking. Recent publications have described the molecular mechanisms of troponin and phospholamban phosphorylation modulation of function (6, 7).

## Evidence that lusitropy is necessary from PLB loss of function models

The key studies of the role of phospholamban in cardiac muscle regulation are based on a PLB knockout (KO) mouse model (8). In unloaded assays (e.g., myocytes) the relaxation rate is completely unresponsive to isoprenaline (Iso) compared with a 30% increase in WT myocytes. However, in isometric contractions lusitropy is merely blunted: decrease in tau relax was 17% vs. 30–50% in non-transgenic littermates (NTG). PLB KO has additional actions, since it activated SERCA2a: tau is lower than NTG and there is a substantial inotropic effect. However, it can be concluded that PLB phosphorylation is a mechanism for lusitropy. Pathogenic, exonic variants have been identified in the PLB gene associated with DCM; to date, there are six known *PLN* mutations linked to dilated cardiomyopathy (p.R9C, R9L, R9H, R14del, R25C, L39X) (9–11) with several more candidate mutations suggested from large scale surveys [e.g., (12)].

The PLB R9C variant associated with DCM has been extensively studied for its inotropic and lusitropic effects in transgenic mice, cardiomyocytes and human iPSC-derived

cardiomyocytes. Cardiomyocytes isolated from transgenic mice bearing the PLB R9C in the heart display prolonged  $\text{Ca}^{2+}$  transients. Upon further investigation it was found that the PLB R9C mutation “traps” PKA and inactivates it, preventing phosphorylation. This has an constitutive inotropic and lusitropic effect but yields negative consequences of impaired frequency potentiation and blunted  $\beta$ -adrenergic responsiveness (9). Another report suggested that acute expression of PLB R9C in cardiomyocytes enhances inotropic and lusitropic responses of the transfected cells but also blunts the response to the frequency of stimulation and isoproterenol stimulation (13). The PLB R9C mutation was also shown to cause a blunted  $\beta$ -agonist response in human iPSC-CMs in experiments performed using 3D human EHTs (14).

## Evidence that lusitropy is necessary from TnI phosphorylation sites serine 22/23 loss of function models

The role of TnI phosphorylation in modulating contractility has been studied in several transgenic mouse models either substituting the unphosphorylatable slow skeletal TnI for native cardiac TnI or by modifying the phosphorylatable serines, to non-phosphorylatable (Ala substitution) or pseudophosphorylated (Asp or Glu substitution) forms.

One of the most extensively studied models is the slow skeletal troponin overexpression model where cTnI in the heart is completely replaced with ssTnI that does not have the N-terminal phosphorylatable peptide (15–17). The substitution increases  $\text{Ca}^{2+}$  sensitivity of isometric tension in myofibrils ( $\text{pCa}_{50}$  is 5.81 WT, 6.13 TG) but also blunts the effect of PKA phosphorylation ( $\Delta \text{pCa}_{50} = 0.146$  in WT but 0.08 in TG). In myocytes, isoprenaline stimulation accelerated relaxation 1.7-fold in WT but only 1.3-fold in TG indicating a blunting of the lusitropic response that is also indicated by measurements of contraction kinetics on intact heart muscle strips ( $f_{\min}$ ). In Langendorf working heart studies the effect of Iso on  $\text{LVdp}/\text{dt}_{\min}$  is also blunted and the blunting of lusitropy is also evident in PV loops. The inotropic effect of Iso is not greatly altered in unloaded studies but, like the PLB KO, is partially blunted in loaded (auxotonic) muscles (Figure 1).

Substituting a non-native TnI and overexpression may have unforeseen physiological off target effects. Better models have been produced by mutating the phosphorylatable serines in native cTnI. The model described by Pi et al. overexpressed cTnI with ser22 and 23 mutated to Alanine (unphosphorylatable); moreover the transgenic mice were bred with cTnI null mice to avoid any interactions between native and transgenic cTnI (18, 19). The blunting of lusitropy was clear: as measured by ATPase in myofibrils or tension in skinned muscle fibers, the

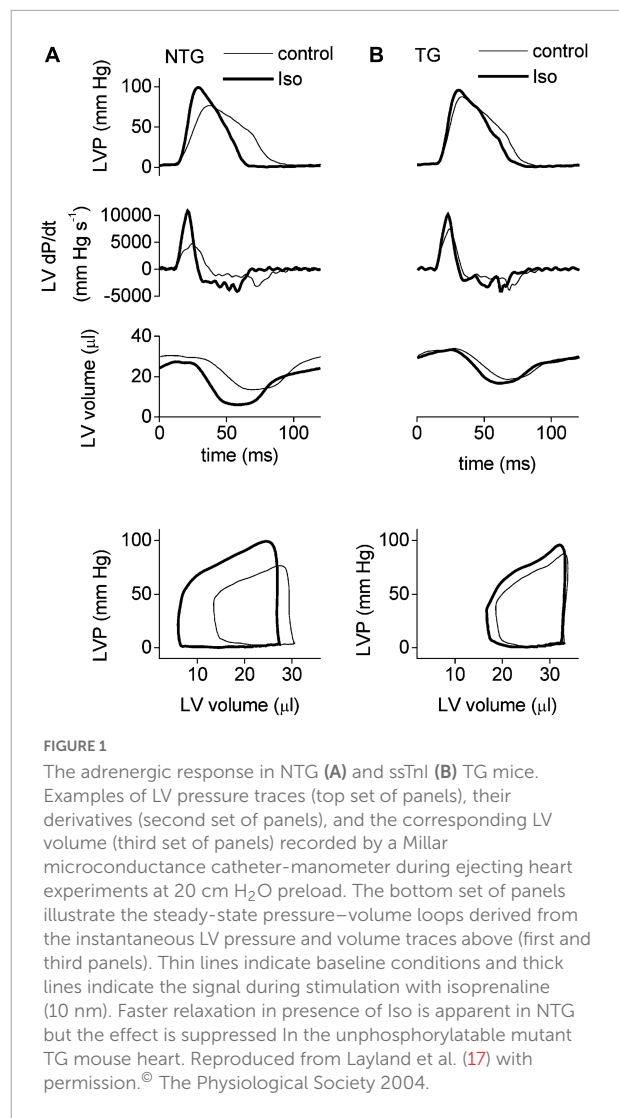


FIGURE 1

The adrenergic response in NTG (A) and ssTnI (B) TG mice. Examples of LV pressure traces (top set of panels), their derivatives (second set of panels), and the corresponding LV volume (third set of panels) recorded by a Millar microconductance catheter-manometer during ejecting heart experiments at 20 cm  $\text{H}_2\text{O}$  preload. The bottom set of panels illustrate the steady-state pressure–volume loops derived from the instantaneous LV pressure and volume traces above (first and third panels). Thin lines indicate baseline conditions and thick lines indicate the signal during stimulation with isoprenaline (10 nm). Faster relaxation in presence of Iso is apparent in NTG but the effect is suppressed in the unphosphorylatable mutant TG mouse heart. Reproduced from Layland et al. (17) with permission. © The Physiological Society 2004.

$\text{Ca}^{2+}$ -sensitivity was shifted 1.3-fold in NTG by Iso but no shift was detected in TG (18). In intact myocytes 2.5 nM Iso decreased relaxation time by 37% in WT but only 18% in TG. Yasuda et al. also studied Ser > Ala replacement in transfected myocytes, finding Iso decreased relaxation time by 36% in NTG but only 9% in TG (20).

The alternative model- substituting aspartic acid for the two serines to create a pseudophosphorylated troponin I has also been studied in transgenic mice and transfected myocytes. The first study used a mouse model overexpressing Asp 22/23 (21) and 95% replacement. It was noted that the mouse model was healthy but had enhanced cardiac function (as measured by Millar catheter) with faster contraction and slower relaxation, however, the response to  $\beta$ -adrenergic stimulation was not significantly different from NTG. Another group produced a similar model with either Asp 22/23 or Asp 22/23/43/45/144 overexpressed and studied lines with almost complete protein replacement (22). *In vitro* the Asp22/23

mouse myofibrillar  $\text{Ca}^{2+}$  sensitivity was lower than NTG, as expected for pseudophosphorylation ( $\Delta\text{pCa}_{50} = 0.20$ ), but upon PKA phosphorylation the  $\text{Ca}^{2+}$  sensitivity was not changed compared with  $\Delta\text{pCa}_{50}$  of 0.23 in NTG. In the intact beating heart (Millar catheter), the rate of relaxation ( $\text{dP/dT}_{\text{min}}$ ) was increased from  $-6,869$  to  $-8,651$  mmHg/s by Iso in NTG and  $-10,598$  to  $-12,099$  in Asp22/23 mouse. Although the studies of Takimoto et al. and Sakthivel et al. show little evidence that loss of the TnI  $\text{Ca}^{2+}$ -sensitivity shift causes lusitropy, the study by Yasuda et al. (20) using the same Asp22/23 model did show a blunting of lusitropy in myocytes. Myocyte twitch tension was measured by attaching microfibre probes. In Wild-type,  $\text{ttb}_{75}$  was decreased from 69 to 39 ms on treatment with Iso, a 44% change, whilst in Asp22/23 myocytes,  $\text{ttb}_{75}$  was decreased from 44 to 38 ms, a 14% change. A similar blunting was measured

in myocytes transfected with Asp22/23: Iso produced a 33% reduction in relaxation time in WT but only 16% in Asp22/23. In addition, this study recapitulated the previous results with Ala22/23 and with ssTnI substitutions in both TG mouse and transfected myocytes (Table 1).

## “Is PLB or TnI the prima donna in $\beta$ adrenergic induced lusitropy?”

This question was raised in a key Circulation Research editorial that discussed the findings of Yasuda in relation to the other published work at the time (23). It is still a very pertinent question. Essentially we need to know whether the release of  $\text{Ca}^{2+}$  from troponin or the removal of  $\text{Ca}^{2+}$  from

TABLE 1 Animal models of impaired lusitropy.

References	Model	$\text{Ca}^{2+}$ sensitivity shift on phosphorylation, $\Delta\text{pCa}_{50}$ , WT > mutant	Lusitropy, % reduction of relaxation time, $100 \times (1 - \text{relaxation time} + \text{dobu or Iso} / \text{relaxation time baseline})$ , WT > mutant
(60)	PLB KO		30% > 0, isometric 40% > 17%
(15)	Ss TnI mouse	0.15 > 0.07	Unloaded 41% > 23%
(17)	ssTnI		$\text{dP/dT}_{\text{min}}$ 39% > 13%
(16)	Ss TnI	0.15 > 0.05	$\text{ttb}_{50}$ skinned fibre 41% > 23%
(18)	cTnI Ser 23/24 Ala <sub>2</sub>	0.08 > 0	Unloaded 37% > 18%
(21)	cTnI 23,24 Asp <sub>2</sub>		
(22)	cTnI 23/24 Asp <sub>2</sub>	0.23 > 0.20	Loaded 26% > 14%
(20)	cTnI 23/24 Asp <sub>2</sub> and Ala <sub>2</sub>		Asp <sub>2</sub> isometric 44% > 14% Ala <sub>2</sub> isometric 36% > 9%
(9)	PLB R9C		$\text{Ca}^{2+}$ uptake rate, 20% > 0
(13)	PLB R9C		Unloaded, 29% > 24%
(14)	PLB R9C		Loaded EHT 25% > 4%
(61)	TnT I79N		26% > 9%, Langendorf 34% > 29%
(62)	TnT R278C		Langendorf 34% > 32%
(7)	TnT R92Q Guinea pig		Myocytes 24% > -9%
(63)	TnT R92Q	0.30 > -0.04	Langendorf 45% > 13%
(53)	TnI P83S		Myofibrils: $k_{\text{RELslow}}$ 56% > 9%
(55)	MYBPC3KI		IPSC eht 19% > 2%
(64)	TnT $\Delta$ 160E		Millar catheter 28% > 19%
(44)	Actin E99K	IVMA 0.46 > 0.06 (mouse), -0.03 (human)	Echo, all $\Delta$ on dob suppressed
(65)	TnI R21C	0.25 > 0.05	32% > 5% (skinned fiber) 16% > 13% (myocytes)
(51)	TnI R21C		Exchanged myofibrils $k_{\text{RELslow}}$ 39% > 8%, $k_{\text{RELfast}}$ 14% > 5%
(59)	Actin E361G		Papillary muscle (10 Hz) 17.5% > 5% Millar catheter 22.4% > 7.5%
(66)	Actin E361G	Myofibrils 0.26 > -0.05	$K_{\text{RELfast}}$ 34% > 0%
(37)	Actin E361G	IVMA 0.47 > 0.017	Cardiac output, dob effect Echo, 14% > 0%, MRI 19% > 8%

Where possible  $\text{ttb}_{90}$  is used. If not available, parameter is given in this table. All studies in mouse models unless otherwise stated. In paired *t*-test, wild-type mean lusitropy is  $28.1\% \pm 1.8$  (sem), mutant mean lusitropy is  $11.0\% \pm 1.8$  (sem),  $n = 25$ . *t* probability < 0.0001.



the sarcoplasm by SERCA is rate limiting for relaxation. The answer to the question depends on the balance of rates of these two processes, which themselves depend on conditions, especially temperature since many experiments are conducted at below normal body temperature but also force, since these rates are different in unloaded and isometric muscle. Measurement technique, experimental medium and most likely also the animal model that is used are also critical.

Two studies have indicated that (in unloaded rat myofibrils at least)  $\text{Ca}^{2+}$  dissociating from TnC becomes rate limiting at 37°C whereas SERCA activity is limiting at lower, non-physiological temperatures (24, 25). Experiments do not support a dominating role for either PLB or TnI phosphorylation. Li et al.

(8) proposed TnI phosphorylation contributes just 14–18% of lusitropy in unloaded muscle but nothing in isometric muscle based on comparison of WT with PLB-KO mouse. Yasuda et al. (20) predicted an opposite pattern with 75% contributed by TnI phosphorylation in unloaded myocytes. Layland et al. (17) argue that cTnI has the pivotal role in the positive inotropic response of the murine heart to  $\beta$ -adrenergic stimulation, under all loading conditions but agree that it is most evident in the auxotonically loaded ejecting heart.

It seems unlikely that either TnI or phospholamban phosphorylation is actually the “prima donna” but rather that the control of lusitropy is a duet. Wolska et al. (26) studied a transgenic mouse with both a PLB KO and ssTnI substitution.

TABLE 2 Mutations that have been reported to cause uncoupling.

Mutation	Effect of phosphorylation on $\text{Ca}^{2+}$ -sensitivity, $\text{pCa}_{50}$ uP- $\text{pCa}_{50}$ P	Measurement method	Publication
<b>DCM</b>			
ACTC E361G	0.017	<i>In vitro</i> motility assay (IVMA)	(37, 38)
TPM1 E54K	0.021	IVMA	(38)
TPM1 E40K	0.00	IVMA	(38)
TPM1 D230N	−0.013	IVMA	(38)
TNNC1 G159D	−0.013	IVMA/ $\text{Ca}^{2+}$ binding	(29, 30, 38, 39)
TNNC1 Y5H	0.068	Skinned fiber	(40)
TNNC1 M103I	0.017	Skinned fiber	(40)
TNNC1 I148V	0.053	Skinned fiber	(40)
TNNT2 $\Delta$ K210	−0.009	IVMA/skinned fiber	(38, 41, 42)
TNNT2 R141W	−0.022	IVMA	(38)
TNNI3 K36Q	−0.009	IVMA/ATPase	(38, 43)
<b>HCM</b>			
ACTC E99K	−0.004	IVMA	(44, 45)
TPM1 E180G	−0.009	Skinned fiber	(45, 46)
TNNC1 L29Q	−0.036	$\text{Ca}^{2+}$ binding/ATPase	(30, 47, 48)
TNNT2 R92Q	0.041	IVMA	(49)
TNNT2 $\Delta$ 14	0.000	IVMA	(49)
TNNT2 $\Delta$ 28 + 7	0.000	IVMA	(49)
TNNT2 $\Delta$ E160Q	0.000	IVMA	(49)
TNNT2 S179F	0.041	IVMA	(49)
TNNT2 K273E	0.041	IVMA	(49)
TNNT2K280N	0.041	IVMA	(49, 50)
TNNI3 R145G	0.000	IVMA/ATPase	(27, 51)
TNNI3 R145W	0.045	IVMA/ATPase	(52)
TNNI3 P83S	0.000	Exchanged myofibrils	(53)
TNNI3 R21C	0.049	Skinned fiber	(35, 51)
TNNI3 G203S	0.057	ATPase/IVMA	(28)
TNNI3 K206Q	0.000	ATPase/IVMA	(28)

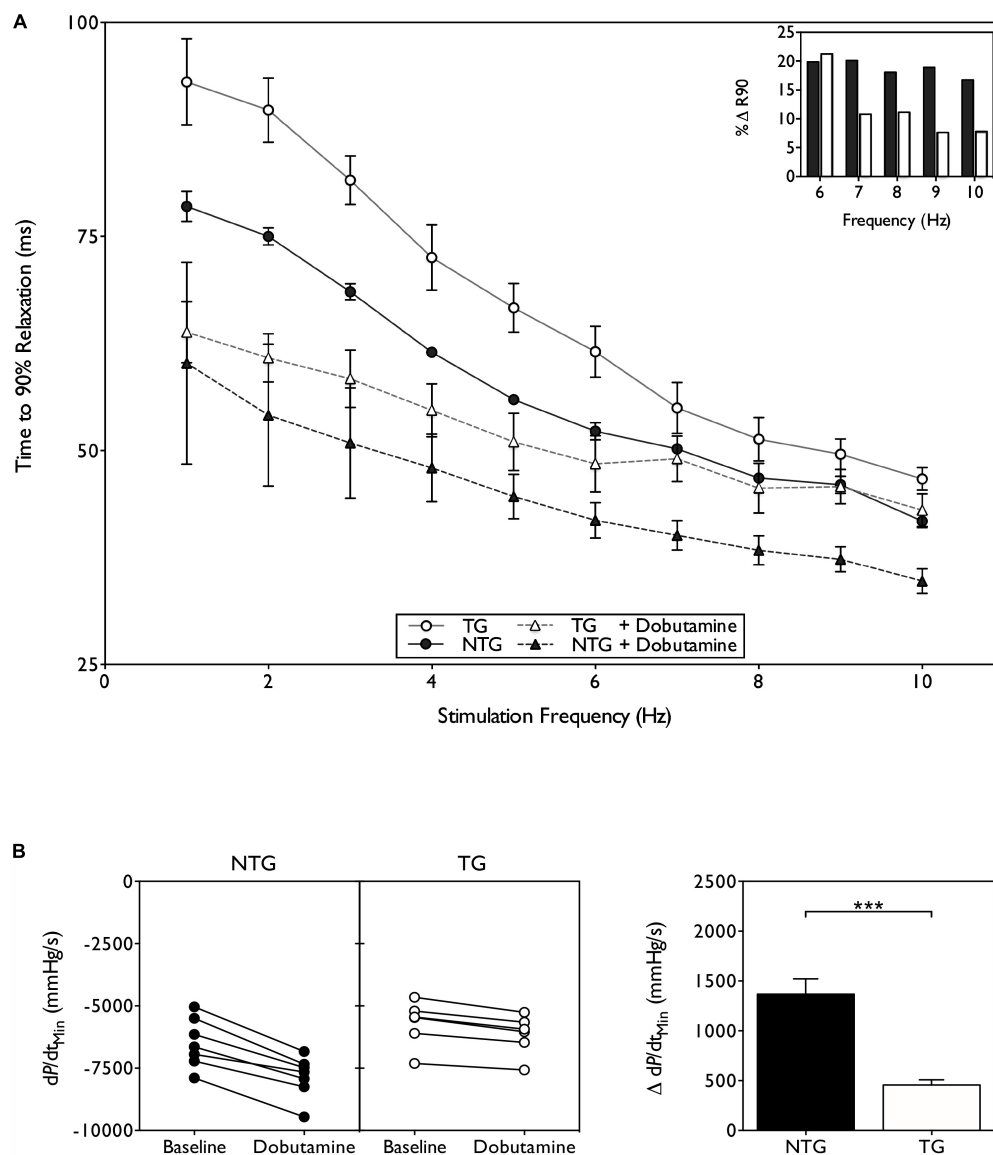


FIGURE 2

Suppression of lusitropy in ACTC E361G transgenic mouse. **(A)** Effect of dobutamine on intact papillary muscle contractility. Papillary muscles, isolated from both ACTC E361G ( $n = 5$ ) and NTG mice ( $n = 5$ ), were stimulated with the addition of  $10 \mu\text{M}$  dobutamine to the perfusion solution at  $37^\circ\text{C}$ . Time to 90% relaxation is plotted against stimulation frequency; (inset) percent change of  $ttb_{90}$  with dobutamine treatment at physiologically relevant frequencies. **(B)** The effect of acute dobutamine treatment on cardiac performance determined by Millar catheter. Data are presented as mean  $\pm$  SE of 6 ACTC E361G (open bars) mice and 7 NTG (solid bars) mice. The change of rate of pressure decline ( $dP/dt_{min}$ ) on treatment with dobutamine is plotted (left) and mean values plotted in a bar chart (right). \*\*\* $P = 0.001$ , unpaired student's  $t$ -test. Data from Wilkinson et al. (59).

In isolated papillary muscle, the study confirmed that single mutant PLB KO enhances relaxation rate but uncouples it from Iso stimulation whilst single mutant ssTnI replacement slows relaxation and also uncouples. In the double mutant (PLBKO/ssTnI) relaxation is enhanced relative to wild-type (like the PLBKO) but the relaxation rate is still uncoupled from Iso stimulation. Thus, in the double KO TnI and PLB appear to act independently and additively. It is likely that phosphorylation of both PLB and cTnI contribute to the increased rate of relaxation

during  $\beta$ -adrenergic stimulation and that deficiency of either will lead to suppression of lusitropy (23).

Somewhat disappointingly, none of these studies looked at the effects of chronic adrenergic stimulation. The transgenic mouse models often showed no cardiac phenotype at rest and this is entirely to be expected since sedentary mouse in the typical animal cage environment are not subjected to any stress. However, studies on mutations in troponin and other thin filament proteins that are demonstrated to be causative

of dilated cardiomyopathy have provided a link between suppression of lusitropy and heart failure.

## Mutations can also suppress lusitropy

Many *in vitro* studies have demonstrated that mutations in thin filament proteins associated with inherited cardiomyopathies abolish the relationship between  $\text{Ca}^{2+}$  sensitivity and TnI phosphorylation by PKA and would therefore likely impair lusitropy. This trait, which we have termed “uncoupling,” was first noted in 2001 (27, 28). In 2007–8 three publications studying the recently discovered TNNC1 G159D mutation showed uncoupling with recombinant mutant troponin, with troponin extracted from a patient with the mutation and with rat trabecula with the mutation exchanged in myocytes (29–31). Subsequently, almost every thin filament mutation that was tested proved to be uncoupled. This was summarized by Messer and Marston (1) and Table 2 lists all the reports of uncoupling to date. In wild-type the mean  $\Delta\text{pCa}_{50}$  is  $-0.31$  (mean of 8 studies) (32) whereas it is close to zero in the mutations studied. It is relevant to note that in *in vitro* experiments, uncoupling is always complete, irrespective of the mutation and that uncoupling is associated with both HCM and DCM-causing mutations. In the case of DCM mutations a case can be made that this is causative of the disease since it is the only mutation-related property that is common to every thin-filament related DCM mutation (1, 33, 38), whereas for HCM, the increase in  $\text{Ca}^{2+}$ -sensitivity is probably the key driver of the cardiomyopathy. Mechanistically, uncoupling usually involves an impaired response of the thin filaments to TnI phosphorylation (34), however, the cTnI R21C mutation has a mechanism whereby the mutation interferes with the phosphorylation process itself (35). Another mechanism that could generate impaired lusitropy is if the balance of phosphorylation of TnI and PLB in response to Iso is disturbed as suggested by Najafi et al. (36).

There are a few reported cases of uncoupling where the mutation is in thick filament or cytoskeletal proteins or occurs with no known mutation (50, 54, 55), however, there is also clear evidence that DCM-associated titin truncation (TTNtv) mutations are fully coupled and that abnormal stiffness and disabled length-dependent activation may be more important for the pathology (56, 57).

Uncoupling implies impaired lusitropy but this has only been tested in a few instances, listed in Table 1. Methodology varies widely: myofibril, iPSC contractility and myocyte contractility, trabecula and papillary muscles and Langendorf-mounted heart. In intact animal, Millar catheter, Echocardiography and Cine-MRI have been used. It is remarkable that mostly these techniques give a uniform result: a 30–50% reduction in  $\text{tTb}_{90}$  on adding PKA or  $\beta 1$  adrenergic stimulation in the WT compared to a 10–20%

reduction in the HCM or DCM mutant animal. Figure 2 shows an example from the work of Wilkinson et al. A possible exception is the DCM-causing D230N mutations in tropomyosin (58) which is uncoupled in single filament assays (Table 2) but shows very little blunting of lusitropy in unloaded myocytes. In general, the range of the lusitropy parameter in cardiomyopathic mutant studies is very similar to the phosphomimetic transgenic animals, confirming that uncoupling due to mutations suppresses lusitropy (59) and revealing this important role for cTnI phosphorylation in cardiac muscle regulation.

The next stage is to determine whether impaired lusitropy can lead to cardiac dysfunction. The transgenic mice studies have found that the majority of DCM mutations in thin filament proteins produce little or no cardiac phenotype, with the exception of a few TnT and Tm mouse models (41, 67, 68). This is to be expected if the defect is in the response to stress.

Very few studies have considered whether chronic stress could induce cardiac dysfunction. The most well documented study is by Wilkinson et al. (59). This study used the ACTC E361G DCM-associated mouse model with the mutant expressed at 50% of total actin, as was commonly found in patients. Initial studies indicated that the loss of lusitropy was the only cardiac dysfunction linked to the mutation and that the mice had a normal phenotype at rest up to 22 months (37). It was hypothesized that the loss of cardiac reserve due to suppressed lusitropy would predispose the ACTC E361G mouse hearts to failure under chronic adrenergic stress. Mice were treated with high doses of Angiotensin II applied by osmotic minipump for 4 weeks. In E361G mice the angiotensin II treatment induced mild systolic dysfunction, as measured by Millar catheter, whilst having no effect on the NTG controls. Compared with the NTG mice ACTC E361G mice had significantly lower rates of pressure increase and decrease as well as reduced end-systolic pressure. As a result cardiac output and ejection fraction were approximately half the value in NTG, indicating that uncoupling had induced contractile dysfunction under chronic stress, characteristic of the early stages of DCM.

## Restoration of lusitropy as a potential treatment for cardiomyopathies

Studies on the effects of mutations that uncouple TnI phosphorylation from the  $\text{Ca}^{2+}$ -sensitivity shift indicate that they probably act by inducing a subtle, phosphorylation-dependent change in the dynamics of troponin (69–74), most clearly indicated by a recent study on the TnC G159D mutation (34). Remarkably, it has been found that several small molecules are capable of fully restoring the  $\text{Ca}^{2+}$ -sensitivity shift *in vitro* and restoring lusitropy to mutated cardiomyocytes (7, 45, 75, 76). These small molecules (EGCG, SilybinB, Resveratrol) therefore have potential for treatment of cardiac dysfunction

**TABLE 3** Studies showing that reduced response to adrenergic stimulation is correlated with cardiac adverse outcome in patients with idiopathic DCM.

Paper	Non-responders, responders	Outcome measured	Follow up time	Adverse events (responders)	Adverse events (non-responders)
(84)	38, 33	Cardiac mortality	60 mo	9%	42%
(85)	11, 10	$\Delta$ LVEF, $\Delta$ LV sphericity	6 mo	0%	45%
(86)	11, 7	$\Delta$ LVEF improvement	15 mo	0%	36%
(87)	83, 103	Cardiac mortality	15 mo	3%	25%
(88)	89, 43	Mortality and/or hospitalization	40 mo	16%	49%
(89)	13, 24	Cardiac mortality	60 mo	34%	76%
(90)	15, 28	Mortality and/or hospitalization	23–67 mo	11%	67%

Data partially based on Waddington (81).

due to suppression of lusitropy, particularly by thin filament mutations but also as a tool for probing for cardiac dysfunction due to suppression of lusitropy. For instance, Tadano et al. in HCM mouse (77) and Mou et al. (78), using a rat abdominal aortic constriction model of heart failure, have demonstrated that EGCG corrects cardiac systolic and diastolic dysfunction and prevents cardiac remodeling.

## Is there a connection between suppression of lusitropy and human cardiomyopathy?

Based on the animal studies of the consequences of uncoupling, we have proposed that patients with uncoupling mutations that are associated with DCM would have impaired lusitropy and that this could contribute to the heart failure phenotype. A thorough investigation of the state of knowledge of idiopathic DCM around this possibility has revealed no direct evidence for the possibility since the question has not been investigated.

There is indirect evidence compatible with our hypothesis, although, of course, other mechanisms may play a part. Mutations that cause suppressed lusitropy also have a reduced contractile reserve when challenged with  $\beta$ 1 agonists in transgenic mouse models (59, 79). A significant association between the absence of left ventricular contractile reserve and increased rate of cardiovascular events, cardiac death and all-cause mortality has been demonstrated (80). Several studies have reported that IDCM patient cohorts tend to segregate in to two groups: those that respond normally to dobutamine and those with a reduced response, usually measured as contractile reserve (Table 3). Moreover, the patients with a reduced response to dobutamine have a more severe prognosis than the other group and also do not respond to standard heart failure medication [see meta-analysis by Waddingham et al. (81)].

The behavior of the non-responders matches that which would be expected if they had familial DCM mutations

that suppressed lusitropy whereas the responders probably correspond to patients with idiopathic DCM caused by non-genetic factors where, both at the single filament and patient levels, lusitropy has been demonstrated to be normal (82, 83).

Unfortunately this hypothesis has not been tested in IDCM patients. There is no clinical study that correlates thin filament mutations with reduced response to  $\beta$ 1 stimulation, nor is lusitropy (relaxation rate increase or twitch duration decrease) commonly measured in Echo or MRI analysis of patients although protocols to do so are available. To test this hypothesis we need to know whether cases of familial DCM caused by mutations correlate with the non-responders group and also whether lusitropy is suppressed in the non-responders.

It is possible that suppression of lusitropy could also play a role in other cardiomyopathies. It is consistently observed that thin filament mutations that cause HCM are associated with uncoupling (Table 2) and loss of lusitropy in cells and intact animals (see ACTC E99K, TNNT2 R92Q in Table 1). Enhanced  $\text{Ca}^{2+}$ -sensitivity is the predominant effect of HCM mutations (91–95). Impaired relaxation is characteristic of HCM. Suppression of lusitropy may play a role here, however, it would be very difficult to unravel what contribution loss of lusitropy makes to the HCM phenotype since the increased  $\text{Ca}^{2+}$  sensitivity and the suppressed lusitropy would both compromise relaxation.

HFpEF is a heterogeneous disease associated with diastolic dysfunction. HFpEF patients have a high prevalence of a blunted response to exercise which may be linked to suppressed lusitropy. However, this has not been measured in any of the studies to date (96, 97).

## Conclusion

Basic and animal studies indicate that specific suppression of lusitropy can induce symptoms of heart failure under stress. In the human heart, where stress is far more common than in laboratory animals, there is considerable

circumstantial evidence that impaired lusitropy whether due to cardiomyopathic mutation or other causes, can contribute to heart failure. It is predicted that such symptoms of heart failure would not be amenable to conventional heart failure therapy but may benefit from small molecules that have been shown to restore lusitropy in laboratory studies. We believe these issues should be taken into account in clinical investigations of cardiomyopathy.

## Author contributions

Both authors listed have made a substantial, direct, and intellectual contribution to the work, and approved it for publication.

## Funding

This work was funded by the British Heart Foundation Programme (grant RG/11/20/29266) to SM and the National Institutes of Health, National Heart, Lung and Blood Institute (grant RO1 HL128683, RO1 HL160966 and RO1 AR077802) awarded to JP.

## References

- Messer A, Marston S. Investigating the role of uncoupling of troponin I phosphorylation from changes in myofibrillar  $\text{Ca}^{2+}$ -sensitivity in the pathogenesis of cardiomyopathy. *Front Physiol.* (2014) 5:315. doi: 10.3389/fphys.2014.00315
- Zabrouskov V, Ge Y, Schwartz J, Walker JW. Unraveling molecular complexity of phosphorylated human cardiac troponin I by top down electron capture dissociation/electron transfer dissociation mass spectrometry. *Mol Cell Proteomics.* (2008) 7:1838–49. doi: 10.1074/mcp.M700524-MCP200
- Chen Y-C, Sumandea MP, Larsson L, Moss RL, Ge Y. Dissecting human skeletal muscle troponin proteoforms by top-down mass spectrometry. *J Musc Res Cell Motil.* (2015) 36:169–81. doi: 10.1007/s10974-015-9404-6
- Robertson SP, Johnson JD, Holroyde MJ, Kranias EG, Potter JD, Solaro RJ. The effect of troponin I phosphorylation on the  $\text{Ca}^{2+}$ -binding properties of the  $\text{Ca}^{2+}$ -regulatory site of bovine cardiac troponin. *J Biol Chem.* (1982) 257:260–3.
- Weiss S, Oz S, Benmocha A, Dascal N. Regulation of cardiac L-Type  $\text{Ca}^{2+}$  channel  $\text{Ca}_v1.2$  via the beta-adrenergic-cAMP-protein kinase A pathway. *Circ Res.* (2013) 113:617–31. doi: 10.1161/circresaha.113.301781
- Ablorh N-AD, Thomas DD. Phospholamban phosphorylation, mutation, and structural dynamics: a biophysical approach to understanding and treating cardiomyopathy. *Biophys Rev.* (2015) 7:63–76. doi: 10.1007/s12551-014-0157-z
- Marston S. Recent studies of the molecular mechanism of lusitropy due to phosphorylation of cardiac troponin I by protein kinase A. *J Muscle Res Cell Motil.* (2022) 43:doi: 10.1007/s10974-022-09630-4
- Li L, Chu G, Kranias EG, Bers DM. Cardiac myocyte calcium transport in phospholamban knockout mouse: relaxation and endogenous  $\text{CaMKII}$  effects. *Am J Physiol.* (1998) 274(4 Pt 2):H1335–47. doi: 10.1152/ajpheart.1998.274.4.H1335
- Schmitt JP, Kamisago M, Asahi M, Li GH, Ahmad F, Mende U, et al. Dilated cardiomyopathy and heart failure caused by a mutation in phospholamban. *Science.* (2003) 299:1410–3.
- Medeiros A, Biagi DG, Biagi DG, Sobreira TJP, de Oliveira PSL, Negrão CE, et al. Mutations in the human phospholamban gene in patients with heart failure. *Am Heart J.* (2011) 162:1088.e–95.e. doi: 10.1016/j.ahj.2011.07.028
- Fish M, Shaboodien G, Kraus S, Sliwa K, Seidman CE, Burke MA, et al. Mutation analysis of the phospholamban gene in 315 South Africans with dilated, hypertrophic, peripartum and arrhythmogenic right ventricular cardiomyopathies. *Sci Rep.* (2016) 6:22235. doi: 10.1038/srep22235
- Walsh R, Thomson KL, Ware JS, Funke BH, Woodley J, McGuire KJ, et al. Reassessment of mendelian gene pathogenicity using 7,855 cardiomyopathy cases and 60,706 reference samples. *Genet Med.* (2017) 19:192–203. doi: 10.1038/gim.2016.90
- Abrol N, de Tombe PP, Robia SL. Acute inotropic and lusitropic effects of cardiomyopathic R9C mutation of phospholamban. *J Biol Chem.* (2015) 290:7130–40. doi: 10.1074/jbc.M114.630319
- Ceholski DK, Turnbull IC, Kong C-W, Koplev S, Mayourian J, Gorski PA, et al. Functional and transcriptomic insights into pathogenesis of R9C phospholamban mutation using human induced pluripotent stem cell-derived cardiomyocytes. *J Mol Cell Cardiol.* (2018) 119:147–54. doi: 10.1016/j.jmcc.2018.05.007
- Fentzke RC, Buck SH, Patel JR, Lin H, Wolska BM, Stojanovic MO, et al. Impaired cardiomyocyte relaxation and diastolic function in transgenic mice expressing slow skeletal troponin I in the heart. *J Physiol (Lond).* (1999) 517(Pt 1):143–57. doi: 10.1111/j.1469-7793.1999.0143z.x
- Kentish JC, McCloskey DT, Layland J, Palmer S, Leiden JM, Martin AF, et al. Phosphorylation of troponin I by protein kinase A accelerates relaxation and crossbridge cycle kinetics in mouse ventricular muscle. *Circ Res.* (2001) 88:1059–65. doi: 10.1161/hh1001.091640
- Layland J, Grieve DJ, Cave AC, Sparks E, Solaro RJ, Shah AM. Essential role of troponin I in the positive inotropic response to isoprenaline in mouse hearts contracting auxotonically. *J Physiol.* (2004) 556:835–47. doi: 10.1113/jphysiol.2004.061176
- Pi Y-Q, Kemnitz KR, Zhang D, Kranias EG, Walker JW. Phosphorylation of troponin I controls cardiac twitch dynamics. Evidence from phosphorylation site mutants expressed on a troponin I-null background in mice. *Circ Res.* (2002) 90:649–56. doi: 10.1161/01.res.0000014080.82861.5f

## Acknowledgments

We are grateful to Profs. M. Kaski (University College London), J. Cleland (University of Glasgow), and G. Limongelli (University Campania) for informed discussions.

## Conflict of interest

The authors declare that the research was conducted in the absence of any commercial or financial relationships that could be construed as a potential conflict of interest.

## Publisher's note

All claims expressed in this article are solely those of the authors and do not necessarily represent those of their affiliated organizations, or those of the publisher, the editors and the reviewers. Any product that may be evaluated in this article, or claim that may be made by its manufacturer, is not guaranteed or endorsed by the publisher.



19. Pi Y, Zhang D, Kemnitz KR, Wang H, Walker JW. Protein kinase C and A sites on troponin I regulate myofilament Ca<sup>2+</sup> sensitivity and ATPase activity in the mouse myocardium. *J Physiol.* (2003) 552:845–57. doi: 10.1113/jphysiol.2003.045260
20. Yasuda S, Coutu P, Sadayappan S, Robbins J, Metzger JM. Cardiac transgenic and gene transfer strategies converge to support an important role for troponin I in regulating relaxation in cardiac myocytes. *Circ Res.* (2007) 101:377–86. doi: 10.1161/CIRCRESAHA.106.145557
21. Takimoto E, Soergel DG, Janssen PM, Stull LB, Kass DA, Murphy AM. Frequency- and afterload-dependent cardiac modulation in vivo by troponin I with constitutively active protein kinase A phosphorylation sites. *Circ Res.* (2004) 94:496–504. doi: 10.1161/01.res.0000117307.57798.f5
22. Sakthivel S, Finley NL, Rosevear PR, Lorenz JN, Gulick J, Kim S, et al. In vivo and in vitro analysis of cardiac troponin I phosphorylation. *J Biol Chem.* (2005) 280:703–14. doi: 10.1074/jbc.M409513200
23. Ramirez-Correa GA, Murphy AM. Is phospholamban or troponin I the &quot;prima donna&quot; in beta-adrenergic induced lusitropy? *Circ Res.* (2007) 101:326–7. doi: 10.1161/CIRCRESAHA.107.158873
24. Janssen PML, Stull LB, Marbain E. Myofilament properties comprise the rate-limiting step for cardiac relaxation at body temperature in the rat. *Am J Physiol Heart Circ Physiol.* (2002) 282:H499–507. doi: 10.1152/ajpheart.00595.2001
25. Little SC, Biesiadecki BJ, Kilic A, Higgins RSD, Janssen PML, Davis JP. The rates of Ca<sup>2+</sup> dissociation and cross-bridge detachment from ventricular myofibrils as reported by a fluorescent cardiac troponin C. *J Biol Chem.* (2012) 287:27930–40. doi: 10.1074/jbc.M111.337295
26. Wolska BM, Arteaga GM, Peña JR, Nowak G, Phillips RM, Sahai S, et al. Expression of slow skeletal troponin I in hearts of phospholamban knockout mice alters the relaxant effect of beta-adrenergic stimulation. *Circ Res.* (2002) 90:882–8. doi: 10.1161/01.res.0000016962.36404.04
27. Deng Y, Schmidtman A, Redlich A, Westerdorf B, Jaquet K, Thieleczek R. Effects of phosphorylation and mutation R145G on human cardiac troponin I function. *Biochemistry.* (2001) 40:14593–602. doi: 10.1021/bi0115232
28. Deng Y, Schmidtman A, Kruse S, Filatov V, Heilmeyer LM Jr., Jaquet K, et al. Phosphorylation of human cardiac troponin I G203S and K206Q linked to familial hypertrophic cardiomyopathy affects actomyosin interaction in different ways. *J Mol Cell Cardiol.* (2003) 35:1365–74. doi: 10.1016/j.yjmcc.2003.08.003
29. Biesiadecki BJ, Kobayashi T, Walker JS, John Solaro R, de Tombe PP. The troponin C G159D mutation blunts myofilament desensitization induced by troponin I Ser23/24 phosphorylation. *Circ Res.* (2007) 100:1486–93. doi: 10.1161/01.RES.0000267744.92677.f7
30. Dong W, Xing J, Ouyang Y, An J, Cheung HC. Structural kinetics of cardiac troponin C mutants linking to familial hypertrophic and dilated cardiomyopathy in troponin complexes. *J Biol Chem.* (2008) 283:3424–32. doi: 10.1074/jbc.M703822200
31. Dyer E, Jacques A, Burch M, Kaski J, Marston S. \*Functional effects of DCM mutation G159D in troponin C from an explanted heart. *J Mol Cell Cardiol.* (2008) 44:729–30.
32. Marston S. Why is there a limit to the changes in myofilament Ca<sup>2+</sup>-sensitivity associated with myopathy causing mutations? *Front Physiol.* (2016) 7:415. doi: 10.3389/fphys.2016.00415
33. Memo M, Messer AE, Leung M-C, Marston SB. Mutations in thin filament proteins that cause familial dilated cardiomyopathy uncouple troponin I phosphorylation from changes in myofibrillar Ca<sup>2+</sup>-Sensitivity. *Biophys J.* (2012) 102:614a. doi: 10.1016/j.bpj.2011.11.3348
34. Yang Z, Marston S, Gould I. Modulation of structure and dynamics of cardiac troponin by phosphorylation and mutations revealed by molecular dynamics simulations. *ChemRxiv [Preprint].* (2022). doi: 10.26434/chemrxiv-2022-kngl7
35. Wang Y, Pinto J, Sancho Solis R, Dweck D, Liang J, Diaz-Perez Z, et al. The generation and functional characterization of knock in mice harboring the cardiac troponin I-R21C mutation associated with hypertrophic cardiomyopathy. *J Biol Chem.* (2011) 287:2156–67. doi: 10.1074/jbc.M111.294306
36. Najafi A, Sequeira V, Helmes M, Bollen IAE, Goebel M, Regan JA, et al. Selective phosphorylation of PKA targets after  $\beta$ -adrenergic receptor stimulation impairs myofilament function in Mybpc3-targeted HCM mouse model. *Cardiovasc Res.* (2016) 110:200–14. doi: 10.1093/cvr/cvv026
37. Song W, Dyer E, Stuckey D, Leung M-C, Memo M, Mansfield C, et al. Investigation of a transgenic mouse model of familial dilated cardiomyopathy. *J Mol Cell Cardiol.* (2010) 49:380–9. doi: 10.1016/j.yjmcc.2010.05.009
38. Memo M, Leung M-C, Ward DG, dos Remedios C, Morimoto S, Zhang L, et al. Mutations in thin filament proteins that cause familial dilated cardiomyopathy uncouple troponin I phosphorylation from changes in myofibrillar Ca<sup>2+</sup>-sensitivity. *Cardiovasc Res.* (2013) 99:65–73. doi: 10.1093/cvr/cvt071
39. Dyer E, Jacques A, Hoskins A, Ward D, Gallon C, Messer A, et al. Functional analysis of a unique troponin C mutation, Gly159Asp that causes familial dilated cardiomyopathy, studied in explanted heart muscle. *Circ Heart Fail.* (2009) 2:456–64. doi: 10.1161/CIRCHEARTFAILURE.108.818237
40. Pinto JR, Siegfried JD, Parvatiyar MS, Li D, Norton N, Jones MA, et al. Functional characterization of TNNC1 rare variants identified in dilated cardiomyopathy. *J Biol Chem.* (2011) 286:34404–12. doi: 10.1074/jbc.M111.267211
41. Du CK, Morimoto S, Nishii K, Minakami R, Ohta M, Tadano N, et al. Knock-in mouse model of dilated cardiomyopathy caused by troponin mutation. *Circ Res.* (2007) 101:185–94.
42. Inoue T, Kobirumaki-Shimozawa F, Kagemoto T, Fujii T, Terui T, Kusakari Y, et al. Depressed Frank-Starling mechanism in the left ventricular muscle of the knock-in mouse model of dilated cardiomyopathy with troponin T deletion mutation  $\Delta$ K210. *J Mol Cell Cardiol.* (2013) 63:69–78. doi: 10.1016/j.yjmcc.2013.07.001
43. Carballo S, Robinson P, Otway R, Fatkin D, Jongbloed JD, de Jonge N, et al. Identification and functional characterization of cardiac troponin I as a novel disease gene in autosomal dominant dilated cardiomyopathy. *Circ Res.* (2009) 105:375–82. doi: 10.1161/CIRCRESAHA.109.196055
44. Song W, Dyer E, Stuckey D, Copeland O, Leung M, Bayliss C, et al. Molecular mechanism of the Glu99lys mutation in cardiac actin (ACTC gene) that causes apical hypertrophy in man and mouse. *J Biol Chem.* (2011) 286:27582–93. doi: 10.1074/jbc.M111.252320
45. Papadaki M, Vikhorev PG, Marston SB, Messer AE. Uncoupling of myofilament Ca<sup>2+</sup> sensitivity from troponin I phosphorylation by mutations can be reversed by epigallocatechin-3-gallate. *Cardiovasc Res.* (2015) 108:99–110. doi: 10.1093/cvr/cvv181
46. Alves ML, Dias FAL, Gaffin RD, Simon JN, Montminy EM, Biesiadecki BJ, et al. Desensitization of myofilaments to Ca<sup>2+</sup> as a therapeutic target for hypertrophic cardiomyopathy with mutations in thin filament proteins. *Circ Cardiovasc Genet.* (2014) 7:132–43. doi: 10.1161/CIRCGENETICS.113.000324
47. Schmidtman A, Lindow C, Villard S, Heuser A, Mügge A, Gessner R, et al. Cardiac troponin C-L29Q, related to hypertrophic cardiomyopathy, hinders the transduction of the protein kinase A dependent phosphorylation signal from cardiac troponin I to C. *FEBS J.* (2005) 272:6087–97. doi: 10.1111/j.1742-4658.2005.05001.x
48. Li AY, Stevens CM, Liang B, Rayani K, Little S, Davis J, et al. Familial hypertrophic cardiomyopathy related cardiac troponin C L29Q mutation alters length-dependent activation and functional effects of phosphomimetic troponin I\*. *PLoS One.* (2013) 8:e79363. doi: 10.1371/journal.pone.0079363
49. Messer AE, Bayliss CR, El-Mezgueldi M, Redwood CS, Ward DG, Papadaki M, et al. Mutations in troponin T associated with hypertrophic cardiomyopathy increase Ca<sup>2+</sup>-sensitivity and suppress the modulation of Ca<sup>2+</sup>-sensitivity by troponin I phosphorylation. *Arch Biochem Biophys.* (2016) 601:113–20. doi: 10.1016/j.abb.2016.03.027
50. Bayliss CR, Jacques AM, Leung M-C, Ward DG, Redwood CS, Gallon CE, et al. Myofibrillar Ca<sup>2+</sup>-sensitivity is uncoupled from troponin I phosphorylation in hypertrophic obstructive cardiomyopathy due to abnormal troponin T. *Cardiovasc Res.* (2012) 97:500–8. doi: 10.1093/cvr/cvs322
51. Cheng Y, Rao V, Tu A-Y, Lindert S, Wang D, Oxenford L, et al. Troponin I mutations R146G and R21C alter cardiac troponin function, contractile properties and modulation by PKA-mediated phosphorylation. *J Biol Chem.* (2015) 290:27749–66. doi: 10.1074/jbc.M115.683045
52. Dvornikov AV, Smolin N, Zhang M, Martin JL, Robia SL, de Tombe PP. Restrictive cardiomyopathy troponin-I R145W mutation does not perturb myofilament length dependent activation in human cardiac sarcomeres. *J Biol Chem.* (2016) 291:21817–28. doi: 10.1074/jbc.M116.746172
53. Cheng Y, Lindert S, Oxenford L, Tu A-Y, McCulloch AD, Regnier M. Effects of cardiac troponin I mutation P83S on contractile properties and the modulation by PKA-mediated phosphorylation. *J Phys Chem B.* (2016) 120:8238–53. doi: 10.1021/acs.jpcc.6b01859
54. Knoell R, Kostin S, Klede S, Savvatis K, Klinge L, Stehle I, et al. A common MLP (muscle LIM protein) variant is associated with cardiomyopathy. *Circ Res.* (2010) 106:695–704. doi: 10.1161/CIRCRESAHA.109.206243
55. Stöhr A, Friedrich FW, Flenner F, Geertz B, Eder A, Schaaf S, et al. Contractile abnormalities and altered drug response in engineered heart tissue from Mybpc3-targeted knock-in mice. *J Mol Cell Cardiol.* (2013) 63:189–98. doi: 10.1016/j.yjmcc.2013.07.011
56. Vikhorev PG, Smoktunowicz N, Munster AB, Copeland O, Kostin S, Montgiraud C, et al. Abnormal contractility in human heart myofibrils from patients with dilated cardiomyopathy due to mutations in TTN and contractile protein genes. *Sci Rep.* (2017) 7:14829. doi: 10.1038/s41598-017-13675-8

57. Vikhorev PG, Vikhoreva NN, Yeung W, Li A, Lal S, Remedios CGD, et al. Titin-truncating mutations associated with dilated cardiomyopathy alter length-dependent activation and its modulation via phosphorylation. *Cardiovasc Res.* (2020) 118:241–53. doi: 10.1093/cvr/cvaa316
58. Lynn ML, Grinspan LT, Holeman TA, Jimenez J, Strom J, Tardiff JC. The structural basis of alpha-tropomyosin linked (Asp230Asn) familial dilated cardiomyopathy. *J Mol Cell Cardiol.* (2017) 108:127–37. doi: 10.1016/j.yjmcc.2017.06.001
59. Wilkinson R, Song W, Smoktunowicz N, Marston S. A dilated cardiomyopathy mutation blunts adrenergic response and induces contractile dysfunction under chronic angiotensin II stress. *Am J Physiol Heart Circ Physiol.* (2015) 309:H1936–46. doi: 10.1152/ajpheart.00327.2015
60. Li L, Desantiago J, Chu G, Kranias EG, Bers DM. Phosphorylation of phospholamban and troponin I in  $\beta$ -adrenergic-induced acceleration of cardiac relaxation. *Am J Physiol Heart Circ Physiol.* (2000) 278:H769–79. doi: 10.1152/ajpheart.2000.278.3.h769
61. Schober T, Huke S, Venkataraman R, Gryshchenko O, Kryshchal D, Hwang HS, et al. Myofilament Ca sensitization increases cytosolic Ca binding affinity, alters intracellular Ca homeostasis, and causes pause-dependent Ca triggered arrhythmia. *Circ Res.* (2012) 111:170–9. doi: 10.1161/CIRCRESAHA.112.270041
62. Sirenko SG, Potter JD, Knollmann BC. Differential effect of troponin T mutations on the inotropic responsiveness of mouse hearts—role of myofilament  $Ca^{2+}$  sensitivity increase. *J Physiol.* (2006) 575(Pt 1):201–13. doi: 10.1113/jphysiol.2006.107557
63. Javadpour MM, Tardiff JC, Pinz I, Ingwall JS. Decreased energetics in murine hearts bearing the R92Q mutation in cardiac troponin T. *J Clin Invest.* (2003) 112:768–75.
64. Moore RK, Grinspan LT, Jimenez J, Guinto PJ, Ertz-Berger B, Tardiff JC. HCM-linked  $\Delta 160E$  cardiac troponin T mutation causes unique progressive structural and molecular ventricular remodeling in transgenic mice. *J Mol Cell Cardiol.* (2013) 58:188–98. doi: 10.1016/j.yjmcc.2013.02.004
65. Dweck D, Sanchez-Gonzalez MA, Chang AN, Dulce RA, Badger CD, Koutnik AP, et al. Long term ablation of protein kinase A (PKA)-mediated cardiac troponin I phosphorylation leads to excitation-contraction uncoupling and diastolic dysfunction in a knock-in mouse model of hypertrophic cardiomyopathy. *J Biol Chem.* (2014) 289:23097–111. doi: 10.1074/jbc.M114.561472
66. Vikhorev PG, Song W, Wilkinson R, Copeland O, Messer AE, Ferenczi MA, et al. The dilated cardiomyopathy-causing mutation ACTC E361G in cardiac muscle myofibrils specifically abolishes modulation of  $Ca^{2+}$  regulation by phosphorylation of troponin I. *Biophys J.* (2014) 107:2369–80. doi: 10.1016/j.bpj.2014.10.024
67. Juan F, Wei D, Xiongzi Q, Ran D, Chunmei M, Lan H, et al. The changes of the cardiac structure and function in cTnTR141W transgenic mice. *Int J Cardiol.* (2008) 128:83–90. doi: 10.1016/j.ijcard.2008.03.006
68. Tal L, Jimenez J, Tardiff JC. DCM-linked D230N tropomyosin mutation results in early dilatation and systolic dysfunction in mice. *Biophys J.* (2012) 102:356A.
69. Baryshnikova OK, Li MX, Sykes BD. Modulation of cardiac troponin C function by the cardiac-specific N-terminus of troponin I: influence of PKA phosphorylation and involvement in cardiomyopathies. *J Mol Biol.* (2008) 375:735–51. doi: 10.1016/j.jmb.2007.10.062
70. Dong X, Sumandea CA, Chen Y-C, Garcia-Cazarin ML, Zhang J, Balke CW, et al. Augmented phosphorylation of cardiac troponin I in hypertensive heart failure. *J Biol Chem.* (2012) 287:848–57. doi: 10.1074/jbc.M111.293258
71. Matsuo T, Takeda S, Oda T, Fujiwara S. Structures of the troponin core domain containing the cardiomyopathy-causing mutants studied by small-angle X-ray scattering. *Biophys Physicobiol.* (2015) 12:145–58. doi: 10.2142/biophysico.12.0\_145
72. Mahmud Z, Dhami PS, Rans C, Liu PB, Hwang PM. Dilated cardiomyopathy mutations and phosphorylation disrupt the active orientation of cardiac troponin C. *J Mol Biol.* (2021) 433:167010. doi: 10.1016/j.jmb.2021.167010
73. Keken-Huskey PM, Lindert S, McCammon JA. Molecular basis of calcium-sensitizing and desensitizing mutations of the human cardiac troponin C regulatory domain: a multi-scale simulation study. *PLoS Comput Biol.* (2012) 8:e1002777. doi: 10.1371/journal.pcbi.1002777
74. Stevens CM, Rayani K, Singh G, Lotfalimalasi B, Tieleman DP, Tibbitts GF. Changes in the dynamics of the cardiac troponin C molecule explain the effects of  $Ca^{2+}$ -sensitizing mutations. *J Biol Chem.* (2017) 292:11915–26. doi: 10.1074/jbc.M116.770776
75. Sheehan A, Messer AE, Papadakis M, Choudhry A, Kren V, Biedermann D, et al. Molecular defects in cardiac myofilament  $Ca^{2+}$ -regulation due to cardiomyopathy-linked mutations can be reversed by small molecules binding to troponin. *Front Physiol.* (2018) 9:243. doi: 10.3389/fphys.2018.00243
76. Alsulami K, Marston S. Small molecules acting on myofilaments as treatments for heart and skeletal muscle diseases. *IJMS.* (2020) 21:9599. doi: 10.3390/ijms21249599
77. Tadano N, Du C, Yumoto F, Morimoto S, Ohta M, Xie M, et al. Biological actions of green tea catechins on cardiac troponin C. *Br J Pharmacol.* (2010) 161:1034–43. doi: 10.1111/j.1476-5381.2010.00942.x
78. Mou Q, Jia Z, Luo M, Liu L, Huang X, Quan J, et al. Epigallocatechin-3-gallate exerts cardioprotective effects related to energy metabolism in pressure overload-induced cardiac dysfunction. *Arch Biochem Biophys.* (2022) 723:109217. doi: 10.1016/j.abb.2022.109217
79. Haddad F, Vrtovc B, Ashley EA, Deschamps A, Haddad H, Denault AY. The concept of ventricular reserve in heart failure and pulmonary hypertension: an old metric that brings us one step closer in our quest for prediction. *Curr Opin Cardiol.* (2011) 26:123–31. doi: 10.1097/hco.0b013e3283437485
80. Thein PM, Mirzaee S, Cameron JD, Nasir A. Left ventricular contractile reserve as a determinant of adverse clinical outcomes: a systematic review. *Intern Med J.* (2022) 52:186–97. doi: 10.1111/imj.14995
81. Waddingham PH, Bhattacharyya S, Zalen JV, Lloyd G. Contractile reserve as a predictor of prognosis in patients with non-ischaemic systolic heart failure and dilated cardiomyopathy: a systematic review and meta-analysis. *Echo Res Pract.* (2018) 5:1–9. doi: 10.1530/erp-17-0054
82. Messer AE, Jacques AM, Marston SB. Troponin phosphorylation and regulatory function in human heart muscle: dephosphorylation of Ser23/24 on troponin I could account for the contractile defect in end-stage heart failure. *J Mol Cell Cardiol.* (2007) 42:247–59. doi: 10.1016/j.yjmcc.2006.08.017
83. Parker JD, Landberg JS, Bittl JA, Mirsky I, Colucci WS. Effects of beta-adrenergic stimulation with dobutamine on isovolumic relaxation in the normal and failing human left ventricle. *Circulation.* (2018) 84:1040–8. doi: 10.1161/01.cir.84.3.1040
84. Nagaoka H, Isobe N, Kubota S, Iizuka T, Imai S, Suzuki T, et al. Myocardial contractile reserve as prognostic determinant in patients with idiopathic dilated cardiomyopathy without overt heart failure. *Chest.* (1997) 111:344–50. doi: 10.1378/chest.111.2.344
85. Naqvi TZ, Goel RK, Forrester JS, Siegel RJ. Myocardial contractile reserve on dobutamine echocardiography predicts late spontaneous improvement in cardiac function in patients with recent onset idiopathic dilated cardiomyopathy. *J Am Coll Cardiol.* (1999) 34:1537–44.
86. Kitaoka H, Takata J, Yabe T, Hitomi N, Furuno T, Doi YL. Low dose dobutamine stress echocardiography predicts the improvement of left ventricular systolic function in dilated cardiomyopathy. *Heart.* (1999) 81:523. doi: 10.1136/hrt.81.5.523
87. Pratali L, Picano E, Otasevic P, Vigna C, Palinkas A, Cortigiani L, et al. Prognostic significance of the dobutamine echocardiography test in idiopathic dilated cardiomyopathy. *Am J Cardiol.* (2001) 88:1374–8. doi: 10.1016/s0002-9149(01)02116-6
88. Rigo F, Gherardi S, Galderisi M, Sicari R, Picano E. The independent prognostic value of contractile and coronary flow reserve determined by dipyridamole stress echocardiography in patients with idiopathic dilated cardiomyopathy. *Am J Cardiol.* (2007) 99:1154–8.
89. Stipac AV, Otašević P, Popović ZB, Čvorović V, Putniković B, Stanković I, et al. Prognostic significance of contractile reserve assessed by dobutamine-induced changes of Tei index in patients with idiopathic dilated cardiomyopathy. *Eur J Echo.* (2010) 11:264–70. doi: 10.1093/ejehocord/jep208
90. Parthenakis F, Patrianakos A, Nyktari E, Arfanakis D, Zacharis E, Vardas P. Prognostic value of NT-pro BNP, left ventricular inotropic reserve and cardiopulmonary exercise test in patients with non-ischemic dilated cardiomyopathy. *Int J Cardiol.* (2011) 147:326–8. doi: 10.1016/j.ijcard.2010.12.079
91. Huke S, Knollmann BC. Increased myofilament  $Ca^{2+}$ -sensitivity and arrhythmia susceptibility. *J Mol Cell Cardiol.* (2010) 48:824–33. doi: 10.1016/j.yjmcc.2010.01.011
92. Willott RH, Gomes AV, Chang AN, Parvatiyar MS, Pinto JR, Potter JD. Mutations in troponin that cause HCM, DCM AND RCM: what can we learn about thin filament function? *J Mol Cell Cardiol.* (2010) 48:882–92. doi: 10.1016/j.yjmcc.2009.10.031
93. Marston SB. How do mutations in contractile proteins cause the primary familial cardiomyopathies? *J Cardiovasc Transl Res.* (2011) 4:245–55.
94. Spudich JA. Hypertrophic and dilated cardiomyopathy: four decades of basic research on muscle lead to potential therapeutic approaches to these devastating genetic diseases. *Biophys J.* (2014) 106:1236–49. doi: 10.1016/j.bpj.2014.02.011

95. Tadros HJ, Life CS, Garcia G, Pirozzi E, Jones EG, Datta S, et al. Meta-analysis of cardiomyopathy-associated variants in troponin genes identifies loci and intragenic hot spots that are associated with worse clinical outcomes. *J Mol Cell Cardiol.* (2020) 142:118–25. doi: 10.1016/j.jmcc.2020.04.005
96. Kitzman DW, Higginbotham MB, Cobb FR, Sheikh KH, Sullivan MJ. Exercise intolerance in patients with heart failure and preserved left ventricular systolic function: failure of the Frank-Starling mechanism. *J Am Coll Cardiol.* (1991) 17:1065–72. doi: 10.1016/0735-1097(91)90832-t
97. Domínguez E, Palau P, Núñez E, Ramón JM, López L, Melero J, et al. Heart rate response and functional capacity in patients with chronic heart failure with preserved ejection fraction. *ESC Heart Fail.* (2018) 5:579–85.



## OPEN ACCESS

## EDITED BY

Amy Li,  
La Trobe University, Australia

## REVIEWED BY

Jorge Contreras,  
The University of California, Davis,  
United States  
Rob Gourdie,  
Virginia Tech Carilion, United States

## \*CORRESPONDENCE

Brian J. North  
✉ briannorth@creighton.edu

## SPECIALTY SECTION

This article was submitted to  
General Cardiovascular Medicine,  
a section of the journal  
Frontiers in Cardiovascular Medicine

RECEIVED 25 October 2022

ACCEPTED 19 December 2022

PUBLISHED 12 January 2023

## CITATION

Pun R, Kim MH and North BJ (2023)  
Role of Connexin 43 phosphorylation  
on Serine-368 by PKC in cardiac  
function and disease.  
*Front. Cardiovasc. Med.* 9:1080131.  
doi: 10.3389/fcvm.2022.1080131

## COPYRIGHT

© 2023 Pun, Kim and North. This is an  
open-access article distributed under  
the terms of the [Creative Commons  
Attribution License \(CC BY\)](#). The use,  
distribution or reproduction in other  
forums is permitted, provided the  
original author(s) and the copyright  
owner(s) are credited and that the  
original publication in this journal is  
cited, in accordance with accepted  
academic practice. No use, distribution  
or reproduction is permitted which  
does not comply with these terms.

# Role of Connexin 43 phosphorylation on Serine-368 by PKC in cardiac function and disease

Renju Pun<sup>1</sup>, Michael H. Kim<sup>2</sup> and Brian J. North<sup>1\*</sup>

<sup>1</sup>Department of Biomedical Sciences, School of Medicine, Creighton University, Omaha, NE,  
United States, <sup>2</sup>CHI Health Heart Institute, School of Medicine, Creighton University, Omaha, NE,  
United States

Intercellular communication mediated by gap junction channels and hemichannels composed of Connexin 43 (Cx43) is vital for the propagation of electrical impulses through cardiomyocytes. The carboxyl terminal tail of Cx43 undergoes various post-translational modifications including phosphorylation of its Serine-368 (S368) residue. Protein Kinase C isozymes directly phosphorylate S368 to alter Cx43 function and stability through inducing conformational changes affecting channel permeability or promoting internalization and degradation to reduce intercellular communication between cardiomyocytes. Recent studies have implicated this PKC/Cx43-pS368 circuit in several cardiac-associated diseases. In this review, we describe the molecular and cellular basis of PKC-mediated Cx43 phosphorylation and discuss the implications of Cx43 S368 phosphorylation in the context of various cardiac diseases, such as cardiomyopathy, as well as the therapeutic potential of targeting this pathway.

## KEYWORDS

gap junctions, Connexin 43, phosphorylation, protein kinase C, cardiology, cardiac disease

## Introduction

Cell-Cell communication is a well-established process in multicellular organisms and includes mechanisms such as endocrine, paracrine, and autocrine pathways. Gap junctions, composed of connexin proteins, are channels formed on the plasma membranes that can form a contiguous pore between adjacent cells to allow for exchange of ions, metabolic coupling, and electrical impulse propagation (1–3). The connexin gene family consists of 20 members in mice and 21 in humans (4) and are structurally characterized as transmembrane proteins with 9 domains: intercellular N- and C-terminal tails, 4 transmembrane domains (M1–M4), 2 extracellular domains (E1), and one cytoplasmic loop (CL) (1, 5). The amino acid sequences of the transmembrane



domains and extracellular loops between the different family members are highly conserved whereas the amino-terminal domain and cytoplasmic loop show modest conservation. However, the C-terminal tails show little to no conservation, suggesting that they may be subjected to connexin specific regulatory mechanisms (6). The diversity of this domain among connexin family members also includes varying lengths of the C-terminal tail resulting in a range of molecular weights for the various proteins from 23 to 62 kDa. The nomenclature of connexins genes/proteins correspond to their molecular weight. For example, Cx43 and Cx32 have molecular weights of 43 and 32 kDa, respectively (7, 8).

Six connexins can oligomerize to form a hexamer or connexon in the plasma membrane leading to the formation of a hemichannel (9–11). In order to form a gap junction between two cells, hemichannels from adjacent cells dock in a head-to-head manner. Such assembly can be homotypic or heterotypic depending on the connexin composition of docking connexons, which themselves can be homomeric or heteromeric depending on the oligomerization of identical and different connexin proteins, respectively (12). This variability in the composition of these gap junctions affects the permeability and conductance between adjacent cells (13, 14). While genes encoding the various connexins are scattered throughout the genome, most connexins have a similar gene structure consisting of a single intron flanked by two exons (15, 16). The biosynthesis of connexins occurs on ribosomes found associated with the rough endoplasmic reticulum where the connexin coding mRNA gets translated directly into the endoplasmic reticulum membrane. As the connexin passes through the Golgi stacks, they oligomerize into a connexon which is trafficked along microtubules within the Golgi vesicle membrane system. Connexon-containing transport vesicles bud from the *trans*-Golgi and subsequently fuse with the plasma membrane, where they can remain as hemichannels on the plasma membrane or dock to connexons from adjacent cells to form a gap junction (17–19). The nexus region of cell-cell attachment consists of gap junction plaques and their associated proteins while the undocked hemichannels are found in a region surrounding the gap junction plaques termed the perinexus (20, 21). The degradation of connexins is initiated by the internalization of the connexon plaques into cytoplasmic annular junctions (22–24). Each gap junction has a short half-life of a few hours (25, 26), and once internalized connexons are disassembled into connexins that undergo degradation via either proteasomal or lysosomal pathways (27–29).

Connexin proteins differ in their expression patterns across tissues and organs (Table 1). Cx46 and Cx50 are abundantly expressed in the eye lens fiber cells while Cx26, Cx30, and Cx31 are prominently expressed in the organ of Corti within the inner ear (30–32). Mammalian cardiomyocytes express Cx40, Cx43, and Cx45 and the expression pattern of these three isoforms varies within the heart. While connexin isoform expression may


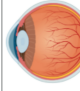




differ between species, mice and human atrial cardiomyocytes express Cx43, Cx45, and Cx40 while ventricular cardiomyocytes express Cx43 and low levels of Cx45 (33–39). The Sino atrial and atrioventricular nodes express Cx45, Cx40, as well as Cx30.2 (33, 35, 37, 40); the His bundle and upper bundle branch express Cx40 and Cx45; whereas the lower bundle branch and Purkinje fibers express Cx40, Cx43, and Cx45 (35, 37, 41–44). Therefore, connexins exert influence within various tissues and organs, and their dysregulation or mutation promotes tissue-specific disease states. For instance, mutations in the *Cx30* gene lead to non-syndromic hearing loss, keratitis ichthyosis deafness (KID), a rare disorder with hearing impairment and rough skin plaques (45, 46). Similarly, mutations in *Cx26* are associated with 50% of non-syndromic hearing loss (47, 48). Cataracts in the eye lens are associated with mutations in *Cx46*, while mutations in the *GJA1* gene which encodes Cx43 lead to a rare autosomal syndrome called oculodentodigital dysplasia (ODD) in which patients display diverse phenotypes such as bone malformations, vision loss, and hypotrichosis (49, 50). Mutations in Cx43 can also cause several skin disorders such as congenital alopecia-1, eczema, and palmoplantar keratoderma (51). Other diseases that have been tied to connexin mutations include Alzheimer's disease and osteoarthritis (52, 53). The expression levels of connexin isoforms differ between organs and the diseases associated with various isoforms are summarized in Table 1.

Cx43 is the most abundantly expressed isoform in the heart. It is localized to the intercalated discs between atrial and ventricular myocytes and connects adjacent cardiomyocytes (54, 55). Mutations in Cx43 have been implicated in myocardial ischemia, cardiomyopathy, and heart failure (56–58). The C-terminal tail of Cx43, comprised of amino acids 232–382, has been extensively studied as it is subjected to various post-translational modifications such as phosphorylation, acetylation, S-nitrosylation, ubiquitination, and SUMOylation (17, 27, 59–65). Multiple serine and tyrosine residues within the Cx43 C-terminal tail are targeted by kinases such as Src, MAPK, and PKC (66, 67), and phosphorylation of these residues plays a key role in regulating the trafficking, assembly, permeability, and disassembly of gap junctions.

Cx43 containing vesicles bring newly formed hemichannels to the plasma membrane after exiting the *trans*-Golgi network during which Cx43 is phosphorylated on Serine-373 by Akt and Serine-365 by PKA (68, 69). 14–3–3 theta recognizes phosphorylated S373 and facilitates the delivery of hemichannels to the plasma membrane by tethering the hemichannels to integrin  $\alpha 5$  (70). 14–3–3 theta is an isoform of the 14–3–3 adapter protein family that functions as critical regulators of a wide range of cellular processes (71, 72). Cx43 hemichannels then dock in the perinexus and translocate into the gap junction plaque (nexus) proper. Older channels are internalized and degraded from the central region of the gap junction plaque (26, 73, 74). Trafficking of Cx43 within the plasma membrane is also regulated by C-terminal tail



**TABLE 1** Prevalence of connexin isoforms in various organs and their expression levels in diseases associated with the organs.

	Disease	Connexin expression	References
	Atrial fibrillation	↓ Cx43	(237)
	Atherosclerosis	↑ Cx43	(238)
	Chronic myocardial infarction	↓ Cx43	(239)
	Retinoblastoma	↑ Cx37	(240)
	Epithelioid melanoma	↑ Cx43	(240)
	Diabetic retinopathy	↓ Cx43	(241)
	Noise induced hearing loss	↓ Cx26 ↓ Cx30	(242)
	Age related hearing loss	↓ Cx26 ↓ Cx30	(243)
	Oculodentodigital dysplasia (ODDD)	↓ Cx43	(244)
	Rheumatoid arthritis	↑ Cx43	(245)
	Acute eczema	↓ Cx43	(246)
	Chronic eczema	↑ Cx43	(246)
	Melanoma	↑ Cx26, Cx30.2 ↓ Cx43	(247)
	Alzheimer's disease	↑ Cx43, Cx30 ↓ Cx47	(248)

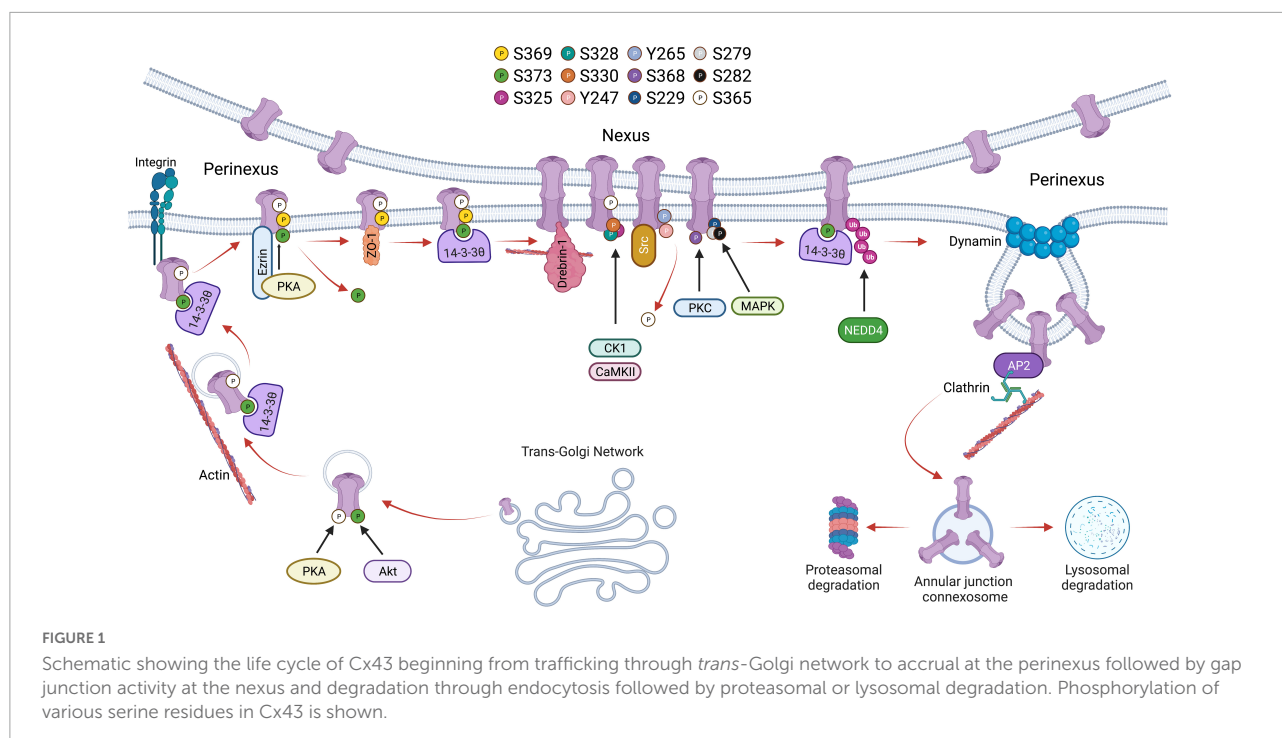
phosphorylation. For instance, phosphorylation of Serine-369 by Protein kinase A (PKA) upregulates hemichannel aggregation in the perinexus. This is aided by the PKA associated protein Ezrin which binds to Cx43 forming a complex bringing PKA and the Cx43 C-terminal tail in close proximity to facilitate phosphorylation at S369 (75). This interaction is thought to precede ZO-1 association with the C-terminal tail of Cx43, which occurs following S373 dephosphorylation (76). ZO-1 is a cytoskeleton binding protein which docks with hemichannels in the periphery of gap junction plaques, scaffolding channels in the perinexus. 14–3–3 theta will again bind Cx43 hemichannels and facilitate their translocation to the nexus. Thus, phosphorylation of S373 is thought to be a trigger that induces the binding of 14–3–3 theta to Cx43 promoting channel translocation from the periphery of the gap junction into the plaque proper (77). As hemichannels of adjacent cells align, the gap junction plaque is stabilized by  $\beta$ -tubulin and Drebrin-1, which binds actin (78). A functional hemichannel is phosphorylated at multiple serine residues including Serine-325, Serine-328, and Serine-330 which are targeted by the kinases CaMKII and CK1 (79). Channel closure is regulated by phosphorylation at Tyrosine-247 and

Tyrosine-265 initiated by the kinase Src. This phosphorylation is followed by PKC-mediated phosphorylation of S368 leading to a reduction in channel permeability (80). Interestingly, S368 phosphorylation occurs only after S365 dephosphorylation suggesting that S365 phosphorylation is a gatekeeper preventing downregulation of Cx43 by PKC (81). Src activity indirectly promotes phosphorylation of other serine sites including S373 by Akt and S225, S279, and S282 by MAPK, which leads to the recruitment of E3 ubiquitin ligase NEDD4 (82). Phosphorylated S279/282 increases the affinity of NEDD4 to the C-terminal tail of Cx43 by twofold (83). Ubiquitination of Cx43 allows for proteins such as Tsg101 and AP2, which are involved in clathrin-mediated endocytosis, to bind to the C-terminal tail of Cx43 (84, 85). During endocytosis, Dynamin serves to initiate scissoring of the gap junction bud and the formation of an annular gap junction (86). Translocation of the annular gap junction from the cell membrane to the cytoplasm is driven by Myosin VI (87) upon which it is subsequently degraded through the proteasomal and lysosomal pathways (88). The Cx43 lifecycle, and the role of C-terminal tail phosphorylation events, is outlined in **Figure 1**.

Amongst the many C-terminal residues targeted for phosphorylation, S368 has been the subject of extensive characterization with a particular emphasis on its role in the heart. For instance, phosphorylation of Cx43 S368 is necessary for myocardial conduction particularly during stress conditions such as metabolic stress (89). Therefore, the remainder of this review will focus on the relationship between Cx43 S368 phosphorylation by PKC isoforms and its consequences in cardiac health and disease.

## Cx43 S368 phosphorylation by PKC isoforms

As an integral gap junction protein, Cx43 plays an important role in intercellular communication, providing a path of least resistance for small molecules and secondary messengers to transit between adjacent cells (2). The phosphorylation/dephosphorylation of Cx43 in its soluble C-terminal tail is a critical regulator of intercellular communication (90). For example, the inositol 1,4,5-trisphosphate receptor (IP<sub>3</sub>R) interacts with, and regulates the phosphorylation of Serine-279/282 in Cx43 in mouse ventricular cardiomyocytes. IP<sub>3</sub>R is a large conductance cationic channel that plays an essential role in controlling Ca<sup>2+</sup> exchange. Blocking IP<sub>3</sub>R with antagonists suppresses Cx43 phosphorylation at S279/282 and hinders intercellular communication (91). As described above, various kinases have been implicated in Cx43-mediated intercellular communication such as the mitogen-activated protein kinase (MAPK), Src, and the Protein Kinase C isozymes (92).



Protein kinase Cs, or PKCs, are a superfamily of Serine/threonine kinases that partake in various signaling transduction pathways and cellular functions such as cell proliferation, migration, and apoptosis (93–95). The PKC family consists of structurally homologous isozymes which are divided into three groups based on their secondary messenger requirements namely: classical, novel, and atypical (96). Classical PKCs, including isoforms  $\alpha$ ,  $\beta_I$ ,  $\beta_{II}$ , and  $\gamma$ , require  $\text{Ca}^{2+}$  and a phospholipid such as DAG for activation in which they harbor a C2 domain that binds  $\text{Ca}^{2+}$  and a C1 domain that binds DAG (97). Novel PKC isoforms include  $\delta$ ,  $\epsilon$ ,  $\eta$ ,  $\theta$ , and  $\mu$  which also contain a C1 domain and a C2-like domain but only require DAG for activation. Atypical PKCs, including  $\zeta$ ,  $\iota$ , and  $\lambda$ , lack a  $\text{Ca}^{2+}$  binding domain and have a C1-like domain that is incapable of binding to DAGs but are activated by other lipid mediators such as sphingosine 1-phosphate (98).

There are multiple downstream targets of PKCs which in turn activate signaling pathways that regulate various cellular activities including cell migration, invasion, survival, and proliferation. PKCs typically recognize 5 consensus motifs: (R/K)X(S/T); (R/K)(R/K)X(S/T); (R/K)XX(S/T); (R/K)X(S/T)R/K; (R/K)XX(S/T)R/K; or (S/T)XR/K (99). For example: EGF receptors are recognized by PKC $\alpha$  through a RKAT sequence corresponding to the motif (R/K)(R/K)X(S/T) while PKC  $\delta$  recognizes a RILT sequence on the insulin receptor tyrosine kinase corresponding to the consensus recognition motif (R/K)XX(S/T) (100). A well-established signaling pathway that is stimulated by PKC is the Raf/Mek/Erk cascade through which survival and proliferation is regulated

in cancer cells (101). PKC overexpression can induce migration and invasion in intestinal epithelial cells while repressing apoptosis through the Ras/PKC $\iota$ /Rac1/MAPK kinase signaling pathway (102). In cardiomyocytes, the JAK/Stat pathway is activated in response to mechanical stretch, and it has been observed that PKC gets activated by mechanical stretch and subsequently phosphorylates Stat1 and Stat3 (103). Similarly, PKCs are involved in the downregulation of p38 MAPK signaling, stabilization of steroid receptor co-activator (src-3), and inhibition of Akt activation in response to growth factors (104–106). These findings highlight the plethora of signaling pathways that PKCs regulate making them essential regulators of cellular function.

Cx43 is directly phosphorylated by PKCs at S368 (107). This phosphorylation leads to a reduction in gap junction permeability affecting intercellular communication (107). The C-terminal tail of Cx43 contains RXSSR repeats that are recognized as PKC phosphorylation consensus sites (108). *In vitro* phosphorylation assays with PKC followed by peptide sequencing demonstrated that S368 of Cx43 is phosphorylated by PKC after treatment with 12-O-tetradecanoylphorbol-13-acetate (TPA) (107), a small diacylglycerol mimetic that induces PKC activity (109, 110). Ectopically expressing wild-type Cx43 in Cx43 deleted cells followed by TPA treatment decreases single channel permeability while expressing a Cx43 S368A mutant version does not affect channel permeability, demonstrating an integral role for Cx43 S368 phosphorylation by PKC to regulate channel permeability and intercellular communication (107).

Further studies observed that S368 phosphorylation reduces Cx43 hemichannel pore diameter/cross sectional area to reduce the incidence of the 100 pS conductance state and an increase in the 50 pS conductance state following TPA treatment. Interestingly, consistent with this notion, mutation of S368 to alanine reduces the incidences of 55–70 pS channels and also reduces the selective permeability of the gap junctions for a cationic dye NBD-M-TMA (111). Similarly, other strategies to reduce S368 phosphorylation such as inhibition of PKC or expression of the C-terminal tail fragment reduces the 50–70 pS conductance state (111). Together, these observations suggest a critical role for S368 phosphorylation in maintaining channel conductance and selective permeability. Consistent with this notion, if all six Cx43 subunits within a hemichannel are phosphorylated at S368, they are shown to lose permeability to sucrose which has a molecular weight of 342 daltons. Whereas, a smaller compound, ethylene glycol with a molecular weight of 62 daltons, was still permeant through these fully phosphorylated hemichannels (112). However, selective permeability of Cx43 hemichannels seems to be independent of the molecular weight of the permeant molecule. When Cx43 was expressed in *Xenopus* oocytes, hemichannels showed higher uptake of ethidium (310 daltons) but restricted uptake of smaller compounds such as glutamate (147 daltons) and Urea (60 daltons) (113). Hence, the selective permeability of Cx43 hemichannels, and its regulation through S368 phosphorylation, to a particular molecule may need to be individually characterized as molecular weight may not be the only determinant involved in dictating selectivity. At the structural level, phosphorylation of Cx43 by PKC at S368 promotes a conformational change in the C-terminal tail of Cx43, while a S368A substitution blocked this conformational change mediated by PKC (114). Studies using a scrape loading dye transfer assay (SL/DY assay) in Cx43 deleted fibroblasts ectopically expressing wild-type Cx43 revealed that dye coupling was reduced in cells reconstituted with Cx43 while dye coupling was not reduced when cells were reconstituted with a Cx43 S368A mutant suggesting that PKC-mediated S368 phosphorylation of Cx43 is a pivotal player in intercellular communication. In further support of this notion, intercellular communication increases in the presence of PKC inhibitors such as Go6976 (107). Furthermore, TPA-induced downregulation of intercellular communication is reversible. Once TPA activates classical and novel PKC isoforms, these isoforms including PKC $\epsilon$  and PKC $\delta$  translocate from the cytosol to the plasma membrane where Cx43 is embedded and phosphorylates S368 (115, 116). However, prolonged TPA activation can lead to the degradation of the PKC isoforms  $\alpha$ ,  $\delta$ ,  $\epsilon$ , and  $\iota$  through the ubiquitin-proteasome system upon which intercellular communication recovers (117, 118). In the rat liver epithelial cell line IAR20, inhibition of the proteasomal degradation pathway with MG132 prolongs PKC activity and prevents intercellular communication. However, inhibiting both the proteasomal

degradation pathway and PKCs, using a non-specific PKC inhibitor GF109203X, reverses the effect of MG132 (119). These studies provide support that PKC regulates intercellular communication through phosphorylating Cx43 on S368.

Several studies have been conducted that reveal regulation of Cx43 phosphorylation at S368 by multiple PKC isozymes. For instance, PKC $\delta$ , a novel PKC isoform, has been shown to phosphorylate S368 leading to gap junction internalization and degradation (120). Using fluorescence energy transfer (FRET) to study the spatiotemporal localization of Cx43 following S368 phosphorylation by PKC $\delta$ , treatment with a phorbol ester compound PDBu led to a decrease in FRET signal within the gap junction followed by internalization of S368 phosphorylated Cx43 containing vesicles that colocalized with proteasomal and lysosomal vesicles suggesting that Cx43 S368 phosphorylation by PKC $\delta$  leads to its internalization and degradation through the proteasomal and lysosomal degradation pathway (120). PKC $\delta$  was shown to directly interact with Cx43 in response to fibroblast growth factor 2 (FGF-2) treatment in osteoblast cell lines (121). FGF-2 treatment induces phosphorylation of PKC $\delta$  at Threonine-505, binding of the C-terminal tail of Cx43 by PKC $\delta$ , and phosphorylation of Cx43 S368. Inhibition of PKC $\delta$  with Rottlerin abolished FGF-2 induced Cx43 phosphorylation, demonstrating that PKC $\delta$  regulates Cx43 phosphorylation in response to FGF-2 (121).

Another novel PKC isoform that has been linked with FGF-2-mediated Cx43 phosphorylation is PKC $\epsilon$ . Upon treatment of cardiomyocytes with FGF-2 and Phorbol 12-myristate 13-acetate (PMA), another DAG mimetic, Cx43 and PKC $\epsilon$  colocalized at sites of intercellular connection. Subsequent coimmunoprecipitation studies revealed that PKC $\epsilon$  physically interacts with Cx43 and an increase in C-terminal tail phosphorylation (using an antibody that recognizes multiple phosphorylated residues) was observed but direct regulation of Cx43 S368 phosphorylation could not be determined (122). In a subsequent study, cardiomyocytes ectopically expressing a dominant-negative version of PKC $\epsilon$  reduced Cx43 phosphorylation levels in response to FGF-2 treatment as observed by incorporation of radiolabeled ATP. FGF-2 treatment was also shown to decrease gap junctional coupling as assessed by monitoring fluorescent dye (6-CF) transfer between cardiomyocytes (123). Ischemic preconditioning (IPC) in the heart is known to induce cardioprotection through gap junction coupling (56, 124). During IPC, the heart is subjected to brief periods of ischemia to increase its resistance toward sustained ischemia (125), and is one of the most effective methods to protect against myocardial ischemic injury (126). Isolated rat ventricular tissues that underwent ischemic preconditioning show enhanced Cx43:PKC $\epsilon$  complex formation as well as PKC $\epsilon$ -mediated phosphorylation of Cx43 at S368 (127). FGF-2 confers cardioprotective effects to ischemic injury in a PKC-dependent manner. Rat hearts perfused with FGF-2 *ex vivo* show upregulated levels of phosphorylated Cx43 on S368 in

intercalated discs suggesting a link between phosphorylation of Cx43 at PKC target sites such as S368 and FGF-2 induced cardioprotection against ischemia (128). PKC can also be activated by cholesterol, and cholesterol treatment reduces dye transfer in the H9c2 cardiomyocyte cell line while PKC inhibition partially restores dye transfer capacity in these cells. Cholesterol treatment upregulates Cx43 S368 phosphorylation in a PKC-dependent manner as PKC antagonists reduces cholesterol induced Cx43 S368 phosphorylation (129). Similarly, lysophosphatidylcholine (LPC) treatment in H9c2 cells induces PKC $\epsilon$  dependent activation of Cx43 S368 phosphorylation and the loss of gap junction intercellular communication through enhancement of Cx43 ubiquitination and proteasomal degradation. Furthermore, treatment with a PKC $\epsilon$  specific inhibitor, eV1-2, prevents the LPC induced reduction of intercellular communication (130).

In addition to gap junctional Cx43, hemichannels containing Cx43 can also be phosphorylated at Serine 368 by PKCs (131). Open hemichannels can conduct ion movement including Na<sup>+</sup>, Ca<sup>2+</sup>, and K<sup>+</sup> (132). Hemichannel opening can be activated by various stimuli such as metabolic inhibition, positive membrane potential, phosphorylation at S368 by PKC, and stimulation by ryanodine (Ryr) receptors (133–135). In ventricular cardiomyocytes, influx of Ca<sup>2+</sup> combined with the activation of Ryr receptors leads to hemichannels opening. Ryr receptors interact with Cx43 hemichannels through its C terminal tail (134). One interesting link between PKC and Cx43 hemichannels is found in mitochondria where Cx43 translocates to during stress conditions such as hypoxia (136). Under hypoxic conditions in cardiomyocytes, PKC $\epsilon$  mediates interaction between mitochondrial Cx43 hemichannels and the ATP regulated mitochondrial potassium ion channel Kir6.1. Phosphorylation of mitochondrial hemichannels increases in response to hypoxia and phosphorylation of Cx43 S262 is involved in the interaction between Cx43 and Kir6.1 in H9c2 rat heart cells (136). Since PKC $\epsilon$  phosphorylates both S262 and S368, it is interesting to speculate that the mitochondrial hemichannels may also be phosphorylated at S368 and may influence the interaction between Cx43 and Kir6.1. In studies assessing the protection conferred by FGF-2 against ischemic insult, PKC $\epsilon$  translocation was reported to increase in the subsarcolemmal mitochondria where Cx43 S262 and S368 phosphorylation is increased by 30- and 8-fold, respectively. PMA stimulation also increased Cx43 hemichannel phosphorylation which is reversed by the PKC $\epsilon$  inhibiting peptide eV1-2 (131). In addition, mitochondrial hemichannel opening is reduced in cardiomyocytes isolated from mice harboring a knockin mutation for Cx43 S368A suggesting further that mitochondrial hemichannels are targeted by PKC in cardiac cells (137), however, more research is necessary to fully understand the role of Cx43 composed hemichannels in regulating mitochondrial biology.

PKC $\gamma$  is a classical PKC isoform and is most abundantly expressed in neurons, the retina, and the eye lens (138, 139).

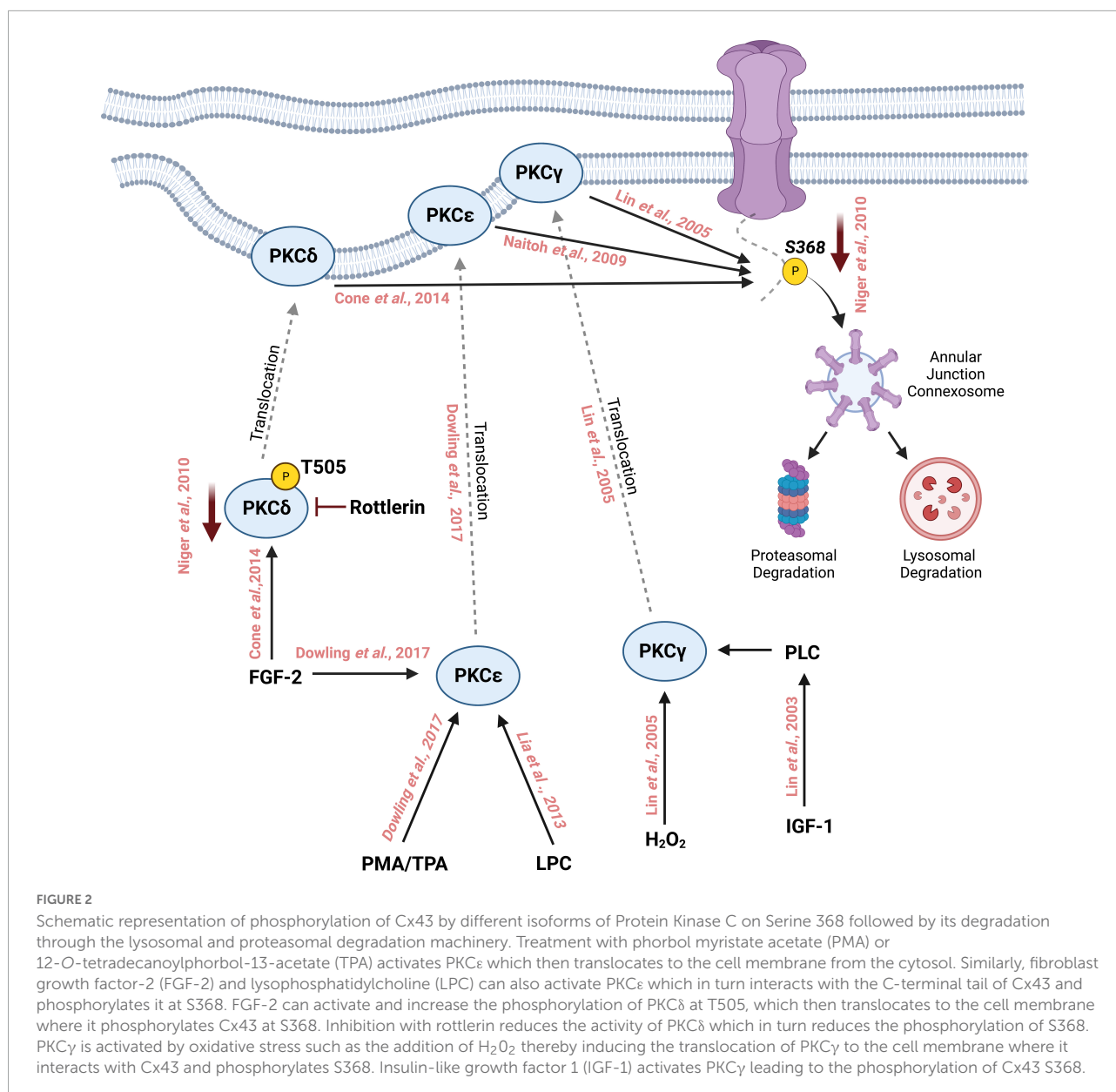
As a classical PKC, it is activated by DAGs (140). Interestingly, PKC $\gamma$  can also be activated by oxidative stress, such as exposure of cells to H<sub>2</sub>O<sub>2</sub>, which stimulates the C1 domain of PKC $\gamma$  to translocate to the plasma membrane where PKC $\gamma$  targets Cx43 for phosphorylation on S368. PKC $\gamma$  physically interacts with Cx43 and drives the disassembly of Cx43 from the membrane leading to a reduction in intercellular communication (141). Interestingly, PKC $\gamma$  led disassembly of Cx43 requires zonula occludens protein-1 (ZO-1), a tight junction protein. In the presence of TPA, ZO-1 interacts with Cx43 through its PDZ binding domain which lies in close proximity to S368 on Cx43. PKC $\gamma$  is able to interact with Cx43 even in the absence of ZO-1 or TPA stimulation. Although Cx43 that is complexed with PKC $\gamma$  in ZO-1 depleted cells lacks S368 phosphorylation, suggesting that ZO-1 may be required for PKC $\gamma$  to phosphorylate Cx43 on S368 (142).

In addition, growth factors such as insulin-like growth factor (IGF-I) induce phosphorylation of Cx43 mediated by PKC $\gamma$ . IGF-1 triggers the production of DAGs through Phospholipases (PLCs) which activate the classical PKCs including PKC $\gamma$  (143). PKC $\beta$ , another classical PKC, has been examined for its role in modulating gap junction intercellular communication through Cx43. Rat R6 fibroblasts overexpressing PKC $\beta$ I did not affect TPA-induced suppression of intercellular communication, suggesting that PKC $\beta$  may not play a major role in Cx43-mediated intercellular communication. Further experiments using the PKC $\beta$ -specific inhibitor LY379196 showed no change in intercellular communication (144). Similarly, PKC $\mu$  was shown to be of minor importance in TPA-mediated downregulation of intercellular communication in this study, since repeated TPA treatments showed little downregulation of PKC $\mu$  unlike other classical isozymes such as PKC $\alpha$  (144). Based on these studies, it can be concluded that several isoforms of PKC play a major role in regulating intercellular communication through the phosphorylation of Cx43 S368 (Figure 2). Further characterization of the roles for various PKC isoforms in regulating Cx43 phosphorylation and subsequent intercellular communication is necessary to understand the complex signaling pathways controlling gap junction function and intercellular communication. The relationship between PKC isozyme expression and Cx43 S368 phosphorylation should be further explored in various organs since the abundance of PKC isozymes differs between tissues and organ. For instance, the expression of PKC  $\alpha$  and  $\beta$  is the highest in the human brain while PKC $\delta$  is abundantly expressed in the adrenal gland (145).

## Cx43-mediated intercellular communication and cardiac conduction

Action potential propagation through both cardiomyocytes and non-cardiomyocytes in the ventricles has long been thought to be mediated by Cx43 (146). Genetic studies have





shown that cardiac-specific Cx43 knockout produces ventricular tachycardia, prolonged PR interval, slowed cardiac conduction, and sudden cardiac death (147, 148). Cx43 is found in the intercalated discs of ventricular cardiomyocytes and is important for electrical impulse propagation. Translocation of Cx43 to and from the plasma membrane is tightly regulated and it has a high turnover rate (25). Any changes to Cx43 distribution can affect intercellular communication and lead to lethal arrhythmias such as ventricular tachyarrhythmia (149). Since phosphorylation of Cx43 at S368 can regulate gap junction pore opening, translocation, and degradation, it suggests that Cx43 phosphorylation at this residue is essential for proper cardiac conduction. Studies in guinea pig hearts following induction with calcium revealed an increase in Cx43

S368 phosphorylation and decrease in gap junction electrical conductance as well as arrhythmias and slower action potential conductance, indicating that Cx43 S368 phosphorylation and cardiac conduction were intimately linked (150). In addition, other phosphorylation sites within the C-terminal tail of Cx43, such as 325/328/330, are also important for gap junctional conductance and the prevention of arrhythmia. Germline knock-in mouse models with phosphomimetic mutation of these three sites display a reduction in arrhythmia and are resistant to gap junctional remodeling (151). Based on these studies, it became widely accepted that Cx43 is indispensable for cardiac conduction.

However, more recent studies have emerged that question this view. For instance, germline Cx43 knockout mice die at



birth due to asphyxia as a result of a defect in the pulmonary outlet and not due to arrhythmia (152). Furthermore, cardiac-specific knockout mice survive up until the fourth week of postnatal life and ultimately die due to fatal arrhythmias (148). However, these mice appear to retain a normal heart rhythm. In humans, Cx43 mutation is tied to Oculodentodigital dysplasia which is a rare congenital autosomal disorder characterized by phenotypic variability. ODDD linked Cx43 mutations G21R and G138R colocalize and coimmunoprecipitate with wild-type Cx43 (153). However, these mutants display a dominant negative effect on gap junctional conductance and yet individuals with these mutations maintain normal cardiac conduction. Similarly, a knockin mouse model where S368 is substituted with an alanine and thus cannot be phosphorylated does not show significant changes in terms of gap junction localization and Cx43 abundance. These studies suggest that Cx43 might not be essential to action potential propagation between cardiomyocytes.

A new model of action potential propagation involving gap junctional structure termed “ephaptic coupling” has emerged which suggests that ionic currents are transmitted between cardiomyocytes through the confined extracellular space at the perinexus which lies at the edge of the gap junction plaque in which adjacent cells are not connected (154–156). Such coupling does not require a continuous pore or direct contact between cells mediated by gap junctions. Manipulation of extracellular volume in the hearts of guinea pigs showed that an increase in extracellular space reduces action potential velocity providing further precedence to determine if other modes of intercellular coupling/communication are present that do not involve the conventional electrotonic mode of conduction through gap junctions but rather through ephaptic coupling (157). Super resolution microscopy of rat ventricular myocytes has shown that the perinexus consists of clusters of Cx43 hemichannels and  $\text{Na}_v1.5$  sodium channels (157).  $\text{Na}_v1.5$  sodium channels contain a  $\beta 1$  subunit which is non-pore forming but acts as an adhesion molecule between cells (158), and also localizes with Cx43 hemichannel clusters within the perinexus. Inhibition of the  $\beta 1$  subunit results in loss of adherence at the perinexus cleft and an increase in the perinexus space in guinea pig ventricles. This de-adherence reduces sodium ion currents in gap junctions adjacent to sodium channels but does not affect the whole cell sodium current further supporting the ephaptic coupling hypothesis. Inhibition of the  $\beta 1$  subunit in guinea pig hearts slows cardiac conduction and causes arrhythmia including prolongation of the QT interval (159). Mathematical modeling suggests that membrane spacing of  $<30$  nm is required for ephaptic coupling (156).  $\beta 1$  subunit adhesion is predicted to provide membrane spacing of less than the 30 nm limit enabling ephaptic coupling to occur (159). Gap junctional structure can therefore support cardiac conduction by providing a perinexus region in which sodium ion channels can propagate action potential through ephaptic coupling. Interestingly, expression

level of  $\text{Na}_v1.5$  is reduced in hearts of mice heterozygous for Cx43 (160) and at the cellular level, this reduction in  $\text{Na}_v1.5$  was observed in regions devoid of Cx43. These mice also had slowed and dispersed conduction suggesting the importance of Cx43 in the expression and function of sodium ion channels in the heart (160). Hence, both electrotonic coupling and ephaptic coupling through Cx43 could exist as a mixed mode of action potential transmission and the balance between these two mechanisms could be key in clarifying our understanding of the role of Cx43 in cardiac conduction (161).

## PKC and Cx43 expression in the healthy heart

The heart predominantly expresses three connexin isoforms, namely Cx40, Cx43, and Cx45, of which Cx43 is the most abundantly expressed (162). Cx43 expression initiates at E8.5 in the mouse embryonic heart and gradually increases throughout development and is found in both the adult atria and ventricles (163). Cx43 is specifically expressed in the trabeculations of embryonic ventricles starting at E10.5 and is expressed by the entire myocardium in the adult heart (42, 163). Similar to its expression pattern, phosphorylation of Cx43 at S368 increases during embryonic development in the heart and it increases significantly in the adult heart. Studies assessing Cx43 S368 phosphorylation between E14.5 embryos and 12-month-old mice revealed an increase in pS368 levels in the adult hearts while the relationship between embryonic and adult tissue was reversed in other tissues such as skin and cornea (164). This increment in phosphorylation of Cx43 in embryonic and adult hearts may be explained by the observed increase in expression of PKC isoforms that directly phosphorylate Cx43 at S368. For example, PKC $\epsilon$  expression increases throughout mouse embryonic development in the heart (165). Furthermore, human heart tissues express several PKC isoforms. Western blot and immunohistochemical analysis show that classical isoforms PKC $\alpha$  and PKC $\beta$  are present in the human heart while PKC $\gamma$  is absent. Novel PKC isoforms  $\delta$ ,  $\epsilon$ ,  $\eta$ , and the atypical PKC isoform PKC $\mu$  are also present in cardiomyocyte homogenates (166). Therefore, co-expression of PKCs and Cx43 are consistent with a regulatory network between PKCs and Cx43 S368 phosphorylation.

## PKC-Cx43 S368 in the diseased heart

### Ischemia

Myocardial ischemia, which refers to the reduction of blood flow and oxygen to the heart, can occur following coronary

artery blockage due to the accumulation of atherosclerotic plaques (167). It is estimated that myocardial ischemia affects around 126 million individuals globally (168). Ischemic insult reduces gap junction intercellular communication between cardiomyocytes which affects electrical impulse propagation leading to arrhythmias (29). Cx43 degradation is dependent upon AMP activated protein kinase (AMPK) during initial periods of ischemia while the later periods require the autophagy regulating protein Beclin-1. Furthermore, degradation of Cx43 due to ischemia also led to an impairment of gap junction intercellular communication in HL-1 mouse cardiomyocytes. Inhibiting autophagy restored intercellular communication indicating that autophagy is involved in ischemia induced Cx43 degradation (29). Reduction of gap junction intercellular communication post ischemia is also observed in neonatal rat heart myofibroblasts. Interestingly, prolonged ischemia led to the opening of hemichannels while gap junctions remained closed. When Cx43 hemichannels are inhibited with Gap26, a connexin derived peptide, infarct size is significantly reduced in isolated perfused rat hearts which suggests that open hemichannels could contribute to the propagation of infarct promoting signals across the heart (169). Studies performed in rat models of ischemia perfusion found an increase in Cx43 S368 phosphorylation at the intercalated discs (ID) of cardiomyocytes which triggers the ubiquitination and subsequent degradation of Cx43 (170). This reduction in Cx43 at the IDs contributes to the electrical uncoupling and reduction in conduction velocity, a hallmark of ischemic hearts (171). In another study in which wild-type mice underwent no-flow ischemia also showed a significant increase in cardiac Cx43 S368 phosphorylation as compared to control mice while total Cx43 levels decreased. This degradation of Cx43 was promoted by 14-3-3 theta which is involved in anterograde transport of Cx43 (70). 14-3-3 theta binds to Cx43 when phosphorylated at S373 (172). Interestingly, S373 acts as a gatekeeper to S368 phosphorylation and S373A substitution impairs PKC induced phosphorylation of S368 in cells exposed to ischemic conditions (173). In contrast to these studies, other studies suggest ischemia has the opposite effect on gap junction intercellular communication. For instance rats subjected to left anterior descending coronary artery (LAD) occlusion showed higher Cx43 levels in the intercalated discs and dye transfer assay revealed an increase in gap junction-mediated intercellular communication after 30 min of LAD occlusion (174). Similarly, adult rat hearts exposed to ischemia undergo electrical uncoupling during which reduced Cx43 phosphorylation is observed. Reperfusion, on the other hand, increases phosphorylated Cx43 at the intercalated discs (25). Mass spectrometry studies on rat hearts that underwent ischemia show that S368 undergoes dephosphorylation within 15–30 min following ischemia, corresponding to the time interval that the majority of gap junction uncoupling occurs. Treatment with an antiarrhythmic peptide analog rotigaptide (ZP123) suppresses dephosphorylation of S368 after 30 min

of ischemia and prevents gap junction uncoupling (175). One mechanism that may promote an increase in Cx43 phosphorylation following reperfusion is through PKCs, such as PKC $\alpha$  and PKC $\epsilon$ , that translocate to the cell membrane upon myocardial ischemia reperfusion. PMA treatment of rat hearts promotes the translocation of PKC isozymes, including  $\alpha$ ,  $\delta$ , and  $\epsilon$ , to the cell membrane (176). All three of these isozymes have been implicated in Cx43 S368 phosphorylation at the cell membrane. In cryoinjured left ventricular tissue treated with  $\alpha$ CT-1, a peptide containing nine amino acids of the Cx43 C-terminal tail, an acute increase in Cx43 S368 phosphorylation is observed (177). However, control hearts treated with  $\alpha$ CT-1 do not show any change in S368 phosphorylation suggesting that Cx43 S368 phosphorylation is dependent on injury (177, 178).  $\alpha$ CT-1 enhances PKC $\epsilon$ -mediated phosphorylation of Cx43 S368 in the injured hearts and prevents arrhythmia (178). In response to injury, PKC $\epsilon$  translocates and phosphorylates Cx43 S368. Interestingly, ischemic injury also induces translocation of PKC $\epsilon$  in the heart of conscious rabbits (179). Similarly, another study demonstrated that ischemic preconditioning in adult rat hearts promoted PKC $\epsilon$ -mediated Cx43 S368 phosphorylation and suppresses Cx43 lateralization (180). Overall, these findings suggest that the increased translocation of PKCs to IDs during ischemia contributes to electrical uncoupling through enhanced Cx43 S368 phosphorylation.

## Myocarditis

Myocarditis is defined as inflammation of the heart muscle which can reduce its ability to pump blood (181). Global trends indicate that myocarditis affected over 3 million people in 2017 alone (182). Cx43 S368 phosphorylation is upregulated in acute myocarditis, which accounts for a majority of sudden cardiac deaths in people without any prior heart conditions (183, 184). Myocarditis is accompanied by abnormal ECG patterns the most common of which is sinus tachycardia associated with non-specific ST/T-wave variations. A study of ECG patterns found in myocarditis revealed multiple characteristics such as depression in precordial and limb leads in the PR segment, pericarditis pattern in the ST segment, and a prolonged QT interval (185). Utilizing a model of rat experimental autoimmune myocarditis (EAM), Cx43 S368 phosphorylation was shown to be elevated in this model (184). Downregulation of Cx43 S368 phosphorylation improves gap junction intercellular communication and reduces the prolonged QRS interval. Since the EAM model is a T cell-mediated inflammatory disorder of cardiac tissues, this study further perfused isolated rat hearts with inflammatory cytokine IL-1 $\beta$  and found that perfusion with IL-1 $\beta$  induces Cx43 S368 phosphorylation in normal rat hearts. EAM models also show upregulation of PKC $\alpha$  in the rat heart, which may provide a mechanism for the increased Cx43

S368 phosphorylation levels. Consistent with this notion, intraperitoneal administration of the PKC inhibitor Ro-32-0432 reduces pro-inflammatory cytokines such as IL-1 $\beta$  which activates Cx43 S368 phosphorylation, as well as reduces biomarkers of heart failure in the EAM model (186). These observations further corroborate the relationship between PKC isozymes and Cx43 S368 phosphorylation in the context of inflammatory cytokines and myocarditis. However, further studies are required to assess the significance of this relationship in myocarditis and if the PKC/Cx43 pathway can serve as a novel therapeutic target to alleviate consequences associated with myocarditis.

## Cardiomyopathy

Cardiomyopathy encompasses a variety of heart conditions that influence the ability of the heart to pump blood into systemic and pulmonary circulation, the most common of which is hypertrophic cardiomyopathy. This condition is caused by the thickening of the left ventricle chamber wall (187, 188). PKC isozymes have been extensively studied in relation to hypertrophy. For instance, adult mice overexpressing classical PKC $\beta$  exhibit mild and progressive ventricular hypertrophy, while overexpression in neonates leads to sudden cardiac death (189). Similarly, neonatal cultured rat cardiomyocytes overexpressing PKC $\alpha$  show hypertrophic cardiomyocyte growth as well as induction of the hypertrophy marker atrial natriuretic factor, whereas overexpression of PKC $\delta$  and PKC $\epsilon$  does not lead to cardiomyocyte hypertrophy. Furthermore, a kinase-inactive mutant of PKC $\alpha$  did not affect cardiomyocyte hypertrophy, indicating downstream phosphorylation events mediated by PKC $\alpha$  are required for its role in cardiac hypertrophy (190). Heart explants from dilated cardiomyopathy and ischemic cardiomyopathy patients have increased levels of PKC $\alpha$  and PKC $\beta$ . Immunoblotting experiments revealed a greater than 40% increase in PKC $\beta$  levels at the membrane, PKC $\alpha$  levels increase by 70% in the cardiomyopathic left ventricles, while PKC $\epsilon$  expression does not significantly change (191).

The DAGs such as PMA have been used to induce hypertrophy since PMA activates most PKCs. Neonatal rat ventricular cardiomyocytes (nrCMCs) treated with PMA show a significant increase in cell size. These cardiomyocytes also have increased markers of pathological hypertrophy such as Nppa, Acta1, and Serca2a. NrCMCs treated with PMA display tachyarrhythmia which is also a characteristic of hypertrophy (192). Given that PKCs activated by PMA directly phosphorylate Cx43 at S368 as described above, one might anticipate that hyperphosphorylation of S368 on Cx43 would promote hypertrophy. A rat model of pressure-overload hypertrophy revealed an initial increase in Cx43 S368 phosphorylation which was followed by a decline after 8 weeks, and these animals were prone to sustained ventricular

tachycardia (193). In contrast, it has also been reported that rats treated with monocrotaline to induce right ventricular hypertrophy show an increase in non-phosphorylated Cx43 and cytosolic annular gap junctions (194). Using inhibitors against protein phosphatase 1 (PP1) suppresses cardiac hypertrophy and heart failure (195). Consistent with this observation, treatment with PP1 inhibitors such as Okadaic acid prevents ischemia-induced Cx43 dephosphorylation in cardiomyocytes (196). Based on these findings, PKC activity may need to be carefully modulated in the heart to maintain Cx43 S368 phosphorylation in equilibrium to ensure appropriate gap junctional communication levels. A more apparent effect of the PKC/Cx43 relationship in cardiomyopathy is observed in mice treated with Furazolidone for 30 weeks to induce dilated cardiomyopathy (197). Mitochondrial dysfunction is a major contributor to dilated cardiomyopathy (198). Furazolidone treatment reduces myocardial mitochondrial Cx43 S368 phosphorylation along with PKC $\epsilon$  levels leading to mitochondrial dysfunction. Treatment with PMA, a PKC activator, increases PKC $\epsilon$  activity and partially reverses Furazolidone inhibition of Cx43 S368 phosphorylation. In contrast, treatment with the Cx43 inhibitor, 18 $\beta$ -glycyrrhetic acid, inhibits the effect of PKC on mitochondrial dysfunction indicating that PKC-mediated Cx43 S368 phosphorylation is essential to reduce mitochondrial dysfunction in dilated cardiomyopathy and therefore could serve as a novel therapeutic target for cardiomyopathy (197).

## Arrhythmias and heart failure

Arrhythmias such as atrial and ventricular tachycardia can lead to heart failure in which the heart fails to pump sufficient blood to the systemic and pulmonary circulation. Heart failure affects around 26 million people worldwide and is considered a global pandemic (199). About 30% of heart failure patients suffer from atrial fibrillation while 50% of sudden death attributed to heart failure is accompanied by ventricular arrhythmias (200–202). Many studies have examined the expression and phosphorylation status of Cx43 in atrial fibrillation and congestive heart failure in various species. However, there are significant variations between species. For instance, expression of Cx43 during atrial fibrillation decreases in rabbits while it increases in dogs (203, 204). Interestingly, congestive heart failure in dogs reduces the phosphorylation of Cx43 at S368 and overall Cx43 in the atria. Ventricular Cx43 undergoes dephosphorylation and lateralization, inducing arrhythmia and slowing conduction during heart failure (205, 206). Along with changes in expression and phosphorylation levels of Cx43, several cardiac diseases such as arrhythmogenic right ventricular cardiomyopathy (ARVC) are accompanied by remodeling of Cx43 (207). Heart failure patients have reduced levels of Cx43 in the gap junction plaques found

at the intercalated discs and an increase in the number of Cx43 in the lateral walls of cardiomyocytes (208, 209). Lateralization of Cx43 is in contrast with the normal distribution of Cx43 which is concentrated at the intercalated disc in the ventricular myocardium (210). Cx43 hemichannels require positive membrane potential of  $>+50$  mV to open. During systole, cardiomyocytes have an elevated level of cytoplasmic  $\text{Ca}^{2+}$  which lowers the membrane potential required to open hemichannels to  $+30$  mV (211). Entry of  $\text{Ca}^{2+}$  into cardiomyocytes further induces the sarcoplasmic reticulum to release more  $\text{Ca}^{2+}$  into the cytoplasm that can lead to the activation of hemichannels. A single open hemichannel can display high conductance of around 220 pS which can allow for the movement of ions such as  $\text{Na}^+$  and  $\text{K}^+$  (132). During pathological conditions, the sarcoplasmic reticulum is spontaneously triggered to release  $\text{Ca}^{2+}$  which leads to the opening of hemichannels and delayed afterdepolarizations that further promotes arrhythmia (212, 213). Caffeine can induce sarcoplasmic reticulum release of  $\text{Ca}^{2+}$  through the activation of ryanodine receptor channels (Ryr2) (214). Ryr2 interacts with and regulates Cx43 hemichannel opening due to elevated  $\text{Ca}^{2+}$  levels in cardiomyocytes. Ventricular cardiomyocytes isolated from heart failure patients display spontaneous  $\text{Ca}^{2+}$  release and hemichannel opening along with delayed afterdepolarizations. In addition, adrenergic stimulation of arterially perfused tissue wedges had higher occurrences of delayed afterdepolarizations which were suppressed by Gap19, a Cx43 hemichannel specific inhibitor (134). This indicates that Cx43 hemichannel lateralization and opening contributes to arrhythmogenic activities. Significant levels of Cx43 lateralization is also observed in mouse models of Duchenne muscular dystrophy (DMD) which is characterized by the loss of dystrophin that stabilizes the sarcolemma in myocytes (207). Cardiac arrhythmias are often seen in young and adolescent individuals with DMD (215). Cx43 lateralization is also observed in mouse models of DMD. Upon isoproterenol treatment, DMD mice develop arrhythmias and die within 24 h. However, treatment with the hemichannel inhibitors Gap19 or Gap26 protects DMD mice from arrhythmogenesis and death suggesting that Cx43 hemichannel activity and lateralization are linked with arrhythmia *in vivo* (207).

Disruption of  $\text{Ca}^{2+}$  homeostasis and Cx43 hemichannel function are also tied to ARVC that is associated with mutations in desmosome proteins such as desmoglein-2, desmoplakin, and Plakophilin-2 (PKP2) (216). ARVC or arrhythmogenic right ventricular dysplasia (ARVD) is characterized by ventricular tachycardia and sudden cardiac death (217). PKP2 knockout mice display higher levels of  $\text{Ca}^{2+}$  levels in the cytoplasm and sarcoplasmic reticulum along with increased duration of  $\text{Ca}^{2+}$  transient currents in right ventricular myocytes (216). Susceptibility to arrhythmia is also significantly higher in PKP2 knockout mice. Interestingly, hemichannel specific inhibition with Gap19 normalizes  $\text{Ca}^{2+}$  homeostasis. Cx43

reduction also decreases  $\text{Ca}^{2+}$  permeability and cytoplasmic  $\text{Ca}^{2+}$  accumulation in right ventricles of PKP2 knockout mice, which was also observed following treatment with the PKC inhibitor GF 109203X (216). Single-molecule localization microscopy indicated that PKC clusters were reduced in the intercalated disc of the PKP2 knockout hearts. Cx43 S368 phosphorylation in the PKP2 knockout group was also lower in both the right and left ventricle which could be due to a reduction in PKC levels at the intercalated disc since PKC phosphorylates Cx43 at S368 (216). Total Cx43 was higher in the PKP2 knockout group as compared to the control group. It is interesting to speculate if this may be due to a reduction in Cx43 hemichannel degradation as S368 phosphorylation is known to play a role in Cx43 degradation (218). Utilizing scanning electron microscopy and Fluoro-Gold labeled Cx43, Cx43 hemichannel abundance was found to be higher in PKP2 deficient hearts (219). However, these Cx43 hemichannels are present in the intercalated disc as “orphan Cx43” and are not docked to form a gap junction. In addition, a widening of the intercellular space in the gap junction plaque in PKP2 deficient hearts suggests a loss of gap junction connection in these spaces (219). Loss of gap junctions in the intercalated discs is also seen in Naxos disease which is a recessive form of ARVC (220). Similarly, Cx43 expression is reduced in cardiomyocytes of cardiomyocyte-specific desmoplakin deficient mice which is compounded by a significant reduction of Cx43 S368 phosphorylation and function (221). Another intriguing observation in patients with ARVC is the reduction in  $\text{Na}_v1.5$  sodium channels which is predicted to mediate ephaptic coupling in the hemichannels in the perinexus (222, 223). Therefore, Cx43 function, mediated by both expression levels and S368 phosphorylation is a critical regulator of  $\text{Ca}^{2+}$  homeostasis in the heart.

The PKC-mediated hyperphosphorylation of Cx43 at S368 in isolated normal heart tissue can also induce lateralization of Cx43 from the intercalated disc to the lateral membrane of the ventricular myocardium (224). This hyperphosphorylation is also associated with arrhythmia with a prolonged QRS complex (184). Immunohistochemical analysis showed redistribution of Cx43 to the lateral membrane in hearts with hyperactivated PKC in response to PMA treatment. Suppression of PKC activity with the PKC inhibitor Ro-32-0432 significantly decreased phosphorylation of Cx43 S368 and suppressed this lateralization (224). In addition, Cx43 lateralization in left ventricle occurs following isoproterenol treatment (225). Isoproterenol is a sympatho-mimetic agent capable of inducing atrial fibrillation and heart failure. Taken together, these studies indicate an important relationship between PKC and Cx43 S368 phosphorylation in arrhythmogenesis promoted by hemichannel lateralization in the heart. Several other PKC isoforms are upregulated in failing hearts including PKC $\alpha$  and PKC $\epsilon$  as observed in a myocardial infarction induced heart failure model in hamsters (226). Similarly, guinea



pig models of heart failure induced by pressure overload also have increased levels of PKC $\alpha$  and PKC $\epsilon$  (227). These findings showcase that Cx43 S368 phosphorylation regulated by PKCs may serve as a therapeutic target in arrhythmias and heart failure.

## PKC/Cx43 pS368 circuit in therapy against cardiac diseases

Peptides that target Cx43 have been extensively studied for their pharmacological benefits in cardiac diseases. These peptides mimic the extracellular loop of Cx43 or the cytoplasmic C terminal domain. For instance, Gap26 and Gap27 are based on the extracellular domains of Cx43 while Gap19 and  $\alpha$ CT1 include amino acids of the C terminal tail of Cx43 (211).  $\alpha$ CT1, or alpha Connexin carboxy terminus 1, has been tested *in vitro* and *in vivo* for its effect against ischemia/reperfusion injury. It was designed to inhibit the interaction of Cx43 with Zona Occludens-1 (ZO-1). Cx43 binds with the postsynaptic density/disk-large/ZO-1 (PDZ2) domain of ZO-1 which results in the remodeling of gap junction plaques. This interaction has been reported to increase cardiomyopathies and heart failure in humans (228). In mouse models of cardiac injury,  $\alpha$ CT1 was shown to interact with the PDZ domain of ZO-1 and induce phosphorylation of Cx43 at S368 which can reduce intercellular communication through Cx43. Cryoinjury CD1 mice treated with  $\alpha$ CT1 display an increase in Cx43 plaques in the intercalated discs while control-treated groups have a higher level of Cx43 remodeling from plaques to lateralized distributions.  $\alpha$ CT1 treatment promoted the level of Cx43 S368 phosphorylation in the plaques in a PKC $\epsilon$  dependent manner (178). Furthermore,  $\alpha$ CT1 can protect hearts from ischemic injury and preserve ventricular function likely due to

its interaction with the Cx43 C-terminal helix 2 domain and not due to its interaction with the PDZ domain of ZO-1.  $\alpha$ CT1 by itself leads to an increase in Cx43 S368 phosphorylation in a concentration-dependent manner (229). *In vivo* studies confirm that  $\alpha$ CT1 reduces arrhythmia in cryo-injured hearts and increases the rate of depolarization (178, 228).  $\alpha$ CT1 has reached Phase III clinical evaluation for healing chronic skin wounds associated with non-cardiac diseases such as cancer and ulcers in which Cx43 plays a prominent role (230, 231). Phase I and Phase II clinical trials with  $\alpha$ CT1 in venous leg ulcers, diabetic foot ulcers, and cutaneous scarring/Laparoscopic incisions showed enhanced wound closure as compared to control-treated patients. However, the phase III clinical trial with  $\alpha$ CT1 was terminated although no adverse toxicity was reported (232). Since  $\alpha$ CT1 has also shown promising results *in vivo* against arrhythmia and ischemia/reperfusion injury, clinical trials utilizing  $\alpha$ CT1 or other agents to promote Cx43 S368 phosphorylation in cardiac diseases seem viable (178, 229).

Another method of increasing Cx43-S368 phosphorylation is by inducing PKC $\epsilon$  activity that directly targets S368. Using  $\psi$  $\epsilon$ RACK, a PKC $\epsilon$  specific activator, revealed that PKC $\epsilon$  activation induces protection against ischemia/reperfusion and hypoxic injury.  $\psi$  $\epsilon$ RACK treatment increases PKC $\epsilon$  translocation to the plasma membrane in isolated cardiomyocytes and in transgenic mouse hearts that express  $\psi$  $\epsilon$ RACK postnatally (233). This activation could be a therapeutic approach toward utilizing PKC $\epsilon$  and Cx43 pS368 relationship against ischemia. Drugs that upregulate PKC $\epsilon$  such as adenosine have been used as an adjunct to thrombolysis or percutaneous intervention to treat acute myocardial infarction in patients. A randomized study showed that adenosine-treated patients had reduced infarct size compared to that observed in the placebo group (234).

TABLE 2 Summary table of the phosphorylation of Cx43-Serine-368 and expression level of PKC isozymes in various cardiac disorders.

Cardiac disease	Species/model	Cx43-serine-368 phosphorylation	PKC isozymes expression	References
Ischemia – reperfusion	Rat (Ischemia – reperfusion model)	↓ Ischemia ↑ Perfusion	↑ Perfusion PKC $\alpha$ and PKC $\epsilon$	(25, 175)
Myocarditis	Rat [experimental autoimmune myocarditis (EAM)]	↑	↑ PKC $\alpha$	(184, 186)
Hypertrophy	Mice	–	↑ PKC $\beta$	(189)
Hypertrophy	Neonatal cultured rat cardiomyocytes	–	↑ PKC $\alpha$	(190)
Dilated cardiomyopathy	Human heart explants	–	↑ PKC $\alpha$ and PKC $\beta$	(191)
Right ventricular hypertrophy	Rats	↓	–	(194)
Congestive heart failure	Dogs	↓	–	(205, 206)
Isoproterenol induced fibrillation	Rats	↑	↑ PKC $\epsilon$	(225)
Myocardial infarction and heart failure	Hamsters	–	↑ PKC $\alpha$ , $\beta$ , $\epsilon$ , $\zeta$	(226)
Pressure overload induced heart failure	Guinea pigs	–	↑ PKC $\alpha$ and PKC $\epsilon$	(227)



Adenosine was administered intravenously to patients which were then followed for new incidences of congestive heart failure after 24 h, or subsequent hospitalization after congestive heart failure, or death due to any causes within 6 months. Although no differences between treated and placebo groups at each of these endpoints were observed, the study did find that higher doses of adenosine correlated with smaller median infarct size. Therefore, pharmacological strategies that promote PKC-mediated Cx43 S368 phosphorylation might be more fruitful based on the importance of this interaction in the heart.

Cx43 S368 phosphorylation is not always reduced in cardiac diseases. For instance, myocarditis and arrhythmia can lead to hyperphosphorylation of Cx43 (184). Despite the presence of various CX43 inhibitors such as carbenoxolone and peptide inhibitors such as Gap26, issues regarding specificity and off-target effects have remained. Interestingly, gap junction inhibitors that show specificity toward the Cx43 S368 phosphorylated confirmation have been generated, such as the lipidated connexin mimetic peptide SRPTEKT-Hdc. Treatment with this peptide leads to a reduction in dye coupling and  $\text{Ca}^{2+}$  wave propagation through Cx43. MDCK cells expressing either phosphodeficient or phosphomimetic mutants of Cx43 S368 were treated with SRPTEKT-Hdc (235). The potency of inhibition by SRPTEKT-Hdc was greater in the phosphomimetic group than in the phosphodeficient group suggesting that SRPTEKT-Hdc had specificity toward the phosphorylated form of Cx43 S368. The cardioprotective effect of this peptide is yet to be examined in cases where hyperphosphorylation of Cx43 S368 is observed. Reduction of Cx43 S368 phosphorylation can also be successfully achieved through the inhibition of PKC using PKC-specific inhibitors such as Calphostin C (108). Since heart failure shows an increase in PKC $\epsilon$  activity, inhibition with PKC $\epsilon$  specific inhibitor  $\epsilon$ V1-2 decreases symptoms associated with heart failure including parenchymal fibrosis and fractional shortening (236). However, the usage of PKC inhibitors should be examined in more depth since most PKC inhibitors affect several PKC isozymes when used at higher concentrations and potentially other kinases as well. Therefore, PKC inhibitors that target the PKC Cx43 S368 phosphorylation circuit should be explored further in cardiac defects as they may provide greater specificity.

## Conclusion

Various PKC isozymes directly target and phosphorylate S368 on the C terminal tail of Cx43 in cardiomyocytes. This acts to regulate gated conductance as well as a degradation signal for the Cx43 plaques to reduce gap junctional coupling in the cardiac system. Here we explored the prevalence of PKC isozymes along with the level of Cx43 S368 phosphorylation in

different cardiac diseases (Table 2). Cx43 S368 phosphorylation occurs in healthy embryonic and adult hearts. However, the level of this phosphorylation varies in different cardiac disease states. Future *in vivo* studies in animal models and therapies based on this PKC/Cx43 pS368 relationship should consider this variation while designing drugs effective toward cardiac diseases.

## Author contributions

RP wrote the initial draft. All authors edited and provided further input in the manuscript preparation.

## Funding

This work was supported by the Nebraska Department of Health and Human Services (DHHS) (LB692) and Creighton University Health Science Strategic Investment Fund Faculty Development Grant to BN. Through LB692, this work was supported by revenue from Nebraska's excise tax on cigarettes awarded to BN of Creighton University through the Nebraska Department of Health and Human Services (DHHS). Its contents represent the view(s) of the author(s) and do not necessarily represent the official views of the State of Nebraska or DHHS.

## Acknowledgments

We thank members of the BN lab for providing helpful comments on this review.

## Conflict of interest

MK reports consulting support from Sanofi.

The remaining authors declare that the research was conducted in the absence of any commercial or financial relationships that could be construed as a potential conflict of interest.

## Publisher's note

All claims expressed in this article are solely those of the authors and do not necessarily represent those of their affiliated organizations, or those of the publisher, the editors and the reviewers. Any product that may be evaluated in this article, or claim that may be made by its manufacturer, is not guaranteed or endorsed by the publisher.

## References

- Goodenough D, Goliger J, Paul D. Connexins, connexons, and intercellular communication. *Annu Rev Biochem.* (1996) 65:475–502. doi: 10.1146/annurev.bi.65.070196.002355
- Lawrence T, Beers W, Gilula N. Transmission of hormonal stimulation by cell-to-cell communication. *Nature.* (1978) 272:501–6. doi: 10.1038/272501a0
- McArthur L, Chilton L, Smith G, Nicklin S. Electrical consequences of cardiac myocyte: fibroblast coupling. *Biochem Soc Trans.* (2015) 43:513–8. doi: 10.1042/BST20150035
- Sohl G, Willecke K. Gap junctions and the connexin protein family. *Cardiovasc Res.* (2004) 62:228–32. doi: 10.1016/j.cardiores.2003.11.013
- Riquelme M, Kar R, Gu S, Jiang J. Antibodies targeting extracellular domain of connexins for studies of hemichannels. *Neuropharmacology.* (2013) 75:525–32. doi: 10.1016/j.neuropharm.2013.02.021
- Omori Y, Yamasaki H. Gap junction proteins connexin32 and connexin43 partially acquire growth-suppressive function in HeLa cells by deletion of their C-terminal tails. *Carcinogenesis.* (1999) 20:1913–8. doi: 10.1093/carcin/20.10.1913
- Beyer E, Paul D, Goodenough D. Connexin43: a protein from rat heart homologous to a gap junction protein from liver. *J Cell Biol.* (1987) 105:2621–9. doi: 10.1083/jcb.105.6.2621
- Dbouk H, Mroue R, El-Sabban M, Talhouk R. Connexins: a myriad of functions extending beyond assembly of gap junction channels. *Cell Commun Signal.* (2009) 7:4. doi: 10.1186/1478-811X-7-4
- Bennett M, Contreras J, Bukauskas F, Saez J. New roles for astrocytes: gap junction hemichannels have something to communicate. *Trends Neurosci.* (2003) 26:610–7. doi: 10.1016/j.tins.2003.09.008
- Cheung G, Chever O, Rouach N. Connexons and pannexons: newcomers in neurophysiology. *Front Cell Neurosci.* (2014) 8:348. doi: 10.3389/fncel.2014.00348
- Ye Z, Wyeth M, Baltan-Tekkok S, Ransom B. Functional hemichannels in astrocytes: a novel mechanism of glutamate release. *J Neurosci.* (2003) 23:3588–96.
- Valiunas V, Weingart R, Brink P. Formation of heterotypic gap junction channels by connexins 40 and 43. *Circ Res.* (2000) 86:E42–9. doi: 10.1161/01.res.86.2.e42
- Koval M, Molina S, Burt J. Mix and match: investigating heteromeric and heterotypic gap junction channels in model systems and native tissues. *FEBS Lett.* (2014) 588:1193–204. doi: 10.1016/j.febslet.2014.02.025
- Smith T, Mohankumar A, Minogue P, Beyer E, Berthoud V, Koval M. Cytoplasmic amino acids within the membrane interface region influence connexin oligomerization. *J Membr Biol.* (2012) 245:221–30. doi: 10.1007/s00232-012-9443-5
- Sohl G, Willecke K. An update on connexin genes and their nomenclature in mouse and man. *Cell Commun Adhes.* (2003) 10:173–80. doi: 10.1080/cac.10.4-6.173.180
- Willecke K, Eiberger J, Degen J, Eckardt D, Romualdi A, Guldenagel M, et al. Structural and functional diversity of connexin genes in the mouse and human genome. *Biol Chem.* (2002) 383:725–37. doi: 10.1515/BC.2002.076
- Aasen T, Johnstone S, Vidal-Brime L, Lynn K, Koval M. Connexins: synthesis, post-translational modifications, and trafficking in health and disease. *Int J Mol Sci.* (2018) 19:1296. doi: 10.3390/ijms19051296
- Salameh A. Life cycle of connexins: regulation of connexin synthesis and degradation. *Adv Cardiol.* (2006) 42:57–70. doi: 10.1159/000092562
- Segretain D, Falk M. Regulation of connexin biosynthesis, assembly, gap junction formation, and removal. *Biochim Biophys Acta.* (2004) 1662:3–21. doi: 10.1016/j.bbame.2004.01.007
- McCutcheon S, Stout R Jr, Spray D. The dynamic Nexus: gap junctions control protein localization and mobility in distinct and surprising ways. *Sci Rep.* (2020) 10:17011. doi: 10.1038/s41598-020-73892-6
- Rhett J, Gourdie R. The perinexus: a new feature of Cx43 gap junction organization. *Heart Rhythm.* (2012) 9:619–23. doi: 10.1016/j.hrthm.2011.10.003
- Catarino S, Ramalho J, Marques C, Pereira P, Girao H. Ubiquitin-mediated internalization of connexin43 is independent of the canonical endocytic tyrosine-sorting signal. *Biochem J.* (2011) 437:255–67. doi: 10.1042/BJ20102059
- Hesketh G, Shah M, Halperin V, Cooke C, Akar F, Yen T, et al. Ultrastructure and regulation of lateralized connexin43 in the failing heart. *Circ Res.* (2010) 106:1153–63. doi: 10.1161/CIRCRESAHA.108.182147
- Leithe E, Rivedal E. Ubiquitination and down-regulation of gap junction protein connexin-43 in response to 12-O-tetradecanoylphorbol 13-acetate treatment. *J Biol Chem.* (2004) 279:50089–96. doi: 10.1074/jbc.M402006200
- Beardslee M, Laing J, Beyer E, Saffitz J. Rapid turnover of connexin43 in the adult rat heart. *Circ Res.* (1998) 83:629–35. doi: 10.1161/01.res.83.6.629
- Gaietta G, Deerinck T, Adams S, Bouwer J, Tour O, Laird D, et al. Multicolor and electron microscopic imaging of connexin trafficking. *Science.* (2002) 296:503–7. doi: 10.1126/science.1068793
- Girao H, Catarino S, Pereira P. Eps15 interacts with ubiquitinated Cx43 and mediates its internalization. *Exp Cell Res.* (2009) 315:3587–97. doi: 10.1016/j.yexcr.2009.10.003
- Lichtenstein A, Minogue P, Beyer E, Berthoud V. Autophagy: a pathway that contributes to connexin degradation. *J Cell Sci.* (2011) 124:910–20. doi: 10.1242/jcs.073072
- Martins-Marques T, Catarino S, Zuzarte M, Marques C, Matafome P, Pereira P, et al. Ischaemia-induced autophagy leads to degradation of gap junction protein connexin43 in cardiomyocytes. *Biochem J.* (2015) 467:231–45. doi: 10.1042/BJ20141370
- Goodenough D. The crystalline lens: a system networked by gap junctional intercellular communication. *Semin Cell Biol.* (1992) 3:49–58. doi: 10.1016/s1043-4682(10)80007-8
- Kikuchi T, Kimura R, Paul D, Adams J. Gap junctions in the rat cochlea: immunohistochemical and ultrastructural analysis. *Anat Embryol.* (1995) 191:101–18. doi: 10.1007/BF00186783
- Lautermann J, ten Cate W, Altenhoff P, Grummer R, Traub O, Frank H, et al. Expression of the gap-junction connexins 26 and 30 in the rat cochlea. *Cell Tissue Res.* (1998) 294:415–20. doi: 10.1007/s004410051192
- Davis L, Rodefeld M, Green K, Beyer E, Saffitz J. Gap junction protein phenotypes of the human heart and conduction system. *J Cardiovasc Electrophysiol.* (1995) 6:813–22. doi: 10.1111/j.1540-8167.1995.tb00357.x
- Dupont E, Matsushita T, Kaba R, Vozzi C, Coppen S, Khan N, et al. Altered connexin expression in human congestive heart failure. *J Mol Cell Cardiol.* (2001) 33:359–71. doi: 10.1006/jmcc.2000.1308
- Greener I, Monfredi O, Inada S, Chandler N, Tellez J, Atkinson A, et al. Molecular architecture of the human specialised atrioventricular conduction axis. *J Mol Cell Cardiol.* (2011) 50:642–51. doi: 10.1016/j.jmcc.2010.12.017
- Kanagaratnam P, Rothery S, Patel P, Severs N, Peters N. Relative expression of immunolocalized connexins 40 and 43 correlates with human atrial conduction properties. *J Am Coll Cardiol.* (2002) 39:116–23. doi: 10.1016/s0735-1097(01)01710-7
- Kreuzberg M, Liebermann M, Segschneider S, Dobrowolski R, Dobrzynski H, Kaba R, et al. Human connexin31.9, unlike its orthologous protein connexin30.2 in the mouse, is not detectable in the human cardiac conduction system. *J Mol Cell Cardiol.* (2009) 46:553–9. doi: 10.1016/j.jmcc.2008.12.007
- Simon A, Goodenough D, Paul D. Mice lacking connexin40 have cardiac conduction abnormalities characteristic of atrioventricular block and bundle branch block. *Curr Biol.* (1998) 8:295–8. doi: 10.1016/s0960-9822(98)70113-7
- Vozzi C, Dupont E, Coppen S, Yeh H, Severs N. Chamber-related differences in connexin expression in the human heart. *J Mol Cell Cardiol.* (1999) 31:991–1003. doi: 10.1006/jmcc.1999.0937
- Kreuzberg M, Sohl G, Kim J, Verselis V, Willecke K, Bukauskas F. Functional properties of mouse connexin30.2 expressed in the conduction system of the heart. *Circ Res.* (2005) 96:1169–77. doi: 10.1161/01.RES.0000169271.33675.05
- Chandler N, Greener I, Tellez J, Inada S, Musa H, Molenaar P, et al. Molecular architecture of the human sinus node: insights into the function of the cardiac pacemaker. *Circulation.* (2009) 119:1562–75. doi: 10.1161/CIRCULATIONAHA.108.804369
- Kaba R, Coppen S, Dupont E, Skepper J, Elneil S, Haw M, et al. Comparison of connexin 43, 40 and 45 expression patterns in the developing human and mouse hearts. *Cell Commun Adhes.* (2001) 8:339–43. doi: 10.3109/15419060109080750
- Severs N, Bruce A, Dupont E, Rothery S. Remodelling of gap junctions and connexin expression in diseased myocardium. *Cardiovasc Res.* (2008) 80:9–19. doi: 10.1093/cvr/cvn133
- van Kempen M, ten Velde I, Wessels A, Oosthoek P, Gros D, Jongsma H, et al. Differential connexin distribution accommodates cardiac function in different species. *Microsc Res Tech.* (1995) 31:420–36. doi: 10.1002/jemt.1070310511
- Jan A, Amin S, Ratajczak P, Richard G, Sybert V. Genetic heterogeneity of KID syndrome: identification of a Cx30 gene (GJB6) mutation in a patient with KID syndrome and congenital atrichia. *J Invest Dermatol.* (2004) 122:1108–13. doi: 10.1111/j.0022-202X.2004.22518.x

46. Shanker V, Gupta M, Prashar A. Keratitis-Ichthyosis-Deafness syndrome: a rare congenital disorder. *Indian Dermatol Online J.* (2012) 3:48–50. doi: 10.4103/2229-5178.93505
47. Rabionet R, Zelante L, Lopez-Bigas N, D'Agruma L, Melchionda S, Restagno G, et al. Molecular basis of childhood deafness resulting from mutations in the GJB2 (connexin 26) gene. *Hum Genet.* (2000) 106:40–4. doi: 10.1007/s004390051007
48. Wingard J, Zhao H. Cellular and deafness mechanisms underlying connexin mutation-induced hearing loss – a common hereditary deafness. *Front Cell Neurosci.* (2015) 9:202. doi: 10.3389/fncel.2015.00202
49. De Bock M, Kerrebrouck M, Wang N, Leybaert L. Neurological manifestations of oculodentodigital dysplasia: a Cx43 channelopathy of the central nervous system? *Front Pharmacol.* (2013) 4:120. doi: 10.3389/fphar.2013.00120
50. Paznekas W, Boyadjiev S, Shapiro R, Daniels O, Wollnik B, Keegan C, et al. Connexin 43 (GJA1) mutations cause the pleiotropic phenotype of oculodentodigital dysplasia. *Am J Hum Genet.* (2003) 72:408–18. doi: 10.1086/346090
51. Cocozzelli A, White T. Connexin 43 Mutations Lead to Increased Hemichannel Functionality in Skin Disease. *Int J Mol Sci.* (2019) 20:6186. doi: 10.3390/ijms20246186
52. Abrams C, Scherer S, Flores-Obando R, Freidin M, Wong S, Lamantea E, et al. A new mutation in GJC2 associated with subclinical leukodystrophy. *J Neurol.* (2014) 261:1929–38. doi: 10.1007/s00415-014-7429-1
53. Quintanilla R, Orellana J, von Bernhardt R. Understanding risk factors for Alzheimer's disease: interplay of neuroinflammation, connexin-based communication and oxidative stress. *Arch Med Res.* (2012) 43:632–44. doi: 10.1016/j.arcmed.2012.10.016
54. Fromaget C, el Aoumari A, Gros D. Distribution pattern of connexin 43, a gap junctional protein, during the differentiation of mouse heart myocytes. *Differentiation.* (1992) 51:9–20. doi: 10.1111/j.1432-0436.1992.tb00675.x
55. van Kempen M, Fromaget C, Gros D, Moorman A, Lamers W. Spatial distribution of connexin43, the major cardiac gap junction protein, in the developing and adult rat heart. *Circ Res.* (1991) 68:1638–51. doi: 10.1161/01.res.68.6.1638
56. Cascio W, Yang H, Muller-Borer B, Johnson T. Ischemia-induced arrhythmia: the role of connexins, gap junctions, and attendant changes in impulse propagation. *J Electrocardiol.* (2005) 38:55–9. doi: 10.1016/j.jelectrocard.2005.06.019
57. Himelman E, Lillo M, Nouet J, Gonzalez J, Zhao Q, Xie L, et al. Prevention of connexin-43 remodeling protects against Duchenne muscular dystrophy cardiomyopathy. *J Clin Invest.* (2020) 130:1713–27. doi: 10.1172/JCI128190
58. Yan J, Killingsworth C, Walcott G, Zhu Y, Litovsky S, Huang J, et al. Molecular remodeling of Cx43, but not structural remodeling, promotes arrhythmias in an arrhythmogenic canine model of nonischemic heart failure. *J Mol Cell Cardiol.* (2021) 158:72–81. doi: 10.1016/j.yjmcc.2021.05.012
59. Johnstone S, Kroncke B, Straub A, Best A, Dunn C, Mitchell L, et al. MAPK phosphorylation of connexin 43 promotes binding of cyclin E and smooth muscle cell proliferation. *Circ Res.* (2012) 111:201–11. doi: 10.1161/CIRCRESAHA.112.272302
60. Lillo M, Himelman E, Shirokova N, Xie L, Fraidenraich D, Contreras J. S-nitrosylation of connexin43 hemichannels elicits cardiac stress-induced arrhythmias in Duchenne muscular dystrophy mice. *JCI Insight.* (2019) 4:e130091. doi: 10.1172/jci.insight.130091
61. Colussi C, Rosati J, Straino S, Spallotta F, Berni R, Stilli D, et al. Nepsilon-lysine acetylation determines dissociation from GAP junctions and lateralization of connexin 43 in normal and dystrophic heart. *Proc Natl Acad Sci U.S.A.* (2011) 108:2795–800. doi: 10.1073/pnas.1013124108
62. Kjenseth A, Fykerud T, Sirnes S, Bruun J, Yohannes Z, Kolberg M, et al. The gap junction channel protein connexin 43 is covalently modified and regulated by SUMOylation. *J Biol Chem.* (2012) 287:15851–61. doi: 10.1074/jbc.M111.281832
63. Lampe P, Lau A. The effects of connexin phosphorylation on gap junctional communication. *Int J Biochem Cell Biol.* (2004) 36:1171–86. doi: 10.1016/S1357-2725(03)00264-4
64. Saez J, Martinez A, Branes M, Gonzalez H. Regulation of gap junctions by protein phosphorylation. *Braz J Med Biol Res.* (1998) 31:593–600. doi: 10.1590/s0100-879x1998000500001
65. Straub A, Billaud M, Johnstone S, Best A, Yemen S, Dwyer S, et al. Compartmentalized connexin 43 s-nitrosylation/denitrosylation regulates heterocellular communication in the vessel wall. *Arterioscler Thromb Vasc Biol.* (2011) 31:399–407. doi: 10.1161/ATVBAHA.110.215939
66. Johnstone S, Ross J, Rizzo M, Straub A, Lampe P, Leitinger N, et al. Oxidized phospholipid species promote in vivo differential cx43 phosphorylation and vascular smooth muscle cell proliferation. *Am J Pathol.* (2009) 175:916–24. doi: 10.2353/ajpath.2009.090160
67. Solan J, Lampe P. Src Regulation of Cx43 Phosphorylation and Gap Junction Turnover. *Biomolecules.* (2020) 10:1596. doi: 10.3390/biom10121596
68. Bruzzone S, Guida L, Zocchi E, Franco L, De Flora A. Connexin 43 hemichannels mediate Ca<sup>2+</sup>-regulated transmembrane NAD<sup>+</sup> fluxes in intact cells. *FASEB J.* (2001) 15:10–2. doi: 10.1096/fj.00-0566fje
69. Vergara L, Bao X, Bello-Reuss E, Reuss L. Do connexin 43 gap-junctional hemichannels activate and cause cell damage during ATP depletion of renal-tubule cells? *Acta Physiol Scand.* (2003) 179:33–8. doi: 10.1046/j.1365-201X.2003.01198.x
70. Batra N, Riquelme M, Burra S, Jiang J. 14-3-3theta facilitates plasma membrane delivery and function of mechanosensitive connexin 43 hemichannels. *J Cell Sci.* (2014) 127:137–46. doi: 10.1242/jcs.133553
71. Obsilova V, Obsil T. Structural insights into the functional roles of 14-3-3 proteins. *Front Mol Biosci.* (2022) 9:1016071. doi: 10.3389/fmolb.2022.1016071
72. Yaffe M, Rittinger K, Volinia S, Caron P, Aitken A, Leffers H, et al. The structural basis for 14-3-3:phosphopeptide binding specificity. *Cell.* (1997) 91:961–71. doi: 10.1016/s0092-8674(00)80487-0
73. Falk M, Baker S, Gumpert A, Segretain D, Buckheit R III. Gap junction turnover is achieved by the internalization of small endocytic double-membrane vesicles. *Mol Biol Cell.* (2009) 20:3342–52. doi: 10.1091/mbc.E09-04-0288
74. Lauf U, Giepmans B, Lopez P, Braconnot S, Chen S, Falk M. Dynamic trafficking and delivery of connexons to the plasma membrane and accretion to gap junctions in living cells. *Proc Natl Acad Sci U.S.A.* (2002) 99:10446–51. doi: 10.1073/pnas.162055899
75. Dukic A, Gerbaud P, Guibourdenche J, Thiede B, Tasken K, Pidoux G. Ezrin-anchored PKA phosphorylates serine 369 and 373 on connexin 43 to enhance gap junction assembly, communication, and cell fusion. *Biochem J.* (2018) 475:455–76. doi: 10.1042/BCJ20170529
76. Thevenin A, Margraf R, Fisher C, Kells-Andrews R, Falk M. Phosphorylation regulates connexin43/ZO-1 binding and release, an important step in gap junction turnover. *Mol Biol Cell.* (2017) 28:3595–608. doi: 10.1091/mbc.E16-07-0496
77. Park D, Wallick C, Martyn K, Lau A, Jin C, Warn-Cramer B. Akt phosphorylates Connexin43 on Ser373, a "mode-1" binding site for 14-3-3. *Cell Commun Adhes.* (2007) 14:211–26. doi: 10.1080/15419060701755958
78. Giepmans B. Role of connexin43-interacting proteins at gap junctions. *Adv Cardiol.* (2006) 42:41–56. doi: 10.1159/000092561
79. Cooper C, Lampe P. Casein kinase 1 regulates connexin-43 gap junction assembly. *J Biol Chem.* (2002) 277:44962–8. doi: 10.1074/jbc.M209427200
80. Saidi Brikci-Nigassa A, Clement M, Ha-Duong T, Adjadj E, Ziani L, Pastre D, et al. Phosphorylation controls the interaction of the connexin43 C-terminal domain with tubulin and microtubules. *Biochemistry.* (2012) 51:4331–42. doi: 10.1021/bi201806j
81. Solan J, Marquez-Rosado L, Sorgen P, Thornton P, Gafken P, Lampe P. Phosphorylation at S365 is a gatekeeper event that changes the structure of Cx43 and prevents down-regulation by PKC. *J Cell Biol.* (2007) 179:1301–9. doi: 10.1083/jcb.200707060
82. Dunn C, Lampe P. Injury-triggered Akt phosphorylation of Cx43: a ZO-1-driven molecular switch that regulates gap junction size. *J Cell Sci.* (2014) 127:455–64. doi: 10.1242/jcs.142497
83. Leykauf K, Salek M, Bomke J, Frech M, Lehmann W, Durst M, et al. Ubiquitin protein ligase Nedd4 binds to connexin43 by a phosphorylation-modulated process. *J Cell Sci.* (2006) 119:3634–42. doi: 10.1242/jcs.03149
84. Auth T, Schluter S, Urschel S, Kussmann P, Sonntag S, Hoher T, et al. The TSG101 protein binds to connexins and is involved in connexin degradation. *Exp Cell Res.* (2009) 315:1053–62. doi: 10.1016/j.yexcr.2008.12.025
85. Fong J, Kells R, Falk M. Two tyrosine-based sorting signals in the Cx43 C-terminus cooperate to mediate gap junction endocytosis. *Mol Biol Cell.* (2013) 24:2834–48. doi: 10.1091/mbc.E13-02-0111
86. Nickel B, Boller M, Schneider K, Shakespeare T, Gay V, Murray S. Visualizing the effect of dynamin inhibition on annular gap vesicle formation and fission. *J Cell Sci.* (2013) 126:2607–16. doi: 10.1242/jcs.116269
87. Piehl M, Lehmann C, Gumpert A, Denizot J, Segretain D, Falk M. Internalization of large double-membrane intercellular vesicles by a clathrin-dependent endocytic process. *Mol Biol Cell.* (2007) 18:337–47. doi: 10.1091/mbc.e06-06-0487



88. Laing J, Tadros P, Westphale E, Beyer E. Degradation of connexin43 gap junctions involves both the proteasome and the lysosome. *Exp Cell Res.* (1997) 236:482–92. doi: 10.1006/excr.1997.3747
89. Nassal M, Werdich A, Wan X, Hoshi M, Deschenes I, Rosenbaum D, et al. Phosphorylation at Connexin43 Serine-368 Is Necessary for Myocardial Conduction During Metabolic Stress. *J Cardiovasc Electrophysiol.* (2016) 27:110–9. doi: 10.1111/jce.12833
90. Solan J, Lampe P. Specific Cx43 phosphorylation events regulate gap junction turnover in vivo. *FEBS Lett.* (2014) 588:1423–9. doi: 10.1016/j.febslet.2014.01.049
91. Kang M, Lin N, Li C, Meng Q, Zheng Y, Yan X, et al. Cx43 phosphorylation on S279/282 and intercellular communication are regulated by IP3/IP3 receptor signaling. *Cell Commun Signal.* (2014) 12:58. doi: 10.1186/s12964-014-0058-6
92. Warn-Cramer B, Cottrell G, Burt J, Lau A. Regulation of connexin-43 gap junctional intercellular communication by mitogen-activated protein kinase. *J Biol Chem.* (1998) 273:9188–96. doi: 10.1074/jbc.273.15.9188
93. Dowling C, Hayes S, Phelan J, Cathcart M, Finn S, Mehigan B, et al. Expression of protein kinase C gamma promotes cell migration in colon cancer. *Oncotarget.* (2017) 8:72096–107. doi: 10.18632/oncotarget.18916
94. Jarzabek K, Laudanski P, Dzieciol J, Dabrowska M, Wolczynski S. Protein kinase C involvement in proliferation and survival of breast cancer cells. *Folia Histochem Cytobiol.* (2002) 40:193–4.
95. Zhu T, Tsuji T, Chen C. Roles of PKC isoforms in the induction of apoptosis elicited by aberrant Ras. *Oncogene.* (2010) 29:1050–61. doi: 10.1038/ncr.2009.344
96. Steinberg S. Structural basis of protein kinase C isoform function. *Physiol Rev.* (2008) 88:1341–78. doi: 10.1152/physrev.00034.2007
97. Corbalan-Garcia S, Gomez-Fernandez J. Protein kinase C regulatory domains: the art of decoding many different signals in membranes. *Biochim Biophys Acta.* (2006) 1761:633–54. doi: 10.1016/j.bbap.2006.04.015
98. Kajimoto T, Caliman A, Tobias I, Okada T, Pilo C, Van An, et al. Activation of atypical protein kinase C by sphingosine 1-phosphate revealed by an aPKC-specific activity reporter. *Sci Signal.* (2019) 12:eaat6662. doi: 10.1126/scisignal.aat6662
99. Kang J, Toita R, Kim C, Katayama Y. Protein kinase C (PKC) isozyme-specific substrates and their design. *Biotechnol Adv.* (2012) 30:1662–72. doi: 10.1016/j.biotechadv.2012.07.004
100. Nishikawa K, Tokar A, Johannes F, Songyang Z, Cantley L. Determination of the specific substrate sequence motifs of protein kinase C isozymes. *J Biol Chem.* (1997) 272:952–60. doi: 10.1074/jbc.272.2.952
101. Ueda Y, Hirai S, Osada S, Suzuki A, Mizuno K, Ohno S. Protein kinase C activates the MEK-ERK pathway in a manner independent of Ras and dependent on Raf. *J Biol Chem.* (1996) 271:23512–9. doi: 10.1074/jbc.271.38.23512
102. Zhang J, Anastasiadis P, Liu Y, Thompson E, Fields A. Protein kinase C (PKC) betaII induces cell invasion through a Ras/ Mek-, PKC iota/Rac 1-dependent signaling pathway. *J Biol Chem.* (2004) 279:22118–23. doi: 10.1074/jbc.M400774200
103. Pan J, Fukuda K, Saito M, Matsuzaki J, Kodama H, Sano M, et al. Mechanical stretch activates the JAK/STAT pathway in rat cardiomyocytes. *Circ Res.* (1999) 84:1127–36. doi: 10.1161/01.res.84.10.1127
104. Baldwin R, Garratt-Lalonde M, Parolin D, Krzyzanowski P, Andrade M, Lorimer I. Protection of glioblastoma cells from cisplatin cytotoxicity via protein kinase Ciota-mediated attenuation of p38 MAP kinase signaling. *Oncogene.* (2006) 25:2909–19. doi: 10.1038/sj.onc.1209312
105. Mao M, Fang X, Lu Y, Lapushin R, Bast R Jr, Mills G. Inhibition of growth-factor-induced phosphorylation and activation of protein kinase B/Akt by atypical protein kinase C in breast cancer cells. *Biochem J.* (2000) 352:475–82.
106. Yi P, Feng Q, Amazil L, Lonard D, Tsai S, Tsai M, et al. Atypical protein kinase C regulates dual pathways for degradation of the oncogenic coactivator SRC-3/AIB1. *Mol Cell.* (2008) 29:465–76. doi: 10.1016/j.molcel.2007.12.030
107. Lampe P, TenBroek E, Burt J, Kurata W, Johnson R, Lau A. Phosphorylation of connexin43 on serine368 by protein kinase C regulates gap junctional communication. *J Cell Biol.* (2000) 149:1503–12. doi: 10.1083/jcb.149.7.1503
108. Bao X, Altenberg G, Reuss L. Mechanism of regulation of the gap junction protein connexin 43 by protein kinase C-mediated phosphorylation. *Am J Physiol Cell Physiol.* (2004) 286:C647–54. doi: 10.1152/ajpcell.00295.2003
109. Goel G, Makkar H, Francis G, Becker K. Phorbol esters: structure, biological activity, and toxicity in animals. *Int J Toxicol.* (2007) 26:279–88. doi: 10.1080/10915810701464641
110. Mochly-Rosen D, Das K, Grimes K. Protein kinase C, an elusive therapeutic target? *Nat Rev Drug Discov.* (2012) 11:937–57. doi: 10.1038/nrd3871
111. Ek-Vitorin J, King T, Heyman N, Lampe P, Burt J. Selectivity of connexin 43 channels is regulated through protein kinase C-dependent phosphorylation. *Circ Res.* (2006) 98:1498–505. doi: 10.1161/01.RES.0000227572.45891.2c
112. Bao X, Lee S, Reuss L, Altenberg G. Change in permeant size selectivity by phosphorylation of connexin 43 gap-junctional hemichannels by PKC. *Proc Natl Acad Sci U.S.A.* (2007) 104:4919–24. doi: 10.1073/pnas.0603154104
113. Hansen D, Braunstein T, Nielsen M, MacAulay N. Distinct permeation profiles of the connexin 30 and 43 hemichannels. *FEBS Lett.* (2014) 588:1446–57. doi: 10.1016/j.febslet.2014.01.036
114. Bao X, Reuss L, Altenberg G. Regulation of purified and reconstituted connexin 43 hemichannels by protein kinase C-mediated phosphorylation of Serine 368. *J Biol Chem.* (2004) 279:20058–66. doi: 10.1074/jbc.M311137200
115. Ohmori S, Shirai Y, Sakai N, Fujii M, Konishi H, Kikkawa U, et al. Three distinct mechanisms for translocation and activation of the delta subtypes of protein kinase C. *Mol Cell Biol.* (1998) 18:5263–71. doi: 10.1128/MCB.18.9.5263
116. Reynolds N, Baldassare J, Henderson P, Shuler J, Ballas L, Burns D, et al. Translocation and downregulation of protein kinase C isoenzymes-alpha and -epsilon by phorbol ester and bryostatin-1 in human keratinocytes and fibroblasts. *J Invest Dermatol.* (1994) 103:364–9. doi: 10.1111/1523-1747.ep12394957
117. Lu Z, Liu D, Hornia A, Devonish W, Pagano M, Foster D. Activation of protein kinase C triggers its ubiquitination and degradation. *Mol Cell Biol.* (1998) 18:839–45. doi: 10.1128/MCB.18.2.839
118. Young S, Parker P, Ullrich A, Stabel S. Down-regulation of protein kinase C is due to an increased rate of degradation. *Biochem J.* (1987) 244:775–9. doi: 10.1042/bj2440775
119. Leithe E, Cruciani V, Sanner T, Mikalsen S, Rivedal E. Recovery of gap junctional intercellular communication after phorbol ester treatment requires proteasomal degradation of protein kinase C. *Carcinogenesis.* (2003) 24:1239–45. doi: 10.1093/carcin/bgg066
120. Cone A, Cavin G, Ambrosi C, Hakozaki H, Wu-Zhang A, Kunkel M, et al. Protein kinase Cdelta-mediated phosphorylation of Connexin43 gap junction channels causes movement within gap junctions followed by vesicle internalization and protein degradation. *J Biol Chem.* (2014) 289:8781–98. doi: 10.1074/jbc.M113.533265
121. Niger C, Hebert C, Stains J. Interaction of connexin43 and protein kinase C-delta during FGF2 signaling. *BMC Biochem.* (2010) 11:14. doi: 10.1186/1471-2091-11-14
122. Doble B, Ping P, Kardami E. The epsilon subtype of protein kinase C is required for cardiomyocyte connexin-43 phosphorylation. *Circ Res.* (2000) 86:293–301. doi: 10.1161/01.res.86.3.293
123. Doble B, Chen Y, Bosc D, Litchfield D, Kardami E. Fibroblast growth factor-2 decreases metabolic coupling and stimulates phosphorylation as well as masking of connexin43 epitopes in cardiac myocytes. *Circ Res.* (1996) 79:647–58. doi: 10.1161/01.res.79.4.647
124. Dhein S. Cardiac ischemia and uncoupling: gap junctions in ischemia and infarction. *Adv Cardiol.* (2006) 42:198–212. doi: 10.1159/000092570
125. Ishida T, Yanimizu K, Gute D, Korthuis R. Mechanisms of ischemic preconditioning. *Shock.* (1997) 8:86–94. doi: 10.1097/00024382-199708000-00003
126. Iliodromitis E, Lazou A, Kremastinos D. Ischemic preconditioning: protection against myocardial necrosis and apoptosis. *Vasc Health Risk Manag.* (2007) 3:629–37.
127. Naitoh K, Yano T, Miura T, Itoh T, Miki T, Tanno M, et al. Roles of Cx43-associated protein kinases in suppression of gap junction-mediated chemical coupling by ischemic preconditioning. *Am J Physiol Heart Circ Physiol.* (2009) 296:H396–403. doi: 10.1152/ajpheart.00448.2008
128. Srisakuldee W, Nickel B, Fandrich R, Jiang Z, Kardami E. Administration of FGF-2 to the heart stimulates connexin-43 phosphorylation at protein kinase C target sites. *Cell Commun Adhes.* (2006) 13:13–9. doi: 10.1080/15419060600631326
129. Zou J, Yue X, Zheng S, Zhang G, Chang H, Liao Y, et al. Cholesterol modulates function of connexin 43 gap junction channel via PKC pathway in H9c2 cells. *Biochim Biophys Acta.* (2014) 1838:2019–25. doi: 10.1016/j.bbame.2014.04.016
130. Liao C, Cheng H, Wang S, Yeih D, Wang S. PKCvarepsilon mediates serine phosphorylation of connexin43 induced by lysophosphatidylcholine in neonatal rat cardiomyocytes. *Toxicology.* (2013) 314:11–21. doi: 10.1016/j.tox.2013.08.001
131. Srisakuldee W, Makazan Z, Nickel B, Zhang F, Thliveris J, Pasumarthi K, et al. The FGF-2-triggered protection of cardiac subsarcolemmal mitochondria from calcium overload is mitochondrial connexin 43-dependent. *Cardiovasc Res.* (2014) 103:72–80. doi: 10.1093/cvr/cvu066

132. De Smet M, Lissoni A, Nezlobinsky T, Wang N, Dries E, Perez-Hernandez M, et al. Cx43 hemichannel microdomain signaling at the intercalated disc enhances cardiac excitability. *J Clin Invest.* (2021) 131:e137752. doi: 10.1172/JCI137752
133. Contreras J, Sanchez H, Eugenin E, Speidel D, Theis M, Willecke K, et al. Metabolic inhibition induces opening of unapposed connexin 43 gap junction hemichannels and reduces gap junctional communication in cortical astrocytes in culture. *Proc Natl Acad Sci U.S.A.* (2002) 99:495–500. doi: 10.1073/pnas.012589799
134. Lissoni A, Hulpiau P, Martins-Marques T, Wang N, Bultynck G, Schulz R, et al. RyR2 regulates Cx43 hemichannel intracellular Ca<sup>2+</sup>-dependent activation in cardiomyocytes. *Cardiovasc Res.* (2021) 117:123–36. doi: 10.1093/cvr/cvz340
135. Schalper K, Sanchez H, Lee S, Altenberg G, Nathanson M, Saez J. Connexin 43 hemichannels mediate the Ca<sup>2+</sup> influx induced by extracellular alkalization. *Am J Physiol Cell Physiol.* (2010) 299:C1504–15. doi: 10.1152/ajpcell.00015.2010
136. Waza A, Andrabi K, Hussain M. Protein kinase C (PKC) mediated interaction between connexin43 (Cx43) and K<sup>+</sup>(ATP) channel subunit (Kir6.1) in cardiomyocyte mitochondria: implications in cytoprotection against hypoxia induced cell apoptosis. *Cell Signal.* (2014) 26:1909–17. doi: 10.1016/j.cellsig.2014.05.002
137. Hirschhauser C, Lissoni A, Gorge P, Lampe P, Heger J, Schluter K, et al. Connexin 43 phosphorylation by casein kinase 1 is essential for the cardioprotection by ischemic preconditioning. *Basic Res Cardiol.* (2021) 116:21. doi: 10.1007/s00395-021-00861-z
138. Yevseyenkov V, Das S, Lin D, Willard L, Davidson H, Sitaramayya A, et al. Loss of protein kinase Cgamma in knockout mice and increased retinal sensitivity to hyperbaric oxygen. *Arch Ophthalmol.* (2009) 127:500–6. doi: 10.1001/archophthalmol.2009.31
139. Zhang B, Li Z, Zhang R, Hu Y, Jiang Y, Cao T, et al. PKCgamma promotes axonal remodeling in the cortico-spinal tract via GSK3beta/beta-catenin signaling after traumatic brain injury. *Sci Rep.* (2019) 9:17078. doi: 10.1038/s41598-019-53225-y
140. Aslam N, Alvi F. Simplified Model of PKCgamma Signaling Dysregulation and Cytosol-to-Membrane Translocation Kinetics During Neurodegenerative Spinocerebellar Ataxia Type 14 (SCA14). *Front Neurosci.* (2019) 13:1397. doi: 10.3389/fnins.2019.01397
141. Lin D, Takemoto D. Oxidative activation of protein kinase Cgamma through the C1 domain. Effects on gap junctions. *J Biol Chem.* (2005) 280:13682–93. doi: 10.1074/jbc.M407762200
142. Akoyev V, Takemoto D. ZO-1 is required for protein kinase C gamma-driven disassembly of connexin 43. *Cell Signal.* (2007) 19:958–67. doi: 10.1016/j.cellsig.2006.11.007
143. Lin D, Boyle D, Takemoto D. IGF-I-induced phosphorylation of connexin 43 by PKCgamma: regulation of gap junctions in rabbit lens epithelial cells. *Invest Ophthalmol Vis Sci.* (2003) 44:1160–8. doi: 10.1167/iovs.02-0737
144. Husoy T, Cruciani V, Sanner T, Mikalsen S. Phosphorylation of connexin43 and inhibition of gap junctional communication in 12-O-tetradecanoylphorbol-13-acetate-exposed R6 fibroblasts: minor role of protein kinase C beta I and mu. *Carcinogenesis.* (2001) 22:221–31. doi: 10.1093/carcin/22.2.221
145. Fagerberg L, Hallstrom B, Oksvold P, Kampf C, Djureinovic D, Odeberg J, et al. Analysis of the human tissue-specific expression by genome-wide integration of transcriptomics and antibody-based proteomics. *Mol Cell Proteomics.* (2014) 13:397–406. doi: 10.1074/mcp.M113.035600
146. Mahoney V, Mezzano V, Mirams G, Maass K, Li Z, Cerrone M, et al. Connexin43 contributes to electrotonic conduction across scar tissue in the intact heart. *Sci Rep.* (2016) 6:26744. doi: 10.1038/srep26744
147. Eloff B, Lerner D, Yamada K, Schuessler R, Saffitz J, Rosenbaum D. High resolution optical mapping reveals conduction slowing in connexin43 deficient mice. *Cardiovasc Res.* (2001) 51:681–90. doi: 10.1016/s0008-6363(01)00341-8
148. Gutstein D, Morley G, Tamaddon H, Vaidya D, Schneider M, Chen J, et al. Conduction slowing and sudden arrhythmic death in mice with cardiac-restricted inactivation of connexin43. *Circ Res.* (2001) 88:333–9. doi: 10.1161/01.res.88.3.333
149. Peters N, Coromilas J, Severs N, Wit A. Disturbed connexin43 gap junction distribution correlates with the location of reentrant circuits in the epicardial border zone of healing canine infarcts that cause ventricular tachycardia. *Circulation.* (1997) 95:988–96. doi: 10.1161/01.cir.95.4.988
150. Jabr R, Hatch F, Salvage S, Orlowski A, Lampe P, Fry C. Regulation of gap junction conductance by calcineurin through Cx43 phosphorylation: implications for action potential conduction. *Pflugers Arch.* (2016) 468:1945–55. doi: 10.1007/s00424-016-1885-7
151. Remo B, Qu J, Volpicelli F, Giovannone S, Shin D, Lader J, et al. Phosphatase-resistant gap junctions inhibit pathological remodeling and prevent arrhythmias. *Circ Res.* (2011) 108:1459–66. doi: 10.1161/CIRCRESAHA.111.244046
152. Reaume A, de Sousa P, Kulkarni S, Langille B, Zhu D, Davies T, et al. Cardiac malformation in neonatal mice lacking connexin43. *Science.* (1995) 267:1831–4. doi: 10.1126/science.7892609
153. Gong X, Shao Q, Langlois S, Bai D, Laird D. Differential potency of dominant negative connexin43 mutants in oculodentodigital dysplasia. *J Biol Chem.* (2007) 282:19190–202. doi: 10.1074/jbc.M609653200
154. Hichri E, Abriel H, Kucera J. Distribution of cardiac sodium channels in clusters potentiates ephaptic interactions in the intercalated disc. *J Physiol.* (2018) 596:563–89. doi: 10.1113/jp275351
155. Kucera J, Rohr S, Rudy Y. Localization of sodium channels in intercalated disks modulates cardiac conduction. *Circ Res.* (2002) 91:1176–82. doi: 10.1161/01.res.0000046237.54156.0a
156. Mori Y, Fishman G, Peskin C. Ephaptic conduction in a cardiac strand model with 3D electrodiffusion. *Proc Natl Acad Sci U.S.A.* (2008) 105:6463–8. doi: 10.1073/pnas.0801089105
157. Veeraraghavan R, Lin J, Hoeker G, Keener J, Gourdie R, Poelzing S. Sodium channels in the Cx43 gap junction perinexus may constitute a cardiac ephapse: an experimental and modeling study. *Pflugers Arch.* (2015) 467:2093–105. doi: 10.1007/s00424-014-1675-z
158. Brackenbury W, Isom L. Na channel beta subunits: overachievers of the ion channel family. *Front Pharmacol.* (2011) 2:53. doi: 10.3389/fphar.2011.00053
159. Veeraraghavan R, Hoeker G, Alvarez-Laviada A, Hoagland D, Wan X, King D, et al. The adhesion function of the sodium channel beta subunit (beta1) contributes to cardiac action potential propagation. *eLife.* (2018) 7:e37610. doi: 10.7554/eLife.37610
160. Jansen J, Noorman M, Musa H, Stein M, de Jong S, van der Nagel R, et al. Reduced heterogeneous expression of Cx43 results in decreased Nav1.5 expression and reduced sodium current that accounts for arrhythmia vulnerability in conditional Cx43 knockout mice. *Heart Rhythm.* (2012) 9:600–7. doi: 10.1016/j.hrthm.2011.11.025
161. Gourdie R. The Cardiac Gap Junction has Discrete Functions in Electrotonic and Ephaptic Coupling. *Anat Rec.* (2019) 302:93–100. doi: 10.1002/ar.24036
162. Fontes M, van Veen T, de Bakker J, van Rijen H. Functional consequences of abnormal Cx43 expression in the heart. *Biochim Biophys Acta.* (2012) 1818:2020–9. doi: 10.1016/j.bbame.2011.07.039
163. Delorme B, Dahl E, Jarry-Guichard T, Briand J, Willecke K, Gros D, et al. Expression pattern of connexin gene products at the early developmental stages of the mouse cardiovascular system. *Circ Res.* (1997) 81:423–37. doi: 10.1161/01.res.81.3.423
164. King T, Lampe P. Temporal regulation of connexin phosphorylation in embryonic and adult tissues. *Biochim Biophys Acta.* (2005) 1719:24–35. doi: 10.1016/j.bbame.2005.07.010
165. Carracedo S, Braun U, Leitges M. Expression pattern of protein kinase C during mouse embryogenesis. *BMC Dev Biol.* (2013) 13:16. doi: 10.1186/1471-213X-13-16
166. Shin H, Barnett J, Chang P, Reddy S, Drinkwater D, Pierson R, et al. Molecular heterogeneity of protein kinase C expression in human ventricle. *Cardiovasc Res.* (2000) 48:285–99. doi: 10.1016/s0008-6363(00)00185-1
167. Shao C, Wang J, Tian J, Tang Y. Coronary artery disease: from mechanism to clinical practice. *Adv Exp Med Biol.* (2020) 1177:1–36. doi: 10.1007/978-981-15-2517-9\_1
168. Khan M, Hashim M, Mustafa H, Baniyas M, Al Suwaidi S, AlKatheeri R, et al. Global epidemiology of ischemic heart disease: results from the Global Burden of Disease Study. *Cureus.* (2020) 12:e9349. doi: 10.7759/cureus.9349
169. Johansen D, Cruciani V, Sundset R, Ytrehus K, Mikalsen S. Ischemia induces closure of gap junctional channels and opening of hemichannels in heart-derived cells and tissue. *Cell Physiol Biochem.* (2011) 28:103–14. doi: 10.1159/000331719
170. Martins-Marques T, Catarino S, Marques C, Matafome P, Ribeiro-Rodrigues T, Baptista R, et al. Heart ischemia results in connexin43 ubiquitination localized at the intercalated discs. *Biochimie.* (2015) 112:196–201. doi: 10.1016/j.biochi.2015.02.020
171. Kleber A, Janse M, Wilms-Schopmann F, Wilde A, Coronel R. Changes in conduction velocity during acute ischemia in ventricular myocardium of the isolated porcine heart. *Circulation.* (1986) 73:189–98. doi: 10.1161/01.cir.73.1.189
172. Park D, Freitas T, Wallick C, Guyette C, Warn-Cramer B. Molecular dynamics and in vitro analysis of Connexin43: a new 14-3-3 mode-1 interacting protein. *Protein Sci.* (2006) 15:2344–55. doi: 10.1110/ps.062172506



173. Smyth J, Zhang S, Sanchez J, Lamouille S, Vogan J, Hesketh G, et al. A 14-3-3 mode-1 binding motif initiates gap junction internalization during acute cardiac ischemia. *Traffic*. (2014) 15:684–99. doi: 10.1111/tra.12169
174. Shintani-Ishida K, Unuma K, Yoshida K. Ischemia enhances translocation of connexin43 and gap junction intercellular communication, thereby propagating contraction band necrosis after reperfusion. *Circ J*. (2009) 73:1661–8. doi: 10.1253/circj.cj-09-0079
175. Axelsen L, Stahlhut M, Mohammed S, Larsen B, Nielsen M, Holstein-Rathlou N, et al. Identification of ischemia-regulated phosphorylation sites in connexin43: a possible target for the antiarrhythmic peptide analogue rotigaptide (ZP123). *J Mol Cell Cardiol*. (2006) 40:790–8. doi: 10.1016/j.yjmcc.2006.03.005
176. Albert C, Ford D. Protein kinase C translocation and PKC-dependent protein phosphorylation during myocardial ischemia. *Am J Physiol*. (1999) 276:H642–50. doi: 10.1152/ajpheart.1999.276.2.H642
177. Palatinus J, Rhett J, Gourdie R. Enhanced PKCepsilon mediated phosphorylation of connexin43 at serine 368 by a carboxyl-terminal mimetic peptide is dependent on injury. *Channels*. (2011) 5:236–40. doi: 10.4161/chan.5.3.15834
178. O'Quinn M, Palatinus J, Harris B, Hewett K, Gourdie R. A peptide mimetic of the connexin43 carboxyl terminus reduces gap junction remodeling and induced arrhythmia following ventricular injury. *Circ Res*. (2011) 108:704–15. doi: 10.1161/CIRCRESAHA.110.235747
179. Ping P, Zhang J, Qiu Y, Tang X, Manchikalapudi S, Cao X, et al. Ischemic preconditioning induces selective translocation of protein kinase C isoforms epsilon and eta in the heart of conscious rabbits without subcellular redistribution of total protein kinase C activity. *Circ Res*. (1997) 81:404–14. doi: 10.1161/01.res.81.3.404
180. Srisakuldee W, Jeyaraman M, Nickel B, Tanguy S, Jiang Z, Kardami E. Phosphorylation of connexin-43 at serine 262 promotes a cardiac injury-resistant state. *Cardiovasc Res*. (2009) 83:672–81. doi: 10.1093/cvr/cvp142
181. Cooper L Jr. Myocarditis. *N Engl J Med*. (2009) 360:1526–38. doi: 10.1056/NEJMra0800028
182. Wang X, Bu X, Wei L, Liu J, Yang D, Mann D, et al. Global, regional, and national burden of myocarditis From 1990 to 2017: a systematic analysis based on the global burden of disease study 2017. *Front Cardiovasc Med*. (2021) 8:692990. doi: 10.3389/fcvm.2021.692990
183. Lynge T, Nielsen T, Gregers Winkel B, Tfelt-Hansen J, Banner J. Sudden cardiac death caused by myocarditis in persons aged 1–49 years: a nationwide study of 14 294 deaths in Denmark. *Forensic Sci Res*. (2019) 4:247–56. doi: 10.1080/20961790.2019.1595352
184. Zhong C, Chang H, Wu Y, Zhou L, Wang Y, Wang M, et al. Up-regulated Cx43 phosphorylation at Ser368 prolongs QRS duration in myocarditis. *J Cell Mol Med*. (2018) 22:3537–47. doi: 10.1111/jcmm.13631
185. Butta C, Zappia L, Larterra G, Roberto M. Diagnostic and prognostic role of electrocardiogram in acute myocarditis: a comprehensive review. *Ann Noninvasive Electrophysiol*. (2020) 25:e12726. doi: 10.1111/anec.12726
186. Zhong C, Wu Y, Chang H, Liu C, Zhou L, Zou J, et al. Effect of PKC inhibitor on experimental autoimmune myocarditis in Lewis rats. *Oncotarget*. (2017) 8:54187–98. doi: 10.18632/oncotarget.17018
187. Maron B, Maron M. Hypertrophic cardiomyopathy. *Lancet*. (2013) 381:242–55. doi: 10.1016/S0140-6736(12)60397-3
188. Tuohy C, Kaul S, Song H, Nazer B, Heitner S. Hypertrophic cardiomyopathy: the future of treatment. *Eur J Heart Fail*. (2020) 22:228–40. doi: 10.1002/ehf.1715
189. Bowman J, Steinberg S, Jiang T, Geenen D, Fishman G, Buttrick P. Expression of protein kinase C beta in the heart causes hypertrophy in adult mice and sudden death in neonates. *J Clin Invest*. (1997) 100:2189–95. doi: 10.1172/JCI119755
190. Braz J, Bueno O, De Windt L, Molkentin J. PKC alpha regulates the hypertrophic growth of cardiomyocytes through extracellular signal-regulated kinase1/2 (ERK1/2). *J Cell Biol*. (2002) 156:905–19. doi: 10.1083/jcb.200108062
191. Bowling N, Walsh R, Song G, Estridge T, Sandusky G, Fouts R, et al. Increased protein kinase C activity and expression of Ca<sup>2+</sup>-sensitive isoforms in the failing human heart. *Circulation*. (1999) 99:384–91. doi: 10.1161/01.cir.99.3.384
192. Neshati Z, Schallij M, de Vries A. The proarrhythmic features of pathological cardiac hypertrophy in neonatal rat ventricular cardiomyocyte cultures. *J Appl Physiol*. (2020) 128:545–53. doi: 10.1152/jappphysiol.00420.2019
193. Jin H, Chemaly E, Lee A, Kho C, Hadri L, Hajjar R, et al. Mechanoelectrical remodeling and arrhythmias during progression of hypertrophy. *FASEB J*. (2010) 24:451–63. doi: 10.1096/fj.09-136622
194. Sasano C, Honjo H, Takagishi Y, Uzzaman M, Emdad L, Shimizu A, et al. Internalization and dephosphorylation of connexin43 in hypertrophied right ventricles of rats with pulmonary hypertension. *Circ J*. (2007) 71:382–9. doi: 10.1253/circj.71.382
195. Pathak A, del Monte F, Zhao W, Schultz J, Lorenz J, Bodi I, et al. Enhancement of cardiac function and suppression of heart failure progression by inhibition of protein phosphatase 1. *Circ Res*. (2005) 96:756–66. doi: 10.1161/01.RES.0000161256.85833.f
196. Jeyaraman M, Tanguy S, Fandrich R, Lukas A, Kardami E. Ischemia-induced dephosphorylation of cardiomyocyte connexin-43 is reduced by okadaic acid and calyculin A but not fostriecin. *Mol Cell Biochem*. (2003) 242:129–34.
197. Shan H, Wei J, Zhang M, Lin L, Yan R, Zhang R, et al. Suppression of PKCepsilon-mediated mitochondrial connexin 43 phosphorylation at serine 368 is involved in myocardial mitochondrial dysfunction in a rat model of dilated cardiomyopathy. *Mol Med Rep*. (2015) 11:4720–6. doi: 10.3892/mmr.2015.3260
198. Jefferies J, Towbin J. Dilated cardiomyopathy. *Lancet*. (2010) 375:752–62. doi: 10.1016/S0140-6736(09)62023-7
199. Savarese G, Lund L. Global public health burden of heart failure. *Card Fail Rev*. (2017) 3:7–11.
200. Kemp C, Conte J. The pathophysiology of heart failure. *Cardiovasc Pathol*. (2012) 21:365–71. doi: 10.1016/j.carpath.2011.11.007
201. Rewiuk K, Wizner B, Fedyk-Lukasik M, Zdrojewski T, Opolski G, Dubiel J, et al. Epidemiology and management of coexisting heart failure and atrial fibrillation in an outpatient setting. *Pol Arch Med Wewn*. (2011) 121:392–9.
202. Santangeli P, Rame J, Birati E, Marchlinski F. Management of Ventricular Arrhythmias in Patients With Advanced Heart Failure. *J Am Coll Cardiol*. (2017) 69:1842–60. doi: 10.1016/j.jacc.2017.01.047
203. Elvan A, Huang X, Pressler M, Zipes D. Radiofrequency catheter ablation of the atria eliminates pacing-induced sustained atrial fibrillation and reduces connexin 43 in dogs. *Circulation*. (1997) 96:1675–85. doi: 10.1161/01.cir.96.5.1675
204. Haugan K, Miyamoto T, Takeishi Y, Kubota I, Nakayama J, Shimojo H, et al. Rotigaptide (ZP123) improves atrial conduction slowing in chronic volume overload-induced dilated atria. *Basic Clin Pharmacol Toxicol*. (2006) 99:71–9. doi: 10.1111/j.1742-7843.2006.pto\_432.x
205. Akar F, Nass R, Hahn S, Cingolani E, Shah M, Hesketh G, et al. Dynamic changes in conduction velocity and gap junction properties during development of pacing-induced heart failure. *Am J Physiol Heart Circ Physiol*. (2007) 293:H1223–30. doi: 10.1152/ajpheart.00079.2007
206. Burstein B, Comtois P, Michael G, Nishida K, Villeneuve L, Yeh Y, et al. Changes in connexin expression and the atrial fibrillation substrate in congestive heart failure. *Circ Res*. (2009) 105:1213–22. doi: 10.1161/CIRCRESAHA.108.183400
207. Gonzalez J, Ramachandran J, Xie L, Contreras J, Fraidenraich D. Selective Connexin43 Inhibition Prevents Isoproterenol-Induced Arrhythmias and Lethality in Muscular Dystrophy Mice. *Sci Rep*. (2015) 5:13490. doi: 10.1038/srep13490
208. Seidel T, Salameh A, Dhein S. A simulation study of cellular hypertrophy and connexin lateralization in cardiac tissue. *Biophys J*. (2010) 99:2821–30. doi: 10.1016/j.bpj.2010.09.010
209. Severs N, Dupont E, Coppen S, Halliday D, Inett E, Baylis D, et al. Remodelling of gap junctions and connexin expression in heart disease. *Biochim Biophys Acta*. (2004) 1662:138–48. doi: 10.1016/j.bbame.2003.10.019
210. Severs N, Coppen S, Dupont E, Yeh H, Ko Y, Matsushita T. Gap junction alterations in human cardiac disease. *Cardiovasc Res*. (2004) 62:368–77. doi: 10.1016/j.cardiores.2003.12.007
211. Wang N, De Bock M, Antoons G, Gadicherla A, Bol M, Decrock E, et al. Connexin mimetic peptides inhibit Cx43 hemichannel opening triggered by voltage and intracellular Ca<sup>2+</sup> elevation. *Basic Res Cardiol*. (2012) 107:304. doi: 10.1007/s00395-012-0304-2
212. Antoons G, Willems R, Sipido K. Alternative strategies in arrhythmia therapy: evaluation of Na/Ca exchange as an anti-arrhythmic target. *Pharmacol Ther*. (2012) 134:26–42. doi: 10.1016/j.pharmthera.2011.12.001
213. Landstrom A, Dobrev D, Wehrens X. Calcium Signaling and Cardiac Arrhythmias. *Circ Res*. (2017) 120:1969–93. doi: 10.1161/CIRCRESAHA.117.310083
214. Reggiani C. Caffeine as a tool to investigate sarcoplasmic reticulum and intracellular calcium dynamics in human skeletal muscles. *J Muscle Res Cell Motil*. (2021) 42:281–9. doi: 10.1007/s10974-020-09574-7
215. Nigro G, Comi L, Politano L, Bain R. The incidence and evolution of cardiomyopathy in Duchenne muscular dystrophy. *Int J Cardiol*. (1990) 26:271–7. doi: 10.1016/0167-5273(90)90082-g

216. Kim J, Perez-Hernandez M, Alvarado F, Maurya S, Montnach J, Yin Y, et al. Disruption of Ca(2+)<sub>i</sub> Homeostasis and Connexin 43 Hemichannel Function in the Right Ventricle Precedes Overt Arrhythmogenic Cardiomyopathy in Plakophilin-2-Deficient Mice. *Circulation*. (2019) 140:1015–30. doi: 10.1161/CIRCULATIONAHA.119.039710
217. Cadrin-Tourigny J, Bosman L, Wang W, Tadros R, Bhonsale A, Bourfiss M, et al. Sudden cardiac death prediction in arrhythmogenic right ventricular cardiomyopathy: a multinational collaboration. *Circ Arrhythm Electrophysiol*. (2021) 14:e008509. doi: 10.1161/CIRCEP.120.008509
218. Falk M, Bell C, Kells Andrews R, Murray S. Molecular mechanisms regulating formation, trafficking and processing of annular gap junctions. *BMC Cell Biol*. (2016) 17(Suppl. 1):22. doi: 10.1186/s12860-016-0087-7
219. van Opbergen C, Sall J, Petzold C, Dancel-Manning K, Delmar M, Liang F. “Orphan” Connexin43 in Plakophilin-2 Deficient Hearts Revealed by Volume Electron Microscopy. *Front Cell Dev Biol*. (2022) 10:843687. doi: 10.3389/fcell.2022.843687
220. Kaplan S, Gard J, Protonotarios N, Tsatsopoulou A, Spiliopoulou C, Anastasakis A, et al. Remodeling of myocyte gap junctions in arrhythmogenic right ventricular cardiomyopathy due to a deletion in plakoglobin (Naxos disease). *Heart Rhythm*. (2004) 1:3–11. doi: 10.1016/j.hrthm.2004.01.001
221. Lyon R, Mezzano V, Wright A, Pfeiffer E, Chuang J, Banares K, et al. Connexin defects underlie arrhythmogenic right ventricular cardiomyopathy in a novel mouse model. *Hum Mol Genet*. (2014) 23:1134–50. doi: 10.1093/hmg/ddt508
222. Desplantez T, McCain M, Beauchamp P, Rigoli G, Rothen-Rutishauser B, Parker K, et al. Connexin43 ablation in foetal atrial myocytes decreases electrical coupling, partner connexins, and sodium current. *Cardiovasc Res*. (2012) 94:58–65. doi: 10.1093/cvr/cvs025
223. Sato P, Musa H, Coombs W, Guerrero-Serna G, Patino G, Taffet S, et al. Loss of plakophilin-2 expression leads to decreased sodium current and slower conduction velocity in cultured cardiac myocytes. *Circ Res*. (2009) 105:523–6. doi: 10.1161/CIRCRESAHA.109.201418
224. Zhong C, Zhao H, Xie X, Qi Z, Li Y, Jia L, et al. Protein Kinase C-mediated hyperphosphorylation and lateralization of Connexin 43 are involved in autoimmune myocarditis-induced prolongation of QRS complex. *Front Physiol*. (2022) 13:815301. doi: 10.3389/fphys.2022.815301
225. Viczenczova C, Kura B, Chaudagar K, Szeiffova Bacova B, Egan Benova T, Barancik M, et al. Myocardial connexin-43 is upregulated in response to acute cardiac injury in rats. *Can J Physiol Pharmacol*. (2017) 95:911–9. doi: 10.1139/cjpp-2016-0680
226. Wang J, Liu X, Arneja A, Dhalla N. Alterations in protein kinase A and protein kinase C levels in heart failure due to genetic cardiomyopathy. *Can J Cardiol*. (1999) 15:683–90.
227. Takeishi Y, Bhagwat A, Ball N, Kirkpatrick D, Periasamy M, Walsh R. Effect of angiotensin-converting enzyme inhibition on protein kinase C and SR proteins in heart failure. *Am J Physiol*. (1999) 276:H53–62. doi: 10.1152/ajpheart.1999.276.1.H53
228. Bruce A, Rothery S, Dupont E, Severs N. Gap junction remodelling in human heart failure is associated with increased interaction of connexin43 with ZO-1. *Cardiovasc Res*. (2008) 77:757–65. doi: 10.1093/cvr/cvm083
229. Jiang J, Hoagland D, Palatinus J, He H, Iyyathurai J, Jourdan L, et al. Interaction of alpha Carboxyl Terminus 1 Peptide With the Connexin 43 Carboxyl Terminus Preserves Left Ventricular Function After Ischemia-Reperfusion Injury. *J Am Heart Assoc*. (2019) 8:e012385. doi: 10.1161/JAHA.119.012385
230. Ghatnekar G, Grek C, Armstrong D, Desai S, Gourdie R. The effect of a connexin43-based Peptide on the healing of chronic venous leg ulcers: a multicenter, randomized trial. *J Invest Dermatol*. (2015) 135:289–98. doi: 10.1038/jid.2014.318
231. Grek C, Montgomery J, Sharma M, Ravi A, Rajkumar J, Moyer K, et al. A Multicenter randomized controlled trial evaluating a Cx43-mimetic peptide in cutaneous scarring. *J Invest Dermatol*. (2017) 137:620–30. doi: 10.1016/j.jid.2016.11.006
232. Montgomery J, Ghatnekar G, Grek C, Moyer K, Gourdie R. Connexin 43-Based Therapeutics for Dermal Wound Healing. *Int J Mol Sci*. (2018) 19:1778. doi: 10.3390/ijms19061778
233. Gray M, Karliner J, Mochly-Rosen D. A selective epsilon-protein kinase C antagonist inhibits protection of cardiac myocytes from hypoxia-induced cell death. *J Biol Chem*. (1997) 272:30945–51. doi: 10.1074/jbc.272.49.30945
234. Ross A, Gibbons R, Stone G, Kloner R, Alexander R, Investigators A. A randomized, double-blinded, placebo-controlled multicenter trial of adenosine as an adjunct to reperfusion in the treatment of acute myocardial infarction (AMISTAD-II). *J Am Coll Cardiol*. (2005) 45:1775–80. doi: 10.1016/j.jacc.2005.02.061
235. Cotter M, Boitano S, Lampe P, Solan J, Vagner J, Ek-Vitorin J, et al. The lipidated connexin mimetic peptide SRPTEKT-Hdc is a potent inhibitor of Cx43 channels with specificity for the pS368 phospho-isoform. *Am J Physiol Cell Physiol*. (2019) 317:C825–42. doi: 10.1152/ajpcell.00160.2019
236. Inagaki K, Koyanagi T, Berry N, Sun L, Mochly-Rosen D. Pharmacological inhibition of epsilon-protein kinase C attenuates cardiac fibrosis and dysfunction in hypertension-induced heart failure. *Hypertension*. (2008) 51:1565–9. doi: 10.1161/HYPERTENSIONAHA.107.109637
237. Bikou O, Thomas D, Trappe K, Lugenbiel P, Kelemen K, Koch M, et al. Connexin 43 gene therapy prevents persistent atrial fibrillation in a porcine model. *Cardiovasc Res*. (2011) 92:218–25. doi: 10.1093/cvr/cvr209
238. Kwak B, Mulhaupt F, Veillard N, Gros D, Mach F. Altered pattern of vascular connexin expression in atherosclerotic plaques. *Arterioscler Thromb Vasc Biol*. (2002) 22:225–30. doi: 10.1161/hq0102.104125
239. Peters N. Myocardial gap junction organization in ischemia and infarction. *Microsc Res Tech*. (1995) 31:375–86. doi: 10.1002/jemt.1070310507
240. Zuzul M, Lozic M, Filipovic N, Canovic S, Didovic Pavicic A, Petricevic J, et al. The Expression of Connexin 37, 40, 43, 45 and Pannexin 1 in the early human retina and choroid development and tumorigenesis. *Int J Mol Sci*. (2022) 23:5918. doi: 10.3390/ijms23115918
241. Bobbie M, Roy S, Trudeau K, Munger S, Simon A, Roy S. Reduced connexin 43 expression and its effect on the development of vascular lesions in retinas of diabetic mice. *Invest Ophthalmol Vis Sci*. (2010) 51:3758–63. doi: 10.1167/iov.09-4489
242. Wang Y, Qu Y, Chen X, Zhang P, Su D, Wang L, et al. Effects of D-methionine in mice with noise-induced hearing loss mice. *J Int Med Res*. (2019) 47:3874–85. doi: 10.1177/0300060519860679
243. Tajima S, Danzaki K, Ikeda K, Kamiya K. Degradation and modification of cochlear gap junction proteins in the early development of age-related hearing loss. *Exp Mol Med*. (2020) 52:166–75. doi: 10.1038/s12276-020-0377-1
244. McLachlan E, Plante I, Shao Q, Tong D, Kidder G, Bernier S, et al. ODDD-linked Cx43 mutants reduce endogenous Cx43 expression and function in osteoblasts and inhibit late stage differentiation. *J Bone Miner Res*. (2008) 23:928–38. doi: 10.1359/jbmr.080217
245. Matsuki T, Arai Y, Tsuchida S, Terauchi R, Oda R, Fujiwara H, et al. Expression of Connexin 43 in Synovial Tissue of Patients With Rheumatoid Arthritis. *Arch Rheumatol*. (2016) 31:55–63. doi: 10.5606/ArchRheumatol.2016.5597
246. Tan M, Kwong H, Ang C, Tey H, Lee J, Becker D. Changes in connexin 43 in inflammatory skin disorders: eczema, psoriasis, and Steven-Johnson syndrome/toxic epidermal necrolysis. *Health Sci Rep*. (2021) 4:e247. doi: 10.1002/hsr2.247
247. Kiszner G, Balla P, Wichmann B, Barna G, Baghy K, Nemeth I, et al. Exploring Differential Connexin Expression across Melanocytic Tumor Progression Involving the Tumor Microenvironment. *Cancers*. (2019) 11:165. doi: 10.3390/cancers11020165
248. Angeli S, Kousiappa I, Stavrou M, Sargiannidou I, Georgiou E, Papacostas S, et al. Altered Expression of Glial Gap Junction Proteins Cx43, Cx30, and Cx47 in the 5XFAD Model of Alzheimer's Disease. *Front Neurosci*. (2020) 14:582934. doi: 10.3389/fnins.2020.582934



## OPEN ACCESS

EDITED BY  
Junbao Du,  
First Hospital, Peking University, China

REVIEWED BY  
Yuh-Cherng Chai,  
John Carroll University, United States  
Samantha P. Harris,  
University of Arizona, United States  
J. Carter Ralphe,  
University of Wisconsin-Madison, United States

\*CORRESPONDENCE  
R. John Solaro  
✉ solarorj@uic.edu

SPECIALTY SECTION  
This article was submitted to  
General Cardiovascular Medicine,  
a section of the journal  
Frontiers in Cardiovascular Medicine

RECEIVED 03 October 2022  
ACCEPTED 29 December 2022  
PUBLISHED 24 January 2023

CITATION  
Rosas PC and Solaro RJ (2023) Implications  
of S-glutathionylation of sarcomere proteins  
in cardiac disorders, therapies, and diagnosis.  
*Front. Cardiovasc. Med.* 9:1060716.  
doi: 10.3389/fcvm.2022.1060716

COPYRIGHT  
© 2023 Rosas and Solaro. This is an  
open-access article distributed under the terms  
of the [Creative Commons Attribution License](#)  
(CC BY). The use, distribution or reproduction in  
other forums is permitted, provided the original  
author(s) and the copyright owner(s) are  
credited and that the original publication in this  
journal is cited, in accordance with accepted  
academic practice. No use, distribution or  
reproduction is permitted which does not  
comply with these terms.

# Implications of S-glutathionylation of sarcomere proteins in cardiac disorders, therapies, and diagnosis

Paola C. Rosas<sup>1</sup> and R. John Solaro<sup>2\*</sup>

<sup>1</sup>Department of Pharmacy Practice, College of Pharmacy, Chicago, IL, United States, <sup>2</sup>Department of Physiology and Biophysics, College of Medicine, University of Illinois at Chicago, Chicago, IL, United States

The discovery that cardiac sarcomere proteins are substrates for S-glutathionylation and that this post-translational modification correlates strongly with diastolic dysfunction led to new concepts regarding how levels of oxidative stress affect the heartbeat. Major sarcomere proteins for which there is evidence of S-glutathionylation include cardiac myosin binding protein C (cMyBP-C), actin, cardiac troponin I (cTnI) and titin. Our hypothesis is that these S-glutathionylated proteins are significant factors in acquired and familial disorders of the heart; and, when released into the serum, provide novel biomarkers. We consider the molecular mechanisms for these effects in the context of recent revelations of how these proteins control cardiac dynamics in close collaboration with Ca<sup>2+</sup> fluxes. These revelations were made using powerful approaches and technologies that were focused on thin filaments, thick filaments, and titin filaments. Here we integrate their regulatory processes in the sarcomere as modulated mainly by neuro-humoral control of phosphorylation inasmuch evidence indicates that S-glutathionylation and protein phosphorylation, promoting increased dynamics and modifying the Frank-Starling relation, may be mutually exclusive. Earlier studies demonstrated that in addition to cTnI as a well-established biomarker for cardiac disorders, serum levels of cMyBP-C are also a biomarker for cardiac disorders. We describe recent studies approaching the question of whether serum levels of S-glutathionylated-cMyBP-C could be employed as an important clinical tool in patient stratification, early diagnosis in at risk patients before HFpEF, determination of progression, effectiveness of therapeutic approaches, and as a guide in developing future therapies.

## KEYWORDS

myosin binding protein C, titin, cardiac troponin I, protein phosphorylation, cross-bridge kinetics, length dependent activation

## 1. Introduction: S-glutathionylation as a potential modifier of sarcomere protein function

In view of evidence discussed below that cardiac myosin binding protein C (cMyBP-C), actin, cardiac troponin I (cTnI) and titin are modified by S-glutathionylation, we focus here on these sarcomere proteins in physiological control of cardiac function by this oxidative related and potentially maladaptive post-translational modification. A prevalence of reduced

glutathione (GSH) is critical to maintain the reducing environment in cardiac myocytes. With a loss of redox balance and exposure of proteins to reactive oxygen species (ROS), there is a promotion of a reversible oxidation of targeted Cys residues that may be adaptive or maladaptive (1). Redox homeostasis and modifications of the cardiac myocyte depend strongly on a balance between reduced (GSH) and oxidized glutathione (GSSG). Reaction of GSSG with proteins, which is reversible, may be beneficial by protecting Cys residues from irreversible modification such as carbonylation (1). However, with persistent and severe oxidative stress the balance of GSH/GSSG tilts unfavorably leading to pathological consequences in a variety of mechanisms as reviewed by Pastore and Piemonte (1). Although early studies emphasized the significance of S-glutathionylation in cell signaling involving myofilament proteins, the functional significance of this post-translational modification in cardiac sarcomeres remained unclear (2, 3). Our discovery reported in 2012 of a role of S-glutathionylation of cMyBP-C in control of sarcomere response to  $\text{Ca}^{2+}$  and cross-bridge kinetics provided a new understanding of the effects oxidative stress on cardiac function especially diastolic function (4). Our findings were confirmed and extended by other laboratories. However, more work needs to be carried out to understand the role of S-glutathionylation more completely in early and late stages of cardiac disorders, in therapies, and in their usefulness as serum biomarkers in diagnosis and stratification of patients.

Advances in the understanding of molecular control processes in sarcomere function demand a new look at the integrated interactions among the proteins modified by S-glutathionylation in mechanisms of control of the heartbeat and beat-to-beat regulation. With the development of better high-resolution imaging techniques such as cryo-electron microscopy (cryo-EM) (5) together with atomistic molecular modeling (6), molecular-dynamics (MD) simulations (7, 8), and interrogating protein-protein interactions with fluorescent probes (9, 10), there have been significant investigations contributing to a new and dynamic evolution in understanding the structure and function of all three of the filaments of the cardiac sarcomere. Detailed accounts of these advances are in recent publications to which we refer in the present paper in the context of our focus on oxidative modifications of cMyBP-C, actin, cTnI, and titin by S-glutathionylation.

## 2. Transitions in thin, thick, and titin filament states in the heartbeat and beat to beat regulation

### 2.1. The diastolic states and transitions to systole

**Figure 1** illustrates integrated function of proteins in the sarcomere filaments in establishing the diastolic and systolic states. We first discuss a current perception of the transition between these states in a basal level of contractility and heart rate, in which there exists a contraction and relaxation reserve. Shown are functional units in a sarcomere consisting of thin filaments with a 7:1:1 ratio of actins: tropomyosin and troponin (Tn) complex (cTnI), the inhibitory unit; cTnC, the Ca-binding unit, and cTnT, named for its binding to tropomyosin (Tm). Sarcomeres illustrated in **Figure 1** are in the C-zone, where cMyBP-C localizes (11). Titin, which stretches from the Z-disk to the M-band and establishes passive tension in diastole is shown extending from the sarcomeres in **Figure 1** and discussed in detail below. In each functional unit, **Figure 1** shows the head, hinge, and extended tail of two headed myosin (cross-bridges) with associated light chain proteins. The reaction of myosin cross-bridges with actin generates tension, shortening, and thus the power to eject blood. In relaxed sarcomeres thin filaments are in a “B” or myosin blocked state. cMyBP-C is in the central so-called C-zone of the sarcomere, and as discussed below interacts both with the thin, thick, and titin filaments. At end diastole, sarcomere length is relatively long, the stretch of titin elastic domains induces resting tension and diastolic pressure (12). In the B-state, there is a dominant obstruction of Tm movement away from its blocking configuration resulting in inhibition of the actin-cross-bridge reaction (13). This inhibition depends on weak interactions with the cTnI-switch peptide (SwP) with cTnC and strong interactions of the cTnI inhibitory peptide (Ip) and C-terminal mobile domain extending from the cTn core domain and holding Tm in a blocking position. There are also interactions of cTnI-cTnC with a cTnT peptide known as the IT arm. Relaxation also depends on a peptide of cTnT located at the overlap of contiguous Tms. As emphasized by Tobacman (14), recent studies of the thin filament structure revealed that each of the cTns on opposite faces of the thin filament interact with both Tm strands. The Tn complexes on opposite sides the thin filament are not in perfect register. It is now recognized that processes at the level of the thick filament proper also play a role in the relaxed states. Evidence has shown that cardiac myosin can exist in either a sequestered super-relaxed state (SRX) with very low ATPase activity with the heads folded back toward the thick filament, or in a disordered relaxed state (DRX) with heads poised to interact with thin filaments in the transition to the active state of the actin-myosin cross-bridge reaction (15, 16). Physiological and pathological mechanisms modulate the population of these states in thick filament related control processes (15).

With its release into the sarcoplasm,  $\text{Ca}^{2+}$  binds to the N-lobe of cTnC promoting a tight binding of cTnI SwP and releasing the tether of the mobile domain to actin; the N-lobe of cTnC now binds to actin-Tm in association with a pivot of the core domain of cTn (5, 7, 14). Current theories suggest that these actions of the cTn complex of proteins induce a Ca-activated or “C” state but do not fully release the thin filament from inhibition. A requirement for interactions of

Abbreviations: cMyBP-C, cardiac myosin binding protein-C; cTnI, cardiac troponin I; cTnC, cardiac troponin C; cTnT, cardiac troponin T; Tm, tropomyosin; Tn, troponin; GSH, reduced glutathione; GSSG, oxidized glutathione; Cys, cysteine; MD, molecular dynamics; B-state, blocked state; SwP, switch peptide; Ip, inhibitory peptide; SRX, super-relaxed state; DRX, disordered relaxed state; M state, myosin activated; FN, fibronectin; Ig, immunoglobulin; LMM, light meromyosin; LDA, length dependent activation; MLC2, myosin light chain 2; FRET, fluorescence resonance energy transfer; RBM20, RNA binding motif protein 20; PTMs, post-translational modifications; cryo-EM, cryogenic electron microscopy; PKC, protein kinase C; CaMKII, calcium/calmodulin-dependent protein kinase II; PEVK domain, Pro-Glu-Val-Lys domain; PKA, protein kinase A; cGMP, cyclic guanosine monophosphate; DOCA, deoxycorticosterone; HF, heart failure; HSE, high stress exercise; UnDOx, unfolded domain oxidation; eNOS, endothelial nitric oxide synthase; NAC, N-acetyl cysteine; DHF, dyssynchronous heart failure; HCM, hypertrophic cardiomyopathy; BiV, bi-ventricular pacing; CRT, cardiac resynchronization therapy; LV, left ventricle; WT, wild type; HFD, high fat diet; Mito TEMPO, mitochondrially targeted antioxidant.



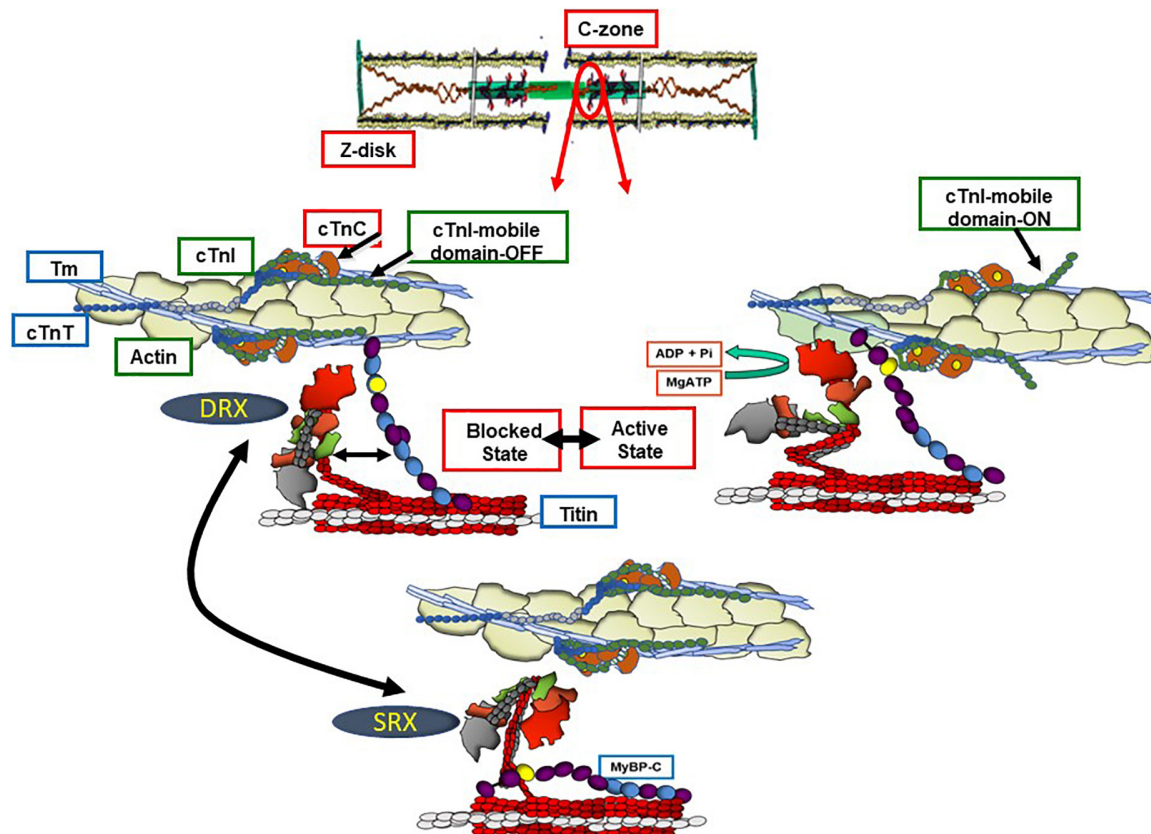


FIGURE 1

Functional units of C-zone sarcomeres in relaxed and active states. Shown are functional units of cardiac sarcomeres in the C-zone containing c(MyBP-C). The **bottom panel** shows a sarcomere the Ca-regulatory site on cTnC not occupied and with myosin in a super relaxed state (SRX) in which the heads are sequestered and not participating in the heartbeat. In the **left middle panel**, the cross-bridges are in a disordered relaxed state (DRX) poised to interact with the thin filament but blocked by the actions of the troponin complex proteins with an inhibitory peptide (Ip) and mobile domain of troponin I (cTnI) locking tropomyosin (Tm) a position sterically blocking the actin-cross-bridge interaction. This blocking position of Tm relies on an interaction of troponin T (cTnT) with the overlap region of Tm. In this state there is an interaction of the N-terminal domain of myosin binding protein C (cMyBP-C) with actin-Tm moving Tm away from its steric blocking position. As indicated, there are also interactions between the middle regions of cMyBP-C and myosin producing a drag on shortening capability. The **right middle panel** shows that with Ca-binding to the N-terminal domain of troponin C (cTnC) the thin filament is released from inhibition permitting activation of cross-bridge interactions with actin promoting force and shortening of sarcomere. The kinetics of the actin-cross-bridge reaction depend on interactions with the N-terminus of cMyBP-C (see text and **Figure 2** for discussion).

the cross-bridge with actin-Tm has been proposed to move Tm fully from its obliteration of myosin binding inducing a myosin activated or “M” state (13). Although not indicated in **Figure 1**, activation of a functional unit may induce cooperative spread of activation along the thin filament to other functional units (17).

Complex interactions among titin, cMyBP-C and the thin filament in control of contraction and relaxation dynamics and in the Frank-Starling relation are in a state of evolution in our understanding and require discussion. A comprehensive summary of mechanisms of cMyBP-C structure and function has been recently published by Suay-Corredera and Alegre-Cebollada (18). Interactions of cMyBP-C with thin, thick, and titin filaments provide an array of mechanisms to maintain homeostasis over a range of physiological states. These mechanisms are associated with domains in N-terminal, central, and C-terminal domains. As emphasized by the studies by Mun et al. (19), these regions of cMyBP-C control sarcomere activity by multiple and independent mechanisms. Moreover, these interactions comprise sites of vulnerability associated with familial cardiac disorders (20). **Figures 1, 2** depict a current perspective the disposition of cMyBP-C in regions of a sarcomere with functional

units in various states of activity. Ten regions consisting of fibronectin III (FN) and immunoglobulin (Ig) domains are indicated. Unique aspects of cMyBP-C are indicated at the N-terminal domain with phosphorylation sites and in an Ig domain with a loop present in the middle of the cardiac isoform (**Figure 2**). Cys residues identified to be modified by S-glutathionylation are also indicated and discussed below. It is accepted that that cMyBP-C extends from C-terminal anchoring sites on titin and light meromyosin (LMM) across the inter-filament space to the thin filament with N-terminal sites binding alternatively with the head-neck region of myosin and actin-Tm (21–23). At low  $\text{Ca}^{2+}$  evidence indicates that the flexible N-terminus of cMyBP-C scans the thin filament seeking binding sites (24, 25). Binding of the N-terminus of some cMyBP-C molecules to actin-Tm moves Tm away from full inhibition, thereby activating the thin filament independently of the Ca-cTnC interaction (26, 27). Regions of cMyBP-C in the central middle domains have multiple functional roles acting in concert with N- and C-terminal domains. Importantly, compared to other regions, middle regions C2C4 and C5C7 have the highest affinity for tail regions of myosin S2 with both regions binding strongly with myosin light chains attached. C5C7



binds strongly to this S2 regions even without the myosin light chains present (28). There is evidence for multiple mechanisms modified by these interactions that have functional effects on sarcomere activity. These mechanisms, which modulate power and energy consumption, include the generation of an internal load inducing a drag on sarcomere shortening, an inhibition of actomyosin ATPase activity, and an induction of the SRX state (29, 30). There is also a proposal that the interaction between central domains of cMyBP-C with myosin steers cross-bridges to and from thin filaments thereby controlling the rate of recruitment and exit from force generating state (31). C-terminal interactions modulate thick filament packing and specific interactions of 3 C-terminal domains with specific super-repeats on titin establish localization of cMyBP-C in its striped configuration in the C-zone of the sarcomere (32). As discussed below, there is evidence that these interactions are modulated by mechanical stress and by phosphorylation. There are also interactions of cMyBP-C domains with the regulatory light chain of myosin in a phosphorylation dependent manner (33). In summary, it is apparent that the population of cMyBP-C molecules in a sarcomere consists of some with N-terminal flexible regions interacting with the thin filament and others interacting with various regions of thick filament proteins slowing cross-bridge kinetics and some inducing an SRX state (34). Adding to the complexity of the disposition of proteins in relaxed and active sarcomeres is evidence, that these interactions are biased toward interactions with actin-Tm in the low  $\text{Ca}^{2+}$  inhibited state of the thin filament and more toward interactions with myosin heads at activating levels of  $\text{Ca}^{2+}$ . As discussed below these interactions are also modified by phosphorylation and by titin induced strain with stretch.

Titin is the major protein establishing passive tension in the diastolic state but also may be a participant in feedback signaling from the systolic state to the thick filament cross-bridges and signaling in communication with cMyBP-C and the thin filament (35–37). Regions of titin that are significant in passive tension are illustrated in **Figure 3**. Recent reviews provide a picture of this giant protein and its modulation by stretch, phosphorylation, and oxidant stress (12, 38).

As discussed below, complex interactions among titin, cMyBP-C, and the thin filament, which occur in control of contraction and relaxation dynamics and in the Frank-Starling relation, are in a state of evolution in our understanding. This discussion includes descriptions of accessible Cys residues expressed in each of these proteins that are targeted by S-glutathionylation. Addition of the negatively charged GSH tripeptide modifies function alters signaling *via* protein phosphorylation.

## 2.2. Beat-to-beat regulation and the Frank-Starling relation

An emerging concept under discussion in the literature is related to the signaling pathway from titin to cMyBP-C and the thin filament in their roles in length dependent activation (LDA), the basis of the Frank-Starling relation. Elegant studies by Reconditi et al. (35) employed X-ray diffraction and mechanics to reveal that a length dependent mechanism governs entry of cross-bridges into the systolic state. They elucidated the concept that a mechano-sensing mechanism rapidly responds to changes in systolic peak force and induces variations in the number of myosin heads in the off state in diastole thereby matching ejection to the hemodynamic

task. In this concept of the Frank-Starling law, cross-bridges sense thick filament stress in systole, which in turn introduces variations in the number cross-bridges in the off state. Reconditi et al. (35) speculate that interactions among titin, MyBP-C, and cross-bridges may form the stress sensing mechanism. This view leaves open the question of how modifications in the thin filament affect LDA. A different view has been presented by Irving and Craig (36) in discussing the X-ray diffraction studies together with evidence from studies using fluorescent probes to monitor changes in thin and thick filaments. Ait-Mou et al. (39) employed X-ray diffraction and reported molecular rearrangements in both thin and thick filaments with changes in length. Fluorescent probe on cTnC confirmed these effects in skinned single cells. This signaling was absent in myofilaments containing a highly compliant splice variant of titin, which generated relative low passive tension. Zhang et al. (9) used polarization of probes on cTnC and MLC2 in skinned cardiac preparations and concluded that whereas length changes in peak tension mainly affect the thick filament, length changes at sub-maximal levels of activation mainly affect the thin filament. An important finding in the study of Zhang et al. was that the changes in the thin filaments occurred independently of active interactions of cross-bridges with the thin filament. In our studies (10), carried out in collaboration with Wenji Dong's laboratory, we employed fluorescence resonance energy transfer (FRET) to probe cTnI interactions with cTnC in skinned fiber preparations containing wild-type titin or highly compliant titin in recombinant binding motif 20 (RBM20) deficient mice. Results showed that the cTnI-cTnC interaction senses sarcomere length with a dependence on the strain induced by stretch of titin. Recent studies report no LDA in skinned fiber preparations from human heart samples containing a truncating titin mutant (40). Based on all these observations, a unifying theory, depicted in **Figure 3**, of LDA discussed by Irving and Craig (36) is that LDA involves mechanisms involving all three sarcomere filaments. The idea is that with stretch interactions of regions of titin with cMyBP-C induce a steering of its N-terminal domain toward the thin filament, where it interacts with actin-Tm to modulate Ca-response independently of cross-bridge interactions. This mechanism may work in conjunction with strain dependent effects on thick filaments depending on the level of Ca-activation. Mamidi et al. (26) concluded from their studies that at maximum tension, LDA is dominated by feedback effects of active tension on entry of cross-bridge into force generation, whereas at submaximal levels of activation LDA is dominated by altered Ca-sensitivity. Data demonstrating that adult cardiac myofilaments regulated by slow skeletal TnI, the fetal/neonatal isoform, show blunted LDA (41) provide support for this idea. Moreover, LDA is significantly blunted in muscle preparations with ablation of cMyBP-C (42). The concept includes the idea that a diastolic mechanism governed by modifications in titin, thick filaments, MyBP-C, and troponin-tropomyosin engages ahead of and controlling the systolic state.

## 3. Protein phosphorylation as a major mechanism modifying sarcomere function

There are data indicating that S-glutathionylation and phosphorylation of sarcomere proteins may be mutually exclusive PTMs or at least need to be considered in integrative control of

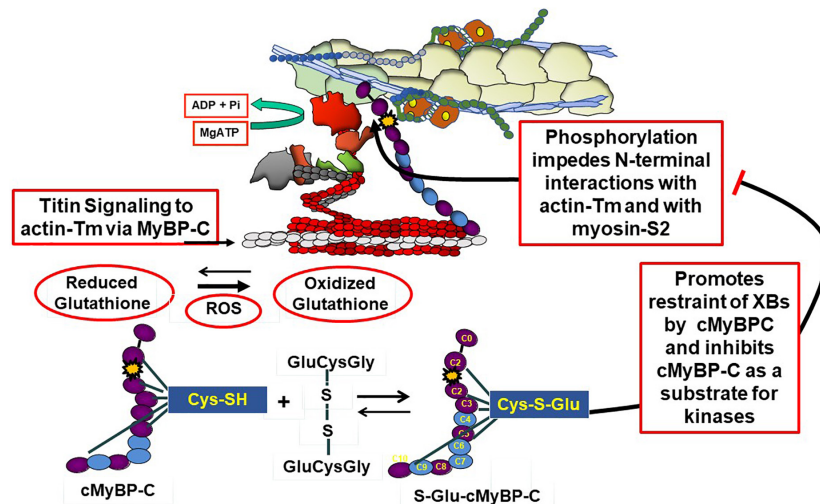


FIGURE 2

Modulation of cMyBP-C by phosphorylation and oxidative stress. The **top panel** shows an active sarcomere emphasizing cMyBP-C interactions at the N-terminal domains with the thin filament and myosin and C-terminal domains interacting with tails of myosin and titin. These interactions are inhibited with site specific phosphorylations (yellow star) of an N-terminal domain (yellow star) and modulated by oxidative stress demonstrated by the action reactive oxygen species (ROS) to increase the ration of reduced glutathione to oxidized glutathione. As shown the oxidized glutathione reacts with available Cys residues generating S-glutathionylated (S-Glu) cMyBP-C, which, as discussed in the text, may block the effects of phosphorylation to increase cross-bridge kinetics. Cys residues identified in various studies (41, 42, 57) are shown to exist in N-terminal and C-terminal regions as well as domains in the **middle panel**.

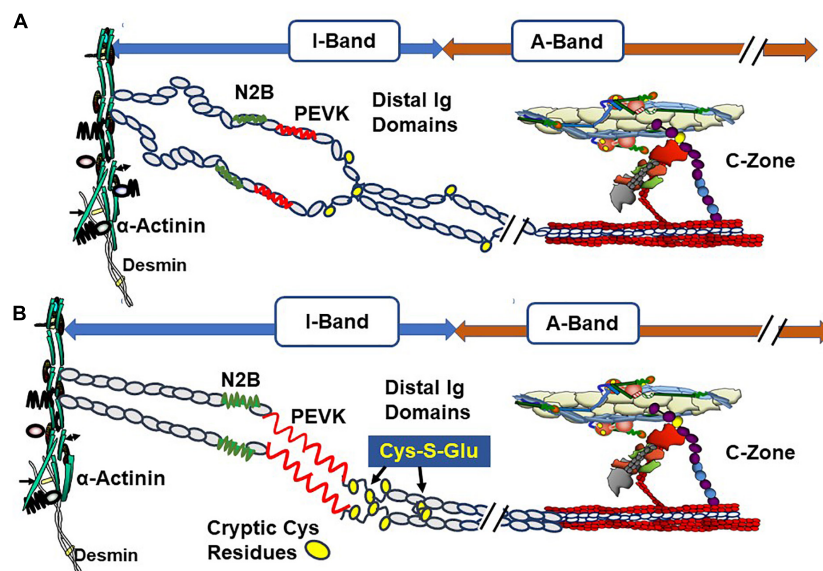


FIGURE 3

Oxidative stress and length dependent stabilization of an unfolded state of titin distal Ig domains induced by exposure and S-glutathionylation of cryptic cysteine residues. (A) Illustration of stretch of titin in diastolic conditions with oxidant stress at a relatively short sarcomere length showing few exposed cysteines (yellow circles). (B) Illustration of stretch of titin with oxidant stress to a relatively long sarcomere length showing exposure of buried cysteine residues and S-glutathionylation. This figure is based on evidence reported by Loescher et al. (12) demonstrating that with mechanical and oxidant stress, stabilization of the state of distensibility of titin occurs with aggregation of distal Ig domains of parallel titin strands. Variations in this mechanism produce a range of values of passive tension and can affect length dependent activation (LDA). Evidence indicates that stretch of titin signals interactions with the C-terminal domains of cMyBP-C that are transmitted to the cMyBP-C N-terminal domains, which promote interactions with actin-Tm and activation of the thin filament. See text for further discussion.

cardiac function in oxidative stress (43–45). Post-translational modifications of cMyBP-C especially by neural and hormonal regulation of protein phosphorylation by kinases and phosphatases modulate its interactions in complex mechanisms (46–49). **Figure 2** illustrates phosphorylation dependent modifications of interactions of cMyBP-C with its neighbors in the sarcomere. Site specific

phosphorylations have been identified at Ser 275, 284, and 304 in the human sequence and a hierarchy of mechanisms defined stressing a role of cMyBP-C in integration of diverse signaling cascades (49, 50). Importantly, as shown in **Figure 2**, phosphorylations release the inhibitory effect of cMyBP-C on cross-bridge kinetics and impeded interactions of the N-terminal domain with actin-Tm (30, 46–48).

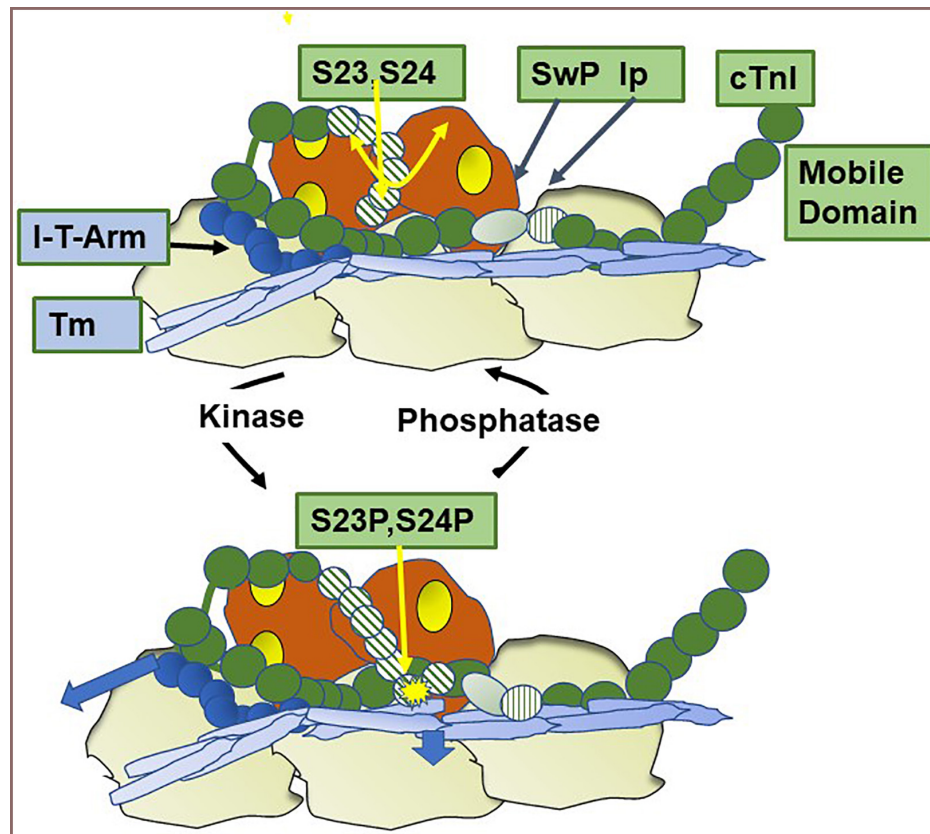


FIGURE 4

Modulation of thin filament activation by cTnI N-terminal phosphorylation. Shown is a cartoon based on recent studies (7) of a region of a Ca-activated thin filament showing the effect of phosphorylation of Ser 23 and Ser 24 in the unique N-terminal peptide of cardiac troponin I (cTnI). In the dephosphorylated state the N-terminal peptide is mobile as indicated by the double yellow arrow. Also shown are the positions of the cardiac troponin I switch peptide (Sw), inhibitory peptide (Ip), and troponin I-troponin T interaction (I-T arm) described in **Figure 1**. Phosphorylation induces an interaction of the N-terminal peptide with actin-tropomyosin and as shown by the arrow in the figure moves tropomyosin (Tm) to a position favoring the off state of the thin filament, thereby decreasing myofilament response to  $\text{Ca}^{2+}$  and promoting relaxation. Cys residues reported to be S-glutathionylated (42) are located in the region of the I-T arm (Cys-80) and in a helix N-terminal to the Ip (Cys 97). See text for further discussion.

cTnI is unique among isoforms in expressing a ~30 amino acid N-terminal peptide containing two sites of phosphorylation (Ser 23, Ser 24 in the human sequence). Phosphorylation of these sites reduces myofilament  $\text{Ca}$ -sensitivity and enhances relaxation (51, 52). **Figure 4** shows results of experiments revealing a new concept of thin filament regulation by the unique N-terminal peptide of cTnI (7) that has modified concepts of mechanisms of its control of sarcomere kinetics (52). Cys residues in cTnI that may participate in S-glutathionylation are indicated (44). Building on previous solution NMR structures, sequence analysis, and molecular dynamic simulations (8, 53) together with the Yamada et al. (5) cryo-EM structures of the thin filament, Pavada et al. (7) reported the novel demonstration of interactions of a pseudo-phosphorylated N-cTnI at Ser23 and Ser24 with actin-Tm. They employed protein-protein docking and molecular dynamic simulations of the disposition of N-cTnI in Ca-activated thin filaments functional units. Pavada et al. (7) concluded that together with Arg residues in the N-terminal peptide, phosphorylated Ser 23, Ser 24 act to hinder an electrostatic interaction between cTnC and Tm in the Ca-activated state. In this disposition, phosphorylated cTnI interacts with actin-Tm moving it away from its steric blocking position thus affecting relaxation kinetics without affecting maximum tension as previously reported by Cheng et al. (8). This mechanism does not include an

effect of cTnI phosphorylation on SwP peptide interactions with cTnC, an effect included in early theories. These findings alter thinking regarding the role of cTnI phosphorylation in affecting the binding of the SwP to cTnC, which was not seen in the studies of Pavada et al. (7).

As expected, phosphorylation of cardiac titin presents as a complex array of sites with variable effects on passive tension. These have been extensively reviewed and related to cardiac disorders in a review by Koser et al. (38). Important findings summarized are that PKC $\alpha$  and CaMKII dependent phosphorylations that occur near the PEVK domain depress passive tension, whereas PKA, cGMP, and CamKII dependent phosphorylations occur in the N2B domains and decrease passive tension. As summarized by Koser et al. (38) large changes in phosphorylation in these sites occur in HFpEF. Moreover, enhancing cGMP dependent phosphorylation of titin has been considered as a therapeutic target in HFpEF (54).

Changes in passive tension induced by titin phosphorylation in conjunction with phosphorylation of cMyBP-C and cTnI are also expected to influence the LDA signaling mechanisms discussed above. Concepts related to this signaling cascade discussed include an effect of protein phosphorylation of cMyBP-C and cTnI on the “gain” in the process of communication of the energies of activation from titin stretch to thin filament  $\text{Ca}$ -sensitivity. Konhilas et al. (55)



reported an enhancement of LDA by cTnI phosphorylation and a blunting of LDA in skinned fibers regulated by slow skeletal TnI. Along these lines, Shaffer et al. demonstrated that phosphorylation of N-terminal residues of cMyBP-C blunted LDA, a finding corroborated by studies of Mamidi et al. (56). Kumar et al. (57) investigated relative roles of cTnI and cMyBP-C phosphorylation on LDA. They concluded that with beta-adrenergic stimulation, phosphorylation of cMyBP-C is mainly responsible for the effect to increase LDA and the Frank-Starling mechanism.

## 4. Modulation of sarcomere function by S-glutathionylation of cMyBP-C, actin, cTnI, and titin

### 4.1. Functional effects of S-glutathionylation of cMyBP-C, actin, and cTnI

To our knowledge, our determination of effects of oxidative stress in a DOCA-salt mouse model with unilateral nephrectomy provided the first report in 2012 of a functional effect of cMyBP-C S-glutathionylation (4). The DOCA-salt model exhibits slight hypertension with diastolic dysfunction and preserved ejection fraction. Cardiac myocytes isolated from the DOCA-salt model had no differences from controls in  $\text{Ca}^{2+}$ -currents,  $\text{Ca}^{2+}$ -transient dynamics, and late  $\text{Na}^+$  currents. These results indicated an altered myofilament  $\text{Ca}^{2+}$ -response. We therefore compared properties of detergent-extracted (skinned) fiber bundles from controls and DOCA-salt hearts. We measured tension and ATPase activity simultaneously over a range of  $\text{Ca}^{2+}$  concentrations. Compared with controls, fiber bundles from DOCA-salt hearts showed an increase in  $\text{Ca}^{2+}$ -sensitivity and a decrease in the slope of plots of tension vs. ATPase rate indicating a reduction in tension cost (unit tension developed/unit ATP hydrolyzed) and slowing of cross-bridge kinetics. Determination of Ktr (the transition of cross-bridges into the force generating state) showed no differences between controls and DOCA-fibers. These findings supported our conclusion that the diastolic dysfunction in the DOCA-salt hearts was due to a slowing of cross-bridge in their exit from the force generating state. We hypothesized that the oxidative stress induced post-translational modification in the myofilament proteins. We found no differences in phosphorylation among the proteins in controls and DOCA-fibers, but there was an S-glutathionylation of cMyBP-C that correlated with the extent of change in tension cost. In subsequent experiments we confirmed these results in which we treated the DOCA-salt mice with tetra-hydro biopterin (BH4) to suppress the oxidative stress (58). Inasmuch as oxidative stress affects multiple pathways, we tested for direct effects of S-glutathionylation of myofilament tension and ATPase activity by incubating skinned fibers and myofibrillar fractions with oxidized glutathione (GSSG) (59). We also determined sites of S-glutathionylation employing mass spectrometry. As with the preparations isolated from DOCA-salt hearts, myofilaments incubated in GSSG had an increased  $\text{Ca}^{2+}$ -sensitivity. Sites of S-glutathionylation as determined by mass spectrometry occurred at cysteines 655, 479, and 627.

Follow-up studies comparing samples of donor controls with samples of human hearts with dilated and ischemic cardiomyopathy

extended and confirmed these results and identified a potential interaction between S-glutathionylation and protein phosphorylation that appeared mutually exclusive. In 2016, Stathopoulou et al. (43) reported a correlation with a decrease in site specific phosphorylation of cMyBP-C with increases in S-glutathionylation of cMyBP-C. In general agreement with this study, Budde et al. (44) reported studies of a role S-glutathionylation of myofilaments in single cardiac myocytes harvested from human heart samples from control donors and patients with end-stage heart failure (HF). As reported previously they found the HF cells had reduced maximum tension and  $\text{Ca}$ -sensitivity. By treating the myocytes with reduced GSH they were able to correct these changes. They found increased S-glutathionylation of both cTnI and cMyBP-C in the HF samples compared to the donor samples. Treatment with PKA failed to phosphorylate these proteins in the HF samples but worked in the donor samples. Moreover, there was increased titin stiffness in the HF samples that could be suppressed by treatment with PKA and GSH. These data indicated a significant role for interactions of S-glutathionylation and phosphorylation in end stage human heart failure.

In another study extending understanding of a role of S-glutathionylation in cardiac function, Cazorla and colleagues compared redox related modifications in sedentary rats and rats stressed with moderate and exhaustive, high stress exercise (HSE) (45). Compared to controls, bouts of HSE induced large changes in oxidative stress markers together with depressed diastolic and systolic function in isolated perfused hearts. Hearts of HSE mice also demonstrated significantly increased S-glutathionylation of cMyBP-C and a depression cMyBP-C phosphorylation that could not be increased by activation of PKA. There was also a decrease in cTnI phosphorylation although there was no report of S-glutathionylation of cTnI. These data fit with findings in human hearts samples at end stage failure (43).

There are several lines of evidence indicating that post-translational modification of actin by S-glutathionylation may also be an important factor in control of cardiac dynamics. However, effects of actin S-glutathionylation on sarcomere function have not been a consistent finding. An early report by Chen and Ogut (60) identified S-glutathionylation of cardiac actin associated with ischemia suggesting this effect as a possible contributor to the decline in function resulting from myocardial infarction (60). Follow up studies reported that compared to controls there was a depression of acto-myosin S-1-ATPase activity of *in vitro* reconstituted preparations containing S-glutathionylated actin (61). In support of these findings, Passarelli et al. (3) reported a depression in force generation of cardiac myofibrils treated with agents promoting S-glutathionylation. Analysis of mechanism indicated actin S-glutathionylation as the main effector of this depression. Human heart samples analyzed by histochemical techniques showed evidence for *in situ* actin S-glutathionylation. A depression in actin polymerization has also been reported as an associated effect of actin S-glutathionylation at Cys 374 (60, 62). In our investigation of sites of S-glutathionylation determined by mass spectrometry together with functional effects on tension and ATPase activity of cardiac skinned fibers and myofibrils incubated with GSSG, we found no evidence of S-glutathionylation of cardiac actin at Cys 376 (59). There was a correlation of cMyBP-C S-glutathionylation with increased  $\text{Ca}$ -response of tension and ATPase activity with no change in maximum or minimum values. Moreover, we found no evidence of actin S-glutathionylation in hearts expressing the HCM linked mutant TmE180G discussed below. A main conclusion from

publications from our and other laboratories is a dominant and consistent modification of sarcomere proteins by S-glutathionylation is at cMyBP-C and titin. Existing evidence does indicate a need for further investigation of the potential role of actin-S-glutathionylation of integrated function of cardiac myocytes.

## 4.2. Functional effects of S-glutathionylation of titin

Investigations of possible role of S-glutathionylation in the control of stiffness of cardiac titin began with oxidative stress by acute coronary artery occlusion in a mouse acute myocardial infarction model (63). Taking note of this finding, Alegre-Cebollada et al. (64) established a collaboration with our laboratory in confirming and extending this finding. The studies employed a fragment of I-band titin region rich in Cys residues as illustrated in **Figure 3**. Stretch of the fragment exposed cryptic Cys residues making them substrates for GSSG and inducing S-glutathionylation. This modification decreased the mechanical stability of the domain and suppressed folding ability. Studies with isolated human cardiac myocytes demonstrated that this effect is translated to the intact system thereby enhancing titin elasticity (64). These results provide new understanding of the effects of oxidative stress on titin compliance, which had been reported to be due largely to S-S bonds between clusters of Cys residues. In the case of Cys residues of Ig domains the Cys residues are separated enough to be substrates for GSSG when exposed by stretch. Loescher et al. (12) investigated multiple models of oxidative stress together with altered mechanical unloading in an extensive investigation in which they described this mechanism as unfolded domain oxidation (UnDOx). Important findings described in detail in the publication provided evidence that with altered mechanical loading of cardiac myocytes, UnDOx in a distal titin spring region can either up or down regulate titin compliance affecting passive tension and enhancing titin phosphorylation. These findings established the relative significance of UnDOx in regulation of passive tension and thereby filling of the ventricle with blood in diastole. Modifications in titin phosphorylation have been reported with oxidant stress, but whether there is an interaction between S-glutathionylation and phosphorylation remains unclear (65).

## 5. Avenues of future research in cardiac physiology and pathology

### 5.1. Sarcomere protein S-glutathionylation in hypertrophic cardiomyopathy (HCM)

Results of our investigations of oxidative stress induced S-glutathionylation of cMyBP-C in a mouse model of hypertrophic cardiomyopathy expressing  $\alpha$ Tm-E180G (Tm-180) provided insights into the complexities of this PTM in a common cardiac disorder. Compared to wild-type, myofilaments controlled by Tm-180 have increased Ca-sensitivity. This biophysical signal triggers a pathological progression inducing diastolic dysfunction with preserved ejection fraction, oxidative stress, hypertrophic signaling with remodeling, and fibrosis. There is also oxidative stress together with S-glutathionylation of cMyBP-C because of increased eNos

activity. We approached suppressing the oxidative stress either by treatment with NAC (N-acetyl cysteine; promotes GSH synthesis) (66, 67) or with FTY-720 (Fingolimod) (68). FTY-720 is an immuno-modulator approved for use in multiple sclerosis. We previously reported FTY-720 to be effective reducing remodeling and improving function in a pressure-overload mouse model (69). FTY-720 affects sphingolipid signaling by interaction with receptors for sphingosine-1-phosphate. FTY-720 treatment reduced the elevated serum leucocyte population occurring in Tm-180 mice. In both approaches there was an improvement in diastolic dysfunction and a reduction in oxidative stress that was correlated with a reduction in levels of cMyBP-C S-glutathionylation. With FTY-720 treatment there was no change in phosphorylation of sarcomere proteins including total cMyBP-C, titin, and cTnI. Moreover, restoration of diastolic function to control levels occurred with no change in fibrosis. However, in the study with NAC treatment, site specific phosphorylation of cTnI at Ser 23 and Ser 24 was increased in the controls but not in the Tm-180 mice. We found no S-glutathionylation of cTnI suggesting that in this case altered kinase or phosphatase activity was in play and not direct interference of phosphorylation by S-glutathionylation. We also found a significant increase in site specific phosphorylation of cMyBP-C at Ser 282 that occurred in the Tm-180 filaments and was reduced substantially with NAC. These results indicate that levels of sarcomere protein phosphorylation may be directly affected by alterations of Cys residues by S-glutathionylation, but the net effects may also depend on oxidative stress effects on kinase/phosphatase pathways (70).

Apart from the suggestions above about use of serum levels of S-glutathionylated cMyBP-C in diagnosis and patient stratification, there are several gaps in our understanding of the role of S-glutathionylation of major sarcomere proteins in cardiac physiology and pathology. The unique ability of S-glutathionylation to modify Cys residues reversibly and to protect against irreversible oxidative modifications needs to be more completely understood in relation to physiological processes for example, in exercise and aging. Whereas correlations with diastolic dysfunction remain a strong possibility, there is evidence that this PTM may occur in a variety of cardiac disorders many of which display oxidative stress. More studies on early-stage cardiac diseases are in order. These studies need to integrate S-glutathionylation in the major affected proteins, cMyBP-C and titin as well as cTnI.

We think an important unexplored avenue of research is S-glutathionylation induced modulation of sarcomere length dependent activation (LDA), i.e., the Frank-Starling mechanism. Evidence of a role for titin (10, 71), cMyBP-C (56, 57), and cTnI (41, 55, 57) in altering LDA provides a rationale for this suggestion. A further rationale that is unexplored is the possible modification of LDA in the oxidative stress associated with cardiac disorders demonstrating mechanical dyssynchrony. Early activation of the septum associated with late activation of the left ventricular free wall characterizes dyssynchronous heart failure (DHF). A common cause is abnormal Purkinje fiber conduction. However, there is also evidence that DHF occurs with altered sarcomere mechano-biochemical signaling. Although bi-ventricular pacing can suppress the DHF, a significant number of patients do not respond to this treatment. Understanding of this lack of responsiveness may involve abnormal LDA and engagement of the Frank-Starling mechanism.

In testing patients with non-obstructive but symptomatic HCM, Ahmed et al. (72) applied CRT (bi-ventricular pacing, BiV) and tested for improvements in LV diastolic filling and exercise capacity.



Their approach was based on evidence of a significant incidence of dyssynchrony in HCM patients without obstructive outflow disorders. The dyssynchrony manifests at rest in a maladaptive interaction between the RV and LV in diastole inducing a failure of the LV to fill properly during exercise resulting in a failure to employ the Frank-Starling mechanism. After 8 months of sham or BiV, there was an improvement in LV volume during exercise, an increase in exercise capacity, and quality of life scores. The authors did not investigate molecular mechanisms but did evaluate the effects of BiV on LV contractility. At rest, there was no change in mechanical dyssynchrony in the study groups and no change in systolic elastance associated with BiV indicating no change in contractility. Thus, with some allusions to limitation of the study, the authors conclude that major mechanisms for the improvements in exercise were the effect of BiV to engage the Frank-Starling mechanism. Inasmuch as length dependent sarcomere activation is the basis of the Frank-Starling mechanism, this conclusion emphasizes consideration of LDA in sarcomeres with HCM-linked mutations.

The significance of LDA in CRT has been investigated by Niederer et al. (73). By employing a patient specific model of excitation and mechanics from the level of cellular mechanisms to heart function determined in patients before and after CRT. Sensitivity of the model to various elements in cellular control mechanisms demonstrated LDA as a significant contributor to the therapeutic benefit of CRT. The computations indicated a reduced effect of CRT in patients with dysfunctions in LDA. A significant contribution of these findings is the idea that the Frank-Starling relation is not only important in beat-to-beat control of cardiac function but a significant mechanism in synchrony of the heartbeat. Mechanical LDA and other sub-cellular mechanisms are downstream to electrical stimulation and thus dampened or amplified LDA appears to be a relatively important contributor to the efficacy of CRT. This study indicates that despite the electrical effects of CRT, it is critical for the heart to have robust LDA.

Our studies with models of HCM are relevant to these concepts. Early studies from our lab investigated the LDA of myofilaments expressing cTnT-R92Q. The data indicated a higher level of LDA in the R92Q skinned fibers compared to WT fibers (74). Other studies reported an attenuation of LDA in HCM models cTnT-R95H and cTnT-F88L (75, 76). It would be of interest to determine a role of oxidative stress and potential S-glutathionylation of sarcomere proteins in these models.

## 5.2. Potential use of S-glutathionylated sarcomere proteins as biomarkers of oxidative stress and diastolic dysfunction

Reports of determination of cMyBP-C and its fragments as a biomarker for cardiac disorders provide a proof of concept that determination of serum levels of S-glutathionylated cMyBP-C may be a biomarker with functional implications. Studies identified serum cMyBP-C as a biomarker of severe cardiovascular diseases and in acute myocardial infarction (77–80). Based on our studies of S-glutathionylation of cMyBP-C in a model of diastolic dysfunction, Dudley and colleagues (81) further investigated changes in cMyBP-C in cardiac samples of mice fed on normal chow or a high fat diet (HFD) inducing diastolic dysfunction and insulin resistance. One group of mice were also given Mito TEMPO, an

investigational agent not approved by the FDA, concurrently to suppress mitochondrial induced oxidative stress. The results showed an increase in S-glutathionylation of cMyBP-C with the HFD that was reversed or prevented in the mice on the HFD with mito TEMPO. These data encouraged an effort to develop antibody detection of S-glutathionylated cMyBP-C using an immune-precipitation approach in serum of models of cardiometabolic syndrome and in humans (82). Compared to controls with no diastolic dysfunction, levels of serum S-glutathionylated cMyBP-C were elevated in the serum of mice, monkeys, and in a cohort of 24 humans with diastolic dysfunction. These promising preliminary data require verification in larger cohort of patients and measurements need to be made to determine specificity, and biological variation in healthy individuals as has been carried out for comparisons of cTnT and cMyBP-C (80). Knowledge of epitopes employed in antibody detection as well as quantification of levels of S-glutathionylation in relation to severity of disease. The vast literature on serum cTnI and cTnT as biomarkers (83) provides an example of the dimensions of the information and effort required to establish confidence in the use of S-glutathionylated cMyBP-C as a serum biomarker for cardiac disorders. An issue requiring further investigation is the stability of S-glutathionylated cMyBP-C in muscle and serum samples. To reduce thiol oxidative degradation in serum samples, non-reducing preservative reagents, N-Methylmaleimide, neocupporine, and diethylenetriaminepentaacetic acid were added to samples in the determination of serum levels of cMyBP-C prior to binding to primary antibodies (82). We have investigated the stability of post-translational modifications of cardiac/myofibril samples from hearts of mice treated with different euthanizing agents. Our findings indicate a fall in levels of glutathionylation of cMyBP-C between 30 and 90 days of storage (84).

## 6. Summary and conclusion

Results of studies presented here show progress identifying S-glutathionylation of sarcomeric proteins in advanced understanding of physiological stressors and common cardiac disorders. An example is insights into the relation between mechano-biology and S-glutathionylation of titin that provide a novel perspective on relations between protein folding and oxidative stress. This finding may have application to mechano-biology and S-glutathionylation of many other proteins including cMyBP-C, which expresses stretch sensitive regions analogous to the PEVK region of titin (85). Studies summarized here also provide an account of translation of laboratory experiments on S-glutathionylation of sarcomere proteins to clinical applications. Among the various sarcomere modifications discussed, the data indicate that S-glutathionylation of cMyBP-C is a significant regulator of cardiac function and the most promising candidate to add to the list of biomarkers now in use or development. We have stressed S-glutathionylated cMyBP-C as a biomarker in metabolic syndrome and HFpEF, but other uses are evident in cardiac disorders with oxidative stress as a hallmark of the pathology. As we have discussed previously in the case of use of troponins as cardiac injury biomarkers, it is possible that the S-glutathionylated cMyBP-C biomarker may find use in conditions such as cardio-renal syndrome or in SARS-CoV-2 infections (83, 86). We think our discussions here provide a rationale for continued investigation of this powerful post-translational mechanism in sarcomere proteins.

## Data availability statement

The original contributions presented in this study are included in the article/supplementary material, further inquiries can be directed to the corresponding author.

## Author contributions

RS decided on the topic idea and after discussions with PR wrote a first draft. PR read and edited the first draft and finalized the manuscript with the RS. Both authors contributed to the manuscript and approved the submitted version.

## Funding

This work was supported by K01 HL155241 (PR), AHA CDA849387 (PR), RO1 HL 158634 (RS), and PO1 HL62426 (RS).

## References

- Pastore A, Piemonte F. Protein glutathionylation in cardiovascular diseases. *Int J Mol Sci.* (2013) 14:20845–76. doi: 10.3390/ijms141020845
- Dalle-Donne I, Rossi R, Giustarini D, Colombo R, Milzani A. S-glutathionylation in protein redox regulation. *Free Radic Biol Med.* (2007) 43:883–98. doi: 10.1016/j.freeradbiomed.2007.06.014
- Passarelli C, Di Venere A, Piroddi N, Pastore A, Scellini B, Tesi C, et al. Susceptibility of isolated myofibrils to *in vitro* glutathionylation: potential relevance to muscle functions. *Cytoskeleton.* (2010) 67:81–9. doi: 10.1002/cm.20425
- Lovelock J, Monasky M, Jeong E, Lardin H, Liu H, Patel B, et al. Ranolazine improves cardiac diastolic dysfunction through modulation of myofilament calcium sensitivity. *Circ Res.* (2012) 110:841–50. doi: 10.1161/CIRCRESAHA.111.258251
- Yamada Y, Namba K, Fujii T. Cardiac muscle thin filament structures reveal calcium regulatory mechanism. *Nat Commun.* (2020) 11:153. doi: 10.1038/s41467-019-14008-1
- Williams M, Lehman S, Tardiff J, Schwartz S. Atomic resolution probe for allostery in the regulatory thin filament. *Proc Natl Acad Sci USA.* (2016) 113:3257–62. doi: 10.1073/pnas.1519541113
- Pavada E, Rynkiewicz M, Yang Z, Gould I, Marston S, Lehman W. Modulation of cardiac thin filament structure by phosphorylated troponin-I analyzed by protein-protein docking and molecular dynamics simulation. *Arch Biochem Biophys.* (2022) 725:109282. doi: 10.1016/j.abb.2022.109282
- Cheng Y, Lindert S, Keken-Huskey P, Rao V, Solaro R, Rosevear P, et al. Computational studies of the effect of the S23D/S24D troponin I mutation on cardiac troponin structural dynamics. *Biophys J.* (2014) 107:1675–85. doi: 10.1016/j.bpj.2014.08.008
- Zhang X, Kampourakis T, Yan Z, Sevriva I, Irving M, Sun Y. Distinct contributions of the thin and thick filaments to length-dependent activation in heart muscle. *eLife.* (2017) 6:e24081. doi: 10.7554/eLife.24081
- Li K, Methawasin M, Tanner B, Granzier H, Solaro R, Dong W. Sarcomere length-dependent effects on Ca(2+)-troponin regulation in myocardium expressing compliant titin. *J Gen Physiol.* (2019) 151:30–41. doi: 10.1085/jgp.201812218
- Luther P, Winkler H, Taylor K, Zoghbi M, Craig R, Padrón R, et al. Direct visualization of myosin-binding protein C bridging myosin and actin filaments in intact muscle. *Proc Natl Acad Sci USA.* (2011) 108:11423–8. doi: 10.1073/pnas.1103216108
- Loescher C, Breitkreuz M, Li Y, Nickel A, Unger A, Dietl A, et al. Regulation of titin-based cardiac stiffness by unfolded domain oxidation (UnDOx). *Proc Natl Acad Sci USA.* (2020) 117:24545–56. doi: 10.1073/pnas.2004900117
- Rynkiewicz M, Pavada E, Lehman W. Modeling human cardiac thin filament structures. *Front Physiol.* (2022) 13:932333. doi: 10.3389/fphys.2022.932333
- Tobacman L. Troponin revealed: uncovering the structure of the thin filament on-off switch in striated muscle. *Biophys J.* (2021) 120:1–9. doi: 10.1016/j.bpj.2020.11.014
- Schmid M, Toepfer C. Cardiac myosin super relaxation (SRX): a perspective on fundamental biology, human disease and therapeutics. *Biol Open.* (2021) 10:bio057646. doi: 10.1242/bio.057646
- Craig R, Padrón R. Structural basis of the super- and hyper-relaxed states of myosin II. *J Gen Physiol.* (2022) 154:e202113012. doi: 10.1085/jgp.202113012
- Solis C, Solaro R. Novel insights into sarcomere regulatory systems control of cardiac thin filament activation. *J Gen Physiol.* (2021) 153:e202012777. doi: 10.1085/jgp.202012777
- Suay-Corredera C, Alegre-Cebollada J. The mechanics of the heart: zooming in on hypertrophic cardiomyopathy and cMyBP-C. *FEBS Lett.* (2022) 596:703–46. doi: 10.1002/1873-3468.14301
- Mun J, Previs M, Yu H, Gulick J, Tobacman L, Beck Previs S, et al. Myosin-binding protein C displaces tropomyosin to activate cardiac thin filaments and governs their speed by an independent mechanism. *Proc Natl Acad Sci USA.* (2014) 111:2170–5. doi: 10.1073/pnas.1316001111
- Yotti R, Seidman C, Seidman J. Advances in the genetic basis and pathogenesis of sarcomere cardiomyopathies. *Annu Rev Genomics Hum Genet.* (2019) 20:129–53. doi: 10.1146/annurev-genom-083118-015306
- Mun J, Gulick J, Robbins J, Woodhead J, Lehman W, Craig R. Electron microscopy and 3D reconstruction of F-actin decorated with cardiac myosin-binding protein C (cMyBP-C). *J Mol Biol.* (2011) 410:214–25. doi: 10.1016/j.jmb.2011.05.010
- Flashman E, Watkins H, Redwood C. Localization of the binding site of the C-terminal domain of cardiac myosin-binding protein-C on the myosin rod. *Biochem J.* (2007) 401:97–102. doi: 10.1042/BJ20060500
- Alyonycheva T, Mikawa T, Reinach F, Fischman D. Isoform-specific interaction of the myosin-binding proteins (MyBPs) with skeletal and cardiac myosin is a property of the C-terminal immunoglobulin domain. *J Biol Chem.* (1997) 272:20866–72. doi: 10.1074/jbc.272.33.20866
- Inchingolo A, Previs S, Previs M, Warshaw D, Kad N. Revealing the mechanism of how cardiac myosin-binding protein C N-terminal fragments sensitize thin filaments for myosin binding. *Proc Natl Acad Sci USA.* (2019) 116:6828–35. doi: 10.1073/pnas.1816480116
- Lu Y, Kwan A, Trewhella J, Jeffries C. The C0C1 fragment of human cardiac myosin binding protein C has common binding determinants for both actin and myosin. *J Mol Biol.* (2011) 413:908–13. doi: 10.1016/j.jmb.2011.09.026
- Mamidi R, Gresham K, Stelzer J. Length-dependent changes in contractile dynamics are blunted due to cardiac myosin binding protein-C ablation. *Front Physiol.* (2014) 5:461. doi: 10.3389/fphys.2014.00461
- Herron T, Rostkova E, Kunst G, Chaturvedi R, Gautel M, Kentish J. Activation of myocardial contraction by the N-terminal domains of myosin binding protein-C. *Circ Res.* (2006) 98:1290–8. doi: 10.1161/01.RES.0000222059.54917.ef
- Ponnam S, Kampourakis T. Microscale thermophoresis suggests a new model of regulation of cardiac myosin function via interaction with cardiac myosin-binding protein C. *J Biol Chem.* (2022) 298:101485. doi: 10.1016/j.jbc.2021.101485
- Whitten A, Jeffries C, Harris S, Trewhella J. Cardiac myosin-binding protein C decorates F-actin: implications for cardiac function. *Proc Natl Acad Sci USA.* (2008) 105:18360–5. doi: 10.1073/pnas.0808903105

## Conflict of interest

RS was a member of the Scientific Advisor Board of Cytokinetics, Inc. and a consultant to MyoKardia/Bristol-Myers-Squibb, and Edgewise Pharmaceuticals.

The remaining author declares that the research was conducted in the absence of any commercial or financial relationships that could be construed as a potential conflict of interest.

## Publisher's note

All claims expressed in this article are solely those of the authors and do not necessarily represent those of their affiliated organizations, or those of the publisher, the editors and the reviewers. Any product that may be evaluated in this article, or claim that may be made by its manufacturer, is not guaranteed or endorsed by the publisher.

30. Shaffer J, Kensler R, Harris S. The myosin-binding protein C motif binds to F-actin in a phosphorylation-sensitive manner. *J Biol Chem.* (2009) 284:12318–27. doi: 10.1074/jbc.M808850200
31. Tanner B, Previs M, Wang Y, Robbins J, Palmer B. Cardiac myosin binding protein-C phosphorylation accelerates  $\beta$ -cardiac myosin detachment rate in mouse myocardium. *Am J Physiol Heart Circ Physiol.* (2021) 320:H1822–35. doi: 10.1152/ajpheart.00673.2020
32. Tonino P, Kiss B, Gohlke J, Smith J III, Granzier H. Fine mapping titin's C-zone: matching cardiac myosin-binding protein C stripes with titin's super-repeats. *J Mol Cell Cardiol.* (2019) 133:47–56. doi: 10.1016/j.yjmcc.2019.05.026
33. Ratti J, Rostkova E, Gautel M, Pfuhl M. Structure and interactions of myosin-binding protein C domain C0: cardiac-specific regulation of myosin at its neck? *J Biol Chem.* (2011) 286:12650–8. doi: 10.1074/jbc.M110.156646
34. Witt C, Gerull B, Davies M, Centner T, Linke W, Thierfelder L. Hypercontractile properties of cardiac muscle fibers in a knock-in mouse model of cardiac myosin-binding protein-C. *J Biol Chem.* (2001) 276:5353–9. doi: 10.1074/jbc.M008691200
35. Reconditi M, Caremani M, Pinzauti F, Powers J, Narayanan T, Stienen G, et al. Myosin filament activation in the heart is tuned to the mechanical task. *Proc Natl Acad Sci USA.* (2017) 114:3240–5. doi: 10.1073/pnas.1619484114
36. Irving T, Craig R. Getting into the thick (and thin) of it. *J Gen Physiol.* (2019) 151:610–3. doi: 10.1085/jgp.201812307
37. Farman G, Gore D, Allen E, Schoenfelt K, Irving T, de Tombe P. Myosin head orientation: a structural determinant for the frank-starling relationship. *Am J Physiol Heart Circ Physiol.* (2011) 300:H2155–60. doi: 10.1152/ajpheart.01221.2010
38. Koser F, Loescher C, Linke W. Posttranslational modifications of titin from cardiac muscle: how, where, and what for? *FEBS J.* (2019) 286:2240–60. doi: 10.1111/febs.14854
39. Ait-Mou Y, Hsu K, Farman G, Kumar M, Greaser M, Irving T, et al. Titin strain contributes to the frank-starling law of the heart by structural rearrangements of both thin- and thick-filament proteins. *Proc Natl Acad Sci USA.* (2016) 113:2306–11. doi: 10.1073/pnas.1516732113
40. Vikhorev P, Vikhoreva N, Yeung W, Li A, Lal S, Dos Remedios C, et al. Titin-truncating mutations associated with dilated cardiomyopathy alter length-dependent activation and its modulation via phosphorylation. *Cardiovasc Res.* (2022) 118:241–53. doi: 10.1093/cvr/cvaa316
41. Arteaga G, Palmer K, Leiden J, Solaro R. Attenuation of length dependence of calcium activation in myofilaments of transgenic mouse hearts expressing slow skeletal troponin I. *J Physiol.* (2000) 526(Pt. 3):541–9. doi: 10.1111/j.1469-7793.2000.t01-1-00541.x
42. Mamidi R, Li J, Gresham K, Stelzer J. Cardiac myosin binding protein-C: a novel sarcomeric target for gene therapy. *Pflügers Archiv.* (2014) 466:225–30. doi: 10.1007/s00424-013-1412-z
43. Stathopoulou K, Wittig I, Heidler J, Piasecki A, Richter F, Diering S, et al. S-glutathionylation impairs phosphoregulation and function of cardiac myosin-binding protein C in human heart failure. *FASEB J.* (2016) 30:1849–64. doi: 10.1096/fj.201500048
44. Budde H, Hassoun R, Tangos M, Zhazykbayeva S, Herwig M, Varatnitskaya M, et al. The interplay between S-glutathionylation and phosphorylation of cardiac troponin i and myosin binding protein C in end-stage human failing hearts. *Antioxidants.* (2021) 10:1134. doi: 10.3390/antiox10071134
45. Chakouri N, Reboul C, Boulghobra D, Kleindienst A, Nottin S, Gayraud S, et al. Stress-induced protein S-glutathionylation and phosphorylation crosstalk in cardiac sarcomeric proteins - Impact on heart function. *Int J Cardiol.* (2018) 258:207–16. doi: 10.1016/j.ijcard.2017.12.004
46. Main A, Fuller W, Baillie G. Post-translational regulation of cardiac myosin binding protein-C: a graphical review. *Cell Signal.* (2020) 76:109788. doi: 10.1016/j.cellsig.2020.109788
47. Barefield D, Sadayappan S. Phosphorylation and function of cardiac myosin binding protein-C in health and disease. *J Mol Cell Cardiol.* (2010) 48:866–75. doi: 10.1016/j.yjmcc.2009.11.014
48. Rosas P, Liu Y, Abdalla M, Thomas C, Kidwell D, Dusio G, et al. Phosphorylation of cardiac myosin-binding protein-C is a critical mediator of diastolic function. *Circ Heart Fail.* (2015) 8:582–94. doi: 10.1161/CIRCHEARTFAILURE.114.001550
49. Ponnamp S, Sevrieva I, Sun Y, Irving M, Kampourakis T. Site-specific phosphorylation of myosin binding protein-C coordinates thin and thick filament activation in cardiac muscle. *Proc Natl Acad Sci USA.* (2019) 116:15485–94. doi: 10.1073/pnas.1903033116
50. Gautel M, Zuffardi O, Freiburg A, Labeit S. Phosphorylation switches specific for the cardiac isoform of myosin binding protein-C: a modulator of cardiac contraction? *EMBO J.* (1995) 14:1952–60. doi: 10.1002/j.1460-2075.1995.tb07187.x
51. Solaro R, Moir A, Perry S. Phosphorylation of troponin I and the inotropic effect of adrenaline in the perfused rabbit heart. *Nature.* (1976) 262:615–7. doi: 10.1038/262615a0
52. Solaro R, Henze M, Kobayashi T. Integration of troponin I phosphorylation with cardiac regulatory networks. *Circ Res.* (2013) 112:355–66. doi: 10.1161/CIRCRESAHA.112.268672
53. Howarth J, Meller J, Solaro R, Trewhella J, Rosevear P. Phosphorylation-dependent conformational transition of the cardiac specific N-extension of troponin I in cardiac troponin. *J Mol Biol.* (2007) 373:706–22. doi: 10.1016/j.jmb.2007.08.035
54. Kovács Á, Alogna A, Post H, Hamdani N. Is enhancing cGMP-PKG signalling a promising therapeutic target for heart failure with preserved ejection fraction? *Neth Heart J.* (2016) 24:268–74. doi: 10.1007/s12471-016-0814-x
55. Konhilas J, Irving T, Wolska B, Jweid E, Martin A, Solaro R, et al. Troponin I in the murine myocardium: influence on length-dependent activation and interfilament spacing. *J Physiol.* (2003) 547(Pt. 3):951–61. doi: 10.1113/jphysiol.2002.038117
56. Mamidi R, Gresham K, Verma S, Stelzer J. Cardiac myosin binding protein-C phosphorylation modulates myofilament length-dependent activation. *Front Physiol.* (2016) 7:38. doi: 10.3389/fphys.2016.00038
57. Kumar M, Govindan S, Zhang M, Khairallah R, Martin J, Sadayappan S, et al. Cardiac myosin-binding protein C and troponin-I phosphorylation independently modulate myofilament length-dependent activation. *J Biol Chem.* (2015) 290:29241–9. doi: 10.1074/jbc.M115.686790
58. Jeong E, Monasky M, Gu L, Taglieri D, Patel B, Liu H, et al. Tetrahydrobiopterin improves diastolic dysfunction by reversing changes in myofilament properties. *J Mol Cell Cardiol.* (2013) 56:44–54. doi: 10.1016/j.yjmcc.2012.12.003
59. Patel B, Wilder T, Solaro R. Novel control of cardiac myofilament response to calcium by S-glutathionylation at specific sites of myosin binding protein C. *Front Physiol.* (2013) 4:336. doi: 10.3389/fphys.2013.00336
60. Chen F, Ogut O. Decline of contractility during ischemia-reperfusion injury: actin glutathionylation and its effect on allosteric interaction with tropomyosin. *Am J Physiol Cell Physiol.* (2006) 290:C719–27. doi: 10.1152/ajpcell.00419.2005
61. Pizarro G, Ogut O. Impact of actin glutathionylation on the actomyosin-S1 ATPase. *Biochemistry.* (2009) 48:7533–8. doi: 10.1021/bi900669m
62. Dalle-Donne I, Giustarini D, Rossi R, Colombo R, Milzani A. Reversible S-glutathionylation of Cys 374 regulates actin filament formation by inducing structural changes in the actin molecule. *Free Radic Biol Med.* (2003) 34:23–32. doi: 10.1016/S0891-5849(02)01182-6
63. Avner B, Shioura K, Scruggs S, Grachoff M, Geenen D, Helseth D Jr, et al. Myocardial infarction in mice alters sarcomeric function via post-translational protein modification. *Mol Cell Biochem.* (2012) 363:203–15. doi: 10.1007/s11010-011-1172-z
64. Alegre-Cebollada J, Kosuri P, Giganti D, Eckels E, Rivas-Pardo J, Hamdani N, et al. S-glutathionylation of cryptic cysteines enhances titin elasticity by blocking protein folding. *Cell.* (2014) 156:1235–46. doi: 10.1016/j.cell.2014.01.056
65. Kovács Á, Herwig M, Budde H, Delalat S, Kolijn D, Bódi B, et al. Interventricular differences of signaling pathways-mediated regulation of cardiomyocyte function in response to high oxidative stress in the post-ischemic failing rat heart. *Antioxidants.* (2021) 10:964. doi: 10.3390/antiox10060964
66. De Flora S, Balansky R, La Maestra S. Rationale for the use of N-acetylcysteine in both prevention and adjuvant therapy of COVID-19. *FASEB J.* (2020) 34:13185–93. doi: 10.1096/fj.202001807
67. Wilder T, Ryba D, Wiecek D, Wolska B, Solaro RJ. N-acetylcysteine reverses diastolic dysfunction and hypertrophy in familial hypertrophic cardiomyopathy. *Am J Physiol Heart Circ Physiol.* (2015) 309:H1720–30. doi: 10.1152/ajpheart.00339.2015
68. Ryba D, Warren C, Karam C, Davis R III, Chowdhury S, Alvarez M, et al. Sphingosine-1-phosphate receptor modulator, FTY720, improves diastolic dysfunction and partially reverses atrial remodeling in a Tm-E180G mouse model linked to hypertrophic cardiomyopathy. *Circ Heart Fail.* (2019) 12:e005835. doi: 10.1161/CIRCHEARTFAILURE.118.005835
69. Liu W, Zi M, Tsui H, Chowdhury S, Zeef L, Meng Q, et al. A novel immunomodulator, FTY-720 reverses existing cardiac hypertrophy and fibrosis from pressure overload by targeting NFAT (nuclear factor of activated T-cells) signaling and perlestin. *Circ Heart Fail.* (2013) 6:833–44. doi: 10.1161/CIRCHEARTFAILURE.112.000123
70. Cuello F, Herberg F, Stathopoulou K, Henning P, Diering S. Regulation of cardiac PKA signaling by cAMP and oxidants. *Antioxidants.* (2021) 10:663. doi: 10.3390/antiox10050663
71. Methawasin M, Hutchinson K, Lee E, Smith J III, Saripalli C, Hidalgo C, et al. Experimentally increasing titin compliance in a novel mouse model attenuates the frank-starling mechanism but has a beneficial effect on diastole. *Circulation.* (2014) 129:1924–36. doi: 10.1161/CIRCULATIONAHA.113.005610
72. Ahmed I, Loudon B, Abozguia K, Cameron D, Shivu G, Phan T, et al. Biventricular pacemaker therapy improves exercise capacity in patients with non-obstructive hypertrophic cardiomyopathy via augmented diastolic filling on exercise. *Eur J Heart Fail.* (2020) 22:1263–72. doi: 10.1002/ehf.1722
73. Niederer S, Plank G, Chinchapatnam P, Ginks M, Lamata P, Rhode K, et al. Length-dependent tension in the failing heart and the efficacy of cardiac resynchronization therapy. *Cardiovasc Res.* (2011) 89:336–43. doi: 10.1093/cvr/cvq318
74. Chandra M, Rundell V, Tardiff J, Leinwand L, De Tombe P, Solaro R. Ca(2+) activation of myofilaments from transgenic mouse hearts expressing R92Q mutant cardiac troponin T. *Am J Physiol Heart Circ Physiol.* (2001) 280:H705–13. doi: 10.1152/ajpheart.2001.280.2.H705
75. Mickelson A, Chandra M. Hypertrophic cardiomyopathy mutation in cardiac troponin T (R95H) attenuates length-dependent activation in guinea pig cardiac muscle

- fibers. *Am J Physiol Heart Circ Physiol*. (2017) 313:H1180–9. doi: 10.1152/ajpheart.00369.2017
76. Reda S, Chandra M. Cardiomyopathy mutation (F88L) in troponin T abolishes length dependency of myofilament Ca(2+) sensitivity. *J Gen Physiol*. (2018) 150:809–19. doi: 10.1085/jgp.201711974
77. Tong C, Dusio G, Govindan S, Johnson D, Kidwell D, De La Rosa L, et al. Usefulness of released cardiac myosin binding protein-C as a predictor of cardiovascular events. *Am J Cardiol*. (2017) 120:1501–7. doi: 10.1016/j.amjcard.2017.07.042
78. Govindan S, Kuster D, Lin B, Kahn D, Jeske W, Walenga J, et al. Increase in cardiac myosin binding protein-C plasma levels is a sensitive and cardiac-specific biomarker of myocardial infarction. *Am J Cardiovasc Dis*. (2013) 3: 60–70.
79. Marber M, Mills N, Morrow D, Mueller C. Cardiac myosin-binding protein C as a biomarker of acute myocardial infarction. *Eur Heart J Acute Cardiovasc Care*. (2021) 10:963–5. doi: 10.1093/ehjacc/zuab086
80. Alaour B, Omland T, Torsvik J, Kaier T, Sylte M, Strand H, et al. Biological variation of cardiac myosin-binding protein C in healthy individuals. *Clin Chem Lab Med*. (2022) 60:576–83. doi: 10.1515/cclm-2021-0306
81. Jeong E, Chung J, Liu H, Go Y, Gladstein S, Farzaneh-Far A, et al. Role of mitochondrial oxidative stress in glucose tolerance, insulin resistance, and cardiac diastolic dysfunction. *J Am Heart Assoc*. (2016) 5:e003046. doi: 10.1161/JAHA.115.003046
82. Zhou X, Jeong E, Liu H, Kaseer B, Liu M, Shrestha S, et al. Circulating S-glutathionylated cMyBP-C as a biomarker for cardiac diastolic dysfunction. *J Am Heart Assoc*. (2022) 11:e025295. doi: 10.1161/JAHA.122.025295
83. Solaro C, Solaro R. Implications of the complex biology and micro-environment of cardiac sarcomeres in the use of high affinity troponin antibodies as serum biomarkers for cardiac disorders. *J Mol Cell Cardiol*. (2020) 143:145–58. doi: 10.1016/j.yjmcc.2020.05.010
84. Utter M, Warren C, Solaro R. Impact of anesthesia and storage on posttranslational modifications of cardiac myofilament proteins. *Physiol Rep*. (2015) 3:e12393. doi: 10.14814/phy2.12393
85. Karsai A, Kellermayer M, Harris S. Mechanical unfolding of cardiac myosin binding protein-C by atomic force microscopy. *Biophys J*. (2011) 101:1968–77. doi: 10.1016/j.bpj.2011.08.030
86. Solaro R, Rosas P, Langa P, Warren C, Wolska B, Goldspink P. Mechanisms of troponin release into serum in cardiac injury associated with COVID-19 patients. *Int J Cardiol Cardiovasc Dis*. (2021) 1:41–7. doi: 10.46439/cardiology.1.006





## OPEN ACCESS

## EDITED BY

Alexander E. Berezin,  
Zaporizhia State Medical University, Ukraine

## REVIEWED BY

Thomas E. Sharp III,  
Louisiana State University, United States  
Elisabeth Ehler,  
King's College London, United Kingdom

## \*CORRESPONDENCE

Michelle Peckham  
✉ m.peckham@leeds.ac.uk

## SPECIALTY SECTION

This article was submitted to  
Heart Failure and Transplantation,  
a section of the journal  
Frontiers in Cardiovascular Medicine

RECEIVED 10 November 2022

ACCEPTED 30 January 2023

PUBLISHED 14 February 2023

## CITATION

Parker F, Tang AAS, Rogers B, Carrington G,  
dos Remedios C, Li A, Tomlinson D and  
Peckham M (2023) Affimers targeting proteins  
in the cardiomyocyte Z-disc: Novel tools that  
improve imaging of heart tissue.  
*Front. Cardiovasc. Med.* 10:1094563.  
doi: 10.3389/fcvm.2023.1094563

## COPYRIGHT

© 2023 Parker, Tang, Rogers, Carrington, dos  
Remedios, Li, Tomlinson and Peckham. This is  
an open-access article distributed under the  
terms of the [Creative Commons Attribution  
License \(CC BY\)](#). The use, distribution or  
reproduction in other forums is permitted,  
provided the original author(s) and the  
copyright owner(s) are credited and that the  
original publication in this journal is cited, in  
accordance with accepted academic practice.  
No use, distribution or reproduction is  
permitted which does not comply with  
these terms.

# Affimers targeting proteins in the cardiomyocyte Z-disc: Novel tools that improve imaging of heart tissue

Francine Parker<sup>1</sup>, Anna A. S. Tang<sup>1</sup>, Brendan Rogers<sup>1</sup>,  
Glenn Carrington<sup>1</sup>, Cris dos Remedios<sup>2</sup>, Amy Li<sup>3,4,5</sup>,  
Darren Tomlinson<sup>1</sup> and Michelle Peckham<sup>1\*</sup>

<sup>1</sup>School of Molecular and Cellular Biology, Faculty of Biological Sciences, University of Leeds, Leeds, United Kingdom, <sup>2</sup>Mechanobiology Laboratory, Victor Chang Cardiac Research Institute, Darlinghurst, NSW, Australia, <sup>3</sup>Sydney Heart Bank, The University of Sydney, Sydney, NSW, Australia, <sup>4</sup>Department of Pharmacy & Biomedical Sciences, La Trobe University, Bendigo, VIC, Australia, <sup>5</sup>Centre for Healthy Futures, Torrens University Australia, Surrey Hills, NSW, Australia

Dilated Cardiomyopathy is a common form of heart failure. Determining how this disease affects the structure and organization of cardiomyocytes in the human heart is important in understanding how the heart becomes less effective at contraction. Here we isolated and characterised Affimers (small non-antibody binding proteins) to Z-disc proteins ACTN2 ( $\alpha$ -actinin-2), ZASP (also known as LIM domain binding protein 3 or LDB3) and the N-terminal region of the giant protein titin (TTN Z1-Z2). These proteins are known to localise in both the sarcomere Z-discs and the transitional junctions, found close to the intercalated discs that connect adjacent cardiomyocytes. We use cryosections of left ventricles from two patients diagnosed with end-stage Dilated Cardiomyopathy who underwent Orthotopic Heart Transplantation and were whole genome sequenced. We describe how Affimers substantially improve the resolution achieved by confocal and STED microscopy compared to conventional antibodies. We quantified the expression of ACTN2, ZASP and TTN proteins in two patients with dilated cardiomyopathy and compared them with a sex- and age-matched healthy donor. The small size of the Affimer reagents, combined with a small linkage error (the distance from the epitope to the dye label covalently bound to the Affimer) revealed new structural details in Z-discs and intercalated discs in the failing samples. Affimers are thus useful for analysis of changes to cardiomyocyte structure and organisation in diseased hearts.

## KEYWORDS

Dilated Cardiomyopathy, Affimer, Z-disc, intercalated disc, fluorescence microscopy, cardiac actinin, ZASP and the N-terminal region of titin (TTN)

# 1. Introduction

Dilated Cardiomyopathy (DCM) is a major cause of heart failure worldwide. It has a prevalence of between 1 in 250 to 1 in 400 people (1, 2) and is the leading cause of Orthotopic Heart Transplantation (OHT). It is characterised as systolic dysfunction and dilation usually of the left ventricle (LV). It is commonly associated with arrhythmias and sudden death (3). In the US the prevalence of familial dilated cardiomyopathy (FDCM) was recently reported at 29.7% (4) but this figure may increase with time. A mutation in cardiac actin (ACTC) was the first to be identified as a possible cause of DCM (5) followed by reports of mutations in cardiac myosin heavy chain (MYH6 and MYH7), troponin T, troponin I and  $\alpha$ -tropomyosin (6). Genetic variants in MYH7 are reported to be the third most common cause of DCM (7), about 10% of all cases. The clinical characteristics for these were recently comprehensively evaluated (8).

Since the first report identifying mutations in TTN as a cause of DCM (9), we now know that TTN truncating mutations (TTNtv) account for about 25% of all familial DCMs (10). Titin is the largest known protein with a molecular weight of  $\sim 3$  MDa and a length  $> 1 \mu\text{m}$  (11). It spans from the Z-disc (N-terminus) in striated muscle to the central M-band (C-terminus) of striated muscle sarcomeres and is thought to be a key regulator of sarcomere assembly and function (12, 13). The central A-band region is primarily composed of repeating immunoglobulin (Ig) and fibronectin-3-like (Fn-3) domains that predominantly interact with myosin and myosin-binding protein C in the A band. This region of titin is thought to act as a molecular “ruler,” regulating the formation, length and position of the myosin-containing thick filament (11). Its huge size (363 coding exons) and complexity accounts for alternative splicing that results in at least three different isoforms in cardiac muscle (14). TTNvs were only recently identified as a major cause of disease (15, 16).

TTNvs result in premature stop codons, splice variants and frameshift mutations. TTNvs are more likely to occur some distance from the N-terminus of the protein (17). They are most common in the A-band region of titin, in both N2A and N2B isoforms and are largely absent from Z-disc and M-band regions (16–18). Variants in the A-band region of titin and are the most pathogenic (18). iPSCs and CRISPR studies have been used to evaluate the effects of these mutations in humans (19).

Here, our main objective was to evaluate the usefulness of using novel, antigen binding proteins called Affimers [originally termed Adhirons (20)] in determining the overall organisation of sarcomeric proteins in frozen sections of DCM tissue from the Sydney heart bank. Affimers are much smaller than antibodies, with a molecular mass of 10–12 kDa and dimensions of  $\sim 2$ – $3 \text{ nm}$  (21–23). They are formed of a scaffold consisting of a consensus plant phytocystatin protein sequence, have been engineered to be highly soluble and to have high thermal stability. The binding interface is provided by two regions of variable sequence, approximately 9 residues in length. Affimers to proteins, or protein domains of interest are isolated by screening a phage display Affimer library, in which the amino acids in the regions of variable sequence have been randomised. The ability of the isolated Affimers to bind to their targets are then confirmed by phage ELISA. Each Affimer is then sequenced, and approximately 10 Affimers are then taken forward for further testing. The sequences are subcloned into bacterial expression vectors, to

introduce a His tag for purification, and, in our case, a single unique N- or C-terminal cysteine, to enable direct fluorescent dye labelling. Purified dye labelled Affimers are then tested for their ability to label structures of interest efficiently and specifically, with low background. The best performing Affimer is then used in subsequent experiments.

In this new work, we report that Affimers work better than antibodies in labelling samples of control and DCM tissue from the Sydney Heart Bank (24). We tested Affimers to the cardiac isoform of  $\alpha$ -actinin-2 (25), ZASP (Cypher/Oracle/Enigma: a PDZ-LIM protein) and the Z1Z2 repeats of titin. Samples of DCM tissue from this heart bank have already been shown to be useful in evaluating the effects of mutations on the contractile properties of myofibrils from DCM hearts (26, 27), with some analysis on the morphology of this tissue (28). The small size of the Affimer reagents enhances their ability to penetrate tissue sections and improves their ability to identify regions within the dense cytoskeleton, compared to conventional antibodies or even their small (Fab) fractions. To demonstrate their efficacy, we focused on heart tissue samples derived from two different patients [see (26)], both of which have a single TTNtv frameshift variant implicated in FDCM (p.R23464Tfs\*41) and compared these to samples from an age and sex-matched control.

## 2. Results

### 2.1. Affimers to Z-disc protein domains

We isolated Affimers to three Z-disc proteins, by screening a phage display library against the calponin homology (CH) domains of  $\alpha$ -actinin-2 (ACTN2) the Z1Z2 repeats of titin, and full length ZASP (Isoform 2 of LIM domain-binding protein 3, also known as cypher). ACTN2 crosslinks actin filaments within the Z-disc. The Z1Z2 repeats of titin are formed of Ig domains and are found within the N-terminal region of titin, located in the Z-disc (29). ZASP (Z-disc alternatively spliced PDZ-motif) is a member of the ALP/Enigma family (30), forms a multiprotein complex ACTN2 and is implicated in signalling (31). All the Affimers, confirmed to bind to their protein targets by phage ELISA (data not shown), were subcloned into bacterial expression vectors, expressed, purified, dye labelled and tested for their ability to label Z-discs. A single Affimer for each target, that labelled Z-discs specifically and showed low background staining was then taken forward for further analysis.

Next, we were interested to determine if AlphaFold modelling could be useful in predicting the site of interaction between the Affimer and its target. We already know the site of interaction for the ACTN Affimer as we previously solved a crystal structure of the Affimer bound to the CH domains of ACTN2 [(PDB: 6SWT (25)] and see **Supplementary Figure 1A**). However, we have not yet obtained crystal structures for the ZASP and titin Z1Z2 Affimers, and AlphaFold could provide a good fast alternative approach to crystallisation, to determine the site of interaction.

First, we compared the structures predicted by AlphaFold modelling with our published ACTN2-CH domain-Affimer crystal structure (PDB: 6SWT) to determine the efficacy of AlphaFold in predicting the mode of binding (**Supplementary Figure 1**). AlphaFold did correctly predict the structures of the isolated CH domain structure of ACTN2 (RMSD  $\sim 0.29 \text{ \AA}$ ) and the Affimer (RMSD  $\sim 0.6 \text{ \AA}$ ) with a high degree of accuracy

(**Supplementary Figures 1A, B, 2**). For the CH-domain-Affimer complex, two of the five AlphaFold predictions show a similar interaction of the Affimer with the ACTN2 CH domain to that found in the crystal structure, in which variable loop-1 of the Affimer interacts with a loop within CH domain 2 (**Supplementary Figures 1A, B**). This suggests that AlphaFold can, with some degree of certainty, predict the epitope on the protein of interest that the Affimer is recognising.

Next, we used AlphaFold modelling for the Affimer-Z1Z2 complex and the Affimer-ZASP complexes. From the results, we speculate that the Z1Z2 Affimer likely recognises the C-terminus of Z1Z2 (Z2 domain; 3 hits) or the unstructured loop connecting the 2 domains (2 hits) (**Supplementary Figures 1C, 2**). However, this approach was less successful for ZASP, which is predicted to be largely disordered, with the exception of the first 84 residues that form a PDZ domain, a site of interaction for ACTN2 (32). Not surprisingly, the confidence in ZASP structural prediction is considerably lower, with the regions connecting between the relatively well-structured N- (~1–100aa) and C- (~420–617aa) regions showing per residue confidence (pLDDT) scores below 50% confidence (**Supplementary Figure 2**). Omitting regions with a confidence score of less than 30% suggests that the ZASP Affimer recognises an epitope at the very C-terminus of ZASP (**Supplementary Figure 1D**). Thus, AlphaFold could be useful for predicting sites of interaction in the future, but the degree of confidence in these results is variable. However, knowing the precise site of interaction is not essential to using the Affimers in downstream applications, such as staining of tissue samples.

## 2.2. Affimer tissue penetration is improved compared to antibodies

To determine the specificity of Affimers to effectively label protein structures in human heart sections, we compared the staining results using Affimers and antibodies to ACTN2 and to the Z1Z2 repeats of titin imaged by confocal (Antibodies to ZASP were not available to us). The resulting images showed that fluorescent labelling of the heart sections was much more uniform across the whole section for ACTN2 and Z1Z2 Affimers compared to that for anti-ACTN2 and Z1Z2 antibodies (**Figure 1A**). The fluorescence intensity across the section was highly variable, when the sections were labelled with antibodies against ACTN2 and Z1Z2, followed by secondary fluorescent antibodies, with levels of labelling higher toward the edge, or less dense parts, of the section. In contrast, the fluorescence intensity across the section was much more uniform, when the sections were labelled with Affimers (**Figure 1B**). In addition, the transitional zones close to the intercalated discs (ICD) were labelled well by the Affimer but labelling by the antibody was less uniform (**Figure 1A**: boxed region).

Super-resolution (STED) microscopy was used to further compare the ability of Affimers and antibodies to label the Z-disc. The xy-resolution of confocal microscopy (~200 nm, or ~170 nm in Airyscan mode) is not sufficient to resolve any detail within the Z-disc [approximately 100–140 nm in cardiac tissue (33)]. The xy-resolution for 2D-STED (stimulated emission depletion) microscopy is approximately 50nm and can resolve some structure within the Z-disc.

STED imaging of the same tissue sections used for confocal microscopy (**Figure 1A**) further demonstrates that the small size of

the Affimers allows them to better penetrate the Z-disc structure and label ACTN2 and Z1Z2 repeats of titin, which should be distributed through the Z-disc, compared to antibodies. ACTN2 and Z1Z2 antibodies labelled the edges of Z-discs but were mostly absent from the central region of the Z-disc (**Figures 1C, E**). This variation in staining is demonstrated by intensity profile plots across the Z-disc, which revealed two peaks for the antibody labelling at the edges of the Z-disc (**Figures 1C, E**). In contrast, the Affimers labelled the Z-disc uniformly throughout (**Figures 1C, E**). It is worth noting here that the Z1Z2 repeats were first reported to be located in the central region of the Z-disc (29) whereas a later study using the Z1Z2 antibody used here showed that they were located toward the edge of the Z-disc (34). Our work with the Affimer suggests that the first report is likely to be correct.

The small size and direct labelling of Affimers puts the dye label very close to the epitope that the Affimer recognizes (~4 nm). In contrast, the combination of primary and secondary antibodies typically puts the dye label much further away (~30 nm). The average width of the Z-disc measured from deconvolved STED images, using specimens labelled with both antibody and Affimer, was larger (262 and 238 nm for ACTN2 and Z1Z2 respectively) using the antibody labelling than using the Affimer labelling (163 and 197 nm). The values measured for the Affimers are closer to the 130 nm width measured for the Z-disc in vertebrate cardiac muscle from EM data (35) (**Figures 1D, F**).

## 2.3. Affimers detect molecular changes in sarcomeres from DCM patient samples. Z-discs are thicker and sarcomeres are shorter

Having confirmed that the ACTN2 and Z1Z2 Affimers outperform antibodies in labelling these proteins within the Z-disc, we then used these 2 Affimers and one additional Affimer isolated to ZASP to stain the Z-discs in control samples (age, sex matched) and in two heart samples from two different DCM patients (DCM1 and DCM2) sharing the same A-band titin mutation. All the samples were labelled with the ACTN2 Affimer and co-labelled with either ZASP or Z1Z2 Affimers.

In donors and DCM heart samples, all three Affimers labelled the Z-disc well. The labelling showed the characteristic striated pattern expected for Z-discs in cardiomyocytes in both control and DCM samples (**Figure 2**). In DCM samples, the myofibrils were less well organized with evidence of myofibrillar disarray and misalignment (**Figures 2A, B**). In addition, the width of the Z-disc was increased compared to controls, and the spacing between Z-discs (sarcomere length) decreased. To quantify this, we measured the Z-disc widths and sarcomere length for control and DCM patient tissue using deconvolved 2D-STED images of Z-discs labelled by each of the three Affimers (**Figures 2A, B**). Sarcomere lengths (distance between Z-discs) were significantly decreased (**Figure 2C**) and Z-disc widths significantly increased (**Figure 2D**) in heart samples from the two DCM patients compared to controls.

The Z-disc widths measured for ACTN2 and Z1Z2 in this second dataset for samples co-stained with Affimers are consistent with the measurements for of Z-disc widths measured for the Affimers in the first independent dataset in which samples were co-stained with antibodies and Affimers (**Figures 1D, F**). Interestingly, the Z-disc

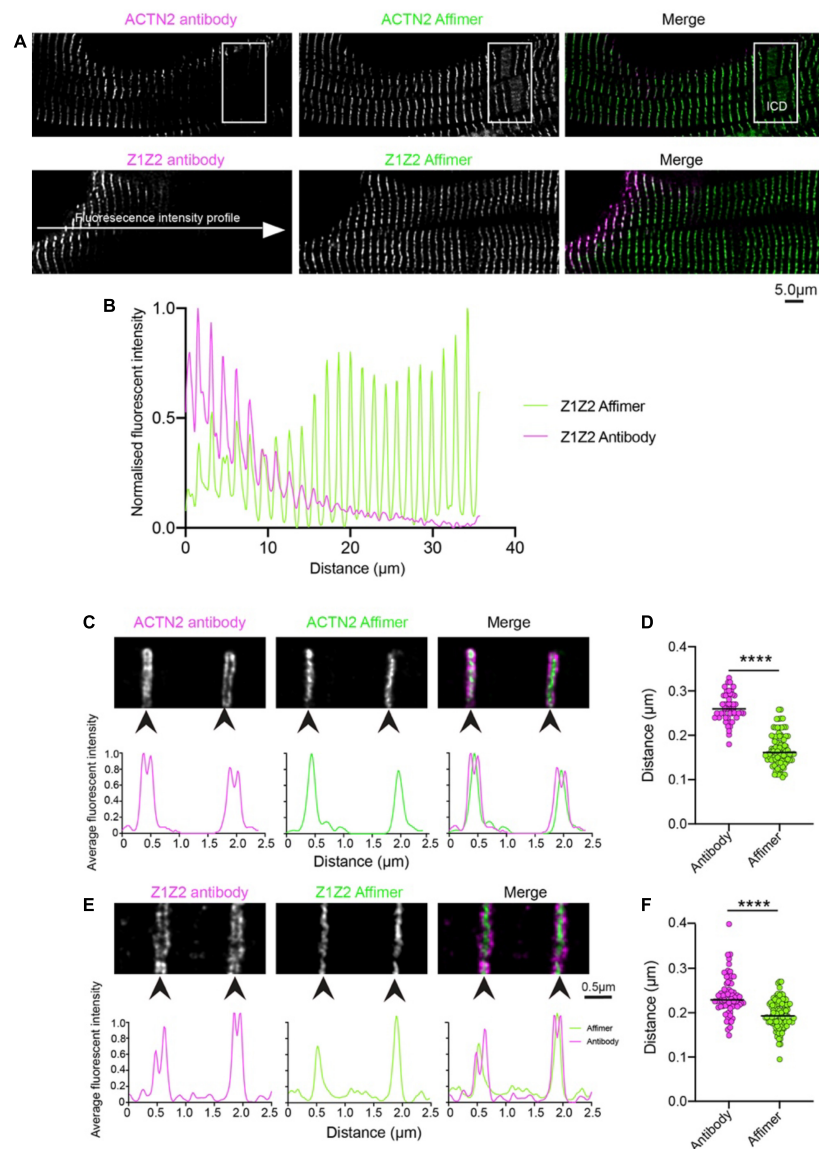


FIGURE 1

Comparison of staining heart sections using antibodies and Affimers to ACTN2 and titin Z1Z2 repeats. (A) Example confocal image of a region of a donor heart section stained using a primary antibody to ACTN2 or the Z1Z2 repeat of titin combined with a secondary fluorescent antibody, and with a dye-labelled Affimer. The boxed region shows the position of the ICD: intercalated disc. (B) Example of fluorescence intensity (normalized) for a line profile drawn across the cell for the ACTN2 antibody (magenta) and Affimer (green). Example 2D-STED images for Z-discs stained using the ACTN2 primary and secondary antibody combination and the dye-labelled ACTN2 Affimer (C) and the titin Z1Z2 antibody combination and Z1Z2 Affimer (E) are shown together with the associated profile plots for the labelling intensity across the Z-disc structures. (D,F) Measurements of the Z-disc widths for multiple Z-discs from sections labelled with the antibody combination and Affimers, using either the antibody images or the Affimer images.

\*\*\*\* $p < 0.0001$ .

width measured for Z1Z2 is increased compared to that measured for ACTN2 in both. Z-disc width measured for Z1Z2 ( $200 \pm 33$  nm, mean  $\pm$  SD) is significantly higher than that measured for ACTN2 ( $170 \pm 0.040$  nm: mean  $\pm$  SD) and may reflect a wider distribution of Z1Z2 titin epitopes across the Z-disc, compared to ACTN2.

## 2.4. Z-disc Affimers label the edges of intercalated discs

Cardiomyocytes connect to each other at the intercalated discs, structures that enable communication between cardiomyocytes. The

plasma membrane in this region is highly folded, and a transitional zone has been reported in which Z-disc proteins (ACTN, titin) assemble into a structure at the position in which the final Z-disc of the muscle sarcomere would be expected to be found (36). A titin antibody (T12) that labels a region of titin just outside of the Z-disc showed a doublet distribution either side of the intercalated disc (36). The thin filaments have been suggested to pass through this transitional zone and insert into the adherens junction in the intercalated disc, to enable effective structural integration of the myofibrils at this junction (36).

Focusing on Affimer labelling at the intercalated disc, which was identified by antibody labelling for desmoglein-2, revealed that ZASP, ACTN2 and Z1Z2 Affimers all label a structure close



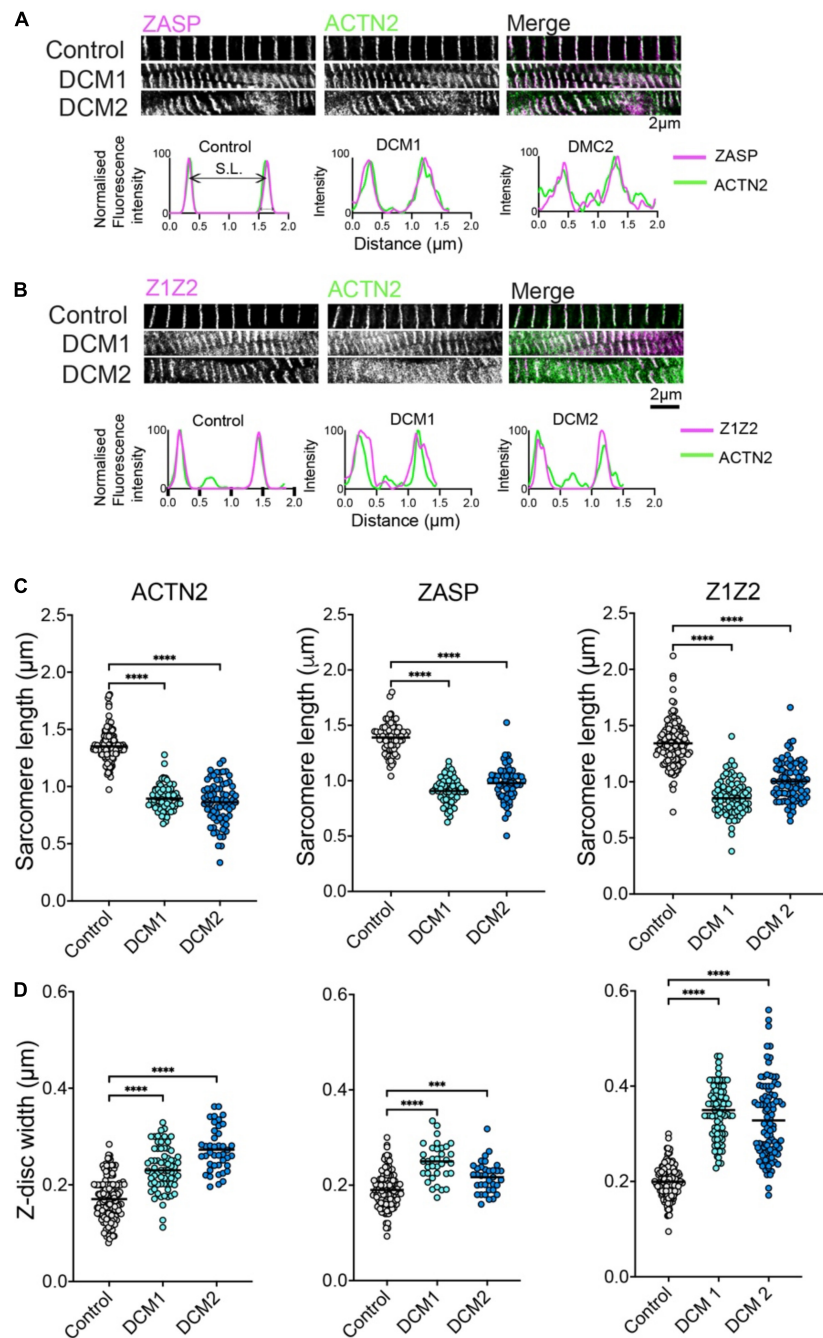


FIGURE 2

ZASP, ACTN2 and titin Z1Z2 Z-disc labelling using Affimer combinations and analysis. **(A)** Example 2D-STED images of heart tissue sections from control (donor tissue) and two independent DCM patients with the same TTN mutation, co-stained using an Affimer to ZASP (magenta in merged image) and ACTN2 (green in merged image). Example line profiles for ZASP and ACTN2 across two a single sarcomere, including both Z-discs at either side are shown below. These profiles were used to estimate Z-disc width and sarcomere length. **(B)** Example images of heart tissue sections from control and DCM patients stained using an Affimer to titin Z1Z2 (Magenta in merged image) and ACTN2 (green in merged image). Example line profile plots are shown below. **(C)** Measurements of Z-disc width for control and DCM patients. **(D)** Measurements of sarcomere lengths for control and DCM patients. Measurements were made from at least 50 sarcomeres from three independently stained heart tissue sections for controls and for each of the DCM patient tissue. \*\*\* $p < 0.001$ , \*\*\*\* $p < 0.0001$  for comparisons of DCM1 and DCM2 to control.

to the ICD (**Figures 3A–C**, WT) likely to be the transitional zone. We also observed that there was some labelling within the ICD, at right-angles to, and crossing the junction, possibly structures within the membrane. The intensity of ICD labelling using an antibody to desmoglein-2 was significantly lower in heart tissue samples from both DCM patients (**Figures 3B, C, F**). In addition, Affimer staining in this region was much

less ordered, especially in DCM2 compared to control samples (**Figure 3F**). Due to the highly disordered nature of the Affimer staining here, it was not possible to quantify the expression levels of the Z-disc proteins. Cardiomyocyte width estimated from the length of desmoglein-2 labelling across the end of the cardiomyocyte within the ICD was slightly increased in DCM samples (**Figure 3E**).

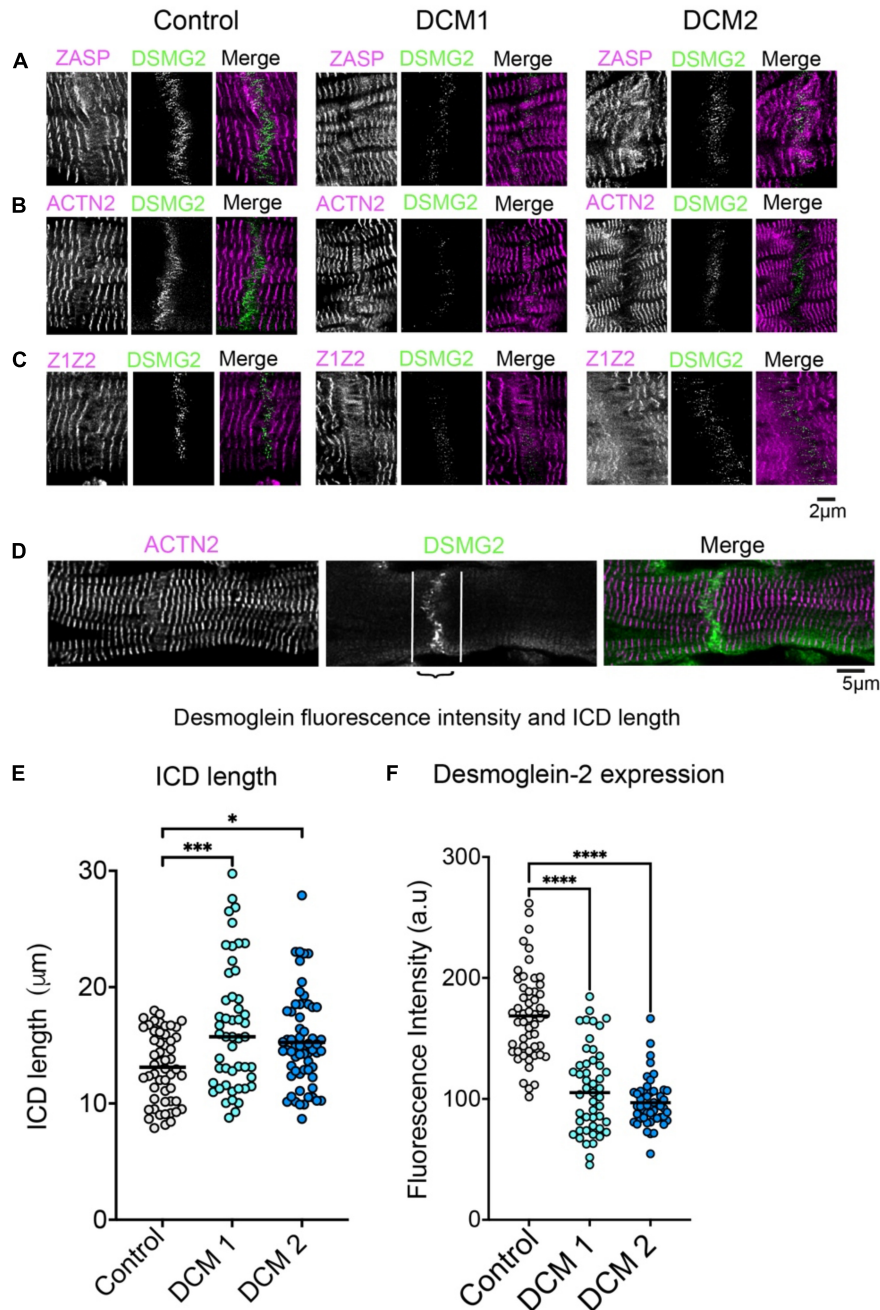


FIGURE 3

Labelling of intercalated discs (ICDs) between cardiomyocytes in heart tissue sections with Z-disc Affimers and desmoglein. Panels (A–C) are examples of labelling for ZASP (A), ACTN2 (B) and titin Z1Z2 (C) for control (normal donor heart) and DCM heart tissue sections. Panel (D) shows desmoglein staining for a single ICD in more detail to show the region of interest used to estimate labelling intensity for desmoglein (DSMG2) in the ICD. Panel (E) shows the average length of the ICD and (F) the fluorescence labelling intensity for desmoglein staining, for controls and DCM patients. A minimum of 50 ICDs were analysed for three independently stained heart tissue sections. \* $p < 0.05$ , \*\*\* $p < 0.001$ , \*\*\*\* $p < 0.0001$  for comparisons of DCM 1 and DCM2 to control.

### 3. Discussion

Here we report that Affimers to ACTN2, ZASP and titin (Z1Z2) are excellent tools for labelling the cardiac cytoskeleton. The Affimers label structures across the tissue sections with better uniformity, and better penetration of the compact Z-disc compared to traditional primary and secondary antibody combinations. The Z-disc widths measured using Affimers are closely aligned with values obtained by electron microscopy. They demonstrate that the Z-disc thickness

increases in DCM patients LV tissue compared to controls, an increase that was consistently observed for the three Affimers, while the sarcomere length was decreased. All three Affimers labelled the transition zone in the intercalated disc, with some Affimer labelling within the disc. Both DCM patients showed alterations to the structure of the intercalated disc.

Z-discs are narrow structures that vary from about 100–140 nm in width in cardiomyocytes to as little as ~30 nm in width in skeletal muscle (33). They are important structural and signalling centres and contain many different proteins. Accurately measuring

the width of Z-discs using the traditional primary and secondary antibody combination is challenging due to their large size which limits penetration of the antibodies into the Z-disc structure, and the positioning of the fluorophore ~30nm away from the target epitope. Here, the combination of STED microscopy and Affimers allowed more accurate measurements of Z-disc width, more consistent with that measured by electron microscopy. The Z-disc width increased for both DCM patients, which both harbour the same TTNtv.

Titin is a key molecule that is assembled into the Z-disc via its N-terminal domains and into the M-band via its C-terminal domains, spanning half a muscle sarcomere (14). In patients with TTNtv variants, not only are levels of wild-type titin reduced, but truncated titin isoforms are also present at least for TTNtv variants, where the truncation is relatively distal to the N-terminus. The p.R23464Tfs\*41 truncation is relatively distal to the N-terminus and can integrate into the muscle sarcomere (reviewed in (37–39)). The increased Z-disc width is consistent with the idea that a full-length intact titin molecule is required to transmit and buffer force generated by myosin during contraction (40) and that shorter variants of TTN such as the TTNtv variants likely result in disordered Z-discs.

Intercalated discs are critical for attachment of cardiomyocytes cell-cell signalling and communication. Here we found ACTN2, ZASP and titin Z1Z2 are all localised to the transition zone of the intercalated discs, consistent with earlier findings (36, 41, 42). We also show evidence of staining within the intercalated discs, not seen before, which highlights their ability to reveal new structures. This transitional zone has been suggested to act as a site for generating a new Z-disc complex and for sarcomere addition (41). Alterations to the structural integrity of the intercalated disc has previously been suggested to be important in cardiomyopathies (43, 44) and mutations in intercalated disc proteins also result in cardiomyopathies (45). More work is needed to understand how TTNtv variants can affect the structure and organisation of the intercalated discs.

In conclusion, we have shown that Affimers are excellent tools in analysing heart samples. Importantly, Affimers are easy to make, stable, and simple to use in labelling proteins in heart tissue sections. They outperform antibodies in imaging these sections, through better penetration, and their small size improves resolution. A simple one-step staining procedure makes staining easier, and overcomes any problems caused by using traditional labelled secondary antibodies. Specifically, we have demonstrated that Affimers can be used to characterise disease phenotype and reveal alterations to the structure and organisation of cardiomyocytes in patients with cardiomyopathies. If used in the clinic, they could be a useful tool to confirm the phenotype and help to diagnose DCM, if, as we anticipate, DCM generally leads to a widening of the Z-disc.

## 4. Materials and methods

### 4.1. Donor tissue and ethical approval

Anonymised tissue samples from explanted and donor hearts in the Sydney Heart Bank were used in this study (Table 1). Two patients with a diagnosis of familial DCM requiring a heart transplant at a young age, both with the same TTN frameshift

mutation (SHB code 4.100 (Male, 22years) and 4.125 (Male, 37 years) were selected together with an age/sex matched non-cardiac death donor (SHB code 6.038 (Male 37 years, non-cardiac death) as a control. Patients were consented under ethical approvals obtained from St Vincent's Hospital, Darlinghurst (HREC #H91/048/1a), the University of Sydney (HREC #2016/923). The heart samples for DCM were snap-frozen within 20–30 min of the loss of coronary blood flow. Frozen samples were shipped to the University of Leeds for analysis and stored and processed under ethical approval BIOSCI 17-015.

### 4.2. Affimer screening and expression

The Affimer reagent to  $\alpha$ -actinin-2 (ACTN2), isolated against the CH domains from ACTN2, has been described previously (25). Two new Affimer reagents were isolated to the N-terminal region of titin (Z1/Z2: residues 1–200) and to the ZASP (isoform 2: NP-001073583: 1–617 residues). To isolate the Affimers, target protein constructs were expressed and purified using *E. coli*. For Z1/Z2, a codon-optimised Z1/Z2 cDNA construct, cloned into pET28a-SUMO vector with a His tag for affinity purification was expressed in BL21 DE3 cells (Novagen), purified using NiNTA chromatography followed by size exclusion chromatography. The purified protein was then biotinylated before using in the Affimer screen. These two Z1Z2 domains of titin are located within the Z-disc (13). For ZASP, the coding sequence was cloned into a pGEX-Avitag vector (a kind gift from Christian Tiede) in frame with a C-terminal 15 residue Avitag (GLNDIFEAQKIEWHE) and a 6-His N-terminal tag for affinity purification. The protein was biotinylated in *E. Coli*, by co-expressing with pBirA using AVB101 bacterial cells (Avidity). Cells were grown in TYH (Tryptone, Yeast Extract, HEPES) medium supplemented with 0.5% glucose until the OD<sub>600</sub> reached 0.7. Protein expression and biotinylation was induced by the addition of 1.5 mM IPTG and 50 mM biotin solution (12 mg of d-biotin in 10 ml of 10 mM bicine buffer, pH 8.3) for 3 h. The expressed protein was purified by NiNTA chromatography. All expressed proteins were checked for purity. Western blots with streptavidin-HRP (Sigma) were performed to confirm the purified protein was the correct size and that it was the only protein that was biotinylated. Approximately 1.0 mg/ml of biotinylated protein were used in an Affimer screen as described (23, 25). Following the screen, approximately 8–10 Affimers that bound to the protein of interest, as demonstrated by ELISA were subcloned into pET11a for bacterial expression, using the *NotI* and *NheI* restriction sites and a unique cysteine residue was added at the C-termini to allow maleimide conjugation to a fluorescent dye.

### 4.3. Expression, purification, and Affimer labelling

Affimer expression was as described previously (23, 25). Cells from the expression cultures were harvested, pellets were frozen and then thawed on ice and lysed by addition of 1ml lysis Buffer (50 mM NaH<sub>2</sub>PO<sub>4</sub>; 500 mM NaCl; 30 mM Imidazole; 20% Glycerol; pH 7.4, supplemented with 1x HALT protease inhibitor cocktail (Promega), 0.1mg/ml lysozyme (Sigma), 1% Triton X-100 and 10 U/ml DNase) for one hour on a rotor mixer at room temperature.



TABLE 1 A summary of the details of the LV samples used in this report.

SHB code	Sex/Age (y)	Diagnosis	LVEF%	NYHA	Mutated gene	LR/RV co-morbidities	Publication
4.100	Male/22	DCM	15–20	IV	TTNtv	No CAD	(26, 48)
4.125	Male/36	DCM	15	IV	TTNtv	Dilated LV-RV. LAD 50% occluded	(27, 49)
6.038	Male/25	Donor	50+	NA	None	No CAD (cervical dislocation)	(50, 51)

The Sydney Heart Bank (SHB) code is an anonymised patient label. Patients were diagnosed with familial Dilated Cardiomyopathy (DCM) with both carrying a truncating mutation of the giant TTNtv gene. The clinical records for patient 4.100 included an unsupported note suggesting it may be “post-viral” but otherwise he exhibited no co-morbidities. The Pathology report for patient 4.125 confirmed he had 50% occlusion of the left anterior descending (LAD) artery only. Publications listed support the DCM and donor status of these patients (column 3). SHB: LVEF: left ventricular ejection fraction. NYHA: New York Heart Association classification of heart failure. (IV: class IV – severe).

Low stability *E. coli* proteins were denatured by heating to 50°C for 20 min (Affimers are stable at 50°C) and the insoluble fraction was pelleted at 16,000 g for 20 min. The supernatant was mixed with 300 mL Ni-NTA resin at room temperature for 1 h, washed in wash buffer (50 mM NaH<sub>2</sub>PO<sub>4</sub>; 500 mM NaCl; 20 mM Imidazole; 20% Glycerol; pH 7.4) and then eluted in the same buffer with 300 mM Imidazole. The concentration of Affimer eluted from the column was monitored by absorbance at A<sub>280</sub> on a NanoDrop spectrophotometer.

Affimer labelling was performed immediately after elution from the Ni-NTA column. Affimers were diluted to 1.0 mg/ml in PBS (phosphate buffered solution) and cysteine activated by mixing with immobilised TCEP (tris(2-carboxyethyl)phosphine) denaturing gel (Thermo Scientific) for 1 h at room temperature. Following a brief centrifugation of 1,000 rpm for 1 min, 130 µl of supernatant was removed and mixed in a 1.5 ml tube with 6 µl of a 2 mM stock maleimide-fluorescent dye (Abberior STAR 580- or STAR 635P-maleimide, Abberior) for 2 h at RT or overnight at 4°C. The reaction was quenched by the addition of 1.3 µl of β-mercaptoethanol for 15 min at room temperature. Labelled Affimers were dialysed against PBS to removed unbound dye (Snakeskin Dialysis Tubing molecular weight cut off 3.5, Pierce) or purified using PD SpinTrap G-25 columns (Cytivia) following manufacturers' instructions. SDS-PAGE was performed to assess Affimer purity and labelling.

#### 4.4. Tissue preparation, staining, and imaging of samples

Each of the 8–10 Affimers, isolated for each of the three protein targets (ACTN2, Z1Z2 and ZASP) were tested for their ability to label Z-discs in heart sections, and from these, the Affimer that gave the best signal, specific Z-disc labelling with low background, was taken forward for the remaining experiments presented here. To prepare sections, frozen left ventricular heart tissue was embedded in O.C.T (optimal cutting temperature) compound and brought up to cryosection temperature of –20°C. 10 µm thick sections were cut using a cryostat (Leica Biosystems) and adhered directly to SuperFrost Plus slides (Fisher Scientific). A PAP pen was used to draw a hydrophobic barrier around the section and the tissue was fixed in 4% paraformaldehyde for 60 min at room temperature before washing three times in PBS containing Tween-20 for 5 min each.

To label sections, the sections were first blocked in in phosphate buffer (PBS) containing 0.5% Triton X-100 and 10% BSA (bovine serum albumin) for 1 h, then incubated with 10 mg/ml Affimer

or primary antibody, diluted in blocking buffer, for 1 h at RT or O/N at 4°C. Following washing, in PBS -Tween, samples were either incubated for an hour with secondary antibody diluted in blocking buffer and either washed again or (for Affimer staining only, where a second incubation step is not required) mounted directly by adding a drop of ProLong Gold Antifade (Invitrogen) onto the section, then placing a cleaned glass coverslip [#1.5: (Scientific Laboratory Supplies)] on top of the samples. All the samples were labelled for identification using an alphanumeric code, to avoid bias in imaging and subsequent analysis.

Confocal imaging used an inverted Zeiss LSM880 in Airyscan mode, using the ×40 N.A. 1.4 objective lens and the same laser power settings for each sample. STED imaging used an Abberior STEDYCON and a ×100, N.A. 1.4 objective lens, with the depletion laser set for ~50nm resolution.

In addition to the Affimers, commercial mouse monoclonal anti-actinin antibody EA-53 (Sigma-Aldrich, 1:500: raised to the full length ACTN protein) and a mouse monoclonal antibody to human desmoglein-2 (CCSTEM28; eBiosciences from Thermo Scientific, 1:200) were used followed by secondary anti-mouse StarRed antibodies (Abberior, 1:100). The rabbit polyclonal titin Z1Z2 antibody was generously provided by Bang et al. (14) (raised against the NH2-terminal 195 residues of the human cardiac titin) and used with secondary anti-rabbit Star Red antibodies. Affimers used in these experiments were directly labelled with STAR 580.

#### 4.5. Sarcomere analysis

STED images were deconvolved using the deconvolution wizard in Huygens software (SVI, Netherlands). For sarcomere length measurements, straight lines were drawn across a run of 10–20 sarcomeres in ImageJ, beginning and ending at a Z-disc. To estimate the average sarcomere length, the lengths of these lines were measured and divided by the number of sarcomeres (Z-discs). Measurements were repeated for a minimum of 50 times with specimens from 3 separate experiments, using a minimum of 3 sections per control and for each of the two DCM patients. Samples were labelled alpha-numerically to prevent user bias.

Z-disc width, intercalated disc length and diameter of the intracellular storage vesicles were also measured using ImageJ using the deconvolved STED images. A thick line (74pt) was drawn across the structures, and plot profile was used to determine the intensity profile and derive the average widths (or lengths) of the structures. To determine the expression levels of desmoglein-2, the average fluorescent intensity along intercalated discs was measured with ImageJ using Airyscan confocal images where the settings



remained constant for each sample. Data was collected from 3 separate experiments using a minimum of 3 sections per control and for each of the two DCM patients. All data was analysed and plotted using Prizm (Graph Pad). Significant changes between samples were tested by Anova with *post hoc* analysis.

## 4.6. Aphafold2

Affimer:protein complexes were generated using the ColabFold implementation of AlphaFold (46, 47). Models of the ACTN:Affimer complex were compared with the published CH domain from actinin in complex with an Affimer crystal structure (6SWT) in Chimera.

## Data availability statement

The original contributions presented in this study are included in the article/**Supplementary material**, further inquiries can be directed to the corresponding author.

## Ethics statement

Patients were consented under ethical approvals obtained from St. Vincent's Hospital, Darlinghurst (HREC #H91/048/1a), the University of Sydney (HREC #2016/923). Frozen samples were shipped to the University of Leeds and stored and processed under ethical approval BIOSCI 17-015. The patients/participants provided their written informed consent to participate in this study.

## Author contributions

DT and AT performed and analysed the Affimer screen to proteins supplied by FP and BR. AL provided the samples from SHB. FP prepared and labelled Affimers, performed the staining, imaging, and analysis of the heart sections. MP performed additional imaging. MP and FP designed the experiments and wrote the manuscript. GC performed the AlphaFold modelling. CR and AL provided the clinical details of the heart samples. All authors reviewed the final version of the manuscript.

## References

1. Hershberger R, Hedges D, Morales A. Dilated cardiomyopathy: the complexity of a diverse genetic architecture. *Nat Rev Cardiol.* (2013) 10:531–47. doi: 10.1038/nrcardio.2013.105
2. McKenna W, Judge D. Epidemiology of the inherited cardiomyopathies. *Nat Rev Cardiol.* (2021) 18:22–36. doi: 10.1038/s41569-020-0428-2
3. Richardson P, McKenna W, Bristow M, Maisch B, Mautner B, O'Connell J, et al. Report of the 1995 world health organization/international society and federation of cardiology task force on the definition and classification of cardiomyopathies. *Circulation.* (1996) 93:841–2. doi: 10.1161/01.cir.93.5.841
4. Huggins G, Kinnamon D, Haas G, Jordan E, Hofmeyer M, Kransdorf E, et al. Prevalence and cumulative risk of familial idiopathic dilated cardiomyopathy. *JAMA.* (2022) 327:454–63. doi: 10.1001/jama.2021.24674
5. Olson T, Michels V, Thibodeau S, Tai Y, Keating M. Actin mutations in dilated cardiomyopathy, a heritable form of heart failure. *Science.* (1998) 280:750–2. doi: 10.1126/science.280.5364.750
6. Kamisago M, Sharma S, DePalma S, Solomon S, Sharma P, McDonough B, et al. Mutations in sarcomere protein genes as a cause of dilated cardiomyopathy. *N Engl J Med.* (2000) 343:1688–96. doi: 10.1056/NEJM200012073432304

## Funding

This work was funded by a BBSRC award to MP and FP BB/S015787/1, and a BBSRC UK-Australia Partnering award BB/T019751/1 to MP, DT, CR, and AL. The STED microscope was funded by a BBSRC Alert award to MP BB/S019464/1 and the Airyscan confocal microscope was funded by the Wellcome Trust, 104918/Z/14/Z. BR was funded by a BBSRC DTP studentship BB/M011151/1. CR acknowledges financial support from Medical Advances Without Animals (MAWA) that funded the nitrogen vapour dewar facility.

## Acknowledgments

We would like to acknowledge the help and support of staff in the BioImaging Facility at Leeds, Daniel Thomas at Leeds for support and training for storing and using human heart samples, and Sean Lai, University of Sydney for advice and help.

## Conflict of interest

The authors declare that the research was conducted in the absence of any commercial or financial relationships that could be construed as a potential conflict of interest.

## Publisher's note

All claims expressed in this article are solely those of the authors and do not necessarily represent those of their affiliated organizations, or those of the publisher, the editors and the reviewers. Any product that may be evaluated in this article, or claim that may be made by its manufacturer, is not guaranteed or endorsed by the publisher.

## Supplementary material

The Supplementary Material for this article can be found online at: <https://www.frontiersin.org/articles/10.3389/fcvm.2023.1094563/full#supplementary-material>

7. Kelly M, Caleshu C, Morales A, Buchan J, Wolf Z, Harrison S, et al. Adaptation and validation of the ACMG/AMP variant classification framework for myh7-associated inherited cardiomyopathies: recommendations by Clingen's inherited cardiomyopathy expert panel. *Genet Med.* (2018) 20:351–9. doi: 10.1038/ngim.2017.218
8. de Frutos F, Ochoa J, Navarro-Penalver M, Baas A, Bjerre J, Zorio E, et al. Natural history of Myh7-related dilated cardiomyopathy. *J Am Coll Cardiol.* (2022) 80:1447–61. doi: 10.1016/j.jacc.2022.07.023
9. Gerull B, Gramlich M, Atherton J, McNabb M, Trombitas K, Sasse-Klaassen S, et al. Mutations of TTN, encoding the giant muscle filament titin, cause familial dilated cardiomyopathy. *Nat Genet.* (2002) 30:201–4. doi: 10.1038/ng815
10. Ware J, Cook S. Role of titin in cardiomyopathy: from DNA variants to patient stratification. *Nat Rev Cardiol.* (2018) 15:241–52. doi: 10.1038/nrcardio.2017.190
11. Tskhovrebova L, Trinick J. Titin: properties and family relationships. *Nat Rev Mol Cell Biol.* (2003) 4:679–89. doi: 10.1038/nrm1198
12. Eldemire R, Sharp C, Taylor M, Sbaizero O, Mestroni L. The sarcomeric spring protein titin: biophysical properties, molecular mechanisms, and genetic mutations associated with heart failure and cardiomyopathy. *Curr Cardiol Rep.* (2021) 23:121. doi: 10.1007/s11886-021-01550-y
13. Tskhovrebova L, Trinick J. Titin and nebulin in thick and thin filament length regulation. *Subcell Biochem.* (2017) 82:285–318. doi: 10.1007/978-3-319-49674-0\_10
14. Bang M, Centner T, Fornoff F, Geach A, Gotthardt M, McNabb M, et al. the complete gene sequence of titin, expression of an unusual approximately 700-KDA titin isoform, and its interaction with obscurin identify a novel Z-line to I-band linking system. *Circ Res.* (2001) 89:1065–72. doi: 10.1161/hh2301.100981
15. Golbus J, Puckelwartz M, Fahrenbach J, Dellefave-Castillo L, Wolfgeher D, McNally E. Population-based variation in cardiomyopathy genes. *Circ Cardiovasc Genet.* (2012) 5:391–9. doi: 10.1161/CIRCGENETICS.112.962928
16. Herman D, Lam L, Taylor M, Wang L, Teekakirikul P, Christodoulou D, et al. Truncations of titin causing dilated cardiomyopathy. *N Engl J Med.* (2012) 366:619–28. doi: 10.1056/NEJMoa1110186
17. Roberts A, Ware J, Herman D, Schafer S, Baksi J, Bick A, et al. Integrated allelic, transcriptional, and phenomic dissection of the cardiac effects of titin truncations in health and disease. *Sci Transl Med.* (2015) 7:270ra6. doi: 10.1126/scitranslmed.3010134
18. Schafer S, de Marvao A, Adami E, Fiedler L, Ng B, Khin E, et al. Titin-truncating variants affect heart function in disease cohorts and the general population. *Nat Genet.* (2017) 49:46–53. doi: 10.1038/ng.3719
19. Romano R, Ghahremani S, Zimmerman T, Legere N, Thakar K, Ladha F, et al. Reading frame repair of Ttn truncation variants restores titin quantity and functions. *Circulation.* (2022) 145:194–205. doi: 10.1161/CIRCULATIONAHA.120.049997
20. Tiede C, Tang A, Deacon S, Mandal U, Nettlehip J, Owen R, et al. Adhiron: a stable and versatile peptide display scaffold for molecular recognition applications. *Protein Eng Des Sel.* (2014) 27:145–55. doi: 10.1093/protein/gzu007
21. Carrington G, Tomlinson D, Peckham M. Exploiting nanobodies and affimers for superresolution imaging in light microscopy. *Mol Biol Cell.* (2019) 30:2737–40. doi: 10.1091/mbc.E18-11-0694
22. Cordell P, Carrington G, Curd A, Parker F, Tomlinson D, Peckham M. Affimers and nanobodies as molecular probes and their applications in imaging. *J Cell Sci.* (2022) 135:jcs259168. doi: 10.1242/jcs.259168
23. Tiede C, Bedford R, Heseltine S, Smith G, Wijetunga I, Ross R, et al. Affimer proteins are versatile and renewable affinity reagents. *Elife.* (2017) 6:e24903. doi: 10.7554/eLife.24903
24. Lal S, Li A, Allen D, Allen P, Bannon P, Cartmill T, et al. Best practice biobanking of human heart tissue. *Biophys Rev.* (2015) 7:399–406. doi: 10.1007/s12551-015-0182-6
25. Curd A, Leng J, Hughes R, Cleasby A, Rogers B, Trinh C, et al. Nanoscale pattern extraction from relative positions of sparse 3d localizations. *Nano Lett.* (2021) 21:1213–20. doi: 10.1021/acs.nanolett.0c03332
26. Vikhorev P, Smoktunowicz N, Munster A, Copeland O, Kostin S, Montgiraud C, et al. Abnormal contractility in human heart myofibrils from patients with dilated cardiomyopathy due to mutations in TTN and contractile protein genes. *Sci Rep.* (2017) 7:14829. doi: 10.1038/s41598-017-13675-8
27. Vikhorev P, Vikhoreva N, Yeung W, Li A, Lal S, Dos Remedios C, et al. Titin-truncating mutations associated with dilated cardiomyopathy alter length-dependent activation and its modulation via phosphorylation. *Cardiovasc Res.* (2022) 118:241–53. doi: 10.1093/cvr/cvaa316
28. Pluess M, Daeubler G, Dos Remedios C, Ehler E. Adaptations of cytoarchitecture in human dilated cardiomyopathy. *Biophys Rev.* (2015) 7:25–32. doi: 10.1007/s12551-014-0146-2
29. Gautel M, Goulding D, Bullard B, Weber K, Furst D. The central Z-disk region of titin is assembled from a novel repeat in variable copy numbers. *J Cell Sci.* (1996) 109(Pt 11):2747–54. doi: 10.1242/jcs.109.11.2747
30. Fisher L, Schock F. The unexpected versatility of Alp/Enigma family proteins. *Front Cell Dev Biol.* (2022) 10:963608. doi: 10.3389/fcell.2022.963608
31. Wadmore K, Azad A, Gehmlich K. The role of Z-disc proteins in myopathy and cardiomyopathy. *Int J Mol Sci.* (2021) 22:3058. doi: 10.3390/ijms22063058
32. Au Y, Atkinson R, Guerrini R, Kelly G, Joseph C, Martin S, et al. Solution structure of ZASP PDZ domain; implications for sarcomere ultrastructure and enigma family redundancy. *Structure.* (2004) 12:611–22. doi: 10.1016/j.str.2004.02.019
33. Luther P. The vertebrate muscle Z-disc: sarcomere anchor for structure and signalling. *J Muscle Res Cell Motil.* (2009) 30:171–85. doi: 10.1007/s10974-009-9189-6
34. Gregorio C, Trombitas K, Centner T, Kolmerer B, Stier G, Kunke K, et al. The Nh2 terminus of titin spans the Z-disc: its interaction with a novel 19-Kd ligand (T-Cap) is required for sarcomeric integrity. *J Cell Biol.* (1998) 143:1013–27. doi: 10.1083/jcb.143.4.1013
35. Burgoyne T, Morris E, Luther P. Three-dimensional structure of vertebrate muscle Z-band: the small-square lattice Z-band in rat cardiac muscle. *J Mol Biol.* (2015) 427:3527–37. doi: 10.1016/j.jmb.2015.08.018
36. Bennett P, Maggs A, Baines A, Pinder J. The Transitional junction: a new functional subcellular domain at the intercalated disc. *Mol Biol Cell.* (2006) 17:2091–100. doi: 10.1091/mbc.e05-12-1109
37. Fomin A, Gartner A, Cyganek L, Tiburcy M, Tuleta I, Wellers L, et al. Truncated titin proteins and titin haploinsufficiency are targets for functional recovery in human cardiomyopathy due to TTN mutations. *Sci Transl Med.* (2021) 13:eabd3079. doi: 10.1126/scitranslmed.abd3079
38. McAfee Q, Chen C, Yang Y, Caporizzo M, Morley M, Babu A, et al. Truncated titin proteins in dilated cardiomyopathy. *Sci Transl Med.* (2021) 13:eabd7287. doi: 10.1126/scitranslmed.abd7287
39. Santiago C, Huttner I, Fatkin D. Titin-related cardiomyopathy: is it a distinct disease? *Curr Cardiol Rep.* (2022) 24:1069–75. doi: 10.1007/s11886-022-01726-0
40. Li Y, Hessel A, Unger A, Ing D, Recker J, Koser F, et al. Graded titin cleavage progressively reduces tension and uncovers the source of a-band stability in contracting muscle. *Elife.* (2020) 9:e64107. doi: 10.7554/eLife.64107
41. Bennett P. From myofibril to membrane; the transitional junction at the intercalated disc. *Front Biosci (Landmark Ed).* (2012) 17:1035–50. doi: 10.2741/3972
42. Wilson A, Schoenauer R, Ehler E, Agarkova I, Bennett P. Cardiomyocyte growth and sarcomerogenesis at the intercalated disc. *Cell Mol Life Sci.* (2014) 71:165–81. doi: 10.1007/s00018-013-1374-5
43. Ehler E. Cardiac cytoarchitecture—why the “hardware” is important for heart function! *Biochim Biophys Acta.* (2016) 1863(Pt B):1857–63. doi: 10.1016/j.bbamcr.2015.11.006
44. Perriard J, Hirschy A, Ehler E. Dilated cardiomyopathy: a disease of the intercalated disc? *Trends Cardiovasc Med.* (2003) 13:30–8. doi: 10.1016/s1050-1738(02)00209-8
45. Zhao G, Qiu Y, Zhang H, Yang D. Intercalated discs: cellular adhesion and signaling in heart health and diseases. *Heart Fail Rev.* (2019) 24:115–32. doi: 10.1007/s10741-018-9743-7
46. Jumper J, Evans R, Pritzel A, Green T, Figurnov M, Ronneberger O, et al. Applying and improving AlphaFold at Casp14. *Proteins.* (2021) 89:1711–21. doi: 10.1002/prot.26257
47. Mirdita M, Schutze K, Moriaki Y, Heo L, Ovchinnikov S, Steinegger M. Colabfold: making protein folding accessible to all. *Nat Methods.* (2022) 19:679–82. doi: 10.1038/s41592-022-01488-1
48. Marston S, Montgiraud C, Munster A, Copeland O, Choi O, Dos Remedios C, et al. OBSCN mutations associated with dilated cardiomyopathy and haploinsufficiency. *PLoS One.* (2015) 10:e0138568. doi: 10.1371/journal.pone.0138568
49. Messer A, Bayliss C, El-Mezgueldi M, Redwood C, Ward D, Leung M, et al. Mutations in troponin T associated with hypertrophic cardiomyopathy increase Ca(2+)-sensitivity and suppress the modulation of Ca(2+)-sensitivity by troponin I phosphorylation. *Arch Biochem Biophys.* (2016) 601:113–20. doi: 10.1016/j.abb.2016.03.027
50. Berecz T, Yiu A, Vittay O, Orsolits B, Mioulane M, Dos Remedios C, et al. Transcriptional co-activators Yap1-Taz of hippo signalling in doxorubicin-induced cardiomyopathy. *ESC Heart Fail.* (2022) 9:224–35. doi: 10.1002/ehf2.13756
51. Bollen I, Ehler E, Fleischanderl K, Bouwman F, Kempers L, Ricke-Hoch M, et al. Myofilament remodeling and function is more impaired in peripartum cardiomyopathy compared with dilated cardiomyopathy and ischemic heart disease. *Am J Pathol.* (2017) 187:2645–58. doi: 10.1016/j.ajpath.2017.08.022



## OPEN ACCESS

EDITED BY  
Sean Lal,  
The University of Sydney, Australia

REVIEWED BY  
Masashi Tawa,  
Osaka Medical and Pharmaceutical University,  
Japan  
Yi-Chou Hou,  
Cardinal Tien Hospital, Taiwan

\*CORRESPONDENCE  
Toshiaki Nakano  
✉ nakano.toshiaki.455@m.kyushu-u.ac.jp

SPECIALTY SECTION  
This article was submitted to  
Heart Failure and Transplantation,  
a section of the journal  
Frontiers in Cardiovascular Medicine

RECEIVED 10 July 2022  
ACCEPTED 18 January 2023  
PUBLISHED 21 February 2023

CITATION  
Kishimoto H, Nakano T, Torisu K, Tokumoto M,  
Uchida Y, Yamada S, Taniguchi M and  
Kitazono T (2023) Indoxyl sulfate induces left  
ventricular hypertrophy via  
the AhR-FGF23-FGFR4 signaling pathway.  
*Front. Cardiovasc. Med.* 10:990422.  
doi: 10.3389/fcvm.2023.990422

COPYRIGHT  
© 2023 Kishimoto, Nakano, Torisu, Tokumoto,  
Uchida, Yamada, Taniguchi and Kitazono. This is  
an open-access article distributed under the  
terms of the [Creative Commons Attribution  
License \(CC BY\)](#). The use, distribution or  
reproduction in other forums is permitted,  
provided the original author(s) and the  
copyright owner(s) are credited and that the  
original publication in this journal is cited, in  
accordance with accepted academic practice.  
No use, distribution or reproduction is  
permitted which does not comply with  
these terms.

# Indoxyl sulfate induces left ventricular hypertrophy via the AhR-FGF23-FGFR4 signaling pathway

Hiroshi Kishimoto<sup>1</sup>, Toshiaki Nakano<sup>1\*</sup>, Kumiko Torisu<sup>1</sup>,  
Masanori Tokumoto<sup>2</sup>, Yushi Uchida<sup>1</sup>, Shunsuke Yamada<sup>1</sup>,  
Masatomo Taniguchi<sup>3</sup> and Takanari Kitazono<sup>1</sup>

<sup>1</sup>Department of Medicine and Clinical Science, Graduate School of Medical Sciences, Kyushu University, Fukuoka, Japan, <sup>2</sup>Fukuoka Red Cross Hospital, Fukuoka, Japan, <sup>3</sup>Fukuoka Renal Clinic, Fukuoka, Japan

**Background:** Patients with chronic kidney disease (CKD) have a high risk of left ventricular hypertrophy (LVH). Fibroblast growth factor 23 (FGF23) and indoxyl sulfate (IS) are associated with LVH in patients with CKD, but the interactions between these molecules remain unknown. We investigated whether IS contributes to LVH associated with FGF23 in cultured cardiomyocytes and CKD mice.

**Methods and results:** In cultured rat cardiac myoblast H9c2 cells incubated with IS, mRNA levels of the LVH markers atrial natriuretic factor, brain natriuretic peptide, and  $\beta$ -myosin heavy chain were significantly upregulated. Levels of mRNA of the polypeptide N-acetylgalactosaminyltransferase 3 (GALNT3), which regulates FGF23 O-glycosylation, and FGF23 were also upregulated in H9c2 cells. Intact FGF23 protein expression and fibroblast growth factor receptor 4 (FGFR4) phosphorylation were increased in cell lysates by IS administration. In C57BL/6J mice with heminephrectomy, IS promoted LVH, whereas the inhibition of FGFR4 significantly reduced heart weight and left ventricular wall thickness in IS-treated groups. While there was no significant difference in serum FGF23 concentrations, cardiac FGF23 protein expression was markedly increased in IS-injected mice. GALNT3, hypoxia-inducible factor 1 alpha, and FGF23 protein expression was induced in H9c2 cells by IS treatment and suppressed by the inhibition of Aryl hydrocarbon receptor which is the receptor for IS.

**Conclusion:** This study suggests that IS increases FGF23 protein expression via an increase in GALNT3 and hypoxia-inducible factor 1 alpha expression, and activates FGF23-FGFR4 signaling in cardiomyocytes, leading to LVH.

## KEYWORDS

indoxyl sulfate, fibroblast growth factor 23, fibroblast growth factor receptor 4, left ventricular hypertrophy, aryl hydrocarbon receptor

## Introduction

Patients with chronic kidney disease (CKD), including those with end-stage kidney disease, have a high risk of cardiovascular disease, which is the major cause of death in these patients (1–5). Traditional cardiovascular risk factors for the general population, such as diabetes mellitus, high blood pressure, and dyslipidemia, are more common in patients with CKD, but cannot entirely explain the increased cardiovascular risk (6). Left ventricular hypertrophy (LVH), which

is a typical pathological feature of uremic cardiomyopathy, is an independent risk factor for mortality in patients with CKD (7).

Dysregulated phosphorus metabolism is a common complication of CKD and is associated with adverse cardiovascular and renal outcomes. Fibroblast growth factor 23 (FGF23), which is a hormone secreted by osteocytes, controls the rate of urinary excretion of phosphate and inhibits renal production of 1,25-dihydroxyvitamin D. This process helps to mitigate hyperphosphatemia in patients with kidney disease. Increased circulating FGF23 concentrations are associated with LVH, kidney disease progression, and mortality in patients with dialysis, predialysis CKD, or non-CKD, independent of risk factors, such as high phosphate and parathyroid hormone concentrations (8–14).

Indoxyl sulfate (IS) is an important uremic solute, which is derived from tryptophan in dietary protein. IS is converted in the liver and excreted into the urine by proximal tubular secretion *via* organic anion transporters (15). Serum IS greatly and progressively increases with increasing CKD stages, and is a predictor of overall and cardiovascular mortality. In addition, the serum IS concentration is independently associated with LVH in patients with CKD (16).

FGF23 and IS are associated with LVH in patients with CKD, but the interactions between these molecules remain unknown. Therefore, we examined whether IS is associated with FGF23 and induces LVH *in vivo* and *in vitro*.

## Materials and methods

### Cell culture

Rat cardiac myoblast (H9c2, 2-1) cells were acquired from the American Type Culture Collection (Manassas, VA) and cultivated in Dulbecco's Modified Eagle Medium (GIBCO, Dublin, Ireland) containing 10% fetal bovine serum (HyClone; GE Healthcare, Bucks, UK), 100 U/mL penicillin, and 100 mg/mL streptomycin (Life Technologies, Carlsbad, CA), in a humidified atmosphere with 5% CO<sub>2</sub> at 37°C. The cells were cultured until 70–80% confluence and were then serum deprived for 24 h before each experiment. The cells were incubated with 0, 0.25, or 1.0 mM IS or 0, 50, or 100 ng/mL recombinant mouse FGF23 (2629-FG; R&D Systems, Minneapolis, MN) diluted in normal saline (NS) and collected after 24 and 72 h for real-time reverse transcription-polymerase chain reaction and western blotting, respectively. To perform small interfering RNA (siRNA) knockdown, the cells were transfected with On-TARGETplus SMARTpool siRNA [non-targeting control, aryl hydrocarbon receptor (AhR), and FGF23; Horizon Discovery, Cambridge, UK] using Dharmafect 1 reagent (Horizon Discovery) in accordance with the manufacturer's instructions.

### Animal experiments and ethics statement

All animal experiments were conducted in accordance with the animal use protocols approved by the Committee on Ethics of Animal Experimentation at Kyushu University Graduate School of Medical Sciences (Approval number: A19-274-0). We used C57BL/6Jcl mice (CLEA Japan, Inc., Tokyo, Japan). They were maintained in an air-conditioned specific pathogen-free room at 21°C and 65% humidity, with a 12:12-h light and dark cycle (lights on at 8:00 a.m., off at 8:00

p.m.) with free access to chow and water. Experiments were reported according to the ARRIVE guidelines.

### Experimental procedures for LVH in mice

To induce LVH, 8-week-old male mice were fed a high phosphorus diet, which contained modified AIN-93G, lactose 20.0%, sucrose 2.023%,  $\beta$ -corn starch 20.3486%,  $\alpha$ -corn starch 7.0%, CaCO<sub>3</sub> 0.55%, Ca(H<sub>2</sub>PO<sub>4</sub>)<sub>2</sub> 5.05%, and phosphate 1.5g/100g (Oriental Yeast, Tokyo, Japan) 1 day after left heminephrectomy (removal of the whole left kidney). This diet was provided for the induction of FGF23 and was administered with a continuous subcutaneous dose of 100 mg/kg IS (I3875; Sigma-Aldrich, St. Louis, MO) or 28  $\mu$ l/day of NS (Otsuka Pharmaceutical Factory, Tokushima, Japan) for 4 weeks using a micro-osmotic pump (2002-0000296; Alzet, Cupertino, CA). Half of the mice were treated with a continuous intraperitoneal dose of 7.5 mg/kg H3B-6527 (H3B), which is an FGFR4 inhibitor (S8675; Selleck Biotech, Tokyo, Japan), or 3.6  $\mu$ l/day of NS using a micro-osmotic pump (1004-0009922; Alzet) for 4 weeks. The 2,002-pumps were replaced biweekly. To examine the effect of IS administration on cardiac hypertrophy and fibrosis, the mice were divided into the five following groups: sham; control; IS + NS; NS + H3B; and IS + H3B. Sham mice were treated with anesthesia, skin incision, and laparotomy, but did not have pumps inserted and were fed a normal phosphorus diet (CRF-1LID10; Oriental Yeast, Tokyo, Japan). The mice were operated on day 0, observed for 4 weeks, and euthanized on day 28. The mice were anesthetized intraperitoneally with medetomidine hydrochloride (0.3 mg/kg body weight; Wako, Osaka, Japan), midazolam (4 mg/kg body weight, Sandoz, Tokyo, Japan), and butorphanol tartrate (5 mg/kg body weight, Wako). The body temperature of the mice was maintained at 37°C during the whole procedure.

### Sample collection

The mice were euthanized on day 28. Blood samples were collected from the inferior vena cava. Serum was separated by centrifugation at 3,000  $\times g$  for 10 min, aliquoted for later analysis, and stored at  $-80^{\circ}\text{C}$ . Immediately after blood collection, 50 mL ice-cold phosphate-buffered saline (14249-24; Nacalai Tesque Inc., Kyoto, Japan) (pH 7.4) was slowly perfused to harvest the heart and kidney. We separated the right kidney in half cross-sectionally for obtaining coronal sections. One half of the kidney and most of the heart were immersed in 10% formaldehyde neutral buffer solution (37152-51; Nacalai Tesque Inc.) for histological analysis. The other half of the kidney and the apex of the heart (one quarter of the heart) were snap-frozen in liquid nitrogen and stored at  $-80^{\circ}\text{C}$  for protein and RNA analysis.

### Heart histology

The hearts of mice were immersed in 10% formaldehyde neutral buffer solution for at least 48 h before being sectioned. The hearts were cut horizontally into four equal sections. The thickest wall of the left ventricle from the four sections was evaluated. Sections from each sample were subjected to hematoxylin–eosin staining using standard



methods. Histological images were captured by light microscopy (Eclipse E800 microscope; Nikon, Tokyo, Japan).

## RNA extraction and quantitative real-time polymerase chain reaction

Total RNA was extracted from H9c2 cells using the MAXWELL®16 LEV simply RNA tissue Kit (Promega, Madison, WI) and the MAXWELL® 16 instrument (Promega) in accordance with the manufacturer's instructions. Complementary DNA was

synthesized from 1 µg of total RNA with the PrimeScript RT Reagent Kit (Takara Bio Inc., Shiga, Japan). Real-time polymerase chain reaction (PCR) was performed using SYBR Premix Ex Taq™ (Takara Bio Inc.) and the Applied Biosystems 7500 Real Time PCR System (Applied Biosystems, Foster, CA). Rat Glyceraldehyde 3-phosphate dehydrogenase (*GAPDH*) was amplified as an internal control. Expression analysis was performed by the Delta-Delta Ct method using 7500 Software v2.3 (Applied Biosystems). The primers used for these experiments were as follows: rat atrial natriuretic factor (*ANF*), forward 5'-ATGGGCTCCTTCTCCATCAC-3' and reverse 5'-TTCATCGGTATGCTCGCTCA-3'; rat brain natriuretic peptide

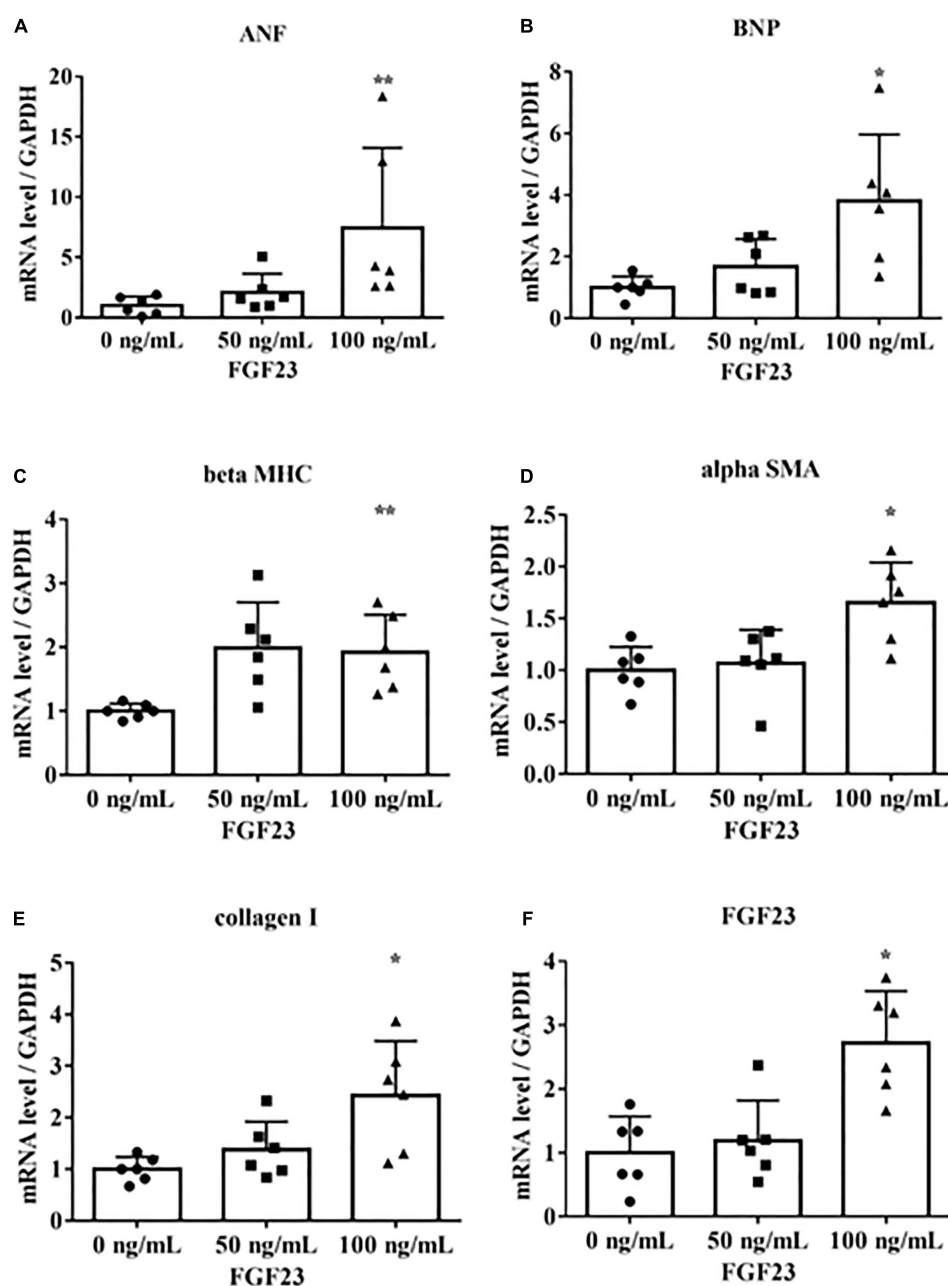


FIGURE 1

Fibroblast growth factor 23 increases mRNA levels of markers of hypertrophy and fibrosis. Rat cardiac myoblast cells (H9c2) were cultured with 0, 50, or 100 ng/mL fibroblast growth factor 3 (FGF23) for 24 h, and mRNA expression levels were analyzed by real-time PCR. (A) Atrial natriuretic factor (*ANF*) ( $n = 6$ ). \*\* $P < 0.05$  versus 0 ng/mL. (B) Brain natriuretic peptide (*BNP*) ( $n = 6$ ). \* $P < 0.01$  versus 0 ng/mL. (C)  $\beta$ -myosin heavy chain (*beta MHC*) ( $n = 6$ ). \*\* $P < 0.05$  versus 0 ng/mL. (D) Alpha smooth muscle actin (*alpha SMA*) ( $n = 6$ ). \* $P < 0.01$  versus 0 ng/mL. (E) Collagen I ( $n = 6$ ). \* $P < 0.01$  versus 0 ng/mL. (F) *FGF23* ( $n = 6$ ). \* $P < 0.01$  versus 0 ng/mL. Data were analyzed by one-way analysis of variance.

(*BNP*), forward 5'-TGGGAAGTCCTAGCCAGTCT-3' and reverse 5'-GATCCGGTCTATCTTCTGCC-3'; rat  $\beta$ -myosin heavy chain (*beta MHC*), forward 5'-CTAGGAGGCGGAGGAACAG-3' and reverse 5'-CTTGGCGCCAATGTCACG-3'; rat alpha smooth muscle actin (*alpha SMA*), forward 5'-GACACCAGGGAGTGATGGTT-3' and reverse 5'-GTTAGCAAGGTCCGATGCTC-3'; rat collagen I, forward 5'-TGCCGTGACCTCAAGATGTG-3' and reverse 5'-CACAAGCGTGCTGTAGGTGA-3'; rat *FGF23*, forward 5'-GCAACATTTTGGATCGTATCA-3' and reverse 5'-GATGCTTCGGTGACAGGTAGA-3'; rat N-acetylgalactosaminyltransferase

3 (*GALNT3*), forward 5'-GTTGCTAGGAGCAACAGTCGCA-3' and reverse 5'-AGTTCACCGTGGTAGTATTGTAGT-3'; and rat *GAPDH*, forward 5'-GGCACAGTCAAGGCTGAGAATG-3' and reverse 5'-ATGGTGGTGAAGACGCCAGTA-3'.

## Western blot analysis

To perform western blot analysis, H9c2 cells were harvested with cell lysis buffer (Mammalian Protein Extraction Reagent, 78501; Pierce Thermo Scientific, Tokyo, Japan) containing protease

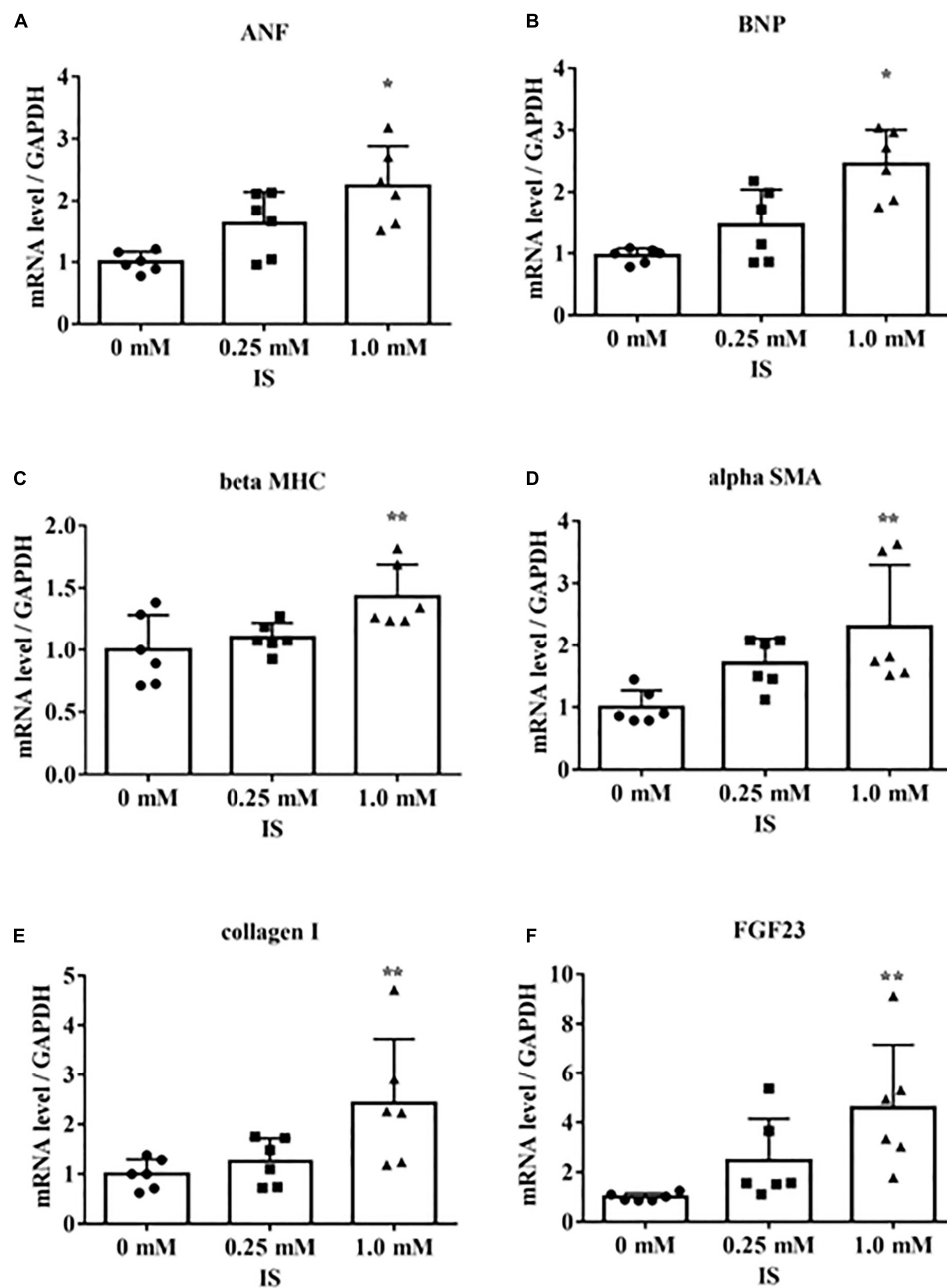


FIGURE 2

Indoxyl sulfate increases mRNA levels of markers of hypertrophy and fibrosis. H9c2 cells were cultured with 0, 0.25, or 1.0 mM indoxyl sulfate (IS) for 24 h, and mRNA expression levels were analyzed by real-time PCR. (A) Atrial natriuretic factor (*ANF*) ( $n = 6$ ). \* $P < 0.01$  versus 0 mM. (B) Brain natriuretic peptide (*BNP*) ( $n = 6$ ). \* $P < 0.01$  versus 0 mM. (C)  $\beta$ -myosin heavy chain (*beta MHC*) ( $n = 6$ ). \*\* $P < 0.05$  versus 0 mM. (D) Alpha smooth muscle actin (*alpha SMA*) ( $n = 6$ ). \*\* $P < 0.05$  versus 0 mM. (E) Collagen I ( $n = 6$ ). \*\* $P < 0.05$  versus 0 mM. (F) *FGF23* ( $n = 6$ ). \*\* $P < 0.05$  versus 0 mM. Data were analyzed by one-way analysis of variance.

inhibitors (#04080-11; Nacalai Tesque Inc.) and phosphatase inhibitors (#07575-51; Nacalai Tesque Inc.) on ice for 15 min. The supernatants of protein lysates were collected after 10 min of centrifugation at  $10,000 \times g$ . The protein concentrations of cell lysates were determined using a bicinchoninic acid (BCA) protein assay kit (Thermo Fisher Scientific). The samples (5  $\mu$ g) were

separated on 5–20% sodium dodecyl sulfate-polyacrylamide gels (#2331830; Atto, Tokyo, Japan) and transferred onto polyvinylidene difluoride membranes (BioRad, Hercules, CA) using Trans-Blot Turbo (BioRad). After being blocked with Blocking One (#03953-95; Nacalai Tesque Inc.) for 30 min at room temperature, the membranes were washed in Tris-buffered saline containing 0.1%

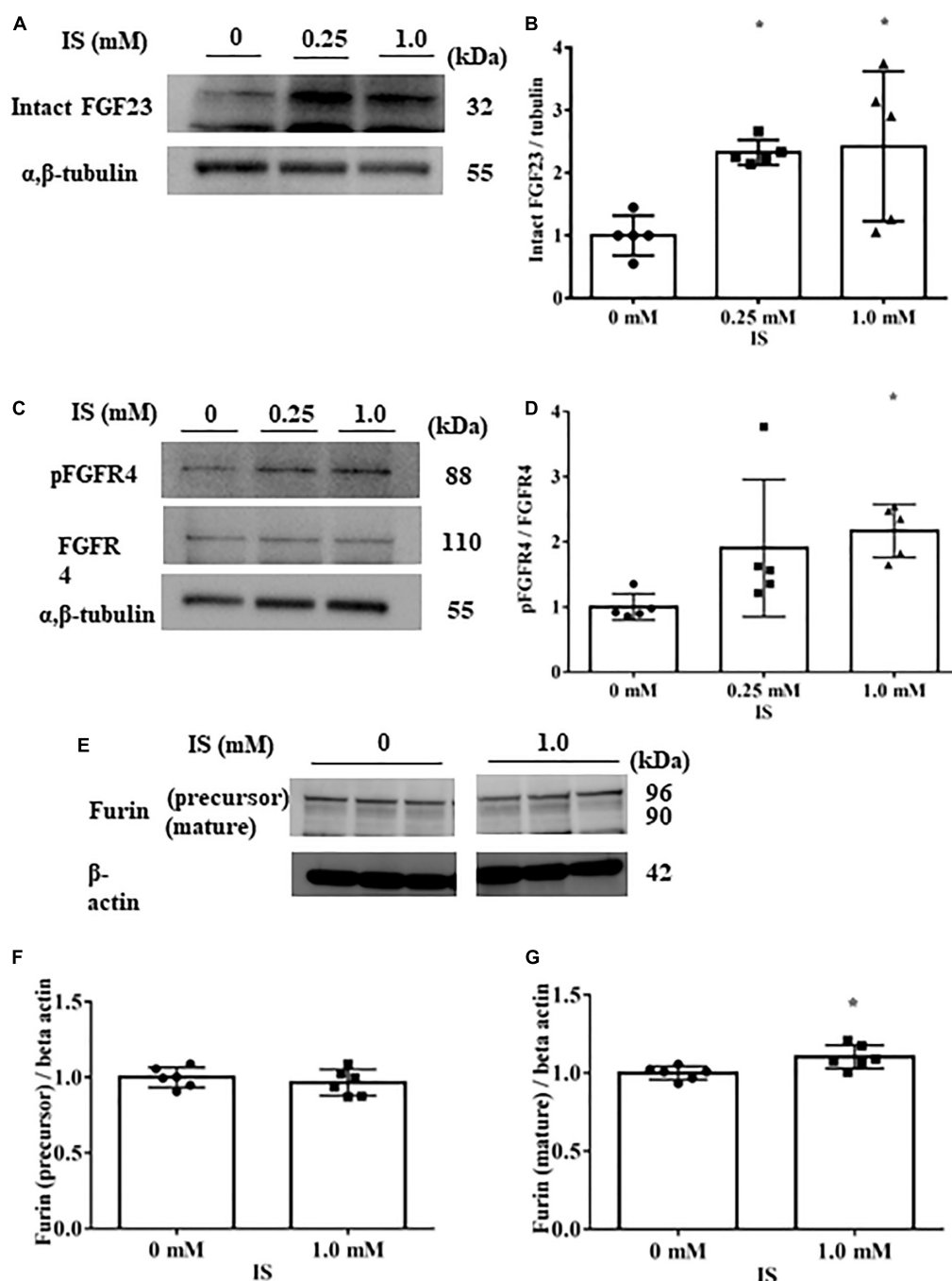


FIGURE 3

Indoxyl sulfate increases fibroblast growth factor 23 protein expression and fibroblast growth factor receptor 4 phosphorylation. (A,B) Western blotting of fibroblast growth factor 3 (FGF23) protein expression in H9c2 cells. H9c2 cells were cultured with 0, 0.25, or 1.0 mM indoxyl sulfate (IS) for 72 h. Alpha, beta-tubulin protein expression was examined as an internal control ( $n = 5$ ). \* $P < 0.05$  versus IS 0 mM. (C,D) Western blotting of fibroblast growth factor receptor 4 (FGFR4) protein expression and FGFR4 phosphorylation in H9c2 cells. H9c2 cells were cultured with 0, 0.25, or 1.0 mM IS for 72 h. Alpha, beta-tubulin protein expression was examined as an internal control ( $n = 5$ ). \* $P < 0.05$  versus IS 0 mM. (E–G) Western blotting of furin protein in H9c2 cells. H9c2 cells were cultured with 0 or 1.0 mM IS for 72 h. The images are from different parts of the same gel. Beta actin protein expression was examined as an internal control ( $n = 6$ ). Furin stained as two bands, furin precursor (96 kDa) and mature (90 kDa) forms. \* $P < 0.05$  versus IS 0 mM. Data were analyzed by one-way analysis of variance.

Tween 20 (polyoxyethylene sorbitan monolaurate, 35624-15; Nacalai Tesque Inc.) three times for 10 min and incubated with primary antibodies at 4°C overnight. The following antibodies were used as primary antibodies: monoclonal anti-rat FGF23 antibody (1:500, MAB2629; R&D Systems); polyclonal anti-goat FGF23 antibody (1:1000, ab123502; Abcam, Cambridge, UK); polyclonal anti-rabbit FGFR4 antibody (1:1000, ab119378; Abcam); polyclonal anti-rabbit FGFR4 (phospho Y642; pFGFR4) antibody (1:1000, ab192589; Abcam); polyclonal anti-rabbit furin antibody (1:1000, PA1-062; Thermo Fisher Scientific); polyclonal anti-rabbit hypoxia-inducible

factor 1 alpha (HIF1 $\alpha$ ) antibody (1:1000, NB100-134; Novus Biologicals, Centennial, CO); polyclonal anti-rabbit polypeptide GALNT3 antibody (1:1000, SAB2106736; Sigma-Aldrich); and anti-rabbit  $\alpha/\beta$  tubulin (1:1000, CST#2148; Cell Signaling Technology, Danvers, MA). After being washed in Tris-buffered saline containing 0.1% Tween 20 three times, the membranes were incubated with the following horseradish peroxidase-conjugated secondary antibodies: donkey anti-rabbit IgG antibody (1:5000, NA934; GE Healthcare, Bucks, UK) and goat anti-rat IgG antibody (1:10,000, NA935; GE Healthcare) for 1 h. The bands were detected by the

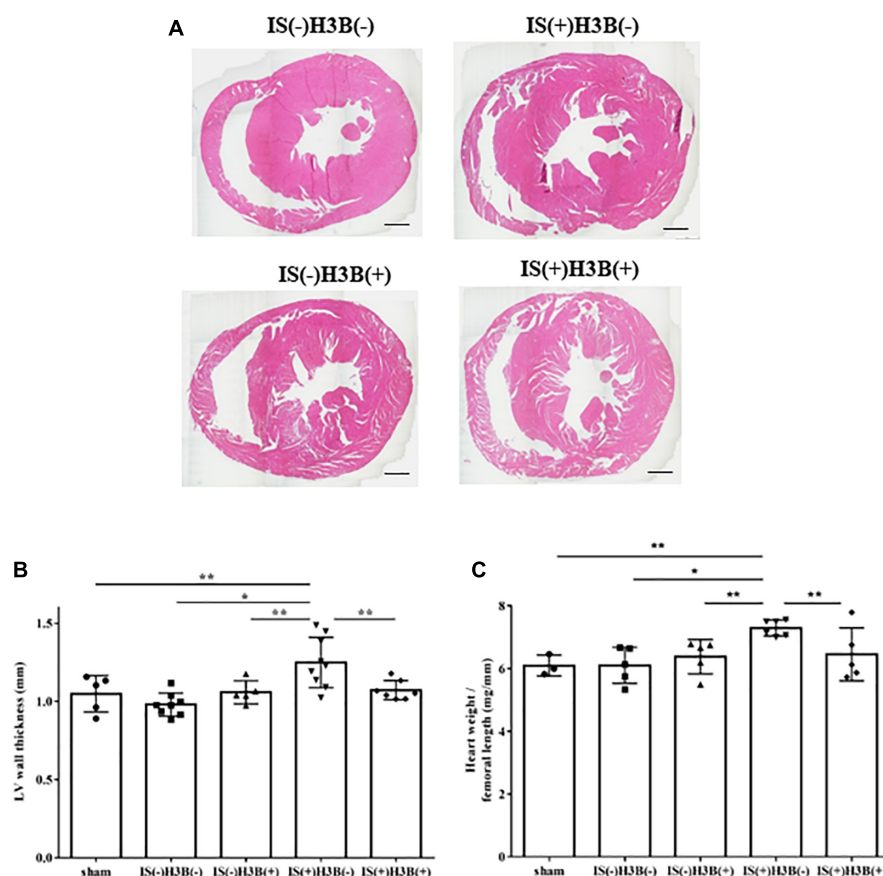


FIGURE 4

Indoxyl sulfate induces LVH in mice with CKD. (A) Mouse hearts were cut horizontally and stained with hematoxylin–eosin. Representative images are shown. Scale bar = 500  $\mu$ m. (B) After hematoxylin–eosin staining, we measured the LV wall thickness for each sample ( $n = 3-6$ ). \* $P < 0.01$ , \*\* $P < 0.05$ . (C) The relative heart weight was markedly increased in indoxyl sulfate (IS)-treated mice and this increase was reduced by FGFR4 inhibition ( $n = 3-6$ ). \* $P < 0.01$ , \*\* $P < 0.05$ . Data were analyzed by one-way analysis of variance.

TABLE 1 Body weight, blood pressure, and laboratory data from animal experiments.

	Sham	IS(-)H3B(-)	IS(-)H3B(+)	IS(+)H3B(-)	IS(+)H3B(+)	$p$
Body weight (g)	24.76 $\pm$ 1.25	22.41 $\pm$ 1.91	23.07 $\pm$ 0.74	24.18 $\pm$ 0.98	23.44 $\pm$ 1.91	0.181
Blood pressure (mmHg)	121.03 $\pm$ 15.5	135.8 $\pm$ 14.7	127.9 $\pm$ 19.0	116.1 $\pm$ 13.4	133.3 $\pm$ 13.8	0.243
Cre (mg/dL)	0.55 $\pm$ 0.38	0.22 $\pm$ 0.17	0.31 $\pm$ 0.22	0.18 $\pm$ 0.03	0.31 $\pm$ 0.24	0.189
Ca (mg/dL)	10.20 $\pm$ 1.04	9.46 $\pm$ 0.59	9.76 $\pm$ 0.47	10.28 $\pm$ 0.78	9.88 $\pm$ 0.63	0.359
P (mg/dL)	13.17 $\pm$ 1.32	12.96 $\pm$ 1.95	16.28 $\pm$ 3.29	17.47 $\pm$ 5.56	17.24 $\pm$ 1.77	0.161
Intact FGF23 (pg/mL)	104.4 $\pm$ 88.5	857.8 $\pm$ 339.5*	728.0 $\pm$ 238.2*	832.7 $\pm$ 257.6*	658.7 $\pm$ 175.1*	0.0047
Indoxyl sulfate ( $\mu$ g/dL)	3.48 $\pm$ 0.99	2.96 $\pm$ 1.13	6.51 $\pm$ 0.99	11.81 $\pm$ 1.11**	9.15 $\pm$ 1.35	0.0072

Data are presented as the mean  $\pm$  standard error. IS, indoxyl sulfate; H3B, H3B-6527; Cre, creatinine; Ca, calcium; P, phosphorus. Comparisons of groups were analyzed with one-way analysis of variance followed by Tukey's test. \* $P < 0.01$  versus the sham group. \*\* $P < 0.05$  versus the sham group and the IS(-)H3B(-) group.



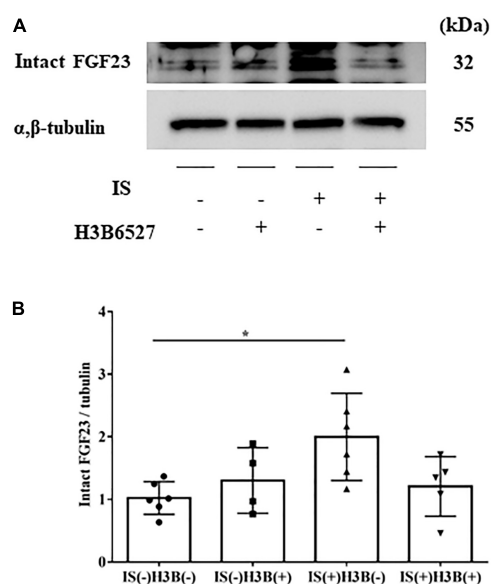


FIGURE 5

(A,B) IS increases intact FGF23 expression in the heart. The expression of intact FGF23 in the heart was significantly increased after IS treatment. This effect was abrogated by FGFR4 inhibition as shown by Western blotting ( $n = 3-6$ ). Data were analyzed by one-way analysis of variance.  $*P < 0.05$ .

enhanced chemiluminescent method (ECL prime; GE Healthcare or Chemi-Lumi One Ultra; Nacalai Tesque Inc.), captured using a chemiluminescence imaging system (AE-9300 Ez-capture MG;

Atto), and analyzed with ImageJ Software (National Institutes of Health, Bethesda, MD).

## Statistical analysis

Data were analyzed using the JMP 14.0 software program (SAS Institute, Tokyo, Japan). Continuous variables are expressed as the mean  $\pm$  standard error. Differences between two groups were compared by Student's  $t$ -test. Differences among groups were compared by one-way analysis of variance followed by Tukey's honest significant difference tests.  $P < 0.05$  was considered statistically significant for all tests.

## Results

### FGF23 Promotes hypertrophic and pro-fibrotic signaling in cultured cardiomyocytes

To determine if FGF23 is associated with hypertrophic signaling in cultured rat cardiac myoblast cells (H9c2), we incubated H9c2 cells with 0, 50, or 100 ng/mL recombinant mouse FGF23. These concentrations were chosen on the basis of previous reports (17–19). The cells were collected after 24 h for real-time PCR. The mRNA levels of *FGF23*, the LVH markers *ANF*, *BNP*, and *beta MHC*, and the fibrotic markers *alpha SMA* and collagen I were upregulated (Figure 1).

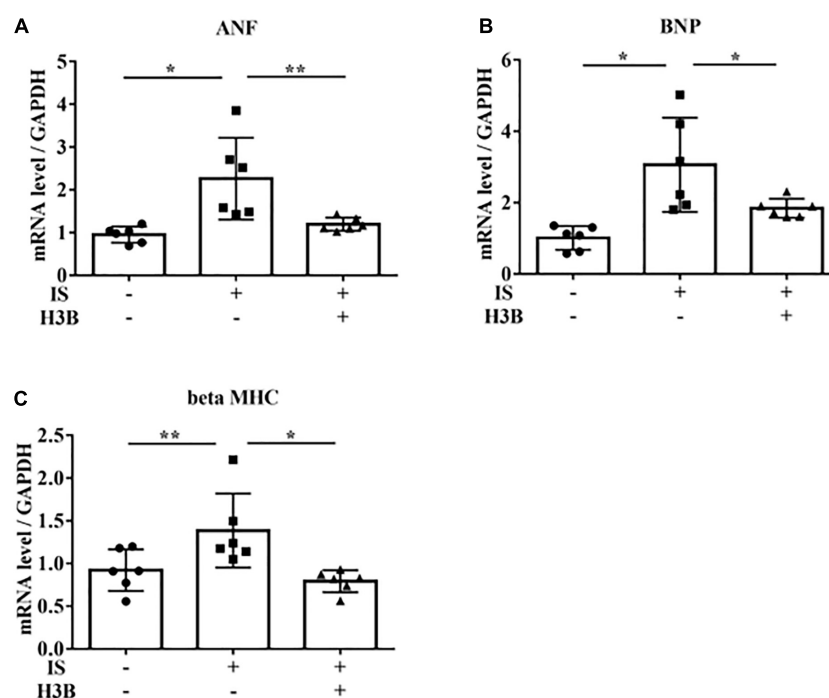


FIGURE 6

IS increases hypertrophic markers via FGFR4 *in vitro*. H9c2 cells were cultured with 0 or 1 mM IS and 0 or 10  $\mu$ M H3B-6527 (FGFR4 inhibitor) for 6 h. (A) *ANF* mRNA levels were significantly increased by IS and downregulated with H3B-6527 ( $n = 6$ ).  $*P < 0.01$ ,  $**P < 0.05$ . (B) *BNP* mRNA levels were significantly increased by IS and downregulated with H3B-6527 ( $n = 6$ ).  $*P < 0.01$ . (C) *beta MHC* mRNA levels were significantly increased by IS and downregulated with H3B-6527 ( $n = 6$ ).  $*P < 0.01$ ,  $**P < 0.05$ . Data were analyzed by one-way analysis of variance.

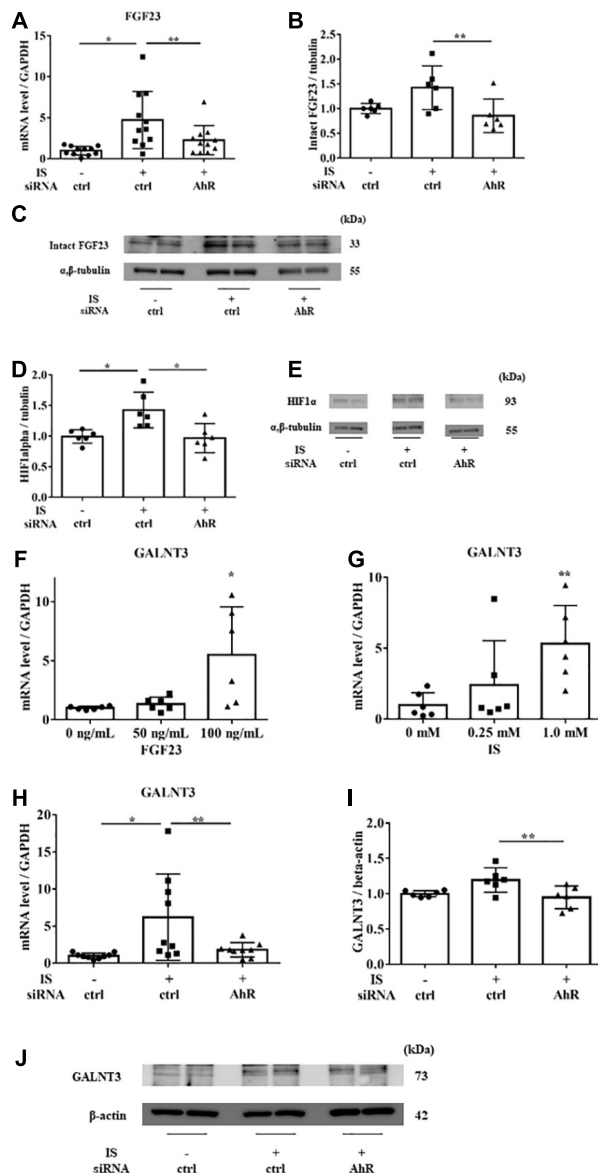


FIGURE 7

IS induces FGF23 via AhR *in vitro*. H9c2 cells were cultured with 0 or 1 mM IS for 6 h (for mRNA) or 48 h (for protein) after pretreatment with AhR siRNA or control siRNA (ctrl). (A) FGF23 mRNA levels were significantly increased by IS and downregulated with AhR siRNA ( $n = 11$ ).  $*P < 0.01$ ,  $**P < 0.05$ . (B,C) Western blotting of FGF23 protein expression in H9c2 cells. Alpha, beta-tubulin protein expression was examined as an internal control ( $n = 6$ ).  $*P < 0.01$ ,  $**P < 0.05$ . (D,E) Western blotting of HIF1 $\alpha$  protein expression in H9c2 cells. The images are different parts of the same gel. Alpha, beta-tubulin protein expression was used as an internal control ( $n = 6$ ).  $*P < 0.01$ ,  $**P < 0.05$ . (F) H9c2 cells were cultured with 0, 50, or 100 ng/mL FGF23 for 24 h, and mRNA expression levels were analyzed by real-time PCR. Levels of polypeptide N-acetylgalactosaminyltransferase 3 (GALNT3) mRNA ( $n = 6$ ).  $*P < 0.01$ ,  $**P < 0.05$ . (G) H9c2 cells were cultured with 0, 0.25, or 1.0 mM IS for 24 h, and mRNA expression levels were analyzed by real-time PCR. Levels of GALNT3 mRNA ( $n = 6$ ).  $*P < 0.01$ ,  $**P < 0.05$ . (H) Levels of GALNT3 mRNA ( $n = 9$ ).  $*P < 0.01$ ,  $**P < 0.05$ . (I,J) Western blotting of GALNT3 protein expression in H9c2 cells. Alpha, beta-tubulin protein expression was used as an internal control ( $n = 6$ ).  $*P < 0.01$ ,  $**P < 0.05$ . Data were analyzed by one-way analysis of variance.

## IS upregulates hypertrophic and pro-fibrotic signaling and increases FGF23 expression in cultured cardiomyocytes

We determined the underlying mechanisms by which IS induces cardiomyocyte hypertrophy by treating H9c2 cells with IS. The H9c2 cells were cultured with 1 mM IS for 24 h, which has been reported as a clinically relevant concentration of IS in severe CKD (20–23). The mRNA levels of *beta MHC*, *BNP*, *alpha SMA*, collagen I, and *FGF23* were upregulated (Figure 2). We also examined whether IS affects the cell size in cultured cardiomyocytes. We found that IS induced hypertrophy in H9c2 cells (Supplementary Figure 1). IS is known as a protein-bound toxin (20). Therefore, we examined whether IS induces hypertrophic and pro-fibrotic signaling in H9c2 cells with 4% albumin-containing medium as previously reported (23). IS induced hypertrophic and pro-fibrotic signaling in H9c2 cells in the 4% albumin-containing medium (Supplementary Figure 2).

In H9c2 cells cultured with 1 mM IS for 72 h, FGF23 protein expression and FGFR4 phosphorylation were elevated in cell lysates (Figures 3A–D). This FGFR4 phosphorylation by IS also occurred even in the 4% albumin-containing medium (Supplementary Figure 3). Furin, which is a protein that cleaves intact FGF23, was not downregulated by IS (Figures 3E, F).

These data suggest that IS increases FGF23 protein expression and FGFR4 phosphorylation in cardiomyocytes, and induces hypertrophic and pro-fibrotic signaling in cardiomyocytes.

## IS induces LVH and FGFR4 inhibition reduces this effect

In our mild CKD mouse model, we observed a heavier heart weight and greater left ventricular wall thickness in IS + NS mice than in the other mice (Figures 4A–C). Body weight, blood pressure, creatinine concentrations, calcium concentrations, and phosphate concentrations were not significantly different among the groups (Table 1). Serum IS concentrations tended to be increased in the IS-treated groups (Table 1). Inhibition of FGFR4 reduced heart weight and left ventricular wall thickness in the IS-treated groups (Figures 4A–C). Although serum FGF23 concentrations were not significantly different among the experimental groups (Table 1), FGF23 protein expression in the heart was markedly increased in IS-injected mice (Figures 5A, B). To examine the relationship between IS and FGFR4, we treated H9c2 cells with IS with or without an FGFR4 inhibitor for 24 h (Figure 6). IS upregulated mRNA expression levels of the hypertrophic markers *ANF*, *BNP*, and *beta MHC*, and FGFR4 inhibition reduced their expression.

## IS stimulates AhR and the FGF23-FGFR4 signaling pathway

To examine the relationship between IS and FGF23, we suppressed AhR, which is the receptor of IS, by siRNA in H9c2 cells and then treated cells with 1 mM IS for 6 h (for mRNA) or 48 h (for protein expression). The increase in FGF23 expression in IS-treated myocytes was suppressed by AhR siRNA (Figures 7A–C). HIF1 $\alpha$ ,

which is a hypoxic stress marker that regulates FGF23 production (24), was upregulated by IS. This effect was suppressed by AhR siRNA (Figures 7D, E). GALNT3, which regulates FGF23 O-glycosylation (25), was also upregulated by FGF23 and IS (Figures 7F, G). The increased expression of GALNT3 in IS-treated myocytes was suppressed by AhR siRNA (Figures 7H–J). These data suggest that IS affects FGF23 processing by upregulating GALNT3 and by an inflammatory effect.

## The increase in hypertrophic and pro-fibrotic signaling by IS depends on FGF23 in cultured cardiomyocytes

To examine the relationship between IS and FGF23, we suppressed FGF23 by siRNA in H9c2 cells and then treated cells with 1 mM IS for 24 h (for mRNA) or 48 h (for protein expression) (Figures 8F, 9A). The increase in mRNA levels of *ANF*, *beta MHC*, *BNP*, *alpha SMA*, collagen I, and *FGF23* was suppressed by FGF23 siRNA (Figures 8A–F). The increase in FGF23 and FGFR4

phosphorylation in IS-treated myocytes was suppressed by FGF23 siRNA (Figures 9A–D).

## Discussion

In this study, we investigated the relationship between IS and FGF23 in LVH. We found that IS increased levels of *FGF23* mRNA and markers of hypertrophy in cardiomyocytes. These data suggest that IS leads to LVH by increasing FGF23 expression.

IS is an endogenous agonist for AhR, (26) which is required for *GALNT3* gene expression. GALNT3 inhibits furin proprotein convertase processing by O-glycosylation of tyrosine at residue 178 of FGF23, which suppresses degradation of FGF23 and increases intact FGF23 (25, 27). Our study showed that IS upregulated GALNT3 and FGF23, and that this effect could be controlled by suppressing AhR (Figures 2, 7), supporting the above-mentioned pathways. Although FGF23 expression increased with IS treatment, furin was also mildly upregulated by IS. This finding suggests that FGF23 is likely to be upregulated by the GALNT3 pathway, not by a reduction in furin,

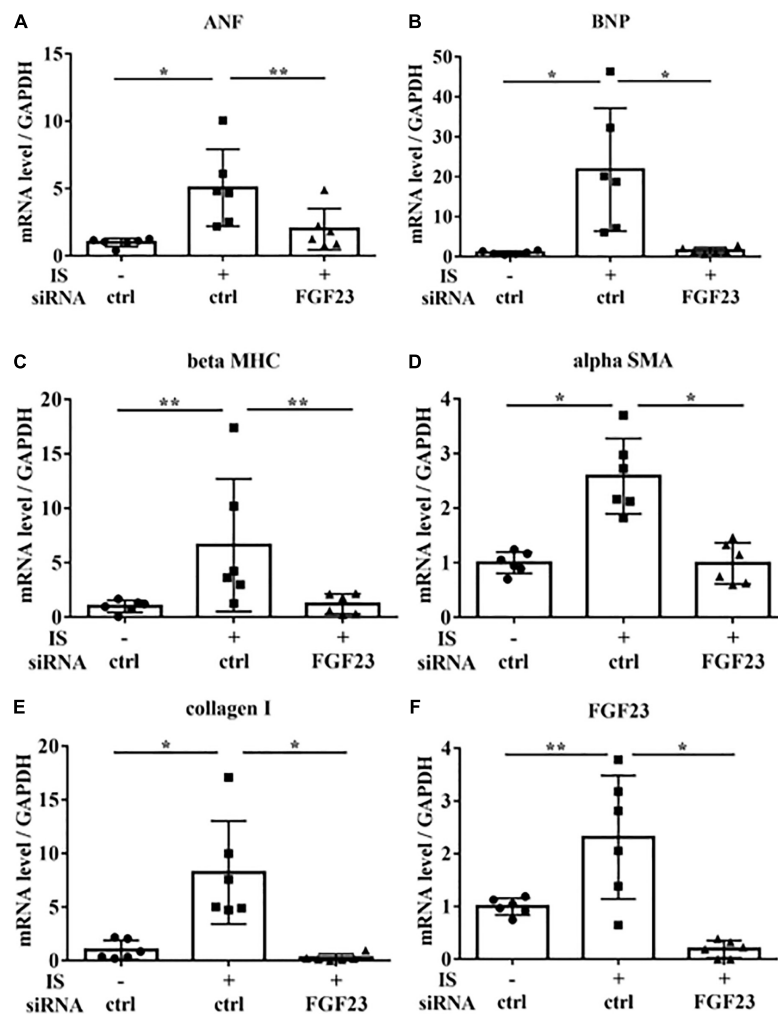


FIGURE 8

IS increases hypertrophic markers via FGF23 *in vitro*. H9c2 cells were cultured with 0 or 1 mM IS for 24 h after pretreatment with FGF23 siRNA or control siRNA (ctrl), and mRNA expression levels were analyzed by real-time PCR. (A) *ANF*, (B) *BNP*, (C) *beta MHC*, (D) *alpha SMA*, (E) collagen I, and (F) *FGF23* mRNA levels were significantly increased by IS and downregulated with FGF23 siRNA ( $n = 6$ ). Data were analyzed by one-way analysis of variance.

\* $P < 0.01$ , \*\* $P < 0.05$ .

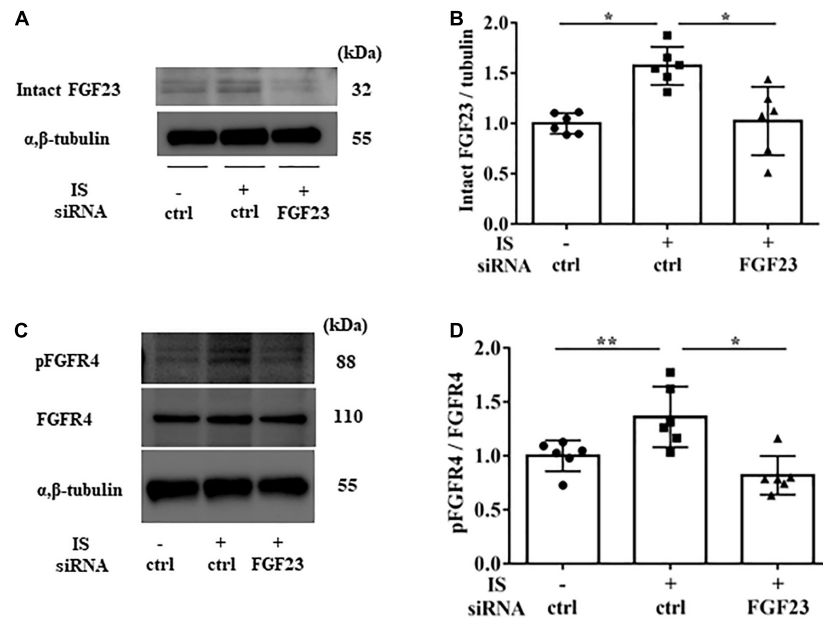


FIGURE 9

IS increases FGFR4 via FGF23 *in vitro*. H9c2 cells were cultured with 0 or 1 mM IS for 48 h after pretreatment with FGF23 siRNA or control siRNA (ctrl). (A,B) Western blotting of FGF23 protein expression in H9c2 cells. (C,D) Western blotting of FGFR4 protein expression and FGFR4 phosphorylation in H9c2 cells. Alpha, beta-tubulin protein expression was examined as an internal control ( $n = 6$ ). Data were analyzed by one-way analysis of variance. \* $P < 0.01$ , \*\* $P < 0.05$ .

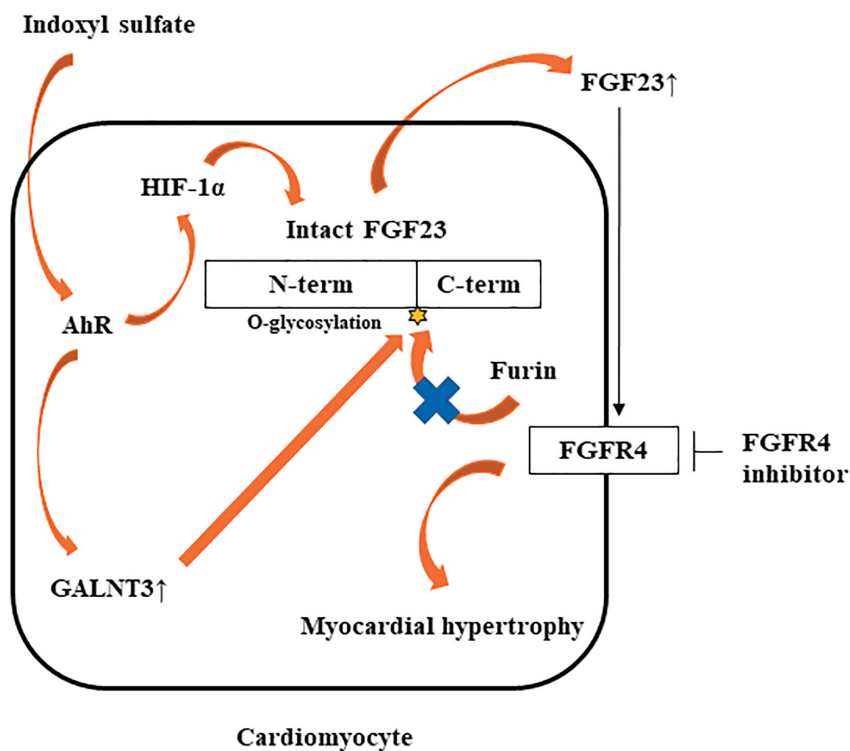


FIGURE 10

Potential mechanism by which IS may induce LVH via the FGF23-FGFR4 pathway. IS upregulates *FGF23* mRNA via AhR and HIF1 $\alpha$ . IS also increases *GALNT3* gene expression, preventing furin-mediated degradation of intact FGF23. Increased FGF23 induces myocardial hypertrophy by FGFR4-dependent activation.

and that increased expression of FGF23 may upregulate furin for negative feedback (Figures 3E, F). IS treatment also accelerated FGFR4 phosphorylation and induced cardiomyocyte hypertrophy.

Furthermore, we demonstrated that IS increased intact FGF23 protein expression in the heart, but not in the serum (Table 1 and Figure 5), suggesting that the effect of IS on FGF23 may be



limited to organs such as the heart. A recent report also showed that FGF23 expression in the heart was associated with LVH using autopsy samples collected from patients with CKD (28). Additionally, rats that undergo nephrectomy show FGF23 expression in the heart (18). This evidence supports the notion that FGF23 expression in the heart is induced by the uremic condition containing higher serum IS concentrations.

In this study, IS increased not only FGF23 protein expression, but also *FGF23* mRNA expression. GALNT3 induced by IS inhibited the degradation of FGF23 protein expression. Therefore, another mechanism was involved in increased *FGF23* mRNA induced by IS. Recent studies showed that inflammatory cytokines were direct regulators of FGF23 production in cardiac fibroblasts (29) and osteoblasts (24, 30). The induction of HIF1 $\alpha$  in osteoblasts and osteocytes, in response to iron deficiency or hypoxia, increases FGF23 production (31). IL-1 $\beta$  significantly increases *FGF23* mRNA expression through a HIF1 $\alpha$ -dependent mechanism (24). Therefore, some inflammatory cytokines induce *FGF23* mRNA *via* HIF1 $\alpha$ . In this study, IS increased HIF1 $\alpha$  *via* the IS-AhR pathway (Figures 7D, E), which suggested that the increase in *FGF23* mRNA induced by IS was partly mediated by HIF1 $\alpha$ . On the basis of these findings, we propose a novel hypothesis on the role of the IS-FGF23-FGFR4 signaling pathway in uremic cardiomyopathy (Figure 10).

FGFR4 is one of four family members harboring tyrosine kinase domains and is most likely expressed only in cardiomyocytes and not in other cardiac cell types (17). Three FGF19 subfamily members (FGF19, FGF21, and FGF23) have the potential to bind FGFR4. H3B-6527 is a selective FGFR4 inhibitor (32). Faul et al. (33) showed that FGF23 caused LVH by FGFR-dependent activation of the calcineurin-NFAT signaling cascade, but it did not require klotho as a coreceptor. FGFR inhibition can reduce LVH caused by FGF23 independent of blood pressure. In our study, IS increased FGFR4 phosphorylation, and FGFR4 inhibition prevented IS-induced LVH, which suggested that IS affected the FGF23-FGFR4 signaling pathway in cardiomyocytes.

A previous report showed that active vitamin D inhibited FGF23-FGFR4 signaling and hypertrophy (18). Paracrine FGF23 activates FGFR tyrosine kinase, and induces activation of the renin-angiotensin system-mitogen-activated protein kinase, phospholipase C-gamma, phosphatidylinositol 3-kinase-AKT, and STAT pathways (34). Active vitamin D also inhibits expression of renin-angiotensin system-associated gene expression and cardiac fibrosis (35). Therefore, active vitamin D may have a role in preventing LVH. However, in our study, IS did not decrease active vitamin D in H9c2 cells (data not shown).

We used the LVH model with heminephrectomy in this study because this model shows mild CKD. Therefore, the elevation in serum FGF23 concentrations is not extremely high. Consequently, we could investigate the IS-FGF23 pathway without the confounding effect of other uremic toxins in this model. In sham mice, serum intact FGF23 concentrations were lower than the other groups. The sham mice were fed a normal phosphorus diet and experienced less stress than the other mice treated by a micro-osmotic pump (Table 1).

Previous studies have shown that FGF23 promotes myocardial fibrosis (36, 37). We also evaluated cardiac fibrosis in the mice in this study, but we found no significant difference among the groups (data not shown). The mouse model in this study is different from that used in previous studies (36, 37). Therefore, we speculate that cardiac fibrosis may occur later than cardiac hypertrophy or *via* another pathway in our model. A possibility is that  $\beta$ -catenin or the local

renin-angiotensin system may induce cardiac fibrosis associated with FGF23 (36, 37).

In summary, this study shows that IS induces LVH *via* AhR and the FGF23-FGFR4 signaling pathway *in vitro* and *in vivo*. IS also upregulates GALNT3 and HIF1 $\alpha$  through AhR, leading to the stabilization of FGF23. These data suggest that blocking the IS-AhR-FGF23-FGFR4 pathway is a new strategy to prevent LVH in patients with CKD.

## Data availability statement

The data that support the findings of this study are available from the corresponding author upon reasonable request.

## Ethics statement

The animal study was reviewed and approved by the Committee on Ethics of Animal Experimentation at Kyushu University Graduate School of Medical Sciences.

## Author contributions

HK performed most of the experiments and drafted the manuscript. TN was responsible for the experimental design, funding of the study, data interpretation, and manuscript development. KT supervised the cell culture experiments and animal experiments. MTo provided advice on the cell culture and animal experiments and contributed to revision of the manuscript. YU assisted with the experiments and data acquisition. SY and MTa contributed to revision of the manuscript. TK contributed to critical revision of the manuscript and supervision of the study. All authors provided critical reviews of the draft and approved the final version.

## Funding

This work was supported by JSPS KAKENHI Grant Number 21K08232.

## Acknowledgments

We thank the Research Support Center and Kyushu University Graduate School of Medical Sciences for technical support. We also thank Mr. M. Munakata and Mrs. M. Tanaka at the Department of Medicine and Clinical Science, Graduate School of Medical Sciences, Kyushu University for assistance with histology. We thank Leah Cannon, Ph.D., from Edanz (<https://jp.edanz.com/ac>) for editing a draft of this manuscript.

## Conflict of interest

The authors declare that the research was conducted in the absence of any commercial or financial relationships that could be construed as a potential conflict of interest.

## Publisher's note

All claims expressed in this article are solely those of the authors and do not necessarily represent those of their affiliated organizations, or those of the publisher, the editors and the reviewers. Any product that may be evaluated in this article, or claim that may be made by its manufacturer, is not guaranteed or endorsed by the publisher.

## Supplementary material

The Supplementary Material for this article can be found online at: <https://www.frontiersin.org/articles/10.3389/fcvm.2023.990422/full#supplementary-material>

## References

- Go A, Chertow G, Fan D, McCulloch C, Hsu C. Chronic kidney disease and the risk of death, cardiovascular events, and hospitalization. *N Engl J Med.* (2004) 351:1296–305. doi: 10.1056/NEJMoa041031
- Manjunath G, Tighiouart H, Ibrahim H, MacLeod B, Salem D, Griffith J, et al. Level of kidney function as a risk factor for atherosclerotic cardiovascular outcomes in the community. *J Am Coll Cardiol.* (2003) 41:47–55. doi: 10.1016/S0735-1097(02)02663-3
- Muntner P, He J, Hamm L, Loria C, Whelton P. Renal insufficiency and subsequent death resulting from cardiovascular disease in the United States. *J Am Soc Nephrol.* (2002) 13:745–53. doi: 10.1681/ASN.V133745
- Ninomiya T, Kiyohara Y, Kubo M, Tanizaki Y, Doi Y, Okubo K, et al. Chronic kidney disease and cardiovascular disease in a general Japanese population: the Hisayama Study. *Kidney Int.* (2005) 68:228–36. doi: 10.1111/j.1523-1755.2005.00397.x
- Collins A, Foley R, Chavers B, Gilbertson D, Herzog C, Johansen K, et al. United States renal data system 2011 annual data report: atlas of chronic kidney disease & end-stage renal disease in the United States. *Am J Kidney Dis.* (2012) 59:e1–420. doi: 10.1053/j.ajkd.2011.11.015
- Longenecker J, Coresh J, Powe N, Levey A, Fink N, Martin A, et al. Traditional cardiovascular disease risk factors in dialysis patients compared with the general population: the choice study. *J Am Soc Nephrol.* (2002) 13:1918–27. doi: 10.1097/01.asn.0000019641.41496.1e
- Silberberg J, Barre P, Prichard S, Sniderman A. Impact of left ventricular hypertrophy on survival in end-stage renal disease. *Kidney Int.* (1989) 36:286–90. doi: 10.1038/ki.1989.192
- Gutierrez O, Mannstadt M, Isakova T, Rau-Hain J, Tamez H, Shah A, et al. Fibroblast growth factor 23 and mortality among patients undergoing hemodialysis. *N Engl J Med.* (2008) 359:584–92. doi: 10.1056/NEJMoa0706130
- Gutierrez O, Januzzi J, Isakova T, Laliberte K, Smith K, Collierone G, et al. Fibroblast growth factor 23 and left ventricular hypertrophy in chronic kidney disease. *Circulation.* (2009) 119:2545–52. doi: 10.1161/CIRCULATIONAHA.108.844506
- Fliser D, Kollerits B, Neyer U, Ankerst D, Lhotta K, Lingenhel A, et al. Fibroblast growth factor 23 (FGF23) predicts progression of chronic kidney disease: the Mild to moderate kidney disease (MMKD) study. *J Am Soc Nephrol.* (2007) 18:2600–8. doi: 10.1681/ASN.2006080936
- Mirza M, Hansen T, Johansson L, Ahlstrom H, Larsson A, Lind L, et al. Relationship between circulating FGF23 and total body atherosclerosis in the community. *Nephrol Dial Transplant.* (2009) 24:3125–31. doi: 10.1093/ndt/gfp205
- Seiler S, Reichart B, Roth D, Seibert E, Fliser D, Heine G. FGF-23 and future cardiovascular events in patients with chronic kidney disease before initiation of dialysis treatment. *Nephrol Dial Transplant.* (2010) 25:3983–9. doi: 10.1093/ndt/gfq309
- Kestenbaum B, Sampson J, Rudser K, Patterson D, Stephen L, Young B, et al. Serum phosphate levels and mortality risk among people with chronic kidney disease. *J Am Soc Nephrol.* (2005) 16:520–8. doi: 10.1681/ASN.2004070602
- Kovesdy C, Ahmadzadeh S, Anderson J, Kalantar-Zadeh K. Secondary hyperparathyroidism is associated with higher mortality in men with moderate to severe chronic kidney disease. *Kidney Int.* (2008) 73:1296–302. doi: 10.1038/ki.2008.64
- Watanabe H, Miyamoto Y, Otagiri M, Maruyama T. Update on the pharmacokinetics and redox properties of protein-bound uremic toxins. *J Pharm Sci.* (2011) 100:3682–95. doi: 10.1002/jps.22592
- Barreto F, Barreto D, Liabeuf S, Meert N, Glorieux G, Temmar M, et al. Serum indoxyl sulfate is associated with vascular disease and mortality in chronic kidney disease patients. *Clin J Am Soc Nephrol.* (2009) 4:1551–8. doi: 10.2215/CJN.03980609
- Grabner A, Amaral A, Schramm K, Singh S, Sloan A, Yanucil C, et al. Activation of cardiac fibroblast growth factor receptor 4 causes left ventricular hypertrophy. *Cell Metab.* (2015) 22:1020–32. doi: 10.1016/j.cmet.2015.09.002
- Leifheit-Nestler M, Grabner A, Hermann L, Richter B, Schmitz K, Fischer D, et al. Vitamin D treatment attenuates cardiac FGF23/FGFR4 signaling and hypertrophy in uremic rats. *Nephrol Dial Transplant.* (2017) 32:1493–503. doi: 10.1093/ndt/gfw454
- Chen W. Soluble Alpha-klotho alleviates cardiac fibrosis without altering cardiomyocytes renewal. *Int J Mol Sci.* (2020) 21:2186. doi: 10.3390/ijms21062186
- Vanholder R, Smet R, Glorieux G, Argile's A, Baurmeister U, Brunet P, et al. Review on uremic toxins: classification, concentration, and interindividual variability. *Kidney Int.* (2003) 63:1934–43. doi: 10.1046/j.1523-1755.2003.00924.x
- Ito S, Higuchi Y, Yagi Y, Nishijima F, Yamato H, Ishii H, et al. Reduction of indoxyl sulfate by AST-120 attenuates monocyte inflammation related to chronic kidney disease. *J Leukoc Biol.* (2013) 93:837–45. doi: 10.1189/jlb.0112023
- Matsuo K, Yamamoto S, Wakamatsu T, Takahashi Y, Kawamura K, Kaneko Y, et al. Increased proinflammatory cytokine production and decreased cholesterol efflux due to downregulation of ABCG1 in macrophages exposed to indoxyl sulfate. *Toxins.* (2015) 7:3155–66. doi: 10.3390/toxins7083155
- Nakano T, Katsuki S, Chen M, Decano J, Haru A, Lee H, et al. Uremic toxin indoxyl sulfate promotes proinflammatory macrophage activation via the interplay of OATP2B1 and Dll4-Notch signaling. *Circulation.* (2019) 139:78–96. doi: 10.1161/CIRCULATIONAHA.118.034588
- David V, Martin A, Isakova T, Spaulding C, Qi L, Ramirez V, et al. Inflammation and functional iron deficiency regulate fibroblast growth factor 23 production. *Kidney Int.* (2016) 89:135–46. doi: 10.1038/ki.2015.290
- de Las Rivas M, Daniel E, Narimatsu Y, Companon I, Kato K, Hermosilla P, et al. Molecular basis for fibroblast growth factor 23 O-glycosylation by GalNAc-T3. *Nat Chem Biol.* (2020) 16:351–60. doi: 10.1038/s41589-019-0444-x
- Schroeder J, Dinatale B, Murray I, Flaveny C, Liu Q, Laurenzana E, et al. The uremic toxin 3-indoxyl sulfate is a potent endogenous agonist for the human aryl hydrocarbon receptor. *Biochemistry.* (2010) 49:393–400. doi: 10.1021/bi901786x
- Kido S, Fujihara M, Nomura K, Sasaki S, Mukai R, Ohnishi R, et al. Molecular mechanisms of cadmium-induced fibroblast growth factor 23 upregulation in osteoblast-like cells. *Toxicol Sci.* (2014) 139:301–16. doi: 10.1093/toxsci/kfu043
- Leifheit-Nestler M, Siemer R, Flasar K, Richter B, Kirchhoff F, Ziegler W, et al. Induction of cardiac FGF23/FGFR4 expression is associated with left ventricular hypertrophy in patients with chronic kidney disease. *Nephrol Dial Transplant.* (2016) 31:1088–99. doi: 10.1093/ndt/gfv421
- Yan L, Bowman M. Chronic sustained inflammation links to left ventricular hypertrophy and aortic valve sclerosis: a new link between S100/RAGE and FGF23. *Inflamm Cell Signal.* (2014) 1:e279. doi: 10.14800/ics.279

### SUPPLEMENTARY FIGURE 1

IS induces hypertrophy *in vitro*. H9c2 cells were cultured with 0 or 1 mM IS for 72 h. Cell surface changes were measured using ImageJ software (National Institutes of Health, 165 Bethesda, MD) ( $n = 10$ ). Student's  $t$ -test was used for analysis. \* $P < 0.01$  versus control.

### SUPPLEMENTARY FIGURE 2

IS increases mRNA levels of markers of hypertrophy and fibrosis in medium with 4% albumin. H9c2 cells were cultured with 0, 0.25, or 1.0 mM IS in medium with 4% albumin for 24 h, and mRNA expression levels were analyzed by real-time PCR. (a) ANF, (b) BNP, (c) beta MHC, (d) alpha SMA, (e) collagen I, and (f) FGF23 mRNA levels were significantly increased by IS ( $n = 6$ ). Data were analyzed by one-way analysis of variance. \* $P < 0.01$ , \*\* $P < 0.05$ .

### SUPPLEMENTARY FIGURE 3

IS increases FGF23 protein expression and FGFR4 phosphorylation in medium with 4% albumin. H9c2 cells were cultured with 0, 0.25, or 1.0 mM IS in medium with 4% albumin for 48 h. Alpha, beta-tubulin protein expression was examined as an internal control ( $n = 6$ ). Data were analyzed by one-way analysis of variance. \* $P < 0.01$ , \*\* $P < 0.05$  versus IS 0 mM. (a,b) Western blotting of FGF23 protein. (c,d) Western blotting of FGFR4 protein expression and FGFR4 phosphorylation.

30. Ito N, Prideaux M, Wijenayaka A, Yang D, Ormsby R, Bonewald L, et al. Sclerostin directly stimulates osteocyte synthesis of fibroblast growth factor-23. *Calcif Tissue Int.* (2021) 109:66–76. doi: 10.1007/s00223-021-00823-6
31. Farrow E, Yu X, Summers L, Davis S, Fleet J, Allen M, et al. Iron deficiency drives an autosomal dominant hypophosphatemic rickets (ADHR) phenotype in fibroblast growth factor-23 (Fgf23) knock-in mice. *Proc Natl Acad Sci USA.* (2011) 108:E1146–55. doi: 10.1073/pnas.1110905108
32. Lang L, Teng Y. Fibroblast growth factor receptor 4 targeting in cancer: new insights into mechanisms and therapeutic strategies. *Cells.* (2019) 8:31. doi: 10.3390/cells8010031
33. Faul C, Amaral A, Oskouei B, Hu M, Sloan A, Isakova T, et al. FGF23 induces left ventricular hypertrophy. *J Clin Invest.* (2011) 121:4393–408. doi: 10.1172/JCI46122
34. Ito N, Nakayama Y, Konishi M. Roles of FGFs as paracrine or endocrine signals in liver development, health, and disease. *Front Cell Dev Biol.* (2016) 13:4–30. doi: 10.3389/fcell.2016.00030
35. Schön A, Leifheit-Nestler M, Deppe J, Fischer D, Bayazit A, Obrycki L, et al. Active vitamin D is cardioprotective in experimental uraemia but not in children with CKD Stages 3–5. *Nephrol Dial Transplant.* (2021) 3:442–51. doi: 10.1093/ndt/gfaa227
36. Hao H, Li X, Li Q, Lin H, Chen Z, Xie J, et al. FGF23 promotes myocardial fibrosis in mice through activation of  $\beta$ -catenin. *Oncotarget.* (2016) 7:64649–64. doi: 10.18632/oncotarget.11623
37. Böckmann I, Lischka J, Richter B, Deppe J, Rahn A, Fischer D, et al. FGF23-mediated activation of local RAAS promotes cardiac hypertrophy and fibrosis. *Int J Mol Sci.* (2019) 20:4634. doi: 10.3390/ijms20184634



## OPEN ACCESS

## EDITED BY

Amy Li,  
La Trobe University, Australia

## REVIEWED BY

Yuka Morikawa,  
Texas Heart Institute, United States  
Jihyun Jang,  
Abigail Wexner Research Institute, United States  
Joshua Travers,  
University of Colorado Anschutz Medical  
Campus, United States

## \*CORRESPONDENCE

Caitlin C. O'Meara  
✉ comeara@mcw.edu

## SPECIALTY SECTION

This article was submitted to Cardiovascular  
Biologics and Regenerative Medicine, a section  
of the journal Frontiers in Cardiovascular  
Medicine

RECEIVED 11 January 2023

ACCEPTED 20 February 2023

PUBLISHED 14 March 2023

## CITATION

Flinn MA, Alvarez-Argote S, Knas MC,  
Almeida VA, Paddock SJ, Zhou X, Buddell T,  
Jamal A, Taylor R, Liu P, Drnevich J,  
Patterson M, Link BA and O'Meara CC (2023)  
Myofibroblast Ccn3 is regulated by Yap and  
Wwtr1 and contributes to adverse cardiac  
outcomes.  
Front. Cardiovasc. Med. 10:1142612.  
doi: 10.3389/fcvm.2023.1142612

## COPYRIGHT

© 2023 Flinn, Alvarez-Argote, Knas, Almeida,  
Paddock, Zhou, Buddell, Jamal, Taylor, Liu,  
Drnevich, Patterson, Link and O'Meara. This is  
an open-access article distributed under the  
terms of the [Creative Commons Attribution  
License \(CC BY\)](#). The use, distribution or  
reproduction in other forums is permitted,  
provided the original author(s) and the  
copyright owner(s) are credited and that the  
original publication in this journal is cited, in  
accordance with accepted academic practice.  
No use, distribution or reproduction is  
permitted which does not comply with these  
terms.

# Myofibroblast Ccn3 is regulated by Yap and Wwtr1 and contributes to adverse cardiac outcomes

Michael A. Flinn<sup>1,2</sup>, Santiago Alvarez-Argote<sup>1,2</sup>, Makenna C. Knas<sup>1,2</sup>,  
Victor Alencar Almeida<sup>1,2</sup>, Samantha J. Paddock<sup>1,2</sup>, Xiaoxu Zhou<sup>3</sup>,  
Tyler Buddell<sup>2,4</sup>, Ayana Jamal<sup>2,4</sup>, Reiauna Taylor<sup>1</sup>, Pengyuan Liu<sup>1,3</sup>,  
Jenny Drnevich<sup>5</sup>, Michaela Patterson<sup>2,4</sup>, Brian A. Link<sup>2,4</sup> and  
Caitlin C. O'Meara<sup>1,2,6\*</sup>

<sup>1</sup>Department of Physiology, Medical College of Wisconsin, Milwaukee, WI, United States, <sup>2</sup>Cardiovascular Center, Medical College of Wisconsin, Milwaukee, WI, United States, <sup>3</sup>Institute of Translational Medicine, Zhejiang University School of Medicine, Hangzhou, China, <sup>4</sup>Department of Cell Biology, Neurobiology, and Anatomy, Medical College of Wisconsin, Milwaukee, WI, United States, <sup>5</sup>High Performance Computing in Biology (HPCBio) and the Roy J. Carver Biotechnology Center, University of Illinois, Urbana-Champaign, Champaign, IL, United States, <sup>6</sup>Genomics Sciences and Precision Medicine Center, Medical College of Wisconsin, Milwaukee, WI, United States

**Introduction:** While Yap and Wwtr1 regulate resident cardiac fibroblast to myofibroblast differentiation following cardiac injury, their role specifically in activated myofibroblasts remains unexplored.

**Methods:** We assessed the pathophysiological and cellular consequence of genetic depletion of Yap alone (*Yap<sup>fl/fl</sup>;Postn<sup>MCM</sup>*) or Yap and Wwtr1 (*Yap<sup>fl/fl</sup>;Wwtr1<sup>fl/+</sup>;Postn<sup>MCM</sup>*) in adult mouse myofibroblasts following myocardial infarction and identify and validate novel downstream factors specifically in cardiac myofibroblasts that mediate pathological remodeling.

**Results:** Following myocardial infarction, depletion of Yap in myofibroblasts had minimal effect on heart function while depletion of Yap/Wwtr1 resulted in smaller scars, reduced interstitial fibrosis, and improved ejection fraction and fractional shortening. Single cell RNA sequencing of interstitial cardiac cells 7 days post infarction showed suppression of pro-fibrotic genes in fibroblasts derived from *Yap<sup>fl/fl</sup>;Wwtr1<sup>fl/+</sup>;Postn<sup>MCM</sup>* hearts. In vivo myofibroblast depletion of Yap/Wwtr1 as well in vitro knockdown of Yap/Wwtr1 dramatically decreased RNA and protein expression of the matricellular factor Ccn3. Administration of recombinant CCN3 to adult mice following myocardial infarction remarkably aggravated cardiac function and scarring. CCN3 administration drove myocardial gene expression of pro-fibrotic genes in infarcted left ventricles implicating CCN3 as a novel driver of cardiac fibrotic processes following myocardial infarction.

**Discussion:** Yap/Wwtr1 depletion in myofibroblasts attenuates fibrosis and significantly improves cardiac outcomes after myocardial infarction and we identify *Ccn3* as a factor downstream of Yap/Wwtr1 that contributes to adverse cardiac remodeling post MI. Myofibroblast expression of Yap, Wwtr1, and Ccn3 could be further explored as potential therapeutic targets for modulating adverse cardiac remodeling post injury.

## KEYWORDS

myofibroblast, pathological remodeling, adverse remodeling, hippo pathway, CCN3 (NOV), YAP, WWTR1, cardiac fibroblast



## Introduction

Following cardiac injury such as myocardial infarction (MI), progressive fibrosis can contribute to adverse ventricular remodeling and ultimately heart failure. Resident cardiac fibroblasts, which directly produce the pro-fibrotic response, are a heterogeneous population of stromal cells. When activated following injury, a subset of resident fibroblasts adopt a myofibroblast phenotype (1, 2) characterized by expression of Periostin (Postn) and alpha smooth muscle actin [ $\alpha$ SMA (1)], increased production of extracellular matrix (ECM) proteins [primarily collagens (3, 4)], and secretion of metalloproteases (1), inflammatory chemokines, and cytokines (5, 6). While myofibroblast function is critical for wound contraction, initial scar formation, and to prevent catastrophic heart rupture (1, 7), extended myofibroblast proliferation and activation can lead to persistent matrix protein secretion causing exacerbated scar formation, myocyte uncoupling, decreased cardiac compliance, and progressive heart failure (5). There is currently an un-met need to identify molecular mediators of myofibroblast activity so that we can therapeutically target these pathways and regulate the fibrotic response following cardiac injury.

The Hippo-Yap/Wwtr1 pathway (herein referred to as “Hippo-Yap”) is a highly conserved signaling pathway consisting of core protein kinases; Stk3, Stk4, Lats1, and Lats2, and scaffolding proteins; Sav1, Mob1a, and Mob1b, whose kinase activity suppresses function of the transcriptional co-activators Yap and Wwtr1 (8). Phosphorylation of Yap and Wwtr1 by the Hippo pathway kinases prevents nuclear localization and promotes phospho-degradation of Yap and Wwtr1, thereby inhibiting nuclear transcriptional activity. It has been demonstrated in mice Lats1/2 deletion specifically in resident cardiac fibroblasts promotes Yap and Wwtr1 activity, driving proliferation and cell fate transition to a myofibroblast state in a cell autonomous manner and resulting in deleterious fibrosis in mice (9, 10). Inhibiting the Hippo-Yap pathway by verteporfin following myocardial infarction reduces fibrosis and injury size (11). Furthermore, depletion of Yap/Wwtr1 in Tcf21 or Collagen (Col1a2 or Col1a1) positive cells attenuated pathological remodeling and improved cardiac function (9, 10, 12, 13). However, Tcf21, Col1a2 and Col1a1 target all fibroblast populations and the role of endogenous Yap and Wwtr1 in differentiated cardiac myofibroblasts specifically has not been investigated. Here, we take the novel approach of investigating the role of endogenous Yap/Wwtr1 expression in activated cardiac myofibroblasts (Postn+) following MI. We demonstrate a cooperative role for myofibroblast Yap and Wwtr1 in scar size, interstitial fibrosis, and cardiac function post MI.

The downstream pathways modulated by Hippo-Yap activity in myofibroblasts are poorly understood. We found that depletion of Yap/Wwtr1 in myofibroblasts both *in vivo* and *in vitro* strongly suppresses expression of the secreted matricellular protein Ccn3 (also known as nephroblastoma overexpressed—Nov), suggesting Ccn3 expression might contribute to adverse outcomes post MI. Indeed, global administration of recombinant CCN3 to mice post MI significantly exacerbates adverse cardiac function and scarring.

CCN3 signaling to myocardial tissue post MI promoted expression of pro-fibrotic genes. Collectively, we identify a novel factor expressed downstream of Yap/Wwtr1 in cardiac fibroblasts that independently promotes adverse cardiac wound healing dynamics.

## Methods

### Animals

The following mouse lines from The Jackson Laboratory were utilized: stock 027929 *Yap<sup>fl</sup>*, 029645 *Postn<sup>MCM</sup>*, 030532 *Yap<sup>fl</sup>*; *Wwtr1<sup>fl</sup>*, and 004077 *Rosa26-eGFP<sup>fl</sup>*. Sprague Dawley neonatal rats (Charles River Laboratories) were used for cardiac fibroblast cell isolation. Adult mice were euthanized by administration of isoflurane and subsequent thoracotomy, neonatal mice and rats were euthanized by decapitation.

### Isoflurane administration

During echocardiography, surgical MI, or euthanasia, adult mice were anesthetized *via* inhalation of 1%–3% isoflurane vaporized with compressed O<sub>2</sub> at a flow rate of 1 L/min.

### Myocardial infarction

Six- to ten-week-old mice were used for adult MI studies. The left anterior descending (LAD) coronary artery was ligated using the “Rapid Method” originally described by Gao et al. (14). Briefly, a 1–2 cm incision was made in the skin on the left lateral side of the thorax. The heart was retracted from the thoracic cavity *via* the 5th intercostal space and a surgical needle with 6-0 prolene suture was inserted under the LAD artery. The vessel was then tied off to create a permanent infarction. The heart was returned to the thorax and the chest wall compressed along the sternal midline to force out excess air. The outer incision of the skin was closed using monofilament nonabsorbable nylon suture. The mouse was removed from anesthesia and returned to a cage to recover under a warming lamp. Immediately following surgery animals were administered 1.5 mg/kg slow-release Buprenorphine and the following day received oral administration of 5 mg/kg Meloxicam.

P6 neonatal MI surgeries were performed as described in Mahmoud et al. (15). Briefly, methods were similar to that of adult MI except P6 mice were anesthetized on ice. Following surgery, mice recovered under a heat lamp. When animals were sternal and active, they were returned to their mother.

### Tamoxifen treatment

Mice of all genotypes were treated with tamoxifen to induce Cre expression and excision of floxed genes following MI. Cre negative controls received identical tamoxifen dosing. For neonatal mice, tamoxifen (Sigma) was dissolved into a mixture of

25% ethanol and 75% sunflower oil at a concentration of 1.5 mg/ml and injected subcutaneously at a dosage of 30 mg/kg. Postnatal day 6 (P6) neonatal mice were administered with tamoxifen 1, 3, and 5 days post injury (dpi). For adult mice, a diet of 0.4 g/kg tamoxifen citrate chow (Envigo) was provided *ad libitum* starting immediately after MI and continued for the duration of the study.

## CCN3 mouse administration

Following MI in 8 week-old C57/B6J mice, recombinant CCN3 (R&D Systems 1640-NV-050) was resuspended in PBS at a concentration of 0.01 µg/µl, and 6 µg/kg was administered by intraperitoneal injection following surgical MI (Tuesday) and subsequently three times weekly (Monday, Wednesday, Friday) as described in Riser et al. (16) over the course of 28 days. At this concentration, intraperitoneal injection of CCN3 was shown to localize to the heart, liver, and kidneys and to elicit renal phenotypes but not overt adverse effects in mice (16). PBS was administered by intraperitoneal injection to vehicle control animals.

## Echocardiography

Echocardiograms were obtained from adult mice using a Vevo 770 with an RMV 707 transducer or Vevo 3,100 with an MX550D transducer. Scans were taken of the parasternal long axis and short axis at the papillary muscle level in triplicate and measured in a genotype or treatment blinded manner. We calculated ejection fraction (%EF) based on measurements from tracing the circumference of the LV chamber in long axis mode during systole and diastole. Measurements based on internal diameters in short axis mode at the mid-papillary level were used to calculate fractional shortening (%FS), left ventricular internal diameter during diastole (LVID-d), and systole (LVID-s).

## Histological analysis

Hearts were fixed in 10% formalin for 48 h at room temperature prior to processing and paraffin embedding. Sectioning was performed starting at the apex and progressing towards the base of the heart in 250 µm steps. 4 µm sections were collected at each level. Gömöri trichrome staining was performed to assess scar size. Slides were scanned using a Super Coolsan 9,000 (Nikon) or for higher resolution slides were scanned using a NanoZoomer 2.0-HT (Hamamatsu Photonics K.K.). For scar size quantification, four sections starting at 1,000 µm from the apex and proceeding every 500 µm toward the papillary muscles were averaged to quantify fibrotic area and midline percentage using MIquant (17). Interstitial fibrosis was quantified from five representative images in the remote region of the left ventricle and quantified using Fiji ImageJ colorimetric analysis. Immunohistology was evaluated using a Nikon A1 confocal microscope or Eclipse 80i fluorescent microscope (Nikon) and Panda sCMOS camera (PCO). Immunostaining was

performed with antibodies described in **Supplementary Table S1**. Click-iT (Thermo Fisher) 5-ethynyl-2'-deoxyuridine (EdU) staining was performed according to the manufacturer's recommendations. Two to five regions within the scar were averaged per heart to assess EdU incorporation in non-myocyte scar associated cells. Wheat germ agglutinin (WGA) staining was used to identify the cell surface of cardiomyocytes to assess cross sectional area from five representative images within the remote region of the left ventricle. For denatured collagen assessment, serial sections of the left ventricle containing robust scar regions (~2,000 µm from the apex) were treated with collagen hybridizing peptide with Cy3 conjugate (3Helix) according to the manufacturer's recommendations. Representative images of the injury were quantified for presence of Cy3 vs. scar area. Yap and Wwtr1 staining was assessed by confocal microscopy and intensities were quantified by mean grey value *via* ImageJ in either the cytoplasm or nuclei, delineated by DAPI, in GFP+ cells. Confocal microscopy was used to verify measured nuclei were inside of GFP+ cells.

## siRNA knockdown in cultured rat cardiac fibroblasts

Primary cardiac fibroblasts were isolated from 2-day-old rats using a neonatal heart dissociation kit (Miltenyi Biotec) according to the manufacturer's protocol, followed by percoll gradient separation. 24 h after plating, cultured cells were transfected for 48 h with 25 nM siRNAs designed against Yap and/or Wwtr1, or with universal negative control siRNAs (**Supplementary Table S2**) as detailed in Flinn, et al. (18). Untreated cells were cultured in Dulbecco's modified eagle medium (DMEM, Life Technologies) supplemented with 7.5% fetal bovine serum without siRNA.

## <sup>3</sup>H thymidine incorporation in cultured rat cardiac fibroblasts

Forty-eight hours post siRNA transfection cells were treated with DMEM containing <sup>3</sup>H thymidine for DNA synthesis quantification. Cells were exposed to <sup>3</sup>H thymidine treated media for 16 h, fibroblasts were then washed with PBS and lysed with 0.1 M NaOH + 0.1% Sodium Dodecyl Sulfate (SDS). <sup>3</sup>H thymidine incorporation was quantified on the LS 6,500 MultiPurpose Scintillation Counter (Beckman Coulter).

## CCN3 administration to cultured rat cells

Twenty-four hours after plating P2 neonatal rat cardiac fibroblasts or cardiomyocytes, cells were serum starved for 1 h and then administered CCN3 at either 0.1 µg/ml or 1.0 µg/ml or PBS as a control. Cells were incubated for 5 h after which they were collected and stored in TRIzol (Thermo Fisher) for RNA extraction.

## Single cell RNA sequencing (scRNAseq)

To identify differentially expressed genes (DEGs) in cardiac myofibroblasts between *Postn*<sup>MCM</sup> and *Yap*<sup>fl/fl</sup>;*Wwtr1*<sup>fl/+</sup>;*Postn*<sup>MCM</sup> *in vivo* we performed scRNAseq on interstitial cells from hearts following MI. Both strains carried *R26-eGFP* transgene. MI was performed on 8–10 week old mice as described above and animals were put on tamoxifen citrate chow immediately following surgery. At 7 dpi hearts were extracted and retrograde perfused with 50 ml of 1 mg/ml Collagen type II to digest hearts. Following digestion, atria and valves were removed and ventricular tissue was resuspended in PBS and filtered through a 40 µm cell strainer to remove cardiomyocytes and undigested tissue. Single cells were resuspended in 1 ml of ACK (ammonium-chloride-potassium) lysis buffer (ThermoFisher Cat# A1049201) for 2 min at room temperature and washed with 2 ml of FACS buffer— 1% fetal bovine serum, 0.1% Na3 Dulbecco's Phosphate Buffered Saline (DBPS) without Calcium and Magnesium (Lonza). Cells were resuspended in 4 ml of FACS buffer for cell counting, which was performed using the LUNA<sup>TM</sup> automated cell counter (Logos Biosystems) using 0.4% trypan blue (ThermoFisher Cat# T10282) and the LUNA<sup>TM</sup> cell counter bright field feature. Subsequently, samples were resuspended to a concentration of one million cells per 100 µl of FACS buffer. Samples were stained with 3 µM of [4',6-Diamidino-2-Phenylindole, Dilactate (DAPI, Biolegend Cat# 422801)], in a volume of 1 ml of DAPI-FACS buffer per sample for 15 min. Then samples were washed with 1 ml of FACS buffer and resuspended again in 1 ml of FACS buffer for cell sorting. Samples were sorted using BD FACS Aria II Cell Sorter (BD Biosciences) and collected in 3–5 ml of FACS buffer.

Single cell capture, cDNA synthesis, barcoding, and library preparation was performed using the 10x Chromium system using V3.1 chemistry according to the manufacturer's recommendation (10x Genomics). Each sample was loaded onto a single lane of a Chromium Next GEM chip G to target 3,000 cells per sample. Cells were captured in single GEMs and lysed followed by cDNA synthesis using 12 amplification cycles, followed by library construction per manufacturer's protocol. An i7 multiplex single index kit was used to generate the libraries over 14 cycles of sample index PCR. Fragment size of cDNA and libraries was assessed using Agilent's 5,200 Fragment Analyzer System.

## scRNAseq data analysis

Libraries were sequenced at the Roy J. Carver Biotechnology Center at the University of Illinois, Urbana Champaign on a NovaSeq 6,000 using one S4 lane with 2X150nt reads. Samples were demultiplexed using Cell Ranger v6.1.1 (10X Genomics). A custom reference was made using NCBI's GRCm39 genome and Annotation Release 109, along with Cloning vector pEGFP-1 (GenBank: U55761.1) and SA-betageo synthetic construct [full details of modifications in Supplemental R file, (19)]. The "cellranger count" pipeline with default parameters was run separately on each sample to call cells and collapse reads to unique molecular identifiers (UMIs). Both samples were combined using "cellranger aggr" with "–normalize = none".

The UMI counts per gene for all called cells were read into R [v4.1.2, (20)] and analyzed using Seurat [v4.0.6, (21)]. Genes were filtered out if they did not have at least 1 UMI in at least 20 cells, leaving 16,855 genes. Initial quality control involved performing SCTransform normalization (22), principal components analysis, shared nearest neighbor cluster calling, and Uniform Manifold Approximation and Projection [UMAP, (23)] dimension reduction (hereafter referred to as the "Seurat pipeline"). One cluster of cells had extremely high percentage of UMIs in mitochondrial genes (likely dead/dying cells) and two other clusters had extremely low numbers of genes detected and total number of UMIs (likely stripped nuclei). These 3 clusters were removed completely along with a few other cells that had total numbers of UMIs > 54,742 or percentage of UMIs in mitochondrial genes > 4.58 (thresholds set at 6 median absolute deviations). The remaining cells were re-run through the Seurat pipeline to create the final clustering and dimension reduction.

Marker genes per cluster were found by recursively comparing each cluster's cells against all other clusters combined using a Wilcoxon Rank Sum test. Within each cluster, gene expression differences between *Yap*<sup>fl/fl</sup>;*Wwtr1*<sup>fl/+</sup>;*Postn*<sup>MCM</sup> and *Postn*<sup>MCM</sup> cells were tested also using a Wilcoxon Rank Sum test. The cells that expressed *Postn* were overwhelmingly in one cluster, so this one cluster was run by itself through the Seurat pipeline to find sub-clusters of cells. Sub-cluster marker genes and within-subcluster *Yap*<sup>fl/fl</sup>;*Wwtr1*<sup>fl/+</sup>;*Postn*<sup>MCM</sup> and *Postn*<sup>MCM</sup> DEGs were calculated as before. Full R codes for all Seurat analyses are in the Supplemental Methods.

## Western blot

Cultured rat cardiac fibroblasts or mouse left ventricles were collected in RIPA buffer. Rat cardiac fibroblasts were collected 48 h post siRNA transfection. Protein lysates were combined with Laemmli buffer and separated on a 4%–15% Mini-PROTEAN TGC precast gel (Bio-Rad) by electrophoresis. Proteins were then transferred to a 0.45 µm pore size nitrocellulose membrane (Bio-Rad). Western blots were processed according to Li-Cor's Near-Infrared Western Blot Detection protocol and blocked using TBS based Intercept buffer (Li-Cor Biosciences). Protein detection was performed using an Odyssey-CLx infrared imager (Li-Cor Biosciences). Uncropped blots are provided in the supplemental data.

## RNA extraction and qRT-PCR

Twenty-four hours post siRNA transfection media was changed to DMEM with 7.5% FBS, and forty-eight hours later cells were collected for gene expression analysis by either qRT-PCR or RNAseq. CCN3 administered cells were collected 5 h after treatment. Cells were washed in PBS and collected in TRIzol for RNA extraction according to the manufacturer's recommendations. For qRT-PCR analysis RNA was reverse transcribed using a high-capacity cDNA reverse transcription kit (Applied Biosystems). qRT-PCR was performed with SybrGreen (Invitrogen) and primers listed in **Supplementary Table S3** and

amplification was detected on the QuantStudio 6 Flex (Thermo Fisher). Gene expression was normalized to 18s ribosomal RNA expression and analyzed in QuantStudio (Thermo Fisher).

## Bulk RNAsequencing

Two methods were used to attain bulk RNAseq data. First, primary cardiac fibroblasts were isolated from 2-day-old rats, treated with siRNA or a universal negative control, and RNA was extracted from cells using TRIzol extraction protocol according to the manufacturer's recommendations. This process was repeated with separate litters to achieve 3 biological replicates per group. RNA quality was determined using an Agilent BioAnalyzer. RNA libraries were prepared by BGI Americas. Sequencing was performed using a DNBSEQ-G400 platform at 20 M reads per sample. Adapter sequences were removed from the output sequence and reads with low base quality (<13) were further trimmed using Trim\_Galore v0.6.5 (Babraham Bioinformatics). Trimmed reads were then aligned to the rat genome (rn6) using Hisat2 v 2.2.1. Transcripts were assembled from RNA-seq alignments using Stringtie2 v2.1.5. Expression was quantified by fragments per kilobase of transcript per million reads mapped (FPKM). DEGs for each experimental group, as compared to the negative control, were detected using DESeq2.

Second, left ventricles were obtained from 4 dpi adult mice treated with either 6 µg/kg CCN3 or PBS daily starting at 1 dpi. RNA was extracted from homogenized tissue by TRIzol extraction. RNA libraries were prepared by the Roy J. Carver Biotechnology Center at the University of Illinois with the Kapa Hyper mRNA library kit (Roche) and sequenced with a NovaSeq 6,000 with V1.5 sequencing kits. Fastq files were generated and demultiplexed with the bcl2fastq v2.20 Conversion Software (Illumina). Salmon version 1.4.0 was used to quasi-map reads to the GRCm39 transcriptome (NCBI) and quantify the abundance of each transcript. Data was normalized by removing unwanted variation by a factor of 2 (24). Differential gene expression analysis was performed using the edgeR-quasi method using a model of treatment + 2 RUV factors plus False Discovery Rate (FDR) correction on the *P*-values.

For both methods, analysis using the Ingenuity Pathway Analysis (IPA, Qiagen) and Database for Annotation, Visualization and Integrated Discovery [DAVID, (25)] was performed.

## Statistics

Data were analyzed using Prism 8.2.0 (GraphPad). Two-way ANOVA followed by Tukey's multiple comparisons tests were performed on samples with two experimental factors. For data series consisting of two experimental factors assessed at multiple timepoints, a repeated measures Two-way ANOVA was performed followed by Sidak multiple comparisons test. Statistical comparisons between two groups were analyzed by Student's *t*-test, or between three or more groups by one-way ANOVA followed by Tukey's or Dunnett's multiple comparisons

test. Welch's correction was utilized when the variance differed significantly in groups. Assessment of survival curves was performed using a Logrank Mantel-Cox test. Error bars in graphical data represent standard error.

## Study approval

All protocols in these studies were approved by the local Animal Care and Use Committee and conform to the Guide for the Care and Use of Laboratory Animals published by the National Institutes of Health.

## Results

### Yap and Wwtr1 are expressed in myofibroblasts after MI

After an ischemic injury, resident cardiac fibroblasts differentiate into myofibroblasts which aggregate at the site of injury as soon as 1 dpi with a robust presence around 4–7 dpi (1). By comparison, uninjured hearts show little signs of myofibroblast differentiation (<1% of interstitial cells). To assess whether the Hippo-Yap pathway was active in myofibroblasts, we leveraged a myofibroblast specific and tamoxifen inducible *Postn* Cre [*Postn*<sup>MCM</sup>(1)] crossed to a transgenic reporter line containing a floxed stop codon prior an enhanced green fluorescent protein (eGFP) in the *Rosa26* locus (*R26-eGFP*<sup>fl/+</sup>) to express eGFP in myofibroblasts following tamoxifen induction (Figure S1A). This reporter model facilitates reliable identification of myofibroblasts by eGFP expression in tissue sections. *R26-eGFP*<sup>fl/+</sup>; *Postn*<sup>MCM</sup> mice were crossed to Yap and Wwtr1 floxed mice to generate Yap<sup>fl/fl</sup>; Wwtr1<sup>fl/WT</sup>; *R26-eGFP*<sup>fl/+</sup>; *Postn*<sup>MCM</sup> reporter mice that are depleted for Yap and Wwtr1 expression in *Postn* expressing cells following tamoxifen administration (Figure S1B). We performed MI followed by tamoxifen treatment in both postnatal day 6 (P6) and in 8–10 week old adult mice to investigate expression patterns of Yap and Wwtr1 at two developmental timepoints (Figure 1A and Supplementary Figure S1C). At 7 dpi we identified a robust population of GFP+ cells at the site of injury, but not in remote cardiac tissue, in *R26-eGFP*<sup>fl/+</sup>; *Postn*<sup>MCM</sup> mice (Figure 1B and Supplementary Figures S1 D,E). At both timepoints we observed nuclear Yap and Wwtr1 expression in GFP+ myofibroblasts in *R26-eGFP*<sup>fl/+</sup>; *Postn*<sup>MCM</sup> mice while Yap<sup>fl/fl</sup>; Wwtr1<sup>fl/+</sup>; *R26-eGFP*<sup>fl/+</sup>; *Postn*<sup>MCM</sup> mice showed marked decrease in nuclear Yap (Figures 1B,C) and Wwtr1 (Figures 1D,E) expression.

### Depletion of Yap in myofibroblasts results in modest protection against ventricular dilation post MI

To test if Yap deletion in myofibroblasts influences cardiac function we performed MI on Yap<sup>fl/fl</sup>; *Postn*<sup>MCM</sup> and Yap<sup>fl/fl</sup> animals followed by tamoxifen administration provided *ad*



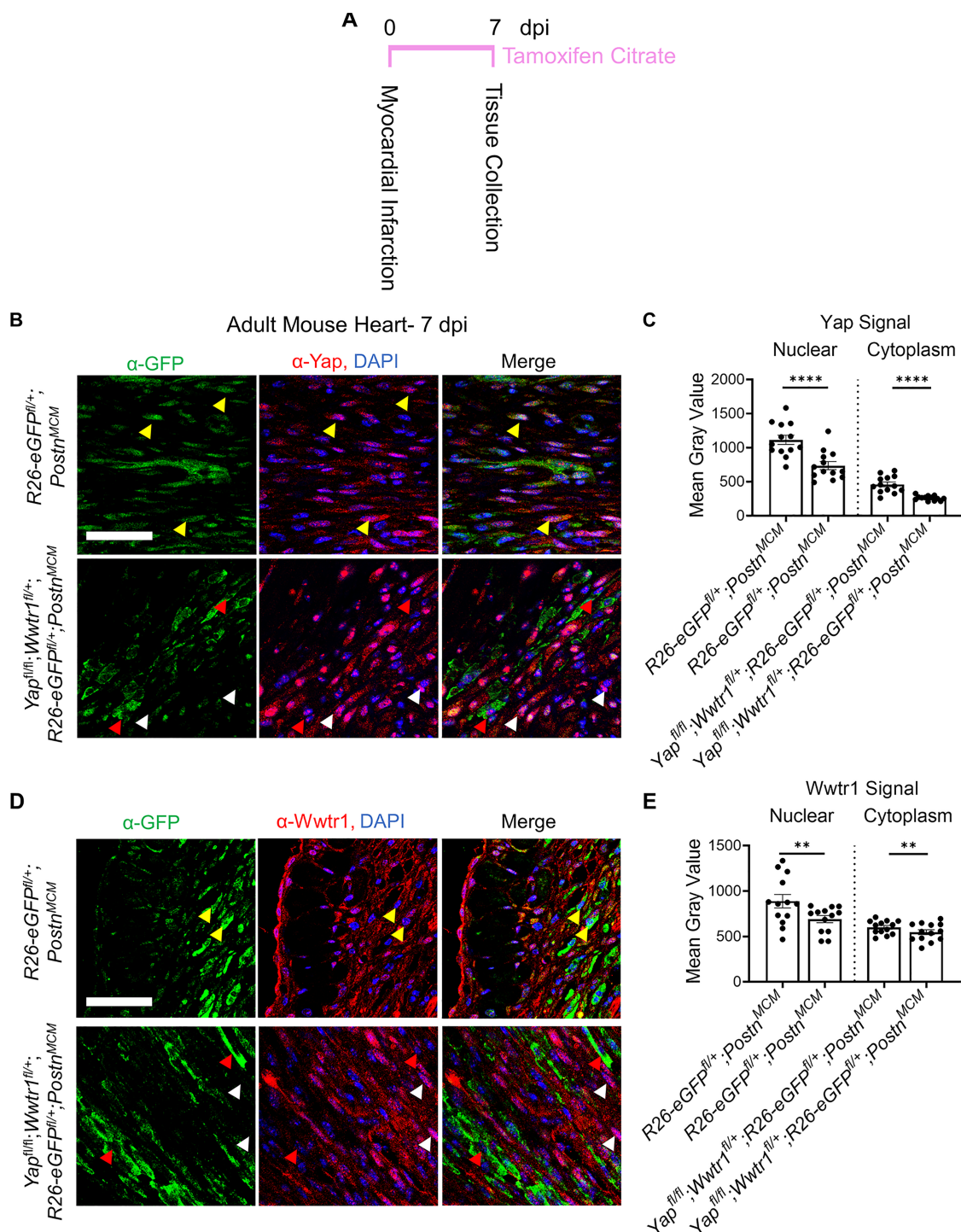


FIGURE 1

Yap and Wwtr1 expression is detected in myofibroblasts after ischemic injury. (A) Experimental timeline of adult MIs and subsequent tamoxifen administration. (B–E) Representative confocal data of the scar region in R26-eGFP<sup>fl/+</sup>;Postn<sup>MCM</sup> and Yap<sup>fl/fl</sup>;Wwtr1<sup>fl/+</sup>;R26-eGFP<sup>fl/+</sup>;Postn<sup>MCM</sup> mice at 7 dpi. Scale = 100 μm. (B) Immunostaining with α-GFP and α-Yap antibodies and DAPI. Yellow arrows denote Yap co-localization in GFP positive cells, red arrows denote absence of Yap colocalization in GFP positive cells, white arrows denote nuclear localized Yap in GFP negative cells. (D) Immunostaining with α-GFP and α-Wwtr1 antibodies and DAPI. Yellow arrows denote Wwtr1 co-localization in GFP positive cells, red arrows denote absence of Wwtr1 colocalization in GFP positive cells, white arrows denote nuclear localized Wwtr1 in GFP negative cells. (C,E) Quantification of Yap and Wwtr1 signal from histological staining in adult mice following MI. *n* = 13 randomly selected GFP + cells. Unpaired student's *t*-test with Welch's correction. \*\**P* < 0.01. \*\*\*\**P* < 0.0001.

*libitum* in chow. We found no difference between genotypes in cardiac function at baseline (3 days before MI) or at 3 dpi indicating similar degree of injury in both groups

(Supplementary Figure S2A). At 28 dpi Yap<sup>fl/fl</sup>;Postn<sup>MCM</sup> animals had significantly smaller left ventricular internal diameters during diastole (LVID-d) compared to Yap<sup>fl/fl</sup>

<sup>fl</sup>(Supplementary Figures S2A,B). LVID-s by comparison was not significantly different ( $P=0.27$ ). While the  $Yap^{fl/fl};Postn^{MCM}$  genotype conferred modest protection against left ventricular dilation, %EF and %FS were not significantly different between  $Yap^{fl/fl};Postn^{MCM}$  and  $Yap^{fl/fl}$  animals (Supplementary Figure S2A) nor were heart weights or body weights (Supplementary Figures S2C,D). At the histological level we found no significant difference in CM cross sectional area between experimental and control animals, suggesting reduced ventricular dilation does not correlate with attenuated CM hypertrophy in our model (Supplementary Figures S2E,F). Together, these data illustrate that Yap depletion from myofibroblasts imparts a slight protection against adverse ventricular dilation after MI, but functional contractility parameters such as %EF and %FS remain comparable to control animals.

Considering  $Yap^{fl/fl};Postn^{MCM}$  animals showed a slight improvement in ventricular dilation following injury, we sought to investigate if cell proliferation or scarring differences could be observed. To assess cell cycle activity, following MI we administered a single dose of EdU at 6 dpi, a time when *Postn* expression and myofibroblast proliferation is high in the heart (1, 2). We found a 70% decrease in EdU+ nuclei in the scar region of  $Yap^{fl/fl};Postn^{MCM}$  mice compared controls (Supplementary Figures S2G,H). Based on the known role of Yap in promoting cell proliferation, we postulated that the significant reduction of scar associated cell EdU incorporation is the result of decreased myofibroblast proliferation. However, despite the reduction in purported myofibroblast proliferation, we did not observe any change in scar size after injury as assessed by both midline scar percentage and the percentage of collagen content within the left ventricle of Gömöri trichrome stained serial sections (Supplementary Figures S2I,J).

## Depletion of both Yap and Wwtr1 in myofibroblasts improves cardiac function following MI

Yap and Wwtr1 share overlapping roles in various cell types. In some cases, depletion of Yap can be compensated by increased Wwtr1 activity and vice versa (26). In vitro knockdown of either Yap or Wwtr1 in neonatal rat cardiac fibroblasts demonstrated a significant decrease in DNA synthesis compared to negative siRNA or non-treated cells while an additive effect was observed with knockdown of both genes suggesting redundant role for Yap and Wwtr1 in fibroblasts (Supplementary Figure S3). We hypothesized that depletion of both Yap and Wwtr1 in myofibroblasts would improve cardiac outcomes post MI compared to Yap depletion alone. To test this hypothesis, we used a genetic mouse model where both copies of *Yap* and a single copy of *Wwtr1* are floxed, as both *Postn*<sup>MCM</sup> and *Wwtr1* are located chromosome 3 in mice at approximately 3 million base pairs apart. This genetic linkage made generating a homozygous floxed *Wwtr1* line with the Cre driver locus impractical, either alone or in combination with *Yap*.

We subjected  $Yap^{fl/fl};Wwtr1^{fl/+};Postn^{MCM}$  or  $Yap^{fl/fl};Wwtr1^{fl/+}$  littermate controls to MI and subsequently fed a continuous diet of tamoxifen citrate chow (Figure 2A). Similar to the loss of Yap alone, depletion of Yap and Wwtr1 did not affect heart weight or body weight at 60 dpi (Figures 2B,C). While we found no difference in cardiac function between genotypes at baseline or 3 dpi,  $Yap^{fl/fl};Wwtr1^{fl/+};Postn^{MCM}$  mice showed significantly improved cardiac function at 60 dpi compared to control (Figures 2D,E). While %FS and %EF declined to ~10% and ~17% respectively in  $Yap^{fl/fl};Wwtr1^{fl/+}$  animals, %EF and %FS in  $Yap^{fl/fl};Wwtr1^{fl/+};Postn^{MCM}$  were maintained at ~18% and ~35% respectively. Both LVID-s and LVID-d also trended downward in  $Yap^{fl/fl};Wwtr1^{fl/+};Postn^{MCM}$  mice at 60 dpi, but were not statistically different from control mice ( $P=0.17$  and  $0.22$  respectively, Supplementary Figure S4). In contrast, when allowed to progress to the 60 dpi timepoint,  $Yap^{fl/fl};Postn^{MCM}$  still showed no difference in %EF or %FS or fibrosis compared to  $Yap^{fl/fl}$  littermates and heart weight and body weight were not affected (Supplementary Figures S5–S7). We tested if the preservation in cardiac function in  $Yap^{fl/fl};Wwtr1^{fl/+};Postn^{MCM}$  as compared to  $Yap^{fl/fl};Wwtr1^{fl/+}$  controls was the result of Cre expression in within myofibroblasts alone by repeating the MI study on *Postn*<sup>MCM</sup> transgenic mice and wildtype littermate controls. We found no difference in %FS or %EF between these genotypes indicating that preserved cardiac function is due to depletion of Yap and Wwtr1, and not due to Cre expression in myofibroblasts (Figure 2E). Together, these data illustrate that depletion of both Yap and Wwtr1 attenuate adverse cardiac remodeling and improve cardiac function after ischemic injury.

Despite the improved cardiac function of  $Yap^{fl/fl};Wwtr1^{fl/+};Postn^{MCM}$  mice after surgical MI, no difference in cardiomyocyte cross sectional area was observed between genotypes (Figures 3A,B). We next tested whether depletion of both Yap and Wwtr1 from myofibroblasts resulted in modulation of cell proliferation, scar formation, or fibrosis in our model. To quantify proliferation of cells within the scar region, adult mice subjected to MI were administered a single dose of EdU at 3 dpi. Consistent with results observed in  $Yap^{fl/fl};Postn^{MCM}$  mice,  $Yap^{fl/fl};Wwtr1^{fl/+};Postn^{MCM}$  mice exhibited a 60% decrease in EdU+ scar associated cells compared to controls, whereas the percentage of EdU+ interstitial cells remained unchanged (Figures 3C,D and Supplementary Figure S8). However, unlike  $Yap^{fl/fl};Postn^{MCM}$  mice which showed no difference in scar size at 28 or 60 dpi (Supplementary Figures S2I,J, S5, S6),  $Yap^{fl/fl};Wwtr1^{fl/+};Postn^{MCM}$  mice displayed significantly reduced scar size as assessed by scar midline length (38% reduction) and fibrotic percentage of the left ventricle (38% reduction) (Figures 3E,F) and a 43% reduction in interstitial fibrosis compared to control (Figure 3G,H). We further characterized scar composition by quantifying denatured collagen, which is more easily turned over and can reduce deleterious fibrosis in the heart, using collagen hybridizing peptide Cy3 conjugate (CHP) (27). CHP binds to the unfolded triple-helix of collagen fibers, thus marking denatured collagen. CHP has been shown to correlate with other assays assessing degradation of collagen post MI such as matrix metalloproteinase activity *in vivo* and zymography (28, 29).

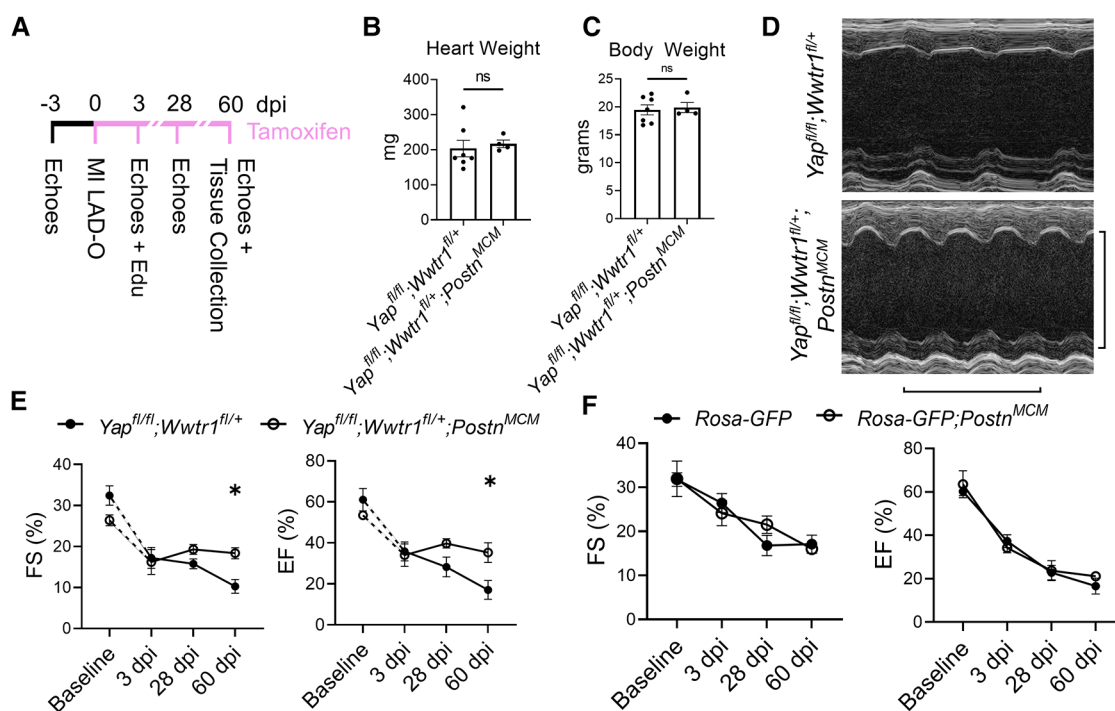


FIGURE 2

Depletion of Yap and a single copy of *Wwtr1* from myofibroblasts improves left ventricular function in response to ischemic injury. (A) Experimental timeline of echocardiography, MIs, tamoxifen chow administration, and EdU administration in adult *Yap<sup>fl/fl</sup>;Wwtr1<sup>fl/+</sup>* and *Yap<sup>fl/fl</sup>;Wwtr1<sup>fl/+</sup>;Postn<sup>MCM</sup>* mice. Quantification of (B) heart and (C) body weights at 60 dpi.  $n = 7$  *Yap<sup>fl/fl</sup>;Wwtr1<sup>fl/+</sup>* and 4 *Yap<sup>fl/fl</sup>;Wwtr1<sup>fl/+</sup>;Postn<sup>MCM</sup>*. Unpaired student's *t*-test. (D) Representative M-mode echocardiograms of left ventricles 60 dpi. Short axis view at mid papillary muscle. Horizontal bar = 500 ms. Vertical bar = 5 mm. (E,F) Quantification of %FS and %EF analyzed by repeated measures two-way ANOVA and Sidak multiple comparisons test.  $n = 7$  *Yap<sup>fl/fl</sup>;Wwtr1<sup>fl/+</sup>*, 4 *Yap<sup>fl/fl</sup>;Wwtr1<sup>fl/+</sup>;Postn<sup>MCM</sup>*, 5 *R26-eGFP<sup>fl/+</sup>*, 4 *R26-eGFP<sup>fl/+</sup>;Postn<sup>MCM</sup>*. A separate subset of animals establishing a baseline for *Yap<sup>fl/fl</sup>;Wwtr1<sup>fl/+</sup>* animals as denoted by the hashed lines and assessed by un-paired student's *t*-test.  $n = 4$  *Yap<sup>fl/fl</sup>;Wwtr1<sup>fl/+</sup>* and 5 *Yap<sup>fl/fl</sup>;Wwtr1<sup>fl/+</sup>;Postn<sup>MCM</sup>*. ns = not significant, \* $P < 0.05$ .

While scars from *Yap<sup>fl/fl</sup>;Postn<sup>MCM</sup>* mice showed no difference in CHP binding compared to controls (Figures 3I,J), *Yap<sup>fl/fl</sup>;Wwtr1<sup>fl/+</sup>;Postn<sup>MCM</sup>* mice displayed ~2.5 fold increase in the amount of denatured collagen in the scar region as compared to *Yap<sup>fl/fl</sup>;Wwtr1<sup>fl/+</sup>* littermates (Figures 3K,L). Thus, depletion of both Yap and Wwtr1 significantly modulated scar size and also collagen composition following MI.

Prior studies have demonstrated that genetic ablation of *Postn* expressing cells (i.e., myofibroblasts) results in a stark decreased survival post MI due to lack of scar deposition and subsequent rupture (1). Importantly, neither depletion of Yap and Wwtr1 nor expression of Cre itself significantly affect survival of infarcted mice (Figure 3M). Collectively, combined depletion of Yap and Wwtr1 in myofibroblasts attenuates fibrosis and improves functional outcomes following MI.

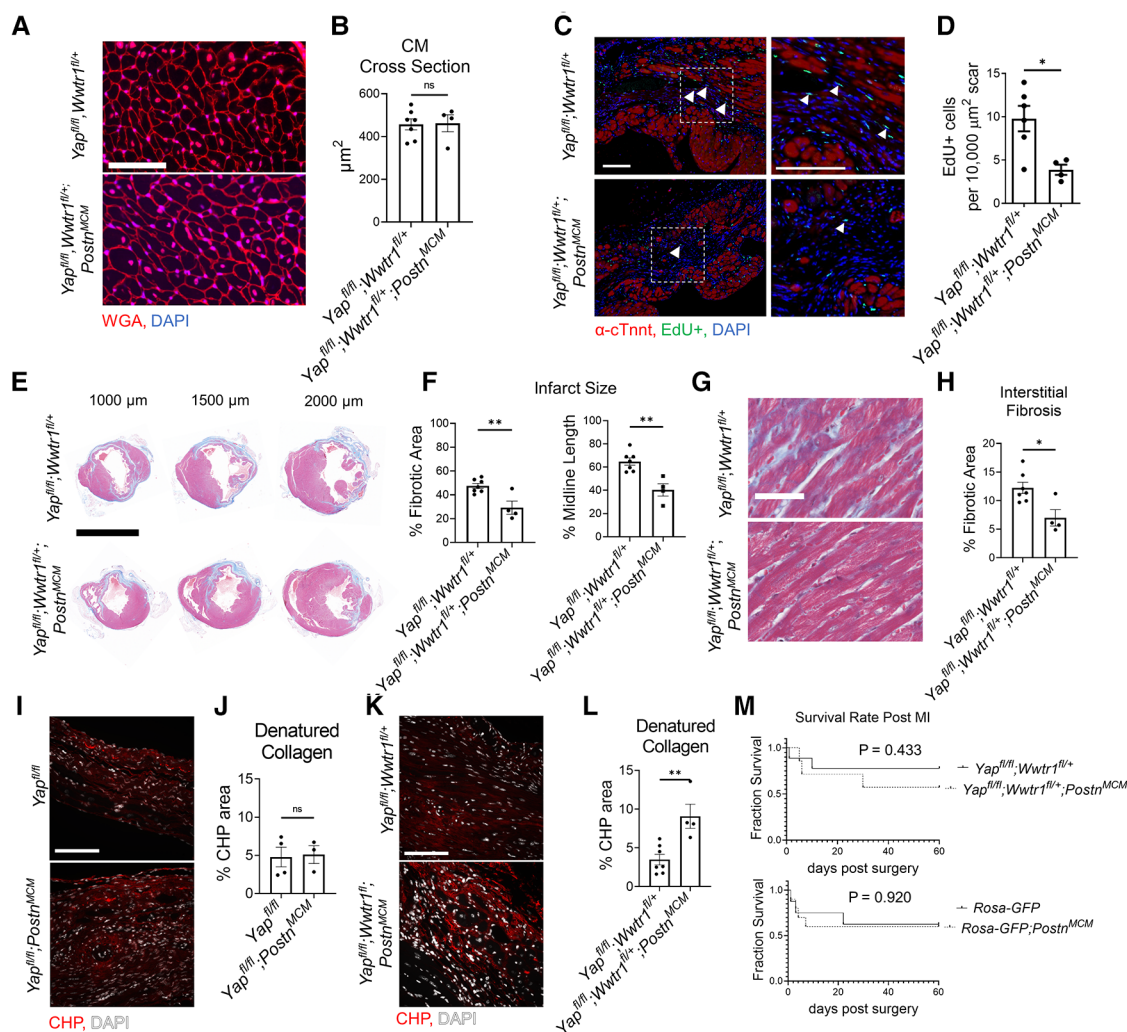
## Single cell analysis defines Yap and Wwtr1 downstream targets in cardiac myofibroblasts post MI

We next performed transcriptomic profiling on interstitial cells from *Postn<sup>MCM</sup>* and *Yap<sup>fl/fl</sup>;Wwtr1<sup>fl/+</sup>;Postn<sup>MCM</sup>* hearts post injury to identify transcriptional changes and differential infiltration of

cell types between genotypes. At 7 days post MI, hearts were extracted, digested into single cell suspension, and FACS sorted for live nucleated cells. We targeted cDNA and library construction of 3,000 cells per genotype on the 10x Chromium Controller for sequencing. We obtained a total of 6,063 high quality sequenced cells, 2,930 from *Postn<sup>MCM</sup>* and 3,133 from *Yap<sup>fl/fl</sup>;Wwtr1<sup>fl/+</sup>;Postn<sup>MCM</sup>* hearts, at an average sequencing depth of 47,945 reads per cell. Cluster analysis of interstitial cells revealed 18 main populations consisting of neutrophils (clusters 1, 18), B cells (cluster 2), macrophages/monocytes (clusters 0, 3, 11, 12, 13), T cells (clusters 4, 7, 8, 10), fibroblasts (cluster 5), natural killer cells (cluster 14), and dendritic cells (cluster 17) (Figures 4A,B and Supplementary Tables S4, S5). Two small clusters (15 and 16) could not be identified or expressed mixed cell type markers. While cells from each genotype were represented in most clusters, clusters 6, 9, and 10 were primarily derived from *Yap<sup>fl/fl</sup>;Wwtr1<sup>fl/+</sup>;Postn<sup>MCM</sup>* (Figures 4C). Cluster 6 and 10 were enriched for proliferation markers (*Top2a* and *Mki67*), suggesting a population of proliferative T cells infiltrate myocardial injury in response to Yap/Wwtr1 myofibroblasts depletion.

We were primarily interested in fibroblast gene expression profiles in *Yap<sup>fl/fl</sup>;Wwtr1<sup>fl/+</sup>;Postn<sup>MCM</sup>* hearts following MI compared to control, as this comparison could provide insights





**FIGURE 3** Depletion of myofibroblast Yap and Wwtr1 decreases fibrosis at 60 dpi. (A) Representative images of WGA staining in the remote zone of the left ventricle at 60 dpi. Scale = 50  $\mu\text{m}$ . (B) Quantification of cardiomyocyte cross sectional area.  $n = 7$   $Yap^{fl/fl}; Wwtr1^{fl/+}$  and 4  $Yap^{fl/fl}; Wwtr1^{fl/+}; Postn^{MCM}$ . Unpaired student's  $t$ -test. (C) Representative images denoting EdU+ nuclei within the scar area. White arrows indicate EdU+ scar associated nuclei. Scale = 100  $\mu\text{m}$ . (D) Quantification of EdU+ scar associated nuclei.  $n = 6$   $Yap^{fl/fl}; Wwtr1^{fl/+}$  and 4  $Yap^{fl/fl}; Wwtr1^{fl/+}; Postn^{MCM}$ . Unpaired student's  $t$ -test. (E) Representative serial sections of Gömöri trichrome stained hearts measured from the apex. Scale = 5 mm. (F) Quantification of infarct scar size by either total fibrotic area or midline size of the left ventricle.  $n = 7$   $Yap^{fl/fl}; Wwtr1^{fl/+}$  and 4  $Yap^{fl/fl}; Wwtr1^{fl/+}; Postn^{MCM}$ . Unpaired student's  $t$ -test. (G) Representative images depicting interstitial fibrosis within the remote zone of Gömöri trichrome stained hearts. Scale = 50  $\mu\text{m}$ . (H) Quantification of the % blue fibrotic area vs. total ventricular tissue.  $n = 7$   $Yap^{fl/fl}; Wwtr1^{fl/+}$  and 4  $Yap^{fl/fl}; Wwtr1^{fl/+}; Postn^{MCM}$ . Unpaired student's  $t$ -test. (I,K) Representative images of CHP staining within the scar region of 60 dpi mice. Scale = 100  $\mu\text{m}$ . (J,L) Quantification of CHP as a % area of the scar region.  $n = 4$   $Yap^{fl/fl}$ , 3  $Yap^{fl/fl}; Postn^{MCM}$ , 7  $Yap^{fl/fl}; Wwtr1^{fl/+}$ , and 4  $Yap^{fl/fl}; Wwtr1^{fl/+}; Postn^{MCM}$ . Unpaired student's  $t$ -test. (M) Survival curve comparing  $Yap^{fl/fl}; Wwtr1^{fl/+}$  and  $Yap^{fl/fl}; Wwtr1^{fl/+}; Postn^{MCM}$  or R26-eGFP $^{fl/+}$  and R26-eGFP $^{fl/+}; Postn^{MCM}$  mice after MI until the 60 dpi end point. Animals that died during surgery were not included.  $n = 9$   $Yap^{fl/fl}; Wwtr1^{fl/+}$ , 7  $Yap^{fl/fl}; Wwtr1^{fl/+}; Postn^{MCM}$ , 8 R26-eGFP $^{fl/+}$ , 10 R26-eGFP $^{fl/+}; Postn^{MCM}$ . Logrank Mantel-Cox test. Ns, not significant, \* $P < 0.05$ , and \*\* $P < 0.01$ .

into the mechanisms downstream of Yap and Wwtr1 that mediate adverse cardiac remodeling or fibrotic phenotypes. Notably, Yap and Wwtr1 expression was almost exclusively detected in fibroblasts (cluster 5) (Figure 4D). Differential expression analysis on fibroblasts (cluster 5) revealed 319 differentially expressed genes (DEGs) between  $Yap^{fl/fl}; Wwtr1^{fl/+}; Postn^{MCM}$  and  $Postn^{MCM}$  genotypes (Supplementary Table S6). Upstream regulator analysis of DEGs indicated fibroblasts from  $Yap^{fl/fl}; Wwtr1^{fl/+}; Postn^{MCM}$  mice upregulated pathways related to proinflammatory cytokines (IFN $\gamma$ , Stat1, Tnf) and downregulated pathways related to cell cycle activation (Myc (30) and Trim24

(31)) and pro-fibrotic cytokine activation such as IL4 (32) (Figure 4E). Furthermore,  $Yap^{fl/fl}; Wwtr1^{fl/+}; Postn^{MCM}$  fibroblasts showed significant negative activation scores for Yap, Wwtr1, and Tead1 as upstream regulators ( $-0.427$ ,  $P$ -value  $1.56\text{E}-16$ ;  $-1.026$ ,  $P$ -value  $7.05\text{E}-03$ ; and  $-1.739$ ,  $P$ -value  $2.44\text{E}-07$  respectively) compared to  $Postn^{MCM}$  fibroblasts, indicating downregulation of reported Yap/Wwtr1/Tead1 target genes in conditional knockout fibroblasts (Supplementary Figure S9). Amongst the most strongly upregulated genes in fibroblasts from  $Yap^{fl/fl}; Wwtr1^{fl/+}; Postn^{MCM}$  hearts included genes associated with collagen secretion and pro-tumorigenic fibroblast properties



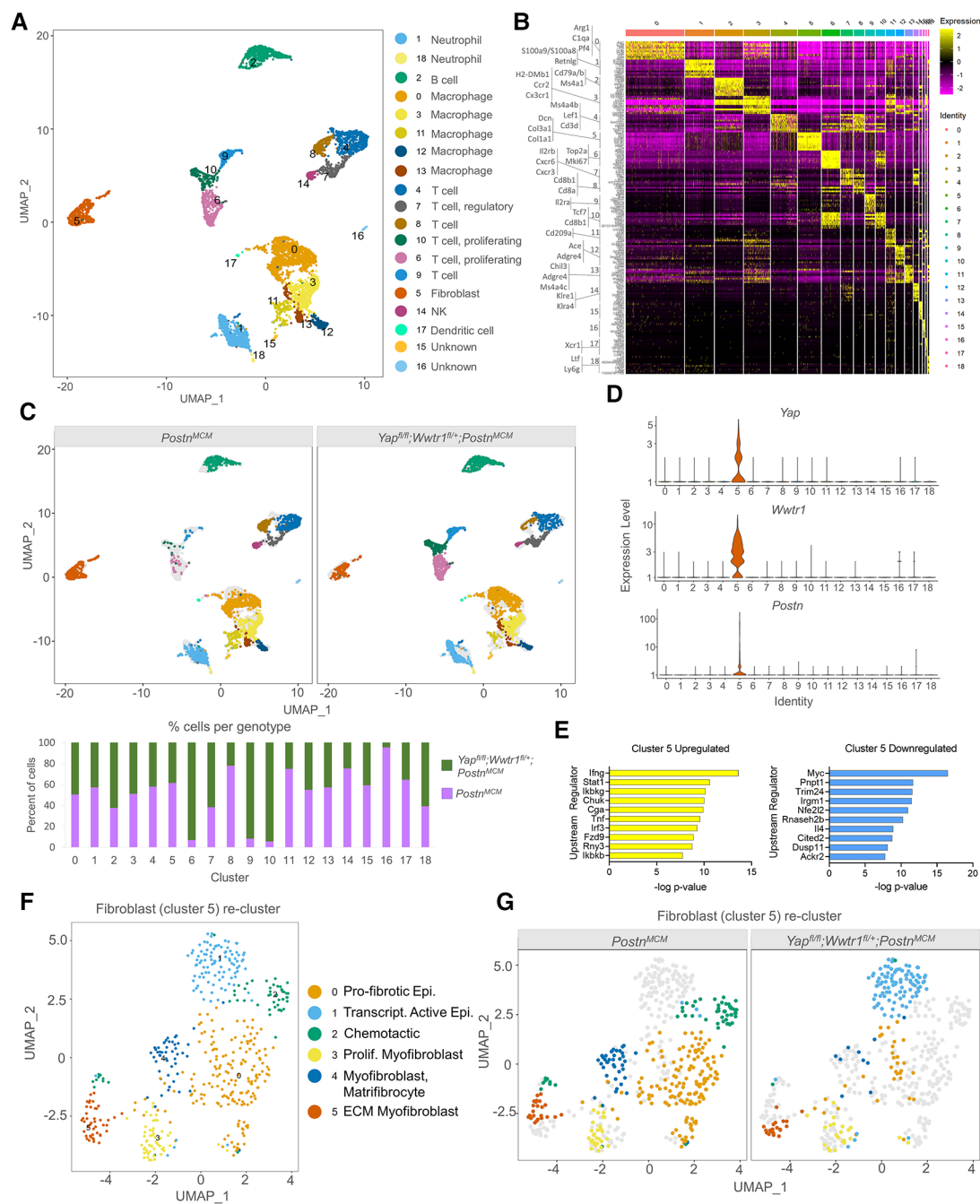


FIGURE 4

scRNAseq reveals Yap and Wwtr1 downstream targets in cardiac fibroblasts post MI. (A) UMAP projection and identification of combined interstitial cardiac cells, post filtering, from *Postn*<sup>MCM</sup> and *Yap*<sup>fl/fl</sup>; *Wwtr1*<sup>fl/+</sup>; *Postn*<sup>MCM</sup> adult mouse heart 7 dpi. Clusters are identified by enriched gene markers in **Supplementary Table S4**. (B) Heatmap of top 10 genes enriched within each cluster. (C) UMAP projection split by genotype and quantification of percent of cells from each genotype for each cell cluster. (D) Violin plots denoting UMI count for *Yap*, *Wwtr1*, or *Postn* for each cluster. (E) IPA analysis of predicted upstream regulators of upregulated or downregulated DEGs (*Yap*<sup>fl/fl</sup>; *Wwtr1*<sup>fl/+</sup>; *Postn*<sup>MCM</sup> vs. *Postn*<sup>MCM</sup>) in fibroblasts (cluster 5). (F) UMAP projection of re-clustering only fibroblasts (cluster 5) and identification of cardiac fibroblast subclusters. Epi., epicardial; Transcript., transcriptionally; Prolif., Proliferating; Myofib., myofibroblast; MFC, matrifibrocyte. (G) UMAP projection split by genotype.

[*Saa3*, *Mpp6*, *Pdgfra* (33, 34)]. Amongst the most downregulated genes included proto-onco genes (*Laptn4b* (35), *Clec3b* (36)) and the myogenic marker, Desmin [*Des* (37)]. Of particular interest, the secreted matricellular protein *Ccn3* was amongst the most strongly suppressed in *Yap*<sup>fl/fl</sup>; *Wwtr1*<sup>fl/+</sup>; *Postn*<sup>MCM</sup>

fibroblasts (average Log<sub>2</sub> fold change = -1.69, adjusted *P*-value  $1.24 \times 10^{-14}$ ). While CCN family members, *Ccn1* [*Cyr61* (38)] and *Ccn2*, [*Ctgf* (39, 40)] are well known transcriptional targets of Yap and Wwtr1, *Ccn3* expression has not been previously linked to the Hippo-Yap pathway.

To improve resolution of fibroblast phenotypes, we re-clustered cells from fibroblast cluster 5 which resulted in 6 distinct clusters 0–5 (Figure 4F). Cells from both *Yap<sup>fl/fl</sup>;Wwtr1<sup>fl/+</sup>;Postn<sup>MCM</sup>* and *Postn<sup>MCM</sup>* genotypes populated clusters 3 and 5 while cluster 0, 2, and 4 were derived primarily from *Postn<sup>MCM</sup>* hearts and cluster 1 derived primarily from *Yap<sup>fl/fl</sup>;Wwtr1<sup>fl/+</sup>;Postn<sup>MCM</sup>* hearts (Figure 4G). Cluster 0 was highly enriched for anti-proliferative and pro-fibrotic IGF binding proteins [*Igfbp5*, *Igfbp6*, *Igfbp3* (41, 42)] as well the epicardial marker *Dmkn* (41, 43–45). Cluster 2 was enriched for genes encoding chemotactic genes (*Cxcl13*, *Cxcl1*, *Cxcl12*, *Apln*), and Cluster 4 was strongly enriched for matrifibrocyte markers (*Angptl7*, *Thbs1*, *Sfrp2*) described by Forte et al. as well as *Vegfc* (46). Thus, fibroblasts derived primarily from *Postn<sup>MCM</sup>* control hearts appear to be enriched for pro-fibrotic and pro-inflammatory genes and more closely resemble matrifibrocyte phenotype designed to support a rigid scar (2). Cluster 1 was enriched for epicardial markers [*Saa3*, *Mpp6* (46)] suggesting distinct activation of epicardial derived fibroblasts in *Yap<sup>fl/fl</sup>;Wwtr1<sup>fl/+</sup>;Postn<sup>MCM</sup>* hearts. Cluster 3 contained cells from both genotypes and was strongly enriched for genes described by Forte et al. as proliferating myofibroblasts [*Cenpa*, *Hmgb2*, *Cdc20*, *Birc5*, *Cks2*, *Stmn1*, *Top2a*, among others (46)]. Cluster 5 contained genes from both genotypes and was strongly enriched for genes encoding ECM components (*Mfap4*, *Col8a1*, *Col14a1*, *Col15a1*) and contractile proteins (*Postn*, *Acta2*, *Tagln*) suggesting a secretory myofibroblast phenotype (47). Collectively, differential gene expression and marker analysis of fibroblast sub-clusters indicates fibroblasts from *Yap<sup>fl/fl</sup>;Wwtr1<sup>fl/+</sup>;Postn<sup>MCM</sup>* hearts are less proliferative and secretory, and display distinct inflammatory chemokines compared to *Postn<sup>MCM</sup>* hearts.

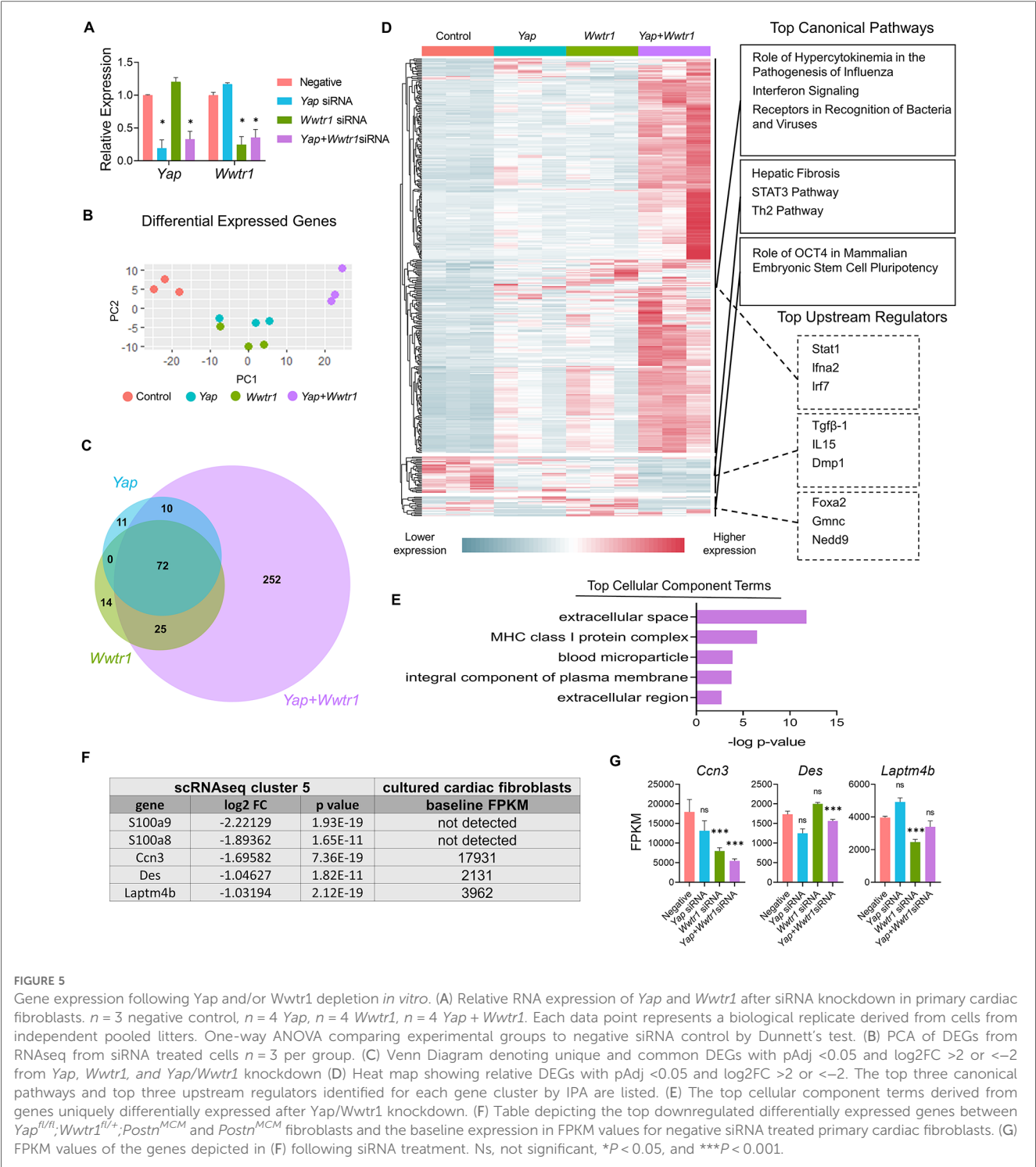
## Yap and Wwtr1 co-depletion synergistically modulates *Ccn3* gene expression in cardiac fibroblasts

We next sought to address if gene expression changes observed *in vivo* in *Yap<sup>fl/fl</sup>;Wwtr1<sup>fl/+</sup>;Postn<sup>MCM</sup>* cells were associated with depletion of either Yap or Wwtr1 individually or required depletion of both factors. We performed siRNA mediated knockdown of *Yap* and/or *Wwtr1* in cultured primary rat neonatal cardiac fibroblasts which resulted in greater than ~70% depletion of *Yap* and *Wwtr1* as verified by qRT-PCR (Figure 5A). Compared to the negative control and single knockdowns of either Yap or Wwtr1, we identified distinct genetic profiles for *Yap/Wwtr1* double knockdown cells as evident by a principal component analysis (PCA) of DEGs (Figure 5B). A relatively large set of significantly DEGs ( $P < .05$ ) with  $\text{Log}_2$  fold change ( $\text{Log}_2\text{FC}$ )  $>2$  or  $<-2$  were unique to *Yap/Wwtr1* double knockdown cells (252 genes) while *Yap* or *Wwtr1* single knockdowns shared the majority of their DEGs (Figure 5C), suggesting high functional redundancy of Yap and Wwtr1 in cardiac fibroblasts. A large gene cluster that was activated only when both Yap and Wwtr1 were knocked down contained genes primarily related to the immune response (Figure 5D). A gene cluster that was significantly downregulated

in the Yap/Wwtr1 knockdown group contained genes primarily regulated by Tgfb-1 and related to “hepatic fibrosis”, Stat3 pathway, and Th2 pathway— illustrating suppression of pro-fibrotic genes with depletion of Yap and Wwtr1. Gene ontology analysis of DEGs unique to Yap and Wwtr1 co-depletion were related to extracellular space (Figure 5E) indicating modulation of matrix or secreted proteins. We specifically measured expression of genes that were most strongly differentially expressed in the fibroblast cluster (cluster 5) from our *in vivo* scRNAseq experiment to determine if their expression was regulated by depletion of Yap, Wwtr1, or both Yap and Wwtr1. Out of the top five downregulated genes from the *in vivo* scRNAseq experiment, *Ccn3* was the most highly expressed in negative siRNA treated cultured cardiac fibroblasts (Figure 5F). Of these genes, only *Ccn3* was robustly suppressed with Yap + Wwtr1 siRNA mediated depletion (Figure 5G). While expression of most genes tested showed a synergistic (*Cfb*, *Mgp*, *Prss23*) or additive (*B2m*, *Irf7*, *Isg15*, *Tnfrsf11b*) response to Yap and Wwtr1 depletion, *Anxa2* appeared primarily regulated by Yap while *Ccn3* and *S100a10* more strongly regulated by Wwtr1 (Supplementary Figures S10A,B). From these data we observed a synergistic role between Yap and Wwtr1 regulating gene expression in cardiac fibroblasts, with *Ccn3* expression of particular interest given its prominence in the datasets and function as a matrix element.

## CCN3 administration contributes to adverse ventricular remodeling and fibrosis post MI in mice

*Ccn3* was the most strongly downregulated gene in *Yap<sup>fl/fl</sup>;Wwtr1<sup>fl/+</sup>;Postn<sup>MCM</sup>* fibroblasts at 7 dpi (Supplementary Table S6 and Figures S11A,B) that was also significantly and robustly decreased following *in vitro* knockdown of Yap + Wwtr1 in cardiac fibroblasts, but not Yap knockdown alone (Figure 5G). To confirm our results from scRNAseq and bulk RNAseq of cultured fibroblasts, we repeated the siRNA knockdown experiment in neonatal rat cardiac fibroblasts and measured *Ccn3* protein levels. In agreements with our RNAsequencing, knockdown of Yap alone showed no change in *Ccn3* protein levels, whereas Yap + Wwtr1 knockdown significantly decreased *Ccn3* protein expression (Figures 6A,B and Supplementary Figure S12). *Ccn3* is a member of the CCN (*Cyr61*, *Ctgf*, *Nov*) family of secreted extracellular proteins (48). While studies have linked *Ccn3* to integrin and Notch1 mediated signaling (49) and prevention of renal fibrosis (16), the role of *Ccn3* in the heart post injury is virtually unexplored. *Ccn3* protein is more abundant in infarcted hearts at 14 dpi compared to uninjured hearts and its expression is decreased in *Yap<sup>fl/fl</sup>;Wwtr1<sup>fl/+</sup>;Postn<sup>MCM</sup>* compared to *Yap<sup>fl/fl</sup>;Wwtr1<sup>fl/+</sup>* mice (Figure 6C and Supplementary Figure S13). These data mirror observations in human patients suffering from dilated cardiomyopathies, who also show elevated cardiac CCN3 expression (50). Furthermore, *Ccn3* expression is strongly enriched in cardiac fibroblasts when compared to other



interstitial cells (Figures 6D and Supplementary Figure S14, Tables S5, S7) suggesting fibroblasts are the primary source of CCN3 in the heart. We hypothesized that *Ccn3* downregulation in *Yap<sup>fl/fl</sup>;Wwtr1<sup>fl/+</sup>;Postn<sup>MCM</sup>* fibroblasts contributes to improved cardiac functional outcomes post MI, and therefore CCN3 overactivation would promote adverse cardiac remodeling. To test this hypothesis, we performed MI on adult C57/B6 mice and subsequently administered mice with either recombinant CCN3 or vehicle (PBS) by intraperitoneal injection 3 times per week,

beginning at 1 dpi (Figure 7A). A prior study performed same protocol to investigate the role of CCN3 on fibrosis linked to diabetic nephropathy, demonstrating its efficacy in localizing to the heart following interperitoneally injection (16). Strikingly, we found at just 3 dpi that compared to vehicle, mice receiving CCN3 already started to show a decline in cardiac function, and by 14 and 28 dpi cardiac function was substantially and significantly worse (Figure 7B and Supplementary Figure S15). LVID-s increased significantly with administration of CCN3 over

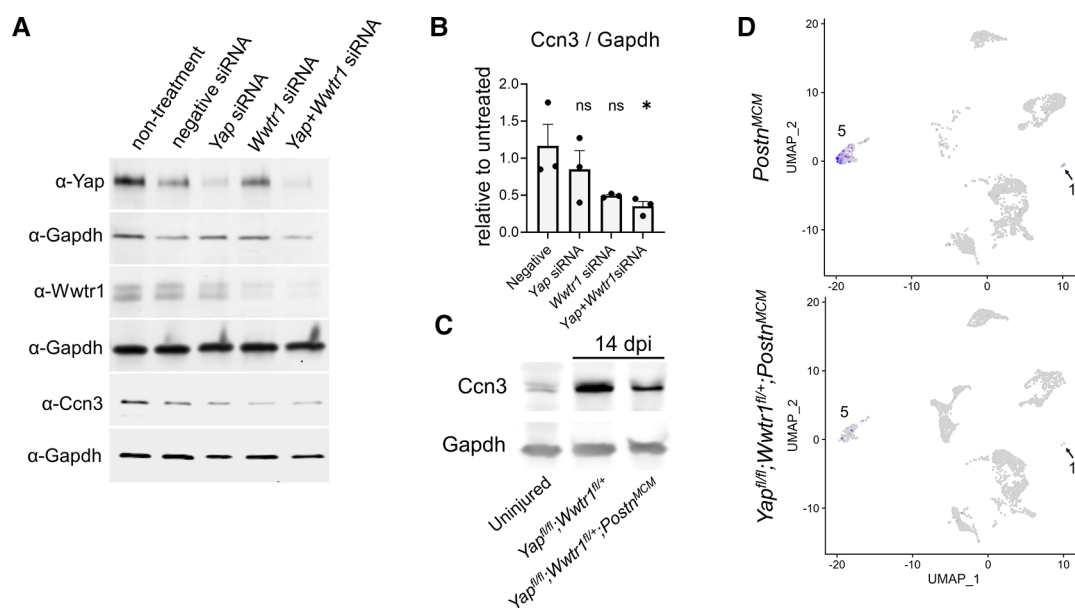


FIGURE 6

Ccn3 abundance decreases with depletion of Yap/Wwtr1. (A) Western blots depicting protein abundance of Yap, Wwtr1, or Ccn3 following siRNA treatment in cultured neonatal rat cardiac fibroblasts with Gapdh loading controls. (B) Quantification of Ccn3 protein from neonatal rat cardiac fibroblasts following siRNA, normalized to non-treated samples.  $n = 3$  biological replicates per group. Each replicate consisted of cells from independent litters. One-way ANOVA comparing experimental groups to negative siRNA control by Dunnett's test. (C) Western blot depicting Ccn3 abundance in left ventricles of uninjured and 14 dpi left ventricles. (D) Feature plot illustrating the abundance of Ccn3 expressing cells by UMI within clusters 5 and 16. Ns, not significant and  $*P < 0.05$ .

the 28-day experiment while LVID-d trended towards being larger ( $P = 0.08$  at 28 dpi, **Figure 7B**). Heart weight and body weight were not significantly different between groups (**Figure 7C**). Histological analysis at 28 dpi revealed significantly larger scars (**Figures 7D,E**) and increased proliferation of scar associated cells in response to CCN3 administration (**Figures 6F,G**) but no difference in cardiomyocyte cross sectional area (**Figures 6H,I**).

We next assessed whether CCN3 administration in mice following infarction resulted in transcriptional changes that promote adverse remodeling. We performed MI and administered CCN3 or PBS for 3 consecutive days starting at 1 dpi. Hearts were collected 4 h after the final injection and left ventricular tissue was processed for bulk RNAsequencing. RNAseq data was normalized to remove unwanted variation, resulting in distinct genetic profiles between CCN3 and PBS control treated animals (**Figure 8A**). We observed extracellular matrix associated genes were predominantly upregulated in ventricles of CCN3 treated mice while transcripts related to mitochondrial function were suppressed (**Figures 8B–D**). Thus, we illustrate CCN3 administration following injury drives fibrotic gene networks in myocardial tissue. Further assessment of DEGs by IPA was performed to identify which pathways were modulated. Tgfβ1, a well characterized promoter of fibrosis, was the most activated upstream regulator while Tead1, a transcription factor activated with Yap/Wwtr1 activity, was the most strongly inhibited (**Figure 8F**) (8, 51). Interestingly, while genes mediated by Tead1 activity were predominantly suppressed, indicating a potential repression of Yap/Wwtr1

activity, the expression of the matrix associated genes and CCN family members, *Ccn1* and *Ccn2*, were significantly increased (**Figure 8G**). Ccn1 is promoted by and subsequently drives Tgfβ1 activity, promoting fibrosis in the heart (52, 53) and our data suggests a novel role for exogenously administered CCN3 in contributing to Ccn1, Ccn2, and Tgfβ1 signaling in the heart and aggravating fibrotic remodeling post MI. We further assessed the cell type on which CCN3 is acting by treating neonatal rat ventricular cardiac fibroblasts or myocytes at two different dosages. At the higher dose, CCN3 drove expression of the pro-fibrotic genes *Fn1*, *Serpine1*, and *Ccn2* as well as *Yap* in cardiac fibroblasts (**Supplementary Figure S16**). CCN3 administration to cardiomyocytes however significantly promoted expression of the cell cycle gene *Aurkb*, the hypertrophic gene *Nppb*, as well as the Hippo-Yap elements *Ccn1*, *Ccn2*, and *Wwtr1* (**Supplementary Figure S17**). Together, our data implicates Ccn3 as an element promoting adverse remodeling.

## Discussion

A nuanced understanding of how myofibroblasts function during wound healing as they proliferate (2), migrate (54), secrete matrix and cytokines (55, 56), recruit immune cells (57), and facilitate a multitude of other roles is salient to understanding the complex nature of progressive heart failure. A therapeutic means to promote the beneficial nature of myofibroblasts (early matrix deposition after injury and recruitment of anti-inflammatory



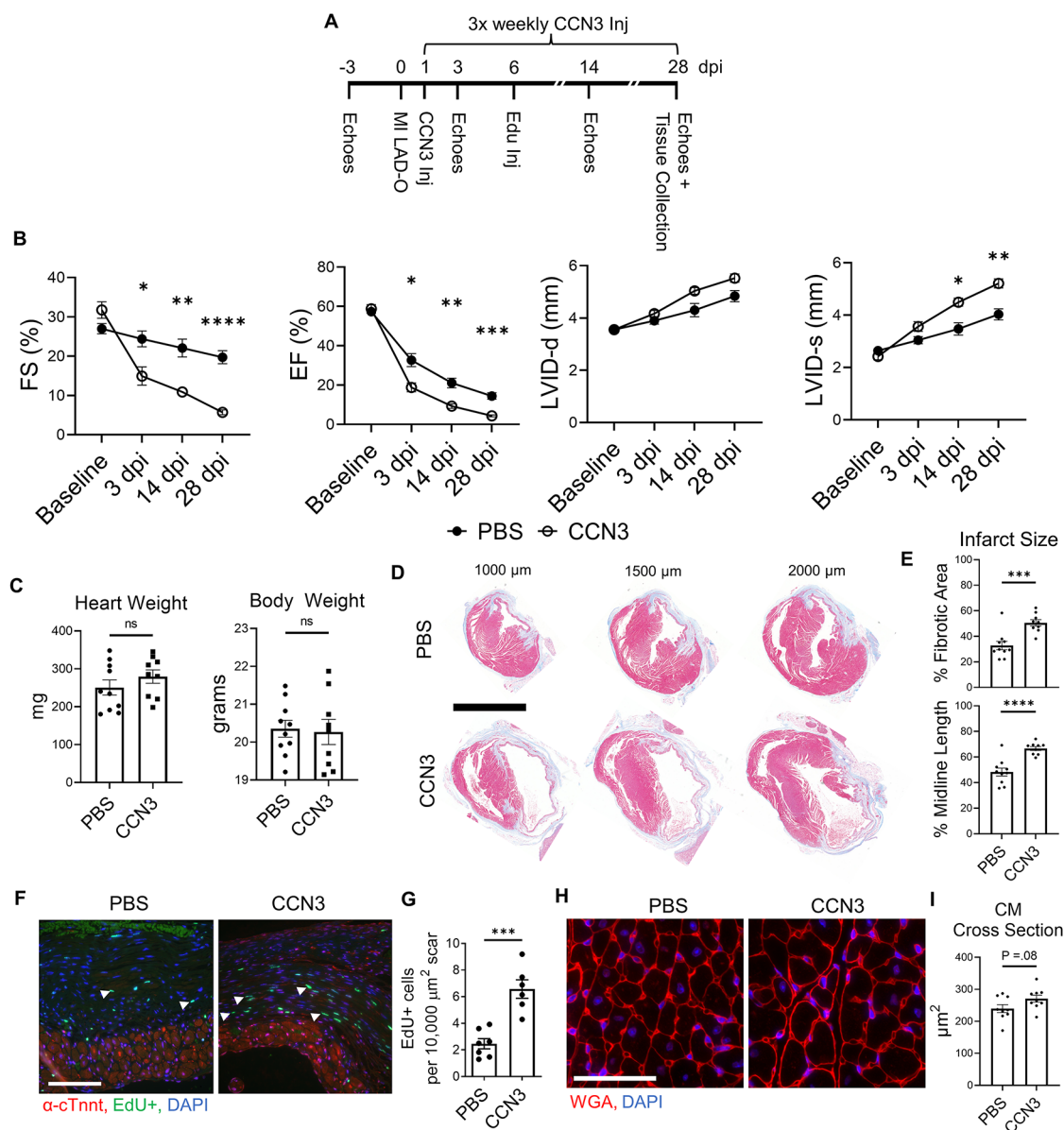
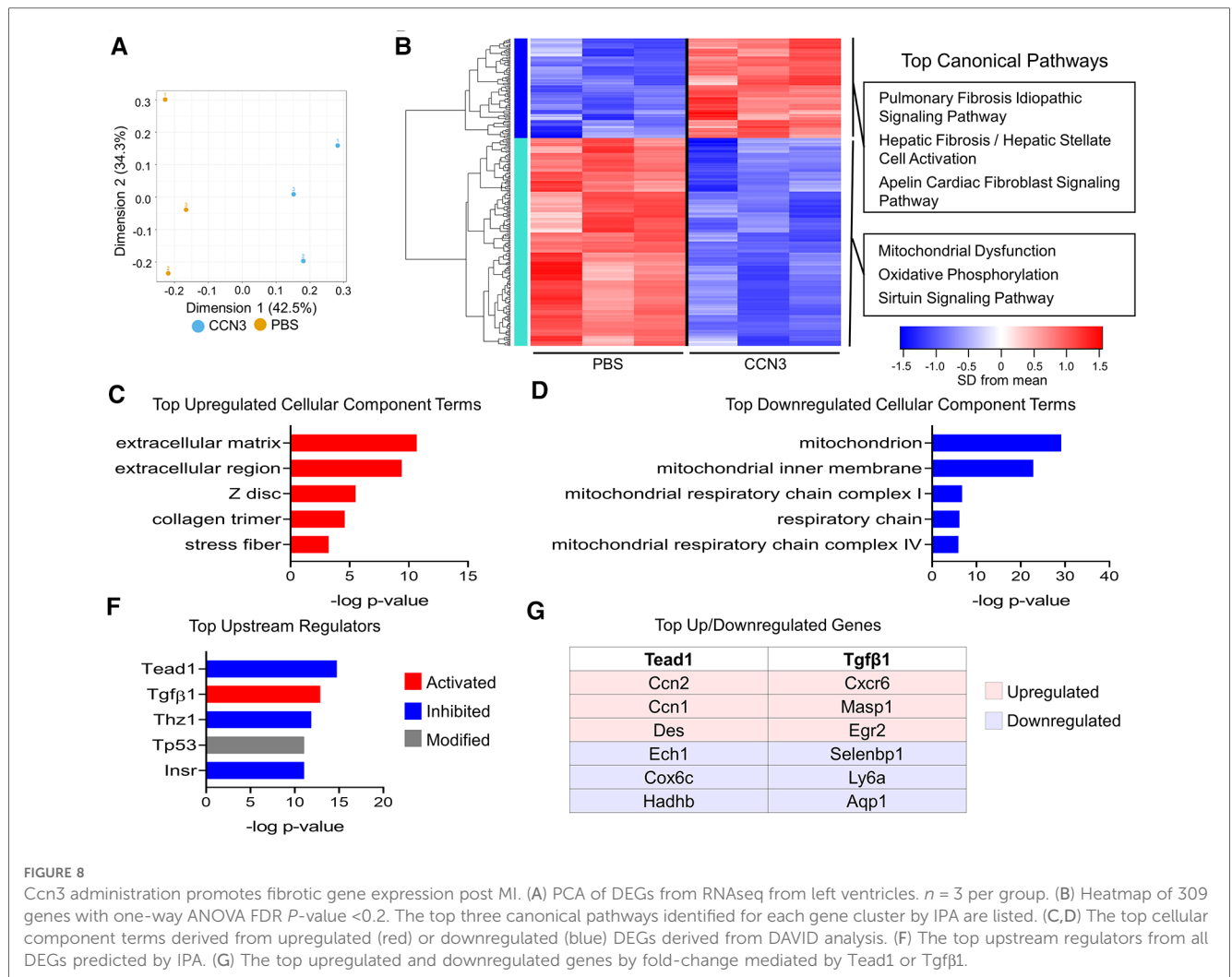


FIGURE 7

Ccn3 administration promotes fibrotic gene expression post MI. (A) Experimental timeline of echocardiography, MIs, CCN3 administration, and EdU administration in adult mice. (B) Quantification of left ventricular function by fractional shortening, ejection fraction, and left ventricular internal diameters during diastole and systole at baseline, 3, 14, and 28 dpi timepoints were analyzed by repeated measures two-way ANOVA and Sidak multiple comparisons test.  $n = 10$  PBS treated, 9 CCN3 treated. (C) Quantification of heart and body weights at 28 dpi.  $n = 10$  PBS treated, 9 CCN3 treated. Unpaired student's  $t$ -test. (D) Representative serial sections of Gömöri trichrome stained hearts measured as distance from the apex. Scale = 5 mm. (E) Quantification of infarct scar size by either total fibrotic area or midline size of the left ventricle.  $n = 10$  PBS treated, 9 CCN3 treated. Unpaired student's  $t$ -test. (F) Representative immunohistological images denoting EdU+ nuclei within the scar area. White arrows indicate EdU+ scar associated nuclei. Scale = 100 μm. (G) Quantification of EdU+ scar associated nuclei.  $n = 7$  PBS treated, 6 CCN3 treated. Scale bar = 100 μm. Unpaired student's  $t$ -test. (H) Representative images and (I) quantification of WGA staining in the remote zone of the left ventricle.  $n = 9$  PBS treated, 9 CCN3 treated. Scale = 100 μm. Unpaired student's  $t$ -test. ns, not significant, \* $P < 0.05$ , \*\* $P < 0.01$ , \*\*\* $P < 0.001$ , \*\*\*\* $P < 0.0001$ .

immune cells) while reducing deleterious aspects (latent fibrosis) would be beneficial to curbing heart failure. To this extent, our studies characterize a means by which myofibroblast proliferation and production of cell matrix genes is regulated by the Hippo-Yap pathway. However, how Hippo-Yap signaling in myofibroblasts affects cardiomyocyte function and whether it elicits an apoptotic response has yet to be determined.

Although the role of the Hippo-Yap pathway has been studied in progenitor epicardial cells and resident cardiac fibroblasts (9, 10, 12, 13), we take the novel approach of assessing the role of endogenous Yap and Wwtr1 expression specifically in myofibroblasts, the cell type responsible for the lion's share of matrix deposition following MI (1). While deletion of Yap alone did not result in observable changes in scar size or fibrosis, co-



disruption of Yap/Wwtr1 resulted in significantly improved cardiac function as well as reduced scar size, interstitial fibrosis, and increased denatured collagen. These results are similar to depletion of Yap and Wwtr1 in resident cardiac fibroblasts whereby Yap and Wwtr1 have been shown to regulate the transition of cardiac fibroblasts to a myofibroblast state (12). However, as therapeutic strategies would likely be implemented after an injury event, once myofibroblast are already activated, our study indicates that inhibiting Yap/Wwtr1 or downstream functional mediators after the transition has already occurred would be a reasonable approach.

We highlight the synergistic role of Yap and Wwtr1 in regulating gene expression in cardiac fibroblasts. Our *in vivo* data demonstrates a significant improvement in cardiac function in  $Yap^{fl/fl}; Wwtr1^{fl/+}; Postn^{MCM}$  whereas minimal improvement was observed in  $Yap^{fl/fl}; Postn^{MCM}$  animals. However, these studies did not include depletion of Wwtr1 alone. Thus,  $Yap^{fl/fl}; Wwtr1^{fl/+}; Postn^{MCM}$  phenotypes could be attributed to either Wwtr1 depletion alone or to Yap and Wwtr1 depletion, necessitating further studies to verify this. Our *in vitro* transcriptomic data elucidated strong synergy in gene regulation with depletion of both Yap and Wwtr1, and enabled us to identify genes

differentially expressed *in vivo* in  $Yap^{fl/fl}; Wwtr1^{fl/+}; Postn^{MCM}$  that were regulated by Wwtr1 or Yap + Wwtr1, but not by Yap alone. This cross-reference approach helped us prioritize candidate factors that might be mediating the effects of Yap/Wwtr1 in cardiac myofibroblasts.

Our *in vitro* and *in vivo* RNA sequencing experiments pointed to candidate genes whose function has been unexplored in the context of cardiac remodeling. Of these genes, *Ccn3* was of particular interest. CCN family members consist of secreted extracellular proteins which have been shown to interact with extracellular matrix components such as Fbln1 and receptors such as integrins and Notch (49). Other members of the CCN family include the well-studied and direct targets of Yap/Wwtr1 mediated transcription *Ccn1* and *Ccn2* (39, 40). Literature on the interaction between *Ccn3* and Hippo-Yap signaling is sparse, but data indicate *Ccn3* expression correlates with Yap/Wwtr1 activity. Administration of the Yap/Wwtr1/Tead inhibitor verteporfin decreases *CCN3* expression in cultured human dermal fibroblasts (58) while a decrease in the ratio of transcriptionally suppressed phosphorylated Yap to unphosphorylated Yap correlated with an increase in *Ccn3* during fragmentation of murine ovaries (59). Similar to our

findings in injured mice, endomyocardial biopsies from patients with dilated cardiomyopathy show significantly increased expression of CCN3 (50). In mice, Ccn3 knockout mutants display endocardial defects and delayed ventricular septum fusion during development, but are viable as adults (60). Adult knockout mice exhibit cardiomyopathy denoted by hypertrophy and calcification of the septal wall, but not overt ventricular fibrosis (60). To our knowledge, MI studies have not been performed in Ccn3 knockout mice. Overall, the consequence of Ccn3 expression on fibrosis across tissues is not well defined in the literature. While it has been documented in some models that Ccn3 reduces fibrosis *via* antagonism with Ccn2 and by extension Tgfb1 signaling (58, 61), this is not always the case (50, 62, 63). Indeed, we illustrate both Tgfb1 signaling and Ccn1 expression are both increased *in vivo* with administration of CCN3. Furthermore, proliferation of interstitial scar cells following cardiac injury was increased. These results mirror those from Lin et al. where CCN3 has been shown to promote DNA synthesis in cultured human skin fibroblasts in the presence of FGF2 (64). However, as systemic administration of CCN3 does affect the renal system and potentially other organ systems and various cell types, we cannot rule out off target effects such as hypertension that may indirectly impact reduced cardiac function we observed in our experiments. Future studies will be aimed at elucidating the how Yap/Wwtr1 modulates Ccn3 expression in cardiac fibroblasts and the collective mechanisms by which Ccn3 contributes adverse cardiac remodeling.

Together, our work illustrates the intrinsic function of Yap and Wwtr1 in myofibroblast activity which promotes fibrosis and deleterious remodeling of the left ventricle after injury. We demonstrate that Ccn3 expression is regulated by Yap and Wwtr1, and CCN3 administration substantially contributes to adverse cardiac function post MI. As such, the Hippo-Yap pathway, Ccn3, or other downstream elements expressed in cardiac myofibroblasts could be attractive targets for modulating adverse remodeling following MI.

## Data availability statement

Data from the bulk *in vitro* RNAseq, bulk left ventricular RNAseq, and scRNAseq have been uploaded to the Gene Expression Omnibus (<https://www.ncbi.nlm.nih.gov/geo/>) and can be accessed under GSE185368, GSE217925, and GSE204712 respectively.

The datasets presented in this study can be found in online repositories. The names of the repository/repositories and accession number(s) can be found in the article/**Supplementary Material**.

## Ethics statement

The animal study was reviewed and approved by The Institutional Animal Care and Use Committee of the Medical College of Wisconsin.

## Author contributions

Conceptualization: CCO, MAF, MP, and BAL; Methodology: MAF, SA-A, JD, and XZ; Investigation: MAF, SA-A, JD, MCK, VAA, SJP, XZ, TB, AJ, and RT; Formal analysis: MAF, SA-A, JD, MCK, VAA, SJP, XZ, TB, AJ and RT; Writing - original draft: MAF, CCO, SA-A, and JD; Writing - review & editing: MAF, SA-A, MCK, VAA, SJP, XZ, TB, AJ, PL, JD, MP, BAL, and CCO; Supervision: CCO, MP, BAL, and PL; Project administration: CCO; Funding acquisition: CCO, BAL, MAF, MP, and SJP. All authors contributed to the article and approved the submitted version.

## Acknowledgments

We thank the Roy J. Carver Biotechnology Center at the University of Illinois, Urbana Champaign for sequencing and bioinformatic support.

## Funding

This work was supported by Advancing a Healthier Wisconsin Co-Investigator Grant (BAL and CCO); by the National Institutes of Health (R01 HL141159 to CCO, R01 HL155085 to MP, T32 HL134643 and F32 HL150958 to MAF, and F31 HL150919 to SJP); by the Cardiovascular Center's A.O. Smith Fellowship Scholars Program (MAF); by the American Heart Association (18CDA34110240 to MP), and by the Medical College of Wisconsin Cardiovascular Center (FP00012308).

## Conflict of interest

The authors declare that the research was conducted in the absence of any commercial or financial relationships that could be construed as a potential conflict of interest.

## Publisher's note

All claims expressed in this article are solely those of the authors and do not necessarily represent those of their affiliated organizations, or those of the publisher, the editors and the reviewers. Any product that may be evaluated in this article, or claim that may be made by its manufacturer, is not guaranteed or endorsed by the publisher.

## Supplementary material

The Supplementary Material for this article can be found online at: <https://www.frontiersin.org/articles/10.3389/fcvm.2023.1142612/full#supplementary-material>.

## References

- Kanisicak O, Khalil H, Ivey MJ, Karch J, Maliken BD, Correll RN, et al. Genetic lineage tracing defines myofibroblast origin and function in the injured heart. *Nat Commun.* (2016) 7:12260. doi: 10.1038/ncomms12260
- Fu X, Khalil H, Kanisicak O, Boyer JG, Vagnozzi RJ, Maliken BD, et al. Specialized fibroblast differentiated states underlie scar formation in the infarcted mouse heart. *J Clin Invest.* 128(5):2127–43. doi: 10.1172/JCI98215
- Schmitt-Gräff A, Desmoulière A, Gabbiani G. Heterogeneity of myofibroblast phenotypic features: an example of fibroblastic cell plasticity. *Virchows Arch.* (1994) 425(1):3–24. doi: 10.1007/BF00193944
- Weber KT, Sun Y, Bhattacharya SK, Ahokas RA, Gerling IC. Myofibroblast-mediated mechanisms of pathological remodeling of the heart. *Nat Rev Cardiol.* (2013) 10(1):15–26. doi: 10.1038/nrcardio.2012.158
- Ma Y, Iyer RP, Jung M, Czubyrt MP, Lindsey ML. Cardiac fibroblast activation post-myocardial infarction: current knowledge gaps. *Trends Pharmacol Sci.* (2017) 38(5):448–58. doi: 10.1016/j.tips.2017.03.001
- Lai SL, Marin-Juez R, Stainier DYR. Immune responses in cardiac repair and regeneration: a comparative point of view. *Cell Mol Life Sci.* (2019) 76(7):1365–80. doi: 10.1007/s00018-018-2995-5
- Van De Water L, Varney S, Tomasek JJ. Mechanoregulation of the myofibroblast in wound contraction, scarring, and fibrosis: opportunities for new therapeutic intervention. *Adv Wound Care (New Rochelle).* (2013) 2(4):122–41. doi: 10.1089/wound.2012.0393
- Flinn MA, Link BA, O'Meara CC. Upstream regulation of the Hippo-Yap pathway in cardiomyocyte regeneration. *Semin Cell Dev Biol.* (2020) 100:11–9. doi: 10.1016/j.semcdb.2019.09.004
- Xiao Y, Hill MC, Zhang M, Martin TJ, Morikawa Y, Wang S, et al. Hippo signaling plays an essential role in cell state transitions during cardiac fibroblast development. *Dev Cell.* (2018) 45(2):153–69.e6. doi: 10.1016/j.devcel.2018.03.019
- Xiao Y, Hill MC, Li L, Deshmukh V, Martin TJ, Wang J, et al. Hippo pathway deletion in adult resting cardiac fibroblasts initiates a cell state transition with spontaneous and self-sustaining fibrosis. *Genes Dev.* (2019) 33(21–22):1491–505. doi: 10.1101/gad.329763.119
- Garoffolo G, Casaburo M, Amadeo F, Salvi M, Bernava G, Piacentini L, et al. Reduction of cardiac fibrosis by interference with YAP-dependent transactivation. *Circ Res.* (2022) 131(3):239–57. doi: 10.1161/CIRCRESAHA.121.319373
- Mia MM, Cibi DM, Ghani SABA, Singh A, Tee N, Sivakumar V, et al. Loss of Yap/Taz in cardiac fibroblasts attenuates adverse remodeling and improves cardiac function. *Cardiovasc Res.* (2022): 118(7):1785–804. doi: 10.1093/cvr/cvab205
- Francisco J, Zhang Y, Jeong JJ, Mizushima W, Ikeda S, Ivessa A, et al. Blockade of fibroblast YAP attenuates cardiac fibrosis and dysfunction through MRTF-A inhibition. *JACC Basic Transl Sci.* (2020) 5(9):931–45. doi: 10.1016/j.jacbs.2020.07.009
- Gao E, Koch WJ. A novel and efficient model of coronary artery ligation in the mouse. *Methods Mol Biol.* (2013) 1037:299–311. doi: 10.1007/978-1-62703-505-7\_17
- Mahmoud AI, Porrello ER, Kimura W, Olson EN, Sadek HA. Surgical models for cardiac regeneration in neonatal mice. *Nat Protoc.* (2014) 9(2):305–11. doi: 10.1038/nprot.2014.021
- Riser BL, Najmabadi F, Garchow K, Barnes JL, Peterson DR, Sukowski EJ. Treatment with the matricellular protein CCN3 blocks and/or reverses fibrosis development in obesity with diabetic nephropathy. *Am J Pathol.* (2014) 184(11):2908–21. doi: 10.1016/j.ajpath.2014.07.009
- Nascimento DS, Valente M, Esteves T, de Fátima de Pina M, Guedes JG, Freire A, et al. MIQuant – semi-automation of infarct size assessment in models of cardiac ischemic injury. *PLoS ONE.* (2011) 6(9):e25045. doi: 10.1371/journal.pone.0025045
- Flinn MA, Jeffery BE, O'Meara CC, Link BA. Yap is required for scar formation but not myocyte proliferation during heart regeneration in zebrafish. *Cardiovasc Res.* (2019) 115(3):570–7. doi: 10.1093/cvr/cvy243
- Friedrich G, Soriano P. Promoter traps in embryonic stem cells: a genetic screen to identify and mutate developmental genes in mice. *Genes Dev.* (1991) 5(9):1513–23. doi: 10.1101/gad.5.9.1513
- Core Team R. R: A language and environment for statistical computing. Vienna, Austria: R Foundation for Statistical Computing (2021). Available from: <https://www.R-project.org/>
- Butler A, Hoffman P, Smibert P, Papalexi E, Satija R. Integrating single-cell transcriptomic data across different conditions, technologies, and species. *Nat Biotechnol.* (2018) 36(5):411–20. doi: 10.1038/nbt.4096
- Hafemeister C, Satija R. Normalization and variance stabilization of single-cell RNA-seq data using regularized negative binomial regression. *Genome Biol.* (2019) 20(1):296. doi: 10.1186/s13059-019-1874-1
- McInnes L, Healy J, Melville J. UMAP: Uniform Manifold Approximation and Projection for Dimension Reduction. arXiv:1802.03426 [cs, stat]. (2020). Available from: <http://arxiv.org/abs/1802.03426> (cited 2022 Mar 2).
- Risso D, Ngai J, Speed TP, Dudoit S. Normalization of RNA-seq data using factor analysis of control genes or samples. *Nat Biotechnol.* (2014) 32(9):896–902. doi: 10.1038/nbt.2931
- Huang DW, Sherman BT, Lempicki RA. Bioinformatics enrichment tools: paths toward the comprehensive functional analysis of large gene lists. *Nucleic Acids Res.* (2009) 37(1):1–13. doi: 10.1093/nar/gkn923
- Qin Z, Xia W, Fisher GJ, Voorhees JJ, Quan T. YAP/TAZ regulates TGF- $\beta$ /Smad3 signaling by induction of Smad7 via AP-1 in human skin dermal fibroblasts. *Cell Commun Signal.* (2018) 16(1):18. doi: 10.1186/s12964-018-0232-3
- Guzzoni V, de Cássia Marqueti R, Durigan JLQ, de Carvalho HF, Lino RLB, Mekaro MS, et al. Reduced collagen accumulation and augmented MMP-2 activity in left ventricle of old rats submitted to high-intensity resistance training. *J Appl Physiol.* (2017) 123(3):655–63. doi: 10.1152/japplphysiol.01090.2016
- Hwang J, Huang Y, Burwell TJ, Peterson NC, Connor J, Weiss SJ, et al. In situ imaging of tissue remodeling with collagen hybridizing peptides. *ACS Nano.* (2017) 11(10):9825–35. doi: 10.1021/acsnano.7b03150
- Chen J, Tung CH, Allport JR, Chen S, Weissleder R, Huang PL. Near-infrared fluorescent imaging of matrix metalloproteinase activity after myocardial infarction. *Circulation.* (2005) 111(14):1800–5. doi: 10.1161/01.CIR.0000160936.91849.9F
- Amati B, Alevizopoulos K, Vlach J. Myc and the cell cycle. *Front Biosci.* (1998) 3:d250–68. doi: 10.2741/A239
- Wang H, Xue W, Jiang X. Overexpression of TRIM24 stimulates proliferation and glucose metabolism of head and neck squamous cell carcinoma. *Biomed Res Int.* (2018) 2018:6142843. doi: 10.1155/2018/6142843
- Gieseck RL, Wilson MS, Wynn TA. Type 2 immunity in tissue repair and fibrosis. *Nat Rev Immunol.* (2018) 18(1):62–76. doi: 10.1038/nri.2017.90
- Mitchell TI, Coon CI, Brinckerhoff CE. Serum amyloid A (SAA3) produced by rabbit synovial fibroblasts treated with phorbol esters or interleukin 1 induces synthesis of collagenase and is neutralized with specific antiserum. *J Clin Invest.* (1991) 87(4):1177–85. doi: 10.1172/JCI115116
- Djurec M, Graña O, Lee A, Troulé K, Espinet E, Cabras L, et al. Saa3 is a key mediator of the protumorigenic properties of cancer-associated fibroblasts in pancreatic tumors. *Proc Natl Acad Sci USA.* (2018) 115(6):E1147–56. doi: 10.1073/pnas.1717802115
- Meng Y, Wang L, Chen D, Chang Y, Zhang M, Xu JJ, et al. LAPTM4B: an oncogene in various solid tumors and its functions. *Oncogene.* (2016) 35(50):6359–65. doi: 10.1038/onc.2016.189
- Liu J, Liu Z, Liu Q, Li L, Fan X, Wen T, et al. CLEC3B is downregulated and inhibits proliferation in clear cell renal cell carcinoma. *Oncol Rep.* (2018) 40(4):2023–35. doi: 10.3892/or.2018.6590
- Goldring K, Jones GE, Sewry CA, Watt DJ. The muscle-specific marker desmin is expressed in a proportion of human dermal fibroblasts after their exposure to galectin-1. *Neuromuscul Disord.* (2002) 12(2):183–6. doi: 10.1016/S0960-8966(01)00280-2
- Park MH, Kim AK, Manandhar S, Oh SY, Jang GH, Kang L, et al. CCN1 Interlinks integrin and hippo pathway to autoregulate tip cell activity. *Elife.* (2019) 8:e46012. doi: 10.7554/eLife.46012
- Lai D, Ho KC, Hao Y, Yang X. Taxol resistance in breast cancer cells is mediated by the hippo pathway component TAZ and its downstream transcriptional targets Cyr61 and CTGF. *Cancer Res.* (2011) 71(7):2728–38. doi: 10.1158/0008-5472.CAN-10-2711
- Kuo CY, Chang YC, Chien MN, Jhuang JY, Hsu YC, Huang SY, et al. SREBP1 Promotes invasive phenotypes by upregulating CYR61/CTGF via the Hippo-YAP pathway. *Endocr Relat Cancer.* (2021) 29(2):47–58. doi: 10.1530/ERC-21-0256
- Nguyen XX, Muhammad L, Nietert PJ, Feghali-Bostwick C. IGFBP-5 Promotes fibrosis via increasing its own expression and that of other pro-fibrotic mediators. *Front Endocrinol (Lausanne).* (2018) 9:601. doi: 10.3389/fendo.2018.00601
- Longhitano L, Tibullo D, Vicario N, Giallongo C, La Spina E, Romano A, et al. IGFBP-6/sonic hedgehog/TLR4 signalling axis drives bone marrow fibrotic transformation in primary myelofibrosis. *Aging (Albany NY).* (2021) 13(23):25055–71. doi: 10.18632/aging.203779
- Sureshbabu A, Okajima H, Yamanaka D, Shastri S, Tonner E, Rae C, et al. IGFBP-5 induces epithelial and fibroblast responses consistent with the fibrotic response. *Biochem Soc Trans.* (2009) 37(Pt 4):882–5. doi: 10.1042/BST0370882
- Yasuoka H, Jukic DM, Zhou Z, Choi AMK, Feghali-Bostwick CA. Insulin-like growth factor binding protein 5 induces skin fibrosis: a novel murine model for dermal fibrosis. *Arthritis Rheum.* (2006) 54(9):3001–10. doi: 10.1002/art.22084
- Yasuoka H, Zhou Z, Pilewski JM, Oury TD, Choi AMK, Feghali-Bostwick CA. Insulin-like growth factor-binding protein-5 induces pulmonary fibrosis and triggers mononuclear cellular infiltration. *Am J Pathol.* (2006) 169(5):1633–42. doi: 10.2353/ajpath.2006.060501



46. Forte E, Skelly DA, Chen M, Daigle S, Morelli KA, Hon O, et al. Dynamic interstitial cell response during myocardial infarction predicts resilience to rupture in genetically diverse mice. *Cell Rep.* (2020) 30(9):3149–63.e6. doi: 10.1016/j.celrep.2020.02.008
47. Hesse J, Owenier C, Lautwein T, Zalfen R, Weber JF, Ding Z, et al. Single-cell transcriptomics defines heterogeneity of epicardial cells and fibroblasts within the infarcted murine heart. *Elife.* (2021) 10:e65921. doi: 10.7554/eLife.65921
48. Bork P. The modular architecture of a new family of growth regulators related to connective tissue growth factor. *FEBS Lett.* (1993) 327(2):125–30. doi: 10.1016/0014-5793(93)80155-N
49. Lombet A, Planque N, Bleau AM, Li C, Perbal B. CCN3 And calcium signaling. *Cell Commun Signal.* (2003) 1(1):1. doi: 10.1186/1478-811X-1-1
50. Tank J, Lindner D, Wang X, Stroux A, Gilke L, Gast M, et al. Single-target RNA interference for the blockade of multiple interacting proinflammatory and profibrotic pathways in cardiac fibroblasts. *J Mol Cell Cardiol.* (2014) 66:141–56. doi: 10.1016/j.yjmcc.2013.11.004
51. Frangogiannis NG. Transforming growth factor- $\beta$  in tissue fibrosis. *J Exp Med.* (2020) 217(3):e20190103. doi: 10.1084/jem.20190103
52. Dean RG, Balding LC, Candido R, Burns WC, Cao Z, Twigg SM, et al. Connective tissue growth factor and cardiac fibrosis after myocardial infarction. *J Histochem Cytochem.* (2005) 53(10):1245–56. doi: 10.1369/jhc.4A6560.2005
53. Daniels A, Van Bilsen M, Goldschmeding R, Van Der Vusse GJ, Van Nieuwenhoven FA. Connective tissue growth factor and cardiac fibrosis. *Acta Physiol.* (2009) 195(3):321–38. doi: 10.1111/j.1748-1716.2008.01936.x
54. Zuo C, Li X, Huang J, Chen D, Ji K, Yang Y, et al. Osteoglycin attenuates cardiac fibrosis by suppressing cardiac myofibroblast proliferation and migration through antagonizing lysophosphatidic acid 3/matrix metalloproteinase 2/epidermal growth factor receptor signalling. *Cardiovasc Res.* (2018) 114(5):703–12. doi: 10.1093/cvr/cvy035
55. Svystonyuk DA, Ngu JMC, Mewhort HEM, Lipon BD, Teng G, Guzzardi DG, et al. Fibroblast growth factor-2 regulates human cardiac myofibroblast-mediated extracellular matrix remodeling. *J Transl Med.* (2015) 13:147. doi: 10.1186/s12967-015-0510-4
56. Landry N, Kavosh MS, Filomeno KL, Rattan SG, Czubyrt MP, Dixon IMC. Ski drives an acute increase in MMP-9 gene expression and release in primary cardiac myofibroblasts. *Physiol Rep.* (2018) 6(22):e13897. doi: 10.14814/phy2.13897
57. Pappritz K, Savvatis K, Koschel A, Miteva K, Tschöpe C, Van Linthout S. Cardiac (myo)fibroblasts modulate the migration of monocyte subsets. *Sci Rep.* (2018) 8(1):5575. doi: 10.1038/s41598-018-23881-7
58. Peidl A, Perbal B, Leask A. Yin/Yang expression of CCN family members: transforming growth factor beta 1, via ALK5/FAK/MEK, induces CCN1 and CCN2, yet suppresses CCN3, expression in human dermal fibroblasts. *PLoS One.* (2019) 14(6):e0218178. doi: 10.1371/journal.pone.0218178
59. Kawamura K, Cheng Y, Suzuki N, Deguchi M, Sato Y, Takae S, et al. Hippo signaling disruption and Akt stimulation of ovarian follicles for infertility treatment. *Proc Natl Acad Sci USA.* (2013) 110(43):17474–9. doi: 10.1073/pnas.1312830110
60. Heath E, Tahri D, Andermarcher E, Schofield P, Fleming S, Boulter CA. Abnormal skeletal and cardiac development, cardiomyopathy, muscle atrophy and cataracts in mice with a targeted disruption of the Nov (Ccn3) gene. *BMC Dev Biol.* (2008) 8:18. doi: 10.1186/1471-213X-8-18
61. Riser BL, Najmabadi F, Perbal B, Rambow JA, Riser ML, Sukowski E, et al. CCN3/CCN2 Regulation and the fibrosis of diabetic renal disease. *J Cell Commun Signal.* (2010) 4(1):39–50. doi: 10.1007/s12079-010-0085-z
62. Zhang C, van der Voort D, Shi H, Zhang R, Qing Y, Hiraoka S, et al. Matricellular protein CCN3 mitigates abdominal aortic aneurysm. *J Clin Invest.* (2016) 126(4):1282–99. doi: 10.1172/JCI82337
63. Borkham-Kamphorst E, van Roeyen CR, Van de Leur E, Floege J, Weiskirchen R. CCN3/NOV Small interfering RNA enhances fibrogenic gene expression in primary hepatic stellate cells and cirrhotic fat storing cell line CFSC. *J Cell Commun Signal.* (2012) 6(1):11–25. doi: 10.1007/s12079-011-0141-3
64. Lin CG, Chen CC, Leu SJ, Grzeszkiewicz TM, Lau LF. Integrin-dependent functions of the angiogenic inducer NOV (CCN3): IMPLICATION IN WOUND HEALING\*. *J Biol Chem.* (2005) 280(9):8229–37. doi: 10.1074/jbc.M404903200



## OPEN ACCESS

## EDITED BY

Amy Li,  
La Trobe University, Australia

## REVIEWED BY

Cristobal Dos Remedios,  
Victor Chang Cardiac Research Institute,  
Australia  
Timothy Spracklen,  
University of Cape Town, South Africa

## \*CORRESPONDENCE

Ivana Purnama Dewi  
✉ dr\_ivanapd@staff.ukdw.ac.id;  
✉ 916ivana@gmail.com

## SPECIALTY SECTION

This article was submitted to Cardiovascular  
Genetics and Systems Medicine, a section of  
the journal Frontiers in Cardiovascular Medicine

RECEIVED 14 November 2022

ACCEPTED 14 March 2023

PUBLISHED 05 April 2023

## CITATION

Dewi IP, Wardhani LFK, Maghfirah I, Dewi KP,  
Subagjo A, Alsagaff MY and Nugroho J (2023)  
Association polymorphism of guanine  
nucleotide-binding protein  $\beta 3$  subunit (*GNB3*)  
C825T and insertion/deletion of the  
angiotensin-converting enzyme (*ACE*) gene  
with peripartum cardiomyopathy.  
Front. Cardiovasc. Med. 10:1096514.  
doi: 10.3389/fcvm.2023.1096514

## COPYRIGHT

© 2023 Dewi, Wardhani, Maghfirah, Dewi,  
Subagjo, Alsagaff and Nugroho. This is an open-  
access article distributed under the terms of the  
Creative Commons Attribution License (CC BY).  
The use, distribution or reproduction in other  
forums is permitted, provided the original  
author(s) and the copyright owner(s) are  
credited and that the original publication in this  
journal is cited, in accordance with accepted  
academic practice. No use, distribution or  
reproduction is permitted which does not  
comply with these terms.

# Association polymorphism of guanine nucleotide-binding protein $\beta 3$ subunit (*GNB3*) C825T and insertion/deletion of the angiotensin-converting enzyme (*ACE*) gene with peripartum cardiomyopathy

Ivana Purnama Dewi<sup>1,2\*</sup>, Louisa Fadjri Kusuma Wardhani<sup>1</sup>,  
Irma Maghfirah<sup>1</sup>, Kristin Purnama Dewi<sup>2,3</sup>, Agus Subagjo<sup>1</sup>,  
Mochamad Yusuf Alsagaff<sup>1</sup> and Johaness Nugroho<sup>1</sup>

<sup>1</sup>Department of Cardiology and Vascular Medicine, Faculty of Medicine, Airlangga University—Dr. Soetomo General Hospital, Surabaya, Indonesia, <sup>2</sup>Faculty of Medicine, Duta Wacana Christian University, Yogyakarta, Indonesia, <sup>3</sup>Department of Pulmonology and Respiratory Medicine, Faculty of Medicine, Airlangga University—Dr. Soetomo General Hospital, Surabaya, Indonesia

**Introduction:** Peripartum cardiomyopathy (PPCM) is a potentially life-threatening pregnancy-related heart disease. Genetic roles such as gene polymorphisms may relate to the etiology of PPCM. This study analyzes the association between single nucleotide gene polymorphism (SNP) guanine nucleotide-binding protein beta-3 subunit (*GNB3*) C825T and insertion/deletion (I/D) of the angiotensin-converting enzyme (*ACE*) gene with the incidence of PPCM.

**Methods:** An analytic observational study with a case-control design was conducted at the Integrated Cardiac Service Center of Dr. Soetomo General Hospital, Surabaya, Indonesia. PPCM patients of the case and control groups were enrolled. Baseline characteristic data were collected and blood samples were analyzed for SNP in the *GNB3* C825T gene and for I/D in the *ACE* gene by using the polymerase chain reaction, restriction fragment length polymorphism, and Sanger sequencing. We also assessed *ACE* levels among different *ACE* genotypes using a sandwich-ELISA test.

**Results:** A total of 100 patients were included in this study, with 34 PPCM cases and 66 controls. There were significant differences in *GNB3* TT and TC genotypes in the case group compared with that in the control group (TT: 35.3% vs. 10.6%,  $p = 0.003$ ; TC: 41.2% vs. 62.5%,  $p = 0.022$ ). The TT genotype increased the risk of PPCM by 4.6-fold. There was also a significant difference in the *ACE* DD genotype in the case group compared with that in the control group (26.5% vs. 9.1%,  $p = 0.021$ ). DD genotypes increased the risk of PPCM by 3.6-fold. *ACE* levels were significantly higher in the DD genotype group than in the ID and II genotype groups ( $4,356.88 \pm 232.44$  pg/mL vs.  $3,980.91 \pm 77.79$  pg/mL vs.  $3,679.94 \pm 325.77$  pg/mL,  $p < 0.001$ ).

**Conclusion:** The TT genotype of *GNB3* and the DD genotype of the *ACE* are likely to increase the risk of PPCM. Therefore, these polymorphisms may be predisposing risk factors for PPCM incidence. *ACE* levels were significantly higher in the DD genotype group, which certainly had clinical implications for the management of PPCM patients in the administration of *ACE* inhibitors as one of the therapy options.

## KEYWORDS

single nucleotide polymorphism, peripartum cardiomyopathy, PPCM, guanine nucleotide-binding protein subunit  $\beta 3$ , angiotensin-converting enzyme

## 1. Introduction

Maternal mortality ratio (MMR) is an indicator that describes national maternal health and welfare. Global MMR reached 214 per 100,000 live births in 2016 (1). In developing countries, MMR is 20 times higher than in developed countries (1). In 2012, Indonesia's MMR was 359 per 100,000 live births (2). An evaluation of the 2015 Millennium Development Goals revealed that 38 mothers in Indonesia died from diseases or complications related to pregnancy and childbirth every day (MMR: 305 per 100,000 live births). The causes of maternal death are mainly bleeding, infection, and cardiovascular disease, including hypertension during pregnancy and heart failure (3).

Peripartum cardiomyopathy (PPCM) is a potentially life-threatening pregnancy-related disease (4). PPCM is characterized by left ventricle (LV) dysfunction in the late peripartum period or in the first months of postpartum without a known history of heart disease (5). To date, there are many hypotheses about the etiology of PPCM, but none is considered as the primary explanation for all cases. PPCM is known to have a pathogenesis that involves many factors such as maternal autoimmune response, inflammation, oxidative stress, imbalance of cardiac proapoptotic factors and anti-angiogenic factors, micronutrient deficiencies, and genetic causes (6). Due to the complexity of the etiology, genetic factor, especially gene polymorphism, may play an essential role (7). Two major PPCM registries, Investigation of Pregnancy Associated Cardiomyopathy (IPAC) (8) and EURObservational Research Programme (EORP) (9), reported various incidence rates of PPCM among countries in different regions, which may be related to genetic predisposition in different races.

The guanine nucleotide-binding protein subunit  $\beta 3$  (*GNB3*) gene encodes the  $\beta 3$  subunit of G protein ( $G\beta 3$ ) located on chromosome 12p13 that consists of 11 exons and 10 introns. The single nucleotide polymorphism (SNP) of *GNB3* at exon 10, C825T, is associated with an increased prevalence and poor outcome of PPCM in individuals of African progeny (10). T allele polymorphisms in the *GNB3* gene are associated with increased intracellular signaling, increased risk of hypertension, low plasma renin, and cardiac remodeling (10). To date, there are no studies on *GNB3* C825T gene polymorphism, especially in Asian populations.

The role of the insertion/deletion (I/D) 287-bp sequence inside intron 16 of the angiotensin-converting enzyme (*ACE*) gene and *ACE* activity in the etiology, pathogenesis, prognosis, and clinical implications of the cardiovascular system has been extensively studied. The deletion polymorphism of the *ACE* allele is associated with increased levels of *ACE* (11). In addition, the *ACE* DD genotype is positively correlated with specific cardiomyopathy such as ischemic cardiomyopathy (ICM), hypertrophic cardiomyopathy (HCM), alcoholic cardiomyopathy, and idiopathic dilated cardiomyopathy (IDCM) (12, 13). IDCM with low ejection fraction (EF) has a phenotype similar to PPCM, suggesting that there may be an association between the I/D of the *ACE* gene and PPCM. This study aims to determine the association between the SNP of the *GNB3* C825T gene and the I/D of the *ACE* gene in women with PPCM.

## 2. Methods

### 2.1. Study design

An analytic observational study with a case-control study was conducted at the Integrated Cardiac Service Center, at Dr. Soetomo General Hospital and Institute of Tropical Diseases (ITD) Laboratory of Airlangga University, Surabaya, Indonesia from January 2021 to June 2022. The case group consisted of all women diagnosed with PPCM, while the control group comprised women without PPCM or a history of PPCM. The study was approved by the Dr. Soetomo General Hospital Surabaya Ethics Committee (0151/KEPK/II/2021). All procedures were approved by the relevant ethics committees and written informed consent was obtained from all study participants.

### 2.2. Patients and controls

All women who were 18–40 years' old and who underwent examination and treatment at the Polyclinic Integrated Cardiac Service Center of Dr. Soetomo General Hospital Surabaya were included. PPCM was diagnosed according to the criteria of the European Society of Cardiology (ESC) Working Group on Peripartum Cardiology in 2010 (14). The criteria were: (1) Heart failure symptoms that appeared in the last 1 month of pregnancy to 5 months' postpartum; (2) No history and other identifiable causes of heart failure; and (3) An left ventricular ejection fraction (LVEF) <45% based on echocardiography. All PPCM patients with previous history of heart failure, a history of coronavirus disease 2019 (COVID-19) infection complicated with any heart problems, and incomplete data were excluded. Controls were women with a history of pregnancy who had never been diagnosed with PPCM.

### 2.3. Detection of *GNB3* C825T gene polymorphisms and *ACE* gene I/D

Patients selected on the basis of inclusion and exclusion criteria and signed a letter of informed consent to participate in the study. A 5 mL sample of cubital venous blood was collected in an ethylenediaminetetraacetic acid (EDTA) tube and rested for about 30 min. The tube was then centrifuged at 300 rpm for 10 min to separate the plasma. DNA extraction was carried out using the QiaAMP DNA Blood Mini Kit (Qiagen, Hilden, Germany) and stored at  $-20^{\circ}\text{C}$ . DNA content was quantified by spectrophotometric absorption (Nanodrop Spectrophotometer, BioLab, Scoresby, VIC, Australia). All DNA samples were blind-tested.

The *GNB3* C825T polymorphism was examined according to the procedure stipulated by Siffert et al. (15). We used 5' TGACCCACTTGCCACCCGTGC 3' as a sense primer and 5' GCAGCAGCCAGGGCTGGC 3' as an antisense primer. The polymerase chain reaction (PCR) was run using a Promega

master mix reagent kit following the manufacturer's instructions (Promega, Madison, WI, United States). Amplifications were carried out in the T100™ Thermal Cycler (Bio-Rad, Hercules, CA, United States) as follows: 35 cycles with denaturation at 94°C for 1 min; annealing at 58°C for 45 s; extension at 72°C for 1 min; and a final extension at 72°C for 7 min. Amplification products were digested by using the restriction endonuclease enzyme, BseDI/BsaJI (MBI Fermentas, St. Leon-Rot, Germany), at 37°C in a water bath for 3 h and 80°C for 5 min. DNA fragments were obtained after the restriction enzyme was electrophoresed on a 2.5% agarose gel and stained with ethidium bromide and the BenchTop 1,000 bp DNA Ladder (Promega, Madison, WI, United States). The DNA fragments were imaged under ultraviolet (UV). The T allele was not digested by using the restriction endonuclease enzyme. It corresponded to the cDNA fragments of 256 bp (TT genotype), whereas the C allele corresponded to 152 bp and 104 bp (CC genotype). Thus, the CT genotype produced three bands, 256 bp, 152 bp, and 104 bp (Figure 1A). Three representative samples of each genotype (TT, TC, and CC) were confirmed with DNA sequencing using the Sanger method. DNA sequencing for the *GNB3* C825T polymorphism was performed by using the ABI Prism 24-capillary 3,500xL Genetic Analyzer to confirm the PCR result. The sequence analysis of the DNA is shown in Figure 1B. The results were

compared with the reference strains of the sequences that were published in GenBank using the Clone Manager Professional version 9.0.

The I/D *ACE* polymorphism was examined as described by Rigat et al. (16). To amplify the *ACE*, a pair of primers 5' CTGGAGACCACTCCCATCCTTTCT 3' and an antisense primer 5' GATGTGGCCATCTTCGTCAGA 3' were used. The PCR amplification was processed as described for *GNB3*. The PCR product is a 490 bp fragment in the presence of the insertion (I) allele and a 190 bp fragment in the presence of the deletion (D) allele. Thus, each DNA sample revealed one of three possible patterns after electrophoresis: a 490 bp band (genotype II), a 190 bp band (genotype DD), or both 490 bp and 190 bp bands (genotype ID) (Figure 1C).

## 2.4. ACE ELISA test

Plasma from the PPCM group sample was separated after centrifugation and stored at −20°C until analysis. To determine the level of the *ACE* between different alleles and the genotype of *ACE* I/D, a sandwich-ELISA test was conducted using a Human Angiotensin-Converting Enzyme 1 ELISA (Elabscience, Hubei, China). The resulting optical density was read by using the BioRad ELISA Reader at 450 nm.

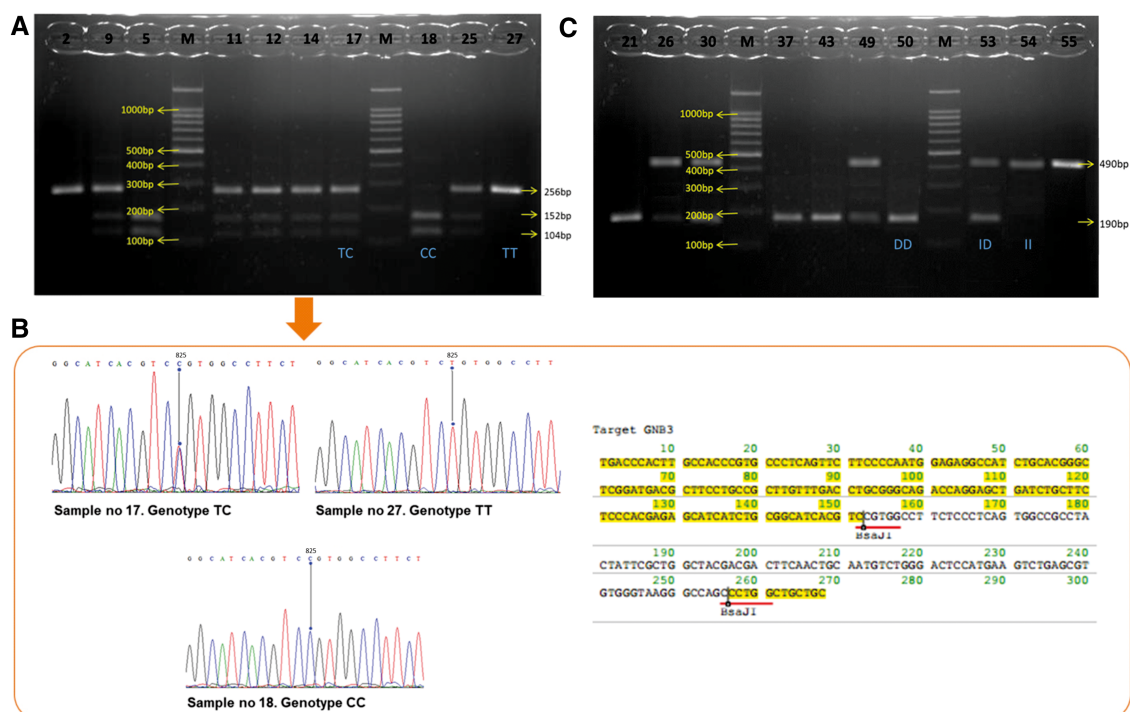


FIGURE 1

(A) Visualization of *GNB3* PCR products. The results from 10 samples show TT genotypes: sample nos. 2 and 27; CC genotypes: sample nos. 5 and 18; TC genotypes: sample nos. 9, 11, 12, 14, 17, and 25. (B) DNA sequencing chromatogram and amino acid sequence restriction of *GNB3*. The lines point to nucleotide 825. Chromatogram of *GNB3* shows TC genotypes at the upper left, TT genotypes at the upper right, and CC genotypes at the middle bottom. (C) Visualization of *ACE* gen PCR products. The results from 10 samples show DD genotypes: sample nos. 21, 37, 43, and 50; II genotypes: sample nos. 54 and 55; TC genotypes: sample nos. 26, 30, 49, and 53. *GNB3*, guanine nucleotide-binding protein beta-3 subunit; PCR, polymerase chain reaction; *ACE*, angiotensin-converting enzyme.



## 2.5. Statistical analysis

The data obtained were processed using SPSS (IBM Statistics 20.0) for Windows. The Hardy–Weinberg Equilibrium (HWE) was used to estimate the number of heterozygous and homozygous variant carriers in non-evolving populations on the basis of allele frequency. The  $\chi^2$  test for the degree of freedom (dF) = 1 and a  $p$ -value = 0.05 were used to determine whether the observed genotypic distribution for *GNB3* and *ACE* agreed with the HWE. The genotypes and alleles of *GNB3* and *ACE* between the PPCM and the control groups were assessed using the  $\chi^2$  test or Fisher's exact test according to the obtained data. Odds ratios (ORs) with a 95% confidence interval (95% CI) were determined to find the association of gene polymorphism intensity with disease. The normality of data was assessed using the Kolmogorov–Smirnov test. An independent Student's  $t$ -test or a Mann–Whitney test was used for numerical data analysis of the two groups. For numerical data with >2 groups, analysis was performed using one-way ANOVA or the Kruskal–Wallis test as appropriate. Univariate and multivariate logistic regression analyses were done to determine whether gene polymorphism was the independent predictor of PPCM. Differences with  $p$ -values <0.05 were considered statistically significant.

## 3. Results

### 3.1. Characteristics of patients

A total of 100 patients were included in the study, of which 34 were PPCM patients and 66 controls, and the characteristics of the case and control group patients are presented in **Table 1**. The mean BMI was higher in the PPCM group than in the control group (29.02 vs. 26.96,  $p = 0.037$ ). The number of patients who had preeclampsia or eclampsia was significantly higher in the PPCM group than in the control group (44.1% vs. 9.1%,  $p < 0.001$ ). The PPCM group had a higher mean systolic blood pressure than the

control group (143.26 mmHg vs. 131.09 mmHg,  $p = 0.007$ ). A total of 91.2% of patients with PPCM were diagnosed antepartum (**Table 1**). We did not find any deviations from the HWE in our population study.

### 3.2. *GNB3* and *ACE* gene polymorphisms and the risk of PPCM

Of the total number of samples, the genotypes of *GNB3* were mostly TC ( $n = 57$ , 57%), followed by CC ( $n = 24$ , 24%) and TT ( $n = 19$ , 19%). There were significant differences in the frequency of TT and TC genotypes of the *GNB3* gene between the PPCM and the control groups (**Table 2**). Individuals with the TT genotype had a higher odds ratio of approximately 4.59 to have PPCM compared with those with the TC and CC genotypes (OR: 4.59; 95% CI: 1.60–13.17,  $p = 0.003$ ) (**Table 2**). Although the frequency of T allele was higher in the PPCM group, the difference was not statistically significant compared with that in the control group (55.9% vs. 43.2%,  $p = 0.088$ ).

Our data indicated that 15 subjects had the DD genotype, 27 had the ID genotype, and 58 the II genotype of the *ACE*. The DD genotype was significantly higher in the PPCM group than in the control group (26.5% vs. 9.1%), and the presence of the DD genotype was associated with a higher risk of PPCM compared with individuals with the ID and II genotypes (OR: 3.60; 95% CI: 1.15–11.18,  $p = 0.021$ ) (**Table 2**). The frequency of D allele was higher in the PPCM group, but the difference was not statistically significant compared with that in the control group (36.8% vs. 24.2%,  $p = 0.063$ ) (**Table 2**). Univariate and multivariate logistic linear regression analyses were done on various variables, as presented in **Table 3**. The analysis from **Table 3** showed that *GNB3* TT and preeclampsia/eclampsia were independent predictors for PPCM.

### 3.3. Subanalysis of the *GNB3* and *ACE* genotypes in the PPCM group

In PPCM patients, the frequency of the *GNB3* genotype was significantly different and was based on BMI and left ventricular internal diameter in diastole (LVIDd) (**Table 4**). The BMI was higher in the TT genotype of *GNB3* than in the TC and CC genotypes (31.73 vs. 27.54 kg/m<sup>2</sup>,  $p = 0.018$ ). The mean of LVIDd was also higher in the TT genotype group than in the TC and CC groups (5.39 ± 0.80 vs. 4.86 cm ± 0.64 cm,  $p = 0.041$ ). Hypertension and a history of preeclampsia/eclampsia were more frequent among those with the *ACE* DD genotype than among those with the ID and II genotypes; 44.4% vs. 8.0%,  $p = 0.031$  and 77.8% vs. 32.0%,  $p = 0.025$ , respectively (**Table 4**).

### 3.4. Comparison of *ACE* levels based on *ACE* genotypes among PPCM patients

The *ACE* levels were measured among 30 of 34 PPCM patients because four subjects received *ACE* inhibitors that may cause bias.

TABLE 1 Baseline characteristics of PPCM and controls.

Characteristics	PPCM ( $n = 34$ ), $n$ (%)	Control ( $n = 66$ ), $n$ (%)	$p$ -value
Age, mean ± SD	29.09 ± 6.16	27.95 ± 5.72	0.362
BMI	29.02 ± 5.04	26.96 ± 4.09	0.037
Parity			0.155
Primiparous	15 (44.1)	39 (59.1)	
Multiparous	19 (55.9)	27 (40.9)	
Multifetal pregnancy	3 (8.8)	2 (3.0)	0.208
History of hypertension	6 (17.6)	4 (6.1)	0.085
Preeclampsia/eclampsia	15 (44.1)	6 (9.1)	<0.001
Systolic blood pressure, mean ± SD	142.03 ± 22.04	131.09 ± 18.69	0.007
Diastolic blood pressure, mean ± SD	84.97 ± 16.08	80.83 ± 11.65	0.144
Diagnosis time			NA
Antepartum	31 (91.2)	NA	
Postpartum	3 (8.8)	NA	

PPCM, peripartum cardiomyopathy; BMI, body mass index.

TABLE 2 Comparison of genotype and allele frequencies of the *GNB3* and *ACE* genes in PPCM and control groups.

Gene	Comparison	PPCM <i>n</i> (%)	Control <i>n</i> (%)	OR	95% CI	<i>p</i> -value
<i>GNB3</i>	Genotype					
	TT vs. TC + CC	12 (35.3)	7 (10.6)	4.59	1.60–13.18	0.003
	TC vs. TT + CC	14 (41.2)	43 (65.2)	0.37	0.16–0.88	0.022
	CC vs. TT + TC	8 (23.5)	16 (24.2)	0.96	0.36–2.54	0.937
	Allele T vs. C					
	T	38 (55.9)	57 (43.2)	1.66	0.92–3.01	0.088
	C	30 (44.1)	75 (56.8)			
<i>ACE</i>	Genotype					
	DD vs. ID + II	9 (26.5)	6 (9.1)	3.60	1.16–11.18	0.021
	ID vs. DD + ID	7 (20.6)	20 (30.3)	0.59	0.22–1.59	0.300
	II vs. DD + ID	18 (52.9)	40 (60.6)	0.73	0.32–1.69	0.462
	Allele D vs. I					
	D	25 (36.8)	32 (24.2)	1.82	0.96–3.42	0.063
	I	43 (63.2)	100 (75.8)			

*GNB3*, guanine nucleotide-binding protein beta-3 subunit; *ACE*, angiotensin-converting enzyme; PPCM, peripartum cardiomyopathy.

TABLE 3 Predictor of the PPCM determinate by univariate and multivariate logistic regression analyses.

Factor	Univariate			Multivariate		
	OR	95% CI	<i>p</i> -value	OR	95% CI	<i>p</i> -value
BMI	1.81	0.73–4.48	0.199			
Parity	1.83	0.79–4.22	0.155			
Multifetal pregnancy	3.10	0.49–19.50	0.208			
History of hypertension	3.32	0.87–12.70	0.085			
Preeclampsia/eclampsia	7.90	2.69–23.21	<0.001	7.55	2.49–22.88	<0.001
<i>GNB3</i> gene polymorphism	4.59	1.60–13.18	0.003	3.74	1.18–11.85	0.025
<i>ACE</i> gene polymorphism	3.60	1.16–11.18	0.021			

*GNB3*, guanine nucleotide-binding protein beta-3 subunit; BMI, body mass index; OR, odds ratio; CI, confidence interval; *ACE*, angiotensin-converting enzyme; PPCM, peripartum cardiomyopathy.

Our data revealed that the *ACE* levels in DD, ID, and II were 4,356.88, 3,980.91, and 3,679.94 pg/mL, respectively. The *ACE* levels were significantly higher in the DD genotype group than

in the ID and II genotype groups,  $p < 0.001$ . The *ACE* levels in individuals with the ID genotype were also higher than in individuals with the II genotype ( $p = 0.020$ ) (Figure 2).

## 4. Discussion

Despite the growing recognition of genetic predispositions as a risk factor for the development of PPCM, little is known about the impact of genomic background on racial differences. Our study was the first one to determine whether there was an association of the SNP *GNB3* C825T gene and the incidence of PPCM in an Asian population. Although the frequency of the TT genotype was relatively rare, this genotype increased the risk of PPCM 4.6 times compared with the other CC and TC genotypes. Multivariate analysis also showed that *GNB3* TT appeared to be an independent predictor for PPCM. A study conducted in North America with 97 subjects (30% were Blacks, 65% were Caucasian, and 5% were others), which assessed the relationship between different *GNB3* genotypic backgrounds and their impact on improvement in LV remodeling in PPCM, found that the *GNB3* TT genotype was more common in Blacks (10). *GNB3* TT

TABLE 4 Comparison of *GNB3* and *ACE* gene genotypes in the PPCM group.

Variable	<i>GNB3</i>			<i>ACE</i>		
	TT <i>n</i> (%)	TC + CC <i>n</i> (%)	<i>p</i> -value	DD <i>n</i> (%)	ID + II <i>n</i> (%)	<i>p</i> -value
Hypertension						
Yes	3 (25.0)	3 (13.6)	0.641	4 (44.4)	2 (8.0)	0.031
No	9 (75.0)	19 (86.4)		5 (55.6)	23 (92.0)	
Preeclampsia/eclampsia						
Yes	4 (30.8)	11 (52.4)	0.296	7 (77.8)	8 (32.0)	0.025
No	9 (69.2)	10 (47.6)		2 (22.2)	17 (68.0)	
BMI (kg/m <sup>2</sup> ), mean ± SD	31.73 ± 5.50	27.54 ± 4.20	0.018	29.88 ± 4.06	28.71 ± 5.40	0.559
Left ventricular ejection fraction (%), mean ± SD	36.92 ± 6.16	38.55 ± 5.50	0.437	36.78 ± 6.12	38.40 ± 5.61	0.506
Left ventricular internal diameter in diastole (cm), mean ± SD	5.39 ± 0.80	4.86 ± 0.64	0.041	5.12 ± 0.85	5.02 ± 0.71	0.726

*GNB3*, guanine nucleotide-binding protein beta-3 subunit; BMI, body mass index; *ACE*, angiotensin-converting enzyme; PPCM, peripartum cardiomyopathy.

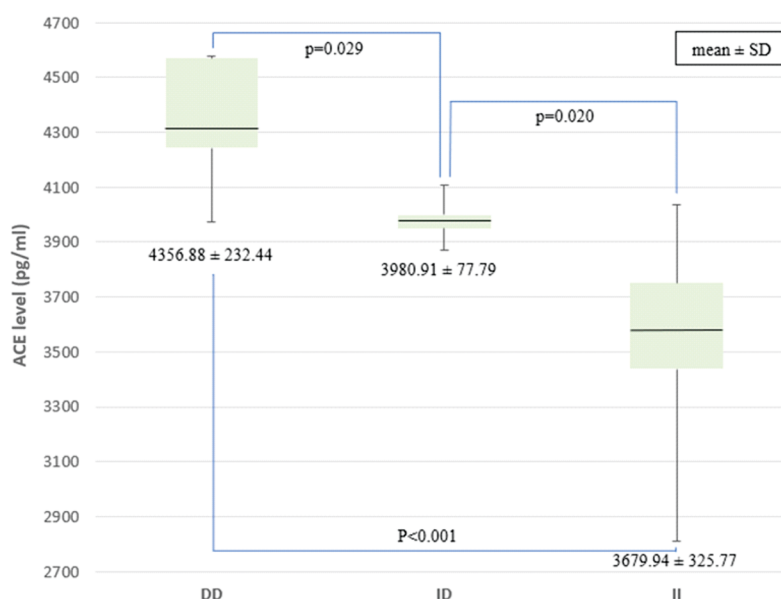


FIGURE 2

Comparison of ACE levels among the genotypes of the I/D ACE gene. ACE, angiotensin-converting enzyme; I/D, insertion/deletion.

was also associated with a much higher incidence of PPCM and lower LVEF recovery (10).

Interestingly, our study found that the TC genotype (57%) was the most frequent genotype and may appear to afford protection from PPCM. However, there is limited evidence of the association between *GNB3* TC polymorphism and PPCM incidence. The exact mechanism by which the *GNB3* polymorphism contributes to the development of PPCM has not been fully understood, but it is thought to involve alterations in the G protein-coupled receptor (GPCR) signaling pathway (17). The *GNB3* protein plays a key role in the signaling pathways through GPCR that control the contraction and relaxation of heart muscle cells (17, 18).

In addition, our study found that the most common genotypes of ACE were II (58%), followed by ID (27%) and DD (15%). The DD genotype increased the risk of PPCM 3.6 times compared with the other genotypes (II and ID). This result was similar to that of a study by Yaqoob et al., which found that the DD genotype was possibly a predisposing and independent risk factor for the pathophysiology of PPCM in the Kashmiri Indian population (13). The frequency of the DD genotype and D allele was also significantly higher in the PPCM population (13). The DD genotype was associated with poorer left ventricle systolic function in terms of ejection fraction, dimension, and left ventricle end-systolic and end-diastolic volumes (13).

Preeclampsia and eclampsia appear to be independent predictors for PPCM, as revealed by multivariate analysis. The pathophysiology of preeclampsia and eclampsia related to PPCM is still poorly understood, but several hypotheses suggest that hemodynamic stress caused by preeclampsia can contribute to the worsening of this condition (19). The EORP study states that the global preeclampsia incidence rate as a comorbid PPCM is 25%. A further investigation reveals that the rate of incidence in

the Asia Pacific population reaches 46% (9). A meta-analysis of 22 observational studies with a total of 979 samples also reveals that 22% of PPCM patients develop preeclampsia/eclampsia (20).

No previous studies have reported an association of the *GNB3* and ACE polymorphisms with hypertension and preeclampsia, specifically in the PPCM population. In our subanalysis, we found that the percentage of PPCM patients with hypertension (44.4% vs. 8%,  $p = 0.032$ ) and a history of preeclampsia (77.8% vs. 32%,  $p = 0.025$ ) was higher in the ACE DD genotype group than in the other genotype groups. A review study found that previous studies reported conflicting results, but the majority found that the DD genotype was associated with the incidence of hypertension and preeclampsia in pregnancy. A study of 121 pregnant women with a gestational age of 27–40 weeks reported a higher frequency of the DD genotype in the essential hypertension group than in the control group (21). A meta-analysis of 40 studies with a total of 3,977 cases and 7,065 controls concluded that the DD genotype increased the risk of preeclampsia compared with the DD and ID genotypes (52% vs. 17%), and D allele increased the risk of preeclampsia 1.29 times more than I allele (22).

Obesity is a risk factor for PPCM. Hemodynamic alterations, apoptosis, and inflammation are three potential causes of pathogenesis. Obesity causes excessive levels of circulating fat to alter blood volume, which increases stroke volume and stresses the LV wall, which, in turn, cause eccentric LV hypertrophy and, eventually, LV dysfunction (23). However, no previous studies have reported an association of the *GNB3* and ACE gene polymorphisms with obesity in the PPCM population. A study of Caucasian, Chinese, and Black populations reported that the TT genotype had a higher mean BMI than other genotypes (TC and CC) (24). In our study, similar results were obtained, where the

mean BMI in the TT genotype was significantly higher than that in the *GNB3* TC and CC genotypes.

Although the mean LVEF in the *GNB3* TT and *ACE* DD genotype groups has been reported to be lower in previous studies (10, 13), our data suggested no significant difference. Our results are in line with those of other studies, which showed no statistically significant difference in LVEF in the *ACE* DD genotype, although the mean LVEF was lower in the *ACE* DD genotype (13). However, the IPAC study reported that PPCM patients with the *GNB3* TT genotype showed a lower LVEF at the initial stage of the study (10). After follow-up, LVEF was found to be significantly lower for *GNB3* TT subjects at 6 months ( $p = 0.007$ ) and 12 months ( $p < 0.001$ ).

The geometry and thickness of the heart wall, especially the LV, are associated with cardiovascular risk. Our study found that *GNB3* genotypes were associated with LVIDd, while the *ACE* was not. In contrast to our finding, a previous study by Poch et al., reported a lower mean of LVIDd in the *GNB3* CC genotype group than in the TT and CT genotype groups in the essential hypertension population (25). Another study by Mahmood et al., also reported that the *GNB3* TT genotype had a strong association with the incidence of LV hypertrophy (26). Similar to our study, a previous study found no difference in mean LVIDd among different genotypes of the *ACE* gene (13).

#### 4.1. Comparison of *ACE* levels in the PPCM group

A study found that the I/D polymorphism of the *ACE* influenced the level of serum *ACE* in a healthy population (16). Observations of genetic polymorphisms may explain the interindividual variability in plasma *ACE*. In our study, the highest mean *ACE* levels were found in the DD group, followed by ID and II. This is in line with a study that found that the *ACE* levels increased twice as high in the DD genotype group as in the ID genotype group (16). Another study of pregnant women with hypertension in India reported significantly higher *ACE* levels in the DD genotype group than in the ID and DD genotype groups (27). The I/D of the *ACE* gene affects not only plasma *ACE* levels but also tissue *ACE* (28). Higher *ACE* levels would increase angiotensin II, which affects various systems, including the cardiovascular system (29). In the PPCM group, elevated *ACE* levels in the *ACE* DD genotype may be associated with the incidence of hypertension. An awareness on the part of clinicians about the existence of differences in *ACE* levels in each genotype will certainly have implications for the management of PPCM patients, one of which is the administration of *ACE* inhibitors as a therapy option in PPCM patients, especially those with the *ACE* DD genotype.

#### 4.2. Limitations

The synergistic relationship between the *GNB3* and the *ACE* gene could not be assessed in this study. In the PPCM group,

only two patients had polymorphisms of both genes, while the control group had none. In this study, we did not analyze the levels of improvement in LVEF function in PPCM patients, which could have provided a better understanding of the issue. The reason for this lack of analysis was that we could not ask these patients to visit the hospital for an echocardiography examination because of the restrictions imposed by the COVID-19 pandemic, which has thrown many facets of the healthcare system out of gear.

## 5. Conclusion

This is a study determining the association of *GNB3* C825T and *ACE* gene polymorphisms and the incidence of PPCM in an Asian population. The presence of the *GNB3* TT genotype increases the risk of PPCM 4.6 times, while the *ACE* DD genotype potentially increases the risk of PPCM by 3.6 times. A subanalysis on PPCM patients found that those with TT had a higher BMI and LVIDd and also that those with the DD genotype were more prone to have hypertension and preeclampsia/eclampsia. *ACE* levels were significantly higher in the DD genotype group than in the ID and II genotype groups. These findings highlight the importance of gene polymorphisms in PPCM and, therefore, might be used as predictors and management strategies in the future.

## Data availability statement

The data analyzed in this study are subject to the following licenses/restrictions: The datasets used are available from the corresponding author on reasonable request. Requests to access these datasets should be directed to the corresponding author.

## Ethics statement

The studies involving human participants were reviewed and approved by the Dr. Soetomo General Hospital Surabaya Ethics Committee. The patients/participants provided their written informed consent to participate in this study.

## Author contributions

All authors listed have made equal substantial, direct, and intellectual contributions to the manuscript and approved the final manuscript for publication.

## Acknowledgments

The authors would like to thank all the patients who were willing to participate in this study. The authors would also like



to thank the staff at Dr. Soetomo Hospital for their cooperation in this study.

## Conflict of interest

The authors declare that the research was conducted in the absence of any commercial or financial relationships that could be construed as a potential conflict of interest.

## References

- World Health Organization. Trends in maternal mortality 2000 to 2017: estimates by WHO, UNICEF, UNFPA, World Bank Group and the United Nations Population Division: executive summary. World Health Organization. (2019). p. 1–12.
- Kementrian Kesehatan Republik Indonesia. Rencana Strategis Kementerian Kesehatan Tahun 2015–2019. (2015). p. 35–41.
- Kotit S, Yacoub M. Cardiovascular adverse events in pregnancy: a global perspective. *Glob Cardiol Sci Pract.* (2021) 2021(1):e202105. doi: 10.21542/gcsp.2021.5
- Arany Z, Elkayam U. Peripartum cardiomyopathy. *Circulation.* (2016) 133(14):1397–409. doi: 10.1161/CIRCULATIONAHA.115.020491
- Stergiopoulos K, Lima FV. Peripartum cardiomyopathy—diagnosis, management, and long term implications. *Trends Cardiovasc Med.* (2019) 29(3):164–73. doi: 10.1016/j.tcm.2018.07.012
- Ntusi NBA, Mayosi BM. Aetiology and risk factors of peripartum cardiomyopathy: a systematic review. *Int J Cardiol.* (2009) 131(2):168–79. doi: 10.1016/j.ijcard.2008.06.054
- Dewi IP, Nugroho J. Genetic polymorphism in peripartum cardiomyopathy. *Gynecol Obstet Reprod Med.* (2021) 27(3):297–301. doi: 10.21613/GORM.2021.1072
- McNamara DM, Elkayam U, Alharethi R, Damp J, Hsich E, Ewald G, et al. Clinical outcomes for peripartum cardiomyopathy in North America: results of the IPAC study (investigations of pregnancy-associated cardiomyopathy). *J Am Coll Cardiol.* (2015) 66(8):905–14. doi: 10.1016/j.jacc.2015.06.1309
- Sliwa K, Petrie MC, van der Meer P, Mebazaa A, Hilfiker-Kleiner D, Jackson AM, et al. Clinical presentation, management, and 6-month outcomes in women with peripartum cardiomyopathy: an ESC EORP registry. *Eur Heart J.* (2020) 41(39):3787–97. doi: 10.1093/eurheartj/ehaa455
- Sheppard R, Hsich E, Damp J, Elkayam U, Kealey A, Ramani G, et al. GNB3 C825T polymorphism and myocardial recovery in peripartum cardiomyopathy: results of the multicenter investigations of pregnancy-associated cardiomyopathy study. *Circ Heart Fail.* (2016) 9(3):1–6. doi: 10.1161/CIRCHEARTFAILURE.115.002683
- Carluccio M, Soccio M, De Caterina R. Aspects of gene polymorphisms in cardiovascular disease: the renin-angiotensin system. *Eur J Clin Invest.* (2001) 31(6):476–88. doi: 10.1046/j.1365-2362.2001.00839.x
- van Spaendonck-Zwarts KY, van Tintelen JP, van Veldhuisen DJ, van der Werf R, Jongbloed JDH, Paulus WJ, et al. Peripartum cardiomyopathy as a part of familial dilated cardiomyopathy. *Circulation.* (2010) 121(20):2169–75. doi: 10.1161/CIRCULATIONAHA.109.929646
- Yaqoob I, Tramboos NA, Bhat IA, Pandith A, Beig JR, Hafeez I, et al. Insertion/deletion polymorphism of ACE gene in females with peripartum cardiomyopathy: a case-control study. *Indian Heart J.* (2018) 70(1):66–70. doi: 10.1016/j.ihj.2017.05.020
- Sliwa K, Hilfiker-Kleiner D, Petrie MC, Mebazaa A, Pieske B, Buchmann E, et al. Current state of knowledge on aetiology, diagnosis, management, and therapy of peripartum cardiomyopathy: a position statement from the heart failure association of the European society of cardiology working group on peripartum cardiomyopathy. *Eur J Heart Fail.* (2010) 12(8):767–78. doi: 10.1093/eurjhf/hfq120
- Siffert W, Rosskopf D, Siffert G, Busch S, Moritz A, Erbel R, et al. Association of a human G-protein  $\beta 3$  subunit variant with hypertension. *Nat Genet.* (1998) 18(1):45–8. doi: 10.1038/ng0198-45
- Rigat B, Hubert C, Alhenc-Gelas F, Cambien F, Corvol P, Soubrier F. An insertion/deletion polymorphism in the angiotensin I-converting enzyme gene accounting for half the variance of serum enzyme levels. *J Clin Invest.* (1990) 86(4):1343–6. doi: 10.1172/JCI114844
- Ricke-Hoch M, Pfeffer TJ, Hilfiker-Kleiner D. Peripartum cardiomyopathy: basic mechanisms and hope for new therapies. *Cardiovasc Res.* (2020) 116(3):520–31. doi: 10.1093/cvr/cvz252
- Wang J, Gareri C, Rockman HA. G-protein-coupled receptors in heart disease. *Circ Res.* (2018) 123(6):716–35. doi: 10.1161/CIRCRESAHA.118.311403
- Martinez BJT, Sison MCC, Acosta CS. Clinical profile and outcome of peripartum cardiomyopathy among teenager patients at the university of the Philippines—Philippine General Hospital. *Acta Med Philipp.* (2022) 56(7):5–11. doi: 10.47895/amp.vi0.3445
- Bello N, Rendon ISH, Arany Z. The relationship between pre-eclampsia and peripartum cardiomyopathy: a systematic review and meta-analysis. *J Am Coll Cardiol.* (2013) 62(18):1715–23. doi: 10.1016/j.jacc.2013.08.717
- Zotova TY, Lapaev NN, Azova MM, Blagoravov ML, Gigani OO, Ait Aissa A, et al. Distribution of polymorphisms of the renin-angiotensin system genes (ACE, AGT, and AGTR1), ITGB3, and FTO in pregnant patients with hypertensive disorders. *Bull Exp Biol Med.* (2019) 167(1):74–8. doi: 10.1007/s10517-019-04464-6
- Wang C, Zhou X, Liu H, Huang S. Three polymorphisms of renin-angiotensin system and preeclampsia risk. *J Assist Reprod Genet.* (2020) 37(12):3121–42. doi: 10.1007/s10815-020-01971-8
- Timoh T, Bloom ME, Siegel RR, Wagman G, Lanier GM, Vittorio TJ. A perspective on obesity cardiomyopathy. *Obes Res Clin Pract.* (2012) 6(3):e175–262. doi: 10.1016/j.orcp.2012.02.011
- Siffert W, Forster P, Jöckel KH, Mvere DA, Brinkmann B, Naber C, et al. Worldwide ethnic distribution of the G protein beta3 subunit 825 T allele and its association with obesity in Caucasian, Chinese, and black African individuals. *J Am Soc Nephrol.* (1999) 10(9):1921–30. doi: 10.1681/ASN.V1091921
- Poch E, González D, Gómez-Angelats E, Enjuto M, Paré JC, Rivera F, et al. G-protein  $\beta 3$  subunit gene variant and left ventricular hypertrophy in essential hypertension. *Hypertension.* (2000) 35(1):214–8. doi: 10.1161/01.HYP.35.1.214
- Mahmood MS, Mian ZSU, Afzal A, Frossard PM. G-protein beta-3 subunit gene 825C > T dimorphism is associated with left ventricular hypertrophy but not essential hypertension. *Med Sci Monit.* (2005) 11(1):CR6–9.
- Aggarwal PK, Jain V, Jha V. Endothelial nitric oxide synthase, angiotensin-converting enzyme and angiotensinogen gene polymorphisms in hypertensive disorders of pregnancy. *Hypertens Res.* (2010) 33(5):473–7. doi: 10.1038/hr.2010.23
- Sayed-Tabatabaei FA, Oostra BA, Isaacs A, Van Duijn CM, Wittman JCM. ACE polymorphisms. *Circ Res.* (2006) 98(9):1123–33. doi: 10.1161/01.RES.0000223145.74217.e7
- Wong MKS. Angiotensin converting enzymes. In: Takei Y, Ando H, Tsutsui K *Handbook of hormones*. Oxford, UK: Elsevier Inc. (2016). p. 263–4. doi: 10.1016/B978-0-12-801028-0.00254-3

## Publisher's note

All claims expressed in this article are solely those of the authors and do not necessarily represent those of their affiliated organizations, or those of the publisher, the editors and the reviewers. Any product that may be evaluated in this article, or claim that may be made by its manufacturer, is not guaranteed or endorsed by the publisher.



## OPEN ACCESS

EDITED BY  
Kenneth Scott Campbell,  
University of Kentucky, United States

REVIEWED BY  
Thomas Kampourakis,  
King's College London, United Kingdom  
Theresia Kraft,  
Hannover Medical School, Germany

\*CORRESPONDENCE  
Aikaterini Kontrogianni-Konstantopoulos  
✉ akontrogianni@som.umaryland.edu

SPECIALTY SECTION  
This article was submitted to  
Heart Failure and Transplantation,  
a section of the journal  
Frontiers in Cardiovascular Medicine

RECEIVED 31 October 2022  
ACCEPTED 26 January 2023  
PUBLISHED 13 April 2023

CITATION  
Grogan A, Huang W, Brong A, Kane MA and  
Kontrogianni-Konstantopoulos A (2023)  
Alterations in cytoskeletal and Ca<sup>2+</sup> cycling  
regulators in atria lacking the obscurin Ig58/59  
module.  
*Front. Cardiovasc. Med.* 10:1085840.  
10.3389/fcvm.2023.1085840

COPYRIGHT  
© 2023 Grogan, Huang, Brong, Kane and  
Kontrogianni-Konstantopoulos. This is an  
open-access article distributed under the terms  
of the [Creative Commons Attribution License](#)  
(CC BY). The use, distribution or reproduction  
in other forums is permitted, provided the  
original author(s) and the copyright owner(s)  
are credited and that the original publication in  
this journal is cited, in accordance with  
accepted academic practice. No use,  
distribution or reproduction is permitted which  
does not comply with these terms.

# Alterations in cytoskeletal and Ca<sup>2+</sup> cycling regulators in atria lacking the obscurin Ig58/59 module

Alyssa Grogan<sup>1</sup>, Weiliang Huang<sup>2</sup>, Annie Brong<sup>1</sup>, Maureen A. Kane<sup>2</sup>  
and Aikaterini Kontrogianni-Konstantopoulos<sup>1\*</sup>

<sup>1</sup>Department of Biochemistry and Molecular Biology, University of Maryland, Baltimore, MD, United States,  
<sup>2</sup>Department of Pharmaceutical Sciences, University of Maryland School of Pharmacy, Baltimore, MD,  
United States

**Introduction:** Obscurin (720–870kDa) is a giant cytoskeletal and signaling protein that possesses both structural and regulatory functions in striated muscles. Immunoglobulin domains 58/59 (Ig58/59) of obscurin bind to a diverse set of proteins that are essential for the proper structure and function of the heart, including giant titin, novex-3, and phospholamban (PLN). Importantly, the pathophysiological significance of the Ig58/59 module has been further underscored by the discovery of several mutations within Ig58/59 that are linked to various forms of myopathy in humans. We previously generated a constitutive deletion mouse model, *Obscn-ΔIg58/59*, that expresses obscurin lacking Ig58/59, and characterized the effects of this deletion on cardiac morphology and function through aging. Our findings demonstrated that *Obscn-ΔIg58/59* male animals develop severe arrhythmia, primarily manifesting as episodes of junctional escape and spontaneous loss of regular p-waves, reminiscent of human atrial fibrillation, accompanied by significant atrial enlargement that progresses in severity with aging.

**Methods and Results:** To comprehensively characterize the molecular alterations responsible for these pathologies, we performed proteomic and phospho-proteomic analyses in aging *Obscn-ΔIg58/59* atria. Our studies revealed extensive and novel alterations in the expression and phosphorylation profile of major cytoskeletal proteins, Ca<sup>2+</sup> regulators, and Z-disk associated protein complexes in the *Obscn-ΔIg58/59* atria through aging.

**Discussion:** These studies implicate obscurin, particularly the Ig58/59 module, as an essential regulator of the Z-disk associated cytoskeleton and Ca<sup>2+</sup> cycling in the atria and provide new molecular insights into the development of atrial fibrillation and remodeling.

## KEYWORDS

obscurin, atrial fibrillation, arrhythmia, Z-disk, Ca<sup>2+</sup> cycling, cytoskeleton

## Introduction

Obscurin (720–870kDa), comprised of 65–67 tandemly arranged immunoglobulin (Ig) domains, 2–3 fibronectin-III motifs, and a unique assortment of signaling domains at its COOH-terminus depending on the isoform, is a giant cytoskeletal protein that localizes to the periphery of M-bands and Z-disks where it modulates diverse structural and regulatory functions in striated muscles (1, 2). Given its large size, modular nature, and unique cellular distribution as a peripheral sarcomeric protein, obscurin is ideally situated to interact with proteins localizing to different cellular compartments, ranging from the sarcomere and the surrounding sarcoplasmic reticulum (SR) membranes to the cytoskeleton and the sarcolemma (1, 2). Accordingly, obscurin serves essential roles in the assembly and stabilization of the myofibril, Ca<sup>2+</sup> signaling, cell adhesion, and the physical integration of the sarcomere with the cytoskeleton and surrounding membrane structures (1, 2).

Over the past several decades, the discovery of >20 missense, splicing, and frameshift mutations spanning the entire length of the obscurin gene (*OBSCN*) in patients with hypertrophic cardiomyopathy (HCM), dilated cardiomyopathy (DCM), left ventricular non-compaction (LVNC), and arrhythmogenic right ventricular cardiomyopathy (ARVC) has increasingly implicated obscurin in the development of cardiac disease in humans (3–5). To date, the disease mechanisms underlying the majority of these mutations have remained entirely uninvestigated, with the exception of the HCM-linked R4344Q variant residing within obscurin Ig58 which our lab has previously characterized (6). Our findings demonstrated that mice carrying the R4344Q variant (*Obscn-R4344Q*) exhibited a “gain-of-function” phenotype wherein enhanced binding between mutant Ig58 and phospholamban (PLN) resulted in disinhibition of the sarco-endoplasmic reticulum  $\text{Ca}^{2+}$  ATPase (SERCA), increased  $\text{Ca}^{2+}$  cycling kinetics, and the development of ventricular arrhythmia through aging (6). The direct binding between obscurin-Ig58/59 and PLN and their enhanced association in the presence of the R4344Q variant was recently corroborated by Fukuzawa and colleagues, reporting a ~2.5-fold decrease in the  $K_d$ ; yet, the physiological relevance of the obscurin/PLN interaction was questioned (7). As a small modulatory protein that is extensively regulated by phosphorylation and assumes multiple oligomeric conformations in physiological settings, PLN inherently interacts weakly and/or transiently with its binding partners. Thus, technical limitations of different *in vitro* systems perhaps mask a complex and dynamically regulated (i.e., on a beat-to-beat basis) interaction between obscurin-Ig58/59 and PLN.

In addition to its binding to PLN, obscurin-Ig58/59 has been reported to interact with the extreme  $\text{NH}_2$ -terminus of titin (3–4 MDa) as well as a unique 198-amino acid long sequence of titin's smaller splice variant, novex-3 (~700 kDa), at the level of the Z-disk (8, 9). Of note, the obscurin/novex-3 interaction was recently contested by Fukuzawa and colleagues (7). Nevertheless, given that obscurin-Ig58/59 may interact with a diverse set of structural and regulatory proteins that are essential for normal muscle function, we generated the *Obscn-ΔIg58/59* model that expresses obscurin constitutively lacking Ig58/59 to extensively characterize the pathophysiological significance of this region in the heart (10). Our studies demonstrated that sedentary *Obscn-ΔIg58/59* males develop severe arrhythmia characterized by frequent episodes of spontaneous junctional escape and atrial fibrillation beginning at 6-months of age accompanied by significantly increased atrial mass and dilated left ventricles by 12-months (10).

Herein, we performed proteomic and phospho-proteomic analysis using 6- and 12-month old *Obscn-ΔIg58/59* atria in order to comprehensively investigate the molecular basis for the prominent atrial arrhythmia and remodeling in aging *Obscn-ΔIg58/59* males. Our studies revealed extensive and novel changes in the expression and phosphorylation profile of the *Obscn-ΔIg58/59* atrial proteome, mainly impacting cytoskeletal and signaling complexes at the Z-disk and  $\text{Ca}^{2+}$  regulating proteins. Together, these results provide new molecular insights into the pathophysiology of spontaneous atrial arrhythmia and remodeling.

## Materials and methods

### *Obscn-ΔIg58/59* constitutive deletion mice

The *Obscn-ΔIg58/59* constitutive deletion model was generated and genotyped as previously described (10). Animal care and procedures

were conducted under protocols approved by the Institutional Animal Care and Use Committee at the University of Maryland, School of Medicine (UMSOM) and in accordance with the NIH guidelines (Guide for the Care and Use of Laboratory Animals).

### Lysate preparation and western blotting

Lysates were prepared from flash frozen cardiac tissue and protein expression was evaluated by immunoblotting as previously described (10). Briefly, frozen right and left atria were combined, ground to a powder in a glass homogenizer while immersed in liquid nitrogen, and incubated at  $-20^{\circ}\text{C}$  for 20 min. The ground tissue was solubilized in urea-thiourea lysis buffer (8 mol/L urea, 2 mol/L thiourea, 3% SDS, 0.05 mol/L tris-HCl, 0.03% bromophenol blue, 0.075 mol/L dithiothreitol, pH 6.8) and 50% glycerol supplemented with protease and phosphatase inhibitors (Halt Protease and Phosphatase Inhibitor Cocktail, Thermo Fisher Scientific, Waltham, MA, United States) in a  $60^{\circ}\text{C}$  water bath. Homogenates were centrifuged and supernatants were aliquoted and flash frozen in liquid nitrogen. For western blotting, equal amounts of protein lysates were thawed at  $55^{\circ}\text{C}$  for 5 min, separated by SDS-polyacrylamide gel electrophoresis, transferred to nitrocellulose membrane, and probed with the respective primary antibodies. Alkaline phosphatase (AP)-conjugated or horseradish peroxidase (HRP)-conjugated secondary antibodies and the respective chemiluminescent reagents (NovaBright; AP, or Pierce ECL; HRP) were used to detect immunoreactive bands. Densitometry was performed using ImageJ and each band was normalized to a loading control (glyceraldehyde 3-phosphate dehydrogenase, GAPDH; heat shock protein 90, Hsp90; or  $\alpha$ -actinin). At least two technical replicates of at least three different biological samples (i.e., hearts) were quantified per genotype for each protein evaluated. The original representative blots shown in Figures 1, 2 and 8 are included in Supplementary Image 1; please note that in some instances, immunoblots were flipped for ease of presentation.

### Antibodies

The following primary antibodies were used for western blotting: rabbit polyclonal antibodies to obscurin Ig58/59 (1  $\mu\text{g/mL}$ ) (11), obscurin Ig67 (1  $\mu\text{g/mL}$ ) (10), novex-3 (1:1000, a generous gift from Dr. Henk Granzier) (9), PLN-pSer16 (1:1000; 07–052, Millipore, Temecula, CA, United States), PLN-pThr17 (1:2000; A010-13AP, Badrilla, Leeds, United Kingdom), sAnk1 (1  $\mu\text{g/mL}$ ) (12), RyR2-pSer2808 (1:2000; ab59225, Abcam, Cambridge, MA, United States), RyR2-pSer2814 (1:500; A010-31AP, Badrilla), sarcolipin (1  $\mu\text{g/mL}$ , a generous gift from Dr. Robert Bloch) (13), ERK2 (1:1000; CST-9108S, Cell Signaling Technology, Danvers, MA, United States), ERK1/2-pThr183/pTyr185 (1:2000; CST-4370 T, Cell Signaling Technology), rabbit monoclonal antibodies to Hsp90 (1:1000; CST-4877, Cell Signaling Technology), and mouse monoclonal antibodies to PLN (1:5000; ab2865, Abcam), SERCA2 (1:1000; MA3-919, Thermo Fisher Scientific, Waltham, MA, United States), RyR2 (1:1000; MA3-925, Thermo Fisher Scientific), GAPDH (1:15000; G8795, Millipore), and  $\alpha$ -actinin (1:2500; A7811, Sigma-Aldrich, St. Louis, MO, United States). The following secondary antibodies were used for western blotting: goat anti-mouse IgG (1:3000; A3688, Sigma-Aldrich), goat anti-rabbit IgG (1:3000; AB\_2337947, Jackson ImmunoResearch, West Grove, PA, United States), goat

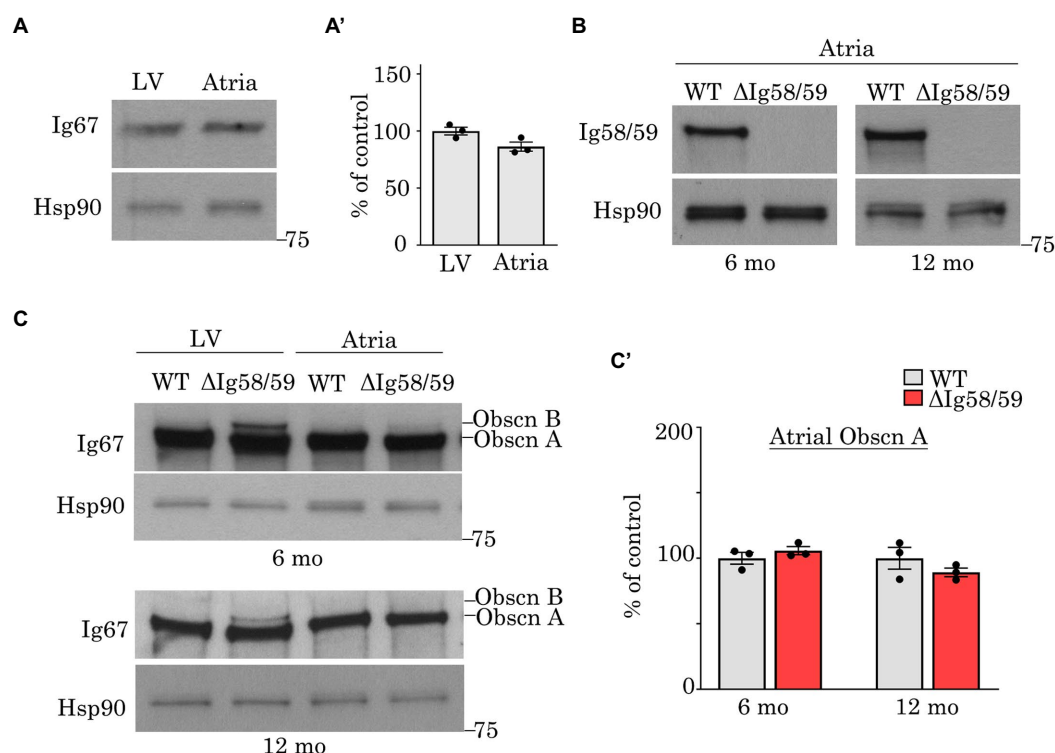


FIGURE 1

Expression levels of obscurin in wild-type and *Obscn-ΔIg58/59* atria. (A,A') Immunoblotting (A) and relative quantification (A') of giant obscurin in wild-type 12-month-old left ventricles (LV) and atrial lysates utilizing antibodies to Ig67 did not reveal significant expression differences; *t*-test, *p*=0.18. (B) Immunoblotting of giant obscurin in 6- and 12-month-old wild-type and *Obscn-ΔIg58/59* atria using antibodies to Ig58/59 confirmed the Ig58/59 deletion. (C,C') Immunoblotting (C) and relative quantification (C') of giant obscurin in 6- and 12-month-old wild-type and *Obscn-ΔIg58/59* LV and atria using antibodies to Ig67 indicated that obscurin A expression is unchanged in *Obscn-ΔIg58/59* atria compared to wild-type; *t*-test, *p*=0.32 (6-months), *p*=0.36 (12-months). Notably, the up-regulation of obscurin B observed in *Obscn-ΔIg58/59* LV was barely detectable in *Obscn-ΔIg58/59* atria; *n*=3 animals per group; data points represent the average of at least two technical replicas; densitometric values were normalized to Hsp90, which was used as loading control.

anti-mouse IgG (1,3,000; CST-7076S, Cell Signaling Technology), and goat anti-rabbit IgG (1,3,000; CST-7074S, Cell Signaling Technology).

## Electrophoresis and Coomassie Blue staining for titin

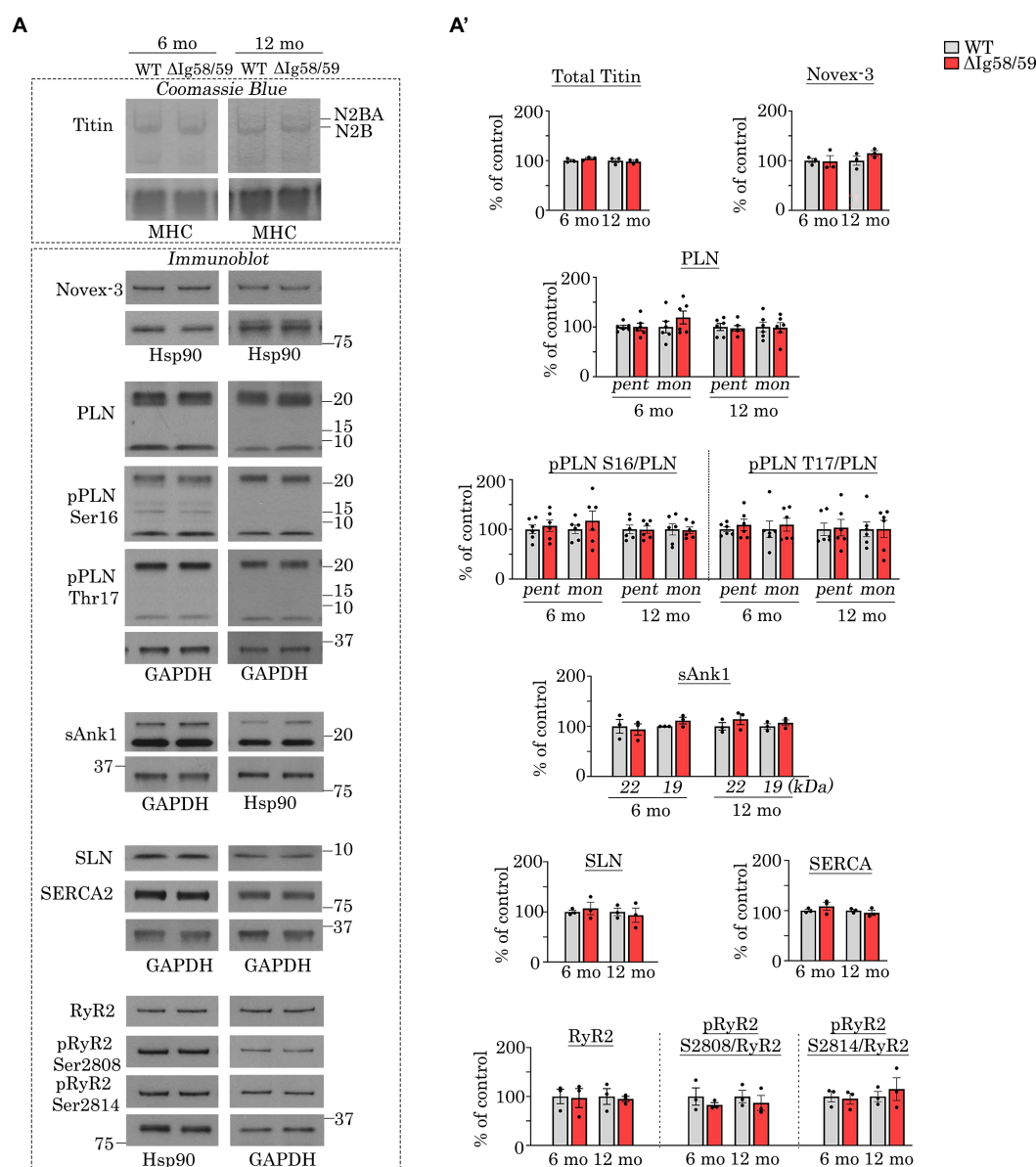
Atrial lysates prepared as described above were separated on 16 × 18 cm gels composed of 1% agarose in 1X running buffer (50 mM tris, 0.384 mol/l glycine, 0.1% SDS) and 30% glycerol using the Hoefer SE600 unit system at 4°C for 3 h as described previously (10). Gels were stained with Coomassie Blue and the bands corresponding to giant titin were quantified using ImageJ and normalized to myosin heavy chain (MHC) as a loading control. Any digital adjustments to promote visualization of the bands were applied uniformly across the entire gel. At least two technical replicates of three different biological samples (i.e., hearts) were quantified for each genotype. The original representative titin gels shown in Figure 2 are included in Supplementary Image 1; please note that in some instances, gels were flipped for ease of presentation.

## Proteomic and phospho-proteomic analysis

Proteomic experiments were performed in the Mass Spectrometry Center at the University of Maryland School of Pharmacy. Atrial tissues

dissected from male wild-type and homozygous *Obscn-ΔIg58/59* mice (*n*=5 hearts per group) were homogenized in phosphate buffered saline using the Precellys CK14 lysing kit (Bertin Corp., Rockville, MD, United States). Proteins were extracted and purified from tissue lysates by trichloroacetic acid precipitation. Protein concentration was measured by bicinchoninic acid assay as described previously (14). Lysates were reduced, alkylated, and trypsinolyzed on a 10 K filter for shotgun proteomics as in (15). Phospho-peptides were enriched by TiO<sub>2</sub> affinity chromatography (Sigma). Tryptic peptides were separated by a nanoACQUITY UPLC analytical column on a Waters nano-ACQUITY UPLC system and analyzed with a coupled Thermo Scientific Orbitrap Fusion Lumos Tribrid mass spectrometer as previously described (16). In detail, tryptic peptides were separated on a nano-ACQUITY UPLC analytical column (BEH130 C18, 1.7 μm, 75 μm × 200 mm, Waters) over a 165-min linear acetonitrile gradient (3–40%) with 0.1% formic acid on a Waters nano-ACQUITY UPLC system and analyzed on a coupled Thermo Scientific Orbitrap Fusion Lumos Tribrid mass spectrometer as previously reported (17). Full scans were acquired at a resolution of 120,000 and precursors were selected for fragmentation by higher-energy collisional dissociation (normalized collision energy at 30%) for a maximum 3-s cycle. Tandem mass spectra were searched against a UniProt reference *Mus musculus* proteome using Sequest HT algorithm (18) and MS Amanda algorithm (19) with a maximum precursor mass error tolerance of 10 ppm. Carbamidomethylation of cysteine was treated as static modification. Phosphorylation of serine (Ser), threonine





**FIGURE 2**  
Expression and phosphorylation status of Ig58/59 binding partners and selected  $\text{Ca}^{2+}$  cycling proteins are unaffected in aged *Obecn-ΔIg58/59* atria. **(A,A')** Representative Coomassie Blue stained agarose gels and immunoblots **(A)** and relative quantifications **(A')** did not reveal statistically significant alterations in the expression or phosphorylation status of giant titins, novex-3, PLN, sAnk1, SLN, SERCA2, or RyR2 in lysates prepared from 6- and 12-month-old *Obecn-ΔIg58/59* atria; MHC, Hsp90, and GAPDH served as loading controls;  $n=3-6$  animals per group; data points represent the average of at least two technical replicates; quantification of phosphorylation levels are normalized to total PLN or RyR2 levels; pent, pentamer; mono, monomer.

(Thr), and tyrosine (Tyr), and deamidation of asparagine and glutamine were treated as dynamic modifications. Resulting hits were validated at a maximum global false discovery rate (FDR) of 0.01 using a semi-supervised machine learning algorithm Percolator (20). Label-free quantifications were performed using Minora, an aligned AMRT (Accurate Mass and Retention Time) cluster quantification algorithm (Thermo Fisher Scientific, 2017). Label-free quantitation of protein abundances was measured by comparing the MS1 peak volumes of peptide ions, whose identities were confirmed by MS2 sequencing.

The above abundance values were imported into Partek GS software for further statistical and bioinformatic analyses (Transcriptomics and Deep Sequencing Core, Johns Hopkins University). There were two mappings of the mass spectra: (a) to individual proteins, and (b) to

unique phospho-peptides, wherein a phospho-peptide represents a unique specific position within its peptide. Both the individual proteins and unique phospho-peptide proteins were annotated with their cognate genes' approved MGI/NCBI nomenclature. Following  $\log_2$  transformation, the abundance values were then quantile normalized for each time point to minimize experimental noise among the lanes that represent replicate samples for the two biological classes (i.e., genotypes), and the *Obecn-ΔIg58/59* samples were compared to the wild type with two-tailed one-way  $t$ -test ANOVA. Each protein or unique phospho-peptide compared received a relative abundance and statistical value, as a fold-change and value of  $p$ , and the  $\log_2$  fold changes were analyzed to determine their standard deviation from the mean value of no change. Proteins and phospho-peptides with a value of  $p$  of  $<0.05$  and  $\log_2$  fold

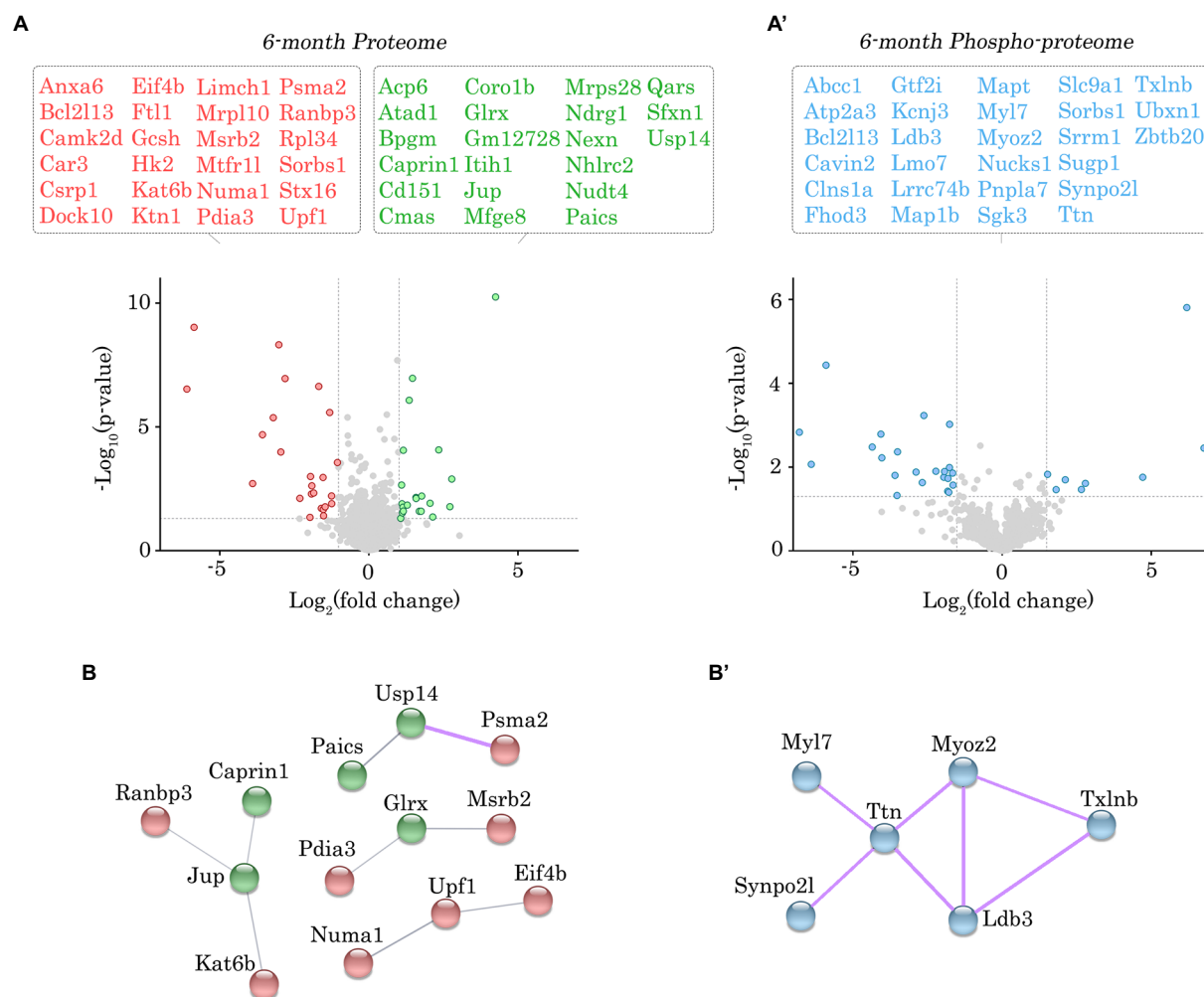


FIGURE 3

Proteomic and phospho-proteomic analysis of *Obecn-Δlg58/59* atria at 6-months. (A,A') Volcano plots of significantly up-regulated (green) or down-regulated (red) proteins (A) and significantly altered phospho-peptides (blue; A') in *Obecn-Δlg58/59* atria at 6-months. A total of 45 proteins out of 1700 detected exhibited significantly altered expression (A), whereas 30 phospho-peptides out of 1401 detected were significantly altered (A') in 6-month-old *Obecn-Δlg58/59* atria compared to wild-type;  $n=5$  biological samples per genotype; grey dotted lines represent thresholds of  $p<0.05$  and  $SD>2$ . (B,B') The physical and functional associations of the deregulated proteins (B) and phospho-proteins (B') in *Obecn-Δlg58/59* atria at 6-months were plotted using the STRING database (v.11.0b). Line thickness corresponds to the strength of the association. Protein networks with a high confidence score ( $>0.7$ ) are highlighted in purple.

changes that differed by  $>2$  standard deviations were deemed to be significantly different. The precise phospho-site residues that exhibited a probability  $>75\%$  are specified, whereas ambiguous phospho-site residues that displayed  $<75\%$  probability are denoted in the associated phospho-peptide when referenced in the text and tables. Phosphorylation sites not previously annotated in PhosphoSitePlus (v. 6.6.0.4.) were denoted as novel. The raw mass spectrometry proteomics data have been deposited to the ProteomeXchange Consortium via the PRIDE (21) partner repository with the dataset identifier PXD028904. A complete list of all proteins and phospho-peptides that were identified at 6- and 12-months are listed with associated statistics in [Supplementary Data Sheets S1–S2](#) and [S3–S4](#), respectively.

## STRING analysis

The physical and functional associations of the proteins and phospho-proteins deemed to be significantly different between

genotypes were plotted using the STRING database (v.11.0b) (22). To be as inclusive as possible, protein–protein interactions with a confidence score of  $>0.4$  (i.e., medium confidence threshold) were plotted for differentially regulated proteins, while those relationships exhibiting high confidence scores ( $>0.7$ ) were highlighted within the network. Only high confidence interactions ( $>0.7$ ) were plotted and highlighted for deregulated phospho-proteins. Disconnected nodes and clusters comprised of less than 3 proteins were excluded.

## Enrichment analysis

The differentially expressed proteins and phospho-proteins were further analyzed with the QIAGEN Ingenuity Pathway Analysis (IPA) platform to determine their biological significance. Due to the large number of significantly altered pathways identified, the top 10 most significant pathways and cellular functions that are relevant to cardiovascular physiology and associated with at least 3 deregulated

proteins/phospho-proteins were included in the text, figures, and tables. A complete list of all significantly altered pathways and cellular functions identified at 6- and 12-months are listed in [Supplementary Data Sheets S5–S6 and S7–S8](#), respectively.

## Results and discussion

### Immunoblot analysis of aging *Obscn-ΔIg58/59* atria did not reveal significant differences in the levels of obscurin, titin, or canonical $\text{Ca}^{2+}$ cycling proteins

We recently generated a constitutive deletion mouse model, *Obscn-ΔIg58/59*, that expresses obscurin lacking the Ig58/59 region and comprehensively evaluated the effects of this deletion on cardiac morphology and function through aging. Our studies showed that male *Obscn-ΔIg58/59* mice exhibit episodes of severe atrial arrhythmia by 6-months, manifesting as junctional escape and spontaneous loss of regular *p*-waves (10). By 12-months, the incidence and severity of arrhythmias intensified accompanied by significant atrial enlargement (10). Notably, female *Obscn-ΔIg58/59* mice do not exhibit any structural or functional deficiencies through aging and develop only mild arrhythmia that occurs less frequently compared to *Obscn-ΔIg58/59* males (10). Therefore, we focus our molecular characterization on *Obscn-ΔIg58/59* males only.

To investigate the mechanistic basis for the development of atrial fibrillation and remodeling in aging *Obscn-ΔIg58/59* males, we first evaluated the expression levels of obscurin, the binding partners of obscurin-Ig58/59, and a panel of  $\text{Ca}^{2+}$  regulators that are commonly associated with the development of atrial fibrillation. Earlier studies assessing the expression of obscurin during embryonic development reported reduced obscurin transcript levels in mouse atria compared to ventricles at embryonic day 12 (23). However, comparison of obscurin expression between adult atrial and ventricular tissues has not yet been experimentally determined. We therefore performed immunoblotting experiments using lysates prepared from 12-month-old wild-type hearts but did not observe significant differences in the levels of giant obscurin between the left ventricle and atria ([Figures 1A,A'](#)).

We next evaluated the impact of the Ig58/59 deletion on atrial obscurin expression in sedentary aging animals. Immunoblotting experiments utilizing antibodies to obscurin-Ig58/59 confirmed the absence of this region in lysates generated from 6- and 12-month-old *Obscn-ΔIg58/59* atria ([Figure 1B](#)). Similar to our prior findings in *Obscn-ΔIg58/59* left ventricles (10), antibodies to obscurin-Ig67 did not reveal significant differences in prototypical obscurin A expression between wild-type and *Obscn-ΔIg58/59* atria at 6- or 12-months ([Figures 1C,C'](#)). Intriguingly, the up-regulation of obscurin B (the largest known isoform containing two serine/threonine, Ser/Thr, kinases) previously reported in *Obscn-ΔIg58/59* left ventricular tissue (10) was barely detectable in *Obscn-ΔIg58/59* atria ([Figures 1C,C'](#)). This finding indicated that the Ig58/59 deletion leads to distinct molecular alterations in *Obscn-ΔIg58/59* atria compared to the ventricle and suggested that *Obscn-ΔIg58/59* atria potentially lack compensatory signaling mechanisms that could be mediated by obscurin-kinase bearing isoforms in *Obscn-ΔIg58/59* left ventricles.

We next evaluated the expression and phosphorylation levels of the known binding partners of Ig58/59 in addition to select  $\text{Ca}^{2+}$  cycling

regulators. Interestingly, there were no statistically significant differences in the levels of giant titin, novex-3, PLN or its phosphorylation at Ser16 or Thr17, small ankyrin 1 (sAnk1), sarcolipin (SLN), SERCA2, RyR2 or its phosphorylation at Ser2808 or Ser2814 in *Obscn-ΔIg58/59* atria compared to age-matched controls at either 6- or 12-months ([Figures 2A,A'](#)). Therefore, the atrial remodeling and arrhythmia in aging *Obscn-ΔIg58/59* male mice cannot be explained by changes in the expression levels and/or canonical phosphorylation sites of these proteins, as is the case for *Obscn-ΔIg58/59* left ventricles (10). This suggested alternative mechanisms in the atria, perhaps involving additional  $\text{Ca}^{2+}$  or cytoskeletal regulators and/or less characterized/novel phosphorylation events. Along these lines, many studies have reported the presence of phosphorylation sites on titin (24), RyR2 (25–27), PLN (28), sAnk1 (29), and SERCA2 (30), for which their (patho)physiological impact has not been established.

### Proteomic and phospho-proteomic analysis revealed deregulated structural and regulatory proteins in aging *Obscn-ΔIg58/59* atria

Given the lack of significant alterations in the levels of obscurin, the binding partners of obscurin-Ig58/59, and canonical  $\text{Ca}^{2+}$  cycling regulators, we performed proteomic and phospho-proteomic experiments using 6- and 12-month-old male wild-type and *Obscn-ΔIg58/59* atrial tissue ( $n = 5$  hearts per group) to obtain a more comprehensive molecular profile of the *Obscn-ΔIg58/59* atria. At 6-months, we identified 45 proteins (out of 1700 detected) that exhibited significantly altered expression levels ([Figure 3A](#); [Supplementary Table S1](#); [Supplementary Data Sheet 1](#)) and 30 phospho-peptides (out of 1,401 detected) originating from 27 different proteins that displayed altered phosphorylation levels ([Figure 3A'](#); [Supplementary Table S2](#); [Supplementary Data Sheet 2](#)). By 12-months, we identified 48 proteins (out of 1708 detected) with altered expression levels ([Figure 4A](#); [Supplementary Table S3](#); [Supplementary Data Sheet 3](#)) and 78 phospho-peptides (out of 2,656 detected) corresponding to 67 different proteins that exhibited altered phosphorylation levels ([Figure 4A'](#); [Supplementary Table S4](#); [Supplementary Data Sheet 4](#)). Of the 45–48 affected proteins and 27–67 affected phospho-proteins in *Obscn-ΔIg58/59* atria, relatively few were commonly deregulated throughout aging ([Figure 5](#)).

In order to discover the functional relationships and/or physical associations shared by the deregulated proteins or phospho-proteins in *Obscn-ΔIg58/59* atria through aging, we performed a network analysis using the publicly available STRING database (v.11.0b) (22). At 6-months, there was a single network exhibiting a high confidence interaction score ( $>0.7$ ) among the proteins displaying deregulated expression in *Obscn-ΔIg58/59* atria ([Figure 3B](#)), which consisted of ubiquitin-specific protease 14 (*Usp14*) and the proteasome subunit alpha type-2 (*Psma2*), possibly reflecting deregulated protein degradation pathways. Also connected to this network, albeit with a medium confidence interaction score ( $>0.4$ ), is the purine biosynthetic enzyme, phosphoribosylaminoimidazole carboxylase/succinocarboxamide synthetase (*Paics*), possibly implicating altered DNA synthesis, intracellular signaling, and/or metabolic processes (31). On the other hand, STRING analysis of the deregulated phospho-proteins at 6-months revealed a high confidence network ([Figure 3B'](#)) comprised of sarcomeric proteins (i.e., titin, *Ttn*; myosin light chain 7, *Myl7*) and cytoskeletal proteins localizing to the Z-disc (i.e., myozenin, *Myoz2*; synaptopodin 2-like, *Synpo2l*; LIM domain binding protein 3, *Ldb3*).

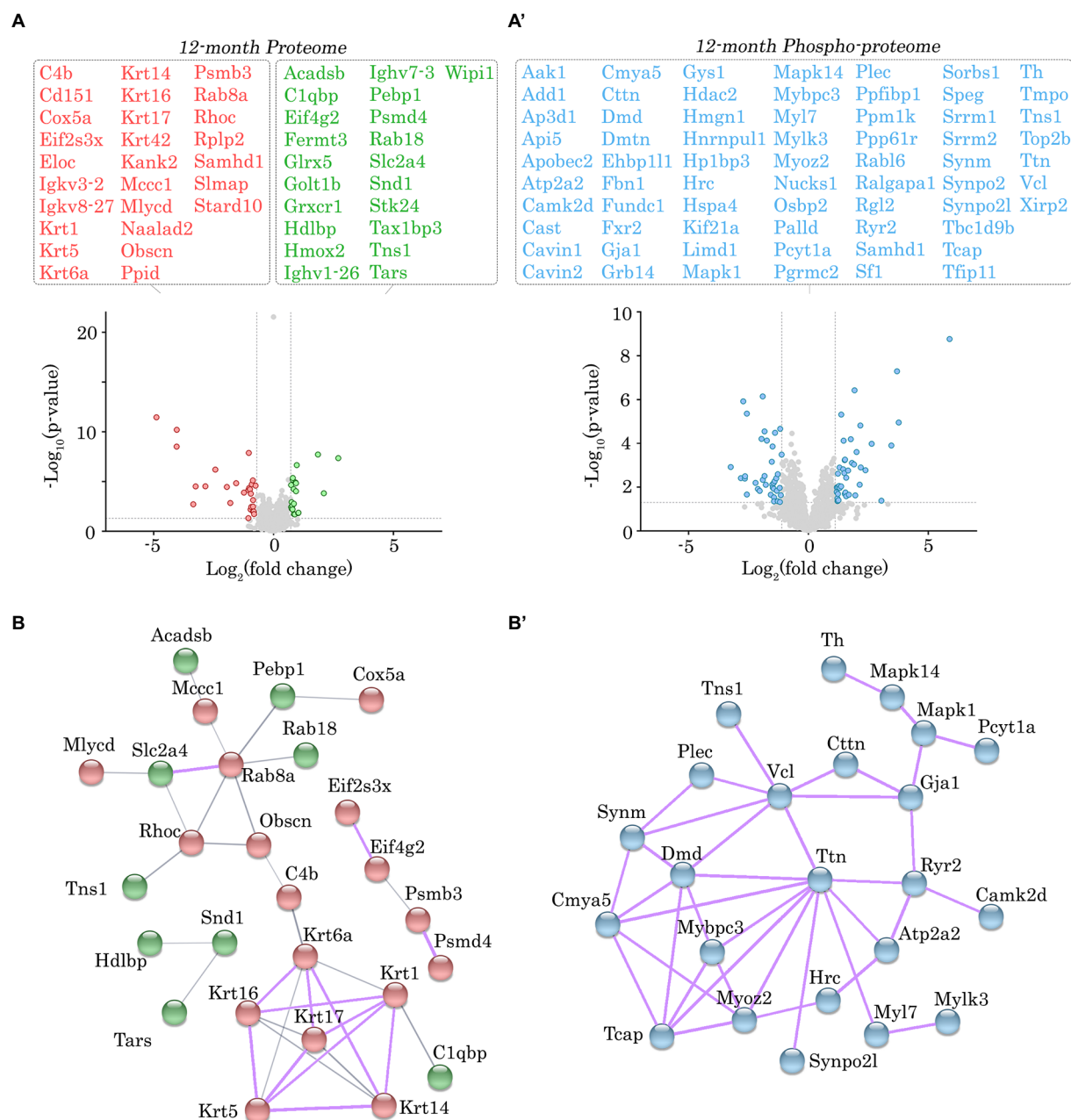


FIGURE 4

Proteomic and phospho-proteomic analysis of *Obscn-ΔIg58/59* atria at 12-months. **(A,A')** Volcano plots of significantly up-regulated (green) or down-regulated (red) proteins **(A)** and significantly altered phospho-peptides (blue; **A'**) in *Obscn-ΔIg58/59* atria at 12-months. A total of 48 proteins out of 1708 detected exhibited significantly altered expression **(A)**, whereas 78 phospho-peptides out of 2,656 detected were significantly altered **(A')** in 12-month-old *Obscn-ΔIg58/59* atria compared to wild-type;  $n=5$  biological samples per genotype; grey dotted lines represent thresholds of  $p<0.05$  and  $SD>2$ . **(B,B')** The physical and functional associations of the deregulated proteins **(B)** and phospho-proteins **(B')** in *Obscn-ΔIg58/59* atria at 12-months were plotted using the STRING database (v.11.0b). Line thickness corresponds to the strength of the association. Protein networks with a high confidence score ( $>0.7$ ) are highlighted in purple.

This network also included  $\beta$ -taxilin, a muscle-specific member of the taxilin family of vesicular trafficking regulators that is proposed to regulate myoblast differentiation (32). At 12-months, we observed a significant clustering of intermediate filament proteins (i.e., keratins, *Krt1*, *Krt5*, *Krt6a*, *Krt14*, *Krt16*, *Krt17*), in addition to a smaller high confidence network of protein homeostasis regulators (i.e., eukaryotic translation initiation factor 2, *Eif2s3x*; eukaryotic translation initiation factor 4 gamma 2, *Eif4g2*; proteasome 20s subunit beta 3, *Psmb3*; 26S proteasome regulatory subunit 4, *Psm4*) that all exhibited reduced

expression levels in *Obscn-ΔIg58/59* atria (Figure 4B). Lastly, STRING analysis of the deregulated phospho-proteins at 12-months revealed an extensive high confidence network comprised of 23 interconnected sarcomeric proteins, cytoskeletal proteins, ion channels,  $Ca^{2+}$  regulators, and kinases (Figure 4B'). Of note, titin represents the most prominent node in the phospho-proteomic network at both timepoints, forming functional and/or physical associations with 4/6 (66%) and 10/23 (43%) of the phospho-proteins that were deregulated at 6- or 12-months, respectively. Given that titin is a binding partner of the obscurin Ig58/59



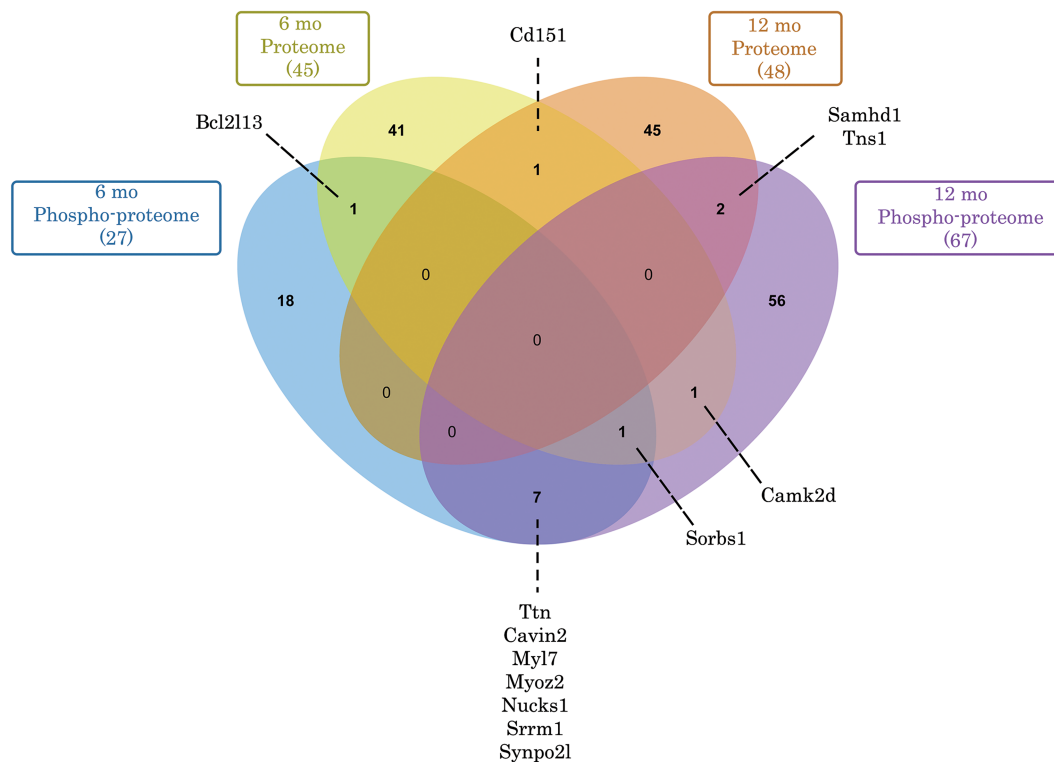


FIGURE 5

Venn diagram depicting commonly deregulated proteins and phospho-proteins in *Obscn-ΔIg58/59* atria through aging. Of the 45 (6-months) and 48 (12-months) proteins that exhibited significantly deregulated expression in *Obscn-ΔIg58/59* atria, only 1 (Cd151) was deregulated at both timepoints. In contrast, of the 27 (6-months) and 67 (12-months) deregulated phospho-proteins in *Obscn-ΔIg58/59* atria, a total of 8 (Ttn, Cavin2, Myl7, Myoz2, Nucks1, Srrm1, Synpo2l, and Sorbs1) were consistently deregulated through aging, albeit at different sites and/or affected in opposite directions at 6- versus 12-months (Supplementary Tables S2, S4). Lastly, CaMKII $\delta$  exhibited deregulated expression at 6-months and altered phosphorylation at 12-months in *Obscn-ΔIg58/59* atria. Venn diagram generated with jvenn (84).

module, this suggests that the disruption of the obscurin/titin complex could be integral to the deregulated phosphorylation events in *Obscn-ΔIg58/59* atria.

To more quantitatively delineate the major molecular pathways and cellular functions that were impacted by the Ig58/59 deletion, we performed an enrichment analysis on the proteins that exhibited significantly altered expression or phosphorylation levels (Figures 6A,B, 7A,B; Supplementary Tables S5–S8). At 6-months, proteins exhibiting altered expression were associated with the regulation of inositol phosphate metabolism (Figures 6A,B; Supplementary Table S5), whereas at 12-months, proteins exhibiting altered expression largely belonged to the keratin subfamily of intermediate filaments (Figures 7A,B; Supplementary Table S7). Additionally, proteins displaying altered phosphorylation were primarily associated with the regulation of cellular assembly/organization (i.e., organization of sarcomeres, filaments, and microtubules), ion transport, and cardiac hypertrophy at 6-months (Figures 6A,B; Supplementary Table S6) and various signaling cascades (i.e., protein kinase A; PKA, integrin, apelin, and Ca<sup>2+</sup> cycling), striated muscle development, formation, morphology, and hypertrophy, as well as cardiomyopathy and familial arrhythmogenic right ventricular dysplasia at 12-months (Figures 7A,B; Supplementary Table S8).

Given the large number of deregulated proteins and phosphorylation events identified in our proteomic screen, we decided to focus on (1) direct alterations to obscurin, and (2) proteins that belong to enriched molecular pathways or cellular functions and represent nodes within high confidence protein networks identified *via* STRING analysis. Of note, we discuss these deregulated proteins and phospho-proteins in

terms of their canonical protein class since many of them belong to multiple affected cellular processes and/or protein interaction networks.

## Alterations in obscurin in aging *Obscn-ΔIg58/59* atria

At 12-months of age, we observed a significant, yet modest, reduction (~1.8 fold) in the expression levels of obscurin in *Obscn-ΔIg58/59* atria compared to wild-type (Figure 4A; Supplementary Table S3). Of note, the lack of statistical significance in our immunoblotting analysis (Figures 1C,C') that revealed only a trend toward decreased obscurin expression in *Obscn-ΔIg58/59* atria (~1.1 fold;  $p = 0.3$ ), is most likely due to the reduced sensitivity of the immunoblotting technique compared to proteomics. Nevertheless, complete knockout or down-regulation of obscurin in striated muscles has been linked to major structural defects, including the disorganization of the longitudinal SR (33), disrupted thick filament assembly (34) and lateral alignment of myofibrils (35), loss of dystrophin at costameres, and alterations in the arrangement of the subsarcolemmal microtubule lattice (36). Therefore, this moderate reduction in obscurin expression in aged *Obscn-ΔIg58/59* atria could indicate a mild loss in the structural integrity of the myofibril, the cytoskeleton, and/or the SR membranes. Accordingly, obscurin expression levels are also reduced in human cardiac biopsies carrying DCM-linked point mutations in *OBSCN* (E963K, V2161D, or D5966N) (37), substantiating that obscurin haploinsufficiency is pathogenic in the heart.

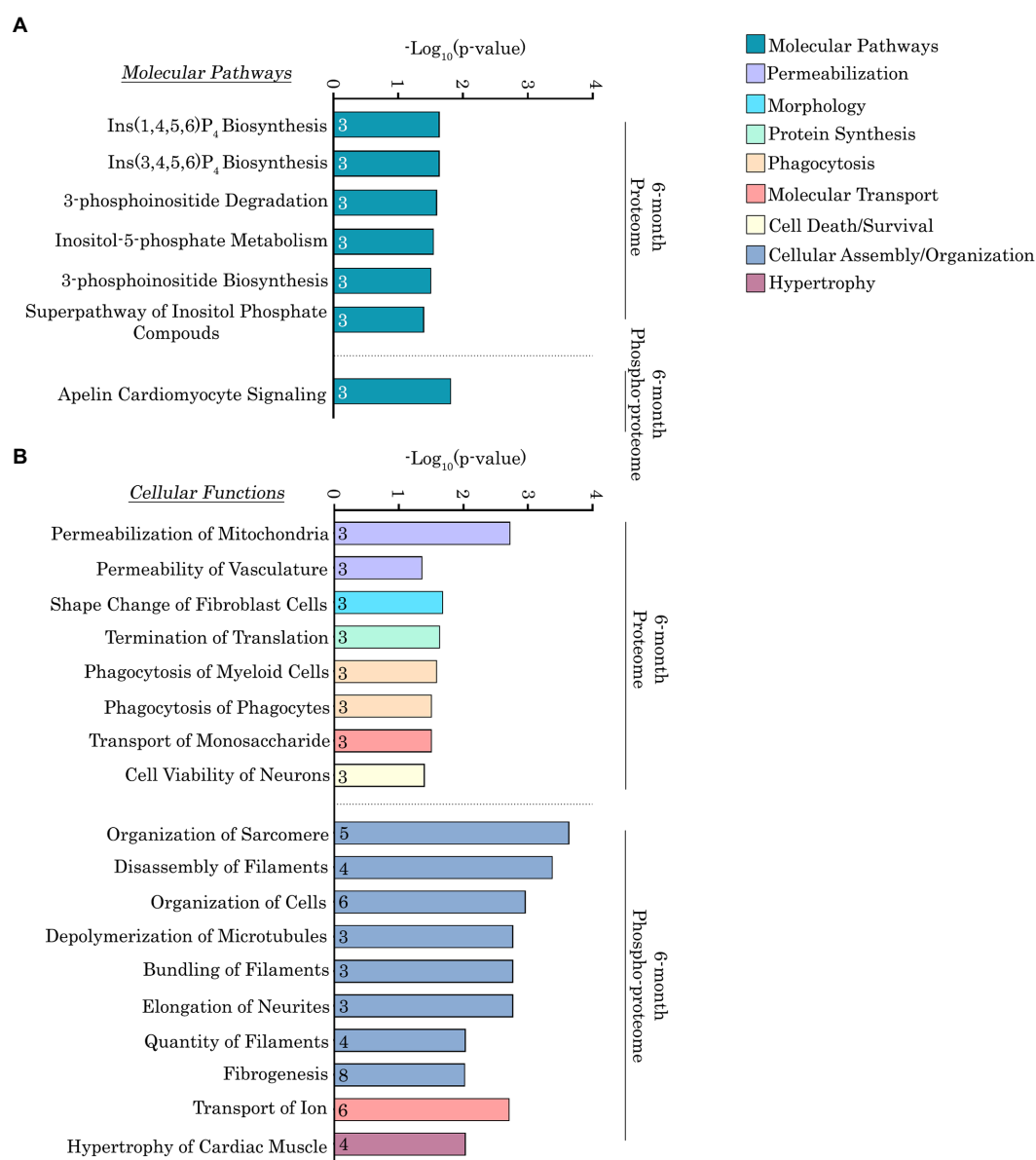


FIGURE 6

Ingenuity pathway analysis of the deregulated proteins and phospho-proteins in *Obscn-ΔIg58/59* atria at 6-months. (A,B) The molecular pathways (A) and cellular functions (B) associated with proteins that exhibited significantly altered expression or phosphorylation in 6-month-old *Obscn-ΔIg58/59* atria. The number of proteins associated with each biological process is indicated within the respective bar.

## Alterations in cytoskeletal and structural regulators in aging *Obscn-ΔIg58/59* atria

In addition to the essential cytoskeletal protein obscurin, a striking portion of the deregulated proteins and phospho-proteins in aging *Obscn-ΔIg58/59* atria were canonical cytoskeletal and structural regulators. In particular, the Ig58/59 deletion induced profound abnormalities in the expression and/or phosphorylation of intermediate filaments, sarcomeric proteins, Z-disk-associated and/or actin-linked cytoskeletal modulators, and structural components of the costamere.

### Intermediate filaments: Keratins

At 12-months, the expression levels of seven different keratin isoforms, including keratins 1, 5, 6A, 14, 16, 17, and 42, were significantly

reduced in *Obscn-ΔIg58/59* atria (Figure 4A; Supplementary Table S3). Although keratins have not been extensively studied in the heart, studies evaluating keratin 19-deficient skeletal muscles show that they contribute to the organization of the costamere and the development of contractile force. Therefore, these findings indicate a drastic loss of intermediate filament proteins that are integral to the organization of costameres and force development in striated muscles (38, 39).

### Sarcomeric cytoskeleton: Titin, T-cap, MyBPC-3, and Myosin Light Chain 7

Our phospho-proteomic analysis revealed age-related alterations in the phosphorylation status of titin in *Obscn-ΔIg58/59* atria. In particular, we observed decreased levels of a bi-phosphorylated peptide, Ser34063/Ser-Thr-Tyr<sub>34062-34,080</sub>, localizing to the titin M-band interdomain

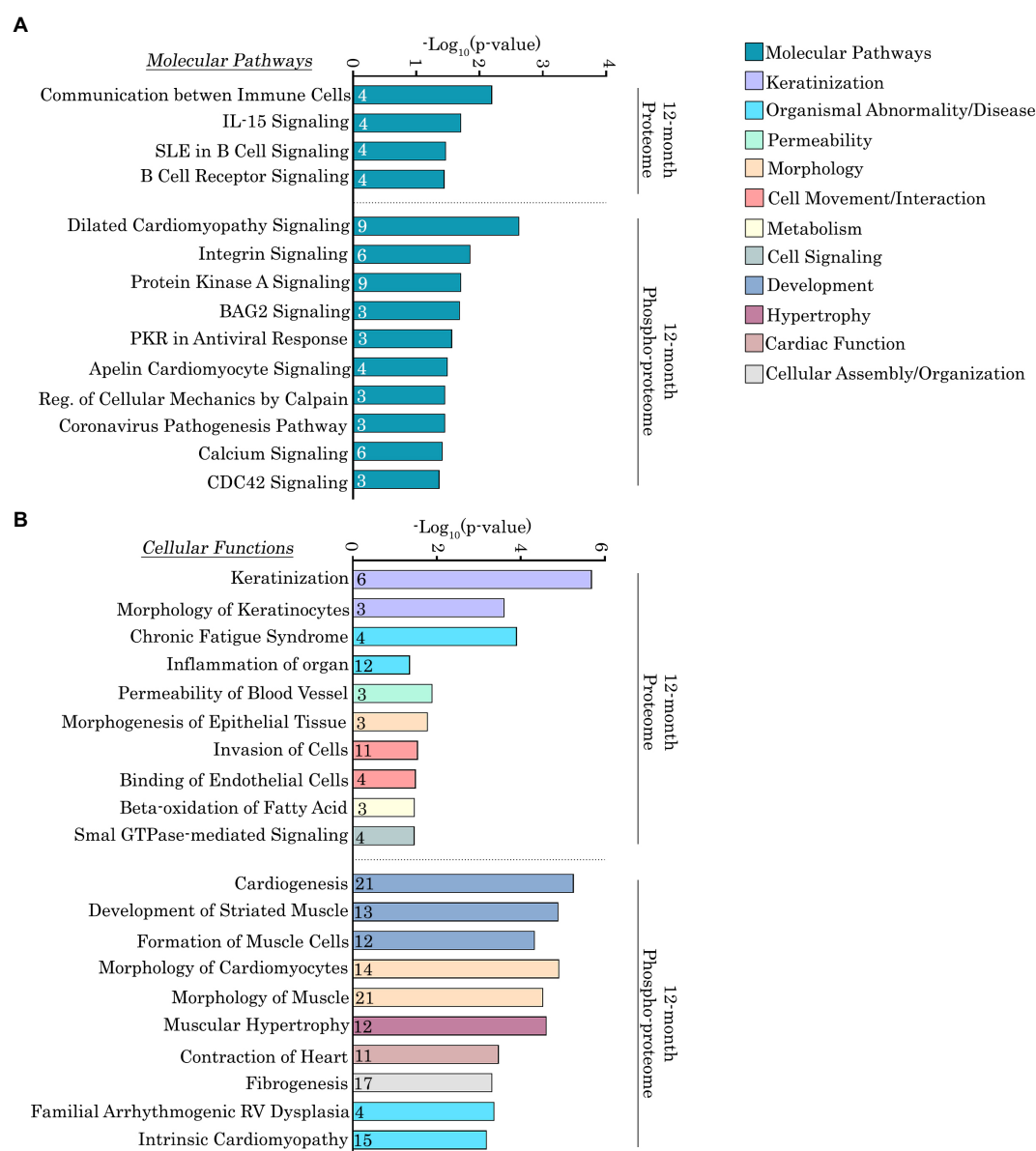


FIGURE 7

Ingenuity pathway analysis of the deregulated proteins and phospho-proteins in *Obscn-ΔIg58/59* atria at 12-months. (A,B) The molecular pathways (A) and cellular functions (B) associated with proteins that exhibited significantly altered expression or phosphorylation in 12-month-old *Obscn-ΔIg58/59* atria. The number of proteins associated with each biological process is indicated within the respective bar.

sequence 2 (Mis2) in *Obscn-ΔIg58/59* atria compared to wild-type at 6-months (Figure 3A; Supplementary Table S2). The physiological function(s) of these phosphorylation events are not yet known, however the titin Mis2 region has been previously established as a binding site for DRAL/FHL2 (40). DRAL/FHL2 is a member of the four and a half LIM domain protein family that is thought to target metabolic enzymes to the M-band *via* binding to titin Mis2 (2, 40). Therefore, the deregulated phosphorylation of titin within Mis2 in *Obscn-ΔIg58/59* atria could potentially influence metabolic complexes that localize to the M-band. Along these lines, recent proteomic studies from our group and others conducted in heart or skeletal muscle where obscurin is either mutated (29) or deleted (41) have also reported alterations in proteins involved in metabolism, specifically lipid catabolism and amino acid metabolism (29) or glycogen metabolism (41).

Titin phosphorylation was also deregulated in *Obscn-ΔIg58/59* atria at 12-months at three distinct locations: a bi-phosphorylated peptide corresponding to the Mis2 region of titin (Ser33875/Ser33880), a site within the M-band (Ser34470), and a site within titin-Ig76/77 (Ser9459; Figure 4A; Supplementary Table S4). Interestingly, the Ser34470 residue which exhibited enhanced phosphorylation resides within the third Lys-Ser-Pro (KSP) motif in titin-Mis4. Of note, the KSP motifs have been shown to be highly phosphorylated during development in muscle and are thought to regulate the assembly of the M-band (42). Thus, these findings are in line with the significantly increased atrial mass observed in *Obscn-ΔIg58/59* atria at 12-months (10) in addition to our pathway analysis that indicated alterations in developmental processes such as cardiogenesis, striated muscle development, and the morphology of cardiomyocytes.

Telethonin, also known as Titin-cap or T-cap, is a Z-disk associated protein that binds to titin's extreme NH<sub>2</sub>-terminal Ig1/2 domains where it is proposed to regulate sarcomeric development, stability, and stretch responses (43, 44). Our proteomic screen revealed reduced phosphorylation of T-cap at Ser161 in *Obscn-ΔIg58/59* atria at 12-months (Figure 4A'; Supplementary Table S4). Candasamy et al. (44) previously reported that endogenous T-cap is constitutively bi-phosphorylated by both protein kinase D and CaMKII at Ser157 and Ser161 in rodent myocardia, and that disruption of these phosphorylation events results in disorganized t-tubule structures and abnormal Ca<sup>2+</sup> cycling. Given that the COOH-terminal region of T-cap containing Ser157/Ser161 binds accessory proteins that localize to t-tubules, it has been further suggested that Ser157/Ser161 phosphorylation may regulate T-cap's ability to serve as an "adapter protein" linking t-tubules to the Z-disk (44). An important observation is that the obscurin-Ig58/59 binding site on titin (Ig9/10) exists in relative proximity to T-cap's binding site to titin (i.e., titin-Ig1/2). It is therefore conceivable that the Ig58/59 deletion could possibly disrupt the titin/T-cap complex at the Z-disk and/or influence the nearby regulatory networks that mediate Ser161 phosphorylation. Along these lines, the observed reduction of Ser161 phosphorylation in 12-month *Obscn-ΔIg58/59* atria could possibly lead to disorganized t-tubule morphology, disrupted Ca<sup>2+</sup>-induced Ca<sup>2+</sup>-release, and potentially contribute to the development of arrhythmia.

Lastly, we saw altered phosphorylation levels of proteins localizing to the thick filament in *Obscn-ΔIg58/59* atria through aging, including myosin light chain 7 and myosin binding protein-C (MyBP-C). In particular, we observed a ~60-fold decrease in the phosphorylation of Ser22 on myosin light chain 7 at 6-months (Figure 3A'; Supplementary Table S2), which is the atrial myosin regulatory light chain isoform. The exact function of this phosphorylation event is not thoroughly characterized, though it was previously shown to be mediated by myosin light chain kinase in response to α-adrenergic signaling (45). Moreover, phosphorylation of Ser23 on myosin light chain 7, immediately adjacent to the phosphorylation site Ser22 that was deregulated in *Obscn-ΔIg58/59* atria at 6-months, was significantly reduced at 12-months (Figure 4A'; Supplementary Table S4). Furthermore, we also identified a novel phosphorylation event on cardiac MyBP-C, Ser268, which exhibited a ~2.5-fold reduction in phosphorylation in 12-month old *Obscn-ΔIg58/59* atria (Figure 4A'; Supplementary Table S4). Importantly, this phosphorylation site localizes within the M-motif (between Ig domains C1 and C2), which is well established as a phosphorylation 'hot-spot' for cardiac MyBP-C. Previous studies have shown that reduced phosphorylation of cardiac MyBP-C within the M-motif is associated with the development of heart failure in mice and results in reduced rates of contraction and relaxation. It is therefore possible that reduced phosphorylation of Ser268 on cardiac MyBP-C and/or Ser23 on myosin light chain 7 could indicate deregulation of contractility in *Obscn-ΔIg58/59* atria at 12-months.

### Actin-linked and/or Z-disk-associated cytoskeleton: Plectin, Cortactin, Myozenin, Synaptopodin 2-l, LIM-domain-binding protein 3, Myospryn

Plectin, a cytoskeletal protein that forms physical links between actin, microtubules, and intermediate filaments, exhibited increased

phosphorylation at Ser4415 in *Obscn-ΔIg58/59* atria at 12-months (Figure 4A'; Supplementary Table S4). Additionally, cortactin, a scaffold protein that regulates the polymerization and stabilization of the actin cytoskeleton, exhibited decreased phosphorylation at a tri-phosphorylated peptide, Thr401/Ser405/Ser407 (Figure 4A'; Supplementary Table S4). Phosphorylation of the Thr401/Ser405 residues on cortactin, mediated by Erk (Ser405) (46), Akt (Thr401/Ser405) (47), and/or PKCδ (Ser405) (48), promotes actin polymerization and cell migration *via* enhancing the interaction between cortactin and actin nucleation promoting factors. Together, these results demonstrate alterations in the phosphorylation status of proteins regulating the assembly and organization of the actin cytoskeleton in 12-month *Obscn-ΔIg58/59* atria.

Our proteomic results indicated deregulated phosphorylation of three additional actin-associated proteins in *Obscn-ΔIg58/59* atria. In particular, phosphorylation of synaptopodin 2-like, which is a member of the synaptopodin family of proteins that regulate actin polymerization at the Z-disk, was altered at Ser89/Ser-Thr<sub>83-126</sub> and Thr88/Ser97 at 6-months and 12-months, respectively (Figures 3A', 4A'; Supplementary Tables S2, S4). Of note, Thr88 represents a novel phosphorylation event on synaptopodin 2-like. In addition, LIM-domain-binding protein 3, also known as Z-band alternatively spliced PDZ motif protein (ZASP), displayed decreased phosphorylation at Thr119/Ser123 in *Obscn-ΔIg58/59* atria at 6-months (Figure 3A'; Supplementary Table S2). LIM-domain-binding protein 3 (ZASP) is a cytoskeletal protein that regulates Z-disk integrity and signal transduction through forming complexes with an array of Z-disk proteins, including α-actinin-2 (49, 50), myozenin (51, 52), myotilins (myotilin, myopalladin, and palladin) (52), and telethonin/Tcap (53). Accordingly, the phosphorylation status of ZASP-interactive myozenin was also disrupted at phosphorylated peptides Ser95/Ser116 and Thr111/Ser116/Ser-Thr-Tyr<sub>92-132</sub> at 6-months, and Thr107 at 12-months (Figures 3A', 4A'; Supplementary Tables S2, S4). Together, these findings provide strong evidence that major cytoskeletal signaling complexes at the level of the Z-disk/thin filament are disrupted in *Obscn-ΔIg58/59* atria throughout aging.

### Dystrophin complex at the costamere: Dystrophin, Vinculin, Synemin

Several proteins that serve as integral components of the dystrophin/dystroglycan complex and/or form structural links between the costamere and the cytoskeleton exhibited altered phosphorylation in *Obscn-ΔIg58/59* atria at 12-months. In particular, synemin, an intermediate filament protein that mediates the lateral transmission of force and maintains the structural integrity of the myofibril during mechanical stress, exhibited increased phosphorylation at Ser1087 in *Obscn-ΔIg58/59* atria (Figure 4A'; Supplementary Table S4). Synemin is present at the level of the Z-disk where it interacts with α-actinin, desmin, vinculin, and components of the dystrophin glycoprotein complex (54). Interestingly, vinculin, which links integrins to the actin cytoskeleton, exhibited increased phosphorylation at Ser721 in *Obscn-ΔIg58/59* atria at 12-months (Figure 4A'; Supplementary Table S4). Furthermore, the abundance of a phospho-peptide corresponding to dystrophin, Ser-Thr<sub>3624-3,664</sub>, was decreased (Figure 4A'; Supplementary Table S4). Together, these results suggest phosphorylation defects in protein complexes that contribute to the formation of cytoskeletal links between the sarcomere and the extracellular matrix.



## Gap junctions: Connexin-43

We also identified altered phosphorylation levels of connexin-43, the core protein that comprises gap junctions, in *Obscn-ΔIg58/59* atria at 12-months. In particular, we saw increased phosphorylation of connexin-43 at Ser325/Thr326, and decreased levels of the phosphopeptide, Ser-Thr<sub>320-345</sub> (Figure 4A'; Supplementary Table S4). Notably, the phosphorylation of Ser325 on connexin-43, along with nearby residues Ser328 and Ser330, is mediated by casein kinase 1 and has been shown to stabilize the formation of gap junctions at the intercalated disc (55). Thus, up-regulation of pSer325 on connexin-43 could indicate enhanced gap junction formation in *Obscn-ΔIg58/59* atria at 12-months and potentially impacting synchronous cardiomyocyte contraction therefore underlying arrhythmic events.

In summary, our proteomic screen revealed extensive abnormalities in the expression and phosphorylation status of major structural regulators in aging *Obscn-ΔIg58/59* atria, including proteins that regulate the assembly and organization of the myofibril, form gap junctions, physically link the sarcomere to the surrounding membranes, and are integral components of the Z-disk associated cytoskeleton. Notably, obscurin and titin, two key cytoskeletal regulators, interact at the level of the Z-disk (8). Given that the Z-disk is a region that integrates proteins of the sarcomere and the surrounding cellular structures, including the cytoskeleton, intercalated disc, and plasma membrane (56), it is interesting to speculate that the disrupted binding between obscurin-Ig58/59 and titin could severely affect the stability and/or regulation of protein complexes that localize to this region. Moreover, many cytoskeletal proteins that localize to the Z-disk, particularly those forming connections to the extracellular matrix *via* costameres, aid in the transmission of force and mediate mechanical transduction pathways (56). Therefore, our proteomics and phospho-proteomics findings could reflect pathological alterations in the stabilization of the myofibril during mechanical stress in *Obscn-ΔIg58/59* atria.

## Alterations in regulatory proteins and signaling mediators in aging *Obscn-ΔIg58/59* atria

Our proteomic and phospho-proteomic analysis also revealed alterations in the expression and phosphorylation of regulatory proteins and signaling mediators in aging *Obscn-ΔIg58/59* atria. Specifically, we observed alterations in canonical regulators of Ca<sup>2+</sup> cycling and major protein kinases that could potentially contribute to the development of atrial fibrillation in *Obscn-ΔIg58/59* mice.

### Calcium cycling proteins: SERCA2, SERCA3, RyR2, HRC

Our phospho-proteomic screen and subsequent enrichment analysis identified several differentially phosphorylated Ca<sup>2+</sup> cycling regulators in *Obscn-ΔIg58/59* atria at 6- and 12-months. At 6-months, we identified a novel phosphorylation site localized within the hydrolase domain of SERCA3, Ser729, which was significantly reduced in *Obscn-ΔIg58/59* atria (Figure 3A'; Supplementary Table S2). SERCA3 was originally thought to be exclusively expressed in non-muscle tissues, however, SERCA3 isoforms were ultimately detected in normal human LV tissue as well (57). Notably, a significant distinction between SERCA3 and the more abundantly expressed SERCA2a isoform is that SERCA3 is unable to bind PLN

(58). Given that loss of binding between Ig58/59 and PLN in *Obscn-ΔIg58/59* atria could lead to enhanced inhibition of SERCA2 (*via* loss of Ig58/59-mediated sequestration of PLN), it is possible that the decreased phosphorylation of SERCA3 at Ser729 at 6-months could serve as a compensatory response. Moreover, at 12-months, we observed a significant reduction in the levels of the SERCA2 phospho-peptide, Ser-Thr-Tyr<sub>372-397</sub>, demonstrating potential abnormalities in Ca<sup>2+</sup> reuptake into the SR through aging (Figure 4A'; Supplementary Table S4).

Histidine rich Ca<sup>2+</sup> binding protein (HRC), a protein that localizes to the SR lumen where it regulates Ca<sup>2+</sup> storage and release (59), exhibited reduced phosphorylation at Ser272 in *Obscn-ΔIg58/59* atria at 12-months (Figure 4A'; Supplementary Table S4). Although this phosphorylation site has not been experimentally characterized, previous studies have suggested that phosphorylation of HRC by casein kinase II regulates RyR2 function in skeletal muscle (59, 60). Importantly, we also observed up-regulation of phosphorylated Ser2810 (Ser2811 in humans) on RyR2 in *Obscn-ΔIg58/59* atria at 12-months (Figure 4A'; Supplementary Table S4). Hyper-phosphorylation of RyR2, specifically at the canonical Ser2808 and Ser2814 sites (human notation), has been strongly linked to enhanced RyR2 open probability and susceptibility to arrhythmia (25, 26). Although there is still controversy regarding the roles of individual RyR2 phosphorylation sites and their potential functional redundancies, it is generally accepted that the “phosphorylation hot-spot” in RyR2 encompassing human Ser2808 through Ser2814 (26) is an effective modulator of Ca<sup>2+</sup> release from the SR. In addition to the Ser2808 and Ser2814 sites which are regulated by CaMKII and/or PKA, there are two additional sites within the hot-spot, Thr2810 and Ser2811, for which less information is known, although both are predicted to impact RyR2 function similarly to Ser2808 and Ser2814 (26, 27). Therefore, hyper-phosphorylation of RyR2 at Ser2810 (human Ser2811) combined with altered HRC phosphorylation in *Obscn-ΔIg58/59* atria could potentially lead to abnormal Ca<sup>2+</sup> release and/or Ca<sup>2+</sup> leak from the SR in *Obscn-ΔIg58/59* atria at 12-months.

### Kinases: CaMKIIδ, SPEG, MAPKs, myosin light chain kinase 3

In addition to proteins directly regulating Ca<sup>2+</sup> homeostasis, we also identified alterations in the expression and phosphorylation of several kinases in our proteomic screen including Ca<sup>2+</sup>/calmodulin-dependent protein kinase δ (CaMKIIδ) and striated muscle preferentially expressed gene (SPEG). CaMKIIδ is one of the major protein kinases that regulates Ca<sup>2+</sup> dynamics in the heart *via* phosphorylation of Ca<sup>2+</sup> handling proteins in response to physiological and/or pathological stimuli (61, 62). Importantly, the expression level of CaMKIIδ was ~2.5 fold lower in *Obscn-ΔIg58/59* atria compared to wild-type at 6-months (Figure 3A; Supplementary Table S1). At 12-months, CaMKIIδ abundance was no longer altered, but its phosphorylation was increased at both Thr331 and another site within the Ser-Thr<sub>323-344</sub> region (Figure 4A'; Supplementary Table S4). The physiological significance of pThr331 has not yet been experimentally determined. However, the deregulation of CaMKIIδ in aged *Obscn-ΔIg58/59* male atria along with its preeminent role in cardiac hypertrophy makes it a key target for future investigation.

Our phospho-proteomic analysis also identified a novel phosphorylation site, Ser2200, that localizes to the inter-kinase

region of SPEG, a paralog of obscurin that arose from gene duplication of *OBSCN*, that was significantly decreased in *Obscn-ΔIg58/59* atria at 12-months (Figure 4A'; Supplementary Table S4). SPEG, sharing high homology to obscurin, also possesses two tandem kinase domains at its COOH-terminus (termed SK1 and SK2, highly homologous to obscurin Kin1 and Kin2) that have been implicated in the regulation of  $\text{Ca}^{2+}$  homeostasis (63). In addition to Ser2200, SPEG also exhibited decreased phosphorylation at Ser2182, which is located within the same inter-kinase region (Figure 4A'; Supplementary Table S4). The functions of these phosphorylation events are not known, but they could potentially affect the substrate specificities and/or activities of SPEG SK1, which phosphorylates junctophilin 2, and/or SPEG SK2, that phosphorylates SERCA2 and possibly RyR2 (63).

Additionally, phosphorylation of myosin light chain kinase 3 was decreased at Ser155 in *Obscn-ΔIg58/59* atria at 12-months (Figure 4A'; Supplementary Table S4). Although the function of this site is not precisely known, this finding could corroborate the reduction in phosphorylation of its substrate, myosin regulatory light chain 7, that we also observed in *Obscn-ΔIg58/59* atria (Figure 4A'; Supplementary Table S4). Lastly, we observed altered phosphorylation levels of mitogen-activated protein kinase 1 (MAPK1) and 14 (MAPK14) at Thr183/Thr188 (up-regulated) and Thr185 (down-regulated), respectively (Figure 4A'; Supplementary Table S4). MAPKs are a family of highly conserved signaling mediators that regulate a diverse set of cellular processes such as proliferation, cell death/survival, transcription, migration, and differentiation by phosphorylating hundreds of downstream targets. In the heart, MAPK1 and MAPK14 isoforms regulate cardiac development and differentiation and promote the hypertrophic response (64). Importantly, Thr183/Thr188 and Thr185 reside within the regulatory loop of MAPK1 and MAPK14. In fact, Thr183 in MAPK1 is part of the canonical Thr-Glu-Tyr motif, which is phosphorylated by the upstream kinase, MEK1/2 (65, 66).

Lastly, tyrosine hydroxylase, the rate limiting enzyme involved in the synthesis of catecholamines such as epinephrine and norepinephrine, exhibited reduced phosphorylation at Thr30 in *Obscn-ΔIg58/59* atria at 12-months (Figure 4A'; Supplementary Table S4). While not a kinase itself, alteration of tyrosine hydroxylase could impact adrenergic activity and/or downstream PKA signaling in *Obscn-ΔIg58/59* atria.

## Conclusion

Collectively, our proteomics and phospho-proteomics data demonstrated extensive alterations in the expression and phosphorylation status of proteins involved in diverse cellular processes, including major  $\text{Ca}^{2+}$  cycling regulators, protein kinases, and cytoskeletal protein complexes associated with the Z-disk that likely drive atrial structural remodeling and arrhythmogenesis in *Obscn-ΔIg58/59* male mice. It is interesting to note the lack of proteins that consistently exhibit altered expression in *Obscn-ΔIg58/59* atria at both timepoints (Figure 5). In contrast, multiple phospho-proteins are affected throughout aging in *Obscn-ΔIg58/59* atria including titin (*Ttn*), caveolae associated protein 2 (*Cavin2*), myosin light chain 7 (*Myl7*), myozenin 2 (*Myoz2*), nuclear casein kinase and cyclin-dependent kinase substrate 1 (*Nucks1*), sorbin and SH3 domain containing 1 (*Sorbs1*), serine/arginine repetitive matrix 1 (*Srrm1*),

and synaptopodin 2-like (*Synpo2l*; Figure 5). Notably, several of these proteins (i.e., titin, myosin light chain 7, myozenin, and synaptopodin 2-like) also constitute core components of the phospho-proteomic STRING networks at both timepoints, comprising 4/6 of the functionally and/or physically interconnected phospho-proteins at 6-months or contribute to a much larger network composed of 23 interconnected phospho-proteins at 12-months. Together, these observations suggest that these commonly deregulated phospho-proteins could represent key players in disease development due to deletion of obscurin-Ig58/59, and that disrupted phosphorylation events could largely contribute to the progressive pathologies that manifest through aging.

Along these lines, our proteomics analysis revealed alterations in the expression and/or phosphorylation status of major protein kinases in aging *Obscn-ΔIg58/59* atria, including CaMKII $\delta$  and MAPK1 and 14. To corroborate our proteomics findings and underscore the contribution of deregulated phosphorylation to the *Obscn-ΔIg58/59* disease phenotype, we performed immunoblots evaluating the expression and phosphorylation levels of two major deregulated kinases in *Obscn-ΔIg58/59* atria that are amenable to validation due to the availability of relevant (phospho)-antibodies. In contrast to our proteomics results (Figure 3A; Supplementary Table S1), we were not able to confirm decreased expression of CaMKII $\delta$  in *Obscn-ΔIg58/59* atria at 6-months *via* immunoblot analysis (Figures 8A,A'), possibly reflecting the reduced sensitivity of immunoblotting techniques compared to proteomics, or a potential artifact in our proteomics data. We next evaluated the phosphorylation levels of MAPK1 (also known as ERK2) at pThr183/pTyr185, given that our phospho-proteomic screen revealed a 2.35-fold increase in the levels of the bi-phosphorylated peptide, Thr183/Thr188, in *Obscn-ΔIg58/59* atria at 12-months (Figure 4A'; Supplementary Table S4). Consistent with our proteomics results, our immunoblotting analysis revealed a 2.89-fold increase in the phosphorylation of the canonical activation motif, pThr183/pTyr185 (Figures 8B,B'), demonstrating up-regulated MAPK1 activity in 12-month *Obscn-ΔIg58/59* atria. Given the established role of MAPK1 in the hypertrophic response and atrial fibrillation (64, 67–69), this may contribute to the development of progressive remodeling and/or arrhythmogenesis in aging *Obscn-ΔIg58/59* atria.

In addition to potential hypertrophic remodeling mediated by MAPKs, the abundance of deregulated cytoskeletal proteins in *Obscn-ΔIg58/59* atria (particularly those localizing to the Z-disk) suggests abnormalities in the organization of sarcomeres and the cellular structures that form connections to the Z-disk (i.e., t-tubules, the intercalated disc, costameres). In particular, the dramatic reduction in keratin protein levels, and decreased phosphorylation of residues with defined (patho)physiological functions such as T-cap (Ser161), cortactin (Thr401/Ser405/Ser407), and connexin-43 (Ser325), implicate disrupted cytoskeletal structures, t-tubules, and intercalated discs in *Obscn-ΔIg58/59* atria at 12-months. Interestingly, we did not observe any major defects in myofibril or sarcomeric ultrastructure in our evaluation of *Obscn-ΔIg58/59* left ventricles (10), suggesting potential distinctions in the cellular and molecular pathogenesis of the Ig58/59 deletion between cardiac chambers. Along these lines, neither our immunoblotting nor our proteomics analysis revealed reduced phosphorylation of PLN (Thr17) or RyR2 (Ser2814) in aging *Obscn-ΔIg58/59* atria, which were both significantly decreased in *Obscn-ΔIg58/59* left ventricles (10). In contrast, RyR2 was hyperphosphorylated at a distinct site, Ser2810

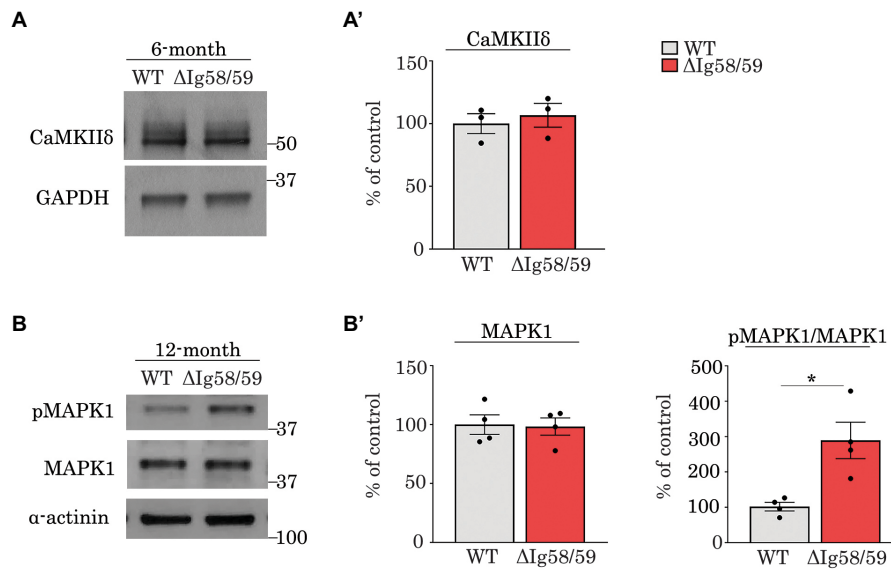


FIGURE 8

Immunoblot analysis confirmed up-regulation of phosphorylated MAPK1 in 12-month old *Obscn-ΔIg58/59* atria. (A,A') Representative immunoblots (A) and relative quantifications (A') did not reveal statistically significant alterations in the expression of CaMKIIδ in lysates prepared from 6-month-old wild-type and *Obscn-ΔIg58/59* atria; *t*-test, *p*=0.62. (B,B') Representative immunoblots (B) and relative quantifications (B') revealed an up-regulation of phosphorylated MAPK1 (also known as ERK2) at its canonical activation motif, pThr183/Tyr185, in *Obscn-ΔIg58/59* atria at 12-months but no differences in total MAPK1/ERK2 levels; *t*-test, *p*<0.05, α-actinin and GAPDH served as loading controls; *n*=3–4 animals per group; data points represent the average of at least two technical replicas; quantification of phosphorylation levels are normalized to total MAPK1/ERK2 levels.

(human Ser2811), in *Obscn-ΔIg58/59* atria at 12-months. Our future studies will more closely interrogate the cellular impacts of the Ig58/59 deletion specifically in atrial tissues to determine how chamber-specific molecular alterations caused by the Ig58/59 deletion affect atrial structure and function.

Our physiological evaluations of the *Obscn-ΔIg58/59* model revealed the presence of severe arrhythmia characterized by episodes of junctional escape and the sporadic loss of regular p-waves reminiscent of atrial fibrillation (10). Atrial fibrillation represents the most common type of sustained arrhythmia in humans and its prevalence increases substantially with aging (70, 71). The entire complex of structural, architectural, contractile, and electrophysiological alterations occurring in diseased atrial myocardium has recently established “atrial cardiomyopathy” as a new disease entity (72). Previous proteomic efforts aiming to characterize the molecular changes underlying atrial fibrillation and/or atrial cardiomyopathy in animals (73, 74) and humans (75–82) have similarly reported alterations in structural and metabolic proteins, ion channels and Ca<sup>2+</sup> regulators (82). However comprehensive phospho-proteomic analyses remain scarce, although they are integral to deciphering the role of phosphorylation in the pathogenesis of atrial fibrillation (83). Nonetheless, the discovery of novel and/or uncharacterized phosphorylation events *via* phospho-proteomic screens must be further validated *in situ* and *in vivo* and investigated in terms of pathophysiological and functional relevance.

In summary, to our knowledge, the present study is the first to evaluate the atrial phospho-proteome through aging using a genetic model of spontaneous atrial arrhythmia and remodeling. Given the presence of both structural and regulatory proteins exhibiting deregulated expression and/or phosphorylation in aging *Obscn-ΔIg58/59* atria (including many phosphorylation events with unknown functions), our present findings reveal numerous molecular

targets associated with novel and/or uncharacterized pathways to be interrogated in future studies and provides new mechanistic insights into atrial remodeling and dysfunction.

## Data availability statement

The data presented in the study are deposited in the Proteome Xchange Consortium via the Pride partner repository, accession number PXD028904.

## Ethics statement

The animal study was reviewed and approved by the Institutional Animal Care and Use Committee at the University of Maryland, School of Medicine. Written informed consent for participation was not obtained from the owners because the animal model that was used was generated in the Senior and Corresponding Author's lab using a commercial source, therefore no written consent was required.

## Author contributions

AG: conceptualization, methodology, validation, formal analysis, investigation, writing original draft, and review and editing. WH: methodology, validation, formal analysis, review and editing. AB: methodology, formal analysis, review and editing. MK: methodology, validation, formal analysis, review and editing. AK-K: conceptualization, review and editing, supervision, project administration, and funding acquisition. All authors contributed to the article and approved the submitted version.



## Funding

This work was supported by the National Institutes of Health Training Program in Muscle Biology, T32 AR007592 to AG, and R01AR077106 to AK-K. Additional support was provided by the University of Maryland School of Pharmacy Mass Spectrometry Center (SOP1841-IQB2014).

## Conflict of interest

The authors declare that the research was conducted in the absence of any commercial or financial relationships that could be construed as a potential conflict of interest.

## References

- Kontogianni-Konstantopoulos, A, Ackermann, MA, Bowman, AL, Yap, SV, and Bloch, RJ. Muscle giants: molecular scaffolds in sarcomerogenesis. *Physiol Rev.* (2009) 89:1217–67. doi: 10.1152/physrev.00017.2009
- Wang, L, Geist, J, Grogan, A, Hu, LR, and Kontogianni-Konstantopoulos, A. Thick filament protein network, functions, and disease association. *Compr Physiol.* (2018) 8:631–709. doi: 10.1002/cphy.c170023
- Grogan, A, and Kontogianni-Konstantopoulos, A. Unraveling obscurins in heart disease. *Pflugers Arch.* (2019) 471:735–43. doi: 10.1007/s00424-018-2191-3
- Chen, P, Xiao, Y, Wang, Y, Zheng, Z, Chen, L, Yang, X, et al. Intracellular calcium current disorder and disease phenotype in OBSCN mutant iPSC-based cardiomyocytes in arrhythmogenic right ventricular cardiomyopathy. *Theranostics.* (2020) 10:11215–29. doi: 10.7150/thno.45172
- Wu, G, Liu, J, Liu, M, Huang, Q, Ruan, J, Zhang, C, et al. Truncating variants in OBSCN gene associated with disease-onset and outcomes of hypertrophic cardiomyopathy. *Circ Genom Precis Med.* (2021) 14:e003401. doi: 10.1161/CIRCGEN.121.003401
- Hu, LR, Ackermann, MA, Hecker, PA, Prosser, BL, King, B, O'Connell, KA, et al. Deregulated  $Ca^{2+}$  cycling underlies the development of arrhythmia and heart disease due to mutant obscurin. *Sci Adv.* (2017) 3:e1603081. doi: 10.1126/sciadv.1603081
- Fukuzawa, A, Koch, D, Grover, S, Rees, M, and Gautel, M. When is an obscurin variant pathogenic? The impact of Arg4344Gln and Arg4444Trp variants on protein-protein interactions and protein stability. *Hum Mol Genet.* (2021) 30:1131–41. doi: 10.1093/hmg/ddab010
- Young, P, Ehler, E, and Gautel, M. Obscurin, a giant sarcomeric rho guanine nucleotide exchange factor protein involved in sarcomere assembly. *J Cell Biol.* (2001) 154:123–36. doi: 10.1083/jcb.200102110
- Bang, ML, Centner, T, Fornoff, F, Geach, AJ, Gotthardt, M, McNabb, M, et al. The complete gene sequence of titin, expression of an unusual approximately 700-kDa titin isoform, and its interaction with obscurin identify a novel Z-line to I-band linking system. *Circ Res.* (2001) 89:1065–72. doi: 10.1161/hh2301.100981
- Grogan, A, Coleman, A, Joca, H, Granzier, H, Russel, MW, Ward, CW, et al. Deletion of obscurin immunoglobulin domains Ig58/59 leads to age-dependent cardiac remodeling and arrhythmia. *Basic Res Cardiol.* (2020) 115:60. doi: 10.1007/s00395-020-00818-8
- Shriver, M, Stroka, KM, Vitolo, MI, Martin, S, Huso, DL, Konstantopoulos, K, et al. Loss of giant obscurins from breast epithelium promotes epithelial-to-mesenchymal transition, tumorigenicity and metastasis. *Oncogene.* (2015) 34:4248–59. doi: 10.1038/onc.2014.358
- Kontogianni-Konstantopoulos, A, Jones, EM, Van Rossum, DB, and Bloch, RJ. Obscurin is a ligand for small ankyrin 1 in skeletal muscle. *Mol Biol Cell.* (2003) 14:1138–48. doi: 10.1091/mbc.e02-07-0411
- Desmond, PE, Labuza, A, Muriel, J, Markwardt, ML, Mancini, AE, Rizzo, MA, et al. Interactions between small ankyrin 1 and sarcolipin coordinately regulate activity of the sarco(endo)plasmic reticulum  $Ca^{2+}$ -ATPase (SERCA1). *J Biol Chem.* (2017) 292:10961–72. doi: 10.1074/jbc.M117.783613
- Huang, W, Yu, J, Jones, JW, Carter, CL, Jackson, IL, Vujaskovic, Z, et al. Acute proteomic changes in the lung after WTLLI in a mouse model: identification of potential initiating events for delayed effects of acute radiation exposure. *Health Phys.* (2019) 116:503–15. doi: 10.1097/HP.0000000000000956
- Defnet, AE, Huang, W, Polischak, S, Yadav, SK, Kane, MA, Shapero, P, et al. Effects of ATP-competitive and function-selective ERK inhibitors on airway smooth muscle cell proliferation. *FASEB J.* (2019) 33:10833–43. doi: 10.1096/fj.201900680R
- Chan, JC, Morgan, CP, Adrian Leu, N, Shetty, A, Cisse, YM, Nugent, BM, et al. Reproductive tract extracellular vesicles are sufficient to transmit intergenerational stress

## Publisher's note

All claims expressed in this article are solely those of the authors and do not necessarily represent those of their affiliated organizations, or those of the publisher, the editors and the reviewers. Any product that may be evaluated in this article, or claim that may be made by its manufacturer, is not guaranteed or endorsed by the publisher.

## Supplementary material

The Supplementary material for this article can be found online at: <https://www.frontiersin.org/articles/10.3389/fcvm.2023.1085840/full#supplementary-material>

- and program neurodevelopment. *Nat Commun.* (2020) 11:1499. doi: 10.1038/s41467-020-15305-w
- Williamson, JC, Edwards, AV, Verano-Braga, T, Schwamm, V, Kjeldsen, F, Jensen, ON, et al. High-performance hybrid Orbitrap mass spectrometers for quantitative proteome analysis: observations and implications. *Proteomics.* (2016) 16:907–14. doi: 10.1002/pmic.201400545
- Eng, JK, Fischer, B, Grossmann, J, and Maccoss, MJ. A fast SEQUEST cross correlation algorithm. *J Proteome Res.* (2008) 7:4598–602. doi: 10.1021/pr800420s
- Dorfer, V, Pichler, P, Stranzl, T, Stadlmann, J, Taus, T, Winkler, S, et al. MS Amanda, a universal identification algorithm optimized for high accuracy tandem mass spectra. *J Proteome Res.* (2014) 13:3679–84. doi: 10.1021/pr500202e
- Kall, L, Canterbury, JD, Weston, J, Noble, WS, and MacCoss, MJ. Semi-supervised learning for peptide identification from shotgun proteomics datasets. *Nat Methods.* (2007) 4:923–5. doi: 10.1038/nmeth1113
- Perez-Riverol, Y, Csordas, A, Bai, J, Bernal-Llinares, M, Hewapathirana, S, Kundu, DJ, et al. The PRIDE database and related tools and resources in 2019: improving support for quantification data. *Nucleic Acids Res.* (2019) 47:D442–50. doi: 10.1093/nar/gky1106
- Szklarczyk, D, Gable, AL, Lyon, D, Junge, A, Wyder, S, Huerta-Cepas, J, et al. STRING v11: protein-protein association networks with increased coverage, supporting functional discovery in genome-wide experimental datasets. *Nucleic Acids Res.* (2019) 47:D607–13. doi: 10.1093/nar/gky1131
- Borisov, AB, Raeker, MO, Kontogianni-Konstantopoulos, A, Yang, K, Kurnit, DM, Bloch, RJ, et al. Rapid response of cardiac obscurin gene cluster to aortic stenosis: differential activation of rho-GEF and MLCK and involvement in hypertrophic growth. *Biochem Biophys Res Commun.* (2003) 310:910–8. doi: 10.1016/j.bbrc.2003.09.035
- Hamdani, N, Herwig, M, and Linke, WA. Tampering with springs: phosphorylation of titin affecting the mechanical function of cardiomyocytes. *Biophys Rev.* (2017) 9:225–37. doi: 10.1007/s12551-017-0263-9
- Dobrev, D, and Wehrens, XH. Role of RyR2 phosphorylation in heart failure and arrhythmias: controversies around ryanodine receptor phosphorylation in cardiac disease. *Circ Res.* (2014) 114:1311–9. doi: 10.1161/CIRCRESAHA.114.300568
- Yuchi, Z, Lau, K, and Van Petegem, F. Disease mutations in the ryanodine receptor central region: crystal structures of a phosphorylation hot spot domain. *Structure.* (2012) 20:1201–11. doi: 10.1016/j.str.2012.04.015
- Camors, E, and Valdivia, HH. CaMKII regulation of cardiac ryanodine receptors and inositol triphosphate receptors. *Front Pharmacol.* (2014) 5:101. doi: 10.3389/fphar.2014.00101
- Colyer, J. Phosphorylation states of phospholamban. *Ann N Y Acad Sci.* (1998) 853:79–91. doi: 10.1111/j.1749-6632.1998.tb08258.x
- Hu, LR, and Kontogianni-Konstantopoulos, A. Proteomic analysis of myocardia containing the Obscurin R4344Q mutation linked to hypertrophic cardiomyopathy. *Front Physiol.* (2020) 11:478. doi: 10.3389/fphys.2020.00478
- Narayanan, N, and Xu, A. Phosphorylation and regulation of the  $Ca^{2+}$ -pumping ATPase in cardiac sarcoplasmic reticulum by calcium/calmodulin-dependent protein kinase. *Basic Res Cardiol.* (1997) 92:25–35. doi: 10.1007/BF00794065
- Pedley, AM, and Benkovic, SJ. A new view into the regulation of purine metabolism: the purinosome. *Trends Biochem Sci.* (2017) 42:141–54. doi: 10.1016/j.tibs.2016.09.009
- Sakane, H, Makiyama, T, Nogami, S, Horii, Y, Akasaki, K, and Shirataki, H. Beta-Taxilin participates in differentiation of C2C12 myoblasts into myotubes. *Exp Cell Res.* (2016) 345:230–8. doi: 10.1016/j.yexcr.2016.05.016
- Lange, S, Ouyang, K, Meyer, G, Cui, L, Cheng, H, Lieber, RL, et al. Obscurin determines the architecture of the longitudinal sarcoplasmic reticulum. *J Cell Sci.* (2009) 122:2640–50. doi: 10.1242/jcs.046193



34. Kontogianni-Konstantopoulos, A, Catino, DH, Strong, JC, Sutter, S, Borisov, AB, Pumpin, DW, et al. Obscurin modulates the assembly and organization of sarcomeres and the sarcoplasmic reticulum. *FASEB J.* (2006) 20:2102–11. doi: 10.1096/fj.06-5761com
35. Raeker, MO, Su, F, Geisler, SB, Borisov, AB, Kontogianni-Konstantopoulos, A, Lyons, SE, et al. Obscurin is required for the lateral alignment of striated myofibrils in zebrafish. *Dev Dyn.* (2006) 235:2018–29. doi: 10.1002/dvdy.20812
36. Randazzo, D, Giacomello, E, Lorenzini, S, Rossi, D, Pierantozzi, E, Blaauw, B, et al. Obscurin is required for ankyrinB-dependent dystrophin localization and sarcolemma integrity. *J Cell Biol.* (2013) 200:523–36. doi: 10.1083/jcb.201205118
37. Marston, S, Montgiraud, C, Munster, AB, Copeland, O, Choi, O, Dos Remedios, C, et al. OBSCN mutations associated with dilated cardiomyopathy and haploinsufficiency. *PLoS One.* (2015) 10:e0138568. doi: 10.1371/journal.pone.0138568
38. Stone, MR, O'Neill, A, Lovering, RM, Strong, J, Resneck, WG, Reed, PW, et al. Absence of keratin 19 in mice causes skeletal myopathy with mitochondrial and sarcolemmal reorganization. *J Cell Sci.* (2007) 120:3999–4008. doi: 10.1242/jcs.009241
39. Muriel, JM, O'Neill, A, Kerr, JP, Kleinhaus-Welte, E, Lovering, RM, and Bloch, RJ. Keratin 18 is an integral part of the intermediate filament network in murine skeletal muscle. *Am J Physiol Cell Physiol.* (2020) 318:C215–24. doi: 10.1152/ajpcell.00279.2019
40. Lange, S, Auerbach, D, McLoughlin, P, Perriard, E, Schafer, BW, Perriard, JC, et al. Subcellular targeting of metabolic enzymes to titin in heart muscle may be mediated by DRAL/FHL-2. *J Cell Sci.* (2002) 115:4925–36. doi: 10.1242/jcs.00181
41. Blondelle, J, Marrocco, V, Clark, M, Desmond, P, Myers, S, Nguyen, J, et al. Murine obscurin and Obsl1 have functionally redundant roles in sarcolemmal integrity, sarcoplasmic reticulum organization, and muscle metabolism. *Commun Biol.* (2019) 2:178. doi: 10.1038/s42003-019-0405-7
42. Gautel, M, Leonard, K, and Labeit, S. Phosphorylation of KSP motifs in the C-terminal region of titin in differentiating myoblasts. *EMBO J.* (1993) 12:3827–34. doi: 10.1002/j.1460-2075.1993.tb06061.x
43. Gregorio, CC, Trombitas, K, Centner, T, Kolmerer, B, Stier, G, Kunke, K, et al. The NH2 terminus of titin spans the Z-disc: its interaction with a novel 19-kD ligand (T-cap) is required for sarcomeric integrity. *J Cell Biol.* (1998) 143:1013–27. doi: 10.1083/jcb.143.4.1013
44. Candasamy, AJ, Haworth, RS, Cuello, F, Ibrahim, M, Aravamudan, S, Kruger, M, et al. Phosphoregulation of the titin-cap protein telethonin in cardiac myocytes. *J Biol Chem.* (2014) 289:1282–93. doi: 10.1074/jbc.M113.479030
45. Grimm, M, Mahnecke, N, Soja, F, El-Armouche, A, Haas, P, Treede, H, et al. The MLCK-mediated alpha1-adrenergic inotropic effect in atrial myocardium is negatively modulated by PK Cepsilon signaling. *Br J Pharmacol.* (2006) 148:991–1000. doi: 10.1038/sj.bjp.0706803
46. Martinez-Quiles, N, Ho, HY, Kirschner, MW, Ramesh, N, and Geha, RS. Erk/Src phosphorylation of cortactin acts as a switch on-switch off mechanism that controls its ability to activate N-WASP. *Mol Cell Biol.* (2004) 24:5269–80. doi: 10.1128/MCB.24.12.5269-5280.2004
47. Wu, X, Renuse, S, Sahasrabudhe, NA, Zahari, MS, Chaerkady, R, Kim, MS, et al. Activation of diverse signaling pathways by oncogenic PIK3CA mutations. *Nat Commun.* (2014) 5:4961. doi: 10.1038/ncomms5961
48. Janjanam, J, Chandaka, GK, Kotla, S, and Rao, GN. PLCbeta3 mediates cortactin interaction with WAVE2 in MCP1-induced actin polymerization and cell migration. *Mol Biol Cell.* (2015) 26:4589–606. doi: 10.1091/mbc.E15-08-0570
49. Zhou, Q, Ruiz-Lozano, P, Martone, ME, and Chen, J. Cypher, a striated muscle-restricted PDZ and LIM domain-containing protein, binds to alpha-actinin-2 and protein kinase C. *J Biol Chem.* (1999) 274:19807–13. doi: 10.1074/jbc.274.28.19807
50. Faulkner, G, Pallavicini, A, Formentin, E, Comelli, A, Ievolella, C, Trevisan, S, et al. ZASP: a new Z-band alternatively spliced PDZ-motif protein. *J Cell Biol.* (1999) 146:465–75. doi: 10.1083/jcb.146.2.465
51. Frey, N, and Olson, EN. Calsarcin-3, a novel skeletal muscle-specific member of the calsarcin family, interacts with multiple Z-disc proteins. *J Biol Chem.* (2002) 277:13998–4004. doi: 10.1074/jbc.M200712200
52. von Nandelstadh, P, Ismail, M, Gardin, C, Suila, H, Zara, I, Belgrano, A, et al. A class III PDZ binding motif in the myotilin and FAT2 families binds enigma family proteins: a common link for Z-disc myopathies. *Mol Cell Biol.* (2009) 29:822–34. doi: 10.1128/MCB.01454-08
53. Xi, Y, Ai, T, De Lange, E, Li, Z, Wu, G, Brunelli, L, et al. Loss of function of hNav1.5 by a ZASP1 mutation associated with intraventricular conduction disturbances in left ventricular non-compaction. *Circ Arrhythm Electrophysiol.* (2012) 5:1017–26. doi: 10.1161/CIRCEP.111.969220
54. Russell, MA. Synemin redefined: multiple binding partners results in multi-functionality. *Front Cell Dev Biol.* (2020) 8:159. doi: 10.3389/fcell.2020.00159
55. Cooper, CD, and Lampe, PD. Casein kinase I regulates connexin-43 gap junction assembly. *J Biol Chem.* (2002) 277:44962–8. doi: 10.1074/jbc.M209427200
56. Hoshijima, M. Mechanical stress-strain sensors embedded in cardiac cytoskeleton: Z disk, titin, and associated structures. *Am J Physiol Heart Circ Physiol.* (2006) 290:H1313–25. doi: 10.1152/ajpheart.00816.2005
57. Dally, S, Monceau, V, Corvazier, E, Bredoux, R, Raies, A, Bobe, R, et al. Compartmentalized expression of three novel sarco/endoplasmic reticulum Ca2+-ATPase 3 isoforms including the switch to ER stress, SERCA3f, in non-failing and failing human heart. *Cell Calcium.* (2009) 45:144–54. doi: 10.1016/j.ceca.2008.08.002
58. Toyofuku, T, Kurzydowski, K, Tada, M, and MacLennan, DH. Identification of regions in the Ca(2+)-ATPase of sarcoplasmic reticulum that affect functional association with phospholamban. *J Biol Chem.* (1993) 268:2809–15. doi: 10.1016/S0021-9258(18)53845-X
59. Arvanitis, DA, Vafiadaki, E, Sanoudou, D, and Kranias, EG. Histidine-rich calcium binding protein: the new regulator of sarcoplasmic reticulum calcium cycling. *J Mol Cell Cardiol.* (2011) 50:43–9. doi: 10.1016/j.yjmcc.2010.08.021
60. Shoshan-Barmatz, V, Orr, I, Weil, S, Meyer, H, Varsanyi, M, and Heilmeyer, LM. The identification of the phosphorylated 150/160-kDa proteins of sarcoplasmic reticulum, their kinase and their association with the ryanodine receptor. *Biochim Biophys Acta.* (1996) 1283:89–100. doi: 10.1016/0005-2736(96)00079-X
61. Beckendorf, J, van den Hoogenhof, MMG, and Backs, J. Physiological and unappreciated roles of CaMKII in the heart. *Basic Res Cardiol.* (2018) 113:29. doi: 10.1007/s00395-018-0688-8
62. Maier, LS. Role of CaMKII for signaling and regulation in the heart. *Front Biosci.* (2009) 14:486–96. doi: 10.2741/3257
63. Grogan, A, Tsakiroglou, P, and Kontogianni-Konstantopoulos, A. Double the trouble: giant proteins with dual kinase activity in the heart. *Biophys Rev.* (2020) 12:1019–29. doi: 10.1007/s12551-020-00715-3
64. Zhang, W, Elimban, V, Nijjar, MS, Gupta, SK, and Dhalla, NS. Role of mitogen-activated protein kinase in cardiac hypertrophy and heart failure. *Exp Clin Cardiol.* (2003) 8:173–83.
65. Prowse, CN, Deal, MS, and Lew, J. The complete pathway for catalytic activation of the mitogen-activated protein kinase, ERK2. *J Biol Chem.* (2001) 276:40817–23. doi: 10.1074/jbc.M105862000
66. Cargnello, M, and Roux, PP. Activation and function of the MAPKs and their substrates, the MAPK-activated protein kinases. *Microbiol Mol Biol Rev.* (2011) 75:50–83. doi: 10.1128/MMBR.00031-10
67. Haas Bueno, R, and Recamonde-Mendoza, M. Meta-analysis of transcriptomic data reveals pathophysiological modules involved with atrial fibrillation. *Mol Diagn Ther.* (2020) 24:737–51. doi: 10.1007/s40291-020-00497-0
68. Li, D, Shinagawa, K, Pang, L, Leung, TK, Cardin, S, Wang, Z, et al. Effects of angiotensin-converting enzyme inhibition on the development of the atrial fibrillation substrate in dogs with ventricular tachypacing-induced congestive heart failure. *Circulation.* (2001) 104:2608–14. doi: 10.1161/hc4601.099402
69. Goette, A, Staack, T, Rocken, C, Arndt, M, Geller, JC, Huth, C, et al. Increased expression of extracellular signal-regulated kinase and angiotensin-converting enzyme in human atria during atrial fibrillation. *J Am Coll Cardiol.* (2000) 35:1669–77. doi: 10.1016/S0735-1097(00)00611-2
70. Andrade, J, Khairy, P, Dobrev, D, and Nattel, S. The clinical profile and pathophysiology of atrial fibrillation: relationships among clinical features, epidemiology, and mechanisms. *Circ Res.* (2014) 114:1453–68. doi: 10.1161/CIRCRESAHA.114.303211
71. Kornej, J, Borschel, CS, Benjamin, EJ, and Schnabel, RB. Epidemiology of atrial fibrillation in the 21st century: novel methods and new insights. *Circ Res.* (2020) 127:4–20. doi: 10.1161/CIRCRESAHA.120.316340
72. Goette, A, Kalman, JM, Aguinaga, L, Akar, J, Cabrera, JA, Chen, SA, et al. Document reviewers: EHRA/HRS/APHS/SOLAECE expert consensus on atrial cardiomyopathies: definition, characterization, and clinical implication. *Europace.* (2016) 18:1455–90. doi: 10.1093/europace/euw161
73. Alvarez-Franco, A, Rouco, R, Ramirez, RJ, Guerrero-Serna, G, Tiana, M, Cogliati, S, et al. Transcriptome and proteome mapping in the sheep atria reveal molecular features of atrial fibrillation progression. *Cardiovasc Res.* (2021) 117:1760–75. doi: 10.1093/cvr/cvaa307
74. De Souza, AI, Cardin, S, Wait, R, Chung, YL, Vijayakumar, M, Maguy, A, et al. Proteomic and metabolomic analysis of atrial fibrillation remodeling in congestive heart failure. *J Mol Cell Cardiol.* (2010) 49:851–63. doi: 10.1016/j.yjmcc.2010.07.008
75. Liu, B, Li, X, Zhao, C, Wang, Y, Lv, M, Shi, X, et al. Proteomic analysis of atrial appendages revealed the pathophysiological changes of atrial fibrillation. *Front Physiol.* (2020) 11:573433. doi: 10.3389/fphys.2020.573433
76. Liu, Y, Bai, F, Tang, Z, Liu, N, and Liu, Q. Integrative transcriptomic, proteomic, and machine learning approach to identifying feature genes of atrial fibrillation using atrial samples from patients with valvular heart disease. *BMC Cardiovasc Disord.* (2021) 21:52. doi: 10.1186/s12872-020-01819-0
77. Cao, H, Zhu, X, Chen, X, Yang, Y, Zhou, Q, Xu, W, et al. Quantitative proteomic analysis to identify differentially expressed proteins in the persistent atrial fibrillation using TMT coupled with nano-LC-MS/MS. *Am J Transl Res.* (2020) 12:5032–47.
78. Jiang, YY, Hou, HT, Yang, Q, Liu, XC, and He, GW. Chloride channels are involved in the development of atrial fibrillation - a transcriptomic and proteomic study. *Sci Rep.* (2017) 7:10215. doi: 10.1038/s41598-017-10590-w
79. Kourliouros, A, Yin, X, Didangelos, A, Hosseini, MT, Valencia, O, Mayr, M, et al. Substrate modifications precede the development of atrial fibrillation after cardiac surgery: a proteomic study. *Ann Thorac Surg.* (2011) 92:104–10. doi: 10.1016/j.athoracsurg.2011.03.071

80. Goudarzi, M, Ross, MM, Zhou, W, Van Meter, A, Deng, J, Martin, LM, et al. Development of a novel proteomic approach for mitochondrial proteomics from cardiac tissue from patients with atrial fibrillation. *J Proteome Res.* (2011) 10:3484–92. doi: 10.1021/pr200108m
81. Mayr, M, Yusuf, S, Weir, G, Chung, YL, Mayr, U, Yin, X, et al. Combined metabolomic and proteomic analysis of human atrial fibrillation. *J Am Coll Cardiol.* (2008) 51:585–94. doi: 10.1016/j.jacc.2007.09.055
82. De Souza, AI, and Camm, AJ. Proteomics of atrial fibrillation. *Circ Arrhythm Electrophysiol.* (2012) 5:1036–43. doi: 10.1161/CIRCEP.112.973008
83. Safabakhsh, S, Panwar, P, Barichello, S, Sangha, SS, Hanson, PJ, Petegem, FV, et al. The role of phosphorylation in atrial fibrillation: a focus on mass spectrometry approaches. *Cardiovasc Res.* (2022) 118:1205–17. doi: 10.1093/cvr/cvab095
84. Bardou, P, Mariette, J, Escudie, F, Djemiel, C, and Klopp, C. jvenn: an interactive Venn diagram viewer. *BMC Bioinformatics.* (2014) 15:293. doi: 10.1186/1471-2105-15-293

# Frontiers in Cardiovascular Medicine

Innovations and improvements in cardiovascular treatment and practice

Focuses on research that challenges the status quo of cardiovascular care, or facilitates the translation of advances into new therapies and diagnostic tools.

## Discover the latest Research Topics

[See more →](#)

### Frontiers

Avenue du Tribunal-Fédéral 34  
1005 Lausanne, Switzerland  
[frontiersin.org](https://frontiersin.org)

### Contact us

+41 (0)21 510 17 00  
[frontiersin.org/about/contact](https://frontiersin.org/about/contact)



### Frontiers in Cardiovascular Medicine

